Thermodynamic study of solid-liquid-vapor equilibrium : application to cryogenics and air separation unit

Marco Campestrini

ParisTech
INSTITUT DES SCIENCES ET TECHNOLOGIES
PARIS INSTITUTE OF TECHNOLOGY

MINES ParisTech

École doctorale n° 432 : Sciences des Métiers de l'ingénieur

Doctorat ParisTech

T H È S E

pour obtenir le grade de docteur délivré par

l'École Nationale Supérieure des Mines de Paris

Spécialité " Energétique et Procédés "

présentée et soutenue publiquement par

Marco CAMPESTRINI

le 9 décembre 2014

Etude thermodynamique des équilibres solide-liquide-vapeur: application à la cryogénie et aux unités de séparation de l'air

(Thermodynamic study of solid-liquid-vapor equilibrium: application to cryogenics and air separation unit)

Directeur de thèse : **Christophe COQUELET**
Maître de thèse : **Paolo STRINGARI**

Jury:

M. Jean-Noël JAUBERT, Pr., Université de Lorraine, Laboratoire Réactions et Génie des Procédés	Président
M. João Araújo Pereira COUTINHO, Pr., University of Aveiro, Department of Chemistry	Rapporteur
Mme. Laura Annamaria PELLEGRINI, Pr., Politecnico of Milan, Department of Chemistry	Rapporteur
M. Philippe ARPENTINIER, Dr., Air Liquide - Centre de Recherche Claude-Delorme	Examinateur
M. Christophe COQUELET, Pr., MINES ParisTech, PSL Research University , CTP	Examinateur
M. Guy DE WEIRELD, Pr., Université de Mons, Department of Thermodynamics	Examinateur
M. Maurizio GRIGIANTE, Dr., University of Trento, Department of Civil and Environmental Engineering	Examinateur
M. Paolo STRINGARI, Dr., MINES ParisTech, PSL Research University, CTP	Examinateur

T H È S E

MINES ParisTech
CTP – Centre Thermodynamique des Procédés
35, rue Saint Honoré, 77300 Fontainebleau

Acknowledgments

I would like to express my gratitude to all the jury members. I am thankful to Pr. João Coutinho and Pr. Laura Annamaria Pellegrini for agreeing to read and evaluate my work, and for the interest shown in being supervisor of this thesis. In addition, a thank you to Pr. Jean-Noël Jaubert and Pr. Guy de Weireld, for accepting to examine this three years work and for the kind cooperation. I wish to thank Dr. Maurizio Grigiante, who in 2010 proposed me to spend a month at the Centre Thermodynamics of Processes, thus giving beginning to my French experience.

I would like to acknowledge the crucial role of Pr. Christophe Coquelet, Dr. Paolo Stringari, and Dr. Philippe Arpentinier. My gratitude is addressed to my project external guide Dr. Philippe Arpentinier from the Air Liquide company, for the useful comments, remarks and engagement during the last three years, especially through the learning process of the cryogenic distillation of air.

I would like to express my special appreciation and thanks to my *directeur de thèse*, Pr. Christophe Coquelet, and my *maître de thèse*, Dr. Paolo Stringari. You have been important mentors for me, and I thank you for your motivating guidance, invaluable constructive criticism and friendly advice during this work. Furthermore, I would like to thank Dr. Paolo Stringari for encouraging my research and for allowing me to grow as a researcher. Your advices on research as well as on my career have been priceless. Thank you for your precious assistance you have been giving me since 2010, and for all the constructive discussions we shared sometimes till night in your office.

I would like to thank all the staff of the Centre Thermodynamics of Processes, who has been receiving me as in a family since the beginning of my thesis. Special thanks go to my friends, colleagues and team mates, Martha, Snaïde, Elise, Fan, Eric, Mauro, Jamal, and Ali. Your support has been fundamental, thank you for remembering me that life is not only work and for making me smiling even in the most busy and stressful periods. I have also to appreciate the assistance provided by Marie-Claude and Jocelyne in dealing with French bureaucracy, and the guidance given by David and Herve in playing football and learning French, respectively.

I would like to express my gratitude to the Air Liquide company, ARMINES, and the Ecole Nationale Supérieure des Mines de Paris for giving me the possibility of doing this work and growing as a researcher.

I want to express my endless gratitude to my wife and my family. You all shared with me these three years, it has not been easy to stay away from you, but you have never ceased to make me feel your love, your support and your encouragement. I will never forget what you have done to allow this aim to be possible. Grazie Fabrizia, Renzo, Maria, e Barbara.

Table of Contents

LIST OF FIGURES ..... **III**

LIST OF TABLES ..... **VII**

PREFACE **1**

INTRODUCTION AND SUMMARY **3**

1 AIR DISTILLATION 5
1.1 Air separation technologies *5*
1.2 Cryogenic air separation unit *6*
1.2.1 ASU block diagram and P-h diagram 8
1.2.2 ASU flow diagram 11
1.2.2.1 Argon and rare gases separation 14
1.2.2.2 Cold box 14
1.2.3 ASU operative conditions 15
1.2.4 Safety problems and contaminants removal 16
1.3 Systems of interest *18*
1.3.1 Bibliographic research 20
2 PHASE DIAGRAMS INCLUDING SOLID PHASE 23
2.1 Aggregation states of the matter *23*
2.2 Phase rule *23*
2.3 First order phase transition *24*
2.4 Phase diagrams *25*
2.4.1 Pure compounds 25
2.4.1.1 Shape of the melting line 26
2.4.2 Binary mixture 28
2.4.2.1 Global phase diagrams for fluid phases 28
2.4.2.2 Solid-liquid temperature-composition projections 29
2.4.2.3 Global phase diagrams for solid and fluid phases 30
2.4.2.4 Type I PT-EP 32
3 PHASE EQUILIBRIUM CALCULATION 33
3.1 Equilibrium condition *33*
3.1.1 Symmetric and asymmetric approach 35
3.1.2 Cubic EoSs 35
3.1.3 Fugacity coefficient from an EoS and Gibbs free energy of mixing 37
3.2 Representation of the solid-liquid equilibrium *40*
3.2.1 Classical approach 40
3.2.2 Solid-fluid equilibrium models 41
3.2.3 Solid-liquid transition 44
3.2.4 SFE models comparison 45
4 REPRESENTATION OF PHASE EQUILIBRIA. I. PURE COMPOUNDS 51
4.1 Yokozeki EoS *51*
4.2 Analytical solution of the SLV EoS *55*
4.3 Setting EoS parameters of the SLV EoS *55*
4.3.1 New procedure for setting EoS parameters 59
4.4 Modeling of phase equilibrium properties *62*
4.4.1 Equilibrium pressures and temperatures 63
4.4.2 Equilibrium densities and enthalpies 65
4.5 Results for pure compounds *67*
4.5.1 Pressure-temperature ranges for the EoS parameters regression 68
4.5.2 Representation of pressure-temperature equilibrium projections 69
5 EXTENSION TO MIXTURES 73
5.1 Mixing rules *73*
5.2 Partial molar fugacity coefficients *76*
5.3 Minimization of the Gibbs free energy of mixing *77*

5.4 Prediction of phase equilibria in binary mixtures *79*
5.5 Mixtures of interest: data assessment *84*
5.6 Application of the SLV EoS to Lennard-Jones mixtures *86*
5.6.1 Lennard-Jones potential 87
5.6.2 Functional form of the LJ-SLV EoS 88
5.6.3 Phase diagram of the LJ fluid from the LJ-SLV EoS 88
5.6.4 Phase diagram of binary LJ mixtures from the LJ-SLV EoS 90
5.6.4.1 Equation for the binary interaction parameters 92
5.6.5 Phase diagram of real binary mixtures from the SLV EoS and predicted binary interaction parameters 92
6 REPRESENTATION OF PHASE EQUILIBRIA. II. BINARY MIXTURES 97
6.1 Evaluation of a three phase line *98*
6.2 Evaluation of then critical loici *98*
6.3 Results for the binary mixtures of interest *99*
6.3.1 Type Ia PT-EP: systems Ar+Kr and N_2+Ar 102
6.3.2 Type Ib PT-EP: system Ar+CH_4 111
6.3.3 Type IIb PT-EP: O_2+C_2H_6 116
6.3.4 Type IIIb+c PT-EP: system N_2+C_2H_6 123
6.3.5 Type IIIb+d PT-EP: system Ar+CO_2 129
6.4 Considerations about the binary interaction parameters *133*
6.5 Modeling O_2+impurity binary mixtures at the reboiler-condenser of the ASU *134*
CONCLUSIONS **137**
BIBLIOGRAPHY **141**
COMMUNICATIONS **147**
APPENDIX A **A1**
APPENDIX B **B1**
APPENDIX C **C1**
APPENDIX D **D1**
APPENDIX E **E1**
APPENDIX F **F1**

List of figures

Figure i.1: Single column apparatus for air separation by Carl von Linde. 2
Figure i.2: Single column apparatus for air separation by Georges Claude. 2
Figure 1.1: Air Liquide MEDAL membrane technology for nitrogen production. 6
Figure 1.2: Principle of the Air Liquide FLOXAL adsorption technology for oxygen and nitrogen production. 6
Figure 1.3: Saturation lines of the three main air components. 7
Figure 1.4: Molar fractions of nitrogen in the liquid and vapor phases in the N_2/O_2 system at 0.1, 0.5 and 1 MPa. 8
Figure 1.5: Molar fractions of argon in the liquid and vapor phases in the Ar/O_2 system at 0.1, 0.5 and 1 MPa. 8
Figure 1.6: ASU main components. 9
Figure 1.7: Pressure-enthalpy diagram of air. 10
Figure 1.8: ASU block diagram: main components and flows within an ASU. 10
Figure 1.9: Air separation unit flow diagram. 12
Figure 1.10: Example of the pressure drop chart of an ASU. 15
Figure 1.11: Qualitative removal efficiency. 18
Figure 2.1: Pressure-temperature equilibrium projection of a phase diagram for a pure substance. 25
Figure 2.2: Qualitative pressure-temperature equilibrium projections of a phase diagram for a pure substance, considering only solid-liquid and liquid-vapor equilibria. 27
Figure 2.3: Qualitative Type I PT-EP systems as presented in van Konynenburg and Scott. 29
Figure 2.4: Types of solid–liquid phase diagrams identified by Matsuoka. 30
Figure 2.5: Qualitative Type I PT-EP systems in case of complete miscibility in the solid phase. 32
Figure 2.6: Qualitative Type I PT-EP systems in case of partial or total immiscibility in the solid phase. 32
Figure 3.1: Qualitative representation of the vapor-liquid equilibrium in a pure compound. 38
Figure 3.2: Qualitative representation of the vapor-liquid equilibrium in a binary mixture. 39
Figure 3.3: SLE of methane from fundamental relation. 40
Figure 3.4: Qualitative subcritical isothermal pressure-volume equilibrium projection of a pure compound. 44
Figure 3.5: Graphical derivation of the Maxwell's equal area rule for phase transition. 44
Figure 3.6: Proposed phase equilibrium behaviors for the solid-liquid transition. 45
Figure 4.1: Schematic *P*-*v* diagram of the Yokozeki EoS at the triple point temperature and $v>b$. 52
Figure 4.2: Qualitative Pressure-residual Gibbs free energy diagram related to the Yokozeki EoS. 52
Figure 4.3: Proper EoS parameter regions for solving the critical point condition with different attractive terms. 57
Figure 4.4: Function $a(T)$ for argon. 58
Figure 4.5: Function $b(T)$ for argon. 58
Figure 4.6: Phase diagram of argon and carbon dioxide in the pressure-temperature equilibrium projection obtained by the Yokozeki EoS with vdW attractive term. 59
Figure 4.7: Flow chart of the proposed procedure for setting the parameters of the SLV EoS. 61
Figure 4.8: Values of the parameter *a* for argon. 64
Figure 4.9: Values of the parameter b for argon. 64
Figure 4.10: Pressure-temperature equilibrium behavior of argon obtained with the SLV EoS and values from auxiliary equations. 65
Figure 4.11: Reduced temperature – reduced density phase equilibrium behavior for argon. 66
Figure 4.12: Latent heats of transition versus reduced equilibrium temperature for argon. 66
Figure 4.13: PT-EP of methane obtained with the SLV EoS. 71
Figure 4.14: PT-EP of carbon dioxide obtained with the SLV EoS. 71
Figure 5.1: Qualitative Gibbs free energy of mixing at the solid-solid-liquid equilibrium. 74
Figure 5.2: Qualitative Gibbs free energy of mixing for the solid, liquid, and vapor phases. 77

Figure 5.3: Main steps of the simplified version of the flow diagram related to the algorithm for the minimization of the Gibbs free energy of mixing. 78
Figure 5.4: Vapor-liquid equilibrium at 138 K for the system Ar + Kr. 79
Figure 5.5: Solid-liquid equilibrium for the system Ar + Kr. 80
Figure 5.6: Vapor-liquid equilibrium at 100 K for the system N_2 + O_2. 80
Figure 5.7: Solid-liquid equilibrium for the system N_2 + O_2. 81
Figure 5.8: Vapor-liquid equilibrium at 253 K for the system N_2 + N_2O. 81
Figure 5.9: Solid-liquid equilibrium for the system N_2 + N_2O. 82
Figure 5.10: Saturation lines of N_2, O_2, and N_2O. 83
Figure 5.11: Lennard-Jones intermolecular potential. 87
Figure 5.12: Reduced pressure, P*, versus reduced temperature, T*; diagram for the pure LJ fluid. 89
Figure 5.13: Temperature vs. composition phase diagrams for two LJ binary mixtures. 91
Figure 5.14: Dependence of the binary interaction parameter k_{ij} from $\varepsilon_{11}/\varepsilon_{22}$ and σ_{11}/σ_{22}. 91
Figure 5.15: Solid-liquid equilibrium for the system Ar – Kr in the temperature-composition diagram. 93
Figure 5.16: Solid-liquid equilibrium for the system Ar – CH_4 in the temperature-composition diagram. 94
Figure 5.17: Solid-liquid equilibrium for the system N_2 – Ar in the temperature-composition diagram. 95
Figure 6.1: Mixture Ar+Kr : comparison between experimental and calculated values of SLE. 102
Figure 6.2: Mixture Ar+Kr: comparison between experimental and calculated values of VLE. 102
Figure 6.3: Mixture Ar+Kr: qualitative pressure-temperature equilibrium projection. 103
Figure 6.4: Mixture Ar+Kr: calculated pressure-temperature equilibrium projection. 104
Figure 6.5: Mixture Ar+Kr: evolution of the phase equilibrium behavior with pressure in the range 70 K – 160 K. 105
Figure 6.6: Mixture N_2+Ar: comparison between experimental and calculated values of SLE. 106
Figure 6.7: Mixture N_2+Ar: comparison between experimental and calculated values of VLE. 106
Figure 6.8: Mixture N_2+Ar: qualitative pressure-temperature equilibrium projection. 107
Figure 6.9: Mixture N_2+Ar: calculated pressure-temperature equilibrium projection. 108
Figure 6.10: Mixture N_2+Ar: calculated pressure-temperature equilibrium projection in the proximity of the triple point of N_2. 109
Figure 6.11: Mixture N_2+Ar: evolution of the phase equilibrium behavior with pressure in the range 55 K – 85 K. 110
Figure 6.12: Mixture Ar+CH_4: comparison between experimental and calculated values of SLE. 111
Figure 6.13: Mixture Ar+CH_4: comparison between experimental and calculated values of VLE. 111
Figure 6.14: Mixture Ar+CH_4: qualitative pressure-temperature equilibrium projection. 112
Figure 6.15: Mixture Ar+CH_4: calculated pressure-temperature equilibrium projection. 113
Figure 6.16: Mixture Ar+CH_4: calculated pressure-temperature equilibrium projection in the proximity of the triple points. 114
Figure 6.17: Mixture Ar+CH_4: evolution of the phase equilibrium behavior with pressure in the range 65 K – 115 K. 115
Figure 6.18: Mixture O_2+C_2H_6: comparison between experimental and calculated values of VLE. 116
Figure 6.19: Mixture O_2+C_2H_6: comparison between experimental and calculated values of SLE. 117
Figure 6.20: Mixture O_2+C_2H_6: qualitative pressure-temperature equilibrium projection. 118
Figure 6.21: Mixture O_2+C_2H_6: calculated pressure-temperature equilibrium projection. 119
Figure 6.22: Mixture O_2+C_2H_6: calculated pressure-temperature equilibrium projection in the proximity of the triple point of O_2. 120
Figure 6.23: Mixture O_2+C_2H_6: evolution of the phase equilibrium behavior with pressure in the range 40 K – 200 K up to 0.2 MPa. 121
Figure 6.24: Mixture O_2+C_2H_6: evolution of the phase equilibrium behavior with pressure in the range 40 K – 320 K for P > 0.2 MPa. 122
Figure 6.25: Mixture N_2+C_2H_6: comparison between experimental and calculated values of SLE. 123
Figure 6.26: Mixture N_2+C_2H_6: comparison between experimental and calculated values of VLE. 123
Figure 6.27: Mixture N_2+C_2H_6: qualitative pressure-temperature equilibrium projection. 124
Figure 6.28: Mixture N_2+C_2H_6: calculated pressure-temperature equilibrium projection. 125
Figure 6.29: Mixture N_2+C_2H_6: calculated pressure-temperature equilibrium projection in the proximity of the triple point of N_2. 126
Figure 6.30: Mixture N_2+C_2H_6: evolution of the phase equilibrium behavior with pressure in the range 50 K – 300 K up to 3 MPa. 127

Figure 6.31: Mixture N_2+C_2H_6: evolution of the phase equilibrium behavior with pressure in the range 50 K – 300 K for P > 3 MPa..... 128
Figure 6.32: Mixture Ar+CO_2: comparison between experimental and calculated values of VLE. 129
Figure 6.33: Mixture Ar+CO_2: qualitative pressure-temperature equilibrium projection. 130
Figure 6.34: Mixture Ar+CO_2: calculated pressure-temperature equilibrium projection. 131
Figure 6.35: Mixture Ar+CO_2: evolution of the phase equilibrium behavior with pressure in the range 50 K – 300 K. 132
Figure 6.36: Form of a typical temperature dependent function used for the binary interaction parameters. 133
Figure 6.37: Phase equilibrium behavior of the system O_2+CH_4 at 94 K. 135
Figure 6.38: Phase equilibrium behavior of the system O_2+C_2H_4 at 94 K. 135
Figure 6.39: Phase equilibrium behavior of the system O_2+C_2H_4 at 94 K for $xO_2 \geq 0.92$. 136

List of tables

Table 1.1: Air composition. 5
Table 1.2: The three processes of air separation. 5
Table 1.3: Abbreviations used in the ASU flow diagram. 11
Table 1.4: Selection of the binary mixtures of interest for the bibliographic study. 19
Table 1.5: Binary mixtures and pure compounds of interest for this study. 20
Table 1.6: Literature review on the kind of equilibrium data for the binary mixtures on interest. 21
Table 2.1: Phase rule scenarios for a pure substance. 25
Table 2.2: Phase rule scenarios for a binary mixture. 31
Table 2.3: Abbreviations, line styles and symbols used in the PT-EP. 31
Table 3.1: Formalisms for the symmetric and asymmetric approaches for the equilibrium condition between a vapor phase and a dense phase in pure compounds and mixtures. 35
Table 3.2: Principal cubic EoSs. 36
Table 3.3: Examples of α–function for subcritical temperatures. 37
Table 3.4: Overview of the main models accounting for the SFE. 43
Table 3.5: SFE models comparison in terms of number of parameters, data involved in the regression of the parameters, and additional fluid-state model. 46
Table 3.6: SFE models comparison in terms of proposed criteria. 48
Table 4.1: Functional forms of the SLV EoS which have been compared in terms of representation of phase equilibrium properties of pure argon. 62
Table 4.2: EoS parameters of the five different SLV EoSs for argon. 62
Table 4.3: Summary of the statistical errors in calculating equilibrium temperatures at fixed pressures for argon. 63
Table 4.4: Summary of the statistical errors in calculating equilibrium pressures at fixed temperatures for argon. 63
Table 4.5: Triple and critical points for the substances of interest. 68
Table 4.6: Minimum SVE and maximum SLE values for the temperature and pressure used for the regression of the SLV EoS parameters. 68
Table 4.7: Summary of the statistical errors in calculating equilibrium pressures at fixed temperatures for the pure compounds of interest. 69
Table 4.8: Summary of the statistical errors in calculating equilibrium temperatures at fixed pressures for the pure compounds of interest. 70
Table 5.1: Temperature ranges of the available experimental values of fluid-fluid and solid-fluid equilibria for the mixtures of interest in this study. 85
Table 5.2: Parameters of the LJ-SLV EoS in reduced variables. 89
Table 5.3: Coefficients for the calculation of the binary interaction parameters from LJ parameters. 92
Table 5.4: Binary interaction parameters for the mixtures Ar + Kr, Ar + CH_4, and N_2 + Ar calculated from LJ parameters. 93
Table 6.1: Binary mixtures represented with regressed binary interaction parameters. 97
Table 6.2: Classification of the binary mixtures of interest according to the encountered pressure-temperature equilibrium behaviors. 100
Table 6.3: Liquid composition at level of the *LPC* sump. 134

Preface

Nowadays, the liquefaction of gases is a key issue in different fields. Several anthropic applications, like metallurgy, chemistry, petrochemistry, health, and electronics, require reasonable supplies of oxygen, nitrogen, and argon. High purity volumes of these substances are obtained from atmospheric air undergoing liquefaction in a cryogenic distillation plant.

At the same time, the world energetic demand is partially satisfied thanks to natural gas, predominantly constituted of methane. In this case, the liquefaction is operated mainly for reducing volumes and consequently abating the transport costs from the areas where natural gas is produced to where it is needed.

The first liquefaction of a gas was achieved by Louis Clouet and Gaspard Monge around 1780. Liquid SO_2 came out from a cooled coil plunged in a bath of salt and ice and fed with compressed gas. Ammonia was liquefied for the first time in 1787 in a bath of snow and hydrochloric calcareous earth. In 1823, Michael Faraday liquefied SO_2, H_2S, CO_2, N_2O, C_2H_2, NH_3, and HCl using a compressor up to 40 bars and cooling the apparatus down to –110°C in a bath of ether and solid carbon dioxide.

Nevertheless, O_2, CO, N_2, He, and H_2 were still considered as "*permanent gases*" since any attempt to liquefy them by means of very high pressures failed due to the incapacity of lowering the temperature under their critical temperatures. It was Thomas Andrews in 1869 who first pointed out that liquefaction of a gas cannot be achieved above the critical temperature even for the highest imposed pressure.

Droplets of liquid oxygen were obtained for the first time in 1877 independently by Louis Paul Cailletet in Paris and Raoul-Pierre Pictet in Geneva. The former physicist allowed cooled and compressed oxygen to rapidly expand, thus exploiting the Joule-Thomson effect for cooling the gas further. Pictet first vaporized SO_2 to liquefy CO_2 and then vaporize CO_2 to liquefy O_2. Based on these insights of introducing an isoenthalpic expansion and subsequent steps of vaporization/liquefaction, the so called "*cascade method*", Sigmund von Wroblewski was able in 1883 in Cracow to collect liquid oxygen and show a meniscus between the liquid and the vapor phases. With the same technique, he liquefied also small quantities of N_2, CO, and CH_4.

The first liquefaction of air in an industrial scale was performed by Carl von Linde in 1895. He used a throttle valve giving the Joule-Thomson isoenthalpic expansion, thereby lowering the temperature of the precooled and compressed feed air till obtaining its partial liquefaction. In 1901, same scientist obtained pure liquid oxygen by a single column apparatus equipped with a reboiler at the bottom, resumed in Figure i.1.

The feed compressed and precooled air is partially liquefied through two heat exchangers and an expansion valve before entering at the top of the distillation column. The first heat exchange occurs in countercurrent with the gaseous products of the process that are moved away from the column. The second heat exchanger is placed at the bottom of the column and it is the centre of the heat exchange between the feed air and the liquid oxygen. The liquid oxygen receives enough heat for reaching its boiling point, and for this reason this exchanger is called reboiler.

The produced oxygen is drawn from the bottom in the vapor state and it may be very pure. The purity of the nitrogen drawn from the top can be improved by increasing the number of trays inside the column, but this stream will still contain high quantity of oxygen owing to the proximity of its extraction point whit the feed air.

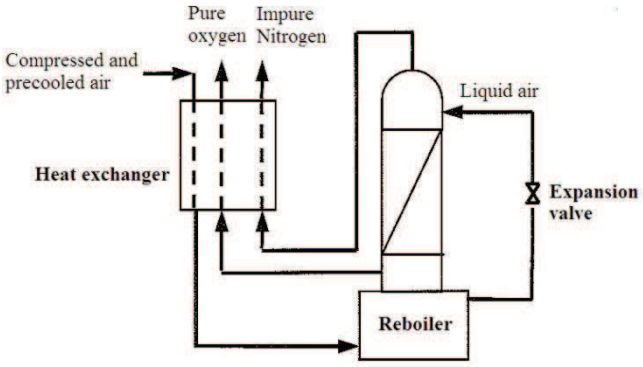

Figure i.1: Single column apparatus for air separation by Carl von Linde [1].

In 1902, George Claude introduced an expansion machine in the liquefaction cycle, thus performing liquefaction by isentropic expansion. Furthermore, he modified the Linde process and proposed the well-known "*Retour en arrière*" configuration for improving the purity of nitrogen, Figure i.2. Claude placed a reflux heat exchanger at the bottom of the distillation column. In this way he obtained an oxygen-enriched liquid and a nitrogen-enriched liquid fed to the middle and to the top of the column, respectively. Using this process it was still no possible to drawn pure nitrogen vapor from the top of the column, even if the oxygen content was reduced.

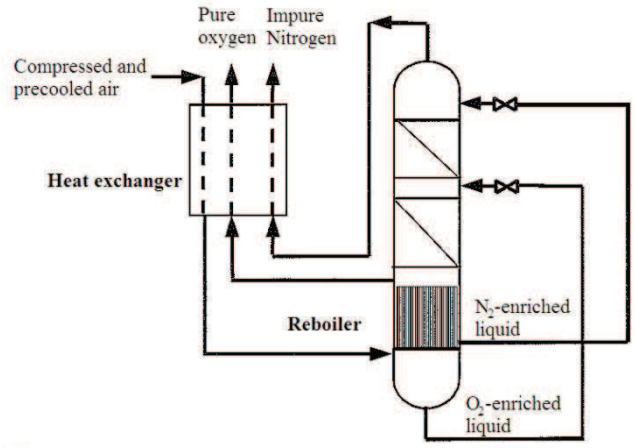

Figure i.2: Single column apparatus for air separation by Georges Claude [1].

All the cryogenic technologies have been successively proposed starting from these two insights and over the years it clearly appeared that two columns were required for producing simultaneously high-purity oxygen and nitrogen by distilling air. Pure liquid nitrogen and oxygen were simultaneously obtained only between 1905 and 1910, when the double column apparatus was conceived.

By the beginning of the 20th century also hydrogen and helium were liquefied, respectively by James Dewar in 1989 and Heike Kamerlingh Onnes in 1908. The work of Onnes introduced also the low temperature physics and the phenomenon of superconductivity in 1911.

Introduction and Summary

Cryogenic distillation of air is the oldest but most highly developed separation technology for the industrial production of oxygen. This technology has not changed fundamentally from that initially developed by Carl von Linde and Georges Claude at the beginning of the 20th century.

Cryogenic air separation is based on fractional distillation in which components of the air mixture are separated on the basis of differences in boiling point and relative volatility. The core of a conventional Air Separation Unit (ASU) is a system of two distillation columns and a reboiler-condenser in between working at about 100 K.

Because of the low temperatures needed in the cryogenic distillation of air, we are faced with the risk of solidification of impurities (CO_2, N_2O) within the process. This phenomenon entails the fouling of the heat transfer surfaces, which worsen the heat exchanges, increases the pressure drops through the process, and causes energy losses and blockages of cryogenic units.

Furthermore, air distillation plants are generally installed on industrial sites and this contributes to air contamination by light hydrocarbons, thus giving a significant safety hazard related to the formation of flammable mixtures in liquid oxygen.

Significant efforts are made by the oxygen producing companies to ensure the safety of cryogenic ASU. Their aim is to avoid that unwanted contaminants reach the reboiler-condenser, are concentrated in liquid oxygen or form a critical mass of solid deposit which could lead to an explosion. Global approaches are developed by these companies to minimize and control that risk. These latter have led to the development of processes equipped with liquid oxygen filters, the development of new adsorbents in the air purification unit and monitoring strategies to track accurately the contaminants from the feed air to the liquid oxygen.

Although the air is sent to a purification unit before entering the double column system, the removal is not complete and some impurities enter in the columns and can accumulate. It is therefore essential for Air Liquide to master the complete phase diagram of the system under the conditions of cryogenic distillation.

Considering the scarcity of experimental values for the binary mixtures hydrocarbons-oxygen, Air Liquide and the Centre Thermodynamics of Processes (CTP) of MINES ParisTech developed a new apparatus for establishing quality data of binary mixtures of interest in the air distillation process.

This apparatus (A. Baba Ahmed, *Appareillage pour l'étude des équilibres liquide-vapeur dans le domaine cryogénique, conception et développement*, Thesis, **1999**), was initially used for the vapor-liquid equilibrium of binary and ternary mixtures of N_2, O_2, and Ar.

More recently (D. Houssin, *Solubilité des hydrocarbures dans l'oxygène liquide*, Thesis, **2007**), same apparatus has been modified and used for the vapor-liquid and liquid-liquid equilibria in binary mixtures of hydrocarbons/nitrogen and hydrocarbons/oxygen.

In a previous work (V. De Stefani, *Etude de la solubilité de solides à pression modérée dans le domaine de la cryogénie: mesures et modélisation*, Thesis, **2003**), the CTP realized a work related to solid-liquid equilibrium with the aim of facing the scarcity of SLE data for the binary mixtures plugging components-oxygen, where plugging components refer to CO_2 and N_2O. A classical approach was adopted for representing the experimental values, then it could not be applied for representing the global phase diagram of the cited mixtures.

The purpose of the present work is to develop and apply a different thermodynamic model for representing, in a wide range of temperature and pressure, the phase equilibrium behavior of the main binary mixtures involved in the cryogenic air distillation process. The main goal is to obtain the global phase diagrams for a selected number of binary mixtures, and the development of the model is proposed in the framework of the research contract between Air Liquide and MINES ParisTech/ARMINES via the CTP.

This manuscript is organized as follows.

Chapter 1 briefly presents the cryogenic air distillation process, and fixes the pure substances and binary mixtures of interest in this work. A bibliographic research has been carried out for collecting experimental values for the systems of interest, and the available literature data are listed in Appendix A.

The presence of the solid phase in the phase equilibrium diagram of pure substances and binary mixtures is presented in Chapter 2. For mixtures, the Pressure-Temperature Equilibrium Projections (PT-EPs) have been qualitatively evaluated starting from the classification of phase diagrams proposed by van Konynenburg and Scott, and most of the obtained PT-EPs have been detailed in Appendix B. These phase diagrams have been produced in a previous work (P. Stringari, M. Campestrini, C. Coquelet, *Etude des équilibres solide–fluide–fluide: diagrammes de phases, inventaire des modèles et banques de données*, Bibliographic Study for Air Liquide, **2012**).

Chapter 3 focuses on the representation of phase equilibria and some literature models proposed for representing the solid-fluid equilibrium. At the end of Chapter 3 some criteria have been proposed for selecting a thermodynamic model, while a detailed presentation of all the considered literature model has been reported in Appendix C. The selected thermodynamic model is the Equation of State (EoS) proposed by Yokozeki in 2003.

The capability of the Yokozeki EoS in representing phase equilibrium properties of pure substances is discussed in Chapter 4. Furthermore, a new procedure for setting the EoS parameters is here presented. The quantitative comparison between model and pure component equilibrium temperature and pressure has been summarized at the end of Chapter 4, whereas details have been reported in Appendix D.

Extension of the Yokozeki EoS to binary mixtures has been considered in Chapter 5. The algorithm for the resolution of the phase equilibrium by means of the minimization of the Gibbs free energy of mixing via the Yokozeki EoS has been detailed in Appendix E. The capability of the EoS in predicting the phase equilibrium behavior in binary mixtures is challenged in Chapter 5, and the necessity of regressing Binary Interaction Parameters (BIPs) is also illustrated. The lack of data suggested applying the EoS to mixtures of Lennard-Jones fluids as device for evaluating BIPs from the LJ parameters σ and ε.

Chapter 6 portrays the application of the Yokozeki EoS for representing the global phase diagram of 5 binary mixtures considered as representative of all the mixtures of interest. The quantitative comparison between model and data for all the mixtures of interest has been presented in Appendix F.

It is worth mentioning that EoS parameters for pure components and BIPs are protected by confidentiality from Air Liquide, so any information concerning their values has been presented within this manuscript.

1 Air distillation

Air is indispensable to life and an important resource at the same time. It is approximately a ternary mixture of nitrogen, oxygen, and argon.

Nevertheless, it contains changeable quantities of many other substances like rare gases, carbon dioxide, hydrogen, methane, carbon monoxide, oxides of nitrogen, NOx, and of sulfur, SOx.

Table 1.1: Air composition [1].

Constituent	Volumetric composition
Fixed components	
N_2	78.084 ± 0.004%
O_2	20.964 ± 0.002%
Ar	0.934 ± 0.001%
CO_2	0.033 ± 0.003%
Ne	18 ± 0.04 ppm
He	5.2 ± 0.05 ppm
Kr	1.14 ± 0.01 ppm
Xe	0.086 ± 0.001 ppm
H_2	0.05 ppm
Impurities(1)	
H_2O	0.1–2.8%
CH_4	1–6 ppm
CO	0.06–1 ppm
SO_x	0.1–1.0%
NO_x	0.52 ppm
O_3	0.01–1 ppm
Rn	6×10^{-3} ppq

(1) In ambient air, including dust, pollen and local pollutants.

To illustrate, Table 1.1 gives an example of an average distribution of the substances in the air mixture. In Table 1.1, distinction is made between fixed components and impurities [1].

Nitrogen and oxygen are among the most common commodity chemicals produced all over the world, and their commercial uses are many. For instance, nitrogen is used to shield materials from contact with oxygen, in ordinary light bulbs, in manufacturing stainless steel, in military aircraft fuel system to reduce fire hazard, to produce ammonia, and as a refrigerant. Refineries, petrochemical plants and marine tankers use nitrogen to remove dangerous vapors and gases from equipments, tanks and pipelines and to maintain an inert and protective atmosphere in tanks storing flammable liquids.

Also oxygen is used in primary metal production and in petroleum refining; others industrial areas are the health services, power generation, catalytic oxidation, oxy-combustion and paper industry.

Taking into account that air contains large amounts of nitrogen and oxygen, it is consequently used for obtaining these compounds and to satisfy practically all the industrial requires. The choice of the production procedure for separating nitrogen and oxygen depends on the quantity and quality that are requested.

1.1 Air separation technologies

Depending on the commercial purposes, a general industrial application could mainly ask two different qualities of oxygen or nitrogen: high-purity and low-purity. For high-purity quality the oxygen (or nitrogen) content must be higher than 98%, while low-purity quality is referred to contents comprised between 85% and 98% [1]. The three main procedures for air separation are membrane, adsorption, and distillation. Table 1.2, a comparison in terms of capacity range and purity of the final products, presents the major advantages of the air separation technologies.

Table 1.2: The three processes of air separation [2].

Process	Development	Purity	Capacity	Advantages
Membrane	1980	N_2: 95% to 99.9%	< 80 T/D to 95% < 5 T/D to 99.9%	Small investment Simple operation
Adsorption	1970	O_2: 90% to 95% N_2: up to 99.9%	5 T/D to 150 T/D	Small investment Quick start up
Distillation	Near 1900	O_2: 85% to 99.7% N_2: up to 10 ppb of Ar, Kr, Xe	100 T/D to more than 4000 T/D	Large production Energy efficient Gaseous and liquid products

Membranes technologies exploit the selective permeation of the substances in the mixture to be separated with respect to porous or non-porous synthetic membranes of polymers such as polyethylene or cellulose acetate. This kind of technology has been developed since the beginning of the 80's, and it is principally used for small operations of hydrogen or moisture removal, and separation of nitrogen from air up to 99.9%. The most advanced membrane technology in the world is the Air Liquide MEDAL hollow fiber membrane, Figure 1.1.

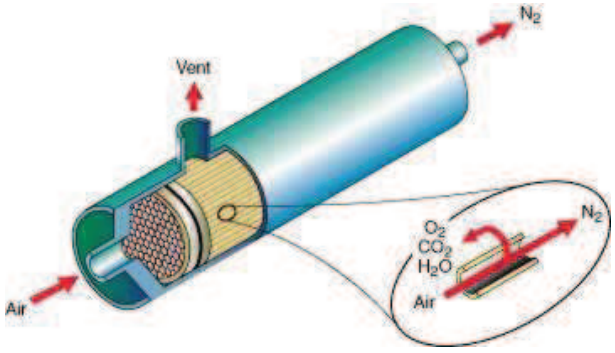

Figure 1.1: Air Liquide MEDAL membrane technology for nitrogen production.

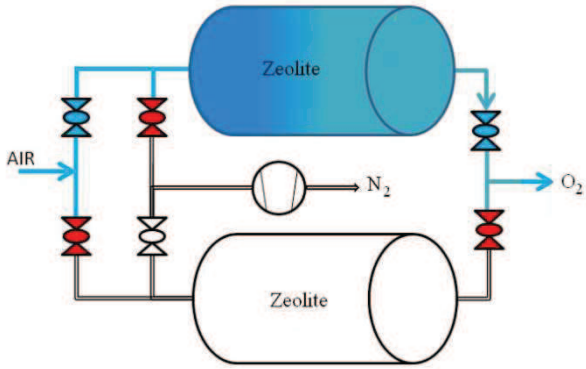

Figure 1.2: Principle of the Air Liquide FLOXAL adsorption technology for oxygen and nitrogen production.

The adsorption separation process is based on fixing nitrogen and air impurities on a porous solid substance called adsorbent, typically zeolite. The separation occurs thanks to electrostatic attraction between these components and the metal cations within the zeolite framework.

Among adsorption plants of various types, Pressure Swing Adsorption (PSA) plants have found the largest application worldwide. A schematic representation of the Air Liquide FLOXAL PSA technology is shown in Figure 1.2. To sum up, in a PSA plant the feed air enters a row of adsorbers wherein water, carbon dioxide and nitrogen are sequentially adsorbed. Oxygen passes through the bed and is collected as final product with purity from 90 to 95%. A mixture with a nitrogen content from 80% to 90% is desorbed from the bed by pumping it with a vacuum pump, while high-purity nitrogen could be obtained by dedicated PSA technologies working on the same principle.

Instead of using pressure swings to selectively adsorb/desorb air components, temperature swing adsorption technologies involve temperature variations. Adsorption technologies are especially used for small to medium requirements, where the high-purity product desired is nitrogen or the low-purity oxygen demand is economically competitive with the cryogenic technologies. The adsorption process has known a rapid growth since the beginning of the 1990's, but it cannot replace the cryogenic processes when a large request of high-purity nitrogen and high-purity oxygen is needed.

The distillation process is a cryogenic technology which has been developed since the beginning of the 20th century, when Carl von Linde (Germany) and George Claude (France) devised processes for the air liquefaction and its subsequent distillation. The importance of this process depends heavily on its capability in providing extremely pure nitrogen and oxygen also in the liquid state. The production capacity ranges from 100 T/D up to more than 4000 T/D, with an energy consumption of only 0.33 kWh for Nm^3 of oxygen produced, [2].

1.2 Cryogenic air separation

Cryogenic air separation is based on the principle of fractional distillation. This process involves liquid and vapor phases and air components are separated on the basis of differences in boiling point and of relative volatility.

The whole process depends consequently on vapor-liquid equilibria occurring within the distillation column, thus important information for the plant design are saturation lines of the main air

components, Figure 1.3, and vapor-liquid equilibria of the nitrogen-oxygen and argon-oxygen mixtures, Figure 1.4 and Figure 1.5.

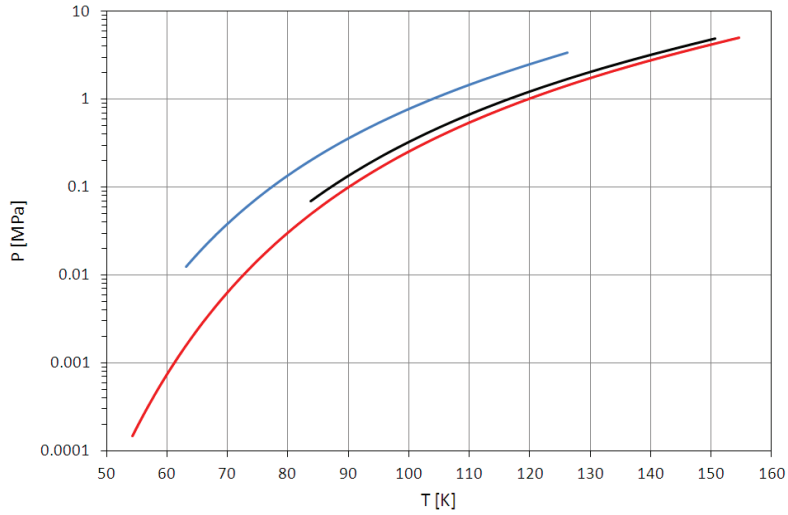

Figure 1.3: Saturation lines of the three main air components, [3].
— : nitrogen; — : argon; — : oxygen.

Each saturation line in Figure 1.3 extends from the triple point up to the critical point of the correspondent substance. These points have not been pointed up in Figure 1.3 because its prior aim is showing the evolution of the saturation lines of the main air components and introducing some important remarks for air distillation.

As stated above, in the distillation process a liquid phase is needed. According to Figure 1.3, the first note is that the process temperature must be at least lower than the critical temperature of oxygen, about 155 K (~ -120 °C), for distillation to be carried out. In this case, pure oxygen can be in the liquid phase depending on the pressure. Furthermore, this temperature should be even lower to keep the operative pressure close to the atmospheric value (0.1 MPa) and limit the operational costs.

As a result, the air distillation is commonly referred as cryogenic separation due to the low operative temperatures, which is about 100 K, (~ -170 °C).

A second important note is the mutual positioning of the three saturation lines. Nitrogen is the most volatile fluid among the main air components, while oxygen is the less volatile. The saturation line of argon is close to the oxygen one, and this fact results in the necessity of realizing further treatments in handling with their small relative volatility.

Assuming air being a ternary mixture of nitrogen, oxygen, and argon, a vapor rich in nitrogen is obtained from a first distillation column, while oxygen and argon feed a second column in the liquid phase to be separated, being less volatile than nitrogen. Details are given in section 1.2.2.

To a fair approximation, the composition of argon in the first column can be neglected, then a nitrogen-oxygen mixture can be considered to account for the equilibrium behavior in this column. The argon-oxygen mixture is instead representative of the equilibria occurring in the second one.

To fix ideas, three equilibrium behaviors of the binary mixtures nitrogen/oxygen and argon/oxygen at three different pressures have been portrayed in Figure 1.4 and Figure 1.5, respectively.

The diagrams in Figure 1.4 and Figure 1.5 are the typical yx equilibrium mole fractions of binary mixtures used for the industrial planning of distillation columns. The shape of a general isobaric yx curve is an important aspect seeing that the height of the distillation column heavily depends on its deviation from the diagonal line, where y=x.

This deviation depends in turn on the difference in boiling points and relative volatility, which directly give a measure of how easily two substances can be separated by distillation. The greater the difference and the relative volatility, the easier the distillation.

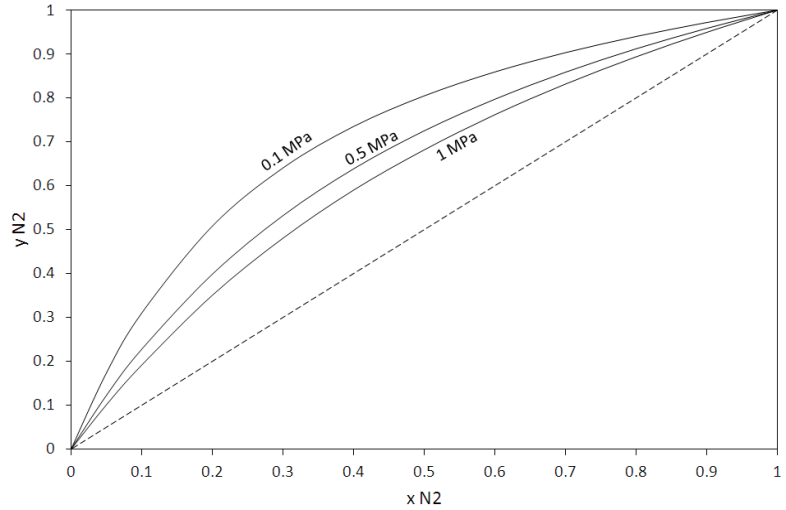

Figure 1.4: Molar fractions of nitrogen in the liquid and vapor phases in the N_2/O_2 system at 0.1, 0.5 and 1 MPa, [4].

Figure 1.4 and Figure 1.5 show that a pressure increase is followed by a leveling of the yx curve towards the x=y line, thus operating distillation at low pressures facilitates cryogenic air separation.

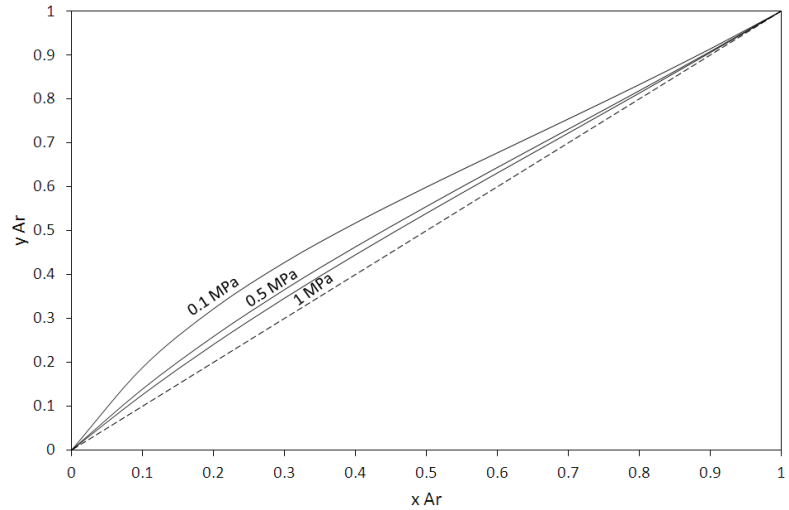

Figure 1.5: Molar fractions of argon in the liquid and vapor phases in the Ar/O_2 system at 0.1, 0.5 and 1 MPa, [5].

A rather complex process is expected for the separation of argon and oxygen because of their small relative volatility, as it can be deduced from Figure 1.5. This results in a more challenging separation and in a higher distillation column.

1.2.1 ASU block diagram and P-h diagram

The previous section places emphases on the cryogenic aspect of the air distillation and the necessity of working at temperatures around 100 K.

Considering that the atmospheric air temperature is usually far away from temperatures needed for its liquefaction, important efforts and investigations have been done by the pioneers of this technology to fill a gap of about 200 degrees.

The result of these researches is an Air Separation Unit (ASU) consisting of five main components, Figure 1.6. The main components are a Compressor *C*, a Purification Unit *PU*, a Heat Exchanger *HE*, an Expander *E*, and the Distillation Column *DC*.

To provide a description of the processes involved in the ASU of Figure 1.6, the Pressure-enthalpy diagram (P-h diagram) of Figure 1.7 and the ASU block diagram resumed in Figure 1.8 have been considered. Numbers and capital letters used in these figures have been reported in their captions.

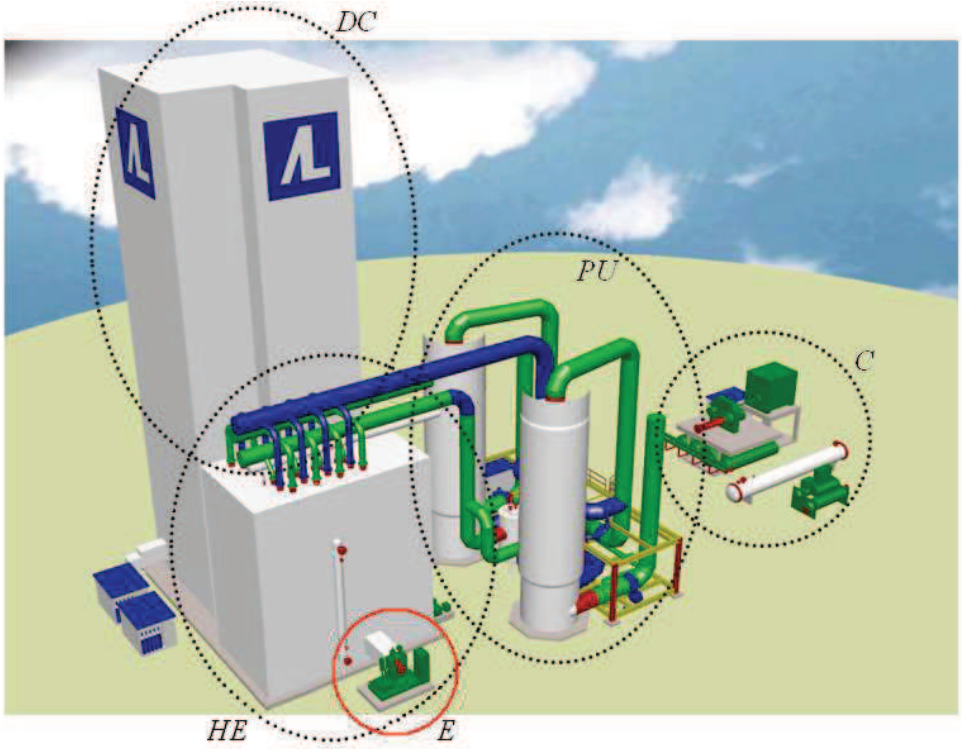

Figure 1.6: ASU main components.
Air Liquide technology, [2]: C: Compressor; PU; Purification Unit; HE: Heat Exchanger; DC; Distillation Column; E: Expander.

Inlet air, point 0 in Figure 1.7, is at atmospheric pressure (0.1 MPa) and a temperature of 27 °C (300 K) has been chosen. At these conditions, the correspondent air entropy and enthalpy are about 6.87 kJ/(kg·K) and 300 kJ/kg, [6].

At 0.1 MPa and 300 K air is in the gaseous state. Keeping constant the pressure, the temperature should be reduced under 82 K for obtaining a liquid phase and entering in the vapor-liquid dome, that is the area underneath the saturated liquid line, in gray, and the saturated vapor line, in red. The saturated lines join together in the air critical point, placed at about 132.6 K and 3.78 MPa, [6].

Each green line within the dome represents a specific quality, which is the ratio between the vapor mass and the total air mass. The quality ratio ranges between 0 on the saturated liquid line and 1 on the saturated vapor line.

The P-h diagram of Figure 1.7 is completed by isentropic curves, in magenta, and isothermal lines, in blue.

When the air temperature is lower than the critical value, the correspondent isotherm splits in two curves: the one on the left of the dome represents air in the liquid phase, whereas the second one is on the right of the dome representing air in the vapor phase. The part of the blue line drawn within the dome is artificial and does not correspond to a real behavior; its only role is to join together the equilibrium saturated phases, placed on the saturated liquid and vapor lines.

Remembering that air distillation requires air liquefaction, the main goal of an ASU is to bring atmospheric air from point 0 to a point somewhere in the vapor-liquid dome.

With reference to Figure 1.6-Figure 1.8, the following processes are involved in an ASU.

The inlet air (0) is compressed by means of the compressor *C* up to point 1 in the P-h diagram. The pressure of point 1 is 0.7 MPa and its temperature is greater than 300 K because air undergoes heating during compression.

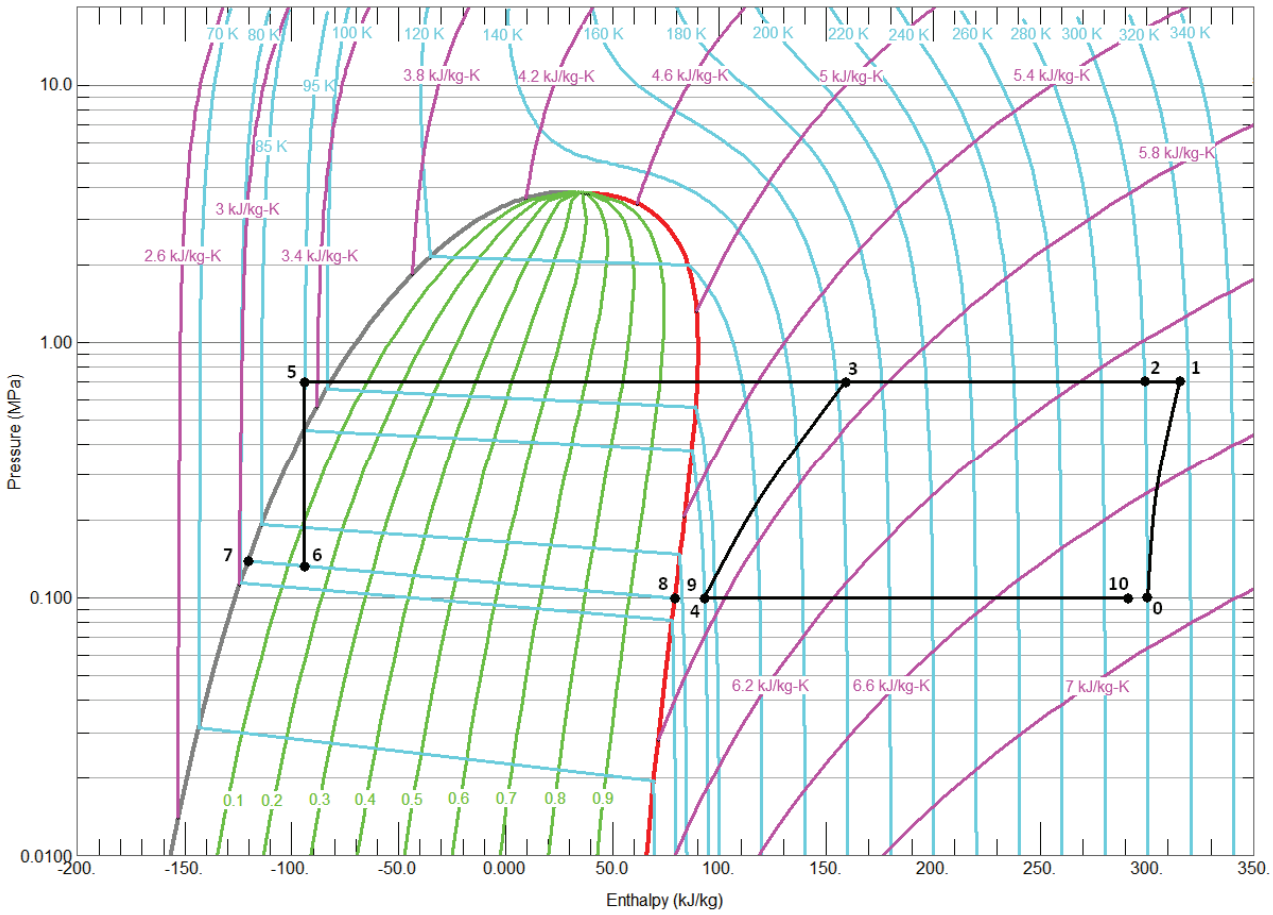

Figure 1.7: Pressure-enthalpy diagram of air, [3].
— : constant entropy lines; — : constant quality lines; — : isotherms; — : saturated vapor line; — : saturated liquid line; — : main ASU processes.
Reference state for air in [3]: T = 298.15 K, P = 0.001 MPa, h = 3453.2 kJ/kg, s = 34.532 kJ/(kg×K).
Flows: 0: inlet air; 1: compressed air; 2 compressed and purified air; 3: cooled vapor; 4; expanded vapor; 5: subcooled liquid; 6: air at vapor-liquid equilibrium; 7: saturated liquid; 8: saturated vapor; 9: cold vapor product; 10: outlet steam.

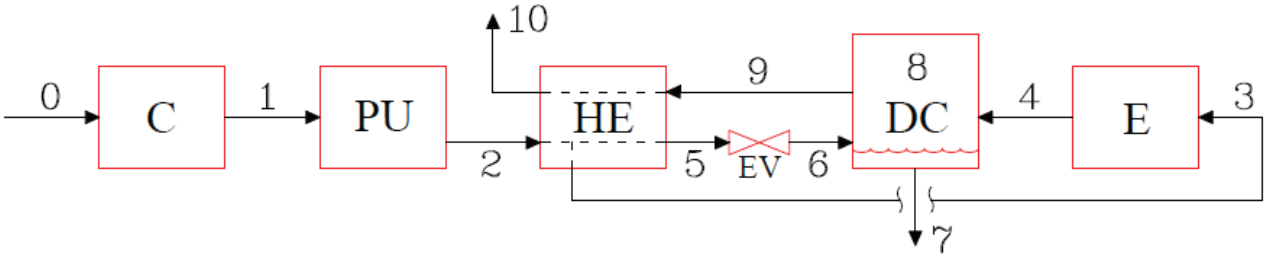

Figure 1.8: ASU block diagram: main components and flows within an ASU.
Components: C: Compressor; PU; Purification Unit; HE: Heat Exchanger; EV: Expansion Valve; DC; Distillation Column; E; Expander;

The compressed air (1), is then purified in the purification unit *PU* in order to remove impurities and cooled typically down to its inlet temperature, 300 K. This compressed and purified air is represented by point 2.

Further cooling is obtained in the heat exchanger *HE* by means of a thermal exchange with the cold vapor product (9) coming from the distillation column *DC*. A part of the compressed and purified air (2) is withdrawn from the *HE* at a temperature of about 160 K, point 3 in Figure 1.7, whereas the remaining flow of air is liquefied and cooled down to 95 K, point 5.

The possibility of heavily reduce the air temperature from point 2 to point 5 is ensured by the expander *E*, where the cooled vapor (3), is isentropically expanded down to atmospheric pressure, point 4. The expanded vapor (4) enters the *DC* lowering the temperature of the cold vapor product

(9) leaving the column. This allows the liquefaction of the compressed and purified air (2) in the *HE*, thus the process within the expander is usually called "*cold production*".

Point 5 is representative of a subcooled liquid which pass through a Joule-Thompson Expansion Valve *EV*, thus the pressure is isoenthalpically reduced towards point 6. Point 6 is underneath the vapor-liquid dome, thus the air feeding the distillation column *DC* splits in a saturated liquid phase (7), and a saturated vapor phase (8). Saturated liquid and vapor phases have two different pressures on the same isotherm: the saturated liquid is at the bubble pressure, whereas the saturated vapor is at the dew pressure of air. According to Figure 1.7, Points 7 and 8 are at about 82 K, and 0.14 MPa and 0.1 MPa, respectively.

The cold vapor product (9) is the result of the mixing between the saturated vapor (8) and the expanded vapor (4), thus its temperature will depend on their flows. Nevertheless, in Figure 1.7 the temperature of point 9 has been approximated to that of point 4.

The cold vapor product (9) feeds the heat exchanger *HE* cooling and liquefying the purified and compressed air (2) coming from the *PU*. As a result, the cold vapor product is heated up to a temperature close to the inlet air temperature. The outlet steam is indicated by point 10 in Figure 1.7.

Points 0 to 10 in Figure 1.7 represent only qualitatively the operative conditions of the air distillation and are not referred to a specific ASU configuration.

The description of the main processes briefly presented here above has been done considering isobaric purification and heat exchange. Furthermore, ideal processes have been considered: for instance, point 4 has been obtained from point 3 considering an ideal isentropic expansion in the *E*.

1.2.2 ASU flow diagram

A detailed representation of a conventional cryogenic ASU is presented in Figure 1.9. In Figure 1.9, capital letters have been used for operating units, while lowercase letters are referred either to liquid or gaseous flows. The abbreviations are summarized in Table 1.3 along with their meaning.

Table 1.3: Abbreviations used in the ASU flow diagram.

Capital letters		Lowercase letters	
Mark	**Meaning**	**Mark**	**Meaning**
F	Filter	w	Waste
C1	Compressor 1	gox	Gaseous oxygen
DCAC	Direct contact aftercooler	lox	Liquid oxygen
CT	Chiller tower	hpgan	High pressure gaseous nitrogen
WT	Waste tower	lpgan	Low pressure gaseous nitrogen
PU	Purification Unit	ncg	Non-condensable gases
C2	Compressor 2	ullq	Upper lean liquid
HE1	Heat exchanger 1	lllq	Lower lean liquid
EV	Expansion Valve	lro	Liquid rich in oxygen
E	Expander	gro	Gas rich in oxygen
TH	Top hat	ca	Crude argon
LPC	Low pressure column	ra	Raw argon
HE2[1]	Heat exchanger 2		
HPC	High pressure column		
CAC	Crude argon column		
HE3	Heat exchanger 3		
HE4	Heat exchanger 4		
P	Pump		

[1] usually called reboiler-condenser.

It is worth mentioning that the flow diagram of an ASU is the result of a detailed design specifically tailored for the on-site customer needs, thus varying from the scheme of Figure 1.9. The intention of the author is to discuss here a general ASU configuration.

Furthermore, in Figure 1.9 the term air has been roughly used without taking into account the specific temperature and pressure conditions of the different air flows within the ASU.

After being filtered, the atmospheric air is compressed in the main air Compressor *C1*. It is then cooled by means of the Direct Contact Aftercooler *DCAC* and the Chiller Tower *CT*. The main objective of such operation is to cool the air before the Purification Unit *PU*. In addition, cooling air allows for a moisture removal by condensation, reducing the water load to be vented in the *PU*.

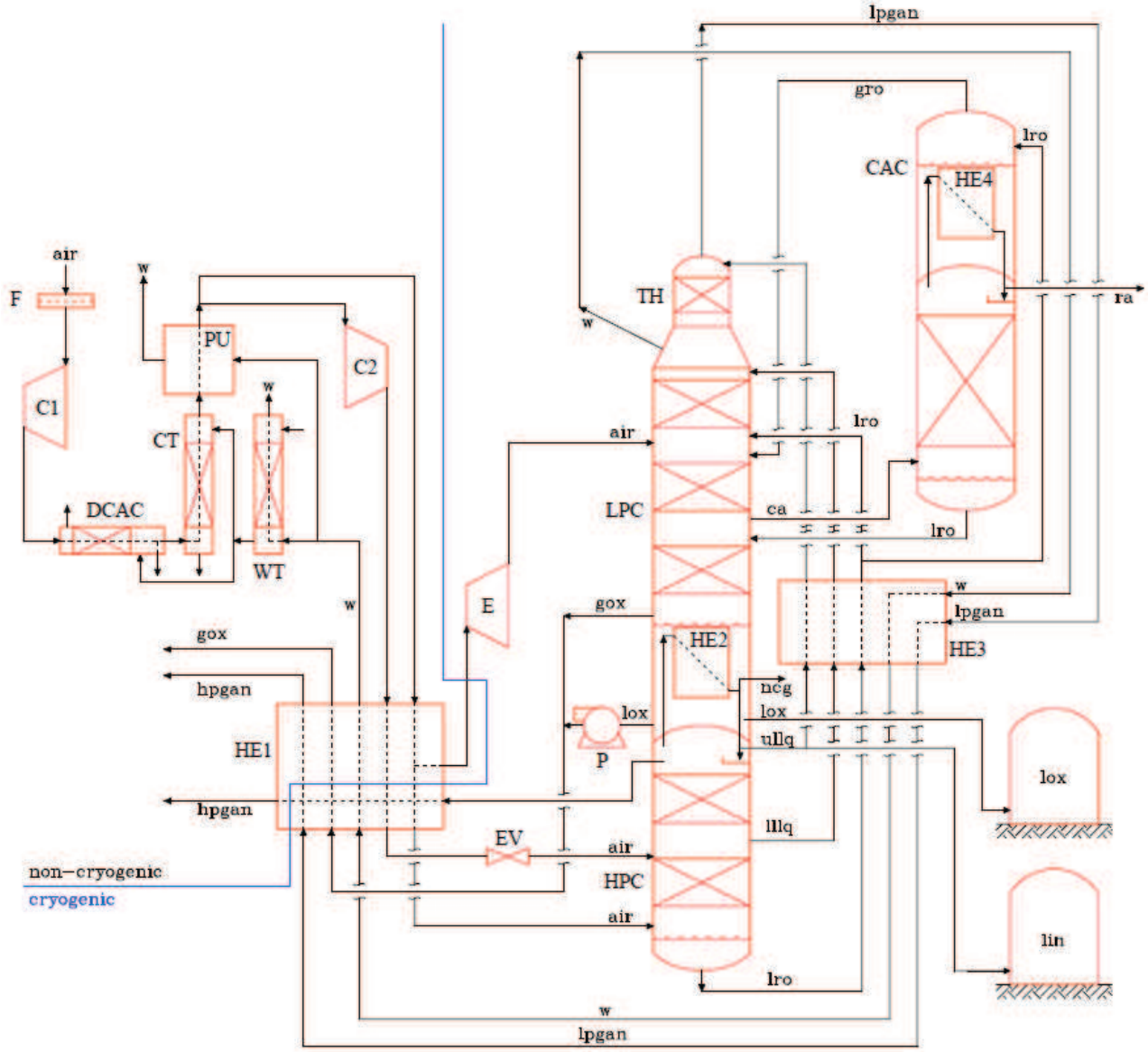

Figure 1.9: Air separation unit flow diagram.

A part of the dry waste gas leaving the ASU is used in the Waste Tower *WT*, to chill a circulating cooling water stream. This latter flows in counter-flow to the air stream in the *DCAC* and the *CT* decreasing the compressed air temperature.

The compressed and precooled air is then sent to the *PU*, where unwanted substances are removed. The importance of this step has been discussed later in section 1.2.4.

Following the diagram of Figure 1.9, a part of the purified air leaving the purification unit is drawn off and compressed in a booster Compressor *C2* before entering the Heat Exchanger *HE1*.

The uncompressed air enters in the Heat Exchanger *HE1* where it is split; a part is drawn off and isentropically expanded, generally by means of a turbine, the Expander *E*.

In the *HE1* all the air streams are cooled in counter-flow to gaseous nitrogen, oxygen, and waste.

The expanded air is sent to the Low Pressure Column *LPC*, while the colder air stream feeds the bottom of the High Pressure Column, *HPC*. The compressed air leaving the *HE1* is expanded in the Expansion Valve *EV* before feeding the middle of the *LPC*.

Both the low pressure and the high pressure columns are provided with many sieve tray sheets on which the rising vapor and the sinking liquid reach the vapor-liquid equilibrium. In some cases, trays are replaced by aluminum structured packing, resulting in a greater contact surface favorable for the heat transfer.

Since nitrogen is more volatile than oxygen, nitrogen moves from the liquid to the vapor phase, while oxygen makes the opposite path. In operative conditions, a nitrogen-enriched vapor is produced at the top of the columns while an oxygen-enriched liquid is produced at their bottoms.

The double column system couples a single condenser column underneath a single boiler column. In a single condenser column fed at the bottom with a gaseous mixture of nitrogen and oxygen, the high-purity distillation product is a nitrogen-enriched gas leaving the top of the column. On the other hand, in a single reboiler column fed at the top with a liquid mixture of a nitrogen and oxygen, the high-purity distillation product is an oxygen-enriched liquid leaving the bottom of the column. As a consequence, the core of the double column ASU is the reboiler-condenser, which provides both heat transfer effects in the same Heat Exchanger, *HE2*. This unit allows achieving the most productive solution in terms of purity and amount of products.

The *HPC* is supplied to the bottom with the compressed and cooled feed air coming from the *HE1*, to the middle with air at the vapor-liquid equilibrium obtained by means of the Expansion Valve *EV*, and to the top with a nitrogen-enriched liquid previously condensed in the *HE2*. It should be noted that gases like hydrogen, helium, and neon, are more volatile than nitrogen and purification units are not designed for their removal. These gases will never condense at the top of the *HPC* because the sinking liquid is not cold enough. Therefore, these Non-Condensable Gases, *ncg*, are vented thanks to a permanent purge installed in the proximity of the *HE2*.

The nitrogen-enriched liquid condensed in the Heat Exchanger *HE2* derives from a gas rich in nitrogen moving from the top of the *HPC* to the *HE2*. The heat of condensation is adsorbed by a liquid rich in oxygen produced at the bottom of the *LPC* which enters in the *HE2*. This liquid partially vaporizes in the *HE2*, providing the rising vapor which exchanges energy and matter with a liquid flow sinking from the top of the low pressure column.

The Liquid Rich in Oxygen, *lro*, leaving the bottom of the high pressure column, has an oxygen content of about 40% [2]. In order to reduce the oxygen losses in the Waste, *w*, and to increase the nitrogen production, two lean liquids are drawn off from the *HPC* and two corresponding refluxes are provided to the *LPC*.

In addition, a third column called top hat or "*minaret*" is introduced in the ASU to further purify waste nitrogen leaving the top of the *LPC*. The Lower Lean Liquid, *lllq*, exits the mid-*HPC* and feeds the top of the *LPC*, while the Upper Lean Liquid, *ullq*, is a high-purity nitrogen liquid feeding the Top Hat, *TH*. A part of this *ullq* is drawn off and sent to the Liquid Nitrogen, *lin*, tank.

Also the remaining high-purity oxygen and nitrogen products are obtained in correspondence of the reboiler-condenser. Liquid Oxygen, *lox*, is drawn off and stored in apposite tank.

With reference to the oxygen production, there are two primary ASU configurations. In the gaseous oxygen process, a cold stream of Gaseous Oxygen, *gox*, is drawn off from the *HE2* area, warmed against incoming air in the *HE1*, and compressed to pressure required by the customer.

In the Liquid Oxygen process, *lox* is pumped to the product pressure and vaporized against incoming air always in the *HE1*. In turn, the gaseous nitrogen demand can be satisfied by means of gaseous streams coming either from the *HPC* or the *LPC*. In this case, it is commonly used referring respectively to High Pressure Gaseous Nitrogen, *hpgan*, and Low Pressure Gaseous Nitrogen, *lpgan*.

A third heat exchanger, *HE3*, is realized for improving the energy efficiency and managing the thermal content of the refluxes moving from the *HPC* to the *LPC*.

1.2.2.1 Argon and rare gases separation

Up to now only nitrogen and oxygen have been considered.

The third main component of air is argon, whose vapor pressure curve is close to the oxygen one. The most of argon entering the column will consequently go to the liquid rich in oxygen, *lro*, thus leaving the bottom of the high pressure column and moving towards the low pressure column.

Composition profiles in the *LPC* show that near the middle of the column the concentration of argon in the gas phase reaches its maximum, around 15%. Because at this point the nitrogen concentration is not negligible, it follows that the gaseous mixture drawn off from *LPC* is made at a lower level, where the nitrogen content is only 0.1%, [2].

This mixture, called Crude Argon, *ca*, is sent to the bottom of the Crude Argon Column, *CAC*, in order to eliminate oxygen. This fourth column is fed at the top with the *lro* coming from the *HPC*, and a fourth heat exchanger, *HE4*, is installed. The *CAC* allows reducing the oxygen content down to 2-3%, thus Raw Argon, *ra*, is drawn off and sent to a further treatment. A Gas Rich in Oxygen, *gro*, and a *lro* stream are sent back to the *HPC*. Furthermore, to a fair approximation, all nitrogen coming in the column comes out in the *gro* stream due to its highest vapor pressure curve.

The further purification of *ra* is made in two alternative ways. In the first case, oxygen removal is given by an exothermic chemical reaction with hydrogen. This process occurs in a "*deoxo*" reactor full of alumina balls covered with palladium. *ra* leaving the *CAC* is heated to ambient temperature and compressed up to 5 bars before entering the reactor, [2].

The final gas contains water steam (which is a product of the reaction between oxygen and hydrogen) and hydrogen seeing that an excess of hydrogen with respect to the stoichiometric quantity is added for a complete oxygen removal. As a consequence, the gas is successively cooled and dried to remove water and then treated in a supplementary column in order to remove any trace of hydrogen and of the remaining nitrogen. The process above is called "*hot purification*" due to the high quantity of heat produced in the deoxo reactor, and the supplementary column where argon is purified is known as the pure argon column.

In order to reduce the hydrogen consumption in hot purification processes and considering its associated difficult operations, it is today preferred to realize taller *CAC*, up to almost the double column height. In this configuration, called "*argon cryogenic separation*", *ca* with less than one ppm of oxygen is obtained from the *CAC* and sent to the pure argon column for nitrogen removal.

The inlet air contains other noble gases then argon. Krypton and xenon are much less volatile than the main air components, thus accumulating in the *lox* at the bottom of the *LPC*. On the other hand, helium and neon are much more volatile then main air components, thus accumulating in the *lpgan* at the top of the *LPC* and as *ncg* in the proximity of the reboiler-condenser, *HE2*. Special units are then designed in the ASU in order to extract raw mixtures of Kr/Xe and He/Ne from an oxygen-enriched flow and a nitrogen-enriched flow, respectively. These raw mixtures are afterwards sent to dedicated separation and purification units.

1.2.2.2 Cold box

The blue line in Figure 1.9 separates the non-cryogenic and the cryogenic areas of an ASU. Operative cryogenic temperatures are required for cooling the air and make the distillation possible. Thus, cold production is needed together with an efficient insulation.

All the cold parts within an ASU are confined in steel boxes in order to maintaining cryogenic temperatures, [2]. These boxes are filled with an insulator like perlite and rock wool, and the whole system undergoing insulation is commonly called "*cold box*".

In spite of the insulation, cold losses not prevented by the insulation must be considered in the cold balance, in addition to thermal losses arising from the incomplete recovery of the cold of the distillation products. These last losses are indicated by the temperature difference at the warm end of all the heat exchangers within the ASU. Therefore, the cold production is designed to cover all the thermal losses and to assure the production of liquid flows required from the customer.

An efficient indicator of the cold balance is the level of *lox* at the bottom of the *LPC*, and it is required to equilibrate the cold balance by increasing the cold production if this level cannot be maintained. In an ASU, cold is produced manly by air expansion through a turbine, the expander *E* in Figure 1.9, and vaporization of the compressed *lox* drawn off from the bottom of the *LPC* against compressed and purified air in the heat exchanger *HE1*.

1.2.3 ASU operative conditions

The reboiler-condenser, *HE2*, is the device needed to condense Gaseous Nitrogen, *gan*, at the top of the *HPC* and to vaporize Liquid Oxygen, *lox*, at the bottom of the *LPC*. The possibility of transferring heat from the *gan* to the *lox* is ensured only by having *gan* warmer than *lox*. As a consequence, the energetic performance of the whole process depends on the temperature difference ΔT between the *lox* at the bottom of the *LPC* and the *gan* at the top of the *HPC*. Furthermore, this ΔT implies a pressure difference between the top and bottom sides of the reboiler-condenser, and this last value is important for determining the pressure at which feed air needs to be compressed.

Considering that nitrogen is more volatile than oxygen, the pressure of the *HPC* must be greater than the *LPC* pressure to get nitrogen warmer than oxygen. This explains why the columns are called high pressure column and low pressure column.

Figure 1.10 is an example of the pressure drop chart used in the planning stage of an ASU. According to Figure 1.10, blue and black lines are referred to the waste and the air circuit, respectively.

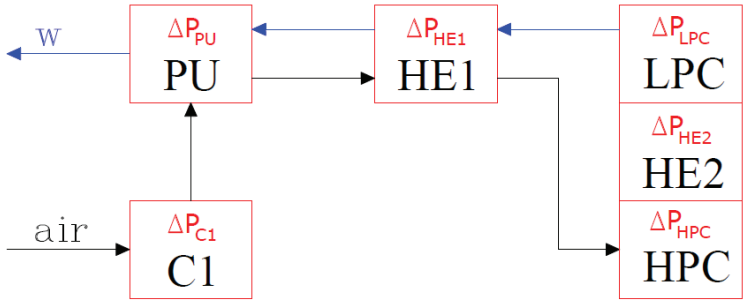

Figure 1.10: Example of the pressure drop chart of an ASU.
ΔP is the pressure drop which occurs in the corresponding unit; w: waste; air: atmospheric air.

Waste are drawn off from the top of the *LPC*, warmed against incoming air in the *HE1*, and sent to the *PU* before leaving the plant. The inlet air is compressed, purified and cooled before entering the bottom of the *HPC*. Cooled waste leaving the *PU* and inlet air are at atmospheric pressure.

Each operation unit occurs with a pressure drop, indicated by the corresponding ΔP in Figure 1.10. The low pressure drops occurring in piping have not been reported in the pressure drop chart of Figure 1.10, but have to be taken into account during the planning stage.

The pressure at the top of the *LPC* is determined by the pressure drops of the waste circuit. Therefore, this pressure is determined from the atmospheric pressure by adding the pressure drops in the *PU*, ΔP_{PU}, in the *HE1*, ΔP_{HE1}, and piping. A pressure drop is required in the *PU* unit in order to provide the minimum pressure needed for the purification.

The pressure at the bottom of the *LPC* is then obtained increasing the *LPC* top pressure by ΔP_{LPC}, the pressure drop of the trays or of the structured packing. This pressure corresponds to the vapor pressure of the liquid oxygen evaporating in the *HE2*, thus imposing the saturation temperature at the bottom of the *LPC*.

The temperature difference, ΔT, between the bottom of the *LPC* and the top of the *HPC* is a proper characteristic of the reboiler-condenser. There are principally two kind of devices used in ASU: bath vaporizers and film condensers. The comparison and the detailed description of their

functioning are beyond the scope of this work, instead it is worth mentioning their working temperature differences. In a bath vaporizer, working in counter-flow and immerged in a bath of liquid oxygen, ΔT is about 3°C. In the most recent technology of film condensers, working in parallel-flow, ΔT is about 1°C. In this discussion, an average ΔT of 2°C can then be fixed.

Having in mind that the *gan* will be 2 degrees warmer than the *lox* at the bottom of the *LPC*, the pressure of the *gan* can be easily obtained from its saturation curve. In such a way, the pressure at the top of the *HPC* and the pressure drop in the reboiler-condenser, ΔP_{HE2}, can be determined.

Similarly to the *LPC*, the pressure at the bottom of the *HPC* is its top pressure increased by the pressure drop of the trays or of the packing, ΔP_{HPC}. Finally, the discharge pressure needed at the outlet of the Compressor *C1* is calculated adding the air circuit drops (ΔP_{PU}, ΔP_{HE1}, and piping drops) to the *HPC* bottom pressure.

One notices at once that the discharge pressure of the compressor depends on the pressure drops of the whole process. For decreasing the energy consumption, the *LPC* top pressure should be set at the lowest value, and the limiting value is the pressure required for air purification.

Secondly, all the pressure drops of Figure 1.10 are functions of the inlet air flow. Therefore, the ASU process together with the choice of the reboiler-condenser will fix the discharge pressure of the compressor for a given air flow.

On average, the absolute pressure on the reboiler-condenser at the bottom of the *LPC* is around 0.14 MPa and the corresponding oxygen boiling temperature is 94 K. The absolute pressure at the top of the *HPC* depends on the working ΔT of the *HE2*. Considering a temperature difference of 2 degrees, 0.56 MPa is the nitrogen saturation pressure at 96 K. It should be kept in mind that all these values are evaluated by considering the saturation curves of pure nitrogen and oxygen.

As stated above, the suction pressure of the compressor *C1* is the atmospheric pressure. Depending on the air flow, pressure drops will change within the ASU making the discharge pressure usually varying from 0.4 to 1 MPa.

1.2.4 Safety problems and contaminants removal

An example of an average distribution of the substances in the air has been presented in Table 1.1. Furthermore, ASUs are typically located in industrial areas, increasing the possibility of air to be polluted by other substances coming from chemical and industrial operation units. These substances are principally light hydrocarbons, and their concentration typically ranges between 0.1 and 0.5 ppm, [1].

As a result, the intake air quality should be carefully evaluated since it can affect the air separation process causing safety and operational problems.

The air contaminants are commonly classified in three categories on the basis of the potential problem they may cause in an ASU. The first category refers to plugging contaminants (such as H_2O, CO_2, SO_2 and $NO_{x(x>1)}$) which can precipitate creating solid deposits. Reactive contaminants groups substances which may react with liquid oxygen. Examples are H_2 and light hydrocarbons. The third category represents corrosive substances with can cause operating problems and reduced plant life. Examples of corrosive substances are SO_x, H_2S, HCl, Cl_2, and NH_3. The presence of these substances in an ASU depends mostly on the peculiar characteristics of the local area where the plant is realized. This makes difficult a generalization for their composition in the atmospheric air, thus these substances, except SO_x, have been omitted in Table 1.1 and not treated in this work.

Rare gases never give safety problems, so any air treatment is provided in an ASU for their removal before feeding the *HPC*. As discussed in section 1.2.2.1, further processes are instead realized for treating and separating Kr/Xe and He/Ne mixtures from the final products.

Plugging and reactive contaminants play together in causing safety and operational problems. It means that safety problems occurred in the past were the combined effects of solid deposits and increased concentration of reactive substances. Except hydrogen, all the contaminants tend to accumulate in the oxygen-rich reboilers within the plant having boiling temperatures higher than liquid oxygen.

The primary hazard is the concentration of hydrocarbons up to their lower explosive limits. In presence of an adequate ignition source, rapid oxidation occurs with a release of a great quantity of energy, in form of pressure or heat, thus giving a significant safety hazard. This hazard increases in presence of high purity phases of hydrocarbons, like solid acetylene and liquid propane droplets, because in this case rapid oxidation requires a lower deal of energy to be ignited.

The quantity of energy released by rapid oxidation and its propagation can also provide the ignition source for the reaction between aluminum and oxygen. This hazard is not negligible considering the huge amount of aluminum used in manufacturing ASU equipments, and the high surface/volume ratios associated to the heat exchangers geometry.

A secondary hazard is the presence of substances like CO_2 and N_2O, which can precipitate out of the liquid solution rich in oxygen if their concentrations reach the solubility limit. Experimental works have also shown that the mutual presence of CO_2 and N_2O in the liquid oxygen lowers their solubility limit, [7]. Therefore, a solid deposit forms more easily when both are present than if either CO_2 or N_2O is present in the same concentration by itself. Although one obvious direct bearing of solid deposits is plugging of piping and equipments, an outcome maybe more dangerous is the promoted accumulation of light hydrocarbons and the following increased possibility of explosions (as for instance the accident of Bintulu in Malaysia in 1997, [8]).

As stated above, accumulation of low boiling substances such as hydrocarbons naturally occurs in distillation. The precipitation of solid deposits facilitate the hydrocarbons accumulation owing to the partial occlusion of the passages where liquid oxygen flows for being vaporized, namely in the reboiler-condenser.

Two main phenomena promote hydrocarbons accumulation: dry boiling ("*vaporisation à sec*") and dead-end distillation ("*distillation en cul de sac*"), [9]. It can occur that liquid oxygen is totally vaporized somewhere within the passages of the reboiler-condenser and impurities accumulate there: this is the phenomenon of dry boiling. The amount of solid deposit increases seeing that fresh liquid is continuously added and totally vaporized in the area, until it clogs the passage leading to the phenomenon of dead-end distillation. As a results, both configurations lead to the concentration of hydrocarbons, thus increasing the risk of rapid oxidation.

It clearly appears that the air contaminant removal is a critical step in dealing with cryogenic air separation. One can classify ways of removing contaminants from feed air into two main types, [2]:

- Front End Purification (*FEP*). A *FEP* is a system of at least two vessels filled with a single or more layers of adsorbents, typically alumina for H_2O removal or molecular sieve for H_2O, CO_2, NO_x, and hydrocarbon removal. The vessels work alternatively in order to provide a constant air flow to the ASU through a TSA process; one vessel is online removing contaminants, the other is offline to be regenerated by the waste N_2 leaving the *LPC* heated at temperatures from 80 and 150°C;
- Reversible Exchangers (*REVEX*). The purification principle is deposition of solid H_2O, and CO_2 by exchange with cold waste from the double column apparatus. Also in this case, two passages are installed, in order to keep a constant air flow sent to the ASU. The passages are then alternatively cleaned up with a waste stream coming from the *LPC*.

Less adopted technologies are caustic scrubbers, where CO_2 is totally removed by a chemical reaction with an aqueous solution of sodium hydroxide, and catalytic oxidizers, used to oxidize hydrocarbons, H_2, and CO, [10].

The choice among different techniques is usually done considering the investment and operational costs, the reactivity ratio, the time at which the system needs to be regenerated, and the removal efficiency.

With reference to the two main technologies, *REVEX* passages require to be regenerated every 5-10 minutes, while a *FEP* have pressure and temperature cycles every 2 to 8 hours before regeneration of the adsorbent layers.

Investment costs of a *FEP* can be from 30 to 50% higher than the corresponding values for the *REVEX*, but *FEP* technology is globally advantageous in terms of energy costs.

The *REVEX* require an average deal of regeneration stream up to 60% of the air flow to be purified, while about 30% is needed in *FEP*. Furthermore, the *FEP* technology allows for a more efficient abatement of hydrocarbons and CO_2 than the *REVEX*. Considering all these points, today *FEP* technologies are preferred to the *REVEX* ones, [2].

The *FEP* is the common technology adopted by the Air Liquide Group for removing contaminants from air. The removal ratios achieved depend on the concentration and operation parameters, but it is possible to state that *FEP* allows almost totally removing H_2O, O_3, C_2H_2, C_3H_6, and CO_2 (>99%), partially removing NO, N_2O (~80%), NO_2, C_2H_4 (~80%), and C_3H_8 (~50%), while H_2, CO, CH_4 and C_2H_6 are even not trapped.

Because the *FPE* does not ensure the total and contemporaneous removal of the different contaminants, it follows that they must be dealt with in the cold box. The plugging components (CO_2, N_2O) enter the double column system and could form a mass of solid deposit in the *LPC* sump. Also the reactive components CH_4, C_2H_4, C_2H_6, and C_3H_8 reach the *LPC* sump, while H_2 and CO do not concentrate there since these compounds follow the stream of N_2 being more volatile than O_2.

In order to improve the removal of unwanted substances, filters are installed for purifying streams of *lox* and *lro* and almost totally removing impurities like N_2O, NO_2 and C_2H_4. Even coupling filters and *FEP*, C_3H_8 and NO are only partially removed, while H_2, CO, CH_4, and C_2H_6 are still not trapped. The qualitative performance of *FEP* and *lox-lro* filters is shown in Figure 1.11.

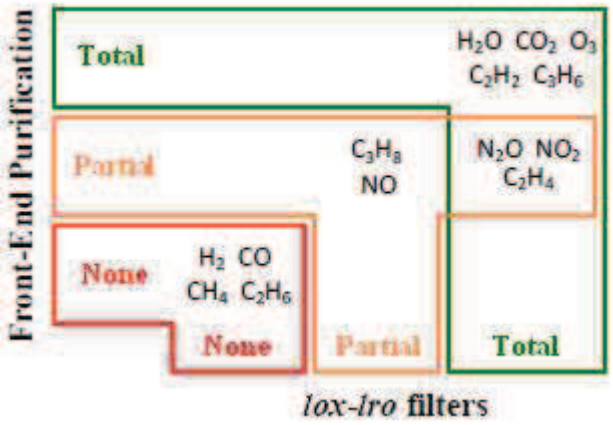

Figure 1.11: Qualitative removal efficiency, [2].

According to Figure 1.11, impurities can in any case enter the distillation column and reach the *LPC* sump. For this reason, a *lox* purge drawn off from the sump of the *LPC* is needed for venting the contaminants and maintaining a safe level of concentration during the distillation process. A minimum continuous *lox* purge rate of the incoming air is then recommended, also in ASU producing predominantly gaseous oxygen.

In spite of these devices, it is sometime necessary to turn to a periodic shutdown of the process to remove accumulated contaminants not trapped in the purification unit, in the cryogenic adsorbers or not vented by the *lox* purge. This operation is called deriming, and usually includes also maintenance checks, repairs, and modifications.

1.3 Systems of interest

Taking into account the outline of Figure 1.11, 15 substances have been considered of interest in this work and divided in the following three categories:

- Main Components (MC): N_2, O_2, Ar;
- Rare Gases (RG): Kr, Xe, Ne, He;
- Impurities (I): CO_2, N_2O, H_2, and light hydrocarbons (CH_4, C_2H_6, C_2H_4, C_3H_8, C_3H_6).

Main components and rare gases, except Rn, have obviously been considered. N_2, O_2, Ar are the main ASU products, and also rare gases have their applications. As previously mentioned, additional processes within an ASU are dedicated at the rare gases separation and purification.

Plugging contaminants, CO_2 and N_2O, reactive contaminants, light hydrocarbons up to propylene, and H_2 have been grouped in the same category. The term impurities, I, refer to unwanted substances that can cause safety and operational problems.

The first aim of the research here presented is improving the knowledge of the contaminant behavior within an ASU, and investigating their binary mixtures phase equilibria with main air components has been judged as starting and fundamental information.

The combinations of the 15 pure substances give 105 possible binary mixtures. Since some components are present only in very small quantities, not all the possible binary mixtures have been judged to have the same relevance in the ASU.

The second aim is proposing a thermodynamic model suitable for being applied in the simulation of cryogenic processes and representing the equilibrium behaviors of the binary mixtures.

According to Table 1.1, the order of magnitude of the contaminants composition is some ppm, thus the model needs to be representative also of infinite dilution behaviors. Furthermore, kinetic aspects are beyond the scope of this work, which is entirely dedicated at thermodynamic ones.

A thermodynamic model usually requires a certain number of parameters for taking into account the interactions between molecule pairs, thus a regression on available experimental values is needed to make the model able to represent the mixture behavior.

The importance of carrying out a regression for the binary interaction parameters, BIPs, and the criteria used in doing the selection of the mixture of interest among the 105 possible combinations are based on the following considerations:

- MC + MC mixture: these mixtures have been considered as fundamental. For the regression of the BIPs, both binary and ternary mixture phase equilibrium data have been used;
- MC + RG or MC + I mixture: all the available binary mixtures phase equilibrium data have been collected and used for the regression of the BIPs;
- RG + RG mixture: only for three mixtures all the available binary mixtures phase equilibrium data have been collected and used for the regression of the BIPs;
- I + I mixtures: experimental data have not been collected because in the process of interest both the components are present in very small mole fractions; null BIPs have been considered;
- RG + I mixture: for 16 mixtures, (Kr or Xe) + (CO_2 or N_2O or CH_4 or C_2H_6 or C_2H_4 or C_3H_8 or C_3H_6) and (Ne or He) + H_2, the phase equilibrium data have been collected and BIPs have been regressed. For the remaining RG + I mixtures, experimental data have not been collected and null BIPs have been considered.

The criteria, summarized in the Table 1.4, give a total of 58 mixtures.

Table 1.4: Selection of the binary mixtures of interest for the bibliographic study.
A data collection has been carried out also for the ternary mixture N_2-O_2-Ar.

Sub. 1	Sub. 2	Data collection	BIPs regression	Mixtures of interest
MC	MC	✓	✓	4[1]
MC	RG	✓	✓	12
MC	I	✓	✓	24
RG[2]	RG[2]	✓	✓	3
RG[3]	I[3]	✓	×	16
I	I	×	×	0

1 Three binary mixtures and one ternary mixture have been considered for the main air components.
2 Except Kr-Ne, Kr-He, and Xe-He.
3 Only mixtures composed by (Kr or Xe) + (CO_2 or N_2O or CH_4 or C_2H_6 or C_2H_4 or C_3H_8 or C_3H_6) and (Ne or He) + H_2.

Table 1.5 shows all the possible binary mixtures obtained as combinations of the 15 pure compounds.

The mixtures of interest are pointed out in red and yellow, while gray has been used for mixtures not of interest in this work. Unlike red mixtures, in yellow ones null BIPs have been considered.

Table 1.5: Binary mixtures and pure compounds of interest for this study.
Data collection has not been carried out for the mixtures pointed out in gray.
Regression of binary interaction parameters has been carried out only for the mixtures pointed out in red.

	N_2	O_2	Ar	Kr	Xe	Ne	He	CO_2	H_2	N_2O	CH_4	C_2H_6	C_2H_4	C_3H_8	C_3H_6
N_2															
O_2															
Ar															
Kr															
Xe															
Ne															
He															
CO_2															
H_2															
N_2O															
CH_4															
C_2H_6															
C_2H_4															
C_3H_8															
C_3H_6															

Next section presents the bibliographic research carried out for collecting data for the 15 pure substances and the 58 binary mixtures of interest.

1.3.1 Bibliographic research

As already introduced, the main objective of this work is to set up a thermodynamic model for the representation of the phase equilibrium behaviors of the pure compounds and the mixtures of interest, see Table 1.5. In particular, this model will be applied to the representation of equilibria involving fluid phases, namely the liquid and the vapor phases, as well as solid phases.

As a consequence, this thermodynamic model needs to be applied in a large temperature range. With reference to pure compounds, this implies to consider the saturation, sublimation, and melting curves of a pressure-temperature phase diagram.

In case of binary mixture, the model is applied for the representation of equilibria occurring at cryogenic conditions up to the binary mixture critical loici. It means that the model has to represent low temperature equilibria involving mostly solid-solid and solid-fluid equilibria, keeping its capability in representing high temperature equilibria between fluid phases.

As a result, a bibliographic research has been carried out in order to collect data concerning solid-solid, solid-fluid, and fluid-fluid equilibria for the binary mixtures of interest.

The details of the bibliographic research of pure compounds and binary mixtures equilibrium values have been included in Appendix A, whereas an overview on the research concerning binary mixture is summarized in Table 1.6. In Table 1.6 different colors are linked to mixtures following these rules:

- gray: binary mixtures not of interest in this study;
- red: no experimental value available in the literature;
- blue: no solid-fluid equilibrium value available in the literature;
- green: no fluid-fluid equilibrium value available in the literature;
- white: both solid-fluid and fluid-fluid equilibria are available in the literature.

Table 1.6 states that solid-fluid equilibrium data are the sole available for the mixtures: N_2+Xe, O_2+Xe, O_2+H_2, O_2+C_3H_6, and Ar+Xe mixtures. 18 mixtures (blue color) lack solid-fluid equilibrium data: 5 of them involve one main components of air coupled with a rare gas or an impurity as second component. The scarcity of this kind of data is also encountered for several mixtures of krypton and xenon.

Table 1.6: Literature review on the kind of equilibrium data for the binary mixtures on interest.
Legend: lack of any kind of data (red), lack of solid-fluid data (blue), lack of fluid-fluid data (green), available data for both solid-fluid and fluid-fluid equilibria (white), mixtures not involved in this study (gray). Check marks are related to mixtures for which the regression of BIPs has been considered relevant.

	N_2	O_2	Ar	Kr	Xe	Ne	He	CO_2	H_2	N_2O	CH_4	C_2H_6	C_2H_4	C_3H_8	C_3H_6
N_2		✓	✓	✓	✓	✓	✓	✓	✓	✓	✓	✓	✓	✓	✓
O_2			✓	✓	✓	✓	✓	✓	✓	✓	✓	✓	✓	✓	✓
Ar				✓	✓	✓	✓	✓	✓	✓	✓	✓	✓	✓	✓
Kr					✓										
Xe						✓									
Ne							✓								
He															

2 Phase diagrams including solid phase

This chapter is organized into four parts. The first three parts present the notions of aggregation state of matter, phase rule, and first order phase transition. Successively, in section 2.4, the presence of the solid phase in phase diagrams has been evaluated. The form of the melting line in the pressure-temperature equilibrium projection of pure compounds has been discussed and a brief debate has been done on the possible presence of a solid-liquid critical point. A preliminary analysis of binary mixtures phase diagrams has been also presented.

2.1 Aggregation states of the matter

Depending on the intensity of the cohesion forces among the molecules, a pure substance can present different aggregation states. In a gaseous state the potential energy of attractive interactions is lower than the kinetic energy and consequently the molecules are in continuous and irregular movement. As a consequence, gaseous molecules occupy all the available volume.

Differently from the gaseous state, a liquid state has its own contour since attractive interactions allow for a spatial arrangement of the molecules. However, these interactions are not enough to give a long-range order and hardness to the matter.

With a small increase of the cohesion forces intensity, the matter assumes some hardness keeping its contour. This state of matter, typical for example for glass and rubber, corresponds to the amorphous or vitreous state.

Further increases of the interactions among the molecules give the density and hardness increases towards a three-dimensional organized distribution of the molecules. The solid is an aggregation state provided with its own shape, rigidity, definite contour, which differs from the amorphous state thanks to its well organized crystal structure.

The regular and recurring distribution of molecules can be described with a regular geometrical model and so schematized with a crystal lattice. Many crystal lattices have been defined in order to describe the schematic distribution of all the known solid state geometries. Moreover, the same pure substance can present two or more crystal structures, depending on temperature and pressure.

In this work, only solid, liquid, and gaseous states have been considered, thus neglecting the amorphous one.

2.2 Phase rule

A pure substance (or a group of substances) organized in a single state of matter is considered a homogeneous system. On the other hand, the system is defined heterogeneous when the matter is organized in different states of aggregation, namely coexisting phases.

A phase is a portion of the system characterized by the same chemical and physical properties, and it is separated from another phase by well-defined contours. For instance, a pure liquid and its solid at the equilibrium (as liquid water and ice) represent the same substance distributed in two phases, and so a heterogeneous system.

The equilibrium state of a system is defined through a certain number of state variables, as the temperature, the pressure, the volume, and the concentration of each single chemical substance present in the system.

$$F = N - \pi + 2 - \varphi \qquad (2.1)$$

The phase rule, eq. (2.1), allows identifying the number of these variables that can be arbitrarily chosen, and that, once fixed, oblige the other variables to assume determined values in order to completely define the system.

In eq. (2.1), F is the variance of the system and represents the number of its degrees of freedom. The variance of the system represents the requisite and sufficient number of variables that is needed to fix for the exact determination of the composition in all the phases of the system. φ is the number

of relations that must be verified in a special state, while N and π are the number of the components and phases, respectively.

2.3 First-order phase transition

Phase transitions can be classified with reference to the discontinuity of the derivatives of the free energy at the transition. Solid-liquid, solid-vapor, and liquid-vapor equilibria are first-order phase transitions as they involve a discontinuous change in density. Conversely, second-order phase transitions are discontinuous in the second derivative and continuous in the first one.

The first-order phase transitions involve an exchange of a well defined quantity of energy, called latent heat, which is absorbed or released from the matter. The matter gradually exchanges this energy with the surrounding environment, thus two phases coexist throughout the transition instead of having an instantaneous change of the whole aggregation state.

At the end of the transition, the system will have completely changed its aggregation state, and the starting state will not be present anymore. The quantity of energy exchanged does not modify the pressure and the temperature of the system, but it is necessary for allowing the modification in the aggregation state.

For example, the temperature and the pressure of a pure fluid do not change during the phase transition from a liquid to its vapor. The molecules of the liquid gradually evaporate by receiving energy from the surrounding system. In such a way, the liquid and vapor molecules will share the whole available volume till all the liquid will be entirely evaporated.

Three are the main latent heats encountered. The latent heat of fusion refers to the melting (solid to liquid) and the freezing (liquid to solid) phase transitions. The latent heat of vaporization refers to the boiling (liquid to vapor) and condensation (vapor to liquid) phase transitions. The latent heat of sublimation refers to the sublimation (solid to vapor) and deposition (vapor to solid).

The equation characterizing a first-order phase transition for equilibria in a pure compound system is the conservation of the free energy G between two equilibrium phases α and β, eq. (2.2). For an infinitesimal change of pressure and temperature along an equilibrium curve, eq. (2.3) must hold, which compared with eq. (2.2) gives eq. (2.4).

Differentiating eq. (2.4) gives eq. (2.5), where the two partial derivates of the Gibbs energy can be related to the system entropy and volume thanks to the well-known Maxwell's relations, eq. (2.6). Eq. (2.5) can then be rewritten as in eqs. (2.7) and (2.8).

Eq. (2.8) is the equation of Clapeyron [11], and for a pure substance this equation describes how the temperature variations modify the pressure at which the aggregation state transition occurs. In eq. (2.8), dP and dT are the pressure and the temperature variations, respectively. λ is the latent heat referred to the specific phase transition, and ΔV is the difference between the volumes of the two phases.

$$G^{\alpha}(T,P) = G^{\beta}(T,P) \tag{2.2}$$

$$G^{\alpha}(T,P) + dG^{\alpha}(T+dT,P+dP) = G^{\beta}(T,P) + dG^{\beta}(T+dT,P+dP) \tag{2.3}$$

$$dG^{\alpha}(T+dT,P+dP) = dG^{\beta}(T+dT,P+dP) \tag{2.4}$$

$$\frac{\partial G^{\alpha}}{\partial T}dT + \frac{\partial G^{\alpha}}{\partial P}dP = \frac{\partial G^{\beta}}{\partial T}dT + \frac{\partial G^{\beta}}{\partial P}dP \tag{2.5}$$

$$\left(\frac{\partial G}{\partial T}\right)_P = -S \quad , \quad \left(\frac{\partial G}{\partial P}\right)_T = V \tag{2.6}$$

$$-S^{\alpha}dT + V^{\alpha}dP = -S^{\beta}dT + V^{\beta}dP \tag{2.7}$$

$$\frac{dP}{dT} = \frac{S^{\alpha} - S^{\beta}}{V^{\alpha} - V^{\beta}} = \frac{\lambda}{T\Delta V} \tag{2.8}$$

2.4 Phase diagrams

As written in section 2.1, the molecules are more or less organized depending on the relation between potential energy of attractive forces and kinetic energy. Neglecting the amorphous state, the matter can organize itself in solid, liquid, or gaseous phases depending on the values of pressure and temperature. It should be noted that, in thermodynamics, the supercritical phase is usually thought as being a special state where liquid and vapor are indistinguishable. The term vapor phase is instead used to indicate the state at the equilibrium with a dense phase, where dense means either liquid or solid.

2.4.1 Pure compounds

The qualitative Pressure-Temperature Equilibrium Projection (*PT-EP*) of a phase diagram for a pure compound is represented in Figure 2.1.

In Figure 2.1, two hypothetical solid phases (solidα, solidβ), with different crystal structures (α , β), and the liquid and vapor phases have been considered.

The *PT-EP* can be examined starting from the phase rule, eq. (2.1), imposing $N = 1$. The degrees of freedom can vary from 0 to 2 depending on the number of phases and constraints. The possible scenarios are summarized in Table 2.1.

The scenario A is representative of a sole homogeneous phase without constraints. This phase has two degrees of freedom, and for being completely defined as many state variables must be fixed.

Referring to the *PT-EP* of Figure 2.1, the regions representative of the scenario A are the surfaces delimited by the curves, namely the homogeneous aggregation states solidα, solidβ, liquid, and vapor.

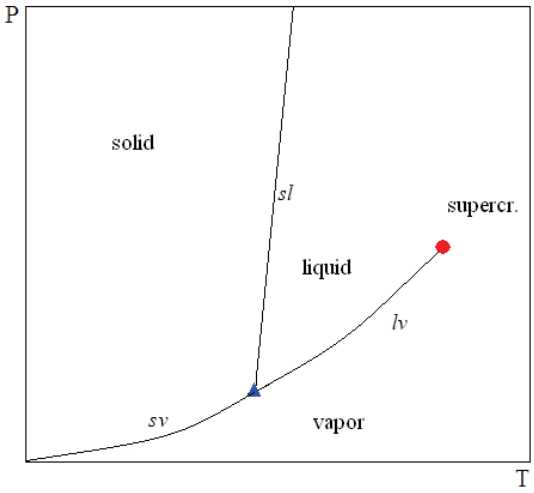

Figure 2.1: Pressure-temperature equilibrium projection of a phase diagram for a pure substance.
—, phase equilibrium boundaries; ▲, triple point; ●, critical point.

A fifth surface is placed on the right of the *PT-EP* and it refers to the supercritical phase, where the liquid and vapor aggregation states are indistinguishable. For high temperatures and low pressures this phase tends to behave like an ideal gas.

The scenario B is represented by the curves in Figure 2.1. Each curve groups the P-T coordinates wherein a pure substance is divided into two coexisting phases at equilibrium, thus representing a phase transition. When a pure substance is distributed in two equilibrium phases, its thermodynamic system has only one degree of freedom, and its corresponding state is completely defined by fixing only one state variable.

Table 2.1: Phase rule scenarios for a pure substance.
The phase rule for a pure compound is $F = 3 - \pi - \varphi$, obtained from eq. (2.1) with ($N = 1$).

Scenario	π	φ	F
A	1	0	2
B	2	0	1
C	3	0	0
D	1	2	0

Referring to the *PT-EP* in Figure 2.1, there are five curves and so there are five equilibria: solidα-solidβ, solidα-liquid, liquid-vapor, solidα-vapor and solidβ-vapor. These curves represent also the limits of existence of the homogeneous phases, which split in two equilibrium phases for P-T couples placed over them.

All curves in Figure 2.1 show a positive slope, thus a temperature increase is followed by a pressure increase. With reference to the Clapeyron equation, eq. (2.8), it follows that by supplying heat to the system, the volume variation will be positive being the latent heat a positive quantity.

This trend is respected for all the pure substances except for some cases, like water, showing a negative slope for the solidα-liquid curve in the proximity of the solidα-vapor-liquid triple point.

The term on the right side of eq. (2.8) is then nearly always a positive quantity, and a positive (negative) temperature variation is combined to a positive (negative) variation in terms of pressure.

In cases like water, where along the melting curve the solid volume is greater than the liquid volume, the volume variation is negative during the phase transition from the solid phase to the liquid phase, and vice-versa. As a consequence, in such a case a temperature variation will be associated to a discordant variation in pressure because of the negative sign of the right side of eq. (2.8).

For a pure substance, three phases can coexist at equilibrium at the same temperature and pressure, the scenario C of Table 2.1. This case is indicated in Figure 2.1 by blue triangles. These points are the solidα-solidβ-vapor and the solidα-liquid-vapor triple points.

Another singular state is the liquid-vapor critical point, represented by the red circle in Figure 2.1. In this case, the scenario D of Table 2.1, $\varphi = 2$ because two constraints $[(\partial P/\partial v)_T,(\partial^2 P/\partial v^2)_T = 0]$ must be matched, and only one phase is present for the correspondent critical temperature and pressure. This point is the first where the vapor and the liquid phases become indistinguishable and above which the liquid-vapor equilibrium cannot exist, and it represents a second-order phase transition. Beyond the critical point it is then usual to speak about the supercritical phase.

The scenario C and D are related to a system without degrees of freedom. In such a case, it is not possible to change a state variable without changing scenario, and triple points and critical point represent the limits of the two phase equilibria. The solidα-solidβ and the solidβ-vapor curves start from the solidα-solidβ-vapor triple point. The solidα-vapor curve starts from the same triple point ending in the solidα-vapor-liquid triple point, where also the solidα-liquid and the liquid-vapor curves start. The liquid-vapor curve ends in the critical point.

In this work, only the solidα has been considered since cryogenic processes usually involve only the first crystal structure. As a consequence, the sublimation curve solidα-vapor is considered to extend down to the low temperature and low pressure region without encountering other crystal structures. Theoretically, one always expects to encounter a solid or a vapor phase (or both of them at equilibrium) below the solid-liquid-vapor triple point as long as the temperature and the pressure are positive.

2.4.1.1 Shape of the melting line

The melting curve, that groups the pressure-temperature conditions for the solid-liquid phase transition, exits the triple point and shows a rising temperature as the pressure increases.

The shape of the melting line has been the object of an important debate since the beginning of the last century, and the different proposed behaviors are portrayed in Figure 2.2.

In 1903, Tammann argued that subjecting a liquid to an isothermal compression will result in a double transition which couple a crystallization followed by a melt, [12]. It means that the melting temperature will first increase and then decrease with pressure, thus the melting line is characterized by a maximum temperature (see graph -a- in Figure 2.2).

In 1968, Leudemann and Kennedy proved this idea through experimental measurements of the melting line of lithium and potassium, [13]. The solid-liquid equilibrium was measured up to 10 GPa, and the maximum temperature for the two compounds was measured at about 9 and 7 GPa, respectively.

In 1995, the theory of maximum melting temperature was further confirmed by Dass, who achieved other experimental works on alkali metals, [14]. Furthermore, he proposed an equation for the melting temperature as function of pressure, and this equation have been applied more recently to hydrogen, deuterium, nitrogen and methane, [15].

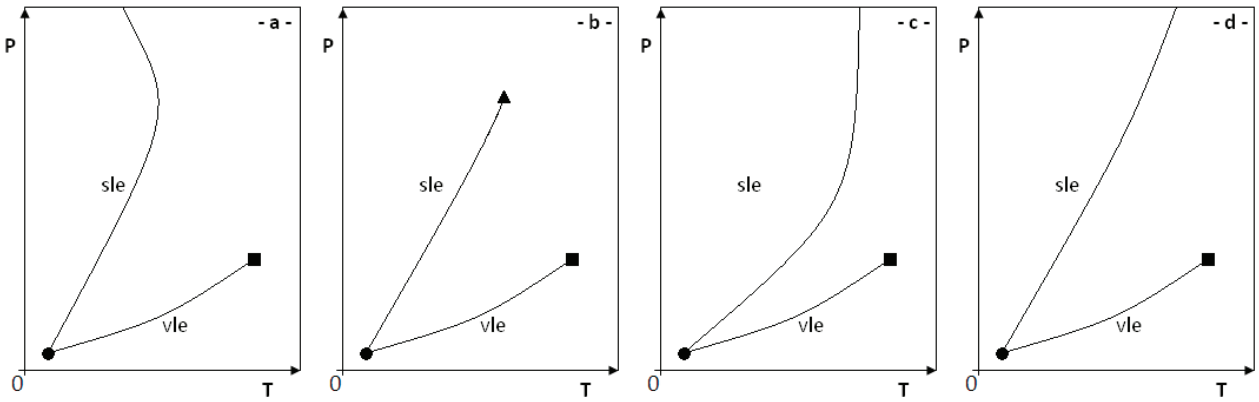

Figure 2.2: Qualitative pressure-temperature equilibrium projections of a phase diagram for a pure substance, considering only solid-liquid and liquid-vapor equilibria.

—, phase equilibrium boundaries; ●, triple point; ■, liquid-vapor critical point; ▲, solid-liquid critial point, -a-, maximum melting temperature; -b-, solid-liquid critical point; -c-, asymptotic temperature; -d-, indifinite rise of the melting curve.

In [15], the capability of the Dass equation in representing solid-liquid equilibrium data of such compounds was proved up to 500GPa for H_2, 8GPa for D_2, and 1GPa for N_2 and CH_4

It is worth mentioning that up to these pressures any reference data confirm the presence of a maximum in the melting temperature. Hence, in [15] the maximum of temperature is a merely consequence of the form of the Dass equation rather than being proved by data. However, the predicted maximum temperatures for H_2, D_2, N_2, and CH_4 are 575GPa, 23, 15.5GPa, and 30.7GPa, respectively.

Graph -c- in Figure 2.2 shows an asymptotic temperature at infinite pressure. This hypothesis was introduced by Schames in 1912, [16], and discussed by Bridgman in 1934, [17]. He carried out experimental measurements on 25 substances, including for instance nitrogen and argon. He measured pressure, temperature, change in volume, and latent heat, finding that the incremental ratio between temperature and pressure is always positive. Hence, this ratio is always convex toward the temperature axis instead of being concave as in the Tammann hypothesis. This also implies the Schames theory is wrong, as in such a case the incremental ratio would cut the temperature axis at some temperature.

Furthermore, Bridgman's opinion about the presence of a solid-liquid critical point was the absence of experimental evidence regarding conditions of vanishing of the change in volume and latent heat, since he never found a change of volume concave toward pressure or temperature.

The presence of a solid-liquid critical point, graph -b- in Figure 2.2, is instead a consequence of the order-disorder theory of Lennard-Jones and Devonshire, [18]. In this theory, there is a temperature beyond which the melting process becomes continuous ceasing to be a first-order transition.

Domb pointed out that in [18] the solid-liquid equilibrium is not always discontinuous because at some conditions the crystal lattice becomes incompressible, and such a case is typical only for hard spheres systems, [19]. Thus, his conclusion was that a melting transition will always be first-order, according also to the melting formula proposed by Simon and Glatzel in 1929, [20].

In 1972, Mori et al. investigated the possibility to improve the Lennard-Jones and Devonshire cell theory for avoiding the presence of a solid-liquid critical point, [21]. In their opinion, the order-disorder model fails in considering the crystal lattice enclosed in a fixed volume. Thus in 1972, authors introduced the concept of expandable lattice model in order to give to volume the possibility of change and ensure the discontinuous character of melting.

Summarizing, up to now there are no experimental works demonstrating the existence of a solid-liquid critical point similar to the well-known liquid-vapor critical point. The maximum melting temperature has been experimentally measured only for alkali metals not involved in this study. When predictions have been made on substances like nitrogen and methane, the correspondent maximum temperatures occur at pressures outside the operative conditions of an air distillation unit. As a consequence of what stated here above, hereafter in this work the melting boundary will be consi-

dered as a curve which merely rises indefinitely to high temperatures and pressure, graph -d- in Figure 2.2.

2.4.2 Binary mixture

The possibility of quantitatively representing phase equilibria of real mixtures is a fundamental and challenging topic in chemical engineering. As a consequence, many efforts have been done in order to improve the ability of thermodynamic models to represent distribution and compositions of the equilibrium phases for given thermodynamic conditions. Moreover, it is required that such models evolve their response to match different types of phase phenomena since the operative conditions can change value over the processes.

The response of a model to thermodynamic conditions can be analyzed in the global phase diagram. This concept was introduced in 1977 by Furman, [22]. It is a kind of phase diagram obtained using the molecular parameters of a model as field variables. Global phase diagrams are considered systematic tools to investigate the real phase behavior, considering that real mixtures can be interpreted as specific realizations of a model provided by particular values of its parameters.

2.4.2.1 Global phase diagrams for fluid phases

The first classification of global phase diagrams has been done by van Konynenburg and Scott in 1980, [23].

Using the van der Waals equation of state (EoS) [24], eq. (2.9), and mixing rules, eqs. (2.10)-(2.11), van Konynenburg and Scott proposed a classification of phase diagrams for binary mixtures of non-polar components with equal-size molecules, considering only the fluid phases.

$$P = \frac{RT}{v-b} - \frac{a}{v^2} \tag{2.9}$$

In eq. (2.9), P, T, R, and v are the pressure, the absolute temperature, the molar gas constant, and the molar volume, respectively. The first term on the right side is the repulsive term and it includes the parameter b, the volume that is occupied from the real molecules. The second term on the right side is the attractive term and it includes the parameter a for taking into account temperature variations and the molecular interactions.

van der Waals proposed the following mixing rules for evaluating the parameters a_{MIX} and b_{MIX} in a binary system composed by the components 1 and 2, [24]:

$$a_{MIX}(x) = (1-x)^2 a_{11} + 2(1-x)x a_{12} + x^2 a_{22} \tag{2.10}$$

$$b_{MIX}(x) = (1-x)^2 b_{11} + 2(1-x)x b_{12} + x^2 b_{22} \tag{2.11}$$

In the previous equations, x is the molar fraction, a_{11} (b_{11}), a_{22} (b_{22}) and a_{12} (b_{12}) are the parameter a (b) evaluated for the pure component 1, the pure component 2, and their combination, respectively.

The analysis of van Konynenburg and Scott is based on the equal-size molecules supposition, then $b_{12} = b_{11} = b_{22}$. They defined the thermodynamic variables ζ and λ as functions of the terms a_{12}, a_{11}, and a_{22}., eqs. (2.12)-(2.13).

$$\zeta = \frac{a_{22} - a_{11}}{a_{22} + a_{11}} \tag{2.12}$$

Thus, they evaluated the influence of the change of the term ζ and λ in modifying the response of the van der Waals EoS in terms of phase equilibria.

$$\lambda = \frac{a_{11} - 2a_{12} + a_{22}}{a_{22} + a_{11}} \tag{2.13}$$

As a result, they obtained a mapping of five topologically different types of pressure-temperature equilibrium projections as function of the thermodynamic variables and the EoS parameters. In their classification, the liquid-liquid and the liquid-vapor equilibria extend down to $T = 0$ and $P = 0$.

Figure 2.3 shows the qualitative pressure-temperature equilibrium projection of the first type phase diagram including only the fluid phases, as proposed by van Konynenburg and Scott. In the field of the cryogenic air distillation this type of diagram is very important because it is typical for the binary mixture nitrogen-oxygen.

As it can be seen in Figure 2.3, this projection presents a liquid-vapor equilibrium curve (*lv*) for each component of the mixture, and a continuous vapor-liquid critical line (*l*=*v*) which joins together their critical points, portrayed by empty circles.

In 1992, Sadus extended the classification proposed by van Konynenburg and Scott including other four typologies of phase diagrams, [25].

Since these pioneering studies, many new types have been discovered by other authors considering different specific EoSs and different compounds.

To the purpose of giving a unified classification scheme, Bolz et al. proposed a new nomenclature for phase diagrams including liquid phases, [26].

In this work the authors deeply discussed the different types of diagrams considering also their subsystems.

Nevertheless, in the present work only six phase diagrams will be considered: the five proposed by van Konynenburg and Scott and type VI.

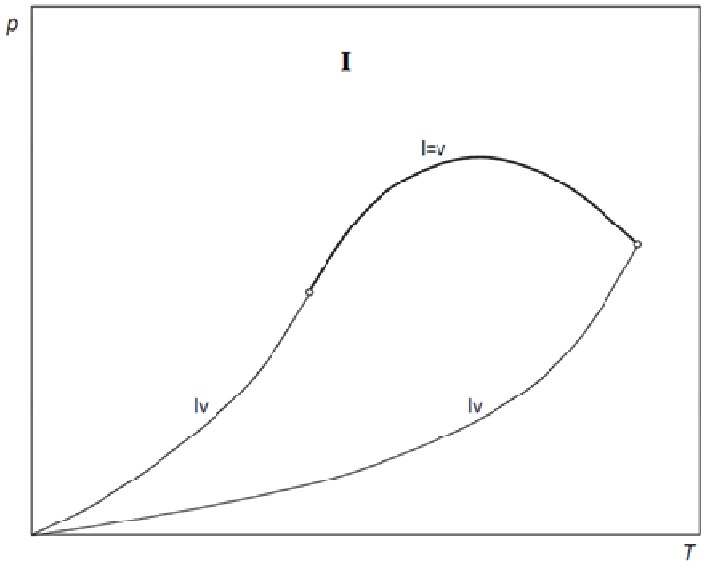

Figure 2.3: Qualitative Type I PT-EP systems as presented in van Konynenburg and Scott, [23].
○, critical points; —, liquid-vapor equilibria for the two compounds; —, liquid-vapor critical locus.

It is worth mentioning that all the selected phase diagrams have been experimentally encountered, and that an equal schematic classification and representation including the solid phase has not been done yet.

2.4.2.2 Solid-liquid temperature-composition projections

One of the first aspects that should be considered for including the solid phase in phase diagrams is the typology of solid-liquid equilibrium. In a temperature-composition cross section (Tx-CS), the *liquidus* and the *solidus* curves represent the lines connecting temperatures at which the melting and the freezing occur for various compositions, respectively. Hence, these curves define the area within the solid-liquid equilibrium (SLE) occurs.

In 1977, Matsuoka classified six types of solid-liquid equilibrium: solid solution, azeotrope, eutectic with partial immiscibility, eutectic with complete immiscibility, peritectic with eutectic, and molecular compound, [27].

Further investigations on binary organic mixtures led Matsuoka to determine the frequencies of occurrence of the Tx-CSs of Figure 2.4, [28]. He affirmed that simple eutectic behavior (type *d*) is the more frequent type among literature systems (more than 50%), followed by molecular compounds (type *f*, 25%). Then peritectic with eutectic behavior (type *e*) occurs in about 7% of the studied systems, whereas the remaining exhibit partial or total miscibility (types *a*-*c*).

Examples of these behaviors are systems Ar-Kr and CH_4-Kr for type *a*, N_2-Ar for type *b*, N_2-O_2 and Ar-CH_4 for type *c*, CO_2-CH_4 for type *d*. Tx-CSs of type *e* and *f* are representative of the mixture water-methanol and tetracloromethane+*p*-xylene, respectively.

It should be remarked that these Tx-CSs have been drawn considering an indefinite amount of matter. They are actually called *solubility diagrams* because they represent the liquidus (solidus) curve when the system has enough matter to respect the conservation matter condition, namely the equilibrium composition of the solid (liquid) phase when a liquid (solid) is cooled (heated). It has

been argued (Shirinyan et al. [29]) that whenever the quantity of matter is limited, as in nanoparticle systems, the solidus and the liquidus curves shift to lower temperatures and split the SLE in two different SLE areas depending on the versus of the transition (liquid to solid, or solid to liquid).

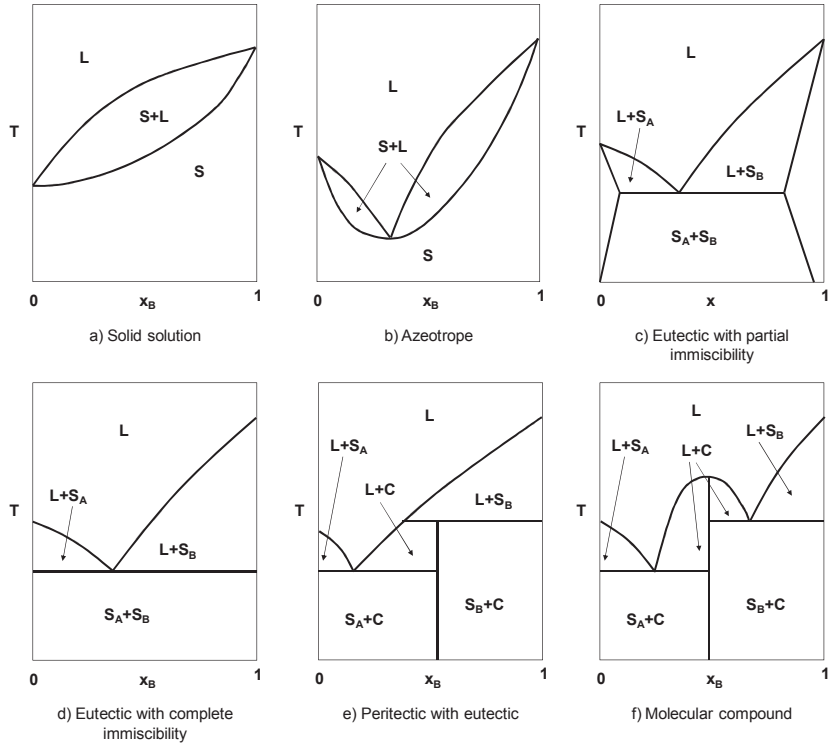

Figure 2.4: Types of solid-liquid phase diagrams identified by Matsuoka, [27].
(a), solid solution; (b), azeotrope; (c), eutectic with partial immiscibility; (d), eutectic with complete immiscibility; (e), peritectic with eutectic; (f), molecular compound. The phase diagrams are shown in the T-x_B plane where x_B is the mole fraction of component B. L = liquid mixture of A and B, S = solid solution of A and B, S_A = solid solution rich in A, S_B = solid solution rich in B, C = ordered solid with fixed stoichiometric ratio A_mB_n

In the present work, indefinite available matter has been considered, and only types *a* to *d* have been considered since the pure substances involved in the cryogenic air distillation present simple molecules which hardly show Tx-Cs of type *e* and *f*.

2.4.2.3 Global phase diagrams for solid and fluid phases

Among all the attempts to include the solid phase in the global phase diagrams it is worth mentioning some works proposed at the end of the 20th century. Garcia and Luks, [30], and Labadie et al., [31], combined the van der Waals equation of state with the classical approach (see Chapter 3) for the solid phase. In such a way, they obtained patterns for the phase equilibrium behaviors sustaining the idea that binary mixtures with the same type of fluid phase diagram can present different behaviors in the low temperature-low pressure region.

From a general point of view, the phase equilibrium behavior of a binary mixture can be qualitatively studied using different diagrams and interpreted always starting with the phase rule with N = 2. The degrees of freedom can vary from 0 to 3 depending on the number of phases and constraints. The possible scenarios are summarized in Table 2.2.

The simplest case is a homogeneous vapor, liquid, or solid phase with three degrees of freedom, scenario A. If a single phase lies on a critical curve two constraints holds, then F = 1, that is the case of scenario B. In the scenario C, two phases coexist at the equilibrium at the same temperature and pressure, and so F = 2. If one of the two phases is a critical phase, there are two constraints that need to be respected, so F = 0; in this case the mixture is identified by a point, called critical endpoint, the scenario D of Table 2.2. In the scenario E the binary mixture presents three phases that

coexist at the equilibrium at the same temperature and pressure, so the system has only one degree of freedom. This is for instance the case of the solid-solid-liquid equilibrium of graph d in Figure 2.4.

Table 2.2: Phase rule scenarios for a binary mixture.
The phase rule for a binary mixture is $F = 4 - \pi - \varphi$, obtained from eq. (2.1) with ($N = 2$).

Scenario	π	φ	F
A	1	0	3
B	1	2	1
C	2	0	2
D	2	2	0
E	3	0	1
F	2	1	1
G	3	1	0
H	1	3	0
I	4	0	0

In the scenario F, two phases at the equilibrium exist and they are placed along the azeotropic curve, wherein the composition of the liquid and vapor phases are the same, thus $\varphi = 1$ and $F = 1$. Starting from this case other two possibilities have to be considered, the scenarios G and H, respectively. If the two phases along the azeotropic curve are at the equilibrium with another phase F becomes 0. The same result is achieved if at the same temperature and pressure the azeotropic curve is tangent to the critical curve and so only a critical phase exists ($\pi = 1$) but three relations hold.

Finally, four phase can coexist at the same temperature and pressure and so $F = 0$. The correspondent couple P-T is usually called quadruple point. This scenario, I in Table 2.2, occurs in case of having partial or total immiscibility in the solid or in the liquid phase.

The phase diagrams for binary mixture including the solid phase have been evaluated starting from the classification proposed by van Konynenburg and Scott [23], some literature diagrams, and the solid-liquid equilibria suggested by Matsuoka, [27]. The solid phase and its equilibria have been added to the original shape of the *PT-EPs* suggested by van Konynenburg and Scott considering total and partial miscibility in the solid phase.

As a result, a classification from type I to type VI *PT-EP* has been proposed. In this chapter, the first type has been reported and briefly discussed, whereas the other *PT-EPs* have been reported in Appendix B. The abbreviations used in the Type I *PT-EP* for indicating the different types of phase equilibria and their meaning are listed in Table 2.3, together with the meaning of different line styles and symbols.

Table 2.3: Abbreviations, line styles and symbols used in the PT-EP.

Abbreviation	Meaning
l=v	Liquid - vapor critical curve
lv	Liquid - vapor equilibrium curve (pure component)
sl	Solid - liquid equilibrium curve (pure component)
sv	Solid - vapor equilibrium curve (pure component)
slv	Solid - liquid - vapor equilibrium curve
ssv	Solid - solid - vapor equilibrium curve
ssl	Solid - solid - liquid equilibrium curve
Equilibrium state	**Representation**
Pure component equilibrium curve	———
Critical curve	———
Three-phase curve	- · - · -
Pure component critical point	○
Pure component triple point	●
Quadruple point	□

It must be kept in mind that for identifying the components of a binary mixture, the subscript 1 indicates the component with the lowest critical temperature and so the subscript 2 means the component with the highest.

2.4.2.4 Type I PT-EP

Figure 2.5 shows the qualitative Type I *PT-EP* in case of solid solution.

According to the classification proposed by van Konynenburg and Scott for Type I, the critical curve *l=v* (Scenario B) joins together the critical points of the two components.

Three phases coexist at equilibrium (Scenario E) along the mixture triple curve *slv* which links the triple points of the two components.

Following the classification suggested by Matsuoka, the solid-liquid equilibrium shows a solid solution for pressure greater than the maximum pressure of the *slv* curve.

If immiscibility exists between two solid phases, like in the CO_2-CH_4 system, a s_1s_2lv quadruple point exists, as qualitatively represented in Figure 2.6. The high temperature equilibrium behavior does not change, while the low temperature equilibrium behavior ceases to show a continuous trend of the *slv* three phase line.

In Figure 2.6, a solid$_2$-liquid-vapor three phase line, s_2lv, exits the triple point of the heavier substance, has a trend with negative slope for decreasing temperatures up to a peak in pressure beyond which it decreases with positive slope down to the quadruple point.

The quadruple point is a singular point where four phases coexist at equilibrium. In this condition the system has no degree of freedom (Scenario I). The coexisting phases are two solids (solid1 and solid2), a vapor, and a liquid phase. From this quadruple point three lines originates.

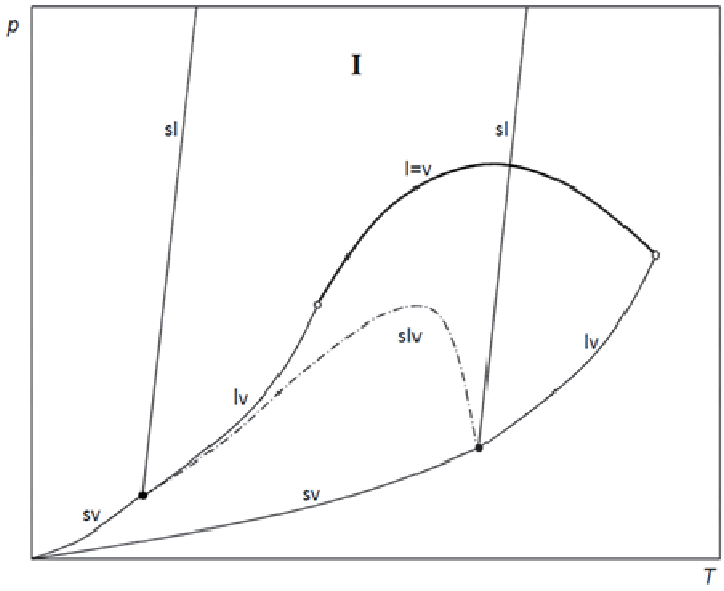

Figure 2.5: Qualitative Type I PT-EP systems in case of complete miscibility in the solid phase.

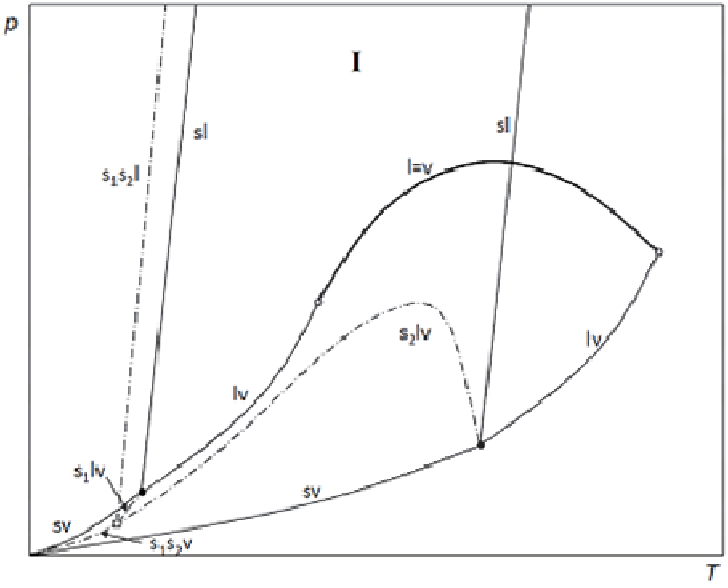

Figure 2.6: Qualitative Type I PT-EP systems in case of partial or total immiscibility in the solid phase.

A s_1lv three phase line joining the triple point of the lighter substance, a s_1s_2v three phase line with positive slop exploring the low temperature-low pressure region, and a s_1s_2l three phase line with a slope similar to the melting lines of the pure substances.

According to the classification suggested by Matsuoka, at any pressure greater than the maximum pressure of the s_2lv curve, the solid-liquid equilibrium can show either a eutectic with or without partial miscibility between the two solid phases.

3 Phase equilibrium calculation

The common formalism used for the equilibrium condition between two phases is discussed in the first part of this section together with a summary of Cubic Equations of State (*CEoSs*).

The second part focuses on literature models proposed to represent equilibria between solid and fluid phases.

3.1 Equilibrium condition

The system in eq. (3.1) resumes the necessary conditions for equilibrium of a heterogeneous closed system consisting of N components arranged in π phases and not allowed to exchange matter with its surroundings, [32]. In eq. (3.1), superscripts and subscripts indicate phase and component, respectively.

$$\begin{cases} T^1 = T^2 = \cdots = T^\pi \\ P^1 = P^2 = \cdots = P^\pi \\ \mu_1^1 = \mu_1^2 = \cdots = \mu_1^\pi \\ \mu_2^1 = \mu_2^2 = \cdots = \mu_2^\pi \\ \vdots \quad \vdots \quad \vdots \\ \mu_N^1 = \mu_N^2 = \cdots = \mu_N^\pi \end{cases} \tag{3.1}$$

Eq. (3.1) expresses the equilibrium condition in terms of intensive quantities: the temperature T, the pressure P, and the chemical potential μ which governs the repartition of the molecules in the different phases.

The chemical potential of a pure compound i is related to the intensive quantities T and P through eq. (3.2), [32], where s_i and v_i are the molar entropy and volume, respectively.

$$d\mu_i = -s_i dT + v_i dP \tag{3.2}$$

According to eq. (3.2), the first derivative of the chemical potential with respect to the pressure at constant temperature is given by eq. (3.3). Eq. (3.4) follows considering the volume of an ideal gas ($v_i = RT/P$) and integrating eq. (3.3) from the reference state P_0 to P. Eq. (3.4) argues that for an ideal gas the isothermal evolution of the chemical potential from its reference value μ_i^0 is a constant (RT) times the logarithm of the final pressure over the pressure at the reference state.

$$\left(\frac{\partial \mu_i}{\partial P}\right)_T = v_i \tag{3.3}$$

$$\mu_i - \mu_i^0 = RT \ln \frac{P}{P_0} \tag{3.4}$$

$$\mu_i - \mu_i^0 = RT \ln \frac{f_i}{f_i^0} \tag{3.5}$$

$$f_i^\alpha = f_i^\beta \tag{3.6}$$

In order to give an expression valid also for dense phases, the pressures ratio in eq. (3.4) has been substituted with the ratio between fugacities f, [32], giving eq. (3.5).

This last equation says that the isothermal change of the chemical potential in a heterogeneous closed system depends on the fugacity ratio of the compound i in the mixture f_i and the fugacity of the same pure compound at a reference state fi^0.

Introducing eq. (3.5) in the system in eq. (3.1) enables us to derive an equivalent criterion for the equilibrium condition, eq. (3.6). Eq. (3.6) tells that for any species i the fugacity must be the same in all phases, and this is the sought-after formalism for the equilibrium condition.

Even if eq. (3.6) gives a simple rule attesting the equilibrium between phases α and β, further details have been provided by means of eqs. (3.7)-(3.13) to handle the importance of fugacity in a real mixture.

The starting point is the relation between the chemical potential of a species and the Gibbs free energy of the system, eq. (3.7). In eq. (3.7), n_i is the number of moles of the component i, whereas S and V are entropy and volume of the system. Eq. (3.8), which can be easily obtained from the previous, states that chemical potential of a compound in a mixture represents the partial molar Gibbs energy, namely the molar Gibbs free energy g_i.

The information contained in eq. (3.8) coupled with eq. (3.5) provide the important relation between the activity a_i and the Gibbs free energy, eq. (3.9). The activity is the ratio between the fugacities of component i in the mixture and in its reference state and represents the *activation* of the compound in a mixture with respect to its reference state.

$$dG = -SdT + VdP + \sum_{i=1}^{N} \mu_i dn_i \tag{3.7}$$

$$\mu_i = \left(\frac{\partial G}{\partial n_i}\right)_{T,P,n_{j\neq i}} = g_i \tag{3.8}$$

$$\mu_i - \mu_i^0 = g_i - g_i^0 = RT \ln \frac{f_i}{f_i^0} = RT \ln a_i \tag{3.9}$$

The second term in eq. (3.9) can be now related to the Gibbs free energy of mixing (ΔG^M), eq. (3.10), that is the difference between the real value, G, and the free energy of each pure compound in the reference state, g_i^0.

$$\Delta G^M = G - \sum_{i=1}^{N} n_i g_i^0 = \sum_{i=1}^{N} n_i g_i - \sum_{i=1}^{N} n_i g_i^0 = \sum_{i=1}^{N} n_i \left(g_i - g_i^0\right) = \sum_{i=1}^{N} n_i RT \ln a_i \tag{3.10}$$

According to eq. (3.10), the activity of each component in a heterogeneous system a_i needs to be evaluated for representing the equilibrium.

The easiest possibility is to consider the mixture behaving as an ideal solution. In a binary mixture of components A and B, the ideal solution model assumes same energy of interactions between couples A-A, A-B, B-A, and B-B, so that the enthalpy change upon mixing is zero, ΔH^M=0. In addition to that, the volume of the ideal mixture is just the sum of the volumes of the individual components, so that also the volume change upon mixing is zero, Δv^M=0. An ideal solution is then a mixture obeying the Raoult's law, and the thermodynamic driving force for mixing is an increase of entropy, eq. (3.11). Eq. (3.12) derives from $\Delta G^M = \Delta H^M - T\Delta S^M$ and eq. (3.11) since ΔH^M=0.

The comparison between eqs. (3.10) and (3.12) states that in a ideal solution $a_i = x_i$, then the activity of each component equals its composition.

$$\Delta S^M = -\sum_{i=1}^{N} n_i R \ln x_i > 0 \tag{3.11}$$

Nevertheless, the enthalpy of mixing is often different from zero, and the ideal solution model is not representative of the real behavior of the mixture.

$$\Delta G^M = \sum_{i=1}^{N} n_i RT \ln x_i < 0 \tag{3.12}$$

In the model of real solution, compositions in mixture are not enough for describing the activation of the compounds with respect to their reference state. To take into account the deviations from ideal behavior an additional factor is used, namely the activity coefficient γ.

For each component, the activity a_i in a real mixture is then expressed as the activity in the ideal mixture, x_i, times an activity coefficient γ_i. In such a case eq. (3.10) becomes:

$$\Delta G^M = \sum_{i=1}^{N} n_i RT \ln a_i = \sum_{i=1}^{N} n_i RT \ln \gamma_i x_i = G^E + \sum_{i=1}^{N} n_i RT ln x_i \tag{3.13}$$

Considering the activity coefficients of the components introduces a new term in ΔG^M; this term is the excess Gibbs free energy of mixing (G^E), which represents the deviation from the ideal solution. Eq. (3.13) states firstly that the Gibbs free energy of mixing is a function of G^E and composition. Keeping in mind that the fugacity of each component must respect eq. (3.6) for the equilibrium condition, and that a_i is related to the fugacity ratio, eq. (3.9), it follows that the value assumed by ΔG^M is a direct consequence of the thermodynamic equilibrium.

On the other hand, the equilibrium condition has been reduced by eq. (3.13) to the evaluation of G^E, which turns in the evaluation of the activity coefficient γ_i. Different G^E models have been proposed to quantify γ, especially in liquid-vapor and liquid-liquid equilibria. Among others, well-know models are the Non Random Two Liquids (*NRTL*), [33], the Universal Quasi Chemical (*UNIQUAC*), [34], and the Universal Functional-group Activity Coefficient (*UNIFAC*), [35].

3.1.1 Symmetric and asymmetric approach

For each compound *i* in the system, the thermodynamic equilibrium between two phases implies an isofugacity condition, eq. (3.6). Two approaches are commonly used for describing this condition: the symmetric and the asymmetric approaches, resumed in Table 3.1.

The difference between these approaches, known respectively also as φ-φ and γ-φ approach, stems from the way used for evaluating the fugacities of eq. (3.6). In the φ-φ approach, the fugacities of both phases are evaluated in terms of fugacity coefficients obtained by solving an EoS. Unlike this case, in the γ-φ approach, the fugacity of one phase is expressed in terms of activity coefficients derived from a G^E model. To fix ideas, let's consider the equation representing the equilibrium between a vapor phase and a dense phase (solid or liquid) in a mixture, eq. (3.14).

Table 3.1: Formalisms for the symmetric and asymmetric approaches for the equilibrium condition between a vapor phase and a dense phase in pure compounds and mixtures.

Isofugacity condition	$f_i^D = f_i^V$			(3.14)
	φ-φ approach		γ-φ approach	
Mixture	$\hat{\varphi}_i^D x_i P = \hat{\varphi}_i^V y_i P$	(3.15)	$\gamma_i x_i P_i^{0,s} \varphi_i^{0,s} exp\left[\frac{v_i^D (P - P_i^{0,s})}{RT}\right] = \hat{\varphi}_i^V y_i P$	(3.16)
Pure compound	$\varphi^D = \varphi^V$	(3.17)	$P^{0,s} \varphi^{0,s} exp\left[\frac{v^D (P - P^{0,s})}{RT}\right] = \varphi^V P$	(3.18)

In both approaches, the non ideality of the vapor phase can be evaluated from a cubic EoS. f_i^V is then expressed as the product between the fugacity coefficient $\hat{\varphi}_i^V$ in the vapor phase and the fugacity in an ideal vapor phase, namely the partial pressure of component *i*. According to the Dalton's rule, the partial pressure in a vapor phase is given by the molar fraction of the component *i*, y_i, times the fugacity of the pure ideal component in the vapor phase, that is the pressure of the system.

In the φ-φ approach also f_i^D is evaluated from an EoS, thus for a mixture eq. (3.15) holds: x_i is the composition of component *i* in the dense phase and $\hat{\varphi}_i^D$ its fugacity coefficient.

Unlike the symmetric approach, the γ-φ approach determines f_i^D from an activity model, and eq. (3.16) can be obtained, [32]. In eq. (3.16), $P_i^{0,s}$ is the saturation (sublimation) pressure of the pure liquid(solid)-vapor equilibrium at *T*, $\varphi_i^{0,s}$ is the pure vapor phase fugacity coefficient at saturation (sublimation), and v_i^D is the molar volume of the compressed liquid (solid) phase. It should be noted that eq. (3.16) has been obtained considering constant volume of the dense phase between the equilibrium pressure *P* and the pure compound properties $P_i^{0,s}$.

When applied to pure compounds, the symmetric and asymmetric approaches give eqs. (3.17) and (3.18), respectively.

3.1.2 Cubic EoSs

The first attempt to describe the thermodynamic behavior of a gas was the ideal gas model. The ideal gas is constituted by mono atoms with same kinetic energy and unable to exert interacting forces. Moreover, the proper volume of these atoms is supposed to be negligible with respect to the total volume of the system. The perfect gas model sets up a relation between intensive properties. It equals the product between the pressure and the molar volume of a system to the gas constant *R* times the temperature, $Pv = RT$.

In order to involve repulsive and attractive forces, van der Waals introduced the parameters *a* and *b*. *a* takes into account the attractive forces among atoms, whereas *b* represents the molar covolume, that is the proper volume occupied by each atom. As a consequence of the introduction of

these two quantities, the pressure of the system is increased by the molecular pressure (a/v^2), while the atoms can space a lower volume than in the perfect gas model ($v–b$).

This equation is the first model able to introduce the liquid phase, and to describe the liquid-vapor first-order transition up to the vapor-liquid critical point. Starting from this EoS, other investigations proposed modified versions of the van der Waals equation of state (vdW EoS) aiming to reach better representations of the fluid thermodynamic properties. These CEoSs are generally written in a pressure-explicit form. Some examples of CEoSs are given in Table 3.2.

Table 3.2: Principal cubic EoSs.

Authors	Reference	Abbreviation	Pressure-explicit form
van der Waals	[24]	vdW EoS	$P(T,v)=\frac{RT}{v-b}-\frac{a(T)}{v^2}$
Soave, Redlich, Kwong	[36]	SRK EoS	$P(T,v)=\frac{RT}{v-b}-\frac{a(T)}{v(v+b)}$
Peng, Robinson	[37]	PR EoS	$P(T,v)=\frac{RT}{v-b}-\frac{a(T)}{v^2+2bv-b^2}$
Patel, Teja	[38]	PT EoS	$P(T,v)=\frac{RT}{v-b}-\frac{a(T)}{v^2+(b+c)v-bc}$
Schmidt, Wenzel	[39]	SW EoS	$P(T,v)=\frac{RT}{v-b}-\frac{a(T)}{v^2+(1+3\omega)bv-3\omega b^2}$
Twu, Sim, Tassone	[40]	TST EoS	$P(T,v)=\frac{RT}{v-b}-\frac{a(T)}{v^2+2.5bv-1.5b^2}$
Trebble, Bishnoi, Salim	[41]	TBS EoS	$P(T,v)=\frac{RT}{v-b}-\frac{a(T)}{v^2+(b+c)v-(bc+d^2)}$

A nomenclature has been proposed in Table 3.2 for each CEoS according to the authors. It should be noticed that Schmidt and Wenzel took into account the *acentric factor*, ω, in giving the expression of their CEoS. As its name suggests, the acentric factor is a measure of the non-sphericity of the atoms, in comparison with simple noble gas which are spherical.

The pressure-explicit expression of a CEoS involves the so-called repulsive and attractive pressures. The repulsive pressure includes the gas constant, whereas the attractive pressure contains the attractive forces.

All the cubic EoSs in Table 3.2 have the same repulsive pressure ($RT/(v–b)$), while the attractive term of the vdW EoS has been the subject of further improvements aimed to improve the representation of the saturation pressure. The underlying reason is the following.

The attractive forces are supposed to vary with temperature, thus $a(T)$ is the correspondent law of variation. This law must match two conditions. The former is that the attractive forces must tend to zero as temperature increases, because the thermal motion becomes more important than the attractive forces. The latter is that the attractive forces increase as temperature decreases.

This is due to the fact that the lower is the temperature, the lower the thermal motion of the atoms, thus static atoms attract themselves more than moving atoms.

Hence, the higher is the temperature, the lower are the mutual attractive forces, and the atoms tend to behave like in the ideal gas. To the contrary, the lower is the temperature, the higher are the attractive forces.

As a consequence, the attractive term becomes more and more important as the temperature decreases, thus the liquid phase undergoes attractive forces higher than those in the vapor phase. Therefore, it has appeared important to modify the attractive term for taking into account the behavior of the attractive forces.

The temperature-dependent function, $a(T)$, present in each cubic EoS of Table 3.2, is usually expressed as the value of the attractive parameter at the critical point, a_c, times the *α–function*, $\alpha(T)$. This means that the temperature dependence of a is traduced in modifications of the α-function. Ta-

ble 3.3 shows some α-functions proposed by different authors. These expressions depend on the acentric factor ω, the reduced temperature T_r (T/T_c), and present adjustable parameters (m_i , c_i , and $N_{0,1}$, $L_{0,1}$ and $M_{0,1}$) which can be tuned on experimental values.

Table 3.3: Examples of α–function for subcritical temperatures.

Authors	Reference	α–function
Soave, et al.[1]	[36]	$\alpha(T) = \left[1 + \left(\sum_{i=0}^{n} m_i \omega^i\right)\left(1 - \sqrt{T_r}\right)\right]^2$
Peng, Robinson[2]	[37]	
Mathias, Copeman	[42]	$\alpha(T) = \left[1 + \sum_{i=1}^{3} c_i \left(1 - \sqrt{T_r}\right)^i\right]^2$
Twu	[43],[44]	$\alpha(T) = \alpha^0(T) + \omega[\alpha^1(T) - \alpha^0(T)]$, where: $\alpha^{0,1} = T_r^{N_{0,1}(M_{0,1}-1)} exp\left[L_{0,1}\left(1 - T_3^{N_{0,1}M_{0,1}}\right)\right]$
Coquelet et al.	[45]	$\alpha(T) = exp[c_1(1 - T_r)]\left[1 + \sum_{i=2}^{3} c_i \left(1 - \sqrt{T_r}\right)^i\right]^2$

[1] – n=3; [2] - n=2.

Cubic EoSs are used for the representation of the liquid-vapor equilibrium not only for pure compounds, indeed they can be extended to mixtures. In this case, the mixing rules provide the values of the EoS parameters (a_{mix} , b_{mix}) starting from the values for the pure compounds involved in the mixture. Thus, these mixing rules take into account the reciprocal interaction between pure compounds. The simplest mixing rules are those proposed by van der Waals, called classical mixing rules. Eq. (3.19) gives the classical mixing rules for a mixture of N compounds.

$$a_{mix} = \sum_{i}^{N}\sum_{j}^{N} x_i x_j \left(1 - k_{ij}\right)\sqrt{a_i a_j} \quad , \quad b_{mix} = \sum_{i}^{N} x_i b_i \tag{3.19}$$

3.1.3 Fugacity coefficient from an EoS and Gibbs free energy of mixing

The fugacity coefficient of a pure compound can be obtained from an EoS and the compressibility factor Z. The relation between φ and Z is presented in eq. (3.20), where $a^R(T,v)$ is the residual Helmholtz energy, estimated by eq. (3.21), [32].

$$\ln \varphi = Z - 1 - \ln Z + a^R(T, v) \tag{3.20}$$

$$a^R(T,V) = \frac{1}{RT}\int_{\infty}^{v}\left[\frac{RT}{v} - P(T,v)\right]dv \tag{3.21}$$

In case of a vapor-liquid equilibrium, eq. (3.17) holds with the dense phase represented by the liquid. Furthermore, it is possible to use twice eq. (3.9) obtaining similar equations for the liquid and the vapor phases, as reported in eq. (3.22).

$$\begin{aligned} g^L - g^0 &= g^L - RTlnf^0 = RTln\varphi^L \\ g^V - g^0 &= g^V - RTlnf^0 = RTln\varphi^V \end{aligned} \tag{3.22}$$

By considering that at equilibrium $f^0 = P^L = P^V = P^{VLE}$, and that $\varphi^L = \varphi^V$, from eq. (3.22) it can be stated that the equality between the fugacity coefficients means the equality of the molar Gibbs free

energies of the two phases, namely $g^L = g^V$. Hence, at equilibrium g is the same for both phases, thus $dg(T,P) = g^L - g^V = 0$.

The first-order transition corresponding to the liquid-vapor equilibrium is described in graphs -a- and -b- of Figure 3.1. Graph -a- shows the qualitative isothermal pressure-density equilibrium projection that can be obtained from one of the cubic EoSs listed in Table 3.2 calculating the pressure for different values of density. This curve links the low and the high density regions by means of the well known S-loop. The red line is representative of the equilibrium pressure for a generic given temperature.

Moving from the vapor phase A towards the liquid phase F, the molar Gibbs free energy evolves like in graph -b-. The lines AB and EF provide the stable vapor and liquid phases, respectively. The lines BCDE in both graphs are a consequence of the pressure-explicit form of a cubic EoS, and are not representative of the real isothermal behavior of a substance. Hence, the line BCDE is a spinodal curve introduced by a cubic EoS to join the liquid and vapor branches, and it is the so-called S-loop. As it can be noticed in Figure 3.1, C and D are the maxiumum and minimum points of the S-loop, which is representend by dashed lines.

B and E represents the liquid-vapor equilibrium: at the same temperature and pressure they present two different densities in graph -a-, one for the vapor and one for the liquid. In graph -b- they have the same molar Gibbs free energy (B=E). As it has been stated before, AB and EF represent the stable vapor and liquid phases. For each positive pressure in graph -b-, the lowest molar Gibbs free energy always belongs to one of lines AB and EF. Therefore, the segments BC, CD, and DE (except points B and E) represent not stable states because for each positive pressure between A and C the correspondent g are greater then the values on the lines AB and EF. Segments BC and DE represent instead metastable states since their correspondent isothermal compressibility is positive. Again, negative pressures in both graphs are the artifice of the S-loop.

Concluding this analysis on pure compounds, one can assert that a pure system organizes itself in order to accommodate the minimum molar Gibbs free energy. When the same minimum is matched by two phases, an equilibrium occurs.

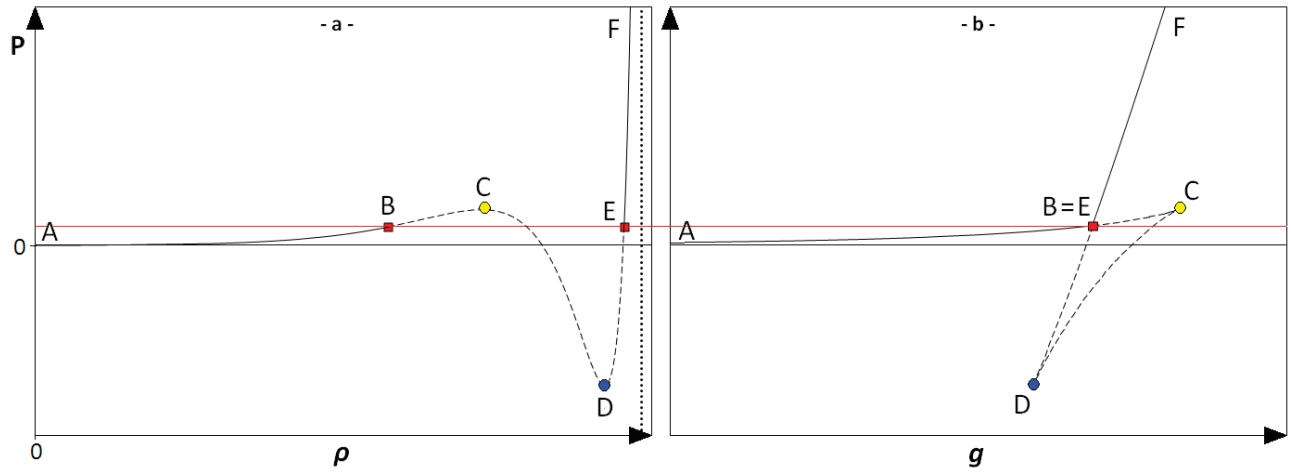

Figure 3.1: Qualitative representation of the vapor-liquid equilibrium in a pure compound.
-a-, isothermal pressure-density equilibrium projection; -b-, evolution of the molar Gibbs free energy along the isotherm; —, equilibrium pressure; A, vapor phase; B, equilibrium vapor phase; C, maximum of the S-loop; D, minimum of the S-loop; E, equilibrium liquid phase; F, liquid phase.

The fugacity coefficient of the i^{th} compound in a mixture $\hat{\varphi}_i$ is given in eq. (3.23). The first term on the right hand side of this equation represents the first derivative of the residual Helmholtz energy with respect to the number of moles of the i^{th} component.

$$\ln \hat{\varphi}_i = \left(\frac{\partial n a^R}{\partial n_i}\right)_{T,nv,j\neq i} - \ln Z \tag{3.23}$$

Let's consider a liquid-vapor equilibrium in a binary mixture and try to describe the equilibrium in term of the Gibbs free energy of mixing (G^M). Graph -a- in Figure 3.2 shows a classical temperature-composition cross section (Tx-CS) representing a simple vapor-liquid lens evaluated including mixing rules in a cubic EoS. The red line in graph -a- is the equilibrium temperature, while x_1 is the composition of one of the two components, ranging from 0 to 1. At the equilibrium temperature the pure component 1 and 2 are homogeneous vapor and liquid phase, respectively.

G^M can be evaluated for both phases by means of eq. (3.13). With reference to graph -b-, G_L^M and G_V^M represent the Gibbs free energy of mixing referred to the bubble line (the convex downward curve) and the dew line (the convex upward curve) of graph -a-, respectively. In a Tx-CS, the bubble (dew) line groups for each composition of the mixture the temperature at which the first bubble (drop) of vapor (liquid) is formed heating (cooling) a homogeneous liquid (vapor) phase.

Since the pure component 1 at the equilibrium temperature is stable in the vapor phase, G_L^M is higher than G_V^M for compositions approaching the limit $x_1 = 1$. Conversely, G_L^M is lower than G_V^M for compositions approaching the limit $x_1 = 0$, owing to the fact that at that temperature the pure component 2 is stable in a homogeneous liquid phase.

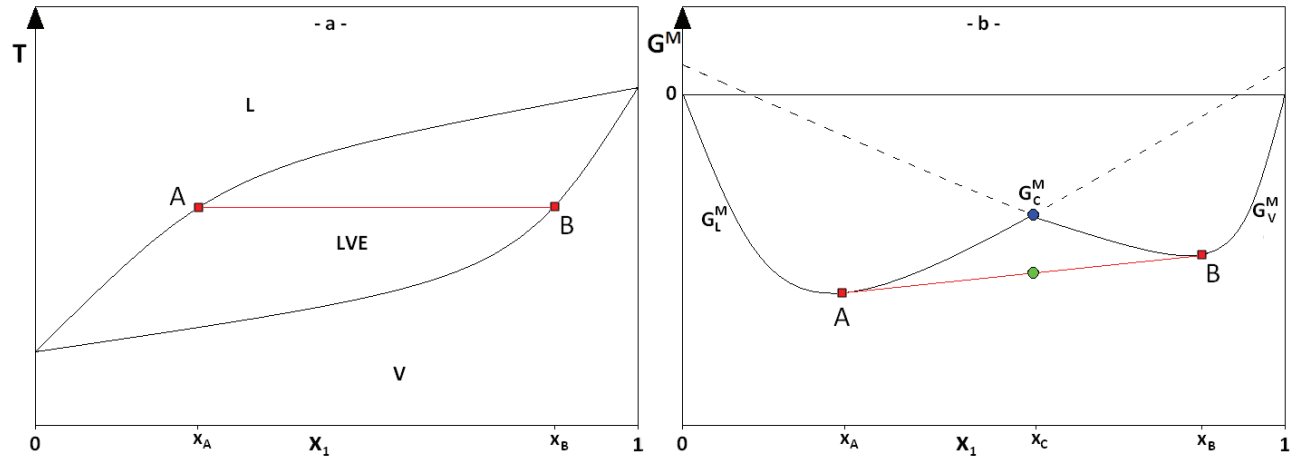

Figure 3.2: Qualitative representation of the vapor-liquid equilibrium in a binary mixture.
-a-, isobaric temperature-composition cross section; -b-, evolution of the mixing Gibbs free energy with the composition at equilibrium pressure and temperature; A, equilibrium liquid phase; B, equilibrium vapor phase; x_A, mole fraction of the component 1 in the liquid phase; x_B, mole fraction of the component 1 in the vapor phase; G_L^M, mixing Gibbs energy for the liquid phase; G_V^M, mixing Gibbs energy for the vapor phase.

As a result, there must be a point (blu point in graph -b-) where the G_L^M and G_V^M curves meet. The Gibbs energy of mixing of this point is indicated as G_C^M, and x_C is the composition in term of component 1.

It has been argued that a pure compound is organized in order to allocate the lowest molar Gibbs energy. By extending this concept on the current example, it can be said that for x_1 ranging from 0 to 1 the mimumum Gibbs energy of mixing ($G^{M,Min}$) corresponds to G_L^M for compositions lower than x_C, whereas $G^{M,Min}$ equals G_V^M from x_C up to $x_1 = 1$. Hence, G_L^M and G_V^M outside these ranges involve unstable liquid and vapor phases, respectively.

In graph -b- of Figure 3.2, by combining a homogeneous liquid mixture of composition x_A and Gibbs energy of mixing $G_L^M(x_A)$ with a homogeneous vapor mixture of composition x_B and mixing Gibbs energy $G_L^V(x_B)$, one obtains a mixture of composition x_C having a free energy lower than G_C^M. Thus, this unstable mixture, the green point in graph -b-, split in two equilibrium phases A (liquid phase) and B (vapor phase).

It is worth noticing that the solution of the equilibrium condition in a mixture, eq. (3.15), is equivalent to solve a mathematical problem of maximization of the distance between $G^{M,Min}$ and the Gibbs energy obtained from $G_L^M(x_A)$ and $G_L^V(x_B)$. Then, the maximization of the distance between blue and green points of graph -b- will provide the maximum instability causing the system splitting in the two stablest equilibrium phases. In other words, the solution of a phase equilibrium problem

can be described mathematically as finding a plane tangent to the Gibbs free energy of mixing G^M which does not intersect G^M at any other point than the stationatory points of equilibria. This concept has been introduced at the beginning of the 80's by Baker, [46], and Michelsen, [47].

As a consequence of this procedure, the maximum distance could not be placed in corrispondence of x_C, depending on the particular shape of the ${G_L}^M$ and ${G_V}^M$ curves.

Concluding this analysis on binary mixtures, one can assert that a binary system organizes itself in order to accommodate the lowest Gibbs free energy of mixing. Unlike the case of a pure compound, the equilibrium phases do not present the same G^M, whereas the underlying foundament is the maximization of difference between G of the homogeneous mixture and G at the same composition obtained combining ${G_L}^M$ and ${G_V}^M$.

Details of this concept have been developed and discussed in chapter 6.

3.2 Representation of the solid-fluid equilibrium

According to Table 3.1, we need fugacities for the prediction of equilibrium, and a relation for representing the solid-liquid equilibrium is still missing. The aim of this section is then to represent the SLE in terms of basic thermodynamic relations, and to illustrate literature models which proposed in dealing with phase equilibria involving solid phase. The mathematical steps needed for obtaining the thermodynamic relations hereafter presented are illustrated in Appendix C.

3.2.1 Classical approach

Eq. (3.24) is the fundamental property relation for the fugacity of a pure compound (f^0) which can be obtained from eq. (3.2). In eq. (3.24), H is the enthalpy and V is the volume. This equation can be applied to the solid and liquid phases and integrated from the pure compound triple point to the SLE temperature and pressure giving eq. (3.25). In eq. (3.25), the latent heat of melting, ΔH, the volume and heat capacity differences between the solid and liquid phase, ΔV and ΔC_P, are triple point properties.

$$dlnf^0 = d\left(\frac{G}{RT}\right) = -\frac{H}{RT^2}dT + \frac{V}{RT}dP \tag{3.24}$$

$$ln\frac{f^{0,L}}{f^{0,S}} = \frac{\Delta H}{RT_t}\left(\frac{T_t}{T} - 1\right) - \frac{\Delta C_P}{R}\left(\frac{T_t}{T} - 1 - ln\frac{T_t}{T}\right) + \frac{\Delta V(P - P_t)}{RT} \tag{3.25}$$

$$ln\frac{f^{0,L}}{f^{0,S}} = 0 \Rightarrow P = P_t + \frac{\Delta H}{\Delta V}\left(\frac{T}{T_t} - 1\right) + \frac{\Delta C_P}{\Delta V}\left(T_t - T - Tln\frac{T_t}{T}\right) \tag{3.26}$$

Eq. (3.25) can also be obtained starting from the differential of the Gibbs free energy, $dG = dH - TdS$.

Derivations of eq. (3.25) from $dG = dH - TdS$ and from eq. (3.24) have been reported in Appendix C.

Eq. (3.26) is the pressure explicit form of eq. (3.25) resulting from the solid-liquid isofugacity condition.

Knowing the triple point properties, the SLE pressure can directly be calculated at fixed temperature from eq. (3.26).

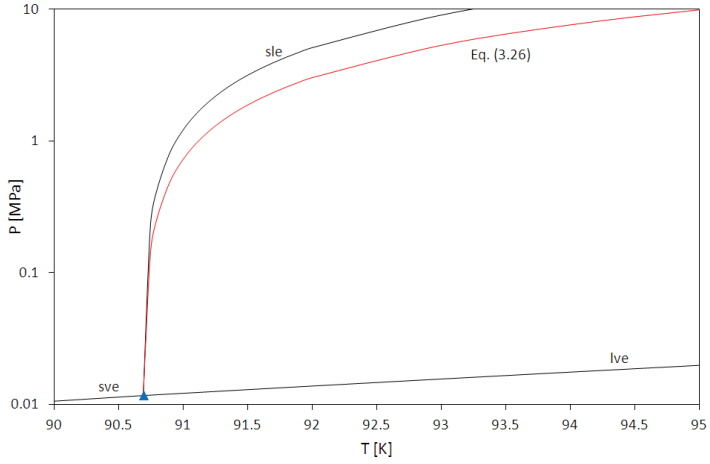

Figure 3.3: SLE of methane from fundamental relation.
— : phase equilibrium boundaries, [3]; ▲ : triple points, [3]; — : sle from eq. (3.26). Molar triple point properties: Δh = 0.9419 kJ/mol [48], $\Delta v = v^L - v^S$ = 0.0044474 dm^3/mol, v^L from [3], v^S from [49], $\Delta C_P = C_P{}^L - C_P{}^S$ = -0.00166 kJ/molK, $C_P{}^L$ and $C_P{}^S$ from [3]. Ratios $\Delta H/\Delta V$ and $\Delta C_p/\Delta V$ in eq. (3.26) are independent from the number of moles.

An example of the application of eq. (3.26) is given in Figure 3.3 for methane. The pressure-temperature equilibrium projection in Figure 3.3 shows (in the range 90K-95K) the SLE, SVE, and VLE equilibria of methane, [3], and the SLE calculated from eq. (3.26). The deviation between SLE from [3] and eq. (3.26) is due to the assumptions made in the integration of eq. (3.24), namely constant ΔC_P and ΔV along the melting line.

The last two terms in eq. (3.25) are usually neglected at temperatures and pressures not too far from the triple point. In this case, the fugacity ratio becomes a merely function of the heat of melting, deeply used in dealing with SLE of mixtures.

Considering x_i and z_i the composition of component i in the liquid and solid phase, respectively, the SLE condition in a mixture can be expressed in terms of activity coefficient, γ, eq. (3.27). In eq. (3.25), the ratio $z_i\gamma_i^S/x_i\gamma_i^L$ can be replaced by $f_i^{0,L}/f_i^{0,S}$ giving eq. (3.28).

$$x_i\gamma_i^L f_i^{0,L} = z_i\gamma_i^S f_i^{0,S} \quad \Rightarrow \quad \frac{f_i^{0,L}}{f_i^{0,S}} = \frac{z_i\gamma_i^S}{x_i\gamma_i^L} \tag{3.27}$$

$$ln\frac{f_i^{0,L}}{f_i^{0,S}} = ln\frac{z_i\gamma_i^S}{x_i\gamma_i^L} = \frac{\Delta H_i^{fus}}{RT_{t,i}}\left(\frac{T_{t,i}}{T} - 1\right) \tag{3.28}$$

Eq. (3.28) relates the equilibrium compositions of the solid and liquid phases with pure component properties ΔH_i^{fus} and $T_{t,i}$. This equation enables the evaluation of SLE in binary mixtures knowing the activity coefficients of the solid and liquid phases. Depending on the values of the activity coefficients, eq. (3.28) can be used for representing solid-solutions as well as eutectic behaviors with total or partial immiscibility. Nevertheless, eq. (3.28) is principally used in cases of total immiscibility in the solid phase where z_i and γ_i^S are 1.

Eqs. (3.25) and (3.28) represent the "*classical approach*" for the SLE seeing that they are derived from classical thermodynamic relations. The classical approach has been widely adopted for the representation of the SLE in cases of total immiscibility in the solid phase where no information are needed concerning the activity coefficient of the solid phase.

At a fixed temperature and pressure, eq. (3.25) allows the evaluation of the fugacity of the pure solid phase from the liquid fugacity, which can be evaluated for example from a CEoS. Nevertheless, eq. (3.24) does not provide information concerning other properties like solid volume or enthalpy. Furthermore, applying the classical approach for mixtures in case of solid solution or partial miscibility needs the evaluation of the activity coefficients of the solid phase, then an activity model is required for describing the non ideality in the solid phase. These features induced other authors to propose other thermodynamic models for representing the SLE.

3.2.2 Solid-fluid equilibrium models

Details of the SLE models discussed in this section are presented in Appendix C, while a summary is reported in Table 3.4. The main models devised to account for the Solid-Fluid Equilibrium (SFE) can be classified in 8 categories:

- Classical Approach (*CA*);
- Modified Cubic Equation of State (*MCEoS*);
- System of Cubic Equations of States (*SCEoSs*);
- Molecular Association (*MA*);
- Quartic Equation of State (*QEoS*);
- Unified Lattice Fluid Equation of State (*ULFEoS*);
- Insertion Probability (*IP*);
- Thermodynamic Perturbation Theory (*TPT*).

Several studies have been proposed for representing the SLE of multicomponent mixtures by means of the *CA*, eq. (3.25). In 1978, Soave applied the SRK EoS to SLE calculations in mixtures

of carbon dioxide and light hydrocarbons, [50]. In [50], ΔH^{fus} and ΔC_P were regressed from experimental SVE pressures of pure CO_2, then the isofugacity condition for CO_2 in the mixture was solved using the *CA* for the fugacity of the pure solid phase and the SRK EoS for the fugacity in the liquid phase.

The *CA* was coupled with the TST EoS to handle solubility in crude oil mixtures by Twu et al. in 2003, [51]. In the mixtures proposed in [51], pure solid phase was considered, and solid fugacities were obtained directly from the expression of the fugacity coefficient related to the TST EoS. The temperature dependence of the attractive forces within the TST EoS for the solid phase was calculated in order to respect eq. (3.28).

Another example of the application of the *CA* has been recently provided by Rodrigues-Reartes et al., [52]. In this work, authors proposed the computation of solid-fluid-fluid equilibria for binary asymmetric mixtures in wide ranges of conditions using eq. (3.25) with ΔC_P linearly dependent on the temperature.

Several works have been proposed by Coutinho concerning SLE in hydrocarbons mixtures. Examples are references [53] and [54]. The *CA* is used to fix the relation between activity coefficients of the solid and liquid phases. The non-ideality in the liquid phase is evaluated by means of the Flory-free volume equation, [55], usually coupled with the UNIFAC model, whereas the solid activity coefficient is defined through the UNIQUAC, the NRTL, or the Wilson model, [56].

Kan's work was the first attempt to develop a unified EoS for representing equilibria involving solid, liquid, and vapor phases, [57]. In [57], a pressure explicit equation was obtained adding a term of order 2 within a CEoS and applied to the phase equilibrium behavior of argon. The result was a Modified CEoS (*MCEoS*), where the last term takes into account the attractive contribution of the solid phase.

Other examples of *MCEoSs* were proposed by Wenzel and Schmidt in 1980, [58], and by Rodriguez and Martinez in 2013, [59]. These authors added a term of order 6 in the SRK EoS and a term of order 10 in a parametric CEoS, respectively. Among the *MCEoSs* here discussed, only the one in reference [58] was applied to SLE of binary mixtures.

In 1994, Salim and Trebble proposed a System of two cubic EoSs (*SCEoSs*) to allow calculation of thermodynamic properties of the three main states of matter as well as the correspondent equilibria, [60]. The two CEoSs within the system, whose functional form is of the TBS EoS type, are used for representing the liquid-vapor and the solid-vapor equilibrium, respectively. The one applied to SVE is obtained translating the TBS EoS at the pure compound triple point, thus forcing it to represent triple point properties by refitting of the parameters. The *SCEoSs* was used in [60] for representing equilibrium behaviors of pure compounds, solubility of solid carbon dioxide in liquid methane, and SVE in the systems carbon dioxide-benzoic acid and ethylene-benzoic acid.

Molecular Association (*MA*) models superimpose the concept of existence of molecular clusters at chemical equilibrium on the basic assumptions of CEoSs, namely the concepts of repulsive and attractive forces. The possibility of having association phenomena in pure fluids containing non polar as well as strongly polar or hydrogen-bonded molecules was argued by Heidemann and Prausnitz in 1976, [61]. In [61], authors proposed a van der Waals-type EoS involving molecular association of monomer molecules to form dimers, trimers, and so on up to *N*-mers, according to chemical equilibria. Lang and Wenzel, [62], and Geaña and Wenzel, [63], coupled molecular association and the SW EoS for determining the SFE behavior of pure compounds and mixtures. The starting points of their models were always the possibility of representing substances as mixtures of their own molecules and to consider the solid phase as the biggest molecular clusters.

In 2003, Yokozeki modified the repulsive term of a CEoS for representing solid, liquid, and vapor phases with a single analytical equation, [64]. The result was a Quartic Equation of State (*QEoS*) involving a discontinuity along the solid-liquid transition while keeping the classic S-loop for the liquid-vapor transition. The *QEoS* has been applied for representing phase equilibrium behavior of pure compounds, [64], mixtures, [64] and [65], mixtures involving hydrates, [66] and [67], hard sphere mixtures, [68], and indoles, [69].

The Unified Lattice Fluid Equation of State (*ULFEoS*) was suggested by Lee et al. in 2010, [70]. First of all, authors adapted the lattice model proposed by Veytsman for fluids with hydrogen bonds, [71], to derive the solid-liquid transition. Secondly, the SLE contribution was incorporated into a lattice based EoS yielding the vapor-liquid transition to account for the three phase behavior. In [70], the *ULFEoS* was tested against equilibrium properties of eight pure compounds, providing a close representation of SLE, VLE, and SVE.

In 2011, Lee and Yoo investigated the possibility of obtaining an EoS applicable to the three phases of matter exploiting the relation between the compressibility factor and the Insertion Probability (*IP*), [72]. In systems of hard spheres, the *IP* is defined as the probability that a randomly selected molecule can enter into the system without overlapping the existing molecules, thus finding a cavity large enough to accommodate it. On the basis of this analysis, same authors reinterpreted the correlated cell model of Alder et a., [73], in terms of *IP*, and proposed an EoS for representing SLE, SVE, and VLE of pure substances ranging from simple gases to organic compounds, [74].

The thermodynamic behavior of a system can be described starting from its Helmholtz free energy. The Helmholtz free energy can be expressed taking the Lennard-Jones (*LJ*) system as the reference one, and considering contributions from other types of interaction as a perturbation, namely a deviation from the properties of the LJ system, [75]. This approach, known as Thermodynamic Perturbation Theory (*TPT*), allows obtaining an EoS from a physical model which describes the complex interaction potential of a fluid.

On the basis of the *TPT*, Adidharma and Radosz in 2004, [76], and Cochran and Chiew in 2006, [77], proposed *TPT* models to represent the thermodynamic behavior of the solid phase, considering the reference system interacting with the LJ potential and made of hard spheres and hard chains, respectively. More recently, Tan et al. coupled the LJ-solid EoS proposed by Adidharma with a *TPT* fluid EoS for representing solid-liquid-vapor equilibria in non-associating and non-polar systems, [78]. In 2007, the perturbed hard chain model proposed by Cochran and Chiew has been coupled with an analogous EoS for the fluid phase and applied to pure compounds and binary mixtures of *n*-alkanes, [79], [80].

Table 3.4: Overview of the main models accounting for the SFE.

Authors	Ref.	Year	Model	System	
				Pure	Mixtures
Soave	[50]	1978	*CA*	✓	✓
Twu et al.	[51]	2003	*CA*	◓	✓
Rodriguez-Reartes et al.	[52]	2011	*CA*	◓	✓
Coutinho et al.	[53],[54]	1996	*CA*	◓	✓
Kan	[57]	1979	*MCEoS*	✓	◓
Wenzel, Schmidt	[58]	1980	*MCEoS*	✓	✓
Rodriguez, Martinez	[59]	2013	*MCEoS*	✓	◓
Salim, Trebble	[60]	1994	*SCEoSs*	✓	✓
Heidemann, Prausnitz	[61]	1976	*MA*	✓	◓
Lang, Wenzel	[62]	1989	*MA*	✓	✓
Geaña, Wenzel	[63]	1999	*MA*	✓	✓
Yokozeki	[64]	2003	*QEoS*	✓	✓
Lee et al.	[70]	2010	*ULFEoS*	✓	◓
Lee et al.	[74]	2011	*IP*	✓	◓
Cochran, Chiew	[79],[80]	2007	*TPT*	✓	✓
Tan et al.	[78]	2013	*TPT*	✓	✓

CA = Classic Approach, *MCEoS* = Modified Cubic EoS, *SCEoSs* = System of Cubic EoSs, *MA* = Molecular Association, *QEoS* = Quartic Equation of State, *IP* = Insertion Probability, *TPT* = Thermodynamic Perturbation Theory.

3.2.3 Solid-liquid transition

Among all the SFE models discussed in the previous section, only some authors provided a description of the Solid-Liquid Transition (*SLT*).

Figure 3.4 represents a qualitative subcritical Pressure-Volume Equilibrium Projection (*PV-EP*) for a temperature greater than the triple point temperature.

In such a case, a VLE and a SLE occur at the saturation (P^{VLE}) and melting pressure (P^{SLE}), respectively.

In the *PV-EP* of Figure 3.4, black-solid lines portray the solid, liquid, and vapor branches, whereas the green-solid line represents the saturated liquid an vapor branches extending from the triple point pressure (black dashed line) up to the vapor-liquid critical point (filled black circle).

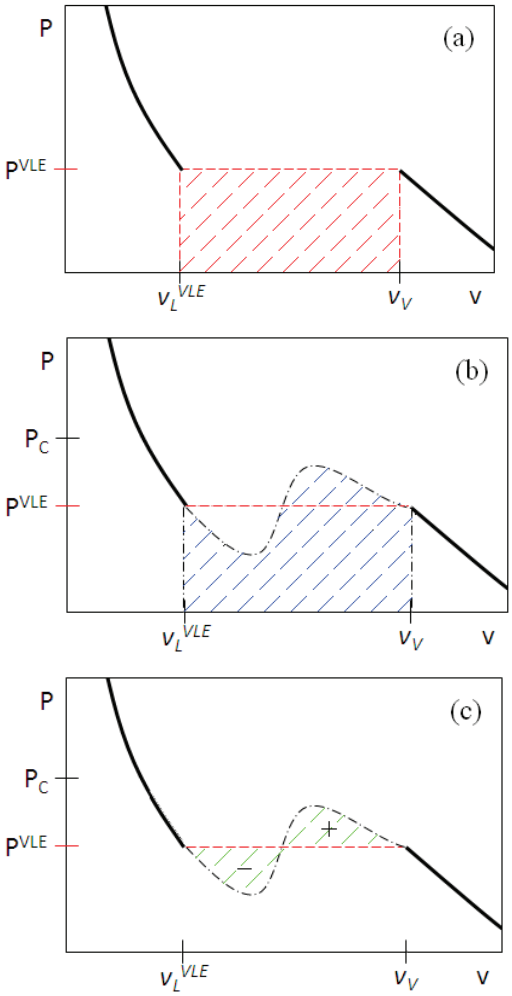

Figure 3.5: Graphical derivation of the Maxwell's equal area rule for phase transition.

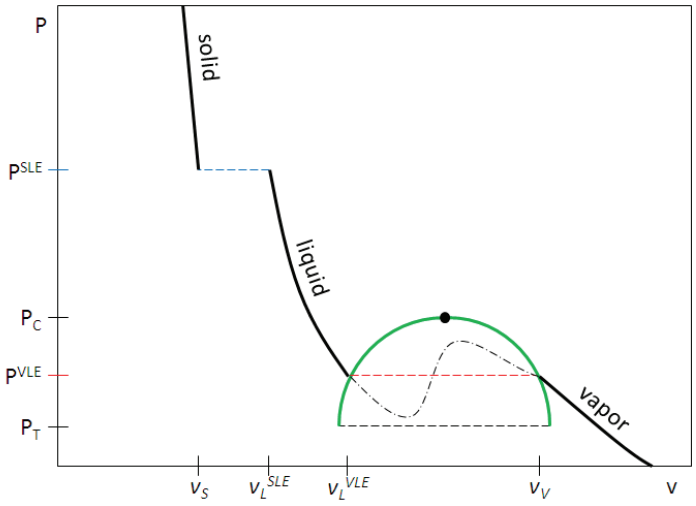

Figure 3.4: Qualitative subcritical isothermal pressure-volume equilibrium projection of a pure compound.

—: solid, liquid, and vapor branches; ● : critical pressure; — : saturated liquid and vapor phases; – – : melting pressure; – –: saturation pressure; – – : triple point pressure; – • – : S-loop.

In Figure 3.4 equilibrium volumes are indicated by v_S and v_L^{SLE} for the SLE, and v_L^{VLE} and v_V for the *VLE*.

When a CEoS is applied for representing the thermodynamic behavior of a pure compound, this turns in joining together v_L^{VLE} and v_V in the *PV-EP* by means of the common S-loop, the dashed-dotted line in Figure 3.4.

The behavior of the S-loop does not reflect the physical equilibrium behavior, which is instead represented by the isothermal-isobaric red dashed line.

The extent of the S-loop decreases for increasing temperatures and disappears at the critical values. From this value, the V-L transition ceases to be first-order.

It is worth mentioning here that the VLE isofugacity condition for a pure compound, eq. (3.17), implies the equal area condition with reference to the S-loop. This condition, known as the Maxwell's Equal Area Rule (*MEAR)*, eq. (3.29), requires the equality of the confined areas between the S-loop and the red dashed line.

$$P^{VLE}(v_V - v_L^{VLE}) - \int_{v_L^{VLE}}^{v_V} P(T,v)dv = 0 \qquad (3.29)$$

The first term of eq. (3.29) involves the real VLE behavior: the pressure equals P^{VLE} for all the duration of the VLE, thus the first term is the red cross-hatched rectangle of graph (a) in Figure 3.5. The integral of eq. (3.29) is the blue cross-hatched area of graph (b) in Figure 3.5. It can be easily inferred that a null difference between these two areas is obtained only in case of equality of the areas confined between the S-loop and P^{VLE}, namely the green cross-hatched areas in graph (c).

The mechanism for the solid-liquid transition involved in some of the SFE models previously discussed are graphically shown in Figure 3.6. These models allow the evaluation of the SLE by means of the Maxwell's Equal Area Rule applied at the melting pressure. Liquid and solid branches are always the black solid lines, the melting pressure is the blue dashed line.

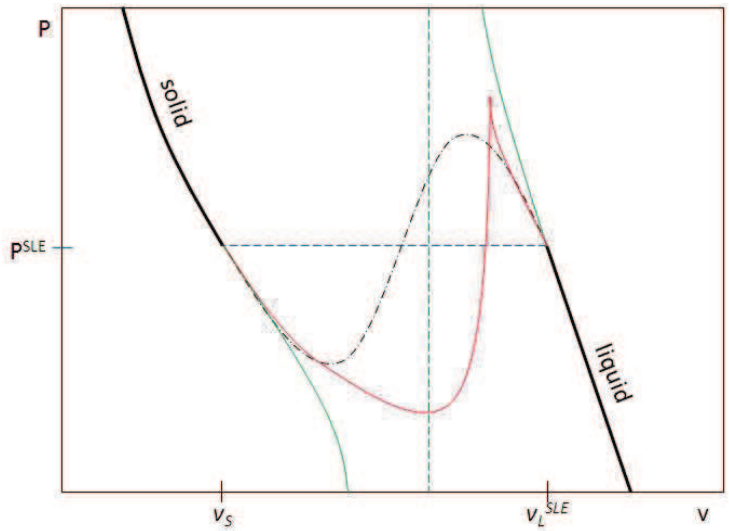

Figure 3.6: Proposed phase equilibrium behaviors for the solid-liquid transition.
— : solid and liquid branches; – – : melting pressure; – • – : solid-liquid transition by S-loop; — : discontinuity between solid branch and liquid branch; — : solid-liquid transition by cusp.

Modifying a CEoS by adding a high order term implies a second S-loop in the high density region. This S-loop allows the evaluation of the SLE by means of the *MEAR* between the equilibrium volumes, v_S and v_L^{SLE}.

In the models of Kan, [57], and Wenzel and Schmidt, [58], the presence of this second S-loop gives a solid-liquid critical point at a certain temperature and pressure conditions.

Also the *MCEoS* of Rodriguez, [59], and the *ULFEoS* of Lee et al., [70], result in a S-loop, but these models provide a first-order transition for the SLE for all temperature and pressure conditions.

Black dashed-dotted line has been used in Figure 3.6 to represent the solid-liquid S-loop.

The *QEoS* of Yokozeki introduces an asymptote in the *PV-EP*, thus the liquid and solid branches never join together, [64]. As a result, the asymptote leads to a discontinuity which avoids any solid-liquid critical point. The isothermal pressure-volume behavior of the *QEoS* in the low volume region is portrayed by green lines in Figure 3.6, with a dashed line for the asymptote.

The EoS proposed by Lee et al. in 2011, [74], is based on the concept of Insertion Probability (*IP*) with reference to the correlated cell model of Alder et al., [73]. As detailed in Appendix C, considering the probability of molecules insertion in a system in dealing with the solid-liquid equilibrium leads to introduce a cusp in the *PV-EP* (red solid line of Figure 3.6). This cusp never disappears, thus allowing the solid-liquid transition to be always first order.

3.2.4 SFE models comparison

Table 3.5 shows a comparison of the SFE models introduced in section 3.2.2.

Columns 1, 2 and 3 correspond to columns 1, 2 and 4 of Table 3.4, namely authors, reference, and category of the model according to the classification previously introduced.

The Number of Parameters (*N PAR*) implied in each model has been introduced in column 4, where distinction is made between parameters needed for applying the model to Pure Compounds (*PC*) from the additional ones required for representing phase equilibria in Mixtures (*M*). A backslash has been used when the model has not been applied for *PC* or *M*.

Column 5 indicates whenever a Regression of the Parameters (*RP*) is required for applying the model, and column 6 points out the kind of data involved in the regression, divided in *PC* or *M* experimental values. Table 3.5 does not report critical point properties of pure compounds since these quantities are used in almost all models.

Abbreviations and superscripts *S*, *L*, *V* are used for indicating experimental values referred to the solid, liquid, or vapor phase, respectively. In addition to that, *TP*, *VLE*, *SLE*, and *SVE* are used for indicating equilibrium data at the triple point, saturation, melting, and sublimation, respectively.

In column 6, backslashes refer to models not applied to the representation of phase equilibrium behaviors of *PC* or *M*, whereas 0 concerns models which do not require regressing parameters to be applied to *PC* or *M*.

Most of the literature works proposed for representing the Solid-Fluid Equilibrium (*SFE*) involves a supplementary model, typically for including the fluid state or the fluid-fluid equilibrium. This Secondary Thermodynamic Model (*STM*) is specified in the last column of Table 3.5.

Table 3.5: SFE models comparison in terms of number of parameters, data involved in the regression of the parameters, and additional fluid-state model.

Column 1	2	3	4		5	6		7
Authors	**Ref.**	**Model**	**N PAR**		**RP**	**Kind of Data**		**STM**
			PC	**M**		**PC**	**M**	
Soave	[50]	*CA*	2	1	✓	*SVE*: P,T *TP*: ΔH^{SLE}, $\Delta C_P{}^{SLE}$	*SLE*: T,x	SRK EoS
Twu et al.	[51]	*CA*	3	3	✓	*SLE*: T *TP*: ΔH^{SLE}	*SLE*: T,x	TST EoS G^E MR[1]
Rodriguez et al.	[52]	*CA*	3	3	✓	*SLE*: P,T	*SLE,VLE*: P,T,x	PR EoS
Coutinho et al.	[53],[54]	*CA*	/	>5	➍	/	0	G^E models
Kan	[57]	*MCEoS*	4	/	✓	*L*: P,V,T *SLE*: P,T	/	/
Wenzel Schmidt	[58]	*MCEoS*	5	2	✓	*S*: ρ *VLE,SLE*: P,ΔH	0	/
Rodriguez, Martinez	[59]	*MCEoS*	7	/	✓	*VLE*: P,ρ^V *TP*: P,T	/	/
Salim, Trebble	[60]	*SCEoSs*	6	3	✓	*TP*: P,ρ^S *SVE*: P,ρ^S,ρ^V,$C_P{}^S$,ΔH	*VLE*: P,T,x *SVE,SLE*: P,T	TST EoS
Heidemann Prausnitz	[61]	*MA*	3	/	➍	0	/	vdW EoS
Lang, Wenzel	[62]	*MA*	5	2	✓	*TP*: T,ΔH^{SLE},ΔV^{SLE}	*SLE*: T,x	SW EoS
Geaña, Wenzel	[63]	*MA*	5	2	✓	*TP*: P,ΔH^{SLE},ΔV^{SLE}	*SVE*: P,T,x	SW EoS
Yokozeki	[64]	*QEoS*	11	1	✓	*TP*: P,T BT^2,IT^3	*SLE,VLE*: P,T,x	/
Lee et al.	[70]	*ULFEoS*	6	/	✓	*VLE*: P,ρ^L *SVE*: P	/	/
Lee et al.	[74]	*IP*	4	/	✓	S: ρ^S *VLE*: P,ρ^L	/	/
Cochran, Chiew	[79],[80]	*TPT*	3	1	✓	*SLE*: T,ρ^S,ρ^L	*SLE*: T,x	LSHSC[4]
Tan et al.	[78]	*TPT*	6	2	✓	*VLE*: P,ρ^L *SVE,SLE*: P	*SLE,VLE*: P,T,x	PC-SAFT

N PAR = Number of Parameters; *PC* = Pure Compound; *M* = Mixture; *RP* = Regression of Parameters; *STM* = Secondary Thermodynamic Model.
CA = Classic Approach, *MCEoS* = Modified Cubic EoS, *SCEoSs* = System of Cubic EoSs, *MA* = Molecular Association, *QEoS* = Quartic Equation of State, *IP* = Insertion Probability, *TPT* = Thermodynamic Perturbation Theory.
TP = Triple Point properties; *VLE*, *SLE*, *SVE* = saturation, melting, sublimation properties.
[1] Mixing Rule
[2] Boyle Temperature
[3] Inversion Temperature of Joule-Thomson coefficient
[4] Liquid State Hard Sphere Chain model

According to Table 3.5, the model of Soave can be applied to represent pure compound phase equilibria by means of the *CA* and the SRK EoS, [50]. Only two Pure Compound (*PC*) parameters need to be regressed, while a binary interaction parameter is tuned on SLE data for extending the model to the binary mixtures presented in [50]. The maximum number of *PC* parameters corresponds to the *QEoS* proposed by Yokozeki in [64].

A variable Number of Parameters (*N PAR*) is involved in the works of Coutinho et al., seeing that it depends on the choice of the activity model. Nevertheless, the main feature of the models re-

ported in [53] and [54] is the possibility of apply the model starting from experimental values without any parameters regression procedure. Thus, in [53] and [54] emphasis is placed on the capability of representing solubility of waxes in hydrocarbon fluids with a predictive approach. Also the *MA* model of Heidemann and Prausnitz does not require fitting parameters, but it has been applied only for pure compounds.

Except for the cases in [53] and [54], by analyzing column 4 it clearly appears that the *N PAR* involved in the different SFE models for the representation of phase equilibrium behaviors in pure compounds varies more than in mixtures, where it varies from 1 to 3. It can then be stated that the main efforts concerned the representation of pure compound properties.

VLE, SLE, and SVE data (temperature, pressure, and composition) have been used for regressing the parameters required for extending the models to equilibrium calculations in mixtures. With reference to column 6 of Table 3.5, triple point properties (like equilibrium densities and latent heats) are the common thermodynamic properties involved in the regression of *PC* parameters. It follows that the literature works here discussed usually started from considering triple point properties to include the solid phase in the phase equilibrium behavior of pure compounds.

Column 7 of Table 3.5 states instead that only six SFE models do not necessitate a *STM* (Secondary Thermodynamic Model) to couple the fluid phases with the solid one, thus representing all the three main states of matter with the same functional form. Among these six models, only the *MCEoS* of Wenzel and Schmidt, [58], and the *QEoS* of Yokozeki, [64], have been extended to phase equilibria in mixtures.

As argued in the first chapter of this manuscript, the main objective of the present work is to develop a thermodynamic model able to represent phase equilibrium behavior of pure compounds and binary mixtures commonly involved in an air separation unit.

A system of 7 criteria has been considered for selecting the best suited model for this purpose among all the literature possibilities (briefly presented in section 3.2.2 and detailed in Appendix C). The Criteria (*C*) have been classified from 1 to 7 in a decreasing order of importance: Criteria 1 (*C1*) is the most important, Criteria 7 (*C7*) is the less important.

The criteria are:

- single functional form for representing solid and fluid phases (*C1*);
- description of the solid-liquid transition (*C2*);
- respect of physical constraints (*C3*);
- model already applied to mixtures (*C4*);
- possibility of representing solid-solution as well as total or partial immiscibility in the solid phase (*C5*);
- possibility of representing thermodynamic properties of the solid phase (*C6*).

The comparison of the SFE models according to these 7 criteria is reported in Table 3.6.

Check marks (✓) or crosses (❹) have been used for models fulfilling or not the above criteria, respectively.

As stated above, only 6 models propose a single functional form for representing solid and fluid phases: *C1* is respected for the *MCEoSs* of Kan, [57], Wenzel and Schmidt, [58], Rodriguez and Martinez, [59], the *QEoS* of Yokozeki, [64], the *ULFEoS* and the *IP* of Lee et al., [70] and [74].

C2 is respected for same SFE models and for all the *MA* models. In the *MCEoSs* and *ULFEoS* models the solid-liquid transition is obtained by a second S-loop; in the *QEoS* a discontinuity is introduced; in the *IP* approach of Lee et al., [74], the Maxwell's equal area rule is applied to a solid-liquid cusp; in *MA* the solid-liquid transition occurs owing to a variation of the self-association mechanism.

Three models violate some physical constraints. *C3* is not matched by the *MCEoSs* of Kan, [57], and Wenzel and Schmidt, [58], whose solid-liquid S-loop leads to a solid-liquid critical point. Conversely, the functional forms of the *MCEoSs* of Rodriguez and Martinez, [59], and the *ULFEoS* of

Lee et al., [70], have been developed in order to keep the S-loop and guarantee always a first order transition for the SLE.

Also the *QEoS* of Yokozeki in some case does not meet *C3*, as discussed by Lee et al. in [72]. In [72], authors found the functional form of the Yokozeki EoS to violate the hard-spheres behavior (the Helmholtz energy convergence condition necessary for describing the solid-liquid transition by means of the Maxwell's equal area rule), and the boundary conditions of the insertion probability when evaluated by the *QEoS*. Details of these limits have been illustrated in Appendix C.

Table 3.6: SFE models comparison in terms of proposed criteria.
Check marks are used for satisfied criteria.

Authors	Ref.	Model	C1	C2	C3	C4	C5	C6
Soave	[50]	*CA*	✗	✗	✓	✓	✗	✗
Twu et al.	[51]	*CA*	✗	✗	✓	✓	✗	✗
Rodriguez-Reartes et al.	[52]	*CA*	✗	✗	✓	✓	✗	✗
Coutinho et al.	[53],[54]	*CA*	✗	✗	✓	✓	✓	✗
Kan	[57]	*MCEoS*	✓	✓	✗	✗		✓
Wenzel, Schmidt	[58]	*MCEoS*	✓	✓	✗	✓	✓	✓
Rodriguez, Martinez	[59]	*MCEoS*	✓	✓	✓	✗		✓
Salim, Trebble	[60]	*SCEoSs*	✗	✗	✓	✓	✓	✓
Heidemann, Prausnitz	[61]	*MA*	✗	✓	✓	✗		✓
Lang, Wenzel	[62]	*MA*	✗	✓	✓	✓	✗	✓
Geaña, Wenzel	[63]	*MA*	✗	✓	✓	✓	✓	✓
Yokozeki	[64],[65]	*QEoS*	✓	✓	✗	✓	✓	✓
Lee et al.	[70]	*ULFEoS*	✓	✓	✓	✗		✓
Lee et al.	[74]	*IP*	✓	✓	✓	✗		✓
Cochran, Chiew	[79],[80]	*TPT*	✗	✗	✓	✓	✓	✓
Tan et al.	[78]	*TPT*	✗	✗	✓	✓	✓	✓

CA = Classic Approach, *MCEoS* = Modified Cubic EoS, *SCEoSs* = System of Cubic EoSs, *MA* = Molecular Association, *QEoS* = Quartic Equation of State, *IP* = Insertion Probability, *TPT* = Thermodynamic Perturbation Theory.
C1 = single functional form for representing solid and fluid phases; C2 = description of the solid-liquid transition; C3 = respect of physical constraints; C4 = model already applied to mixtures; C5 = possibility of representing solid-solution as well as total or partial immiscibility in the solid phase; C6 = possibility of representing thermodynamic properties of the solid phase;

The SFE models in [57], [59], [61], [70], and [74] only pertain the representation of phase equilibria of pure compound, without extensions to mixtures. Consequently, the models of Kan, Rodriguez and Martinez, Heidemann and Prausnitz, and Lee et al. do not satisfy *C4*.

Criteria *C5* has been evaluated only for models applied also to mixtures.

The models of Coutinho et al. provide expressions for the activity coefficients in both the liquid and solid phases, allowing the representation of solid solutions. These expressions are valid for long-chain n-alkanes, namely compounds very different from the simple fluids involved in the present work. The other literature models based on the *CA* have been applied in cases of total immiscibility in the solid phase. Total immiscibility has been considered also in the *MA* of Lang, Wenzel, whereas *C5* is matched by all the remaining *SFE* models dealing with the representation of phase equilibria in mixtures.

The main strength of the *CA* is to require few experimental properties for being applied to solid-solid immiscibility. Nevertheless, the drawbacks are limited capability in describing the complete phase behavior, the need of a solid-state activity model for solid solutions, and inability to predict thermodynamic properties of the solid phase such as density or heat capacity. Therefore, *C6* is not satisfied by the *CA* based models in Table 3.6, while all the other SFE models allow the evaluation of solid state thermodynamic properties.

MCEoSs have the advantage of involving a single functional form, seeing that these EoSs have been obtained adding a high-order term in a *CEoS*. Unfortunately, this high-order term entails a complicated resolution of the *MCEoS* and, in some cases, leads to a solid-liquid critical point.

In the model of Salim and Trebble the problem of solving the functional form is avoided by considering two *CEoSs* in the form of the TST EoS, thus the following inconvenient is to apply twice a *CEoS* instead of having a single EoS.

The fugacity coefficient of a simple *CEoS* is coupled with the chemical equilibrium constants of associating fluids in the *MA* models. In this case, the major drawback is again the need of separately applying the Eos with different degree of associations for representing the three phases of matter.

Same problem arises while applying the *TPT* models of Tan et al., [78], and Cochran and Chew, [79], which additionally do not provide a description of the solid-liquid transition in the isothermal pressure-volume phase diagram.

The main inconvenient of the *IP* model is the presence of a logarithmic term in the functional form of the correspondent EoS, whereas the strength is to respect boundary condition for the insertion probability. Nevertheless, it has been proposed solely for the representation of pure compound equilibria as the *ULFEoS*.

Among all the SFE models discussed in this chapter, the *QEoS* of Yokozeki and the *MCEoS* of Wenzel and Schmidt meet 5 of the 6 criteria proposed. Both models do not respect a physical behavior: positive pressure for a hard spheres system in all the density range and maximum value of the insertion probability equal to 1 for the *QEoS*; absence of the solid-liquid critical point for the *MCEoS* in [58].

Despite the cited problems, the *QEoS* with appropriate values of the parameters presents the simplest functional form among all the SFE models, which make it useful for engineering purposes. In addition to that, under certain conditions the Maxwell's equal area rule can be applied to the *QEoS* for calculating the solid-fluid equilibrium throughout the discontinuity. These features are presented in the next chapter.

The *QEoS* of Yokozeki has been then chosen for being applied to the representation of phase equilibria in the systems of simple molecules usually involved in the cryogenic distillation of air.

4 Representation of phase equilibria. I. Pure compounds

This chapter is organized as follows:

- the functional form of the EoS proposed in 2003 by Yokozeki and the correspondent expressions of fugacity, compressibility factor and residual Helmholtz, Gibbs energy, internal energy, enthalpy, and entropy are introduced in the first part;
- the solution of the 4th order polynomial in terms of volume is illustrated in the second section;
- the third part resumes the regression procedure proposed by Yokozeki and the one proposed in this work for improving the representation of the pressure-temperature equilibrium behavior;
- in part 4, four attractive terms have been considered in the functional form of the EoS while challenging the equation in the representation of equilibrium temperatures, pressures, densities and latent heats of transition;
- results (obtained by applying the final version of the EoS) are shown for methane and carbon dioxide in part 5.

Appendix D contains results for the all the pure compounds of interest and gives a detailed description of mathematical steps involved in parts 1, 2. The EoS parameters for the pure compounds are not introduced in this chapter owing to the confidentiality covering this work. The EoS parameters are property of the Air Liquide Group.

4.1 Yokozeki EoS

The generic functional form of the Yokozeki EoS, here renamed Solid-Liquid-Vapor EoS (SLV EoS), has been questioned by Lee et al., [72], as anticipated in the previous chapter. In order to overcome one of these problems, the form considered in this work is eq. (4.1).

$$P(T,v) = \frac{RT}{v-b}\frac{v-d}{v-c} - \frac{a}{v^2+qbv+rb^2} \tag{4.1}$$

In eq. (4.1), q and r are parameters, R is the gas constant, T the temperature, P the pressure, d the volume where repulsive term becomes 0, c is the liquid covolume, and v is the volume. $a(T)$ and $b(T)$ are T-dependent functions and represent the attractive forces among the molecules and the covolume of the solid phase, respectively.

At each temperature, the solid covolume $b(T)$ must be lower than the liquid covolume, and the relation $b(T) < d < c$ holds.

The pressure-volume behavior of eq. (4.1) at the triple point temperature is portrayed in Figure 4.1. Solid and liquid covolumes entail two asymptotes, which limit the solid and the liquid branch, respectively. The liquid covolume introduces a discontinuity in the dense region, and the Maxwell's equal area rule can be applied for evaluating the solid-liquid transition, which never yields a solid-liquid critical point. In addition to that, the Maxwell's equal area is applied for the S-loop related to the vapor-liquid transition.

The first drawbacks argued by Lee et al. concerns the negative pressures between the asymptotes obtained in the P-v diagram when applying eq. (4.1) for representing hard spheres behavior, namely $a = 0$ in the EoS.

To a fair approximation, the qualitative behavior of eq. (4.1) in the dense region does not change with $a = 0$, so Figure 4.1 can be considered also for the hard-spheres model. The solid branch involves really negative pressures.

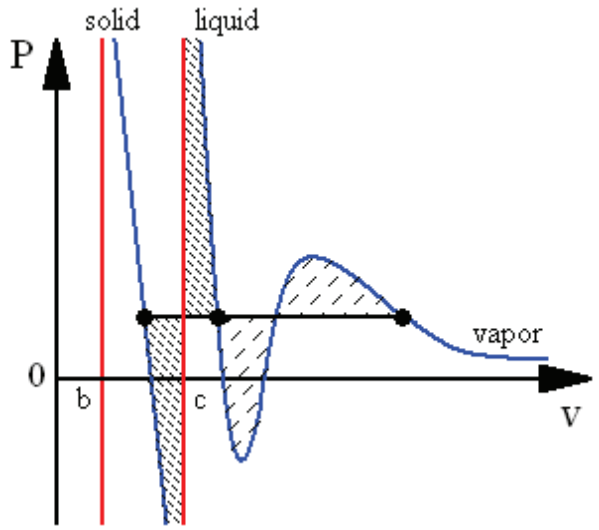

Figure 4.1: Schematic *P-v* diagram of the Yokozeki EoS at the triple point temperature and $v>b$.
— : asymptotes referred to solid and liquid covolumes;
— : isothermal *P-v* diagram of the Yokozeki EoS;
● : solid, liquid and vapor equilibrium phases;
— : triple point pressure;
Hatched areas are the Maxwell's equal area construction.

Always in the framework of the hard spheres models, the second inconvenient of eq. (4.1) is related to the liquid asymptote, which makes the insertion probability exceed 1. For details of the drawbacks refer to Appendix C, section 2.5.1.

Despite these problems, the SLV-EoS of Yokozeki has been chosen principally for its simple functional form. Moreover, it has been considered that negative pressures are encountered also in the liquid-vapor S-loop, which does not represent the real equilibrium behavior, but only a device for solve it.

The Pressure-Gibbs energy diagram (*PG*) related to eq. (4.1) is shown in Figure 4.2 for five temperatures.

If Tt and Tc are triple point and critical point temperature, respectively, the *PG* diagram in Figure 4.2 shows the qualitative trends of the Gibbs energy of a pure compound for a temperature T as follows: T < Tt, T = Tt, Tt < T < Tc, T = Tc, and T > Tc.

Black lines in Figure 4.2 are the Gibbs energy of the solid phase (G^S), while the blue ones are the Gibbs energy of the fluid phases. The energy of the liquid phase (G^L) is the blue line starting at negative pressure, which rapidly extends in the high pressure region cutting somewhere G^S. The energy of the vapor (G^V) is always at positive pressure, and it is represented by the quasi-horizontal lines in Figure 4.2.

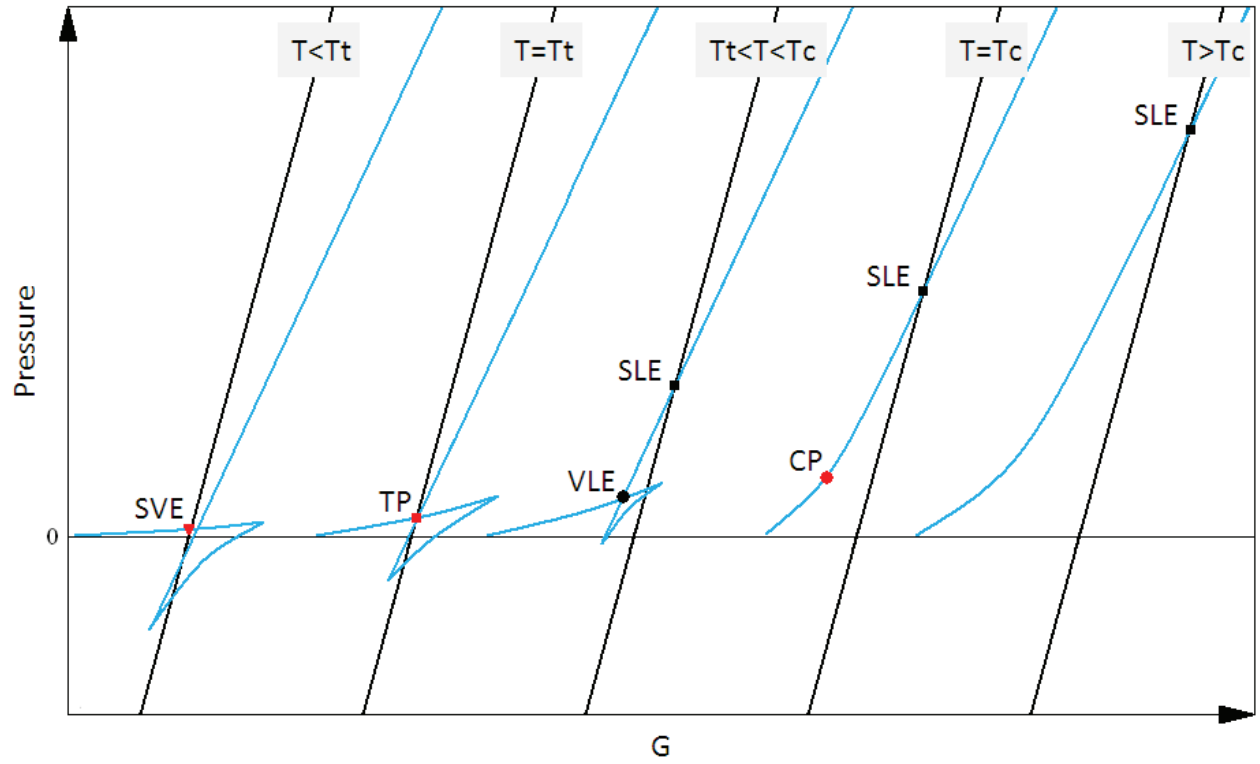

Figure 4.2: Qualitative Pressure-Gibbs free energy diagram related to the Yokozeki EoS.
— : solid phase; — : fluid phases; ▼ : SVE; ■ : SLE; ● : VLE; ■ : Triple Point TP; ● : Critical Point CP; Tt : triple point temperature; Tc : critical point temperature.

For a temperature lower than the triple point temperature, eq. (4.1) gives a liquid-vapor S-loop which does not yield a VLE because G^L is higher than G^S in the positive pressure region. The minimization of the Gibbs energy leads to the SVE, while the fugacity of the liquid phase never meets the solid or the vapor fugacities.

At the triple point temperature, there is a region of positive pressure where G^L shifts on the left of G^S and a solid-liquid-vapor equilibrium occurs. The fugacities of the three phases meet at the triple point pressure.

When Tt < T < Tc, two equilibria occur. A VLE, which pressure is higher than the triple point pressure, and a SLE. Two isofugacity conditions are then applied for evaluating the equilibrium pressures.

The extent of the liquid vapor S-loop decreases to vanish at the critical point temperature. Starting from this temperature, the sole possible first-order transition is the solid-liquid one. The SLE pressure increases towards the supercritical temperature, where the equilibrium involves a solid and a supercritical phase.

Figure 4.2 qualitatively represents the effect of the functional form in eq. (4.1) on the Gibbs free energy of a pure compound. A continuous blue line is used for the Gibbs free energy of the fluid phases, seeing that the S-loop in Figure 4.1 joins together the liquid and vapor phases. It is worth remembering that the segments of the blue lines in Figure 4.2 on the right of G^L and in the negative pressure region are a merely consequence of the S-loop, and do not have any thermodynamic consistency. Since the P-v diagram in Figure 4.1 shows a discontinuity passing from the liquid to the solid phase, G^L and G^S lines are not connected, they only meet at a certain pressure establishing the SLE.

Eq. (4.3) is eq. (4.1) in terms of dimensionless parameters, defined in eq. (4.2). In eqs. (4.2)-(4.3), the subscript *r* refers to the reduced parameters, while *c* refers to the critical point properties.

$$b_r = \frac{b}{v_c} \; ; \; c_r = \frac{c}{v_c} \; ; \; d_r = \frac{d}{v_c} \; ; \; a_r = \frac{aP_c}{R^2T_c^2} \; ; \; P_r = \frac{P}{P_c} \; ; \; T_r = \frac{T}{T_c} \; ; \; Z_c = \frac{P_c v_c}{RT_c} \; ; \; v_r = \frac{v}{v_c} \tag{4.2}$$

$$P_r(T_r, v_r) = \frac{T_r}{Z_c(v_r - b_r)} \frac{v_r - d_r}{v_r - c_r} - \frac{a_r}{Z_c^2(v_r^2 + q v_r b_r + r b_r^2)} \tag{4.3}$$

Eqs. (4.4)-(4.5) are the expressions for the *T*-dependent functions a_r and b_r proposed in [64].

$$a_r(T_r) = [a_0 + a_1 T_r exp(-a_2 T_r^n)] \tag{4.4}$$

$$b_r(T_r) = [b_0 + b_1 exp(-b_2 T_r^m)] \tag{4.5}$$

In eqs. (4.4)-(4.5), T_r is the reduced temperature obtained dividing a general temperature for the critical temperature

Eq. (4.6) is eq. (4.1) in terms of the variables temperature *T* and density ρ. The attractive term in eq. (4.6) has been developed starting from the one in eq. (4.1) considering the relations $q = \varepsilon_1\varepsilon_2$ and $r = \varepsilon_1+\varepsilon_2$. Moreover, a generic covolume *x* has been considered in the attractive term of eq. (4.6), allowing the application of eqs. (4.6)-(4.9) considering either the solid or the liquid covolume. Since only the solid covolume *b* is temperature dependent, *x'* in eq. (4.9) is zero when the liquid covolume is used in the attractive term, while an expression for *b'* must be obtained from eq. (4.5).

Knowing the expressions for the residual Helmholtz free energy a^R and its derivatives with respect to density and temperature, eqs. (4.11)-(4.16) can be used for evaluating the compressibility factor *Z*, the fugacity coefficient φ, the residual Gibbs free energy g^R, the residual internal energy u^R, the residual enthalpy h^R, and the residual entropy s^R.

The derivations of eqs. (4.6)-(4.10) have been detailed in Appendix D.

$$P(T,\rho) = \frac{RT\rho}{1-b\rho}\frac{1-d\rho}{1-c\rho} - \frac{a\rho^2}{(1+\varepsilon_1 x\rho)(1+\varepsilon_2 x\rho)} \tag{4.6}$$

$$a^R(T,\rho) = \frac{1}{b-c}\left[dln\left|\frac{1-b\rho}{1-c\rho}\right| + cln|1-c\rho| - bln|1-b\rho|\right] + \begin{cases} \frac{a}{RTx(\varepsilon_2-\varepsilon_1)} ln\left|\frac{1+\varepsilon_1 x\rho}{1+\varepsilon_2 x\rho}\right| \\ -\frac{a\rho}{RT} \end{cases} \tag{4.7}$$

$$a_\rho^R(T,\rho) = \frac{\partial a^R(T,\rho)}{\partial\rho} = \frac{(b+c-d-\rho bc)}{(1-\rho b)(1-\rho c)} - \begin{cases} \frac{a}{RT(1+qx\rho+rx^2\rho^2)} \\ \frac{a}{RT} \end{cases} \tag{4.8}$$

$$\begin{aligned} a_T^R(T,\rho) = \frac{\partial a^R(T,\rho)}{\partial T} \\ = \frac{b'(c-d)}{(b-c)^2} ln\left|\frac{1-b\rho}{1-c\rho}\right| + \frac{b'\rho(d-b)}{(c-b)(1-b\rho)} \\ + \begin{cases} \frac{a'xT - ax'T - ax}{RT^2x^2(\varepsilon_2-\varepsilon_1)} ln\left(\frac{1+\varepsilon_1 x\rho}{1+\varepsilon_2 x\rho}\right) - \frac{ax'\rho}{RTx(1+qx\rho+rx^2\rho^2)} \\ \frac{\rho(a-a'T)}{RT^2} \end{cases} \end{aligned} \tag{4.9}$$

$$a' = \frac{R^2T_c}{P_c} a_1(1-na_2T_r^n)exp(-a_2T_r^n) \qquad b' = -\frac{v_c}{T_c} b_1b_2mT_r^{m-1}exp(-b_2T_r^m) \tag{4.10}$$

$$Z(T,\rho) = 1 + \rho a_\rho^R(T,\rho) \tag{4.11}$$

$$\ln\varphi\,(T,\rho) = Z(T,\rho) - 1 - \ln Z(T,\rho) + a^R(T,\rho) \tag{4.12}$$

$$\frac{G^R(T,\rho)}{RT} = g^R(T,\rho) = \ln\varphi\,(T,\rho) \tag{4.13}$$

$$\frac{U^R(T,\rho)}{RT} = u^R(T,\rho) = -Ta_T^R(T,\rho) \tag{4.14}$$

$$\frac{H^R(T,\rho)}{RT} = h^R(T,\rho) = Z(T,\rho) - 1 - Ta_T^R(T,\rho) \tag{4.15}$$

$$\frac{S^R(T,\rho)}{RT} = s^R(T,\rho) = -Ta_T^R(T,\rho) - a^R(T,\rho)R^2T^2 \tag{4.16}$$

The residual Helmholtz free energy involves the integral of the pressure-explicit form in eq. (4.6). The integral concerning the attractive term yields two different solutions for $q,r \neq 0$ and $q,r = 0$.

As a consequence, also the derivatives of a^R present different expressions for the attractive term. Each parenthesis in eqs. (4.7)-(4.9) has the term correspondent to $q,r \neq 0$ in the first row, while the second one refers to the attractive term of the vdW EoS, $q,r = 0$.

4.2 Analytical solution of the SLV EoS

Expressions (4.6)-(4.16) require values for the density, thus eq. (4.1) needs to be solved for evaluating the volumes of the phases.

According to Figure 4.1, the subcritical isotherm crosses four times the equilibrium pressure, in that case the triple point pressure. Starting from the solid asymptote, the volumes correspond to the solid phase, the liquid phase, the unphysical volume under the S-loop, and the vapor phase.

When temperature and pressure are fixed, eq. (4.1) can be rearranged for obtaining a 4th order polynomial in terms of volume, eq. (4.17). In eq. (4.17), x is always referred to either the solid or the liquid covolume ($x = b$ or c).

$$v^4 + v^3\alpha + v^2\beta + v\gamma + \delta = 0 \tag{4.17}$$

$$\alpha = qx - c - b - RT/P \tag{4.18}$$

$$\beta = rx^2 - qx(c+b) + cb + (d - qx)\,RT/P + a/P \tag{4.19}$$

$$\gamma = -rx^2(c+b) + qxcb + (qd - rx)\,xRT/P - (c+b)\,a/P \tag{4.20}$$

$$\delta = rx^2cb + rx^2d\,RT/P + acb/P \tag{4.21}$$

Solving eq. (4.1) involves 4 roots from eq. (4.17) for each subcritical temperature. When the liquid and vapor phase merge to give a supercritical phase, the S-loop disappears in the P-v diagram of Figure 4.1, so eq. (4.17) has only two roots. According to what discussed in the previous section, a volume for the liquid phase can always be found even under the triple point, but there this phase is not stable as its Gibbs free energy is greater than the energy of the solid phase.

The solution of eq. (4.17) can be computed converting the quartic polynomial in a correspondent cubic equation, eq. (4.23), by means of the identities in eq. (4.22).

$$\zeta = -\beta \quad , \quad \eta = \alpha\gamma - 4\delta \quad , \quad \vartheta = \delta(4\beta - \alpha^2) - \gamma^2 \tag{4.22}$$

$$v^3 + v^2\zeta + v\eta + \vartheta = 0 \tag{4.23}$$

The roots of the polynomial of order 3 in eq. (4.23) can be calculated using the method of Cardano, [81], and converted in the roots of the 4th order polynomial in eq. (4.17). Details are provided in Appendix D.

4.3 Setting EoS parameters of the SLV EoS

The total number of EoS parameters within the SLV EoS that need to be fixed for representing phase equilibrium behaviors of pure compound is equal to 11: the compressibility factor at the critical point Z_c, the parameters of the T-dependent functions (a_0, a_1, a_2, n, b_0, b_1, b_2, m), the liquid covolume c_r, and d_r.

The procedure proposed by Yokozeki for the regression of these parameters involves three common conditions at the critical point, the vapor-liquid and one solid-fluid isofugacity conditions at the triple point, the Boyle temperature, and the maximum inversion temperature of Joule-Thompson's coefficient [64]. The critical point conditions are resumed in eq. (4.24).

$$P(T_c, v_c) = P_c \quad , \quad \left.\frac{\partial P}{\partial v}\right|_{T_c,v_c} = 0 \quad , \quad \left.\frac{\partial^2 P}{\partial v^2}\right|_{T_c,v_c} = 0 \tag{4.24}$$

By applying the functional form of the reduced pressure in eq. (4.3), constraints in eq. (4.24) turn in eqs. (4.25)-(4.27), where x_r is the reduced solid or liquid covolume, and a_{rc} and b_{rc} are reduced values of a and b at the critical temperature.

Since the following equations are written in terms of reduced quantities, temperature and volume do not appear seeing that at the critical point T_{rc} and v_{rc} are equal to 1. For the mathematical steps for the first and second derivatives with respect to the reduced volume see Appendix D.

$$P_r(T_{rc}, v_{rc}) = \frac{1 - d_r}{Z_c(1 - b_{rc})(1 - c_r)} - \frac{a_{rc}}{Z_c^2(1 + qx_r + rx_r^2)} \tag{4.25}$$

$$\left.\frac{\partial P_r}{\partial v_r}\right|_{T_{rc},v_{rc}} = -\frac{1 - d_r}{Z_c(1 - b_{rc})^2(1 - c_r)} + \frac{d_r - c_r}{Z_c(1 - b_{rc})(1 - c_r)^2} + \frac{a_{rc}(2 + qx_r)}{Z_c^2(1 + qx_r + rx_r^2)^2} \tag{4.26}$$

$$\left.\frac{\partial^2 P_r}{\partial v_r^2}\right|_{T_{rc},v_{rc}} = \frac{2(1 - d_r)}{Z_c(1 - b_{rc})^3(1 - c_r)} - \frac{2(d_r - c_r)}{Z_c(1 - b_{rc})^2(1 - c_r)^2} - \frac{2(d_r - c_r)}{Z_c(1 - b_{rc})(1 - c_r)^3} + \frac{2a_{rc}[(1 + qx_r + rx_r^2) - (2 + qx_r)^2]}{Z_c^2(v_r^2 + qx_r v_r + rx_r^2)^3} \tag{4.27}$$

The system of eqs. (4.25)-(4.27) has five variables: Z_c, a_{rc}, b_{rc}, c_r, and d_r.

An analytic solution of the system can be obtained whenever any two among the five variables are fixed. In such a case the system involves three equations in three variables, which can be uniquely determined. For instance, it is possible to analytically determine the parameters c_r, d_r and a_{rc} starting from values of Z_c and b_{rc}.

Furthermore, eqs. (4.25)-(4.27) can be rearranged to obtain explicit expressions of the parameters c_r (or b_{rc}), d_r and a_{rc}. Details of the mathematical steps are provided in Appendix D.

In the framework of this thesis, it has been considered that solving a system of N equations containing N unknowns leads to an analytical solution of the system, in both cases of having explicit and implicit expressions for the unknowns.

Among all the possible couples of positive real values Z_c and b_{rc} (or Z_c and c_r), only the values allowing $b_{rc} < d_r < c_r < 1$ must be considered in order to respect the constraints required for the applicability of the SLV EoS, as discussed by Yokozeki in [64].

For imposed values of q and r in the attractive term, it is possible to analytically solve the critical point conditions imposing Z_c and b_{rc} (or Z_c and c_r), and checking if the parameters obtained meet the above conditions. The couples Z_c and b_{rc} (or Z_c and c_r) satisfying the conditions can be successively grouped, giving the proper regions for setting the EoS parameters at the critical point.

The proper regions are illustrated in Figure 4.3. Black, red, and blue have been used for the limits of the proper area related to eq. (4.1) with the van der Waals, the Redlich-Kwong, [82], and the Peng-Robinson attractive term, [83], respectively. Dashed and continuous lines are referred to attractive terms involving the liquid covolume and the solid covolume, respectively. The continuous line limits the Z_c-b_{rc} proper area, the dashed one the Z_c-c_r proper area.

By considering for instance the vdW values of q and r, the proper area works as follows. Any couple Z_c-b_{rc} (Z_c-c_r) within the proper region limited by black continuous (dashed) lines allows solving a system of three critical point conditions and as many unknowns, respecting the relations between the parameters ($b_{rc} < d_r < c_r < 1$).

Dashed and continuous lines related to same value of q and r in attractive term join together the couple critical compressibility factor-reduced liquid covolume of the corresponding cubic EoS. For instance, black lines join together $Z_c = 0.375$ and $b_{rc} = 1/3$, which are the parameters of van der Waals cubic EoS.

It is interesting to note that the proper areas shift to the left by modifying the value of q and r, so that the areas approach the experimental values of the critical compressibility factor of the pure fluids of interest.

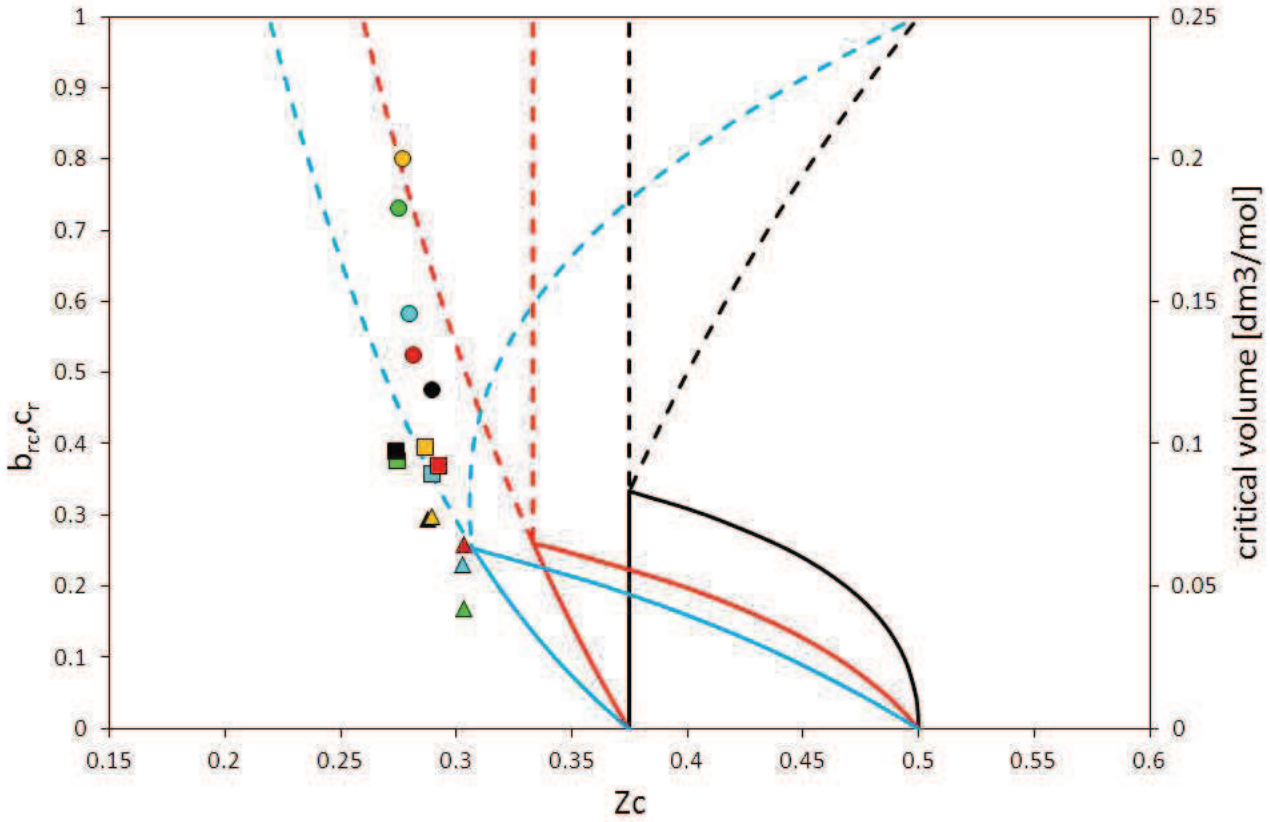

Figure 4.3: Proper EoS parameter regions for solving the critical point condition with different attractive terms.
— : van der Waals (q = 0, r = 0); — : Redlich-Kwong (q = 1, r = 0); — : Peng-Robinson (q = 2, r = -1). Each point represents the couple experimental critical volume-compressibility factor: ■ : N_2; ▲ : O_2; ▲ : Ar; ■ : Kr; ● : Xe; ▲ : Ne; ▲ : He; ■ : CO_2; ▲ : H_2; ■ : N_2O; ■ : CH_4; ● : C_2H_6; ● : C_2H_4; ● : C_3H_8; ● : C_3H_6. Experimental compressibility factor are related to the right y-axis.

These values are illustrated in Figure 4.3 by filled circles, squares and triangles. The correspondent y-axis is the right axis of the Figure 4.3, being the left one related to the proper areas.

The PR values for q and r allows the proper areas to approach the experimental Z_c more than the values of the SRK and vdW *CEoSs*. This fact seems to suggest using the PR values in eq. (4.1) and that a regression could be carried out to fix the parameters q and r in order to match the experimental values of Z_c.

Up to now, three parameters can be analytically calculated starting for instance from values of Z_c and b_{rc} lying in the proper areas of Figure 4.3.

Yokozeki suggested exploiting the information at the solid-liquid-vapor triple point to further setting of the parameters. Three phases coexist at equilibrium at the triple point, thus the existence of this three-phase equilibrium requires solving twice the Maxwell's equal area rule, which corresponds to solve two isofugacity conditions. With reference to the SLE and VLE, the system of triple point conditions involves the solid-liquid and liquid-vapor isofugacity conditions, eqs. (4.28)-(4.29).

$$\varphi^S(P_t, T_t, \rho^S) = \varphi^L(P_t, T_t, \rho^L) \tag{4.28}$$

$$\varphi^V(P_t, T_t, \rho^V) = \varphi^L(P_t, T_t, \rho^L) \tag{4.29}$$

By keeping constant Z_c, c_r and d_r, the system eqs. (4.29)-(4.30) contains only two unknowns, namely the values of a_r and b_r at the triple point, a_{rt} and b_{rt}.

Unlike the critical point conditions, explicit expressions for a_{rt} and b_{rt} cannot be obtained owing to the fact that at fixed temperature and pressure the evaluation of the fugacity coefficient, eq. (4.12), requires the previous solution of the 4th order polynomial in terms of volume, eq. (4.17).

Nevertheless, the system of triple point conditions contains 2 equations in 2 unknowns (a_{rt} and b_{rt}), and this entails an analytical solution of the isofugacity conditions at the triple point.

Regarding the temperature-dependence of the functions $a(T)$ and $b(T)$, Yokozeki assumed finite values for all the temperatures (including T = 0,∞ K), and a maximum for $a(T)$ at a certain temperature, T^*. The $a(T)$ and $b(T)$ proposed in [64] for argon are presented in Figure 4.4 and Figure 4.5, respectively.

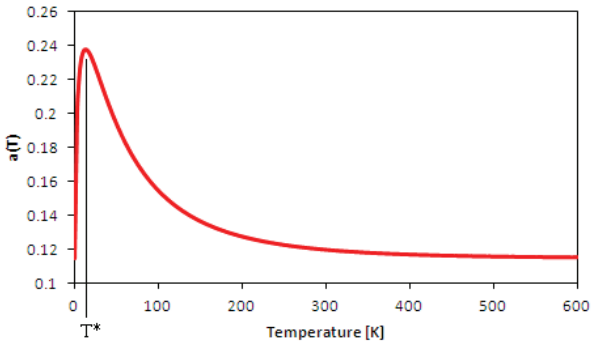

Figure 4.4: Function $a(T)$ for argon, [64].

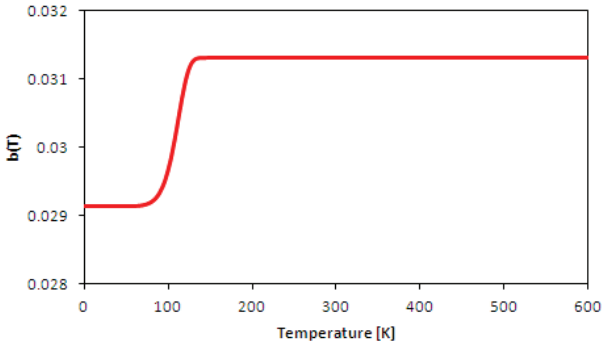

Figure 4.5: Function $b(T)$ for argon, [64].

As $a(T)$ and $b(T)$, or equivalently $a_r(T_r)$ and $b_r(T_r)$, are decreasing and increasing function of temperature, respectively, the analytical solution of the system of eqs. (4.28)-(4.29) needs to meet the isofugacity conditions and the proper order $b_{rt} < b_{rc}$ and $a_{rt} > a_{rc}$. It should be noted that a is a decreasing function of temperature for $T > T^*$.

The analytical solution of the critical and triple point conditions represents the core of the procedure for setting of the EoS parameters proposed by Yokozeki, [64]. Using a minimum amount of information, Yokozeki set up the EoS parameters Z_c, c_r, d_r, the values of a_r and b_r at the critical (a_{rc} - b_{rc}) and triple point (a_{rt} - b_{rt}). Then, two sets of a_r and b_r are available.

The T-dependent functions $a_r(T_r)$ and $b_r(T_r)$, eqs. (4.4)-(4.5), involve eight parameters (a_0, a_1, a_2, n, b_0, b_1, b_2, m). The expressions of a_{rt} and a_{rc} equivalent to eq. (4.4) are:

$$a_r(T_{rt}) = a_{rt} = a_{rc}[a_0 + a_1 T_{rt} exp(-a_2 T_{rt}^n)] \tag{4.30}$$

$$a_r(T_{rc}) = a_{rc} = a_{rc}[a_0 + a_1 exp(-a_2)] \tag{4.31}$$

a_1 and a_0 can be calculated from eqs. (4.30)-(4.31) as functions of a_{rt}, a_{rc}, for imposed values of a_2 and n:

$$a_0 = 1 - a_1 exp(-a_2) \tag{4.32}$$

$$a_1 = \frac{(a_{rt}/a_{rc}) - 1}{T_{rt} exp(-a_2 T_{rt}^n) - exp(-a_2)} \tag{4.33}$$

In the same way the values of b_1 and b_0 can be expressed as functions of b_{rt}, b_{rc}, and calculated for imposed values of b_2, and m:

$$b_0 = 1 - b_1 exp(-b_2) \tag{4.34}$$

$$b_1 = \frac{(b_{rt}/b_{rc}) - 1}{exp(-b_2 T_{rt}^m) - exp(-b_2)} \tag{4.35}$$

By evaluating four parameters of the T-dependent functions (a_0, a_1, b_0, b_1) for fixed values of a_2, n, b_2, and m as in eqs. (4.32)-(4.35), the SLV EoS is forced to meet the values of a_{rc}, a_{rt}, b_{rc}, and b_{rt}, then the critical and triple point conditions. Yokozeki considered the Boyle temperature and the maximum inversion temperature of Joule-Thompson's coefficient for evaluating a_2, n, b_2 and m. The following conditions must be matched: positive values for a_0, a_1, n, b_0, b_2, and m, boundary conditions a_r (T_r = 0,:) = a_0, and b$_r$ (T_r = 0) = $b_0 + b_1 > 0$, [64].

Figure 4.6 shows the representation of the PT-EP of argon and carbon dioxide that Yokozeki obtained using the procedure above and the SLV EoS with vdW attractive term, as published in [64].

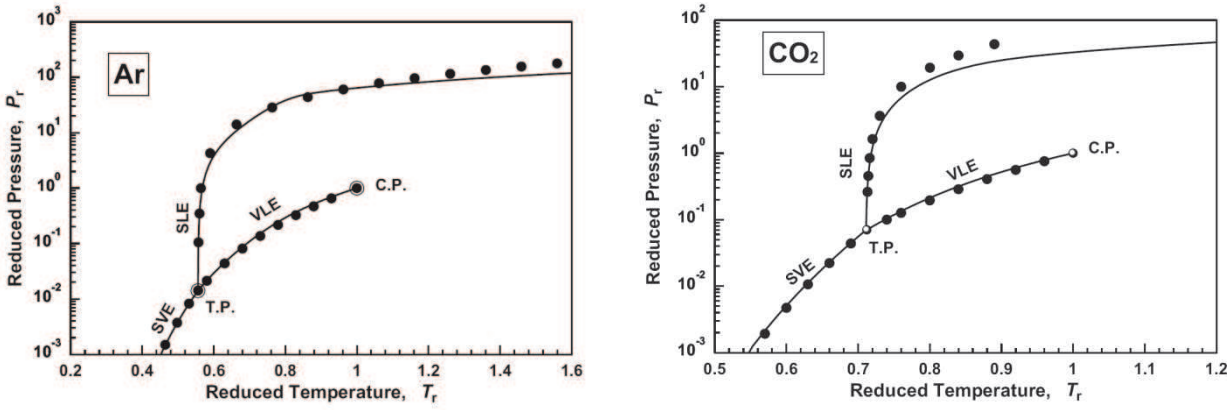

Figure 4.6: Phase diagram of argon and carbon dioxide in the pressure-temperature equilibrium projection obtained by the Yokozeki EoS with vdW attractive term.
Lines: Yokozeki EoS. Symbols: experimental data. Figures have been copied from [64].

The thermodynamic model proposed by Yokozeki represents all the equilibrium branches with the same EoS and it is capable of representing the phase behavior of pure substances in a qualitative correct way, as shown in Figure 4.6. Regarding the solid-liquid equilibria, this model presents some limits and the possibility to improve the representation of the melting line has been verified and discussed in the next section.

4.3.1 New procedure for setting EoS parameters

A new procedure for setting the EoS parameters has been proposed in order to ascertain if the limit of the Yokozeki EoS in representing simultaneously the melting and the vapor pressure curves from the triple point up to the critical point stems from the parameters used in [64] or from the functional form of the EoS. The developed procedure, presented in [84], allows finding, at each temperature from the triple point up to the critical point, the unique solution for both parameters a and b for a suitable value of the compressibility factor Z_c.

This procedure requires the availability of saturation pressure and melting pressure data for the same temperature, which have been obtained from "auxiliary" equations of these properties for the fluids of interest, [3]. These equations are very precise correlations of the available data, hence they can be used for generating equilibrium values, hereafter called "auxiliary" values. Auxiliary equations are resumed in Appendix A, and auxiliary values have been considered as true values of phase equilibria.

This procedure attempts to force the Yokozeki EoS to represent SLE, SVE, and VLE auxiliary values. According to the flow chart in Figure 4.7, this procedure consists of three steps:

1. a value of Z_c within the proper area of Figure 4.3 is chosen as input of a system of four conditions that the SLV EoS is imposed to meet at the critical temperature. Three are the common critical point conditions, eqs. (4.25)-(4.27), the fourth is the solid-liquid isofu-

gacity condition at the melting pressure. Analytical values for the 4 unknowns (a_c, b_c, d, and c) can be obtained from the system of 4 equations:

$$P(T_c, v_c) = P_c \quad , \quad \left.\frac{\partial P}{\partial v}\right|_{T_c,v_c} = 0 \quad , \quad \left.\frac{\partial^2 P}{\partial v^2}\right|_{T_c,v_c} = 0 \quad , \quad \varphi^S(P_{aux}^{SLE}, T_c, \rho^S) = \varphi^L(P_{aux}^{SLE}, T_c, \rho^L) \tag{4.36}$$

In eq. (4.36), $P_{aux}{}^{SLE}$ is the auxiliary pressure of melting. If the condition $b_c < d < c$ is not respected, select another value of the critical compressibility factor[1]. Conversely,

2. a system of two equations is analytically solved (keeping constant Z_c, d and c) in order to find the unique solution for a_i and b_i at each temperature T_i in the domain $T_t \leq T_i < T_c$. The two equations are the solid-liquid and vapor-liquid isofugacity conditions:

$$\varphi^S\left(P_{i,aux}^{SLE}, T_i, \rho^S\right) = \varphi^L\left(P_{i,aux}^{SLE}, T_i, \rho^L\right) \quad , \quad \varphi^V\left(P_{i,aux}^{VLE}, T_i, \rho^V\right) = \varphi^L\left(P_{i,aux}^{VLE}, T_i, \rho^L\right) \tag{4.37}$$

$P_{aux}{}^{SLE}$ and $P_{aux}{}^{VLE}$ are auxiliary melting and saturation pressures. Solving these two equations, continuous functions $a(T)$ and $b(T)$ can be obtained in the domain $T_t \leq T_i < T_c$. If the values of the functions $a(T)$ and $b(T)$ extrapolated to the critical temperature are not equal to the values obtained in step 1, and/or the conditions $b_t < b_c$ and $a_c < a_t$ are not respected, the procedure starts again from step 1 with another Z_c. Otherwise,

3. regress four parameters (a_2, n, b_2 and m) for temperatures ranging from a minimum and a maximum, placed on the sublimation ($T_{min}{}^{SVE}$) and melting branch ($T_{max}{}^{SLE}$), respectively. This regression is necessary seeing that for each $T_i > T_c$ and $T_i < T_t$ only one isofugacity condition (for melting or sublimation) exists, thus impeding the analytical calculation of two parameters (a_i and b_i).
The regression is done imposing the function $a(T)$ and $b(T)$ to match the values of a and b calculated in steps 1 and 2 at the critical and triple points (see eqs. (4.32)-(4.35)). The 4 parameters are regressed by minimization of the following objective function *fob*:

$$fob = \alpha \frac{\sum\left[\ln \varphi^S{}_{(T_i,P_i)} - \ln \varphi^L{}_{(T_i,P_i)}\right]^2}{N_{SLE}} + \beta \frac{\sum\left[\ln \varphi^L{}_{(T_i,P_i)} - \ln \varphi^V{}_{(T_i,P_i)}\right]^2}{N_{LVE}} + \gamma \frac{\sum\left[\ln \varphi^S{}_{(T_i,P_i)} - \ln \varphi^V{}_{(T_i,P_i)}\right]^2}{N_{SVE}} \tag{4.38}$$

N_{SLE}, N_{LVE}, and N_{SVE} are the number of the couples T_i, P_i composing the SLE, LVE and SVE data sets. *fob* in eq. (4.38) involves the average of the square differences between the fugacity coefficients for all the couple T_i, P_i that represents the specific type of equilibrium. For almost all the pure compounds of interest, the weights α, β, and γ are equal to one, while different value have been considered for fluids like CO_2 and N_2O in order to privilege the representation of equilibria involving the solid phase[2].

Figure 4.7 illustrates the flow chart related to the above procedure; *In* and *Out* have been used for underlying the input and output parameters.

Step 1 involves four conditions at the critical temperature, whereas two conditions are involved for each temperature T_i in the range $T_t \leq T_i < T_c$ in step 2. In step 3, the SLV EoS is forced to represent the equilibrium condition between two generic α and β phases at the auxiliary pressure of phase α-phase β Equilibrium, $P_{aux}{}^{\alpha\beta E}$, for T_i in the range $T_{min}{}^{SVE} \leq T_i < T_{max}{}^{SLE}$. $T_{min}{}^{SVE}$ and $T_{max}{}^{SLE}$ are minimum sublimation and maximum melting temperature, respectively.

In addition to that, blue blocks are the check points showing the relations required at the end of each step to proceed in the procedure.

1 : it has been found that values of Z_c allowing the regression of the parameters are close to the edge of the proper area in Figure 4.3. The input values of Z_c are then chosen in the proximity of this point.
2 :this because CO_2 and N_2O are solid at the operative conditions within an ASU.

In addition to that, blue blocks are the check points showing the relations required at the end of each step to proceed in the procedure.

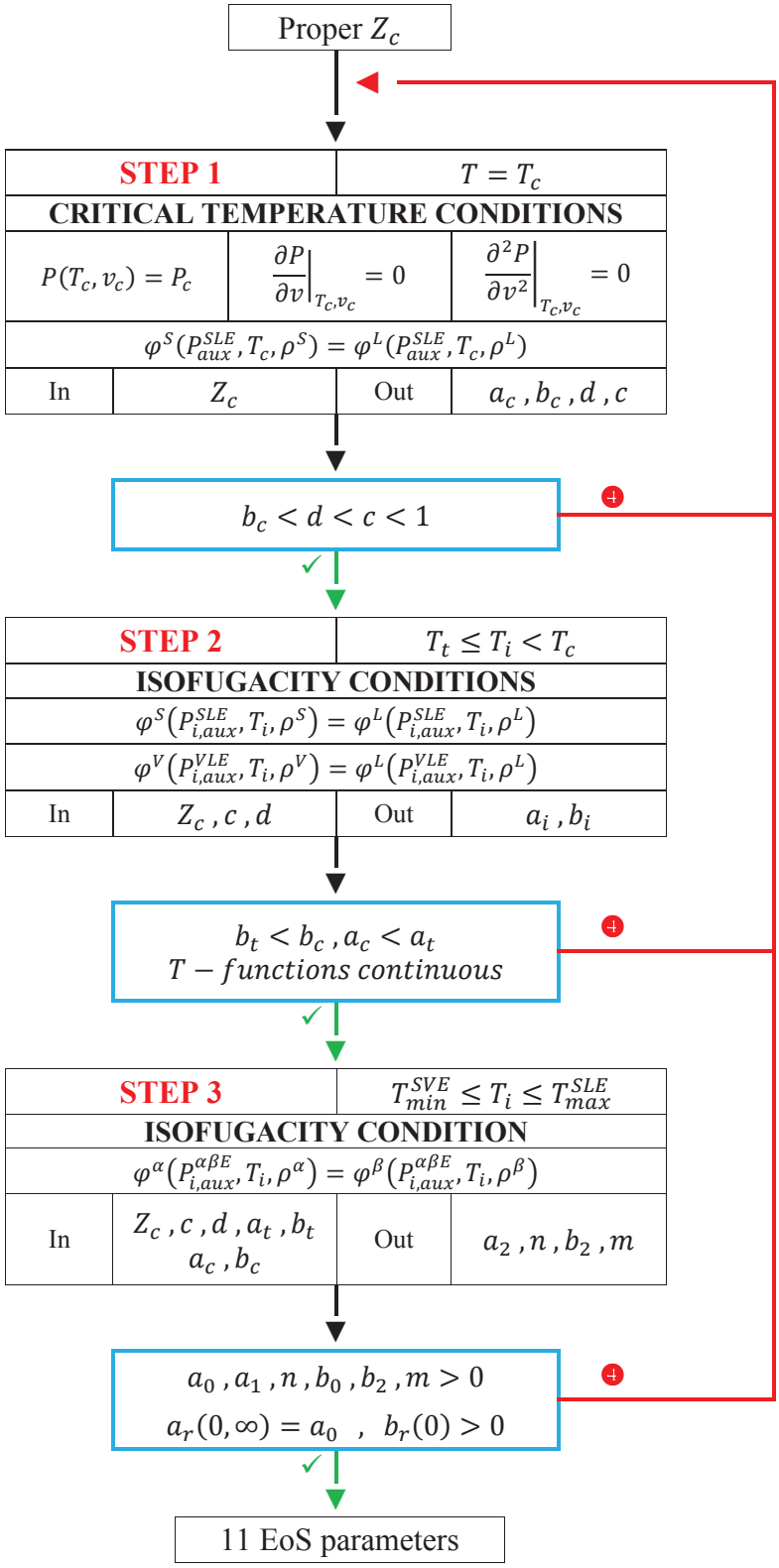

Figure 4.7: Flow chart of the proposed procedure for setting the parameters of the SLV EoS.

By following this procedure for setting the 11 parameters of the SLV EoS (Z_c, a_0, a_1, a_2, n, b_0, b_1, b_2, m, c_r, and d_r), the model proposed by Yokozeki is forced to represent exactly the critical and the triple points, and to reproduce the equilibria generated with the auxiliary equations.

4.4 Modeling of phase equilibrium properties

The new procedure for setting the EoS parameters presented in the previous section has been compared with the one proposed by Yokozeki in terms of the representation of the phase equilibrium behavior of argon (for temperatures from 50 to 160 K and for pressure up to 380 MPa).

Furthermore, tests have been performed for evaluating the possibility of improving the representations by considering not null values for the parameters q and r in the generic EoS, eq. (4.1).

A part of these tests have been presented in reference [84], and here briefly resumed.

Table 4.1 lists five functional forms of the SLV EoS, differing themselves for the regression procedure and/or the attractive pressure. First column illustrates the equations, the second the regression procedures, the third the number of the equations.

In 2003, Yokozeki used the vdW values for q and r and proposed a procedure for setting the EoS parameters. Eq. (4.39) refers hereafter to the functional form and the regression procedure in [64].

Eq. (4.40) involves the same functional form and the procedure proposed in this work. The same proposed procedure is coupled with the Peng-Robinson and Redlich-Kwong values of q and r in eqs. (4.41)-(4.42) and eq. (4.43), respectively. Eqs. (4.41)-(4.42) differ for the covolume involved in the attractive term: the solid covolume in eq. (4.41), the liquid one in (4.42).

Table 4.1: Functional forms of the SLV EoS which have been compared in terms of representation of phase equilibrium properties of pure argon.

Functional form	Regression	Equation
$P(T,v)=\frac{RT}{v-b}\frac{v-d}{v-c}-\frac{a}{v^2}$	[64]	(4.39)
$P(T,v)=\frac{RT}{v-b}\frac{v-d}{v-c}-\frac{a}{v^2}$	[84]	(4.40)
$P(T,v)=\frac{RT}{v-b}\frac{v-d}{v-c}-\frac{a}{v^2+2bv-b^2}$	[84]	(4.41)
$P(T,v)=\frac{RT}{v-b}\frac{v-d}{v-c}-\frac{a}{v^2+2cv-c^2}$	[84]	(4.42)
$P(T,v)=\frac{RT}{v-b}\frac{v-d}{v-c}-\frac{a}{v^2+cv}$	[84]	(4.43)

The EoS parameters of the five EoSs are indicated in Table 4.2. For eq. (4.39), parameters are those presented in [64], whereas the values for the eqs. (4.40)-(4.43) have been obtained following the procedure in [84].

Table 4.2: EoS parameters of the five different SLV EoSs for argon.

Eq.	Zc ($\times10^{-1}$)	b0	b1 ($\times10^{-1}$)	b2	m	d ($\times10^{-2}$)	c ($\times10^{-2}$)	a0 ($\times10^{-2}$)	a1	a2	n
(4.39)	3.751	0.324	-0.225	17.758	10.000	3.258	3.344	35.440	52.5178	6.6546	0.404
(4.40)	3.7507	0.331	-1.483	2.870	1.046	3.202	3.299	1.000	19.677	3.867	0.379
(4.41)	3.06	0.250	-0.366	1.480	2.704	1.972	2.055	45.364	0.294	4.029	2.267
(4.42)	3.06	0.249	-0.398	1.558	1.958	1.966	2.055	1.000	1576.53	8.164	0.161
(4.43)	3.3242	0.256	-1.184	2.561	1.184	2.192	2.287	0.010	30.277	4.260	0.336

4.4.1 Equilibrium pressures and temperatures

First of all, the original SLV EoS presented in [64], eq. (4.39), and the four models, eqs. (4.40)-(4.43), have been compared in terms of the quantitative representation of the pressure-temperature equilibrium behavior of argon.

The quantitative comparison involves equilibrium values (pressure and temperature) calculated from models within Table 4.1 and values produced with the auxiliary equations. The comparison has been done with reference to the percentage deviations: Absolute Average Deviation (AAD), Bias, and Maximum Absolute Deviation (MAD). AAD%, Bias%, and MAD% are defined as in eqs. (4.44)-(4.46).

$$AAD\% = \frac{100}{N}\sum_{i=1}^{N}\left|\left(\frac{M_{calc}-M_{aux}}{M_{aux}}\right)_i\right| \tag{4.44}$$

$$Bias\% = \frac{100}{N}\sum_{i=1}^{N}\left(\frac{M_{calc}-M_{aux}}{M_{aux}}\right)_i \tag{4.45}$$

$$MAD\% = 100 \underset{i=1,N}{max}\left\{\left|\left(\frac{M_{calc}-M_{aux}}{M_{aux}}\right)_i\right|\right\} \tag{4.46}$$

In eqs. (4.44)-(4.46), M is a generic equilibrium property (pressure or temperature), and N is the number of auxiliary values used in the comparison. Subscripts are related to auxiliary (*aux*) or calculated (*calc*) values.

Table 4.3 presents AAD%, Bias%, and MAD% for VLE, SVE, and SLE of argon when equilibrium temperatures are calculated at fixed pressures. Table 4.4 presents the deviations when equilibrium pressures are calculated at fixed temperatures.

Table 4.3: Summary of the statistical errors in calculating equilibrium temperatures at fixed pressures for argon. Deviations are evaluated with respect to values from auxiliary equations.

SLV EoS	VLE (N=107)			SVE (N=35)			SLE (N=116)		
	AAD%	Bias%	MAD%	AAD%	Bias%	MAD%	AAD%	Bias%	MAD%
(4.39)	0.68	-0.67	1.93	0.96	0.96	2.54	2.27	0.73	7.84
(4.40)	0.08	-0.02	0.20	0.35	0.34	0.55	0.26	-0.06	1.04
(4.41)	0.28	0.28	1.29	0.04	0.03	0.09	1.22	-0.35	3.13
(4.42)	0.06	-0.01	0.15	0.28	0.28	0.43	0.17	-0.02	0.89
(4.43)	0.08	-0.04	0.22	0.33	0.23	0.57	0.35	-0.21	1.31

Table 4.4: Summary of the statistical errors in calculating equilibrium pressures at fixed temperatures for argon. Deviations are evaluated with respect to values from auxiliary equations.

SLV EoS	VLE (N=107)			SVE (N=35)			SLE (N=116)		
	AAD%	Bias%	MAD%	AAD%	Bias%	MAD%	AAD%	Bias%	MAD%
(4.39)	4.82	4.75	13.48	14.13	-14.13	40.11	13.89	-6.71	33.17
(4.40)	0.57	0.03	1.18	4.70	-4.61	7.27	1.71	-0.25	4.74
(4.41)	1.65	-1.65	6.40	0.52	-0.38	1.11	7.34	-0.69	12.79
(4.42)	0.44	<0.01	0.91	3.85	-3.85	5.79	1.14	-0.29	3.01
(4.43)	0.58	0.17	1.33	4.53	-2.72	10.46	1.90	0.73	3.30

According to Table 4.3, it clearly appears that it is the procedure for setting the EoS parameters proposed in this work that allows the improvement in the quantitative representation of equilibrium temperatures. In fact, errors related to eqs. (4.40)-(4.43) are almost comparable, and smaller than those of the eq. (4.39), in particular for the solid-fluid equilibrium. As a consequence, any attractive term can be definitely preferred by comparing the models with respect to calculated equilibrium temperatures.

Table 4.4 confirms the improvements also for the quantitative representation of SVE, SLE, and VLE pressures achieved by using the procedure in [84]. With reference to eqs. (4.40)-(4.43), it is possible to argue the following considerations. For VLE, all errors are comparable, except for the MAD%. The maximum value of MAD is found for eq. (4.41), which involves the PR values of q and r and the solid covolume in the attractive term.

Nevertheless, eq. (4.41) allows the best representation of the solid-vapor equilibrium pressures; the worst one is instead related to eq. (4.43), namely RK values of q and r and the liquid covolume in the attractive term. Finally, similar errors are obtained for the SLE by using eqs. (4.40), (4.42), and (4.43), while eq. (4.41) provides the highest errors for all the statistical deviations.

To sum up, Table 4.3 and Table 4.4 confirm the utility of the procedure for setting the EoS parameters proposed in this work.

In addition to that, comparisons in Table 4.3 and Table 4.4 suggest that the generic SLV EoS, eq. (4.1), with the attractive term involving the liquid covolume should be considered for obtaining the best quantitative representations of the pressure-temperature equilibrium behavior.

An additional inconvenient concerning the presence of the solid covolume in the attractive term, eq. (4.41), concerns the functional form $a(T)$ and $b(T)$.

From the author attempts, it was not possible to find a value of Z_c providing a continuous function of $a(T)$ and $b(T)$ across the critical point. This is evidenced in Figure 4.8 for the function $a(T)$ and in Figure 4.9 for the function $b(T)$.

This entails to not meet the condition between steps 2 and 3 in the flow chart of Figure 4.7. As a consequence, eq. (4.1) with $b(T)$ in the attractive term does not allow to meet the critical temperature condition and the SLE and VLE isofugacity conditions in the range $T_t \leq T_i < T_c$ with continuous $a(T)$ and $b(T)$ at the same time.

Author considered this problem as related to the presence of a temperature dependent function, $b(T)$, in the attractive term of eq. (4.1). For these reason, following comparison in this chapter do not concern SLV EoSs involving the solid covolume in the attractive term of the equation.

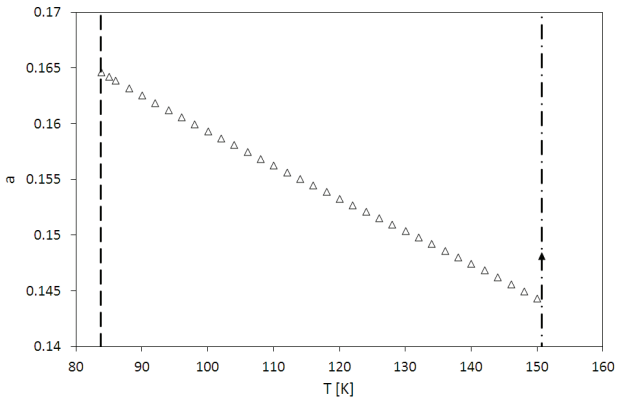

Figure 4.8: Values of the parameter a for argon.
Calculated values: Δ : $a(T_i)$; ▲ : $a(T_c)$.
(− −): triple point temperature;(− • −): critical temperature;
These values have been obtained forcing eq. (4.41) to represent SLE and VLE auxiliary values for a fixed temperature, T_i, see step 2 in the parameters regression procedure.

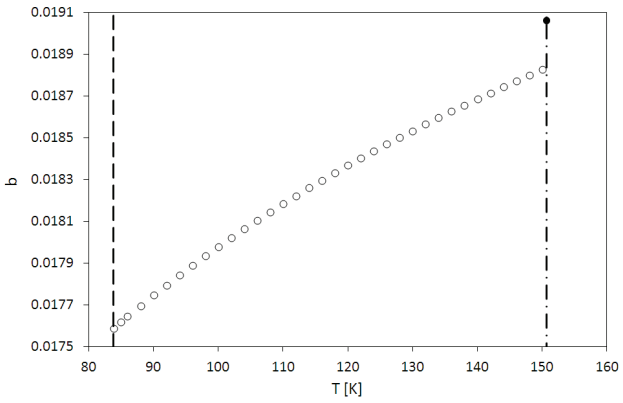

Figure 4.9: Values of the parameter b for argon.
Calculated values: ○ : $b(T_i)$; ● : $b(T_c)$.

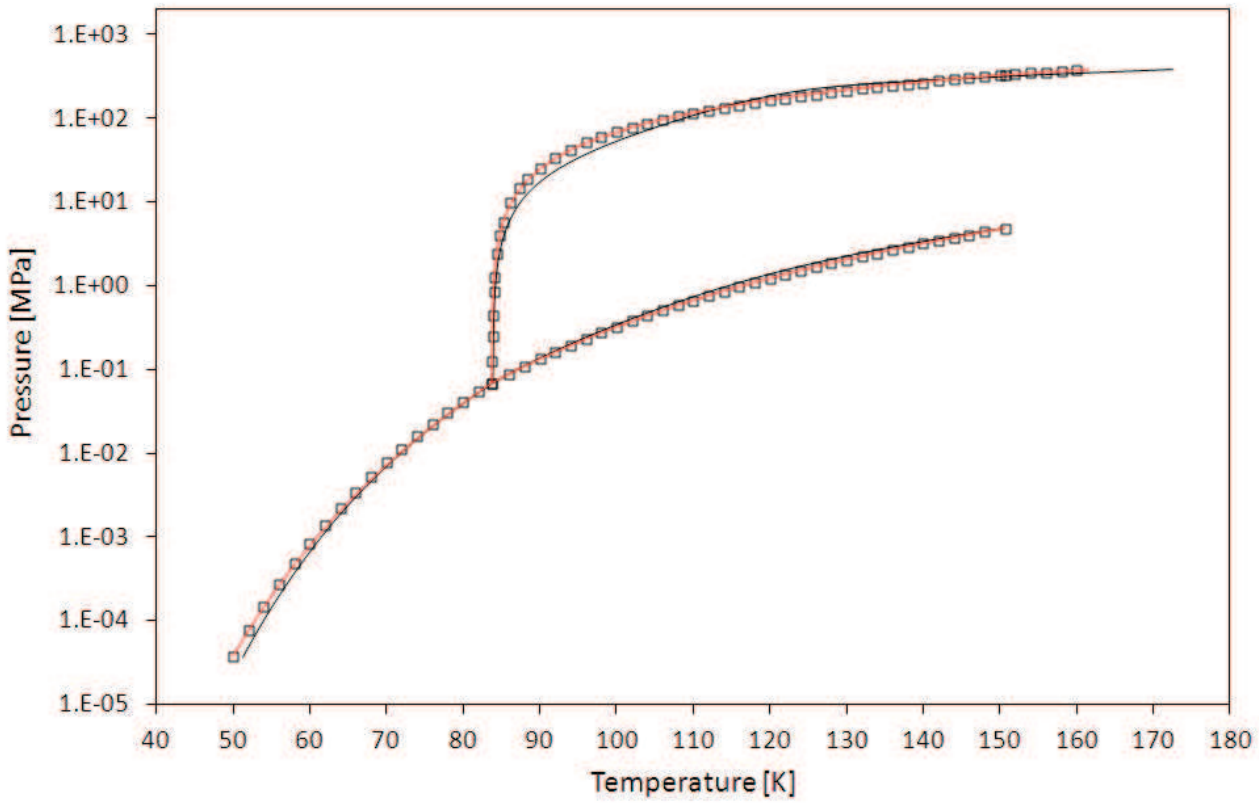

Figure 4.10: Pressure-temperature equilibrium behavior of argon obtained with the SLV EoS and values from auxiliary equations.
— : Yokozeki EoS and procedure for setting the EoS parameter, eq. (4.39), [64];
— : Yokozeki EoS and new procedure for setting the EoS parameter, eq. (4.40), [84];
□ : values form auxiliary equations, [3].

The pressure-temperature equilibrium behavior of argon, as represented by eqs. (4.39), (4.40) and the auxiliary equations, is shown in Figure 4.10. Values calculated from eqs. (4.42)-(4.43) have not been included since the deviations in Table 4.3 and Table 4.4 are similar for eqs. (4.40), (4.42), and (4.43).

4.4.2 Equilibrium densities and enthalpies

The second comparison of the models presented in Table 4.1 (except eq. (4.41)) concerns the qualitative representation of equilibrium density (ρ) and latent heats of transition (Δh) of argon. Calculated values of ρ and Δh are related to EoS parameters within Table 4.2 and the equilibrium pressures, temperatures, and volumes calculated in the framework of the first comparison. Δh have been evaluated by means of eq. (4.15).

Figure 4.11 and Figure 4.12 represent the density-temperature and the latent heat-temperature phase equilibrium behavior of argon, respectively. Reduced quantities have been used in these qualitative comparisons.

Figure 4.11 shows clearly that the representation of reduced densities at equilibrium is better using the attractive term of the van der Waals CEoS, eqs. (4.39)-(4.40). Furthermore, the regression of the EoS parameters proposed in [84] improves the representation of the liquid reduced density at VLE, while worsening that of the solid one at SVE.

Using eqs. (4.42)-(4.43), the value of Z_c that allows satisfying the continuity of the parameters of $a(T)$ and $b(T)$ in the domain $T_t \leq T_i < T_c$ determines a shifting of the reduced density of condensed phases toward higher values.

According to Figure 4.11, it is possible also to state that at SLE all the EoSs here considered show solid density decreasing with increasing pressure, thus deviating from the real trend.

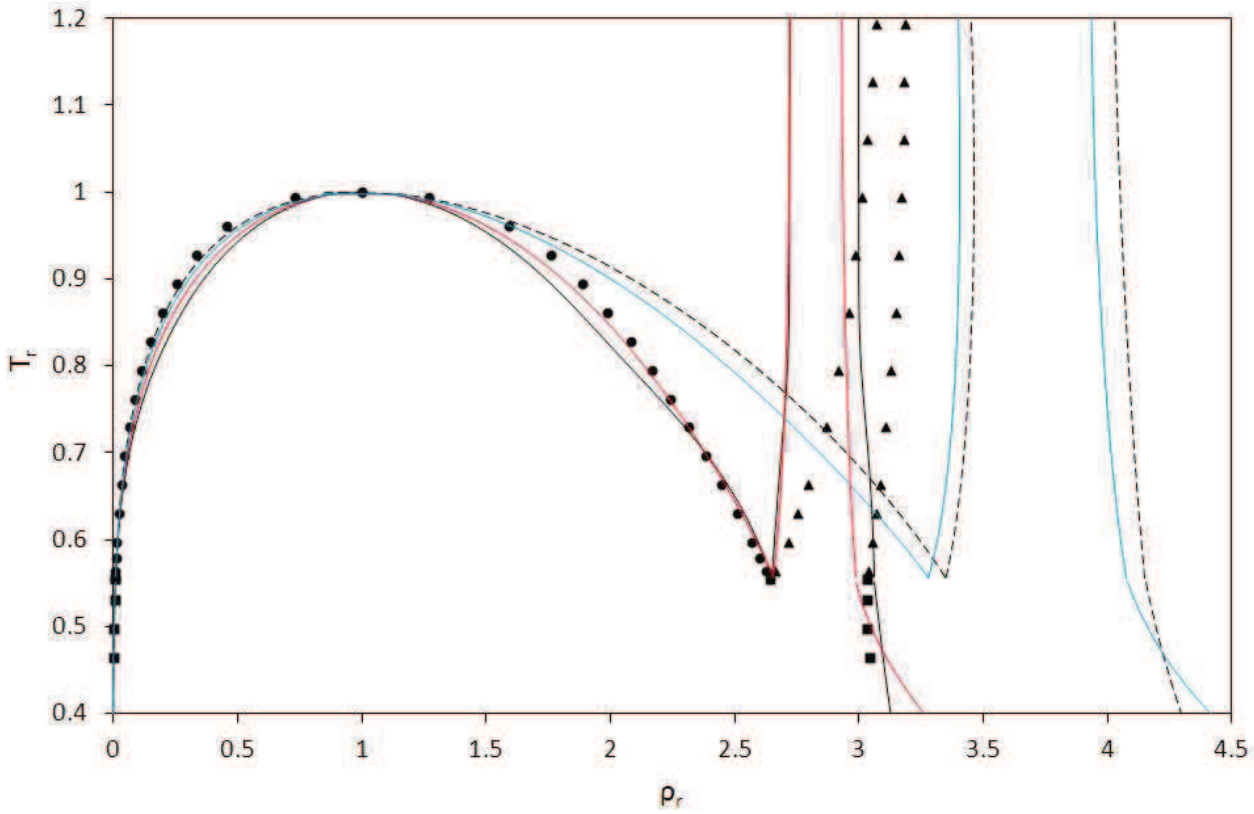

Figure 4.11: Reduced temperature – reduced density phase equilibrium behavior for argon.
Experimental values [48]: ● : VLE; ▲ : SLE; ■ : SVE;
Lines: — : eq. (4.39); — : eq. (4.40); − − : eq. (4.42). — : eq. (4.43).

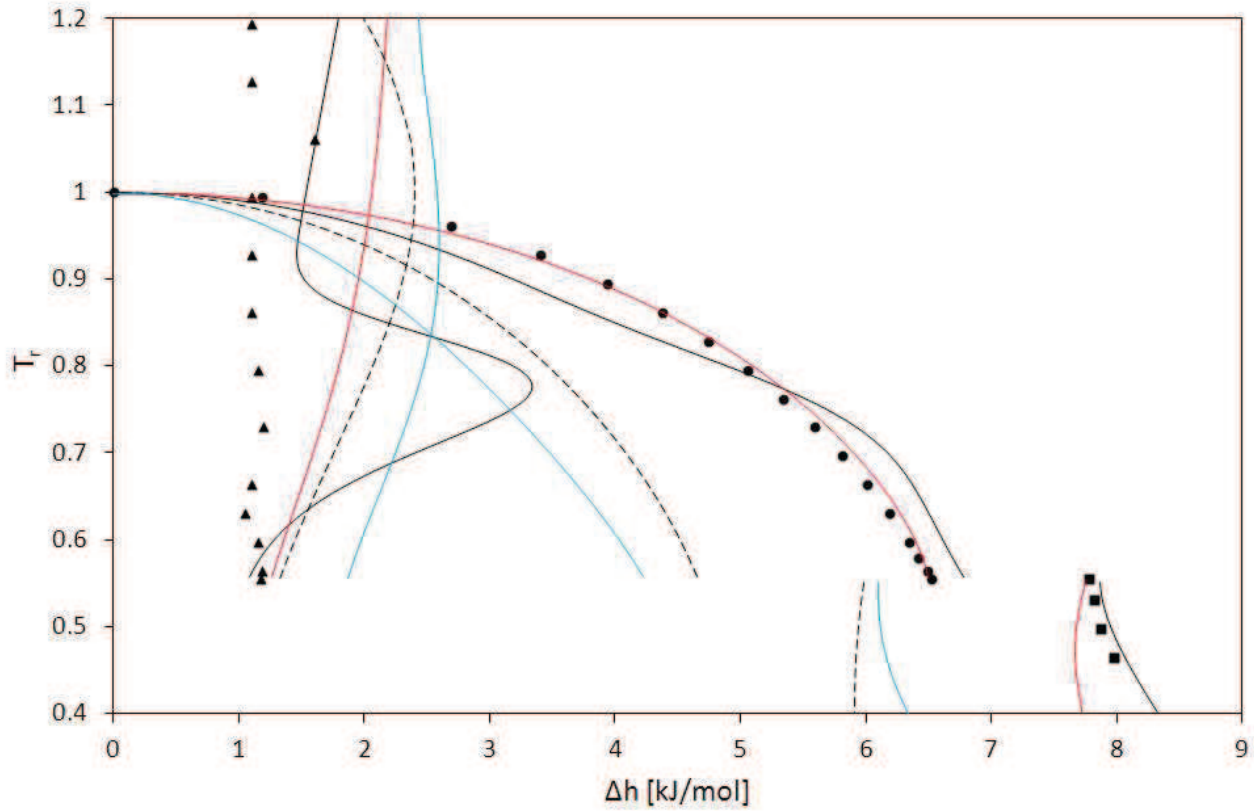

Figure 4.12: Latent heats of transition versus reduced equilibrium temperature for argon.
Experimental values [48]: ● : VLE; ▲ : SLE; ■ : SVE;
Lines: — : eq. (4.39); — : eq. (4.40); − − : eq. (4.42). — : eq. (4.43).

In Figure 4.12 it is possible to observe that the latent heat of vapor-liquid transition is very well represented using eq. (4.40). The original SLV-EoS, eq. (4.39) [64], gives two changes in the second order derivative of the latent heat of liquid–vapor transition with respect to temperature. This problem is probably originated by the changes of the parameters *a* and *b* with temperature.

This can be also the potential origin of the behavior shown for the solid–liquid transition enthalpies, for which eq. (4.39) presents a maximum for reduced temperatures between 0.7 and 0.8. Eqs. (4.42)-(4.43) give correct trends for the latent heat of liquid–vapor transition, but values are not in agreement with the experimental data. Also the experimental values for the latent heats of solid–vapor transition are not well predicted using eqs. (4.42) and (4.43). In general, the four considered equations provide poor results in representing solid-liquid transition enthalpies.

The equilibrium diagrams in Figure 4.11 and Figure 4.12 are referred to argon, but similar diagrams have been encountered also for the other pure compounds of interest in this work.

4.5 Results for pure compounds

The considerations concerning the representation of equilibrium properties (temperature, pressure, density, latent heats of transition) led to choose the functional form of eq. (4.40) for the present work. With the attractive term of the vdW EoS, the model is in agreement at least with equilibrium densities and enthalpies at VLE, even if a slightly better representation of equilibrium pressures and temperatures of argon could be achieved with not null values of q and r in the attractive term. Furthermore, it can be stated that with the functional forms treated above it is not possible to represent all the equilibrium properties, so a universal thermodynamic model still misses.

The final version of the SLV EoS is then the same used by Yokozeki in reference [64]:

$$P(T,v) = \frac{RT}{v-b}\frac{v-d}{v-c} - \frac{a}{v^2} \tag{4.47}$$

The EoS parameters for the pure compounds of interest in this work have been regressed following the procedure introduced in section 4.3.1 and presented in reference [84].

This procedure has been successively improved by adding an additional step. When the first value of Z_c allowing the setting of the EoS parameters is found, the objective function *fob* in eq. (4.38) has a determined value. Iteration can then be conducted for exploring other proper values of Z_c, in order to find the value of Z_c providing the smallest *fob*.

With reference to step 3 of Figure 4.7, the parameters a_2, n, b_2 and m have been regressed considering the saturation branch between the triple and critical point, the sublimation branch down to 10^{-5} MPa, and the melting branch up to 100 MPa. Sublimation and melting lines have been limited for not worsening the representation of the pressure-temperature equilibrium behavior with equilibria occurring at pressures too far from the usual operative conditions of the air distillation process.

In addition to that, the T-dependent function $b_r(T)$ has been modified as in eq. (4.48) in order to automatically match the condition $b_r(T_{ri}) < d_r$.

$$b_r(T_r) = d_r[b_0 + b_1 exp(-b_2 T_r^n)] \tag{4.48}$$

The following section presents the pressure-temperature ranges used for the regression of the EoS parameters.

Section 4.5.2 gives the quantitative comparison between model and the pressure-temperature equilibrium behavior for the compounds of interest. Other equilibrium properties have not been included considering that this work aims principally at the representation of equilibrium temperatures and pressures.

Qualitative representations for methane and carbon dioxide have also been presented in section 4.5.2.

4.5.1 Pressure-temperature ranges for the EoS parameters regression

With the analytic procedure described in section 4.3.1, the values of the parameters a_r and b_r have been determined for each temperature between the triple and the critical temperatures, forcing the SLV EoS, eq. (4.44), to reproduce SLE, and VLE auxiliary values.

The temperature and pressure values of the triple and critical points for the compounds of interest are illustrated in Table 4.5.

Table 4.5: Triple and critical points for the substances of interest, [3].

Fluid	T_t / K	P_t / kPa	T_c / K	P_c / MPa	N VLE
N_2	63.151	12.5198	126.192	3.3958	102
O_2	54.361	0.14628	154.581	5.043	135
Ar	83.8058	68.891	150.687	4.863	107
Kr	115.775	73.5	209.48	5.525	135
Xe	161.405	81.7724	289.733	5.842	167
Ne	24.556	43.368	44.4918	2.6786	135
He	2.1768	5.0428	5.1953	0.22758	173
CO_2	216.592	517.95	304.1282	7.3773	119
H_2	13.957	7.35783	33.145	1.2964	194
N_2O	182.33	87.84	309.52	7.245	96
CH_4	90.6941	11.697	190.56	4.5992	131
C_2H_6	90.368	0.0011421	305.322	4.8722	98
C_2H_4	103.986	0.12196	282.35	5.0418	117
C_3H_8	85.53	1.724×10^{-7}	369.89	4.2512	110
C_3H_6	87.953	7.4717×10^{-7}	364.211	4.555	120

The last column of Table 4.5 indicates the number of VLE auxiliary values used in the regression procedure.

For each pure compound (except helium), Table 4.6 represents the minimum values of sublimation temperature (T_{min}) and pressure (P_{min}) and the maximum values of melting temperature (T_{max}) and pressure (P_{max}) used for the regression of the EoS parameters (in step 3 of Figure 4.7).

Table 4.6: Minimum SVE and maximum SLE values for the temperature and pressure used for the regression of the SLV EoS parameters.

Fluid	SVE			SLE		
	T_{min} / K	P_{min} / kPa	N	T_{max} / K	P_{max} / MPa	N
N_2	41	0.0106	24	82	95.5	56
O_2	48	0.0131	8	65	99.6	43
Ar	48	0.0171	36	106	95.6	59
Kr	66	0.0120	28	143	96.9	56
Xe	91	0.0103	72	197	97.4	59
Ne	14	0.0141	26	37	98.4	82
CO_2	125	0.0112	33	236	99.8	31
H_2	8	0.0131	28	33.145	92.7	194
N_2O	120	0.0207	15	197	95.2	38
CH_4	59	0.0118	33	114	99.4	49
C_2H_6				105	97.4	42
C_2H_4				117	98.7	40
C_3H_8				94	93.2	23
C_3H_6				96	99.5	35

For each compound, the entire saturation line has instead been considered in the regression procedure.

Auxiliary equations for the SVE are not available for helium and light hydrocarbons (except methane), thus the correspondent lower temperature used for the regression is the triple point temperature.

In addition to that, helium has a melting line similar to the one of water, namely a negative slope in the pressure-temperature equilibrium projection.

The classical approach has then been used for generating the melting line of helium, as detailed in Appendix D, and the regression of the EoS parameters involved only saturation auxiliary values once obtained the parameters a and b for temperatures from the triple up to the critical point. For this reason, for helium maximum values of SLE are not indicated in Table 4.6.

In Table 4.6, N is the number of SVE and SLE auxiliary values used for the regression of the parameters.

4.5.2 Representation of pressure-temperature equilibrium projections

As stated above, the EoS parameters have been regressed to fit values from auxiliary equations, and then the model has been quantitatively compared with the auxiliary values.

The comparison via the deviations of eqs. (4.44)-(4.46) has been done twice for each compound:

- by imposing the temperature: in this case the deviations are between calculated equilibrium pressures and auxiliary pressures. It can be said that the deviations are in “terms of pressure”;
- by imposing the pressure: in this case the deviations are between calculated equilibrium temperatures and auxiliary temperatures. In this case, the deviations are in “terms of temperature”.

The last lines of Table 4.7 and Table 4.8 represent a summary of the results obtained for all the compounds. In these lines, the AAD% and the Bias% values are the average of the values related to each compound and weighted on the number of experimental values considered. Conversely, MAD% is the maximum MAD% considering all the fluids. Table 4.7 presents the deviations in terms of pressure.

Table 4.7: Summary of the statistical errors in calculating equilibrium pressures at fixed temperatures for the pure compounds of interest.
Errors are evaluated with respect to the auxiliary equations.

Fluid	VLE			SVE			SLE		
	AAD%	Bias %	MAD%	AAD%	Bias %	MAD%	AAD%	Bias %	MAD%
N_2	0.68	-0.05	1.26	0.44	-0.26	0.94	3.60	-3.41	5.69
O_2	1.49	-0.004	3.00	2.41	-1.52	4.27	4.95	-4.79	11.24
Ar	0.54	0.32	1.36	0.61	-0.24	1.15	2.36	-2.02	3.63
Kr	0.72	0.64	1.75	0.69	-0.21	1.41	2.29	-1.90	5.98
Xe	0.59	0.50	1.39	0.42	-0.10	1.29	4.11	-3.48	27.85
Ne	0.97	0.97	1.89	0.90	-0.33	1.75	1.75	1.01	8.18
He	0.29	0.22	0.42						
CO_2	3.07	3.07	6.22	2.08	1.04	6.43	4.02	4.02	13.57
H_2	0.54	0.31	1.05	0.90	0.47	2.31	0.38	0.33	3.96
N_2O	4.41	4.41	11.41	2.91	1.78	6.48	12.14	12.14	23.74
CH_4	0.71	0.39	1.53	0.37	-0.05	0.89	2.24	-1.64	3.46
C_2H_6	1.22	0.34	3.35				1.22	-0.07	4.11
C_2H_4	0.34	0.19	1.47				3.93	-3.30	5.92
C_3H_8	1.01	0.67	3.34				16.11	-16.11	24.67
C_3H_6	0.82	0.49	3.07				1.69	-0.71	5.25
Overall	**1.06**	**0.75**	**11.41**	**0.91**	**0.08**	**6.48**	**3.07**	**-0.87**	**27.85**

In Table 4.7, for VLE the AAD% averaged with respect to all the compounds is about 1.1% with a Bias% of 0.75% indicating the absence of a systematic error of the SLV EoS with respect to the auxiliary equations for the saturation pressure. The maximum MAD% is about 11%, and it is found for N_2O. For SVE, the AAD% averaged with respect to all the compounds is less than 1%. Bias% is about 0.1% averaged with respect to all the compounds. The maximum value of MAD% is found again for N_2O, and a similar value is obtained for CO_2. For SLE, the AAD% is 3.07% as averaged value for all the compounds; Bias% is less than -1%. Xe shows the maximum value for MAD%, of about 28%, while for N_2O and C_3H_8 also AAD% and Bias% are greater than 10%.

According to Table 4.7, higher deviations usually occur for the SVE and the SLE.

The order of magnitude of the lowest SVE pressure from auxiliary equations considered in the regression procedure is 10^{-5} MPa. When the temperatures are imposed for evaluating the equilibrium pressures via the SLV EoS on the SVE branch, M_{aux} is the auxiliary pressures in eqs. (4.44)-(4.46). If significant percentage errors occur along the SVE branch, they are connected to errors in pressure that are not so relevant in the industrial processes. For example, if the auxiliary pressure P_{aux} is equal to 1×10^{-4} MPa and the calculated pressure P_{calc} is 1.5×10^{-4} MPa, the percentage error will be 50%; the difference between the two pressure would be 50 Pa, and this difference is not so relevant as a percentage error equal to 50% along the vapor-liquid branch.

Understanding why high deviations are obtained for the SLE pressures requires considering that the melting line is practically vertical. A little difference in the triple point coordinates between the values reported in Table 4.5 and values used in the auxiliary equations (see Appendix A) accounts for high percentage errors. This is not due to an incorrect regression of the EoS parameters or to an incorrect functional form of the SLV EoS, but only to the high value of the slope of the solid-liquid branch.

By evaluating the deviations in terms of temperature, the capability of the SLV EoS to represent also SVE and SLE auxiliary values has been proved, as illustrated in Table 4.8. In Table 4.8, for VLE the AAD% averaged with respect to all the compounds is less than 0.2% and also the Bias% is close to zero. The maximum absolute error is about 1.3%. For SVE, the AAD% averaged with respect to all the compounds is 0.06%. The Bias% is again close to zero. The maximum value of MAD% is found for CO_2 and N_2O and it is about 0.3%. AAD% for SLE is about 0.1% with a Bias% of -0.03%. The maximum MAD% is about 1.2%.

Table 4.8: Summary of the statistical errors in calculating equilibrium temperatures at fixed pressures for the pure compounds of interest.
Errors are evaluated with respect to the auxiliary equations.

Fluid	VLE			SVE			SLE		
	AAD%	Bias %	MAD%	AAD%	Bias %	MAD%	AAD%	Bias %	MAD%
N_2	0.08	-0.01	0.20	0.03	0.02	0.07	0.15	0.12	0.33
O_2	0.16	-0.05	0.32	0.13	0.09	0.23	0.17	0.15	0.29
Ar	0.08	-0.06	0.22	0.04	0.02	0.10	0.09	0.04	0.34
Kr	0.11	-0.10	0.28	0.05	0.02	0.10	0.07	0.01	0.28
Xe	0.09	-0.08	0.23	0.03	0.01	0.06	0.09	-0.002	0.33
Ne	0.15	-0.15	0.31	0.07	0.03	0.14	0.30	-0.29	0.68
He	0.07	-0.06	0.11						
CO_2	0.39	-0.39	0.78	0.11	-0.06	0.32	0.16	-0.16	0.84
H_2	0.10	-0.07	0.21	0.09	-0.05	0.26	0.04	-0.03	0.15
N_2O	0.46	-0.46	1.25	0.14	-0.09	0.32	0.26	-0.26	1.21
CH_4	0.10	-0.07	0.24	0.02	0.01	0.05	0.09	-0.004	0.42
C_2H_6	0.12	-0.07	0.45				0.07	-0.05	0.49
C_2H_4	0.04	-0.02	0.22				0.08	0.03	0.38
C_3H_8	0.12	-0.10	0.44				0.32	0.32	0.70
C_3H_6	0.09	-0.07	0.42				0.04	-0.02	0.36
Overall	**0.14**	**-0.11**	**1.25**	**0.06**	**-0.001**	**0.32**	**0.12**	**-0.03**	**1.21**

According to Table 4.7 and Table 4.8, quantitative good agreements have been verified between the SLV EoS and auxiliary values for the solid-vapor and solid-liquid branches in the pressure-temperature ranges in Table 4.6, and for the vapor-liquid branch between the triple and critical points of Table 4.5.

Figure 4.13 and Figure 4.14 portray the *PT-EP* of methane and carbon dioxide, respectively. Analogous diagrams have been reported for the other pure compounds of interest in Appendix D. In Figure 4.13 and Figure 4.14 open circles have been used for a selected number of VLE, SVE, and SLE values from auxiliary equations used for the regression of the EoS parameters. Black lines refer to values calculated from the SLV EoS, eq. (6). Calculation of the solid-liquid equilibrium has been extended up to the critical point temperature, in order to verify the absence of unphysical behaviors along the melting line.

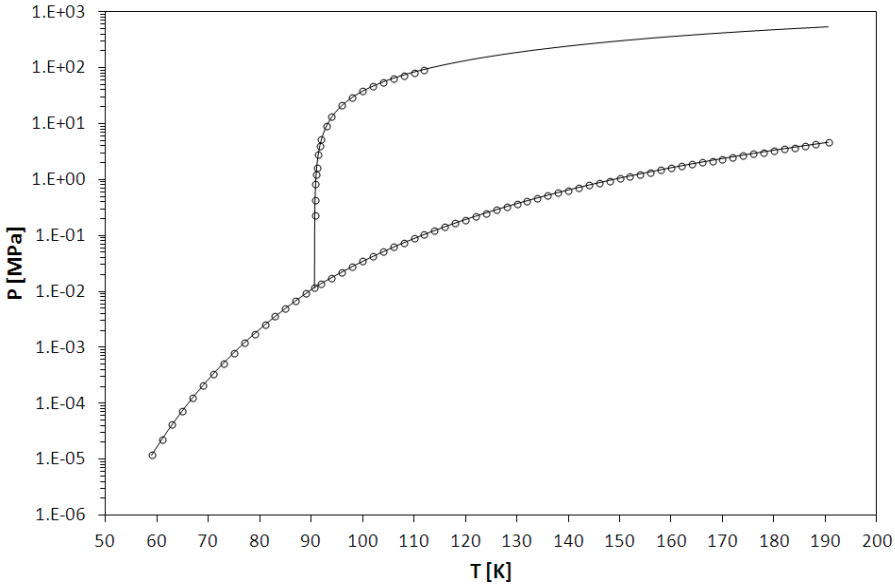

Figure 4.13: PT-EP of methane obtained with the SLV EoS.

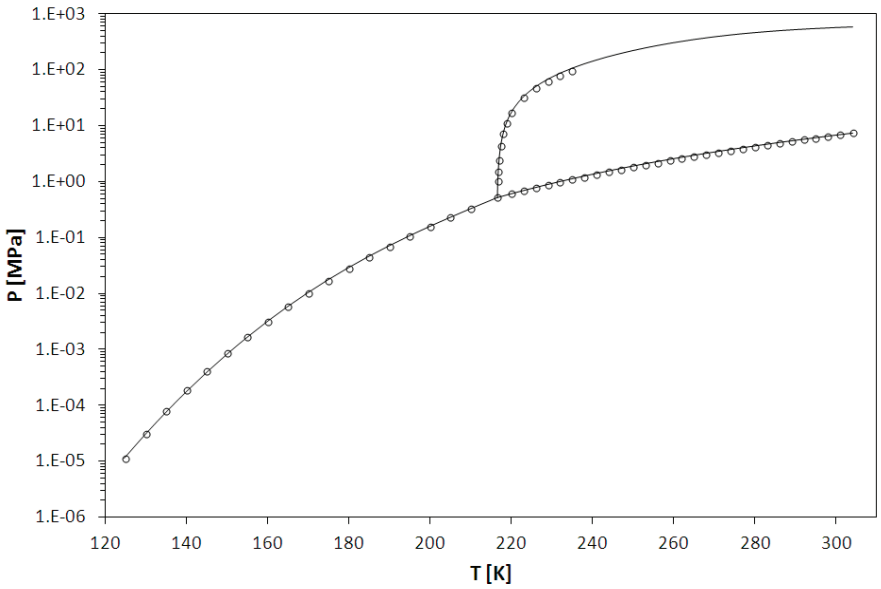

Figure 4.14: PT-EP of carbon dioxide obtained with the SLV EoS.
— : SLV EoS; ○ : selected equilibrium values from auxiliary equations.

5 Extension to mixtures

In the previous chapter, different attractive terms within the solid-liquid-vapor EoS have been tested for the representation of equilibrium properties of pure compounds, and the functional form chosen as best compromise is the one with null values for parameters q and r.

In such a way, the chosen EoS, hereafter called SLV EoS, is identical to the one proposed by Yokozeki in [64]. In addition to that, the capability of SLV EoS in representing quantitatively the pressure-temperature equilibrium behavior for the compound of interest has been detailed at the end of chapter 4.

The first section in Chapter 5 focuses on the mixing rules needed for evaluating the mixtures parameters. The expression of the partial molar fugacity coefficient deriving from the functional form of the SLV EoS is presented in Section 5.2. The minimization of the Gibbs free energy of mixing is partially faced in the third section, while details have been provided in Appendix E.

Comments on the mixtures of interest in terms of available data have been argued in section 5.5. Finally, the application of the SLV EoS to the representation of phase equilibria in binary Lennard-Jones mixtures is presented in the last section of this chapter.

5.1 Mixing rules

In [64], Yokozeki applied the solid-liquid-vapor equation of state with van der Waals attractive term for representing the binary mixture CO_2 + CH_4; the mixing rules in eqs. (5.1)-(5.2) were used for evaluating the mixture parameters a_{mix}, b_{mix}, c_{mix}, and d_{mix} starting from values of the pure compounds, indicated by subscripts i and j. In eqs. (5.1)-(5.2), x is the mole fraction.

$$a_{mix} = \sum_{i=1}^{N}\sum_{j=1}^{N}\sqrt{a_i a_j}\left(1 - k_{ij}\right)x_i x_j \tag{5.1}$$

$$b_{mix} = \sum_{i=1}^{N} b_i x_i \quad , \quad c_{mix} = \sum_{i=1}^{N} c_i x_i , \quad d_{mix} = \sum_{i=1}^{N} d_i x_i \tag{5.2}$$

The only adjustable parameters author used in [64] for representing solid-fluid and fluid-fluid equilibria was then the binary interaction parameter k_{ij} in the quadratic mixing rule of a_{mix}, while the remaining mixture parameters were evaluated as simple molar averages of each pure compound values.

In [67], same mixing rules were adopted for the volumetric parameters b_{mix}, c_{mix}, and d_{mix} by Yokozeki in dealing with the representation of the H_2O + CO_2 system. In [67], Yokozeki used eq. (5.3) for a_{mix}, as a simple quadratic mixing rule in the form of eq. (5.1) was found not be suitable for being applied to highly non-ideal system.

$$a_{mix} = \sum_{i=1}^{N}\sum_{j=1}^{N}\sqrt{a_i a_j}\left(1 - K_{ij}\right)x_i x_j \quad , \quad K_{ij} = \frac{k_{ij}k_{ji}\left(x_i + x_j\right)}{k_{ij}x_j + k_{ji}x_i} \quad , \quad K_{ii} = 0 \tag{5.3}$$

Two different values of the binary interaction parameters, k_{ij} and k_{ji}, can then be fixed, while eq. (5.3) reduces to eq. (5.1) in case of symmetric values, as in that case $K_{ji} = k_{ij} = k_{ji}$. Furthermore, Yokozeki in [67] used a temperature-dependent function and a constant value for k_{12} an k_{21}, respectively.

Yokozeki in [68] applied the equation of state to phase behaviors of hard-sphere mixtures, thus neglecting the attractive term in the functional form. Yokozeki adopted quadratic expressions also for the volumetric parameters b_{mix}, c_{mix}, and d_{mix}, eqs. (5.4)-(5.6).

$$b_{mix} = \frac{1}{2}\sum_{i=1}^{N}\sum_{j=1}^{N}(b_i + b_j)(1 - m_{ij})x_i x_j \tag{5.4}$$

$$c_{mix} = \frac{1}{2}\sum_{i=1}^{N}\sum_{j=1}^{N}(c_i + c_j)(1 - n_{ij})x_i x_j \tag{5.5}$$

$$d_{mix} = \frac{1}{2}\sum_{i=1}^{N}\sum_{j=1}^{N}(d_i + d_j)(1 - l_{ij})x_i x_j \tag{5.6}$$

Eqs. (5.4)-(5.6) contain three new interaction parameters: m_{ij}, n_{ij}, and l_{ij}.

Yokozeki in [68] applied the equation of state with different sets of symmetric binary interaction parameters and represented different types of solid-liquid equilibria, from solid solution to eutectic and peritectic behaviors.

The equations proposed by Yokozeki in 2003, [64], was challenged by same author two years later with reference to the representation of eutectic behaviors in the binary systems benzene+cyclohexane, [65], and indole+aromatics, [69]. In these works, mixing rules in eqs. (5.3)-(5.6) were used. Constant values for the binary interaction parameters m_{ij}, n_{ij}, and l_{ij} were adopted. Furthermore, symmetric and asymmetric values were used for k_{ij} in [65] and [69], respectively.

Despite a rather good representation Yokozeki obtained for solid solutions as well as eutectic behaviors for the considered systems, he used two different sets of k_{ij} for the solid and the liquid phases. It means that the solid-liquid equilibria shown in [65] and [69] have not been represented with the same equation of state, instead Yokozeki applied separately the EoS for the two phases.

Another interesting point is that in [65] and [69] he discussed the capability of the unified EoS in representing eutectic behaviors in real systems. To ease the discussion, let's consider the schematics Gibbs free energy of mixing plotted in Figure 5.1. In Figure 5.1, red and black lines are the Gibbs energy of mixing for the solid, G^S, and the liquid, G^L, respectively. The blue lines are the common tangent line indicating the equilibrium compositions.

At the solid-solid-liquid equilibrium temperature, pure components are stable in the solid phase since the eutectic temperature is lower than their triple point temperatures, while there is a range of composition where G^L is lower than G^S.

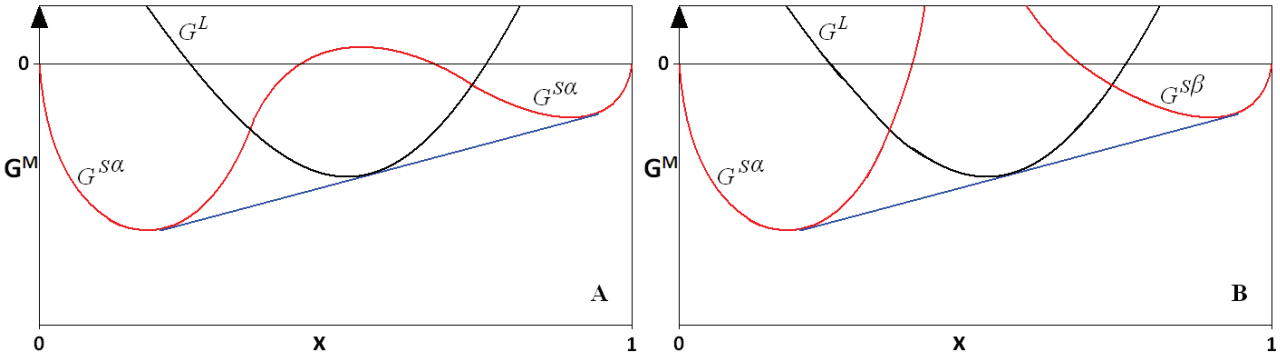

Figure 5.1: Qualitative Gibbs free energy of mixing at the solid-solid-liquid equilibrium, [65].
— : Gibbs energy for the solid phases (G^S); — : Gibbs energy for the liquid phase (G^L); — : tangent line.
A : Eutectic behavior by immiscibility gap in the continuous G^S;
B : Eutectic behavior by presence of two pure crystal lattices (α and β) with different Gibbs energy, $G^{S\alpha}$ and $G^{S\beta}$.

Yokozeki supported the idea that there are two kinds of eutectic behavior with reference to the form of G^S: a single continuous curve (case A) or two different curves $G^{S\alpha}$ and $G^{S\beta}$ for two different crystal lattices (case B). In case A, the immiscibility in the solid phase yielding the eutectic behavior occurs for an immiscibility gap in G^S of the same solid lattice. Conversely, in case B the liquid phase is in equilibrium with two different types of solid structures, α and β. In both cases the liquid

phase must be a homogeneous and continuous state, thus a single curve is always expected in the plots of Figure 5.1.

Yokozeki found binary interaction parameters for representing eutectic behaviors due to immiscibility gap (case A) for the systems indole+aromatics. Conversely, any value for the binary interaction parameters enabled Yokozeki to represent the eutectic point of the system benzene+cyclohexane.

He associated this failure to predict the solid-liquid behavior in the system benzene+cyclohexane to the presence of two different crystal lattices (case B). In order to overcome this problem, Yokozeki introduced a correction term in the fugacity expression of solid cyclohexane, [65].

It is interesting to notice that in the systems indole+aromatics the pure components present a discrete difference in terms of triple point temperatures; for instance, in the systems indole+1-methylnaphtalene, indole+benzene, and indole+biphenyl this difference is about 80, 50, and 20 degrees, respectively. At the same time, the immiscibility gap did not provide the eutectic behavior and two Gibbs energy of mixing ($G^{S\alpha}$ and $G^{S\beta}$) were considered for the system benzene+cyclohexane, components with almost the same triple point temperature.

To sum up, it seems that the higher is the difference between triple point temperatures of the mixture components the higher is the possibility of representing the eutectic behavior thanks to an immiscibility gap without introducing an additional solid structure, case B of Figure 5.1.

This fact could also be confirmed by the capability of the EoS in representing the eutectic behavior due to immiscibility gap in the $CH_4 + CO_2$ system. The difference between pure components triple point temperatures is about 130 degrees, and a single curve for the Gibbs energy of mixing in the solid phase allows the representation of the eutectic, [64].

Coming back to the mixing rules, in this work attempt has been made for representing the phase equilibrium behavior of the mixtures of interest with a unified EoS with parameters a_{mix}, b_{mix}, c_{mix}, and d_{mix} evaluated simultaneously for all the three phases of matter. Same values for the binary interaction parameters have been considered without making difference between the phases. As a consequence, at a fixed pressure and a subcritical temperature the SLV EoS is solved for obtaining the volumes for the three phases.

The mixing rules considered in this work are eq. (5.3) for a_{mix}, and similar expressions have been used for the volumetric parameters, eqs. (5.7)-(5.8). These mixing rules are quadratic functions of compositions and contain the parameters M_{ij}, N_{ij}, and L_{ij} defined as K_{ij} in eq. (5.3).

$$b_{mix} = \frac{1}{2}\sum_{i=1}^{N}\sum_{j=1}^{N}(b_i + b_j)(1 - M_{ij})x_i x_j \quad , \quad M_{ij} = \frac{m_{ij}m_{ji}(x_i + x_j)}{m_{ij}x_j + m_{ji}x_i} \quad , \quad M_{ii} = 0 \tag{5.7}$$

$$c_{mix} = \frac{1}{2}\sum_{i=1}^{N}\sum_{j=1}^{N}(c_i + c_j)(1 - N_{ij})x_i x_j \quad , \quad N_{ij} = \frac{n_{ij}n_{ji}(x_i + x_j)}{n_{ij}x_j + n_{ji}x_i} \quad , \quad N_{ii} = 0 \tag{5.8}$$

$$d_{mix} = \frac{1}{2}\sum_{i=1}^{N}\sum_{j=1}^{N}(d_i + d_j)(1 - L_{ij})x_i x_j \quad , \quad L_{ij} = \frac{l_{ij}l_{ji}(x_i + x_j)}{l_{ij}x_j + l_{ji}x_i} \quad , \quad L_{ii} = 0 \tag{5.9}$$

In the mixing rules presented above, N represents the number of component.

According to eqs. (5.7)-(5.9), each parameters Z_{ij} ($Z = M, N, L$) is a function of two binary interaction parameters, indicated by lowercase letters (k_{ij}, k_{ji}, m_{ij}, m_{ji}, n_{ij}, n_{ji}, l_{ij}, l_{ji}).

These mixing rules involve then 8 binary interaction parameters that can be evaluated for representing the phase equilibrium behavior in mixtures, and allows considering asymmetric values. Furthermore, the relation $k_{ii} = m_{ii} = n_{ii} = l_{ii} = 0$ holds.

As in eq. (5.3), when symmetric values are chosen for the couples ij and ji, the relation $Z_{ij} = z_{ij} = z_{ji}$ holds. As a consequence, the 8 binary interaction parameters reduce to 4.

Since pure compound parameters a_i, a_j, b_i, and b_j are functions of temperature, the temperature variations affect only a_{mix}, b_{mix} when fixed values are imposed for n_{ij}, and l_{ij}.

Nevertheless, it remains the possibility of introducing temperature functions for all the binary interaction parameters within eq. (5.3) and eqs. (5.7)-(5.9), keeping in mind that the resolution of the SLV EoS in terms of volumes in a mixture requires b_{mix}, < d_{mix}, < c_{mix}.

In a recent work, the solid-liquid vapor EoS with the Peng-Robinson and van der Waals attractive terms has been adopted for representing the phase equilibrium behavior in some binary mixtures of CO_2 and light hydrocarbons, [84].

In [84], the mixing rules in the form of eqs. (5.3)-(5.6) have been used, and the thermodynamic consistency test has been provided as supplementary material. This test has been verified also for the volumetric parameters in eqs. (5.7)-(5.9). Details have been reported in Appendix E.

The consistency test concerns both pressure and composition-dependent parameters within an EoS, and focuses on the consequences for thermodynamic properties obtained by derivation or integration of the functional forms. The aim of this test is to assure the absence of inconsistency between the Helmholtz energy and the pressure, which gives erroneous fugacity coefficients, partial molar enthalpies and partial molar volumes, [85].

5.2 Partial molar fugacity coefficients

As discussed in Chapter 3, the necessary and sufficient condition for equilibrium in a mixture is to achieve the global minimum in the Gibbs free energy of mixing. In the φ-φ approach, this makes each component in the mixture to present the same fugacity in all the phases.

The isofugacity condition of component i with reference to equilibrium phases α and β can be expressed as:

$$\hat{\varphi}_i^{\alpha} x_i^{\alpha} P = \hat{\varphi}_i^{\beta} x_i^{\beta} P \tag{5.10}$$

In eq. (5.10), P is the pressure, while x_i and $\hat{\varphi}_i$ are the composition and the partial molar fugacity coefficient of component i in the generic phase.

The partial molar fugacity coefficient of the i^{th} component in a phase α of composition $\bar{x}$ = {x_1, x_2, …, x_N}at temperature T and pressure P is given in eq. (5.11).

$$\ln \hat{\varphi}_i^{\alpha}(T, P, \bar{x}) = \left(\frac{\partial n a^{R,\alpha}}{\partial n_i}\right)_{T,nv,j\neq i} - \ln Z^{\alpha} \tag{5.11}$$

Eq. (5.11) requires the compressibility factor Z and the evaluation of the first derivative of the residual Helmholtz free energy with respect to the number of moles of component i, n_i. Introducing the expression of this derivative associated to the SLV EoS yields the following:

$$\begin{aligned}\ln \hat{\varphi}_i^{\alpha}(T, P, \bar{x}) = a^{R,\alpha} &+ \frac{1}{c-b}\left[\frac{b_i'(d-b)}{(v-b)} + \frac{c_i'(c-d)}{(v-c)}\right] - \frac{a_i'}{RTv} \\ &+ \left[\frac{c_i'(d-b) + d_i'(b-c) + b_i'(c-d)}{(c-b)^2}\right] \ln\left|\frac{v-b}{v-c}\right| - \ln\left|\frac{v}{v-b}\frac{v-d}{v-c} - \frac{a}{RTv}\right|\end{aligned} \tag{5.12}$$

It should be kept in mind that quantities within eq. (5.12) are all evaluated in the phase α.

Eq. (5.12) is related to the SLV EoS with the van der Waals attractive term, which corresponds to the EoS proposed by Yokozeki in [64].

Expression of the partial molar fugacity coefficient with generic values of q and r is provided in Appendix E together with the details of mathematical steps needed for obtaining eq. (5.12).

Eq. (5.12) involves the derivatives of the mixture parameters from eqs. (5.3) and (5.7)-(5.9) with respect to n_i. These derivatives are a_i', b_i', c_i', and d_i'.

Eqs. (5.13)-(5.14) shows the expressions of the derivatives of a_{mix} and b_{mix} in case of symmetric binary interaction parameters, while eqs. (5.15)-(5.16) are referred to the case of asymmetric values.

$$a_i' = \left(\frac{\partial n a_{mix}}{\partial n_i}\right)_{T,nv,j\neq i} = -a_{mix} + 2\left[a_i x_i + \sqrt{a_i a_j}(1-k_{ij})x_j\right] \tag{5.13}$$

$$b_i' = \left(\frac{\partial n b_{mix}}{\partial n_i}\right)_{T,nv,j\neq i} = -b_{mix} + 2b_i x_i + \left(b_i + b_j\right)(1-m_{ij})x_j \tag{5.14}$$

Correspondent expressions for the other two volumetric parameters have not be presented here seeing that c_{mix} and d_{mix} have the same form of b_{mix}. Nevertheless, these expressions are presented in Appendix E containing also the details of the derivation.

$$a_i' = \left(\frac{\partial n a_{mix}}{\partial n_i}\right)_{T,nv,j\neq i} = -a_{mix} + 2\left\{a_i x_i + \sqrt{a_i a_j}x_j\left[1 - K_{ij} - \frac{k_{ij}k_{ji}x_i x_j\left(k_{ij}-k_{ji}\right)}{\left(k_{ij}x_j + k_{ji}x_i\right)^2}\right]\right\} \tag{5.15}$$

$$b_i' = \left(\frac{\partial n b_{mix}}{\partial n_i}\right)_{T,nv,j\neq i} = -b_{mix} + 2b_i x_i + \left(b_i + b_j\right)x_j\left[1 - M_{ij} - \frac{m_{ij}m_{ji}x_j x_i\left(m_{ij}-m_{ji}\right)}{\left(m_{ij}x_j + m_{ji}x_i\right)^2}\right] \tag{5.16}$$

Once all the quantities in eq. (5.12) are defined, the partial molar fugacity coefficient in the generic phase α can be used for evaluating the Gibbs free energy of mixing in that phase, $G^{M\alpha}$. The relation between $\hat{\varphi}_i^{\alpha}$ and $G^{M\alpha}$ is:

$$G^{M\alpha}(T,P,\bar{x}) = \sum_i^N n_i RT \ln\frac{x_i\hat{\varphi}_i^{\alpha}(T,P,\bar{x})}{\varphi_i^0(T,P)} \tag{5.17}$$

At fixed temperature T, pressure P, and composition $\bar{x}$, mixture parameters are evaluated from eqs. (5.3) and (5.7)-(5.9), then the SLV EoS is solved in order to get the volumes. For each phase α, the first derivative of the residual Helmholtz and $\hat{\varphi}_i^{\alpha}$ are evaluated, followed by $G^{M\alpha}$ from eq. (5.17). It should be noted that in eq. (5.17), φ_i^0 is the fugacity coefficient of the pure component i at the same T and P in its stable phase.

Next section presents a schematic flow diagram of the algorithm developed for solving the problem of minimization of the Gibbs free energy of mixing.

5.3 Minimization of the Gibbs free energy of mixing

The details of the algorithm developed for the minimization the Gibbs free energy of mixing G^M in binary mixtures has been presented in Appendix E.

It is worth mentioning here the basic principles on which this algorithm has been developed, together with the main steps. Numerical methods are from [86].

First of all, let's consider the qualitative diagram of G^M in the range of compositions 0 – 1 in Figure 5.2. It refers to specific values of pressure and temperature.

In Figure 5.2, blue, black, and red lines are referred to the solid, liquid, and vapor phases, respectively.

The equilibrium phases are indicated by the points lying on the tangent line which does not cross the G^M curves of the phases in all the range of compositions 0 – 1.

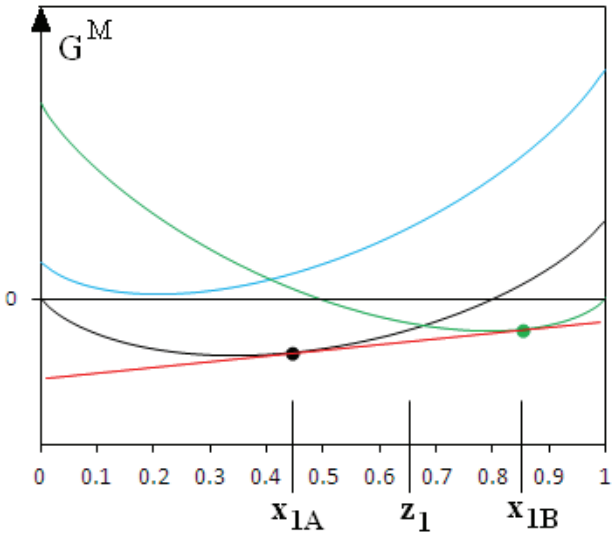

Figure 5.2: Qualitative Gibbs free energy of mixing for the solid, liquid, and vapor phases. G^M for the solid (—), liquid (—), and vapor (—); mole fractions of component 1 in the equilibrium phases (x_{1A} and x_{1B}); z_1 : global composition of the mixture; (—) :tangent line; ● : equilibrium vapor phase; ● : equilibrium liquid phase;

According to Figure 5.2, x_{1A} and x_{1B} are the mole fraction of component 1 in the liquid and in the vapor phase, respectively. z_1 is the mole fraction of component 1 in the global mixture composition.

In all these cases, the mole fraction of component 2 is 1 minus the mole fraction of component 1, thus the vectors of compositions are $\bar{x}_A = \{x_{1A}, x_{2A}\}$ for the liquid phase, $\bar{x}_B = \{x_{1B}, x_{2B}\}$ for the vapor phase, $\bar{z} = \{z_1, z_2\}$ for the global composition. In Figure 5.2, two values for the Gibbs free energy can be evaluated in $\bar{z}$. The first one is the Gibbs free energy of mixing in the stable phase at T and P, that is $G^{M\alpha}(T, P, \bar{z})$ from eq. (5.17). The second value is evaluated by the line passing across points $[x_{1A}, G^{M\alpha}(T, P, \bar{x}_A)]$ and $[x_{1B}, G^{M\alpha}(T, P, \bar{x}_B)]$, with $G^{M\alpha}(T, P, \bar{x}_A)$ and $G^{M\alpha}(T, P, \bar{x}_B)$ the Gibbs free energy of mixing in the stable phase at T and P, and $\bar{x}_A$ and $\bar{x}_B$, respectively.

$$G^M(T, P, \bar{z}) = G^M(T, P, \bar{x}_A) + (z_1 - x_{1A}) \frac{G^{M\alpha}(T, P, \bar{x}_B) - G^{M\alpha}(T, P, \bar{x}_A)}{x_{1B} - x_{1A}} \tag{5.18}$$

The binary mixture splits in the liquid and vapor phases of Figure 5.2 for a z_1 in the range $x_{1A} < z_1 < x_{1B}$, since in this range $G^M(T, P, \bar{z})$ from eq. (5.18) is lower than $G^{M\alpha}(T, P, \bar{z})$ from eq. (5.17).

The goal of the minimization of the G^M is to seek the equilibrium phases whose vector compositions, $\bar{x}_A$ and $\bar{x}_B$, give the lowest possible value of G^M in $\bar{z}$. The input values of the algorithm for the minimization of G^M are temperature T, pressure P, and the vector $\bar{z}$, thus the value of $G^{M\alpha}(T, P, \bar{z})$ is known from eq. (5.17). Two other steps are mainly involved, as illustrated in Figure 5.3.

The algorithm provides the stable equilibrium phases related to $\bar{z}$. It means that compositions x_{1A} and x_{1B} are modified in the range 0 - 1 in order to compare $G^{M\alpha}(T, P, \bar{z})$ with all the possible value of $G^M(T, P, \bar{z})$ from eq. (5.18). The fugacity coefficients of both components are evaluated at T and P considering the phase in which each of them is stable. This stable phase is ascertained comparing P and the equilibrium pressure of the pure component at T, as detailed in Appendix E.

The fugacity coefficients from the second step are needed in eq. (5.17) for evaluating G^M at T, P, for a generic vector of composition.

In the third step, two vectors of compositions are defined in the range $0 < x_1 < 1$. These vectors, here $\bar{x}_A$ and $\bar{x}_B$, are cycled in order to cover the entire range of composition, and each couple $(\bar{x}_A, \bar{x}_B)$ satisfying the relation $x_{1A} < z_1 < x_{1B}$ is modified in order to minimize the G^M in $\bar{z}$ as calculated from eq. (5.18).

In case of having $G^M(T, P, \bar{z}) < G^{M\alpha}(T, P, \bar{z})$, the system presents a local minimum in the Gibbs energy, and the global one is the lowest local minimum among all in the range $0 < x_1 < 1$.

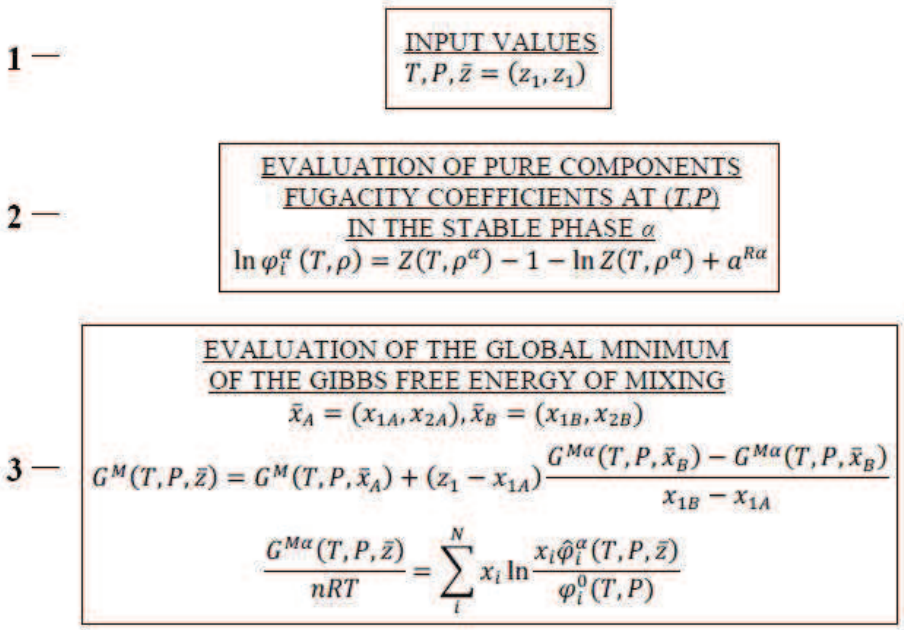

Figure 5.3: Main steps of the simplified version of the flow diagram related to the algorithm for the minimization of the Gibbs free energy of mixing.

5.4 Prediction of phase equilibria in binary mixtures

The algorithm developed for the minimization of the Gibbs free energy of mixing allows applying the SLV EoS for the representation of phase equilibria in binary mixtures. As discussed in the previous section, the algorithm makes use of the expressions of the fugacity coefficient for a pure component (presented in Chapter 4), of the partial molar fugacity of each component in the mixture, eq. (5.12), and the Gibbs free energy of mixing, eq. (5.17).

The functional form of the SLV EoS is the one with the attractive term of the van der Waals cubic EoS, [24], and the mixture parameters are evaluated from the binary mixtures in eq. (5.3) and eqs. (5.7)-(5.9).

This section focuses on the capability of the SLV EoS in predicting the phase equilibrium behavior in binary mixtures. Null binary interaction parameters have been considered in the mixing rules, and three among all the mixtures of interest have been considered: Ar + Kr, N_2 + O_2, and N_2 + N_2O.

The vapor-liquid equilibrium of the mixture Ar + Kr at 138 K is shown in Figure 5.4. Experimental values are from [87]. According to Figure 5.4, it can be stated that the prediction obtained from the SLV EoS is in a very good agreement with the experimental values.

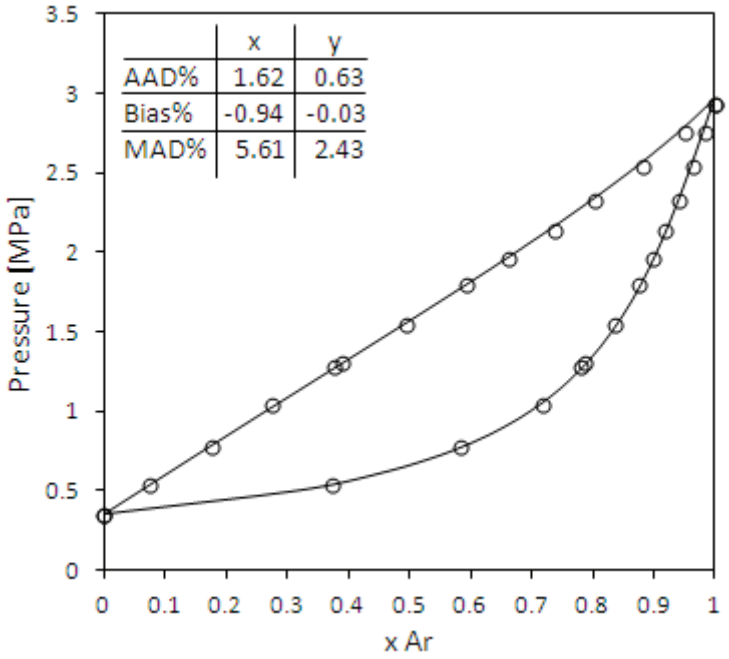

Figure 5.4: Vapor-liquid equilibrium at 138 K for the system Ar + Kr.
○ : data [87]; — : SLV EoS (k_{ij}=m_{ij}=n_{ij}=l_{ij}=*0*).

The Temperature-composition Cross Section (Tx-CS) concerning the solid-liquid equilibrium in the system Ar + Kr is shown in Figure 5.5. The prediction from the SLV EoS is at 1 MPa, value fixed since no information concerning the equilibrium pressures is given in [88], where experimental values refer only to the temperature, and the solid and liquid compositions.

The experimental values in Tx-CS of Figure 5.5 are representative of a solid solution, with a quasi-azeotropic behavior in the region of composition close to pure argon. Null binary interaction parameters do not allow representing the form of the solid-liquid equilibrium, which shows a peculiar shape.

The temperatures of the solidus curve from the SLV EoS are always greater that the experimental values in all the composition range. The liquidus curve slightly approaches the experimental values while reducing the content in argon, but the representation remains poor.

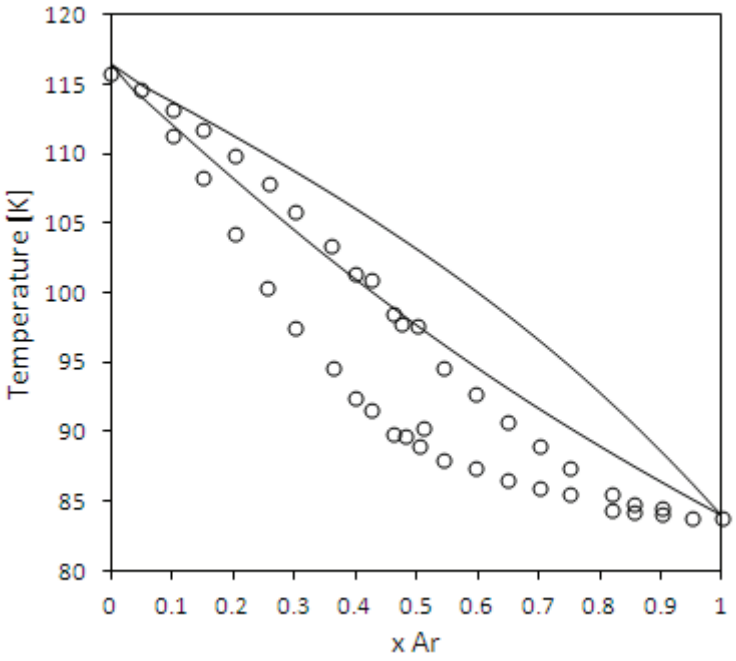

Figure 5.5: Solid-liquid equilibrium for the system Ar + Kr.
○ : data [88]; — : SLV EoS (k_{ij}=m_{ij}=n_{ij}=l_{ij}=*0*).

The experimental values for the vapor-liquid equilibrium at 100 K in the system N_2 + O_2, as presented in [89], are quite well predicted by the SLV EoS with null binary interaction parameters. In Figure 5.6, deviations are mostly concentrated in the oxygen-rich region, and bubble and dew lines from the model are at higher pressures than the experimental values.

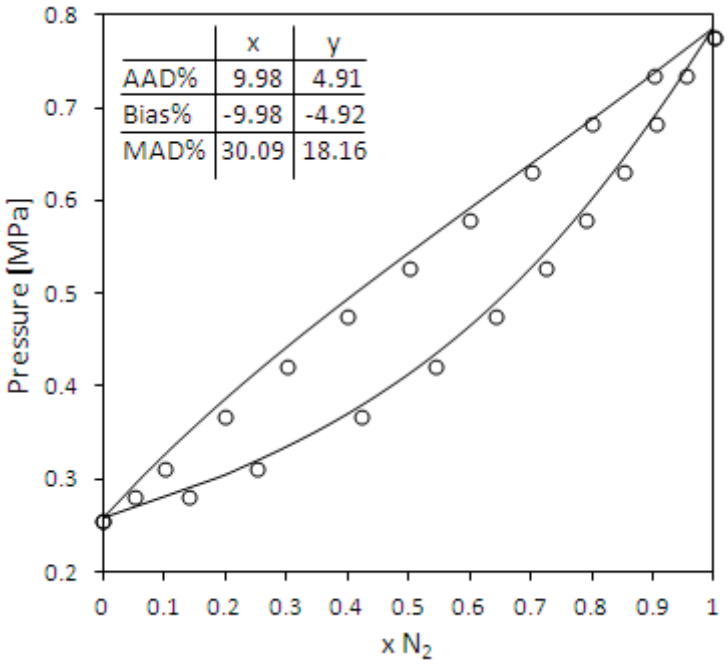

Figure 5.6: Vapor-liquid equilibrium at 100 K for the system N_2 + O_2.
○ : data [89]; — : SLV EoS (k_{ij}=m_{ij}=n_{ij}=l_{ij}=*0*).

The solid-liquid equilibrium for the system N_2 + O_2 is portrayed in the temperature-composition cross section of Figure 5.7. According to the experimental value in [90], this system presents an eutectic point at about 50 K, and the model is not in agreement with data. A solid solution is predicted

by the SLV EoS and the liquid is never stable at temperatures lower than the triple point temperature of pure oxygen (~54 K). As for the case of Ar + Kr, the prediction is made at 1 MPa.

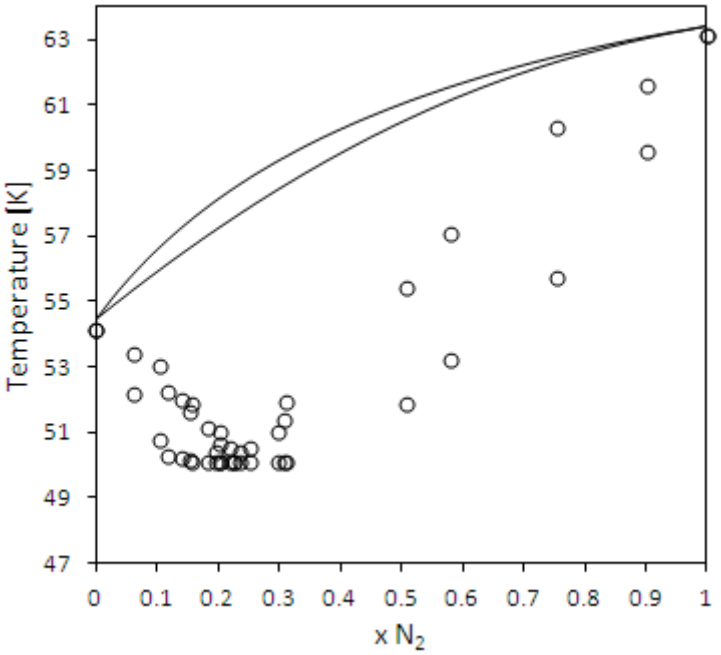

Figure 5.7: Solid-liquid equilibrium for the system $N_2 + O_2$.
○ : data [90]; — : SLV EoS ($k_{ij}=m_{ij}=n_{ij}=l_{ij}=0$).

Figure 5.8 is the Pressure-composition Cross Section (Px-CS) at 253 K for the system $N_2 + N_2O$. The predicted vapor-liquid equilibrium extends at pressures greater than the experimental values, and the predicted critical pressure is at about 17.4 MPa. Experimental values are from [91].

In opposition to what observed for the systems $N_2 + O_2$ and Ar + Kr, in this case the representation of the vapor-liquid equilibrium is not at all satisfactory.

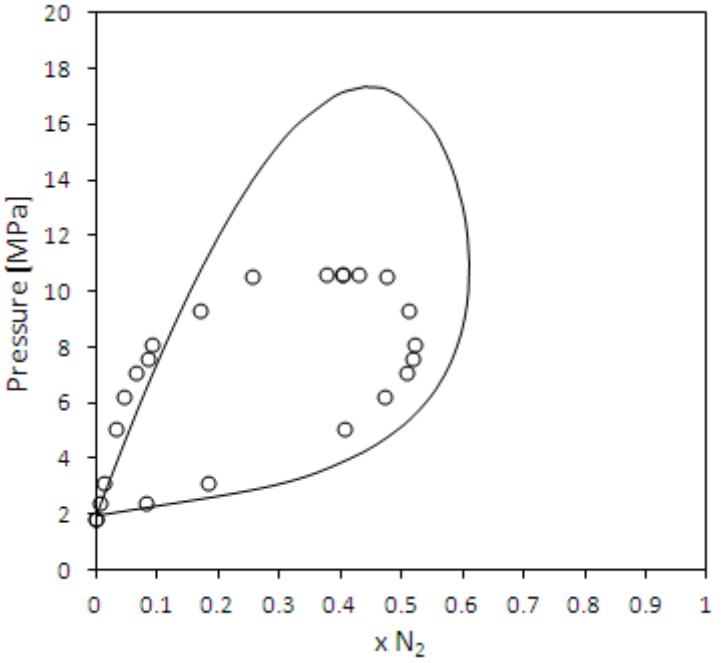

Figure 5.8: Vapor-liquid equilibrium at 253 K for the system $N_2 + N_2O$.
○ : data [91]; — : SLV EoS ($k_{ij}=m_{ij}=n_{ij}=l_{ij}=0$).

Figure 5.9 illustrates the solubility of N_2O in liquid N_2 at 4.05 MPa. Experimental values are from [92], and the x-axis in the Tx-CS is the logarithm of the solubility. Unlike the systems $N_2 + O_2$ and Ar + Kr, in this case the prediction of the solubility is almost satisfactory, considering that the x axis represents the logarithm of the mole fraction of N_2O in the liquid phase rich in N_2.

For instance, the experimental solubility of the mole fraction of N_2O at 85, 100, and 115 K is respectively 1.48×10^{-4}, 6.17×10^{-4}, and 1.72×10^{-3}, while the correspondent predicted values are 2.37×10^{-5}, 1.17×10^{-4}, and 4.47×10^{-4}.

In addition to that, the composition of N_2 in the solid phase, in equilibrium with the liquid phase in Figure 5.9, is close to zero, and the SLV EoS predicts a solid-solid immiscibility at lower temperatures.

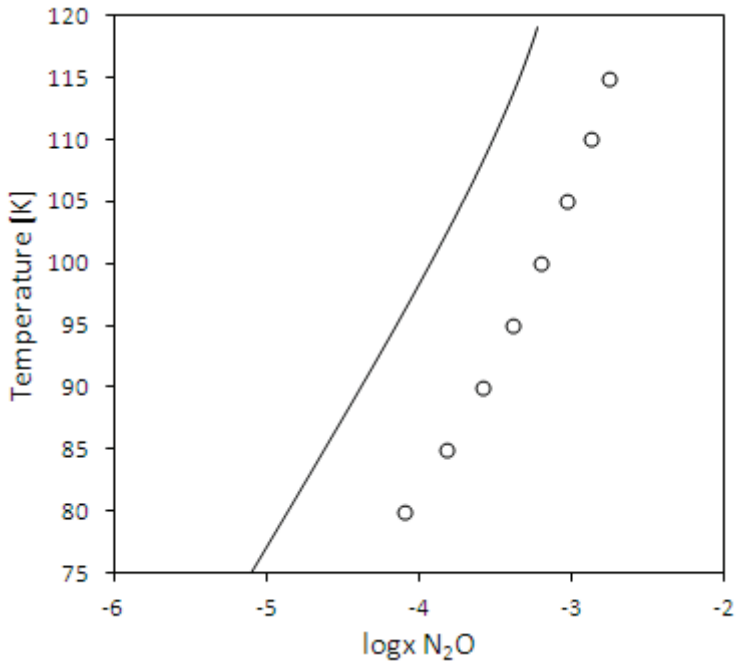

Figure 5.9: Solid-liquid equilibrium for the system $N_2 + N_2O$.
○ : data [92]; — : SLV EoS ($k_{ij}=m_{ij}=n_{ij}=l_{ij}=0$).

The comparisons in Figure 5.4-Figure 5.9 between experimental and predicted values underlines a discrete capability of the SLV in representing vapor-liquid equilibria in the considered systems. It is worth specifying that the equilibrium in Figure 5.8 involves a liquid and a supercritical phase, seeing that 253 K is greater than the critical temperature of pure nitrogen.

With reference to the solid-liquid equilibria, it can be stated that the SLV EoS with null binary interaction parameters fails in matching the kind of behavior in the pressure-composition cross section of the system $N_2 + O_2$, while compositions of the heaviest component are overestimated for the other two systems here treated.

Nevertheless, the experimental values for the solubility of N_2O in liquid N_2, which order of magnitude is around 7×10^{-4} in the range 80-115 K, seem to suggest the presence of a partial or total immiscibility in the solid phase, immiscibility confirmed by the prediction.

Same behavior has been established in [90] for the system $N_2 + O_2$, but the model is far away to predict that the kind of solid-liquid equilibrium.

According to this analysis, it can be supposed that the relevant difference in the capability of predicting the solid-liquid equilibrium for the systems $N_2 + O_2$ and $N_2 + N_2O$ could be somehow associated to the reciprocal position of the pure components in the pressure-temperature equilibrium projection, Figure 5.10.

Figure 5.10 represents the saturation lines of the pure components N_2, O_2, and N_2O. The green line starts in the triple point of nitrogen (63 K, 0.012 MPa), ending in its critical point (126 K, 3.4

MPa). The saturation line of oxygen is the black one origination at 54 K and 1.5×10^{-4} MPa, and ending at 154 K and 5 MPa.

Finally the triple point of nitrous oxide (182 K, 0.088 MPa) and its critical point (309 K, 7.2 MPa) are joined by the red line.

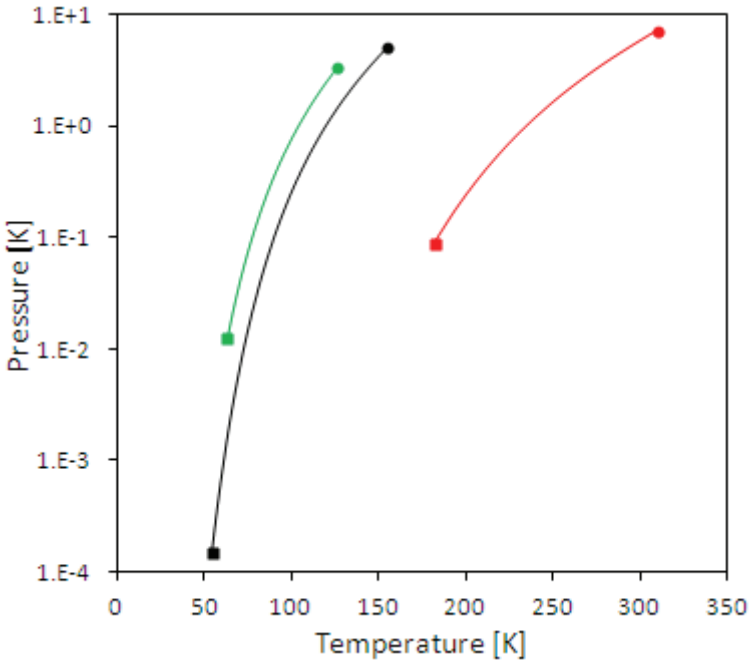

Figure 5.10: Saturation lines of N_2, O_2, and N_2O.
— : nitrogen; — : oxygen; — : nitrous oxide;
Triple points: N_2 (■),O_2 (■), N_2O (■);
Critical points: N_2 (●), O_2 (●), N_2O (●).

The prediction of a probably immiscibility, probably since no experimental values are available for the liquid of a second solid phase, occurs for the system N_2 + N_2O, whose pure components have an important difference in triple and critical point coordinates, especially in terms of temperatures.

Prediction of the solid-liquid equilibrium is totally unsatisfactory for the system N_2 + O_2; the saturation lines of these two components are closer than in the case of N_2 + N_2O, thus a possible explanation for the failure in the prediction can be the similar values for the triple and critical points.

Except for the case Ar + Kr, it appears that discrete variations should be introduced in the binary interaction parameters for keeping a good representation of the equilibria occurring at high temperatures, as in the case of the N_2 + O_2 system, and improving the representation of equilibria occurring in the dense region.

At the same time, in cases like the N_2 + N_2O system, these variations should improve the representation of the high temperature equilibria keeping the representation of low temperature equilibria.

It can then be stated that discrete variations may be considered for the binary interaction parameters in order to represent equilibria among the solid, liquid, and vapor phases in a wide range of temperature and pressure.

Figure 5.4-Figure 5.9 indicate however that null binary interaction parameters cannot provide predictions quantitatively in agreement with experimental values, thus a regression of the parameters needs to be considered.

The algorithm proposed for tuning the binary interaction parameters rests on the algorithm developed for the minimization of the Gibbs free energy of mixing, briefly introduced in section 5.3 and detailed in Appendix E.

In this second algorithm, the binary interaction parameters are tuned minimizing the objective function, fob^{MIX}, presented in eq. (5.19) as the sum of five other objective functions. fob^{MIX} is based on the comparison of the equilibrium temperatures and composition for the Solid-Liquid (SLE), Solid-Vapor (SVE), Vapor-Liquid (VLE), Solid-Solid-liquid (SSLE), and Solid-Liquid-Vapor (SLVE) equilibria.

$$fob^{MIX} = fob^{SLE} + fob^{SVE} + fob^{VLE} + fob^{SSLE} + fob^{SLVE} \tag{5.19}$$

Each term on the right hand side of eq. (5.19) is a function of the absolute value of the percentage deviation with respect to the equilibrium temperature and the absolute errors between experimental and calculated mole fractions. For instance, fob^{SLE} for the SLE is:

$$fob^{SLE} = \sum_{i}^{N_{SLE}} \left\{ 100 \left| \frac{T_{i,EoS} - T_{i,exp}}{T_{i,exp}} \right| + \left| x^{S}_{i,EoS} - x^{S}_{i,exp} \right| + \left| x^{L}_{i,EoS} - x^{L}_{i,exp} \right| \right\} \tag{5.20}$$

In eq. (5.20), N_{SLE} is the number of experimental values used in the regression procedure; T is the solid-liquid equilibrium temperature; x^S and x^L are the compositions of the solid phase and of the liquid phase, respectively. Indexes *EoS* and *exp* indicate SLE properties calculated by the SLV EoS and experimental values, respectively. Analogues expressions have been used for fob^{SVE}, fob^{VLE}, fob^{SSLE}, and fob^{SSVE}.

5.5 Mixtures of interest: data assessment

The regression of binary interaction parameters requires experimental values, and this section provides an analysis on the available data for the mixtures of interest in this work.

As anticipated in Chapter 1, null binary interaction parameters have been considered for the binary mixtures of impurities, thus the regression involves only 42 mixtures.

Table 5.1 portrays these 42 binary mixtures: the first column shows the most volatile component in the mixture, whose triple and critical point temperatures are in columns 2-3, respectively. Same properties for the heaviest component in the mixture are given in columns 4-5. In Table 5.1, 1 and 2 refer to the most volatile and less volatile component, respectively, considering the most volatile the one with the lowest critical temperature.

The range of temperatures (ΔT^{FFE}) for the available Fluid-Fluid Equilibrium (FFE) data are indicated in columns 6; critical point data and FFE data at temperature $T > T_{c2}$ have not been considered. Columns 7-8 refer to the Solid-Fluid Equilibrium (SFE) data; the correspondent ranges of temperature (ΔT^{SFE}) are in column 7, whereas the check marks in column 8 are related to data involving the composition in the solid phase x_S.

First of all, any data is available for the mixtures: Ar+N_2O, Ar+C_2H_4, and Ar+C_3H_8.

Literature experimental values concerning the FFE are available for almost all the binary mixtures in Table 5.1. Lack of FFE data is encountered for the mixtures: N_2+Xe, O_2+Xe, H_2+O_2, O_2+C_3H_6, and Ar+Xe.

For each mixture within Table 5.1, column 6 gives the interval of temperature covered by the experimental values. This range of temperature in most the cases is only a part of the wide range of temperature extending from the triple point temperatures up to the critical point temperatures of the components.

The range of T where the mixture is expected to be present, of course depending on the conditions of pressure and composition, in a fluid phase can be estimated as ranging from the lowest triple point temperature between the two components, up to the highest critical temperatures of the two components.

For instance, the system N_2+O_2 is then supposed to present equilibria involving fluid phases in the range $\min[T_{t1},T_{t2}] < T < \max[T_{c1},T_{c2}]$, namely 54.36 K < T < 154.58 K.

Table 5.1: Temperature ranges of the available experimental values of fluid-fluid and solid-fluid equilibria for the mixtures of interest in this study.

Mixture	T_{t1}	T_{c1}	T_{t2}	T_{c2}	ΔTFFE [K]	ΔTSFE [K]	x_S
N_2+O_2	63.15	126.19	54.36	154.58	60-148	50 – T_{t1}	✓
N_2+Ar	63.15	126.19	83.81	150.69	71- 134	T_{t1} – T_{t2}	✓
N_2+Kr	63.15	126.19	115.76	209.48	100 - 125	70 – T_{t2}	
N_2+Xe	63.15	126.19	161.41	289.73		91 – T_{t2}	
Ne+N_2	24.56	44.49	63.15	126.19	66-121		
He+N_2	2.18	5.19	63.15	126.19	64-126	T_{t2} – 375	
N_2+CO_2	63.15	126.19	216.59	304.12	209-303	T_{t1} – 273	
H_2+N_2	13.96	33.15	63.15	126.19	64-124	25 – T_{t2}	✓
N_2+N_2O	63.15	126.19	182.33	309.52	213-303	T_{t1} – 140	
N_2+CH_4	63.15	126.19	90.69	190.56	82-190	T_{t1} – T_{t2}	✓
N_2+C_2H_6	63.15	126.19	90.35	305.32	93-302	70 – 86	
N_2+C_2H_4	63.15	126.19	103.99	282.35	120-268	69 – 90	
N_2+C_3H_8	63.15	126.19	85.48	369.83	92-350	65 – 101	
N_2+C_3H_6	63.15	126.19	87.95	364.21	78-296	71 – 91	
Ar+O_2	63.15	126.19	54.36	154.58	84-140	T_{t1} – T_{t2}	✓
O_2+Kr	54.36	154.58	115.76	209.48	77-137	53 – 117	
O_2+Xe	54.36	154.58	161.41	289.73		80 – T_{t2}	
Ne+O_2	24.56	44.49	54.36	154.58	63-152		
He+O_2	2.18	5.19	54.36	154.58	65-143		
O_2+CO_2	54.36	154.58	216.59	304.12	218-298	67 – 110	
H_2+O_2	13.96	33.15	54.36	154.58		21 – 55	
O_2+N_2O	54.36	154.58	182.33	309.52	213-293	91 – 113	
O_2+CH_4	54.36	154.58	90.69	190.56	93-153	67 – T_{t2}	
O_2+C_2H_6	54.36	154.58	90.35	305.32	112-139	T_{t1} – 100	
O_2+C_2H_4	54.36	154.58	103.99	282.35	110-140	78 – 90	
O_2+C_3H_8	54.36	154.58	85.48	369.83	110-140	73 – 83	
O_2+C_3H_6	54.36	154.58	87.95	364.21		67 – 92	
Ar+Kr	83.81	150.69	115.76	209.48	88-193	T_{t1} – T_{t2}	✓
Ar+Xe	83.81	150.69	161.41	289.73		81 – 85	
Ne+Ar	24.56	44.49	83.81	150.69	84-138	96 – 123	
He+Ar	2.18	5.19	83.81	150.69	84-150	68 – 86	
Ar+CO_2	83.81	150.69	216.59	304.12	233-299	109 – 116	
H_2+Ar	13.96	33.15	83.81	150.69	84-141	68 – 79	
Ar+N_2O	83.81	150.69	182.33	309.52			
Ar+CH_4	83.81	150.69	90.69	190.56	91-179	70 – T_{t2}	✓
Ar+C_2H_6	83.81	150.69	90.35	305.32	81-116		
Ar+C_2H_4	83.81	150.69	103.99	282.35			
Ar+C_3H_8	83.81	150.69	85.48	369.83			
Ar+C_3H_6	83.81	150.69	87.95	364.21	74-150		
Kr+Xe	115.76	209.48	161.41	289.73	125-270	122 – 158	
Ne+Xe	24.56	44.49	161.41	289.73	163-289	380 – 450	
He+Ne	2.18	5.19	24.56	44.49	25-42	13 – 21	

T_{min} = min[T_{t1},T_{t2}] and T_{max} = max[T_{c1},T_{c2}] have been evaluated for each of the 33 mixtures in Table 5.1 with available FFE data.

With reference to these 33 mixtures, it has been observed that only 7 mixtures (~21%) have experimental values covering the range of temperature $T_{min} < T < T_{max}$ for more than the 80%. Examples are the mixtures N_2+O_2 and Ar+CH_4, whose intervals of experimental temperature of FFE practically cover the whole range $T_{min} < T < T_{max}$.

Continuing with this analysis, the experimental temperatures of FFE cover from the 60% up to the 80% of the range $T_{min} < T < T_{max}$ for 4 mixtures (~12%): N_2+Ar, N_2+C_2H_4, N_2+C_3H_8, and Ne+O_2. For 10 mixtures (~30%) binary interaction parameters can be regressed with reference to the FFE in a range of temperature covering from the 40% up to the 60% of the range $T_{min} < T < T_{max}$. Among others, this is the case of the mixture Ar+O_2, H_2+N_2, and Ne+Ar.

7 mixtures (~21%) have experimental values of FFE temperatures ranging in an interval representing from 20% up to 40% of the range $T_{min} < T < T_{max}$. Examples are the systems Ar+CO_2, N_2+CO_2, and O_2+N_2O. Finally, for 5 mixtures (~15%) the experimental temperatures of FFE cover less than the 20% of the range $T_{min} < T < T_{max}$.

With reference to the experimental values concerning the SFE, from column 8 in Table 5.1 it clearly appears that the solid composition at equilibrium is rarely available in the literature. In addition to that, lack of SFE data is encountered for the systems: Ne+N_2, Ne+O_2, He+O_2, Ar+C_2H_6, Ar+C_3H_6, together with the mixtures Ar+N_2O, Ar+C_2H_4, and Ar+C_3H_8, for which any FFE or SFE data is available.

As pointed out in column 7 of Table 5.1, there are cases showing a restricted range of temperatures of SFE. For instance, the systems O_2+N_2O, N_2+C_2H_6, O_2+C_2H_4, O_2+C_3H_8, and Ar+Ke have experimental values of SFE for temperature ranges of 22, 16, 12, 10, and 4 degrees, respectively.

The main problems concerning the available SFE experimental values is the composition in the solid phase, which remains unknown in the majority of the mixtures presented in Table 5.1.

This fact could entail the possibility of regressing the binary interaction parameters without care about the composition in the solid phase, thus the SLV EoS with regressed interaction parameters could yield unphysical behavior concerning the solid phase in the solid-liquid equilibrium.

As a consequence, considering only the available experimental values for the liquid phase at SFE for the regression of the parameters could then cause the SLV EoS representing the liquid compositions by a solid solution, as well as an eutectic or an azeotrope, especially for cases where the experimental liquid composition does not cover the whole range of composition $0 < x < 1$.

In addition to that, it should be also remembered that the predictions of the model are hardly in agreement with the real behavior of SFE, as presented in section 5.4.

In order to overcome these drawbacks, the SLV EoS has been applied for the representation of binary Lennard-Jones mixtures, as explained in section 5.6.

5.6 Application of the SLV EoS to Lennard-Jones mixtures

The Solid-Fluid Equilibria (SFE) for mixtures involved in cryogenic processes like air distillation and natural gas treatment are poorly investigated from the experimental point of view with respect to the Fluid-Fluid Equilibria (FFE). In addition to that, compositions in the solid phase are rarely available.

The cryogenic air distillation process involves mainly the binary mixture in Table 5.1. These are mixtures of small molecules, which behaviors are characterized by partial or total solubility in the solid phase. It follows that several type of solid-liquid phase diagrams can be formed by these molecules, like solid solutions, eutectic with partial miscibility, or solid-liquid azeotrope.

The combination of these two factors, lack of experimental data from one side, variety of phase equilibrium behaviors from the other side, hinders sometimes the possibility of clearly identifying the type of solid-liquid phase diagram for these molecules.

Nevertheless, the phase behavior of molecules like argon, krypton, xenon, and methane, usually involved in cryogenic processes like air distillation, is well approximated by molecular simulation

of Lennard-Jones (LJ) molecules. LJ fluids have then been considered as very good approximations of the real "simple" molecules objective of this study.

The following sections present the application of the SLV EoS for the representation of phase equilibria in binary mixtures of LJ fluids. Details have been published in [93].

The LJ potential has been described in section 5.6.1. Section 5.6.2 presents the Lennar-Jones Solid-Liquid-Vapor Equation of State (LJ-SLV EoS) used for representing phase equilibria in LJ mixtures; this EoS is a modified version of the SLV EoS proposed by Yokozeki in [64].

Parameters of the LJ-SLV EoS have been regressed for representing the pressure-temperature equilibrium behavior of a pure LJ fluid, as demonstrated in section 5.6.3. Section 5.6.4 shows the application of the LJ-SLV EoS with regressed binary interaction parameters for the representation of phase equilibria in binary mixtures of LJ fluids. Binary interaction parameters have been obtained as functions of the LJ parameters, as illustrated in section 5.6.4.1.

This entails the possibility of evaluating the binary interaction parameters within the EoS starting from the LJ parameters of pure real fluids, and the interaction parameters calculated in such a way have been applied for the prediction of Solid-Liquid Equilibrium (SLE) behavior in real systems of simple molecules, section 5.6.5.

5.6.1 Lennard-Jones potential

In the framework of statistical mechanics, the potential function describing the interaction between molecules can be used for deriving the connection between micro and macroscopic properties in a substance.

One of the most frequently used models in dealing with the molecular interaction in simple fluids of nonbonding atoms is the well-known 12-6 Lennard-Jones (LJ) potential, given by:

$$u_{ij}(r) = 4\varepsilon\left[\left(\frac{\sigma_{ij}}{r}\right)^{12} - \left(\frac{\sigma_{ij}}{r}\right)^{6}\right] \tag{5.21}$$

where ε is the depth of the potential, σ is the distance at which the potential is zero, i and j are two generic particles at the intermolecular distance r, and u_{ij} is the potential interaction energy. The LJ potential in eq. (5.21) is qualitatively portrayed in Figure 5.11.

According to eq. (5.21) and Figure 5.11, the LJ potential involves two contributions: the repulsive and the attractive potentials. The repulsive potential goes with the 12th power of the intermolecular distance (A/r^{12}), whereas the attractive one is a function of the 6th power of r (B/r^{12}).

The attractive potential is a long-range term describing attractions at long ranges, as the van der Waals and dispersion forces.

The term van der Waals forces include forces other than those due to covalent bonds or the electrostatic interaction of ions, namely forces between permanent dipoles, forces between a permanent and a induced dipole, and forces between two induced dipoles.

The LJ potential is a function of the distance r between particles i and j. For $r \to \infty$, the particles are so far away that the potential of interaction is practically zero, or at least close to zero.

For decreasing r the particles come

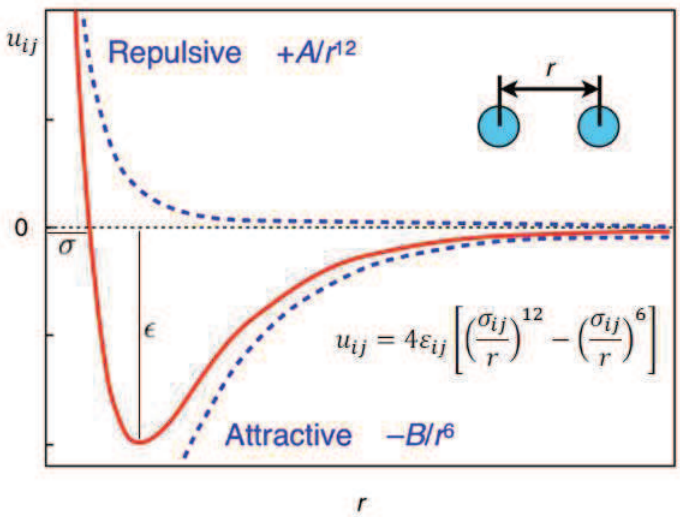

Figure 5.11: Lennard-Jones intermolecular potential. u_{ij} : LJ potential: ε_{ij} : LJ well depth; σ_{ij} : LJ diameter.

closer so that they can reach a distance at which they interact, and the potential energy of interaction becomes negative decreasing from zero.

The distance between the particles is still decreased by the attractive forces until the particles reach an equilibrium distance, which represents the value of r where the minimum potential energy (u_{ij} = - ε) is reached. The lower is ε the stronger the interaction between the particles i and j.

If the distance between the two particles is reduced from the equilibrium position, the repulsive forces begin to rapidly increase due to the overlapping of the electron orbitals. The LJ potential rapidly rises as r approaches zero under the equilibrium value.

The parameter σ is also known as the LJ diameter since it gives a measurement of how close two nonbonding particles can get before having a positive intermolecular potential energy.

5.6.2 Functional form of the LJ-SLV EoS

With the aim of challenging the SLV EoS in the representation of phase diagrams for binary mixtures of Lennard-Jones fluids, the functional form of the EoS proposed by Yokozeki in [64] has been rewritten in terms of reduced variables:

$$P^* = \frac{T^*}{v^* - b^*}\frac{v^* - d^*}{v^* - c^*} - \frac{a^*}{v^{*2}} \tag{5.22}$$

where:

$$P^* = \frac{P\sigma^3}{\varepsilon} \qquad T^* = \frac{k_B T}{\varepsilon} \qquad z^* = \frac{z}{N_A\sigma^3},\ z = v, b, c, d \qquad a^* = \frac{a}{N_A^2\varepsilon\sigma^3} \tag{5.23}$$

Eq. (5.22) is the Lennard-Jones Solid-Liquid-Vapor Equation of State (LJ-SLV EoS) which can easily be obtained from the SLV EoS (with $q = r = 0$) substituting the expressions for the reduced variables, eq. (5.23), and considering the gas constant $R = N_A k_B$. N_A is the Avogadro number, and k_B is Boltzmann constant. ε and σ are respectively the well depth and the collision diameter in the LJ potential.

The derivation of eq. (5.22) from the SLV EoS is presented in Appendix E.

Parameters $a^*$and b^* are functions of temperature, as in the original SLV EoS:

$$a^*(T^*) = a_0 + a_1 T^* exp(-a_2 T^{*n}) \qquad b^*(T^*) = b_0 + b_1 exp(-b_2 T^{*m}) \tag{5.24}$$

where a_0, a_1, a_2, n, b_0, b_1, b_2, and m are adjustable parameters, whose regression for the pure LJ fluid is presented in next section.

5.6.3 Phase diagram of the LJ fluid from the LJ-SLV EoS

In [93], parameters of the SLV EoS in reduced variables, eqs. (2), (4), and (5), have been regressed for reproducing analytically the temperatures and pressures of the critical and triple point of the pure LJ fluid. Temperature and pressure values at the critical point were taken from [94]: $T_c^* = 1.31$ and $P_c^* = 0.126$. Temperature and pressure values at the triple point were taken from [95]: $T_t^* = 0.692$ and $P_t^* = 1.21 \times 10^{-3}$.

Parameters of eqs. (5.22) and (5.24) have been regressed in order to represent saturation, melting, and sublimation equilibrium values of the LJ fluid.

Reduced pressure for vapor-liquid equilibrium data of the pure LJ fluid were produced using eq. (5.25), [94].

$$\ln P_{VLE}^* = 1.2629T^* - \frac{4.8095}{T^*} - \frac{0.15115}{T^{*4}} \tag{5.25}$$

Reduced pressure for solid-liquid and solid-vapor equilibrium data of the pure LJ fluid were taken from [95]. Parameters of eqs. (5.22) and (5.24) have been obtained minimizing an objective function based on the isofugacity condition.

The objective functions has been presented by Stringari and Campestrini in [93], and here not reported for sake of simplicity.

A maximum reduced temperature of about 1.8 has been chosen within the regression as limiting value for the melting line.

The pure LJ parameters of eqs. (5.22)-(5.24) obtained in such a way are summarized in Table 5.2, [93].

Table 5.2: Parameters of the LJ-SLV EoS in reduced variables.

Parameter	Value	Unit
a_0	0.23965	
a_1	467.0981	
a_2	4.34036	
n	0.30353	
b_0	1.27853	
b_1	-0.32365	
b_2	1.99173	
m	1.39554	
c^*	1.33224	
d^*	1.29463	
N_A	$6.022141793 \times 10^{23}$	mol^{-1}
k_B	$1.380648813 \times 10^{-23}$	J/mol

Figure 5.12 presents the qualitative comparison between literature data of VLE, [94], SLE and SVE, [95], and values calculated for the LJ fluid with the LJ-SLV EoS, eq. (5.22). The quantitative deviations in terms of AAD% are: 0.82% (VLE), 1.31% (SVE), and 3.36% (SLE). These AAD% refer to deviations between equilibrium pressures calculated at imposed temperature and pressure from [94] and [95].

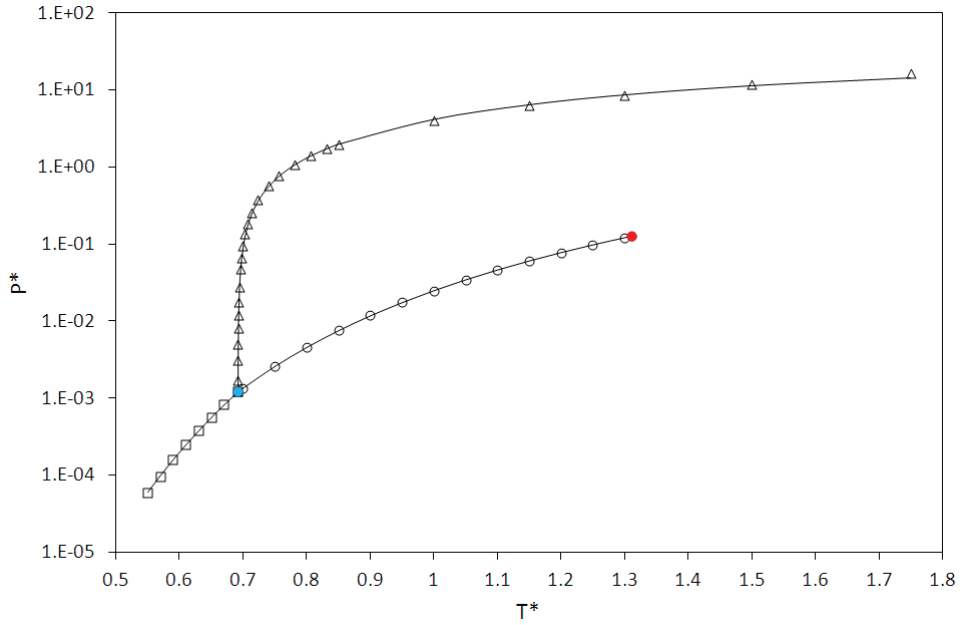

Figure 5.12: Reduced pressure, P*, versus reduced temperature, T*; diagram for the pure LJ fluid.
Symbol represent literature molecular simulation results: ○ : VLE [94]; □ : SVE [95]; Δ : SLE [95]; ● : critical point [94]; ● : triple point [95]; — : LJ-SLV EoS model, eq. (5.22).

5.6.4 Phase diagram of binary LJ mixtures from the LJ-SLV EoS

Several phase diagrams for binary mixtures of LJ fluids were produced using Monte Carlo (MC) simulation for diameter ratios ranging from 0.85 to 1, and well-depth ratios ranging from 0.625 to 1.6 for a reduced pressure P* = 0.002, [96].

Three types of solid-liquid equilibria are encountered in these ranges of σ and ε: solid solutions, solid-liquid azeotrope, and eutectic with partial immiscibility.

In [93], the capability of the LJ-SLV EoS of reproducing the phase diagrams in [96] has been investigated, considering null and regressed binary interaction parameters in the mixing rules.

This comparison allowed verifying the capability of the EoS in predicting qualitatively the phase behavior of binary LJ mixtures varying the ratios $\varepsilon_{11}/\varepsilon_{22}$ and σ_{11}/σ_{22}.

For representing the phase equilibrium of mixtures, the mixing rules in the form proposed in eqs. (5.3)-(5.6) have been used for the parameters a*, b*, c*, and d* in eq. (5.22).

As discussed in [93], the LJ-SLV EoS with null binary interaction parameters never predicts a liquid phase stable at temperatures lower than the lowest melting temperature of the pure solids for the whole range of $\varepsilon_{11}/\varepsilon_{22}$ and σ_{11}/σ_{22}.

This condition is necessary for having eutectic or solid–liquid azeotrope. In addition to that, the solid-solid miscibility is always over-estimated by the LJ-SLV EoS with null binary interaction parameters.

For representing qualitatively the evolution of the MC simulation phase diagrams, all the four interaction parameters in the mixing rules of eqs. (5.3)-(5.6) were used in [93].

This need can be related to the fact that the SLV EoS describes the solid phase as a high-density liquid phase, and mixing rules for the solid and the liquid phases have the same form. This may be the reason of the over-estimated miscibility in the solid phases.

For decreasing the mutual solubility of the solid phases, binary interaction parameters must then be used. As a consequence, the LJ-SLV EoS is mainly adapted to the representation of the phase equilibrium of small, simple molecules, showing partial or total solubility in the solid phases.

In [93], the comparison has been done for all the diagrams proposed in [96], while only two examples have been reported in this section, Figure 5.13. In Figure 5.13 the following reduced variables are used:

$$P^* = \frac{P\sigma_{11}^3}{\varepsilon_{11}} \quad , \qquad T^* = \frac{k_B T}{\varepsilon_{11}} \tag{5.26}$$

In eq. (5.26) ε_{11} refers to the interaction between the particles of the same fluid 1.

Figure 5.13 shows the phase diagrams for two binary LJ mixtures: the binary with $\varepsilon_{11}/\varepsilon_{22} = 1$ and $\sigma_{11}/\sigma_{22} = 0.85$ on the left, and the binary with $\varepsilon_{11}/\varepsilon_{22} = 0.625$ and $\sigma_{11}/\sigma_{22} = 0.9$ on the right.

Empty circles are data from [96], red lines are the LJ-SLV EoS with regressed binary interaction parameters.

A total of 11 binary LJ mixtures have been presented by Lamm and Hall in [96]; all of them have been treated in the framework of the comparison between the EoS and MC simulation data for LJ mixtures, as shown in [93].

With reference to the binary with $\varepsilon_{11}/\varepsilon_{22} = 1$ and $\sigma_{11}/\sigma_{22} = 0.85$ in Figure 5.13, the phase diagram obtained in [96] by MC simulation presents eutectic behavior, and the LJ-SLV EoS model with regressed binary interaction parameters allows representing the eutectic. The eutectic temperature is in agreement with the one predicted by MC simulation.

MC simulation presents two solid-liquid-vapor lines, with a solid-liquid azeotrope at low temperatures for the LJ mixture with $\varepsilon_{11}/\varepsilon_{22} = 0.625$ and $\sigma_{11}/\sigma_{22} = 0.9$. The LJ-SLV EoS in eq. (5.22) with regressed binary interaction parameters matches the temperatures at which the three phase equilibrium exists, together with the solid liquid azeotrope at low temperatures.

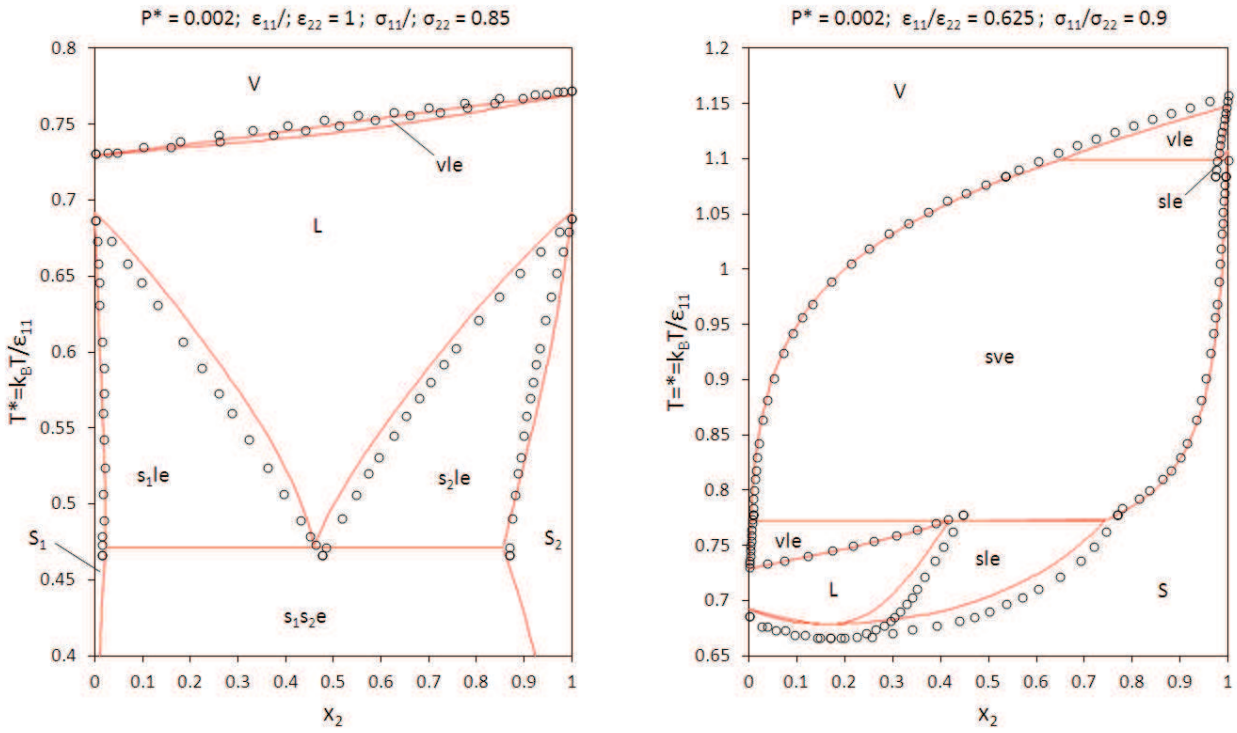

Figure 5.13: Temperature vs. composition phase diagrams for two LJ binary mixtures.
Left graph: $\varepsilon_{11}/\varepsilon_{22} = 0.625$ and $\sigma_{11}/\sigma_{22} = 0.85$; Right graph: $\varepsilon_{11}/\varepsilon_{22} = 0.625$ and $\sigma_{11}/\sigma_{22} = 0.9$. Both graphs are at P* = 0.002. ○ : molecular simulation results from [96]; — : LJ-SLV EoS with regressed binary interaction parameters.

In [93], regressed binary interaction parameters have been portrayed as function of the ratio $\varepsilon_{11}/\varepsilon_{22}$ and σ_{11}/σ_{22}. Here below are the cases for k_{ij}.

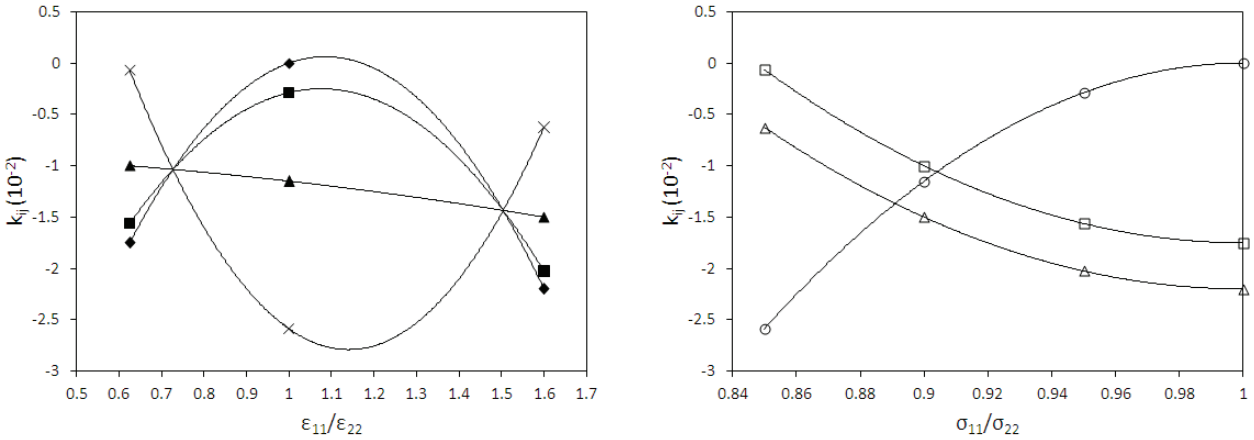

Figure 5.14: Dependence of the binary interaction parameter k_{ij} from $\varepsilon_{11}/\varepsilon_{22}$ and σ_{11}/σ_{22}.
(–×–):σ_{11}/σ_{22}= 0.85; (–▲–): σ_{11}/σ_{22}= 0.9; (–■–): σ_{11}/σ_{22}= 0.95; (–♦–):σ_{11}/σ_{22}= 1; (–Δ–): $\varepsilon_{11}/\varepsilon_{22}$= 1.6; (–◊–):$\varepsilon_{11}/\varepsilon_{22}$= 1; (—):$\varepsilon_{11}/\varepsilon_{22}$= 0.625; (—): correlations.

5.6.4.1 *Equation for the binary interaction parameters*

In [93], binary interaction parameters, k_{ij}, m_{ij}, n_{ij}, and l_{ij}, in the LJ-SLV EoS have been obtained as function of $\varepsilon_{11}/\varepsilon_{22}$ and σ_{11}/σ_{22}. Starting from these functions, eq. (5.27) has been successively formulated for calculating mathematically k_{ij}, m_{ij}, n_{ij}, and l_{ij}, for fixed values of $\varepsilon_{11}/\varepsilon_{22}$ and σ_{11}/σ_{22}.

$$z_{ij} = \sum_{t=1}^{3} \left(\frac{\varepsilon_{11}}{\varepsilon_{22}}\right)^{3-t} \left[A_{t1} + A_{t2}\left(\frac{\sigma_{11}}{\sigma_{22}}\right)^{2}\right] \tag{5.27}$$

For a fixed binary mixture, this equation allows evaluating a general binary interaction parameter, z_{ij} ($z_{ij} = k_{ij}$, m_{ij}, n_{ij}, and l_{ij}), knowing the two ratios $\varepsilon_{11}/\varepsilon_{22}$ and σ_{11}/σ_{22}, and the values of six coefficients (A_{11}, A_{12}, A_{21}, A_{22}, A_{31}, A_{32}). The values of these coefficients for each binary interaction parameter are resumed in Table 5.3. It is worth noting that using a single functional form, eq. (5.27), all the four binary parameters can be evaluated just changing the values of the coefficients.

In such a way, binary interaction parameters can be calculated directly introducing literature values for the pure compounds LJ parameters ε and σ in eq. (5.27).

Table 5.3: Coefficients for the calculation of the binary interaction parameters from LJ parameters.

Binary interaction parameter	A_{11}	A_{12}	A_{21}	A_{22}	A_{31}	A_{32}
k_{ij}	-0.08547	8.35897	0.18555	-18.6500	-0.10008	9.141
m_{ij}	0.01675	4.58119	-0.03522	-8.24440	0.01847	-0.537
n_{ij}	0.05504	3.29914	-0.13478	-8.16110	0.07974	8.412
l_{ij}	0.02530	4.49572	-0.06244	-11.4388	0.03714	8.093

LJ parameters ε and σ from literature have been used for some mixtures of interest in this work, thus the SLV EoS in the form proposed by Yokozeki has been applied to real systems of simple molecules, as presented in section 5.6.5.

5.6.5 Phase diagram of real binary mixtures from the SLV EoS and predicted binary interaction parameters

In previous section, an equation has been presented for calculating the binary interaction parameters from the ratios $\varepsilon_{11}/\varepsilon_{22}$ and σ_{11}/σ_{22}, then the EoS can be applied to mixtures of real "simple" fluids, like the fluids involved in the cryogenic air distillation process (mainly nitrogen, oxygen, noble gases, and light hydrocarbons), once the values of ε and σ are known.

For these fluids, especially noble gases and methane, Lennard-Jones approximation is representative of the real phase equilibrium behavior. Then, the SLV EoS can be applied to mixtures of these real fluids, allowing a prediction of phase equilibrium where experimental data are not available, and for setting starting values while regressing the binary interaction parameters of literature data. Nevertheless, this approach cannot be applied to complex molecules, like waxes and asphaltenes, which differ too much from the mono-atomic Lennard-Jones approximation.

In [97], the SLV EoS with null values for q and r has been applied for representing the solid-liquid equilibrium of a certain number of mixtures. Binary interaction parameters have been evaluated from eq. (5.27) with LJ parameters from Cuadros et al. [98].

In 1995, Cuadros et al. proposed a procedure to determine LJ parameters based on molecular dynamics computer simulation results and the Soave-Redlich-Kwong Equation of State (SRK EoS), [99]. Same authors included a function of temperature and acentric factor in the SRK EoS for extending the LJ model to non-spherical molecules thus obtaining the deviation of intermolecular potential from that of spherical molecules, [98]. As a result, in [98] LJ parameters are tabulated for spherical molecules (as Ar, Kr, and Xe) as well as for diatomic (as N_2, O_2, Cl_2) and multi-atomic molecules (as $C_{10}H_{22}$, $C_4H_{10}O_2$).

Figure 5.15-Figure 5.17 represent the temperature-composition phase diagram of solid-liquid equilibrium for the following binary mixtures: Ar + Kr, Ar + CH_4, and N_2 + Ar.

In Figure 5.15-Figure 5.17, experimental values are indicated by empty symbols, while lines represent values calculated by the SLV EoS using eqs. (5.3) to (5.6) for evaluating the mixture parameters.

The model with binary interaction parameters calculated from eq. (5.27) is represented as continuous lines. The model with null binary interaction parameters has been represented for comparison (dashed lines). The values of the binary interaction parameters obtained from eq. (5.27) and the corresponding ratios σ_{11}/σ_{22} and $\varepsilon_{11}/\varepsilon_{22}$ are indicated in Table 5.4 for the three mixtures.

Table 5.4: Binary interaction parameters for the mixtures Ar + Kr, Ar + CH_4, and N_2 + Ar calculated from LJ parameters.

Mixture	σ_{11}/σ_{22}	$\varepsilon_{11}/\varepsilon_{22}$	Calculated binary Interaction parameter ($\times 10^2$)			
			k_{ij}	m_{ij}	n_{ij}	l_{ij}
Ar – Kr	0.722	0.930	-1.0501	-1.8231	3.1784	1.5859
Ar – CH_4	0.796	0.902	-1.0427	-3.8966	4.5482	2.0943
N_2 – Ar	0.821	1.082	-0.8931	-2.7312	3.2438	1.4479

Figure 5.15 shows the isobaric equilibrium behavior for the mixture Ar + Kr. Experimental values are available for both the solid and the liquid equilibrium phases [88]. The solid phase for this system is a solid-solution with a quasi-azeotropic behavior where argon mole fraction approaches unity.

The SLV EoS with null binary interaction parameters (dashed lines) predicts a solid-solution phase diagram, but it is not able to predict the quasi-azeotropic behavior close to pure argon.

The values of σ_{11}/σ_{22} and $\varepsilon_{11}/\varepsilon_{22}$ obtained from the pure fluid literature values of σ and ε are 0.722 and 0.930, respectively. The binary interaction parameters obtained using these values in eq. (5.27) allow improving the qualitative representation of the solid-liquid equilibrium of Ar + Kr, predicting the quasi-azeotropic behavior close to pure argon.

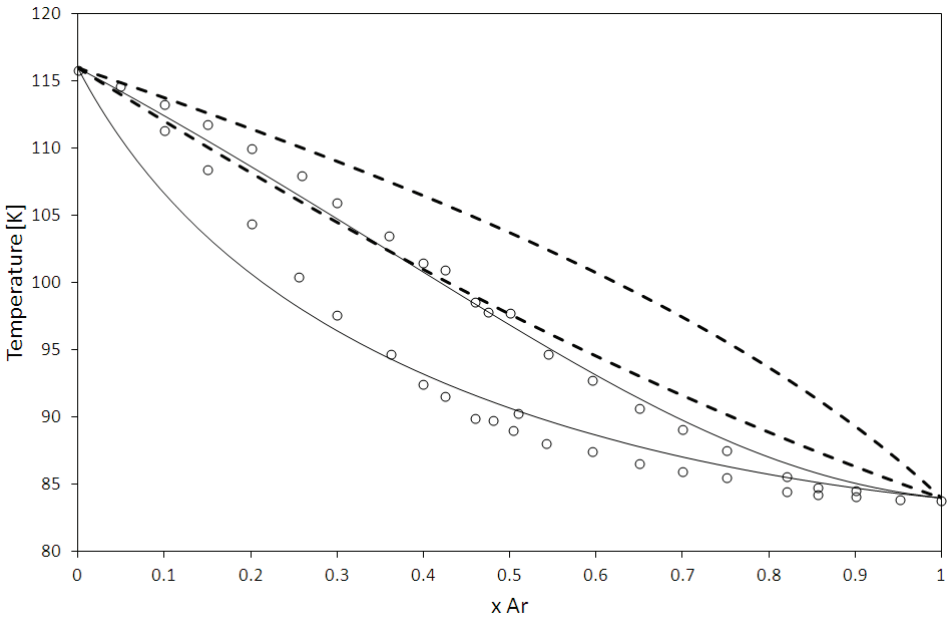

Figure 5.15: Solid-liquid equilibrium for the system Ar – Kr in the temperature-composition diagram.
SLV EoS: (— —): null binary interaction parameters; (——): binary interaction parameters from eq. (5.27). (○): experimental values from Heastie [88].

Figure 5.16 shows the solid-liquid phase diagram for the mixture Ar + CH_4. Also in this case, experimental values are available for both the solid and the liquid equilibrium phases [100], [101]. The presence of experimental values of the liquid phase under the melting temperatures of pure CH_4 and Ar indicates either an azeotrope or an eutectic with partial miscibility in the solid phase.

In [100], Fedorova supported the presence of an azeotrope realizing heat capacity-temperature curves by means of a calorimeter. This azeotrope was localized at about 0.6 in argon mole fraction. The presence of an azeotrope was previously suggested in 1937 by Veith and Schroeder, who did experimental work on the same system [102]. Their results have been omitted in Figure 5.16 for sake of clarity. Nevertheless, Van't Zelde et al. [101] performed experimental works consisting in vapor-pressure measurements in an equilibrium cell concluding that the system presents an eutectic at 71.2 K and for 0.61 in argon mole fraction.

The SLV EoS with null binary interaction parameters predicts a solid solution behavior with a very thin solid-liquid equilibrium lens (see the dashed lines in Figure 5.16). Thus, not only the quantitative prediction is erroneous, but also the qualitative representation is far from the real mixture behavior. In all the range of composition, the SLV EoS with binary interaction parameters equal to zero never gives a liquid phase stable at temperatures lower than the pure argon melting temperature.

The values of σ_{11}/σ_{22} and $\varepsilon_{11}/\varepsilon_{22}$ obtained from the pure fluid literature values of σ and ε are 0.796 and 0.902, respectively. The binary interaction parameters in Table 5.4 allow predicting a solid-liquid azeotrope at about 74.8 K and at 0.58 of argon mole fraction. Even if the liquid curves are qualitatively correct, the two solid-liquid lenses are thinner than the experimental lenses and the predicted azeotrope temperature is about 3 K higher than the experimental value. The prediction, is however in a poor agreement with the eutectic behavior suggested in [101].

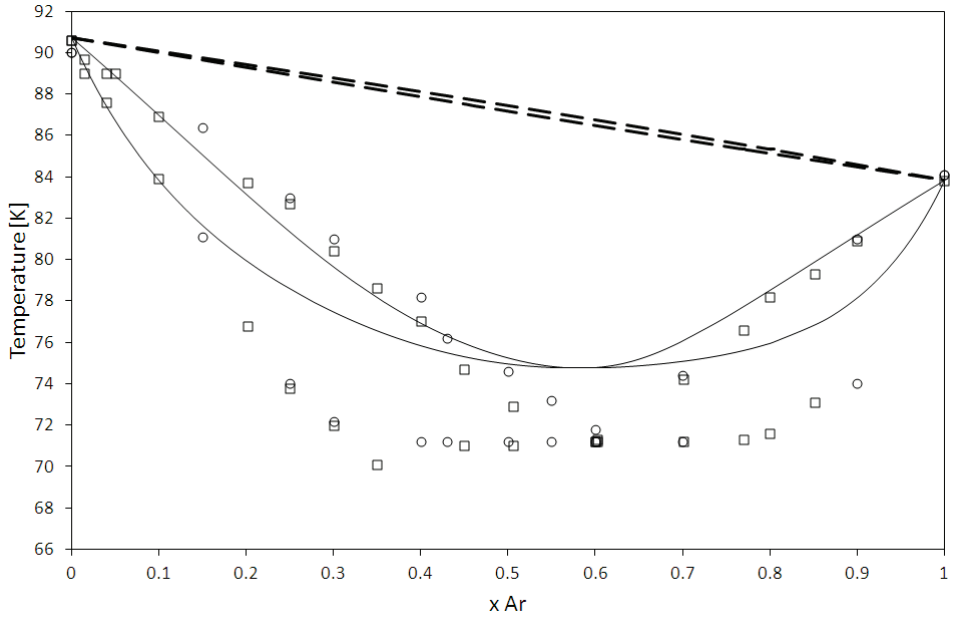

Figure 5.16: Solid-liquid equilibrium for the system Ar – CH_4 in the temperature-composition diagram.
SLV-EoS: (– –): null binary interaction parameters; (——): binary interaction parameters from Eq. (10). Experimental values: (○): Fedorova [100]; (□): Zelde et al. [101].

The experimental values for the mixture N_2 + Ar concerning both the solid and the liquid phases are reported in Figure 5.17. According to [103], this system presents an azeotrope at about 62.7 K and at 0.8 of nitrogen mole fraction, while Long and Di Paolo [104] suggested the presence of partial miscibility in the solid phase in the range 0.55 - 0.60 in nitrogen mole fraction. These authors

supposed two types of solids as a consequence of observed differences in the mode of freezing, which were encountered cooling alternatively nitrogen-rich and argon-rich mixtures.

Again, the prediction with null binary interaction parameters shows a solid-solution. Coupling the SLV-EoS and the binary interaction parameters obtained from the ratios σ_{11}/σ_{22} and $\varepsilon_{11}/\varepsilon_{22}$ allows obtaining a prediction qualitatively representative of the experimental values. The black circle in Figure 5.17 it the solid-liquid azeotrope, calculated at about 62.4 K and 0.8 in nitrogen mole fraction. The model does not predict the peritectic behavior and the partial immiscibility in the solid phase suggested in [104], but it is in agreement with the experimental values for both the liquid and the solid phase.

Furthermore, according to Figure 5.15-Figure 5.17, it can be stated the binary systems Ar - Kr and N_2 – Ar behave like a Lennard-Jones mixture more than Ar – CH_4.

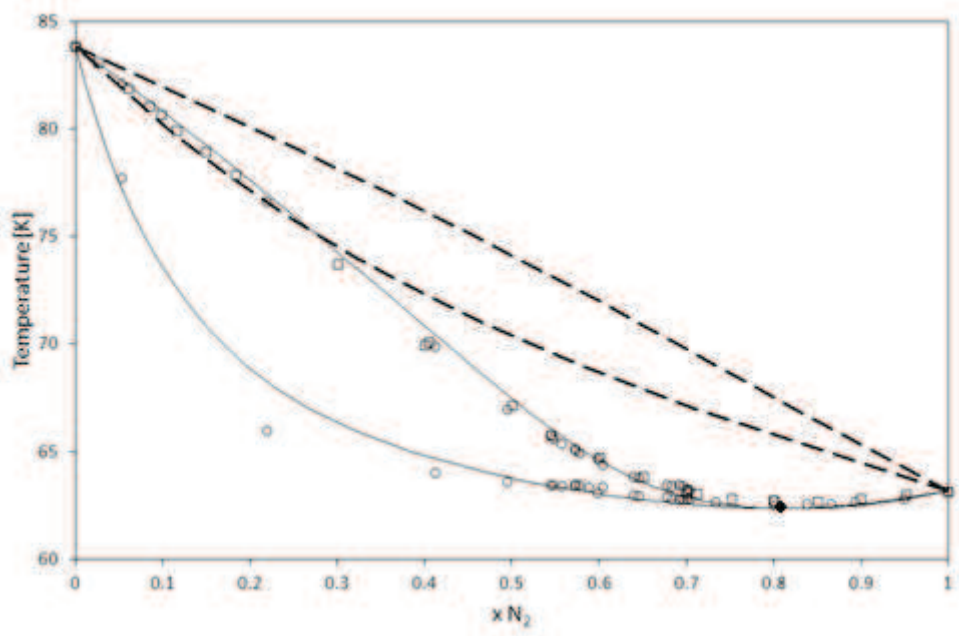

Figure 5.17: Solid-liquid equilibrium for the system N_2 – Ar in the temperature-composition diagram.
SLV-EoS: (– –): null binary interaction parameters; (——): binary interaction parameters from Eq. (10). Experimental values: (□): Din et al. [103]; (○): Long and Di Paolo [104].

The study presented in sections 5.6, coupling the SLV EoS and binary mixtures in LJ systems, tried to answer to the need of knowing, at list qualitatively, the solid-liquid behavior of mixtures for which solid miscibility (partial or total) occurs. The objective of this work has been setting up a method allowing predicting if a mixture forms solid solution, solid-liquid azeotrope, peritectic, or eutectic with partial miscibility.

Analytical developments obtained in [93] allow predicting binary interaction parameters of the SLV EoS. Predicted binary interaction parameters give qualitatively correct representations of the phase diagrams, involving solid phases, for real “simple” fluids.

For real simple fluids are intended small molecules which behavior does not deviate considerably from the Lennard-Jones theory. The model has been applied in [97] to mixtures: Ar – Kr, Ar – CH_4, CH_4 – Kr, N_2 – O_2, N_2 – Ar, and Ar – Xe, and it is capable of predicting the qualitative solid-liquid behavior of the cited mixtures, distinguishing among the different types of phase diagrams.

6 Representation of phase equilibria. II. Binary mixtures

This chapter presents the representation of the phase equilibrium behavior for the main binary mixtures involved in this work. Main binary mixtures are those mixtures for which the regression of the binary interaction parameters has been considered as relevant (42 mixtures), as anticipated in Chapter 1. For the reader convenience, Table 6.1 is a reminder of the cited mixtures.

Table 6.1: Binary mixtures represented with regressed binary interaction parameters.
Binary interaction parameters have been regressed for the mixtures in blue.

	N_2	O_2	Ar	Kr	Xe	Ne	He	CO_2	H_2	N_2O	CH_4	C_2H_6	C_2H_4	C_3H_8	C_3H_6
N_2															
O_2															
Ar															
Kr															
Xe															
Ne															

Among the mixtures in Table 6.1, literature values are not available for three mixtures of argon (Ar+N_2O, Ar+C_2H_4, Ar+C_3H_8) as discussed in Chapter 5.

The present chapter involves then the application of the SLV EoS, eq. (6.1), for the representation of the phase equilibrium behavior of the remaining 39 mixtures. Nevertheless, a quantitative comparison between calculated and experimental values also for the mixtures without binary interaction parameters has been reported in Appendix F.

$$P(T,v) = \frac{RT}{v-b}\frac{v-d}{v-c} - \frac{a}{v^2} \tag{6.1}$$

Eq. (6.1) corresponds to the functional form of the pressure-explicit equation proposed by Yokozeki in 2003, [64]. As detailed in Chapter 4, parameters for the pure components have been tuned according to saturation, melting, and sublimation curves while imposing the EoS to match triple and critical points temperatures and pressures from [3]. The parameters for pure components are protected by confidentiality, and are property of the Air Liquide group.

The mixing rules used for the mixture parameters have been introduced in Chapter 5 and reported here in eqs. (6.2)-(6.5) for the reader convenience. It is also worth remembering that these quadratic mixing rules present a maximum of eight binary interaction parameters, (k_{ij}, k_{ji}, m_{ij}, m_{ji}, n_{ij}, n_{ji}, l_{ij}, l_{ji}), when asymmetric values are considered.

$$a_{mix} = \sum_{i=1}^{N}\sum_{j=1}^{N}\sqrt{a_i a_j}\left(1-K_{ij}\right)x_i x_j \quad , \quad K_{ij} = \frac{k_{ij}k_{ji}\left(x_i+x_j\right)}{k_{ij}x_j + k_{ji}x_i} \quad , \quad K_{ii} = 0 \tag{6.2}$$

$$b_{mix} = \frac{1}{2}\sum_{i=1}^{N}\sum_{j=1}^{N}\left(b_i+b_j\right)\left(1-M_{ij}\right)x_i x_j \quad , \quad M_{ij} = \frac{m_{ij}m_{ji}\left(x_i+x_j\right)}{m_{ij}x_j + m_{ji}x_i} \quad , \quad M_{ii} = 0 \tag{6.3}$$

$$c_{mix} = \frac{1}{2}\sum_{i=1}^{N}\sum_{j=1}^{N}\left(c_i+c_j\right)\left(1-N_{ij}\right)x_i x_j \quad , \quad N_{ij} = \frac{n_{ij}n_{ji}\left(x_i+x_j\right)}{n_{ij}x_j + n_{ji}x_i} \quad , \quad N_{ii} = 0 \tag{6.4}$$

$$d_{mix} = \frac{1}{2}\sum_{i=1}^{N}\sum_{j=1}^{N}\left(d_i+d_j\right)\left(1-L_{ij}\right)x_i x_j \quad , \quad L_{ij} = \frac{l_{ij}l_{ji}\left(x_i+x_j\right)}{l_{ij}x_j + l_{ji}x_i} \quad , \quad L_{ii} = 0 \tag{6.5}$$

The regression of the binary interaction parameters has been carried out in an algorithm not presented in this work. It basically works evaluating the compositions of the equilibrium phases at im-

posed temperature and pressure (flash calculation) by means of the algorithm for the minimization of the Gibbs free energy of mixing. This latter has been presented in Chapter 5 and detailed in Appendix E. The objective function used for tuning the binary interaction parameters has been also presented in the previous chapter.

Once the binary interaction parameters have been regressed, the SLV EoS has been applied for evaluating three phase lines and critical loci. The algorithm developed for the evaluation of the critical loci may yield points that are stable, unstable, or metastable, thus computed solutions have been checked for phase stability via the comparison with results from the minimization of the Gibbs free energy of mixing in order to determine the stable solutions.

6.1 Evaluation of a three phase line

Three phases α, β, and γ coexist at equilibrium if the following relation holds for each component i in the mixture:

$$\hat{\varphi}_i^{\alpha} x_i = \hat{\varphi}_i^{\beta} y_i = \hat{\varphi}_i^{\gamma} z_i \tag{6.6}$$

$\hat{\varphi}_i^{\alpha} x_i - \hat{\varphi}_i^{\beta} y_i = 0$ (6.7)	$\hat{\varphi}_i^{\beta} y_i - \hat{\varphi}_i^{\gamma} z_i = 0$ (6.8)

In eq. (6.6), x_i, y_i , and z_i are composition of component i in the phases α, β, and γ, respectively.

Eq. (6.6) turns in eqs. (6.7)-(6.8), thus $2n$ equilibrium conditions in the form of eqs. (6.7)-(6.8) are needed in a system of n components. As a result, eqs. (6.7)-(6.8) apply twice in a binary systems (respectively for components 1 and 2), giving a system of 4 equilibrium conditions.

For a fixed value of temperature (T), attempt values are imposed for the equilibrium pressure (P) and compositions of component 1 (x_1, y_1, and z_1) in three imposed phases (α, β, and γ). This initial guess vector in four dimensions $\bar{x} = [P, x_1, y_1, z_1]$ is provided to the Broyden's numerical algorithm, implemented as published in [86]. Whenever possible, this recipe zeroes the system of 4 isofugacity conditions modifying the vector $\bar{x}$ while considering the imposed phases α, β, and γ. When the routine has converged to a local minimum, $\bar{x}$ contains the equilibrium pressure and compositions at temperature T for the three phase line involving phases α, β, and γ, and the calculation can be extended to increasing or decreasing temperatures.

Such an algorithm coupled with the expression of the partial molar fugacity coefficient from eq. (6.1) has been applied for evaluating solid-solid-liquid, solid-solid-vapor, solid-liquid-liquid, solid-liquid-vapor, and liquid-liquid-vapor three phase lines. In each of these cases, the initial guess vector $\bar{x}$ has been imposed on the basis of equilibrium values previously evaluated by means of the minimization of the Gibbs free energy of mixing.

6.2 Evaluation of the critical loci

The procedure proposed by Heidemann and Khalil [105] for the calculation of critical points in multicomponent systems has been adopted for the critical loci of the binary mixtures of interest. According to [105], the critical conditions in a binary mixture can be expressed in terms of the Helmholtz free energy as:

$$Q\Delta n = 0 \tag{6.9}$$

$$C = \sum_{i=1}^{2}\sum_{j=1}^{2}\sum_{k=1}^{2} \Delta n_i \Delta n_j \Delta n_k A_{ijk} = 0 \tag{6.10}$$

In eq. (6.9), Q is a 2×2 matrix with elements:

$$Q_{ij} = A_{ij} = \left(\frac{\partial^2 A}{\partial n_i \partial n_j}\right)_{T,v} = RT\left(\frac{\partial \ln f_i}{\partial n_j}\right)_{T,v} \tag{6.11}$$

where n_i and n_j indicate component mole numbers, while $\Delta n = [\Delta n_1, \Delta n_2]^T$ represents a nonzero perturbation vector in the component mole numbers, thus:

$$\Delta n^T \Delta n \neq 0 \tag{6.12}$$

In eq. (6.10):

$$A_{ijk} = \frac{\partial A_{ij}}{\partial n_k} = \left(\frac{\partial^3 A}{\partial n_i \partial n_j \partial n_k}\right)_{T,v} = RT\left(\frac{\partial}{\partial n_k}\left(\frac{\partial \ln f_i}{\partial n_j}\right)_{T,v}\right)_{T,v} \tag{6.13}$$

According to eqs. (6.11) and (6.13), the evaluation of the elements of matrix Q and C requires the first and second order partial composition derivatives of the fugacities f_i at imposed temperature T and volume v.

In binary systems, equations (6.9)-(6.10) and (6.12) represent a system of four equations in the four variables T_c, v_c, Δn_1, and Δn_2. T_c and v_c are the values of temperature and volume at the critical point resulting from the resolution of equations (6.9)-(6.10) and (6.12), and allowing the calculation of the critical pressure P_c directly from the pressure-explicit EoS, eq. (6.1).

Following the procedure proposed in [105], the algorithm for the calculation of critical points makes use of nested iterations. In an inner loop at fixed v, the Newton-Raphson iteration determines a value of temperature such that $\det(Q)=0$, then Δn is determined and normalized, and C is evaluated to adjust v in the outer loop.

In 1980, Michelsen modified the form of C in eq. (6.10), avoiding the need to evaluate the second order partial derivatives of fugacities:

$$C = \sum_{i=1}^{2}\sum_{j=1}^{2} \Delta n_i \Delta n_j \sum_{k=1}^{2} \Delta n_k A_{ijk} = \sum_{i=1}^{2}\sum_{j=1}^{2} \Delta n_i \Delta n_j \, Q^*_{ij} = \Delta n^T Q^* \Delta n \tag{6.14}$$

where:

$$Q^* = \frac{\partial}{\partial s}[Q(n + s\Delta n, T, v)]_{s=0} \tag{6.15}$$

The matrix Q^* involves the partial composition derivative of Q in the direction Δn with respect to a small change s, and it can be computed by numerical differentiation, [106].

The procedure developed in [105]-[106] and here briefly presented has been applied for the mixtures of interest in this work, and results are shown in next sections.

6.3 Results for the binary mixtures of interest

The three phase lines, temperature-composition and pressure-composition cross sections from eq. (6.1) with regressed binary interaction parameters, together with the available literature data suggest that the binary mixtures within Table 6.1 can be grouped in five main pressure-temperature phase equilibrium behaviors. A classification has not been possible for the mixtures Ar+C_2H_6 and Ar+C_3H_6 since few data are available, and considering too hazardous a classification based almost exclusively on the model. Furthermore, classification has not been proposed for the mixtures N_2+He, Ar+He, and Xe+Ne since for the author attempts it has not been possible to represent the phase equilibrium behavior approaching the critical temperatures of the less volatile component.

The classification is emphasized in Table 6.1. First of all, classification has been made with reference to the fluid-fluid equilibrium, hence notations I, II, and III have been assigned according to the classification proposed by van Konynenburg and Scott in 1980, [23].

Secondly, lowercase letters (a, b, c, and d) refer to special kinds of phase equilibrium behavior. Letter a refers to a solid-liquid equilibrium involving a homogeneous solid phase, while b indicates immiscibility in the solid phase. Letter c refers to vapor-liquid equilibria involving a supercritical fluid, whereas d is related to the presence of a liquid-liquid-vapor three phase line in the type III PT-EP.

Mixtures of type I PT-EP present total miscibility in the liquid phase. The mixtures N_2+Ar, Ar+Kr, and Kr+Xe present also total miscibility in the solid phase at the solid-liquid equilibrium (letter a). To the contrary, the other mixtures of type I are characterized by a solid-solid-liquid-vapor quadruple point (with an eutectic or peritectic behavior) occurring in the low temperature-low pressure region (letter b).

Two mixtures involving oxygen have been found to present a type II PT-EP with immiscibility in the solid phase (letter b).

Finally, the majority of the mixtures in Table 6.1 present a type III PT-EP with immiscibility in the solid phase (letter b): some of them (mainly composed by nitrogen or oxygen with hydrocarbons except methane) present a liquid-liquid-vapor three phase line (b+c), whereas the remaining have not (b+d).

Table 6.2: Classification of the binary mixtures of interest according to the encountered pressure-temperature equilibrium behaviors.
I, II, III correspond to the classification of van Konynenburg and Scott, [23].
a = homogeneous solid phase at SLE; b = immiscibility in the solid phase; c = presence of a liquid-liquid-vapor three phase line; d = no liquid-liquid-vapor three phase line.

Mixture	Type of PT-EP				
	I		II	III	
	a	b	b	b+c	b+d
N_2+O_2		■			
N_2+Ar	■				
N_2+Kr		■			
N_2+Xe					■
Ne+N_2					■
N_2+CO_2					■
H_2+N_2					■
N_2+N_2O					■
N_2+CH_4		■			
N_2+C_2H_6				■	
N_2+C_2H_4				■	
N_2+C_3H_8				■	
N_2+C_3H_6				■	
Ar+O_2		■			
O_2+Kr		■			
O_2+Xe		■			
Ne+O_2					■

Mixture	Type of PT-EP				
	I		II	III	
	a	b	b	b+c	b+d
He+O_2					■
O_2+CO_2					■
H_2+O_2					■
O_2+N_2O					■
O_2+CH_4		■			
O_2+C_2H_6			■		
O_2+C_2H_4			■		
O_2+C_3H_8				■	
O_2+C_3H_6				■	
Ar+Kr	■				
Ar+Xe		■			
Ne+Ar					■
Ar+CO_2					■
H_2+Ar					■
Ar+CH_4		■			
Kr+Xe	■				
He+Ne					■

Examples of these PT-EPs are presented in next sections. A binary mixture has been chosen for representing qualitatively each type of PT-EP.

According to Table 6.1, the five PT-EPs are:

- type Ia PT-EP: total miscibility in the liquid phase and in the solid phase at the solid-liquid equilibrium. The mixtures Ar+Kr and N_2+Ar are presented in section 6.3.1. Two mixtures have been chosen as the second one presents a solid-liquid azeotrope, hence differing from the solid solution of the first one;
- type Ib PT-EP: total miscibility in the liquid phase and immiscibility in the solid phase. The mixture Ar+CH_4 is presented in section 6.3.2;
- type IIb PT-EP: mixtures of type II according to van Konynenburg and Scott together with immiscibility in the solid phase. The mixture O_2+C_2H_6 is presented in section 6.3.3;
- type IIIb+c: mixtures of type III according to van Konynenburg and Scott together with a liquid-liquid-vapor triple phase line. The mixture N_2+C_2H_6 is presented in section 6.3.4;
- type IIIb+d: mixtures of type III according to van Konynenburg and Scott together with absence of the liquid-liquid-vapor triple phase line. The mixture Ar+CO_2 is presented in section 6.3.5.

Sections 6.3.1 – 6.3.5 present the qualitative comparison for the cited mixtures. Quantitative comparisons have instead been reported in Appendix E for all the mixtures within Table 6.1, together with examples of pressure-composition and temperature-composition cross sections.

The results in sections 6.3.1 – 6.3.5 have been organized in the following manner:

- a Temperature-composition Cross Section (Tx-CS) reporting the comparison between experimental and calculated values concerning the Solid-Liquid Equilibrium (SLE);
- a Pressure-composition Cross Sections (Px-CSs) providing the comparison between experimental and calculated values concerning the Vapor-Liquid Equilibrium (VLE);
- a schematic representation of the Pressure-Temperature Equilibrium Projection (PT-EP) with the aim of easing the comprehension of the calculated PT-EPs; up to 100 MPa;
- some Tx-CSs at some strategic pressures with reference to the PT-EP in order to appreciate the evolution of the phase equilibrium behavior with pressure in a wide range of temperatures. These strategic pressures usually refer to changes in the phase behavior and appearance of new kinds of equilibrium. As a consequence, these pressures are typically located between invariant points like quadruple points or pure component triple and critical points.

6.3.1 Type Ia PT-EP: systems Ar+Kr and N_2+Ar

The solid solution characterizing the behavior of the system Ar+Kr at SLE is portrayed in Figure 6.1. The SLV EoS with regressed binary interaction parameters is in a good agreement with the data obtained in 1955 by Heastie, [88]. The model well represents the quasi-azeotropic behavior for compositions close to pure Argon, while the solidus line slightly deviate from the experimental values for compositions lower than 0.2 in Ar.

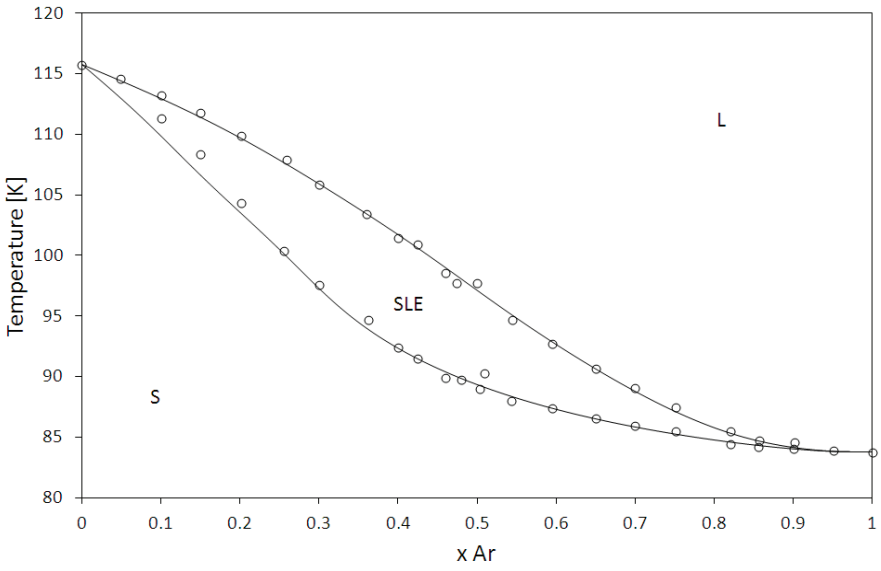

Figure 6.1: Mixture Ar+Kr : comparison between experimental and calculated values of SLE.
○ : experimental values, [88]. — : calculated values.

The VLE obtained with the EoS at 138 K, 148 K, and 153 K are illustrated in Figure 6.2 together with the experimental values published in 1975 by Schouten et al., [87].

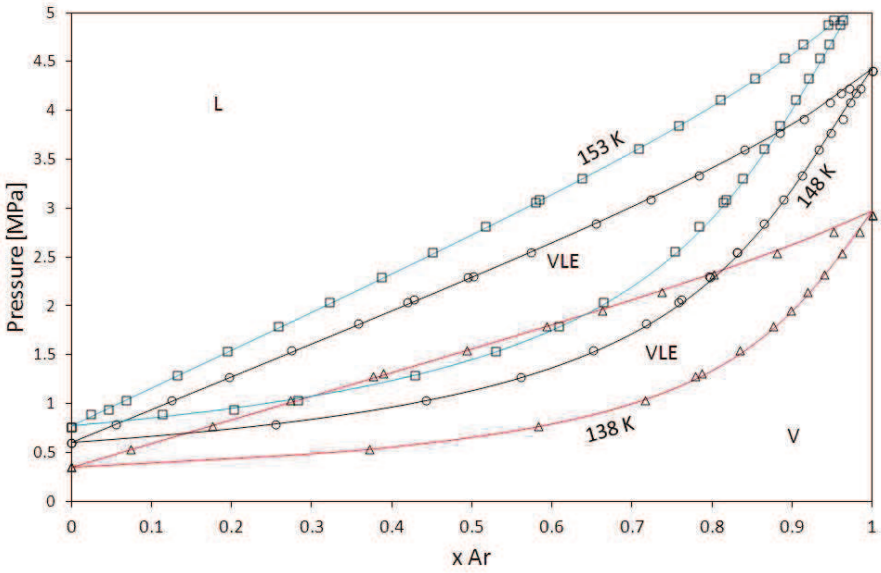

Figure 6.2: Mixture Ar+Kr: comparison between experimental and calculated values of VLE.
Experimental values, [87]: 138.15 K (Δ), 148.15 K (○), 153.15 K (□).
Calculated values: 138.15 K (—), 148.15 K (—), 153.15 K (—).

Figure 6.3 is the qualitative PT-EP representative of the phase equilibrium behavior of the system Ar+Kr. Red and black lines are the saturation, sublimation, and melting lines of Ar and Kr, respectively. Keeping the same distinction in terms of color, triple and critical points are indicated by squares and circles, respectively.

A liquid-vapor critical line (l=v) joins the critical points of the pure components, as well as a single solid-liquid-vapor three phase line runs from the triple point of Ar ending in the one of Kr. The blue line in Figure 6.3 represents the conditions for the solid-liquid-vapor equilibrium (slve) in terms of temperature and pressure.

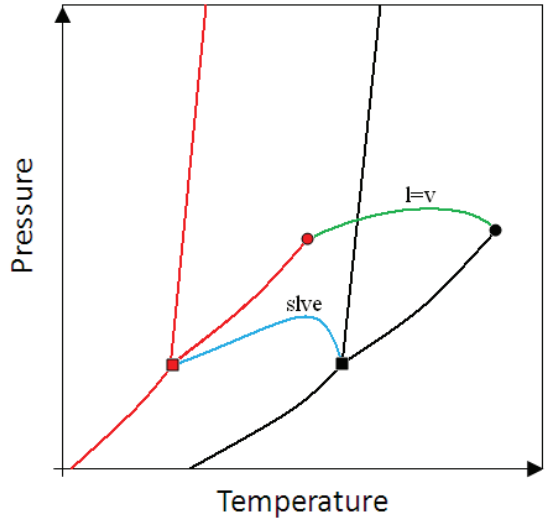

Figure 6.3: Mixture Ar+Kr: qualitative pressure-temperature equilibrium projection.
Ar: triple point ■; critical point ●; equilibria —.
Kr: triple point ■; critical point ●; equilibria —.
— : three phase line; — : critical line.

According to Figure 6.1-Figure 6.3, the system Ar+Kr presents total miscibility in the liquid phase and in the solid phase as well.

The calculated PT-EP for the mixture here treated is in Figure 6.4. Colors are the same of Figure 6.3 to ease the comprehension. The notations sve, sle, and vle have been added in Figure 6.4 for indicating the sublimation, melting, and saturation lines of the two pure components.

The liquid-vapor critical line (l=v) originates at about 151 K, namely the critical temperature of Ar, and ends at about 209 K, the critical value for Kr.

The coexistence of the solid, liquid, and vapor phases at equilibrium (slve) occurs from the triple point temperature of Ar (84 K) up to the one of Kr (116 K). It is worth noting that these temperature are the same values respectively at xAr=1 and xAr=0 in Figure 6.1.

The slve curve exits the triple point of Ar and reaches a maximum in pressure before ending in the triple point of Kr. This maximum has been calculated at about 107 K, 0.17 MPa, and a mole fraction in the liquid phase of 0.27 in Ar.

This behavior entails the presence of two slve temperatures for each pressure between the triple point pressure of Kr (close to 0.07 MPa) and 0.17 MPa.

Four main isobars are indicated in Figure 6.4: P0 (0.02 MPa), P1 (0.1 MPa), P2 (1 MPa), and P3 (10 MPa). The Tx-CSs corresponding to these pressures are portrayed in Figure 6.5 in the range 70 K – 160 K.

In Figure 6.4, considering increasing temperatures from an initial value of 70 K, the line corresponding to P0 meets the sublimation line of Ar and then the one of Kr. These two values are respectively placed at xAr=1 and xAr=0 in the Tx-CS related to pressure P0 in Figure 6.5.

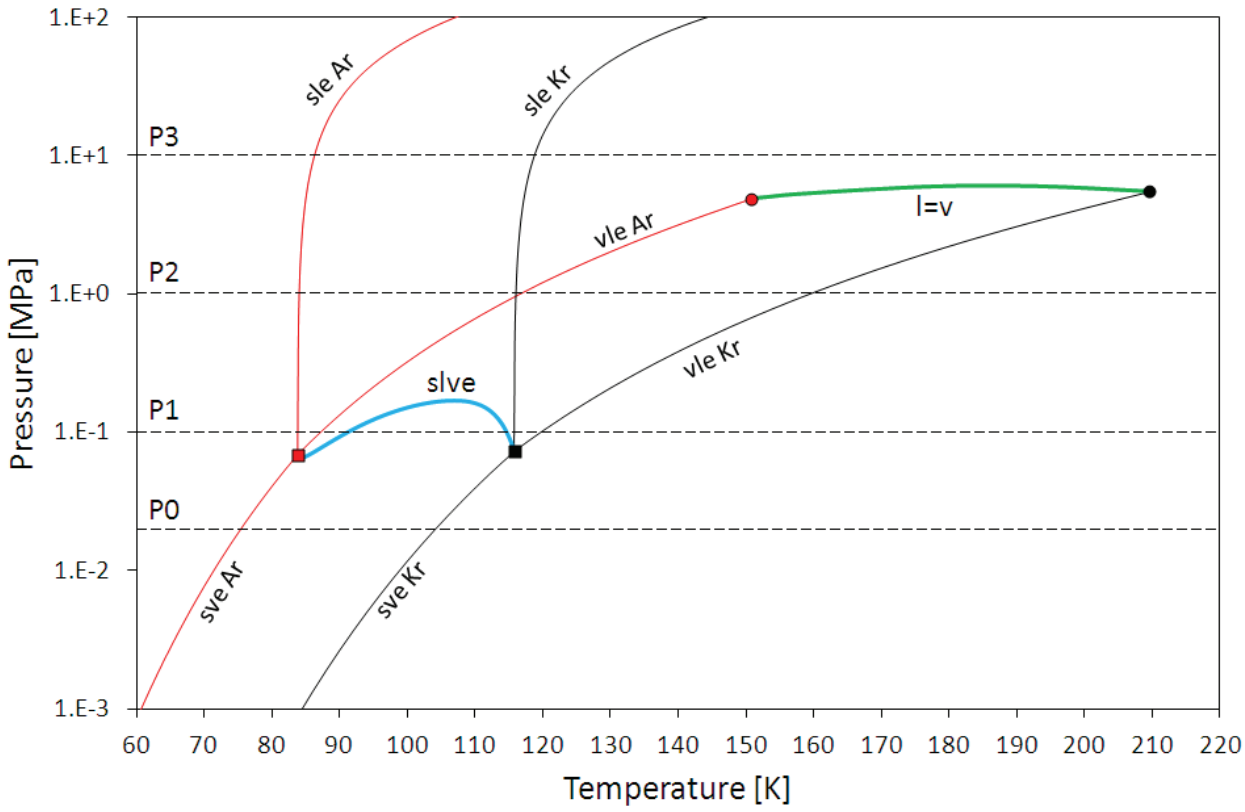

Figure 6.4: Mixture Ar+Kr: calculated pressure-temperature equilibrium projection.
Ar: triple point ■; critical point ●; solid-liquid, solid-vapor, and vapor-liquid equilibria —.
Kr: triple point ■; critical point ●; solid-liquid, solid-vapor, and vapor-liquid equilibria —.
— : slve, solid-liquid-vapor equilibrium. — : l=v, liquid-vapor critical line.

Any three phase line is encountered between the two sve temperatures for the pure components, and the system presents a solid-vapor equilibrium. Any immiscibility in the solid phase occurs.

At P1 (0.1 MPa), both pure components have a solid-liquid and a vapor-liquid equilibrium temperature. With reference to graph P1 in Figure 6.5, it can be stated that at P1 two liquid phases appears. One richer in Ar located between the sle temperature of Ar up to the lower solid-liquid-vapor equilibrium temperature (~91 K). One richer in Kr located between the sle temperature of Kr down to the upper slve temperature (~115 K). At xAr=1 and xAr=0, the ranges of temperature where these two liquid phases are stable are related to the difference between the sle and the vle temperatures of the two pure components at P1. The extent of these ranges reduces while approaching the slve temperatures, and no more liquid exist between the lower and the upper slve temperatures, where the solid is at equilibrium with the vapor.

For increasing pressures, the differences between sle and vle temperatures for the pure compounds increase. The liquid phase rich in Ar moves the upper slve temperature at higher temperatures, while the upper slve temperature is lowered by the liquid rich in Kr. This makes the two slve temperatures meet at a certain pressure, and this value is 0.17 MPa, namely the maximum pressure of the slve curve in Figure 6.4.

Besides this value of pressure, the liquid phase has moved away enough the vapor phase so that the sve ceases to exist in all the range of composition and temperatures, and two distinct phase equilibria occur: a solid-liquid equilibrium at low temperatures, and a vapor-liquid equilibrium at high temperatures. It can be seen in the Tx-CS corresponding to pressure P2 in Figure 6.5.

Above the critical temperatures of the two components, the vle does not exist anymore, and the sole equilibrium remaining is the sle between the sle temperatures of Ar and Kr, Tx-CS at P3 in Figure 6.5.

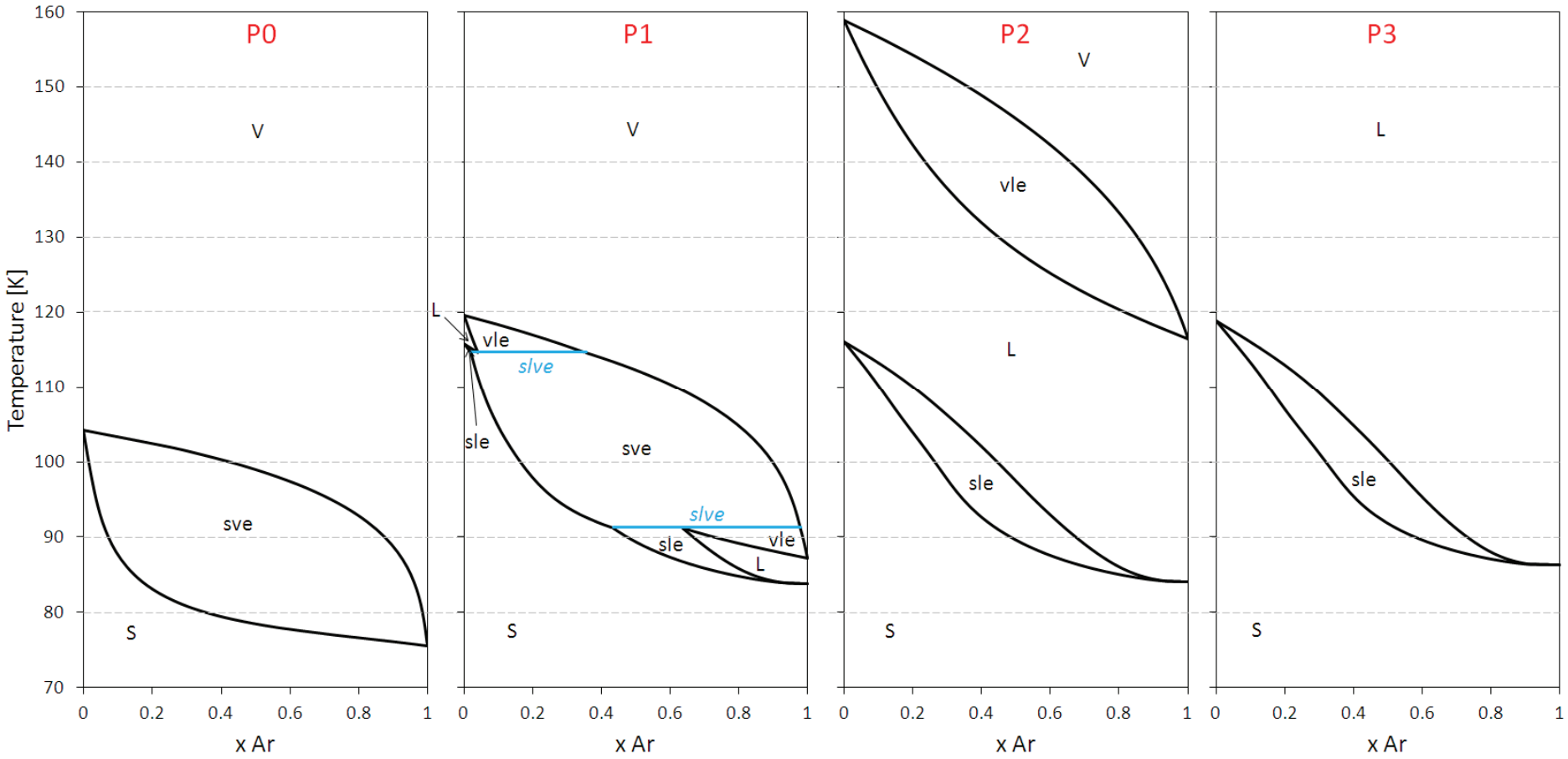

Figure 6.5: Mixture Ar+Kr: evolution of the phase equilibrium behavior with pressure in the range 70 K – 160 K.
P0 = 0.02 MPa; P1 = 0.1 MPa; P2 = 1 MPa; P3 = 10 MPa. — : solid-liquid-vapor equilibrium temperature; S : solid phase; L : liquid phase; V : vapor phase; sve : solid-vapor equilibrium; sle : solid-liquid equilibrium; vle : vapor-liquid equilibrium

The mixture N_2+Ar has a similar equilibrium behavior regarding to the homogeneity of the solid phase at equilibrium with the liquid phase at SLE, as shown in Figure 6.6. As already discussed in Chapter 5, according to the experimental values this system presents a solid-liquid azeotrope at 62.6 K and a N_2 mole fraction of about 0.8.

The SLE calculated by the EoS agrees with the available data for both the liquidus and solidus lines, and the calculated temperature of solid-liquid azeotrope is 62.2 K.

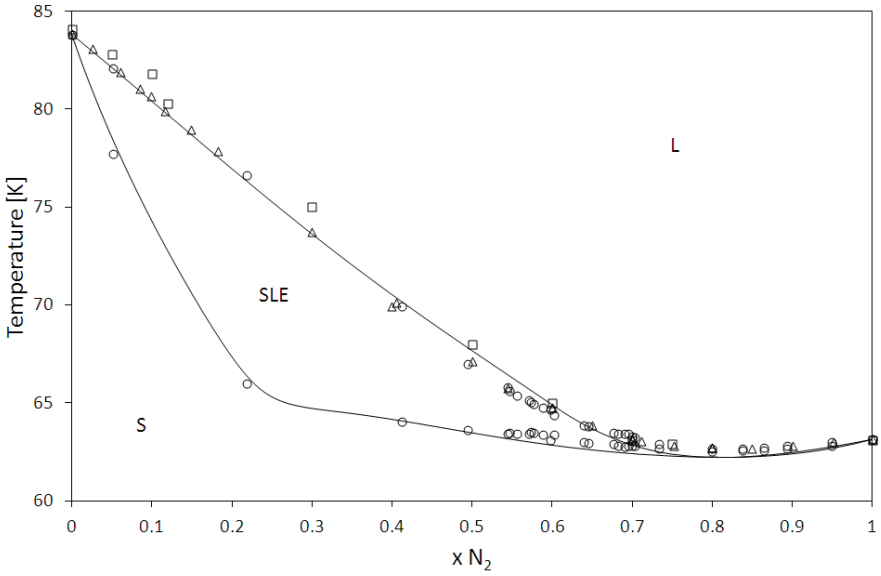

Figure 6.6: Mixture N_2+Ar: comparison between experimental and calculated values of SLE.
Experimental values: ○ [107], □ [100], Δ [108]. — : calculated values.

The comparison between experimental and calculated values of VLE is portrayed in Figure 6.7 for temperatures of 95 K, 115 K, and 121 K. Again, the model is in a quite good agreement with the experimental values.

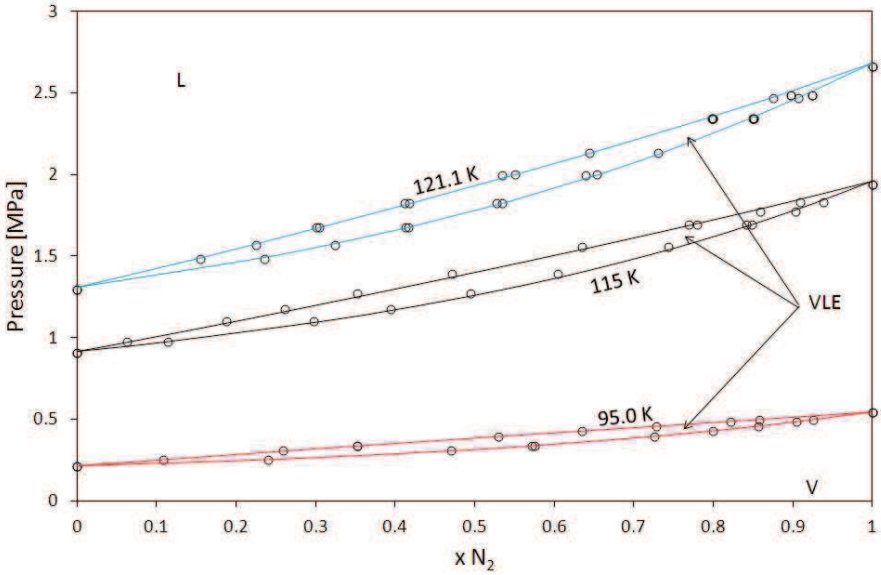

Figure 6.7: Mixture N_2+Ar: comparison between experimental and calculated values of VLE.
Experimental values [109]: 95 K (Δ), 115 K (○), 121.1 K (□).
Calculated values: 95 K (—), 115 K (—), 121.1 K (—).

Figure 6.8 is the qualitative PT-EP showing the phase equilibrium behavior of the system N_2+Ar. Red and black lines are the saturation, sublimation, and melting lines of N_2 and Ar, respectively. As for the previous system, triple and critical points are indicated by squares and circles, respectively.

A liquid-vapor critical line (l=v) joins the critical points of the pure components, and total miscibility occurs in the liquid phase.

The black diamond in Figure 6.8 figures out an upper critical endpoint of solid-solid immiscibility (s_2=s_1). It means that for temperatures and pressures up to this point, two solid phases ($solid_1$ and $solid_2$) coexist at equilibrium with a vapor phase along the $solid_2$-$solid_1$-vapor three phase line. In other words, immiscibility occurs between two solid phases (s_2 and s_1) and these are at equilibrium with the vapor ($s_2s_1$ve).

Nevertheless, these two phases are never in equilibrium with the liquid phase, so that any quadruple point of $solid_2$-$solid_1$-liquid-vapor coexistence occurs. Starting at low temperatures and pressures, the vapor phase is at equilibrium with s_2 and s_1 until immiscibility exists in the solid phase, and above the immiscibility limit in the solid phase (the black diamond) the vapor is in a three phase equilibrium with a liquid phase and a new homogeneous solid phase along the s_2-liquid-vapor three phase line ($s_2$lve in Figure 6.8).

It is worth specifying that the solid s_2 at $s_2$lve is not immiscible with the solid s_1 at equilibrium along the $s_1$lve, although notations 2 and 1 have been maintained in the discussion of the present system. Confirmation of the miscibility of s_2 and s_1 in the solid phase at SLE is provided by Figure 6.6, which shows a homogeneous solid phase at equilibrium with the liquid.

To sum up, two immiscible solid phases s_2 and s_1 exist up their immiscibility limit (the upper critical endpoint s_2=s_1, namely the black diamond in Figure 6.8); any of these two solid phases yield ever a solid-liquid equilibrium; the liquid phase is at equilibrium with a homogeneous solid phase whit s_2 and s_1 meaning the content of N_2.

A solid rich in N_2 (s_1) is at equilibrium with the liquid and the vapor phase from the triple point temperature of N_2 down to the solid-liquid azeotrope, the blue square in Figure 6.8. A solid rich in Ar (s_2) is at equilibrium with the liquid and the vapor phases from the triple point temperature of Ar down to the solid-liquid azeotrope.

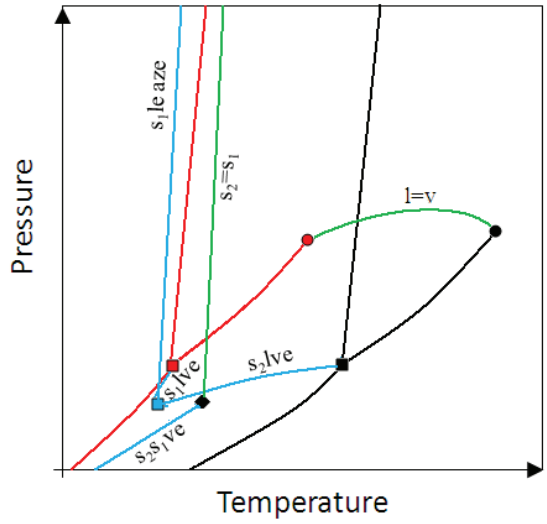

Figure 6.8: Mixture N_2+Ar: qualitative pressure-temperature equilibrium projection.
N_2: triple point ■; critical point ●; equilibria —.
Ar: triple point ■; critical point ●; equilibria —.
■ : solid-liquid azeotrope; ♦ : upper limit of immiscibility in the solid phase; — : three phase lines; — : critical lines.

The calculated PT-EP for the mixture N_2+Ar is in Figure 6.9. Colors and notations are in agreement with Figure 6.8. Different styles have been used for differentiating the three phase lines.

Notations sve, sle, and vle have been added in Figure 6.9 for indicating the sublimation, melting, and saturation lines of the two pure components.

The liquid-vapor critical line (l=v) originates at about 126 K, namely the critical temperature of N_2, and ends at about 151 K, the critical value for Ar.

The coexistence of the $solid_2$, $solid_1$, and vapor phases at equilibrium ($s_2s_1$ve) occurs from the low pressure-low temperature region up to the black diamond (64.2 18 K and 0.0127 MPa) along the dashed-dotted blue line. The composition of the solid at the upper critical endpoint has been evaluated equal to 0.29 in N_2.

The $s_2$lve exits the triple point of Ar (84 K) and reaches the point where the solid-liquid azeotrope originates (T=62.2 K, P=9.86 kPa, xN_2=0.81). Same point is reached by the $s_1$lve three phase line originating from the triple point of N_2 (63 K). The blue dashed line represents the evolution of the s_1l azeotrope with pressure and temperature.

At the upper critical temperature of immiscibility in the solid phase, the pressure is 0.0127 MPa. At same temperature, the pressure of $s_2$lve is 0.0128 MPa, so that the two immiscible solid phases are never in equilibrium with the liquid phase, and a quadruple point is avoided.

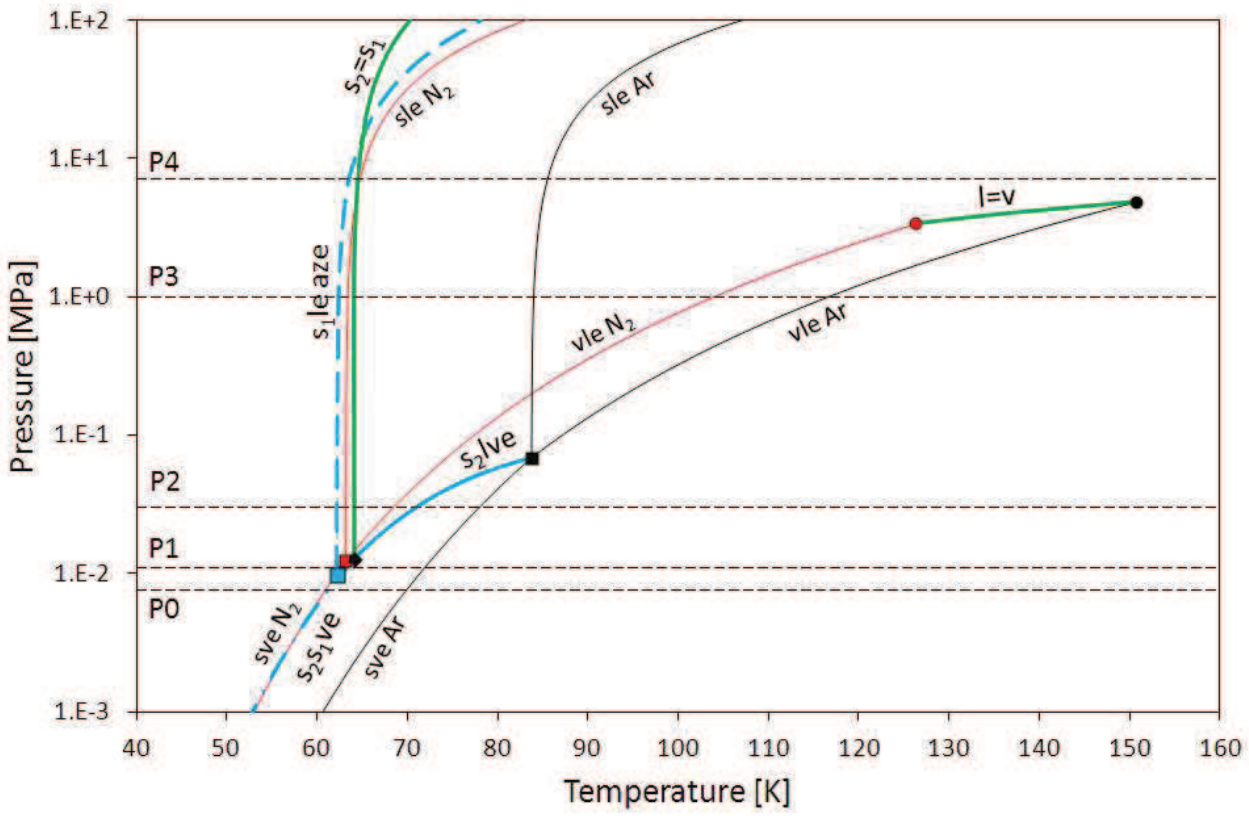

Figure 6.9: Mixture N_2+Ar: calculated pressure-temperature equilibrium projection.
N_2: triple point ■; critical point ●; solid-liquid, solid-vapor, and vapor-liquid equilibria —.
Ar: triple point ■; critical point ●; solid-liquid, solid-vapor, and vapor-liquid equilibria —.
■ : solid-liquid azeotrope; ♦ : upper limit of immiscibility in the solid phase; — : $solid_2$-liquid-vapor three phase line; — — : evolution of the $solid_1$-liquid azeotrope; — • — : $solid_2$-$solid_1$-vapor three phase line; — : critical lines.

The proximity of these two pressures, one related to the upper critical endpoint of immiscibility along the $s_2s_1$ve and the other related to the $s_2$lve at the upper critical endpoint temperature, could be related to the peculiar trend of composition along the solidus line in Figure 6.6. This feature can be appreciated in the isobars of Figure 6.11.

The representative isobars chosen for the system under discussion are portrayed in Figure 6.9; these pressures are P0 (7.5 kPa), P1 (0.011 MPa), P2 (0.03 MPa), P3 (1 MPa), and P4 (10 MPa). All the isobars, except P4, are represented by means of the Tx-CSs in Figure 6.11 in the range 55 K – 85 K. Isobars P4 has been omitted being similar to isobar P3 of the system Ar+Kr: at 10 MPa the system does not present any vapor-liquid equilibrium. Furthermore, the form of the phase diagram is equal to the one at P3. The Tx-CS at 1 MPa, P3, is reported in Figure 6.11 only up to 85 K without considering the vle at higher temperatures, in order to not worsening the representation of the low-temperature phase equilibrium behaviors of the other Tx-CSs.

A zoom of Figure 6.9 in proximity of the triple point of N_2 is given in Figure 6.10.

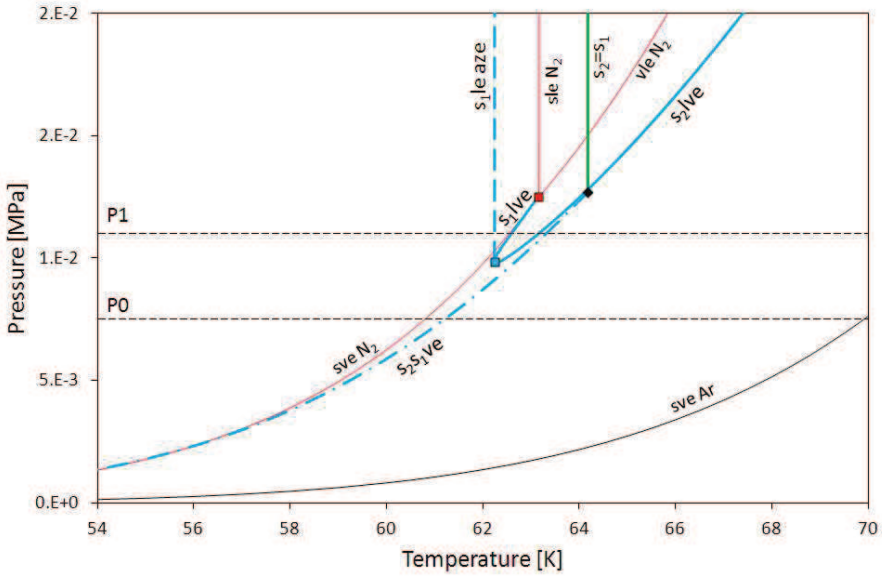

Figure 6.10: Mixture N_2+Ar: calculated pressure-temperature equilibrium projection in the proximity of the triple point of N_2.
N_2: triple point ■; solid-liquid, solid-vapor, and vapor-liquid equilibria —. Ar: solid-vapor equilibria —.
■ : solid-liquid azeotrope; ♦ : upper limit of immiscibility in the solid phase; — : $solid_{1,2}$-liquid-vapor three phase lines; — — : evolution of the $solid_1$-liquid azeotrope; — • — : $solid_2$-$solid_1$-vapor three phase line.

At P0 there is a temperature (61.2 K) at which the two immiscible solid phases (s_2 and s_1) coexist at equilibrium with the vapor phase. The $s_2$ve and the $s_1$ve curves join the sle temperatures of pure Ar and N_2, respectively.

At P1 three phase lines and the $solid_1$-liquid azeotrope ($s_1$le aze) are encountered. The $s_1$le aze is found at about 62.2 K, then two $s_1$lve temperatures are located at about 62.6K and 63.2 K, and finally the $s_2s_1$ve is calculated at about 63.3 K. The liquid phase is bounded between the $s_1$le and the vle.

At P2 the two solid phases join their upper critical temperature of 64.1 K, the $s_1$le aze occurs at 62.4 K, and a $s_2$lve is located at about 71 K.

Finally, at P3 the solid-liquid equilibrium corresponds to the one represented in Figure 6.6, and it can be seen as composed by a $s_2$le for composition lower than the solid-liquid azeotrope, and a $s_1$le for compositions greater than this value (xN_2=0.81).

It should be kept in mind that notations $s_2$le and $s_1$le do not mean presence of a $s_2s_1$le at any temperature and pressure, instead they have been used for emphasizing the content in N_2 when dealing with the solid-liquid equilibrium

Same behavior is showed by the mixture Kr+Xe, which also has an azeotropic behavior. In such a system the $s_2s_1$ve is limited in temperature and pressure, so that the upper critical point of immiscibility in the solid phase is located at lower temperature.

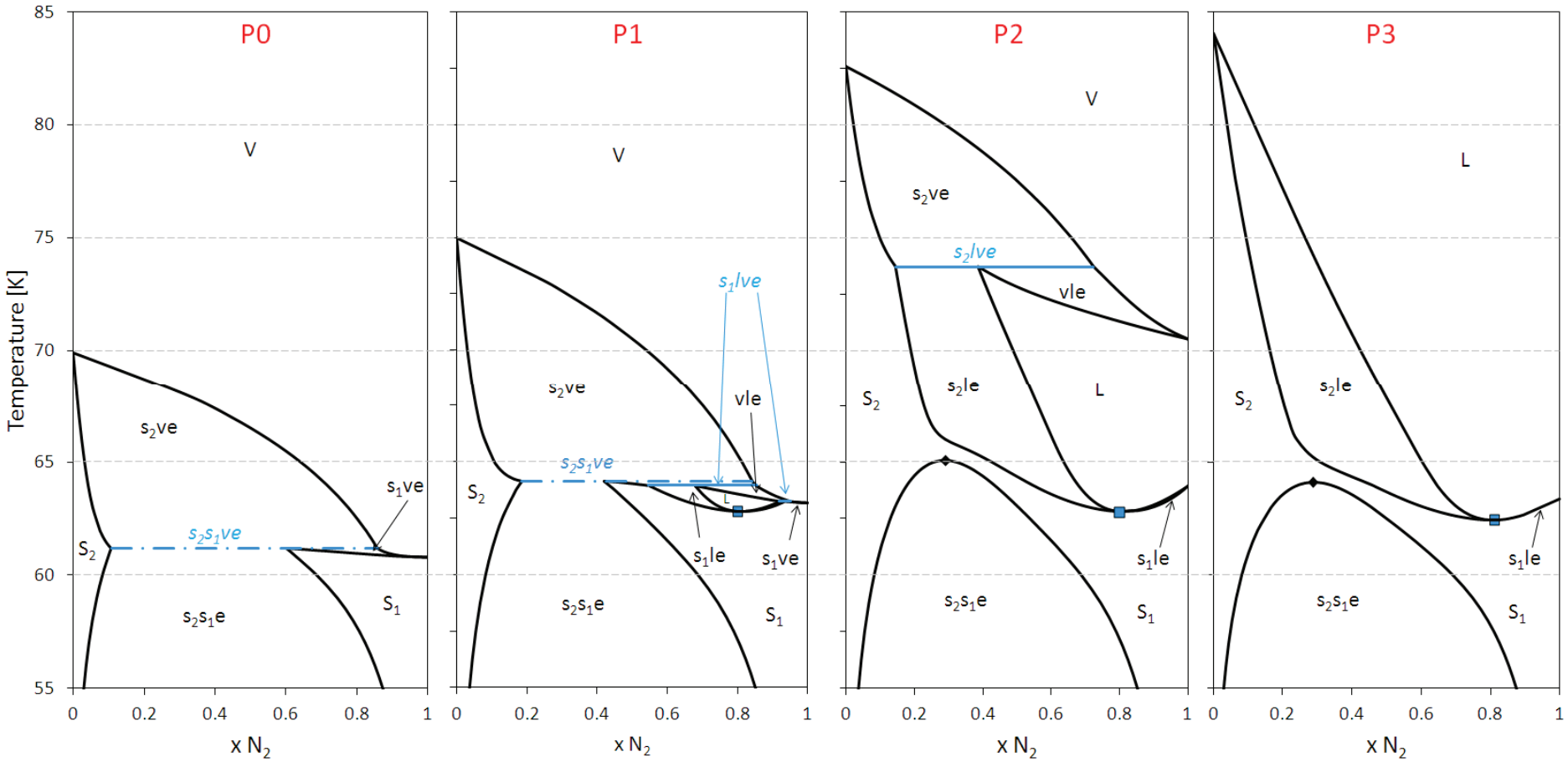

Figure 6.11: Mixture N_2+Ar: evolution of the phase equilibrium behavior with pressure in the range 55 K – 85 K.
P0 = 7.5 kPa; P1 = 0.011 MPa; P2 = 0.03 MPa; P3 = 1 MPa. — : $solid_{1,2}$-liquid-vapor equilibrium temperature; — • — : $solid_2$-$solid_1$-vapor equilibrium temperature; $S_{1,2}$: solid phase; L : liquid phase; V : vapor phase; $s_{1,2}ve$: solid-vapor equilibrium; $s_{1,2}le$: solid-liquid equilibrium; vle : vapor-liquid equilibrium; s_2s_1e : $solid_2$-$solid_1$ equilibrium; ♦ : s_2=s_1 critical endpoint; ■ : solid1-liquid azeotrope.

6.3.2 Type Ib PT-EP: system Ar+CH_4

The SLE for the system Ar+CH4 is shown in Figure 6.12. According to Fedorova, [100], and van't Zelfde et al., [101], the system presents partial immiscibility in the solid phase at about 71.2 K where the composition in Ar are xs_2=0.4, xl=0.6, xs_1=0.7. Binary interaction parameters have been regressed with respect to data from [100] and [101], thus the model is in contrast with the azeotropic behavior obtained by Veith and Schroeder in 1937, [102].

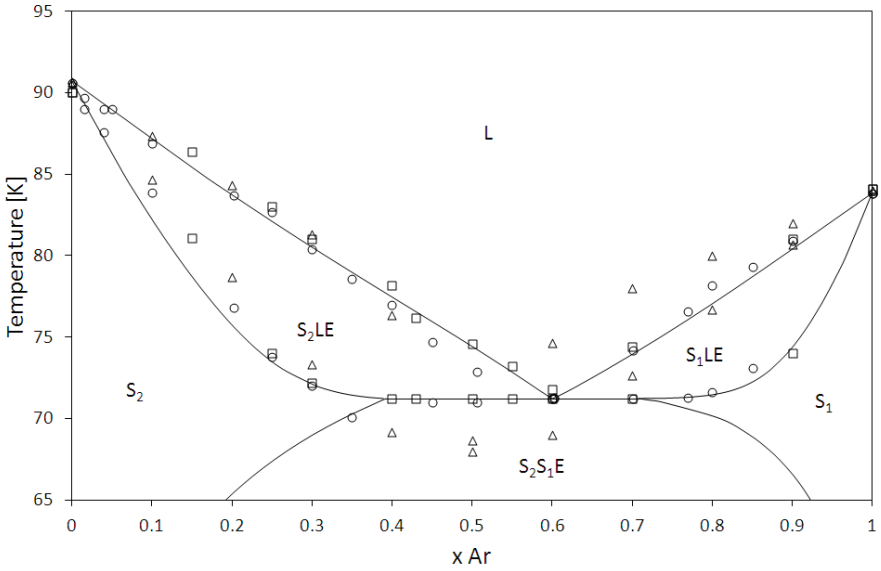

Figure 6.12: Mixture Ar+CH_4: comparison between experimental and calculated values of SLE.
Experimental values: □ [100], ○ [101], Δ [102]. — : calculated values.

The VLE at 151 K, 137 K, and 123 K is illustrated in Figure 6.13 as from experimental values, [110] and [111], and as calculated from the SLV EoS.

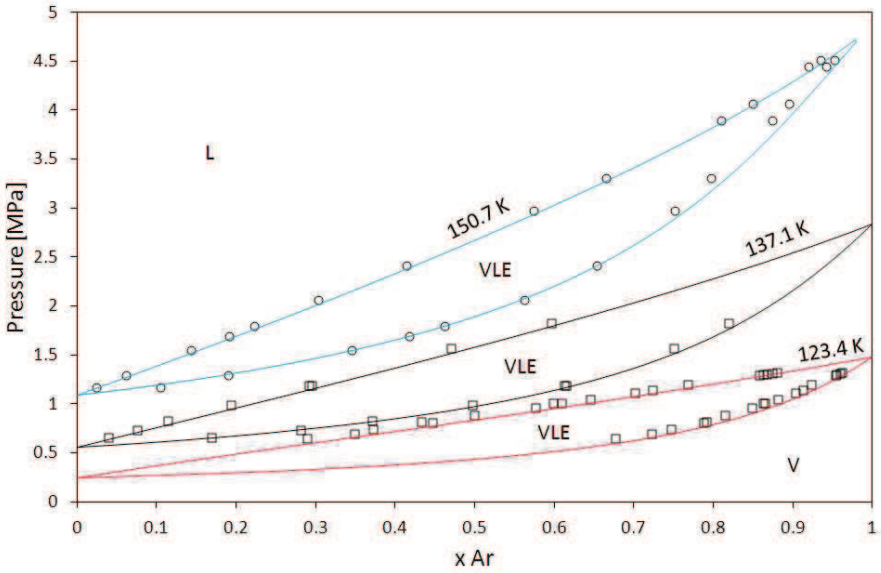

Figure 6.13: Mixture Ar+CH_4: comparison between experimental and calculated values of VLE.
Experimental values: □ : 123.4 K and 137.1 K, [110]; ○ : 150.7 K, [111].
Calculated values: 123.4 K (—), 137.1 K (—), 150.7 K (—).

Figure 6.14 is the qualitative PT-EP portraying the phase equilibrium behavior of the system Ar+CH_4. Red and black lines are the saturation, sublimation, and melting lines of Ar and CH_4, respectively. As for the previous systems, triple and critical points are indicated by squares and circles, respectively.

A liquid-vapor critical line (l=v) joins the critical points of the pure components, then total miscibility occurs in the liquid phase.

The black diamond in Figure 6.14 figures out a quadruple point: here a $solid_2$, a $solid_1$, a liquid, and a vapor phase coexist at equilibrium. From this s_2s_1lv quadruple point four three phase lines originate: a s_1lve ending in the triple point of Ar, a s_2lve ending in the triple point of CH_4, a s_2s_1le extending in the high pressure region, a s_2s_1ve extending in the low pressure region.

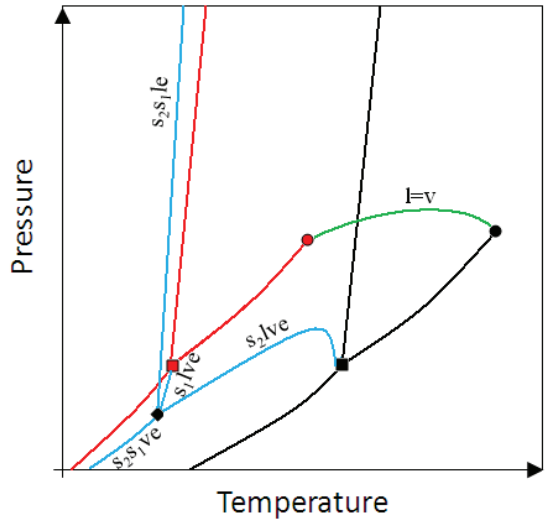

Figure 6.14: Mixture Ar+CH_4: qualitative pressure-temperature equilibrium projection.
Ar: triple point ■; critical point ●; equilibria —.
CH_4: triple point ■; critical point ●; equilibria —.
♦ : solid2-solid1-liquid-vapor equilibrium; — : three phase lines; — : critical line.

According to Figure 6.12-Figure 6.14, the system Ar+CH_4 presents total miscibility in the liquid phase and partial miscibility in the solid phase.

The calculated PT-EP for this mixture is in Figure 6.15. Colors are the same of Figure 6.14. The notations sve, sle, and vle have been added in Figure 6.15 for indicating the sublimation, melting, and saturation lines of the two pure components. A zoom of Figure 6.14 in the proximity of the triple points of the two components is given in Figure 6.16.

The liquid-vapor critical line (l=v) originates at about 151 K, namely the critical temperature of Ar, and ends at about 190 K, the critical value for CH_4.

The s_2lve curve exits the triple point of CH_4 (91 K) and joins the quadruple point, where also the s_1lve arrives after leaving the triple point of Ar (84 K). The s_2lve is portrayed in Figure 6.15 by the dashed-dotted-dotted-dashed blue line, whereas the s_1lve is the continuous blue line.

The s_2s_1ve is the dashed-dotted blue line leaving the black diamond and extending in the low pressure region, and the s_2s_1le is the dashed line moving in the high pressure region.

The coexistence of the $solid_2$, $solid_1$, liquid, and vapor phases at equilibrium has been calculated at 71.2 K and 8.9 kPa; compositions in mole fraction of Ar are xs2= 0.39, xl= 0.6, xs1= 0.71, xv= 0.97.

Similarly to what happens for the slve curve in the system Ar+Kr, the s_2lve reaches a maximum in pressure before ending in the quadruple point. This maximum has been calculated at about 84.5 K, 0.025 MPa, and a mole fraction of Ar in the liquid phase of 0.18.

This behavior entails the presence of two temperatures of $s_2$lve for each pressure between the triple point pressure of CH_4 and 0.025 MPa.

Six main isobars are indicated in Figure 6.15: P0 (4 kPa), P1 (0.011 MPa), P2 (0.02 MPa), P3 (0.04 MPa), P4 (0.1 MPa), and P5 (10 MPa). The Tx-CSs corresponding to these pressures are portrayed in Figure 6.17 in the range 65 K – 115 K. The Tx-CS diagram at P5 is similar to P3 for the system Ar+Kr, seeing that no vle are involved and the s2s1e, s2le, and s1le are similar to those presented in the Tx-CS at 0.1 MPa (P4).

In Figure 6.4, considering increasing temperatures from an initial value of 70 K, the line corresponding to P0 meets the sublimation line of Ar and then the one of Kr. These two values are respectively placed at xAr=1 and xAr=0 in the Tx-CS related to pressure P0 in Figure 6.5.

At P0 the immiscibility in the solid phase entails the presence of a solid$_2$-solid$_1$-vapor equilibrium temperature (66.9 K).

P1 is located slightly under the triple point pressure of pure CH_4 (0.0117 MPa) but above the pressure at the quadruple point. Similarly to the case of N_2+Ar the liquid phase occurring at this pressure is not a consequence of the presence of a stable liquid phase for the pure compounds, what instead has been observed for the case of solid solution in the Ar+Kr system.

As a consequence, also in case of quadruple point and eutectic behavior the liquid phase is confined among other equilibria, as it is possible to appreciate in the Tx-CS relative to P1 in Figure 6.17.

The liquid phase placed in the triangle in the middle of the Tx-CS at about 72 K offers three equilibria: a $s_2$le with a solid rich in CH_4, a $s_1$le with the solid rich in Ar, and a vle with the vapor.

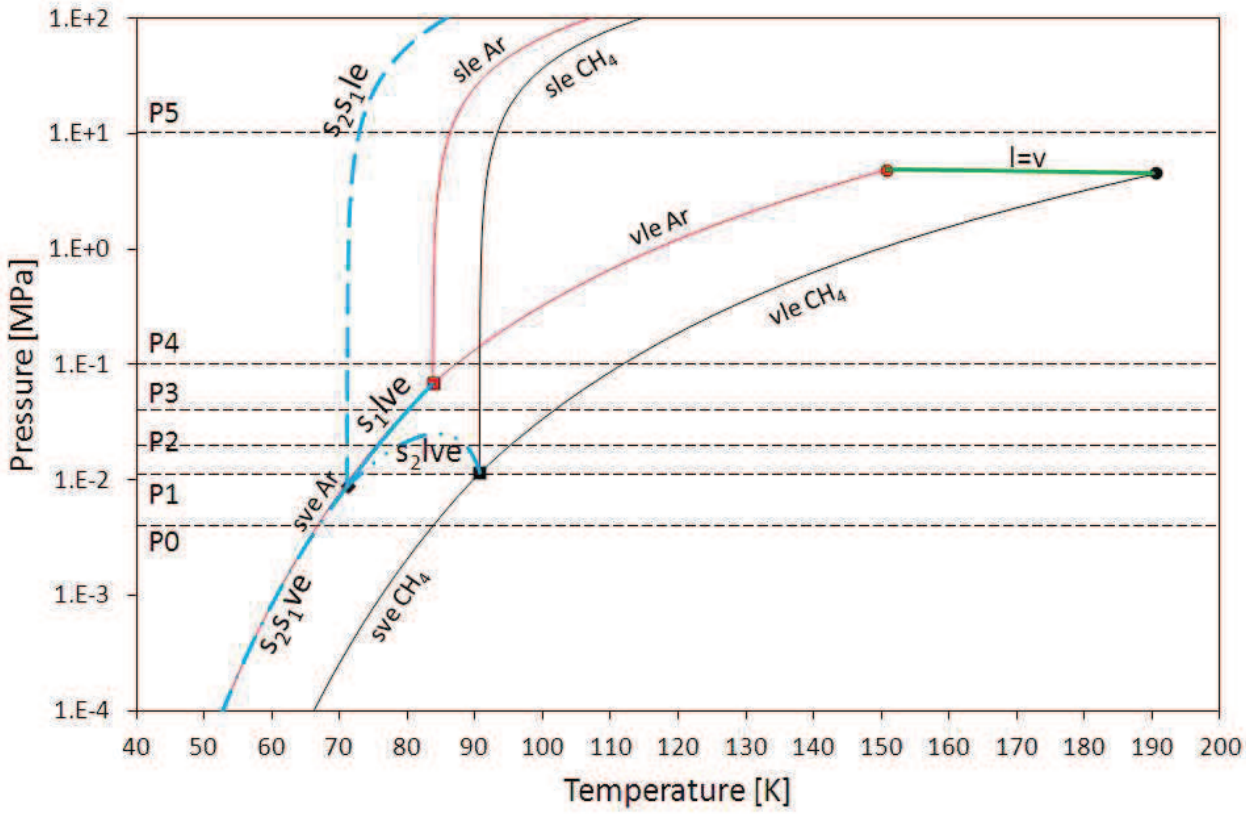

Figure 6.15: Mixture Ar+CH_4: calculated pressure-temperature equilibrium projection.
Ar: triple point ■; critical point ●; solid-liquid, solid-vapor, and vapor-liquid equilibria —.
CH_4: triple point ■; critical point ●; solid-liquid, solid-vapor, and vapor-liquid equilibria —.
♦ : solid$_2$-solid$_1$-liquid-vapor equilibrium; — : solid$_1$-liquid-vapor three phase line; — — : solid$_2$-solid$_1$-liquid three phase line; — • — : solid$_2$-solid$_1$-vapor three phase line; — • • — : solid$_2$-liquid-vapor three phase line; — : critical line.

At P1 three equilibria involving three phases occur: the s_2s_1le (71.2 K), the s_1lve (72.3 K), and the s_2lve (72.9 K).

At P2 one of the two components starts to be stable as pure also in the liquid phase. P2 is greater than the triple point pressure of pure CH_4, so that the pure CH_4 presents a sle and a vle temperatures. A s_2le extend from the sle temperature of pure CH_4 down to an upper s_2lve temperature, where also the vle coming from the vle temperature of pure CH_4 ends. This s_2lve temperature has been calculated at 88.5 K.

The sve is at P2 confined between two s_2lve temperatures, and the lower one has reached a higher temperature (78.8 K) compared to the value previously calculated at P1 (72.9 K). Also the s_1lve temperature has increased (75.7 K), while the s_2s_1le is always constant at 71.2 K. To sum up, at P2 four equilibria involving three phases occur: the s_2s_1le, the s_1lve, and a lower and an upper s_2lve.

Two s_2lve temperatures are present in the Tx-CS up to the maximum pressure of the s_2lve curve (0.025 MPa). When this value is exceeded, P3, the vle has moved enough to make the s_2ve disappear, and the liquid phase that were bounded in the triangle in the middle of the Tx-CS at P2 joins together with the liquid phase rich in CH_4. At P3 Ar still presents a sve temperature, so that a s_1lve occurs (80.1 K).

The extent of the s_1ve progressively reduces from P0 up to P3, disappearing when the system pressure is greater than the triple point pressure of pure Ar (0.069 MPa).

When the pressure is greater than this value, as in the Tx-CS at P4 in Figure 6.17, the vapor phase is not at equilibrium with the solid phase anymore, and a separate vle lens is located at higher temperatures ranging between the vle temperatures of the two pure compounds.

At P4 there is a sole three phase temperature, related to the s_2s_1le equilibrium (71.2 K).

The s_2s_1e, s_2le, and s_1le assume the form of Figure 6.12, and these equilibria remain almost unchanged with increasing pressures, while the vle do not occur for pressure greater than the liquid-vapor critical line (l=v) of Figure 6.15.

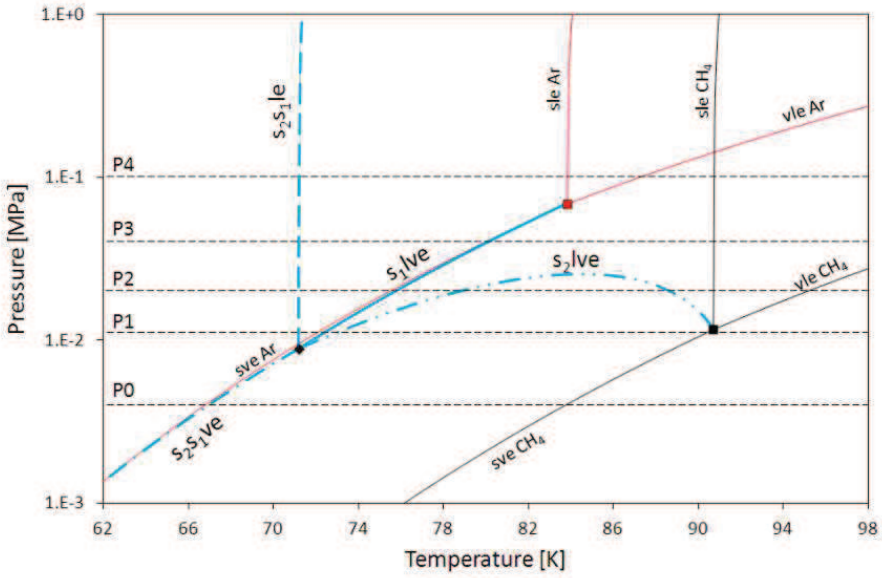

Figure 6.16: Mixture Ar+CH_4: calculated pressure-temperature equilibrium projection in the proximity of the triple points.
Ar: triple point ■; solid-liquid, solid-vapor, and vapor-liquid equilibria —. CH_4: triple point ■; solid-liquid, solid-vapor, and vapor-liquid equilibria —.
♦ : solid2-solid1-liquid-vapor equilibrium; — : $solid_1$-liquid-vapor three phase line; — — : $solid_2$-$solid_1$-liquid three phase line; — • — : $solid_2$-$solid_1$-vapor three phase line; — • • — : $solid_2$-liquid-vapor three phase line.

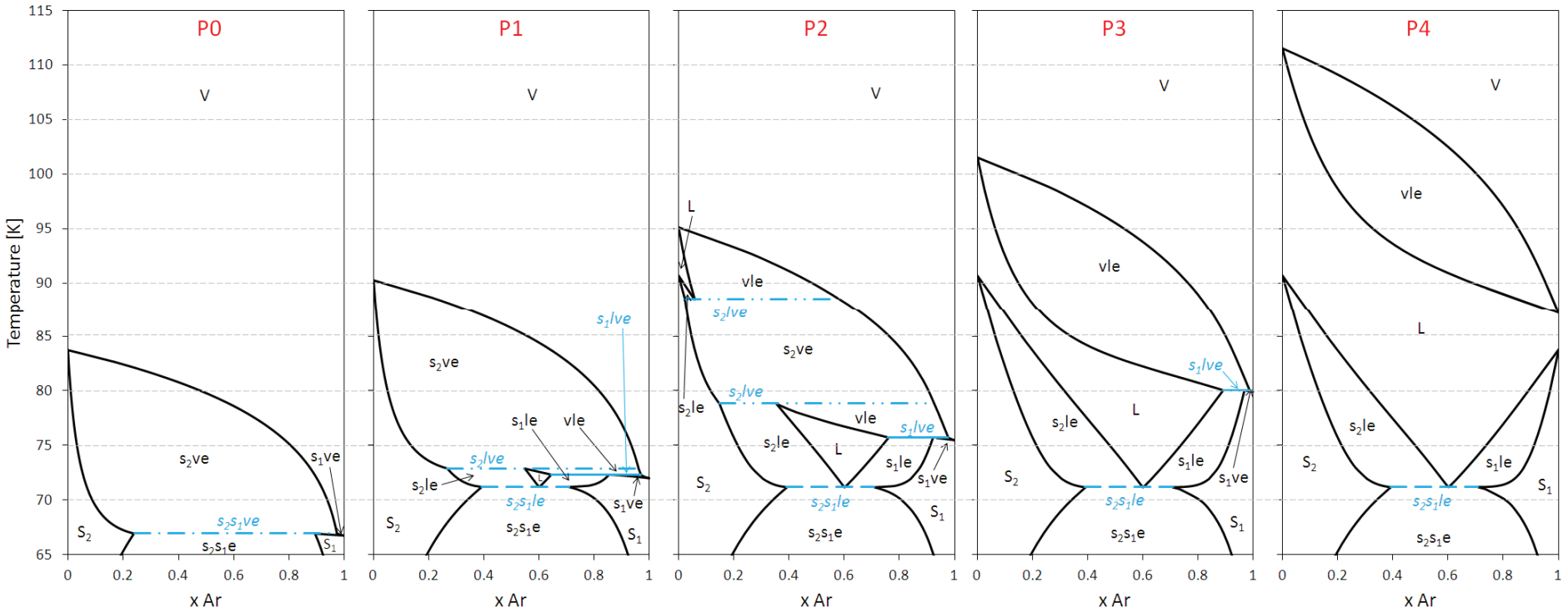

Figure 6.17: Mixture Ar+CH_4: evolution of the phase equilibrium behavior with pressure in the range 65 K – 115 K.
P0 = 4 kPa; P1 = 0.011 MPa; P2 = 0.02 MPa; P3 = 0.04 MPa; P4 = 0.1 MPa. — : $solid_1$-liquid-vapor equilibrium temperature; — • — : $solid_2$-$solid_1$-vapor equilibrium temperature; — • • — : $solid_2$-liquid-vapor equilibrium temperature; — — : $solid_2$-$solid_1$-liquid equilibrium temperature; $S_{1,2}$: solid phase; L : liquid phase; V : vapor phase; $s_{1,2}ve$: solid-vapor equilibrium; $s_{1,2}le$: solid-liquid equilibrium; vle : vapor-liquid equilibrium; s_2s_1e : $solid_2$-$solid_1$ equilibrium.

6.3.3 Type IIb PT-EP: O_2+C_2H_6

In 2007, Houssin-Abbomson published her thesis results concerning the solubility of light hydrocarbons (C_2H_6, C_2H_4, and C_3H_8) in liquid oxygen, [112]. Her work aimed at improving the knowledge of the phase equilibrium behavior in order to better understand the problem related to the accumulation of light hydrocarbons within the reboiler-condenser placed in between the two columns in the air separation unit.

It is worth remembering that the vapor-liquid equilibria published in 2007 represent the only source of experimental values hitherto available for the mixtures of oxygen and C_2H_6, C_2H_4, and C_3H_8.

The results concerning the vapor-liquid equilibrium for the system O_2+C_2H_6 at 112 K, 120K, and 129 K are shown by empty circles in Figure 6.18. The values calculated with the SLV EoS are in rather good agreement with the data, even if model deviates for composition approaching pure oxygen.

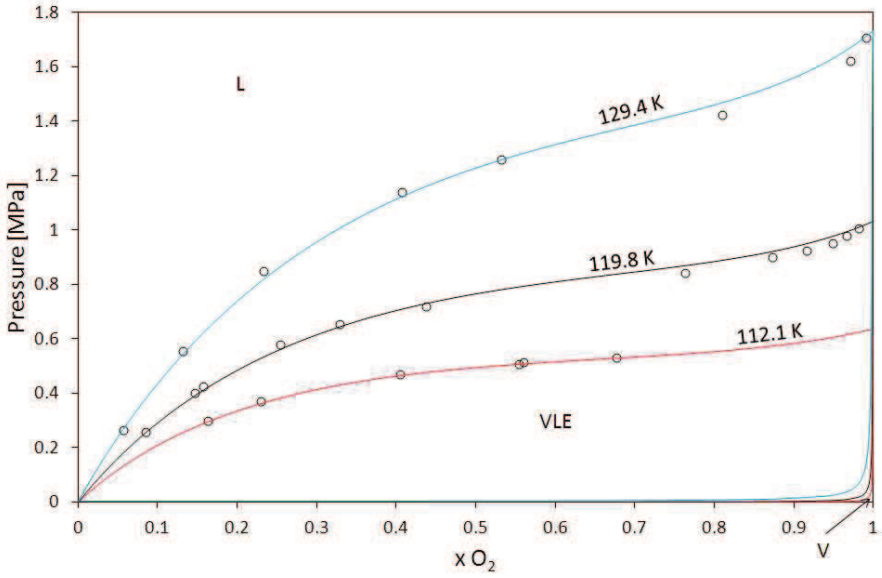

Figure 6.18: Mixture O_2+C_2H_6: comparison between experimental and calculated values of VLE.
Experimental values [112]: 112.1 K (Δ), 119.8 K (○), 129.4 K (□).
Calculated values: 112.1 K (—), 119.8 K (—), 129.4 K (—).

According to Figure 6.18, ethane is totally miscible in liquid oxygen from 112 K up to 130 K.

In [112], the PR EoS (with binary interaction parameters depending on temperature) was used for predicting the phase equilibrium behavior of the mixture at lower temperatures, and immiscibility in the liquid phase was predicted at about 92 K.

The partial immiscibility in the liquid phase had previously been argued by McKinley and Wang, of the Air Products Company, [113]. Those authors realized measures concerning the solubility of solid C_2H_6 in liquid O_2, bearing that the system presents two branches of solubility separated by a region of liquid-liquid immiscibility.

According to McKinley and Wang, at 84.3 K two liquid phases coexist at equilibrium with a solid phase in the system O_2+C_2H_6. These two liquid phases have a O_2 composition of 0.26 and 0.84.

These two compositions are portrayed by red triangles in Figure 6.19 at the solid-liquid$_2$-liquid$_1$ equilibrium temperature.

In Figure 6.19 points represent the available data concerning the solid-liquid equilibrium in the system O_2+C_2H_6. In can be seen that experimental values from different authors are in a poor agreement; the data of Himmelberg, [114], extend at temperatures greater than the triple point temperature of pure C_2H_6 (90.4 K); the compositions in the L_1 phase of Cox and De Vries, [115], Kar-

wat and Klein, [116], and McKinley and Wang [113]-[117] present different solubilities of solid ethane. For xO_2<0.3, the data proposed by McKinley and Wang in [113]-[117] exit the solid-liquid$_2$-liquid$_1$ equilibrium ending at the triple point temperature of C_2H_6.

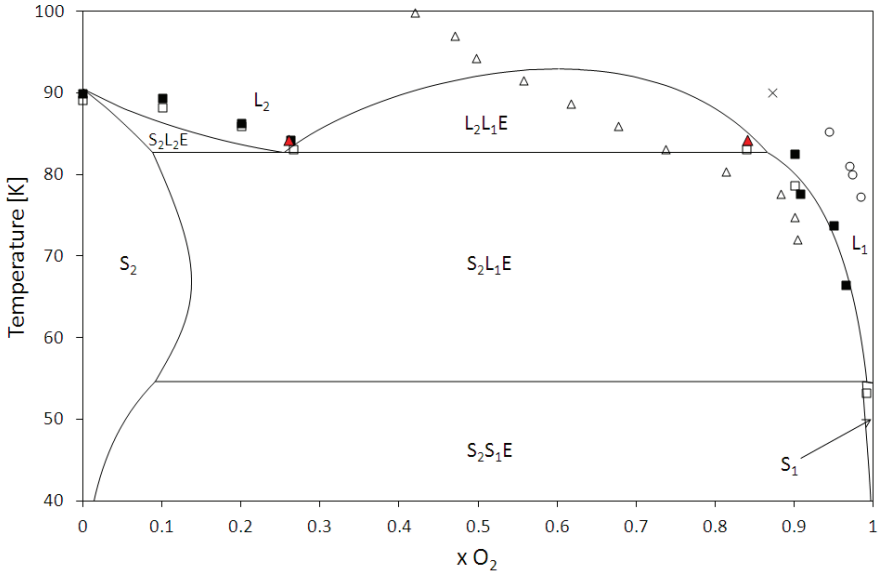

Figure 6.19: Mixture O_2+C_2H_6: comparison between experimental and calculated values of SLE.
Experimental values: ○ [115], × [116], Δ [114], □ [117], ■ and ▲ [113]. — : calculated values.

Binary interaction parameters have been regressed in order to match the phase equilibrium behavior proposed by McKinley and Wang, seeing that data cover a wider range of temperature and composition. As a consequence, the SLV EoS gives a partial immiscibility in the solid phase.

Nevertheless, it has not been possible to tune the parameters in order to match exactly the three phase equilibrium temperature proposed in [113], and also composition in the L_2 phase are only qualitatively representative of the data.

The calculated sl_2l_1e temperature is 82.7 K, and the corresponding compositions in O_2 in the L_2 and L_1 phases are 0.25 and 0.87, respectively. L_2 is the liquid phase rich in C_2H_6, L_1 is the liquid phase rich in O_2. The immiscibility in the liquid phase has been evaluated at 93 K, for xO_2=0.6.

In Figure 6.19, the model gives a stable solid phase S_1 for the one experimental point of [117], which results located under the solid$_2$-solid$_1$-liquid$_1$ equilibrium temperature (about 55 K).

The qualitative pressure-temperature equilibrium behavior for the system O_2+C_2H_6 is the one portrayed in Figure 6.20. Red and black lines are the saturation, sublimation, and melting lines of O_2 and C_2H_6, respectively. As for the previous systems, triple and critical points are indicated by squares and circles, respectively.

With reference to the liquid phases, the PT-EP of the system corresponds to the type II following the notation of van Konynenburg and Scott. A continuous liquid-vapor critical line (l=v) joins together the critical point of the pure components, while a second critical line occurs at lower temperature.

This curve represents the limit of the immiscibility in the liquid phase (l_2=l_1) in terms of temperature and pressure. The system presents total miscibility in the liquid phase for temperature greater than the upper critical endpoint of the liquid$_2$-liquid$_1$-vapor three phase line ($l_2l_1$ve).

The l_2=l_1 critical line extends from the UCEP of the $l_2l_1$ve (the green triangle) up to the UCEP of the solid$_2$-liquid$_2$-liquid$_1$ three phase line ($s_2l_2l_1$e), the green square.

The $l_2l_1$ve and $s_2l_2l_1$e meet together at the solid$_2$-liquid$_2$-liquid$_1$-vapor ($s_2l_2l_1$v) quadruple point (the black triangle of Figure 6.20) together with the solid$_2$-liquid$_2$-vapor ($s_2l_2$ve)and the solid$_2$-

liquid$_1$-vapor (s_2l_1ve) three phase lines. The s_2l_2ve reaches the triple point of C_2H_6, the s_2l_1ve moves down to a lower quadruple point, the black diamond.

In this point, the four coexisting phase are solid$_2$, solid$_1$, liquid$_1$, and vapor ($s_2s_1l_1v$). The qualitative PT-EP is completed by three supplementary three phase lines: the solid$_2$-solid$_1$-vapor (s_2s_1ve), extending at low pressures, the solid$_2$-solid$_1$-liquid$_1$ ($s_2s_1l_1e$), exploring the high pressures, and the solid$_1$-liquid$_1$-vapor (s_1l_1ve), joining the triple point of O_2.

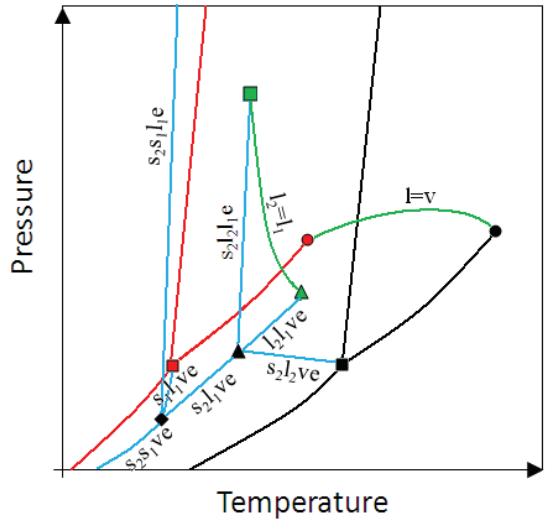

Figure 6.20: Mixture O_2+C_2H_6: qualitative pressure-temperature equilibrium projection.
O_2: triple point ■; critical point ●; equilibria —.
C_2H_6: triple point ■; critical point ●; equilibria —.
♦ : solid$_2$-solid$_1$-liquid$_1$-vapor equilibrium; ▲ : solid$_2$-liquid$_2$-liquid$_1$-vapor equilibrium; — : three phase lines; ▲ : upper critical endpoint of the liquid$_2$-liquid$_1$-vapor three phase line; ■ : upper critical endpoint of the solid$_2$-liquid$_2$-liquid$_1$ three phase line; — : critical lines.

The calculated PT-EP for the mixture is in Figure 6.21. Colors are the same of Figure 6.20. The notations sve, sle, and vle have been added in Figure 6.21 for indicating the sublimation, melting, and saturation lines of the two pure components. A zoom of Figure 6.21 in the proximity of the triple point of O_2 is given in Figure 6.22.

The liquid-vapor critical line (l=v) originates at about 155 K, namely the critical temperature of O_2, and ends at about 305 K, the critical value for C_2H_6.

In Figure 6.21, the black diamond represents the $s_2s_1l_1v$ quadruple point (54.4 K, 0.15 kPa), the black triangle is the $s_2l_2l_1v$ quadruple point (82.7 K, 0.039 MPa), the green triangle is the Upper Critical EndPoint (UCEP) of the l_2l_1ve three phase line (93 K, 0.12 MPa). The UCEP of the $s_2l_2l_1v$ occurs at pressure greater than 100 MPa, thus is not portrayed in Figure 6.21.

The dashed-dotted-dotted-dashed blue line is the s_2l_2ve curve leaving the triple point of C_2H_6 (90 K) and joining the $s_2l_2l_1v$ quadruple point. From this point, the dashed blue line of l_2l_1ve extends up to its UCEP, where the critical line l_2=l_1 originates. For temperatures greater than 93K the system presents total miscibility in the liquid phase, as experimentally proved by the data published in 2007 by Houssin-Abbomson, [112].

The dotted blue line in Figure 6.21 is the evolution of the $s_2l_2l_1e$ from the $s_2l_2l_1v$ quadruple point up to 100 MPa, whereas the continuous blue line is the s_1lve down to the $s_2s_1l_1v$ quadruple point (black diamond). From this lower quadruple point, three lines originate: the dashed-dotted blue line of s_2s_1ve, a dashed-dashed blue line of s_2s_1le, and a third line of s_1l_1ve ending in the triple point of O_2. This last three phase line is not represented in Figure 6.21 since the $s_2s_1l_1v$ quadruple point is close to the triple point of O_2.

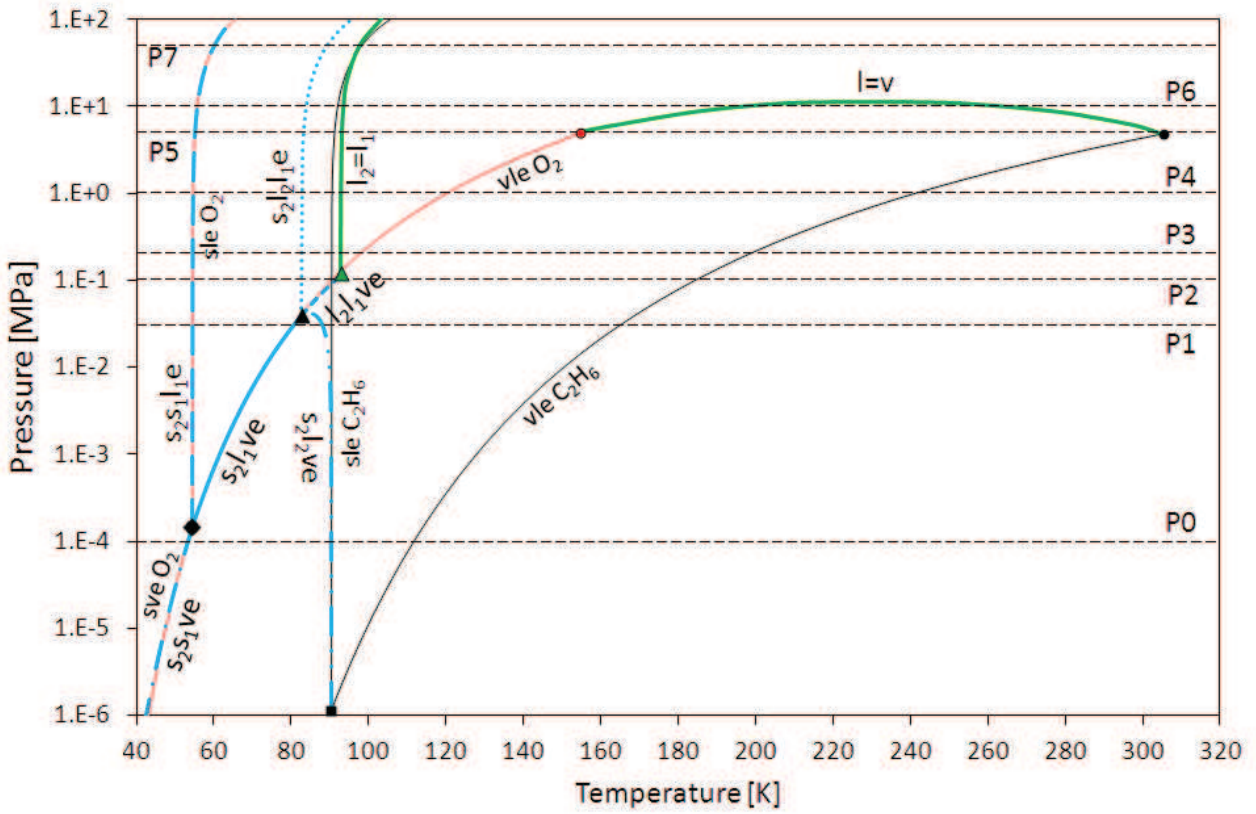

Figure 6.21: Mixture O_2+C_2H_6: calculated pressure-temperature equilibrium projection.
O_2: triple point ■; critical point ●; solid-liquid, solid-vapor, and vapor-liquid equilibria —.
C_2H_6: triple point ■; critical point ●; solid-liquid and vapor-liquid equilibria —.
♦ : solid$_2$-solid$_1$-liquid-vapor equilibrium; ▲ : solid$_2$-liquid$_2$-liquid$_1$-vapor equilibrium; — : solid$_2$-liquid$_1$-vapor three phase line; — — : solid$_2$-solid$_1$-liquid$_1$ three phase line; — • — : solid$_2$-solid$_1$-vapor three phase line; — • • — : solid$_2$-liquid$_2$-vapor three phase line; ••• : solid$_2$-liquid$_2$-liquid$_1$ three phase line; – – : liquid$_2$-liquid$_1$-vapor three phase line; ▲ : upper critical endpoint of the l_2l_1v three phase line; — : critical lines.

Eight main isobars are indicated in Figure 6.21: P0 (0.1 kPa), P1 (0.03 MPa), P2 (0.1 MPa), P3 (0.2 MPa), P4 (1 MPa), P5 (4.9 MPa), P6 (10 MPa), and P7 (50 MPa). The Tx-CSs corresponding to pressures P0, P1, P2, and P3 are portrayed in Figure 6.23 in the range 40 K – 200 K, while the Tx-CSs corresponding to pressures P4, P5, P6, and P7 are portrayed in Figure 6.24 in the range 40 K – 320 K. The first four isobars are also indicated in the calculated PT-EP of Figure 6.22.

In Figure 6.21, considering increasing temperatures from an initial value of 40 K, the line corresponding to P0 meets the sublimation line of O_2, the s_2s_1ve, the s_2l_2ve, and then the sublimation and saturation lines of C_2H_6. The sublimation temperatures of the pure components are placed respectively at xO_2=1 and xO_2=0 in the Tx-CS related to pressure P0 in Figure 6.23. Also the saturation temperature of C_2H_6, is at xO_2=0.

At P0 the immiscibility in the solid phase entails the presence of a s_2s_1ve at 53.3 K, and a s_2l_2ve (90.4 K) occurs seeing that pure C_2H_6 can also be in the liquid phase at P0. To sum up, at P0 there are five equilibria (s_2s_1e, s_1ve, s_2ve, s_2l_2e, and vl_2e) and two three phase equilibria (s_2s_1ve and s_2l_2ve).

P1 is located slightly under the $s_2l_2l_1v$ quadruple point (0.039 MPa). At P1 also O_2 has a melting and a saturation temperature, so that a liquid phase rich in O_2 entails the appearance of additional binary equilibria: s_2l_1e, s_1l_1e, and vl_1e. Conversely, the s_1ve disappears, the extent of the s_2ve reduces, and the s_2s_1ve is replaced by the $s_2s_1l_1e$.

At P1 there are 3 three phase lines: the $s_2s_1l_1e$ (54.6 K), the s_2l_1ve (80.6 K), and the s_2l_2ve (88.2 K). With respect to the s_2l_2ve temperatures at P0 and P1, it can be stated that the s_2l_2v equilibrium moves at lower pressure with increasing pressures.

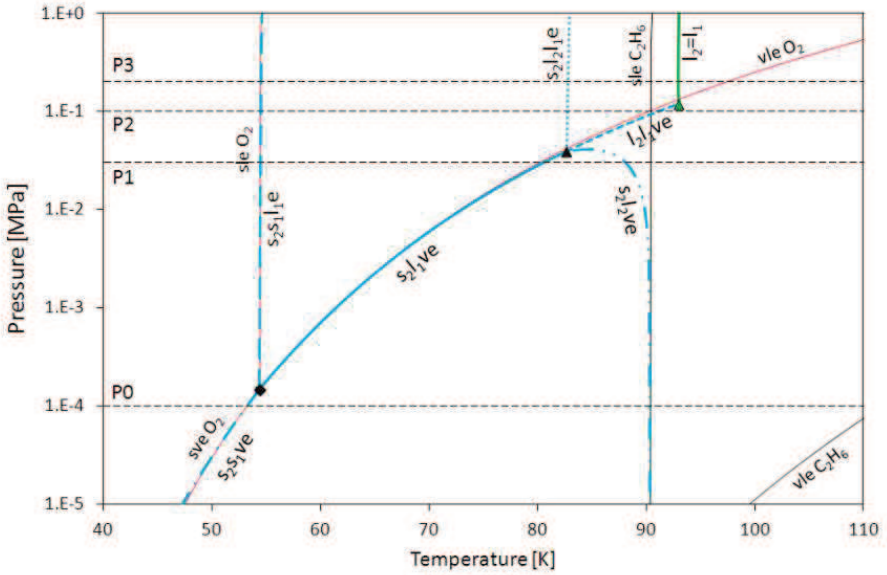

Figure 6.22: Mixture O_2+C_2H_6: calculated pressure-temperature equilibrium projection in the proximity of the triple point of O_2.
O_2: triple point ■; solid-liquid, solid-vapor, and vapor-liquid equilibria —. C_2H_6: vapor-liquid equilibria —.
♦ : solid$_2$-solid$_1$-liquid-vapor equilibrium; ▲ : solid$_2$-liquid$_2$-liquid$_1$-vapor equilibrium; — : solid$_2$-liquid$_1$-vapor three phase line; — — : solid$_2$-solid$_1$-liquid$_1$ three phase line; — • — : solid$_2$-solid$_1$-vapor three phase line; — • • — : solid$_2$-liquid$_2$-vapor three phase line; ••• : solid$_2$-liquid$_2$-liquid$_1$ three phase line; – – : liquid$_2$-liquid$_1$-vapor three phase line; ▲ : upper critical endpoint of the l_2l_2v three phase line;— : liquid$_2$-liquid$_1$ critical line.

At the same moment, the s_2l_1v equilibrium temperature increases with increasing pressures, so that there will be a pressure at which these two three phase lines merge together. This pressure is then related to the $s_2l_2l_1v$ quadruple point, the black triangle of Figure 6.22.

For pressures greater than the pressure at the $s_2l_2l_1v$ quadruple point (0.039 MPa), the solid S_2 is no longer involved in equilibria with the vapor, as indicated in the Tx-CS at P2 in Figure 6.23.

At P2 (0.1 MPa), the three phase lines involved are: the $s_2s_1l_1$ (54.6 K), the $s_2l_2l_1$ (82.7 K), and the l_2l_1v (91.15 K). Immiscibility in the liquid phase occurs, and the immiscibility gap ends in the vapor-liquid lens yielding the l_2l_1ve. The liquid phase rich in O_2 is bounded by the s_1l_1e, the l_2l_1e, and the vl_1e. The liquid phase rich in C_2H_6 is bounded by the s_2l_2e, the l_2l_1e, and the vl_2e.

At P3 (0.2 MPa) the vl_2e extends itself at higher temperatures, so that the liquid$_2$-liquid$_1$ immiscibility ends at the l_2=l_1 critical temperature (93 K), while the two liquid phases are totally miscible at higher temperatures. The Tx-CS related to P3 in Figure 6.23 shows again the $s_2s_1l_1e$ (54.6 K) and the $s_2l_2l_1e$ (82.7 K).

For increasing pressures, the vapor-liquid equilibrium lens moves to higher temperatures following the vle temperatures of the two pure compounds, while the dense region (involving solid-solid and solid-liquid equilibria) remains almost unchanged. At P4 (1 MPa), the vle extends from the saturation temperature of O_2 (119.3 K) up to the saturation temperature of C_2H_6 (240 K), Figure 6.24.

At 4.9 MPa (P5), C_2H_6 is supercritical, and the vle lens originating in the saturation temperature of pure O_2 ends in a vapor-liquid critical point (304.2 K). When the pressure is greater than the critical pressure of O_2 (5 MPa), a second v=l point occurs. This case is portrayed by the Tx-Cs related to pressure P6 (10 MPa). The two critical temperatures are 198.1 K and 262.9 K.

Finally, at 50 MPa (P7 in Figure 6.23) the system presents equilibria only in the dense region.

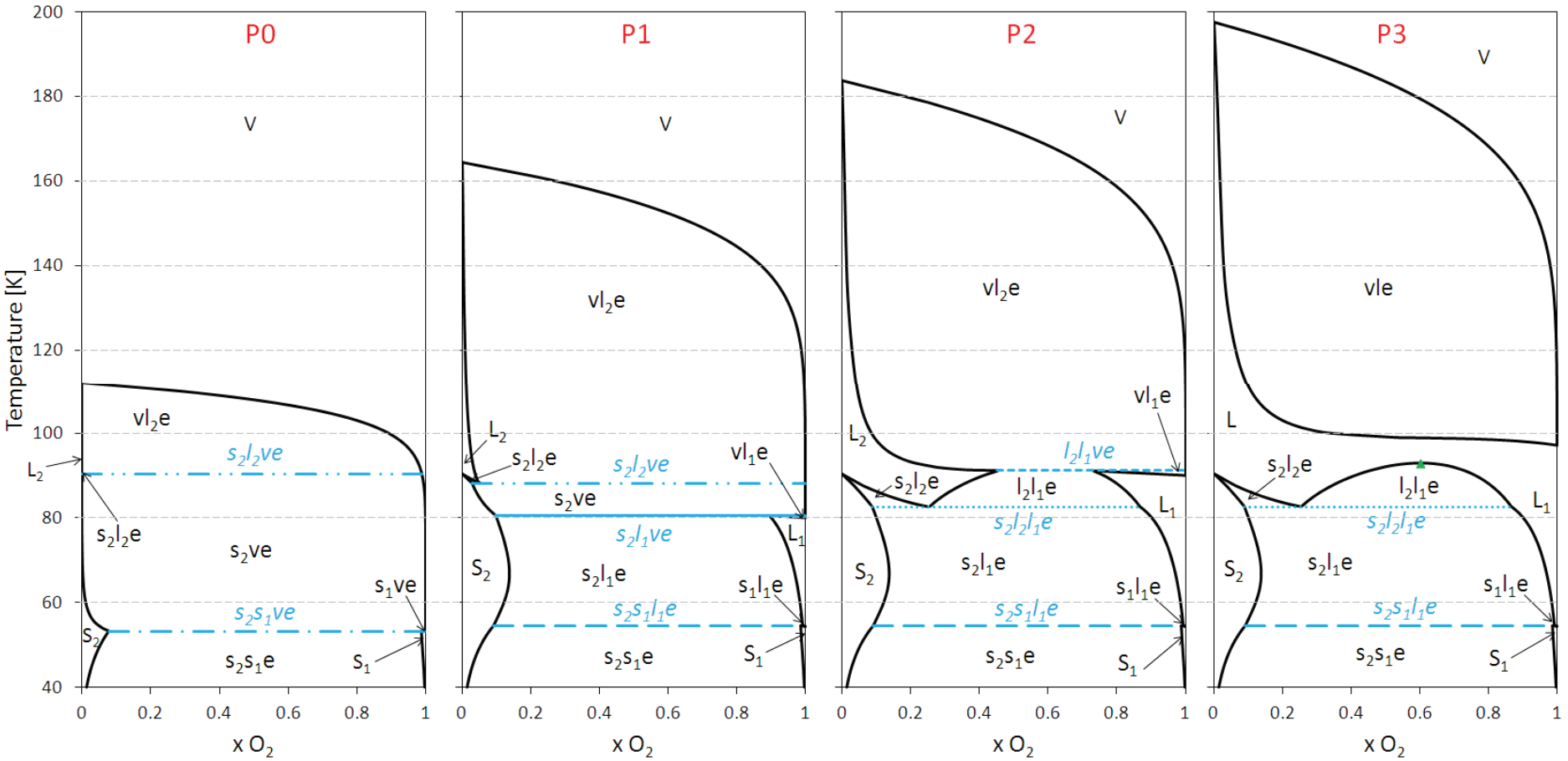

Figure 6.23: Mixture O_2+C_2H_6: evolution of the phase equilibrium behavior with pressure in the range 40 K – 200 K up to 0.2 MPa.
P0 = 0.1 kPa; P1 = 0.03 MPa; P2 = 0.1 MPa; P3 = 0.2 MPa. — : solid$_2$-liquid$_1$-vapor equilibrium temperature; — • — : solid$_2$-solid$_1$-vapor equilibrium temperature; — • • — : solid$_2$-liquid$_2$-vapor equilibrium temperature; — — : solid$_2$-solid$_1$-liquid$_1$ equilibrium temperature; – – : liquid$_2$-liquid$_1$-vapor equilibrium temperature; ••• : solid$_2$-liquid$_2$-liquid$_1$ equilibrium temperature; $S_{1,2}$: solid phase; $L_{1,2}$: liquid phases; V : vapor phase; $s_{1,2}$ve : solid-vapor equilibrium; $s_{1,2}l_{1,2}$e : solid-liquid equilibrium; $vl_{1,2}$e : vapor-liquid equilibrium; s_2s_1e : solid$_2$-solid$_1$ equilibrium; l_2l_1e : liquid$_2$-liquid$_1$ equilibrium; ▲ : critical point.

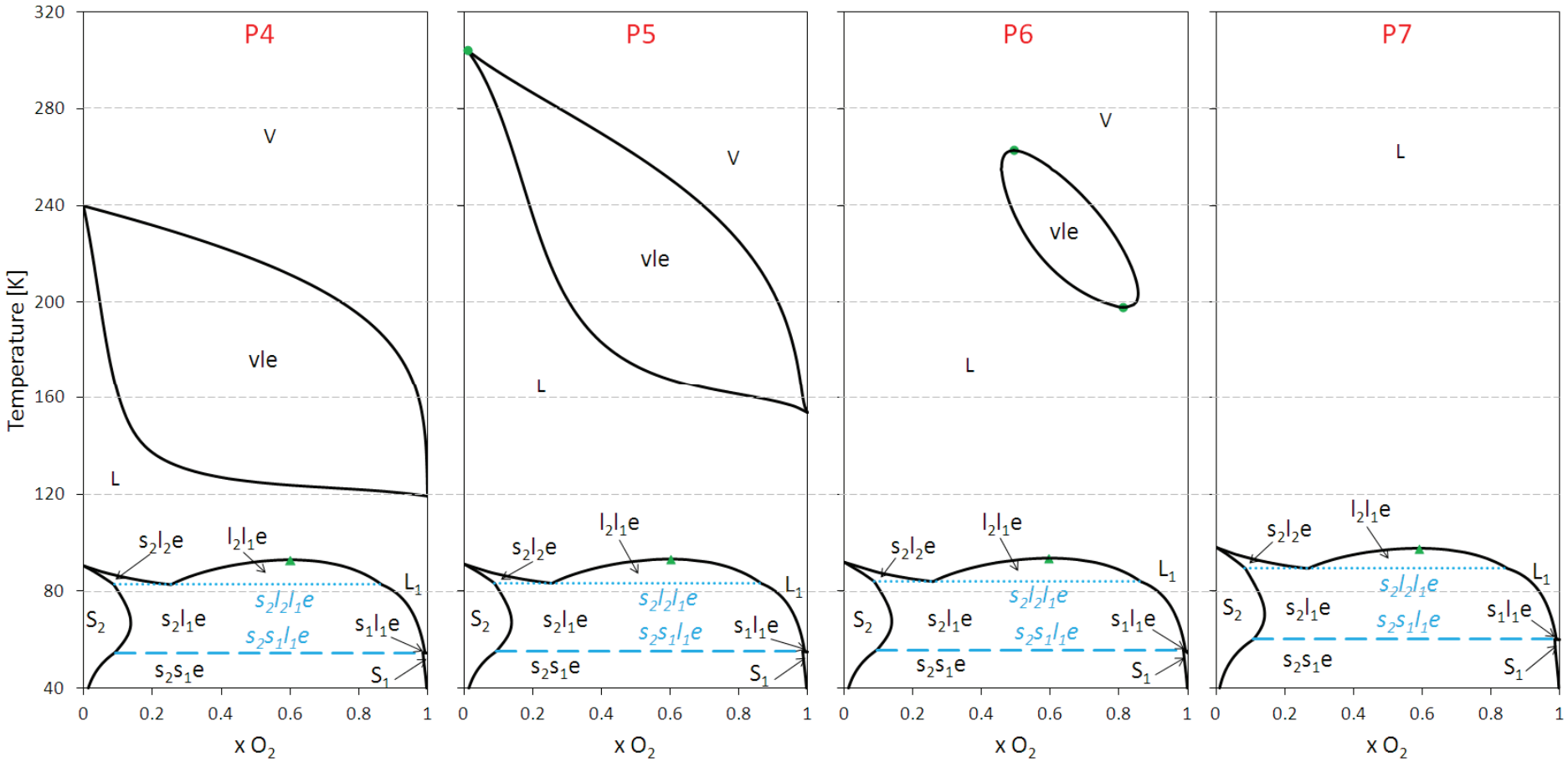

Figure 6.24: Mixture O_2+C_2H_6: evolution of the phase equilibrium behavior with pressure in the range 40 K – 320 K for P > 0.2 MPa.
P4 = 1 MPa; P5 = 4.9 MPa; P6 = 10 MPa; P7 = 50 MPa. — — : solid$_2$-solid$_1$-liquid$_1$ equilibrium temperature; ••• : solid$_2$-liquid$_2$-liquid$_1$ equilibrium temperature; $S_{1,2}$: solid phase; $L_{1,2}$: liquid phases; V : vapor phase; $s_{1,2}l_{1,2}e$: solid-liquid equilibrium; vle : vapor-liquid equilibrium; s_2s_1e : solid$_2$-solid$_1$ equilibrium; l_2l_1e : liquid$_2$-liquid$_1$ equilibrium; ▲ : critical points.

6.3.4 Type IIIb+c PT-EP: system N_2+C_2H_6

The comparison between the few experimental values of the solubility of solid C_2H_6 in liquid N_2 and the model is illustrated in Figure 6.25. The experimental values are located along the liquidus line of the solid$_2$-liquid$_1$ equilibrium, seeing that the system presents immiscibility in both the liquid and the vapor phases.

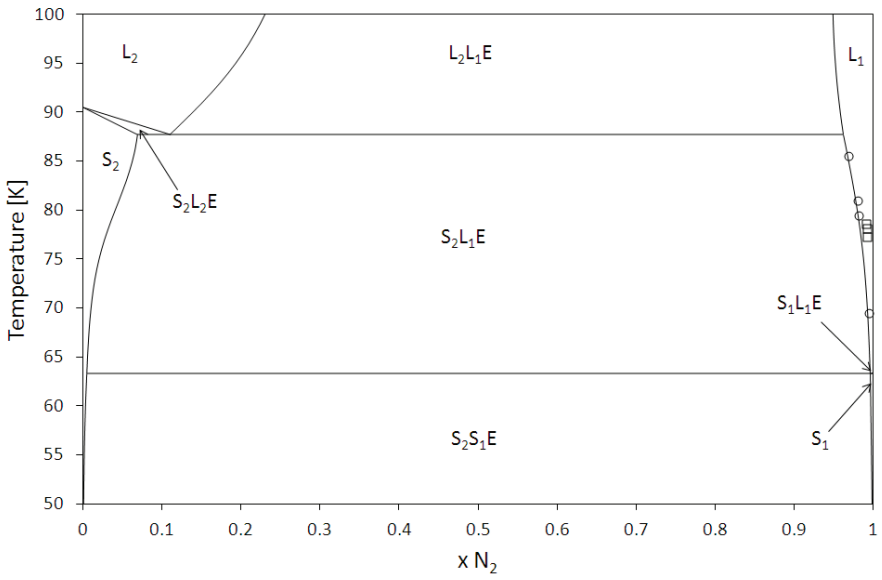

Figure 6.25: Mixture N_2+C_2H_6: comparison between experimental and calculated values of SLE.
Experimental values: □ [115], ○ [118]. — : calculated values.

The qualitative comparison between the experimental isotherms at 172 K, 220 K, and 260 K and values calculated by the SLV EoS can be appreciated in Figure 6.26. N_2 is supercritical at all the three temperatures and the vapor-liquid lenses ends at a vapor-liquid critical pressure.

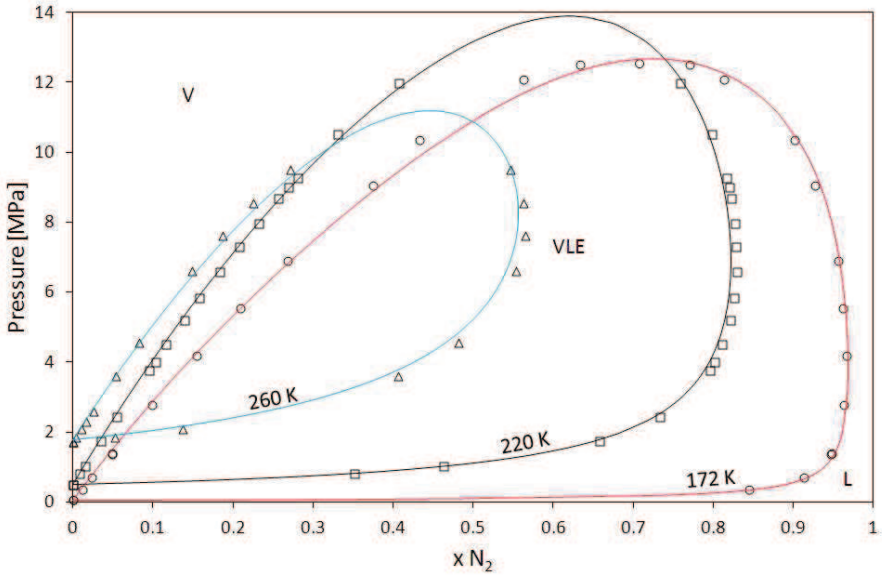

Figure 6.26: Mixture N_2+C_2H_6: comparison between experimental and calculated values of VLE.
Experimental values: ○ : 172 K, [119]; □ : 220 K, [120]; Δ : 260 K, [121].
Calculated values: 172 K (—), 220 K (—), 260 K (—).

Figure 6.27 is the qualitative PT-EP representative of the phase equilibrium behavior of the system N_2+C_2H_6. Red and black lines are the saturation, sublimation, and melting lines of N_2 and C_2H_6, respectively. Keeping the same distinction in terms of color, triple and critical points are indicated by squares and circles, respectively.

With reference to the liquid phases, the PT-EP of the system corresponds to the type III following the notation of van Konynenburg and Scott.

A liquid-vapor critical line (l=v) joins the critical point of C_2H_6 and the upper critical endpoint (UCEP) of the solid$_2$-liquid$_2$-liquid$_1$ three phase line.

A second l=v line joins the critical point of N_2 and the UCEP of the liquid$_2$-liquid$_1$-vapor three phase line. The UCEPs of the $s_2l_2l_1e$ and the l_2l_1ve are represented in Figure 6.27 by green square and green triangle, respectively.

The blue lines in Figure 6.27 represent the conditions for three coexisting phases at equilibrium in terms of temperature and pressure.

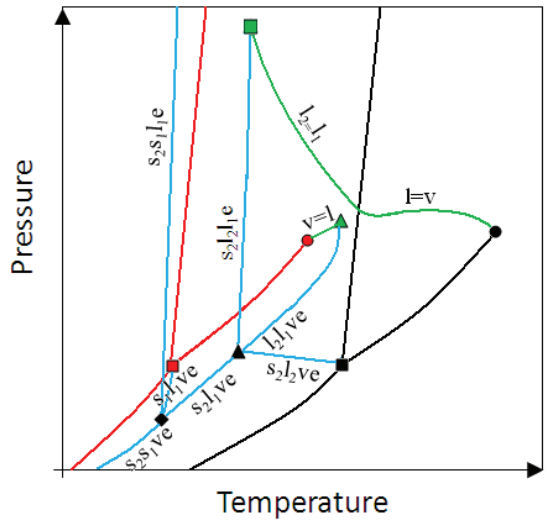

Figure 6.27: Mixture N_2+C_2H_6: qualitative pressure-temperature equilibrium projection.
N_2: triple point ■; critical point ●; equilibria —.
C_2H_6: triple point ■; critical point ●; equilibria —.
♦ : solid$_2$-solid$_1$-liquid-vapor equilibrium; ▲ : solid$_2$-liquid$_2$-liquid$_1$-vapor equilibrium; — : three phase lines; ■ , ▲ : upper critical endpoints; — : critical lines.

Except for the critical lines, the PT-EP of the system N_2+C_2H_6 is similar to that representative of the system O_2+C_2H_6.

There are 7 blue lines indicating seven different three phase equilibria: s_2s_1ve, $s_2s_1l_1e$, s_1l_1ve, s_2l_1ve, s_2l_2ve, $s_2l_2l_1e$, and l_2l_1ve. In addition to that there are two quadruple points: the $s_2s_1l_1v$ (black diamond) and the $s_2l_2l_1v$ (black triangle.)

The s_2s_1ve joins the $s_2s_1l_1v$ quadruple point from the low temperature region. From this quadruple point, the $s_2s_1l_1e$ extends in the high pressure region, the s_1l_1ve joins the triple point of N_2, the s_2l_1ve reaches the second quadruple point.

From the $s_2l_2l_1v$ quadruple point the $s_2l_2l_1e$ extends evolves at higher pressures up to its UCEP, the s_2l_2ve ends in the triple point of C_2H_6, the l_2l_1ve outgoes the critical point of N_2 and joins its UCEP.

Conversely to the system O_2+C_2H_6, the system N_2+C_2H_6 presents total immiscibility in the liquid phase up to the $s_2l_2l_1e$ UCEP, so that the l_2l_1ve line extends up to an UCEP placed besides the critical temperature of pure N_2. The critical line (l=v) coming from the critical point of pure C_2H_6 "feels" the immiscibility with the liquid rich in N_2 and move upwards joining the UCEP of the $s_2l_2l_1e$. In the last part, the l=v curve represents the limit of immiscibility in the liquid phase (l_2=l_1).

At pressure greater than the pressure of the $s_2l_2l_1e$ UCEP the immiscibility in the liquid phase ceases, and the system presents only a $s_2s_1l_1e$ temperature.

The calculated PT-EP for the mixture is in Figure 6.28. Colors are the same of Figure 6.27. The notations sve, sle, and vle have been added in Figure 6.28 for indicating the sublimation, melting, and saturation lines of the two pure components. A zoom of Figure 6.28 in the proximity of the triple point of N_2 is given in Figure 6.29.

The liquid-vapor critical line (l=v) originates at about 305 K, namely the critical temperature of C_2H_6, and joins the $s_2l_2l_1e$ at the corresponding UCEP at pressure greater than 100 MPa.

In Figure 6.28, the black diamond represents the $s_2s_1l_1v$ quadruple point (63.2 K, 0.012 MPa), the black triangle is the $s_2l_2l_1v$ quadruple point (87.6 K, 0.28 MPa), the green triangle is the UCEP of the l_2l_1ve three phase line (130 K, 3.8 MPa). The UCEP of the $s_2l_2l_1v$ occurs at pressure greater than 100 MPa, thus is not portrayed in Figure 6.28.

The dashed-dotted-dotted-dashed blue line is the s_2l_2ve curve leaving the triple point of C_2H_6 (90 K) and joining the $s_2l_2l_1v$ quadruple point. From this point, the dashed blue line of l_2l_1ve extends up to its UCEP, where the critical line l=v originates ending at the critical point of N_2 (126 K).

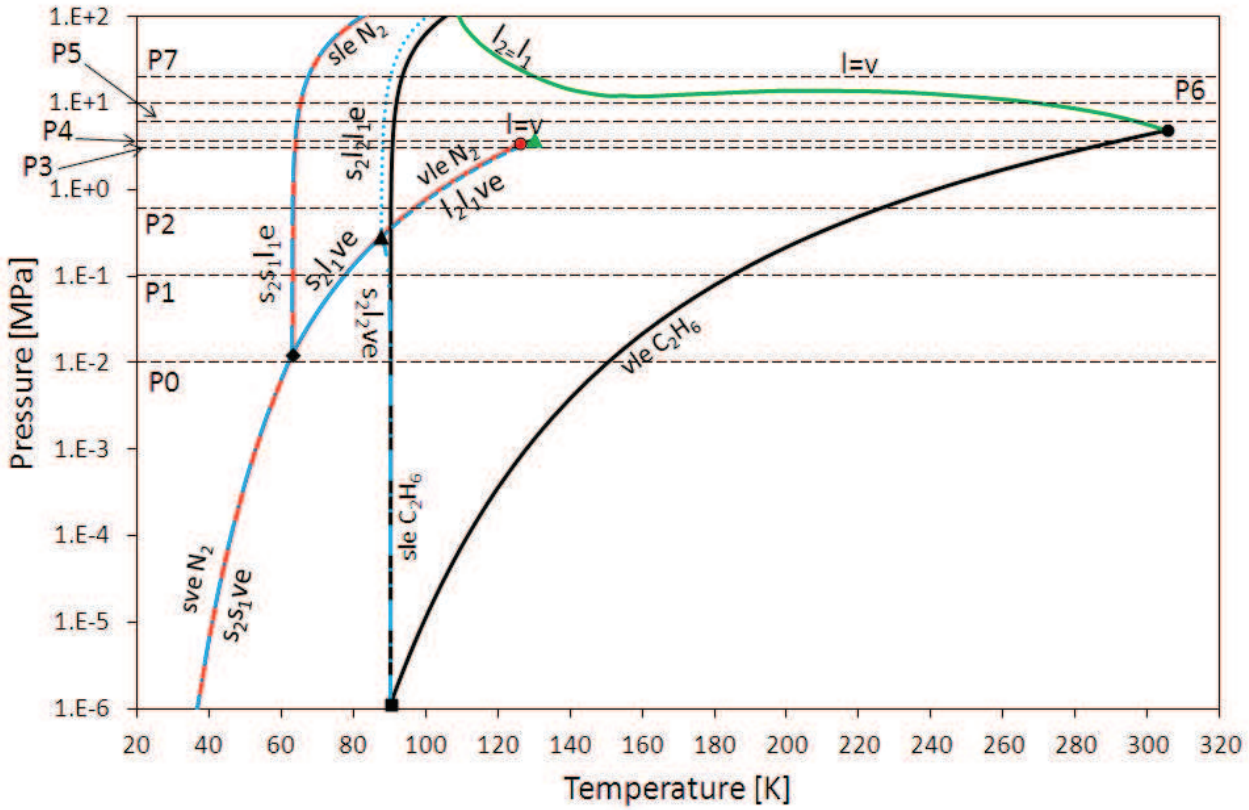

Figure 6.28: Mixture N_2+C_2H_6: calculated pressure-temperature equilibrium projection.
N_2: triple point ■; critical point ●; solid-liquid, solid-vapor, and vapor-liquid equilibria —.
C_2H_6: triple point ■; critical point ●; solid-liquid and vapor-liquid equilibria —.
♦ : solid$_2$-solid$_1$-liquid$_1$-vapor equilibrium; ▲ : solid$_2$-liquid$_2$-liquid$_1$-vapor equilibrium; — : solid$_2$-liquid$_1$-vapor three phase line; — — : solid$_2$-solid$_1$-liquid$_1$ three phase line; — • — : solid$_2$-solid$_1$-vapor three phase line; — • • — : solid$_2$-liquid$_2$-vapor three phase line; ••• : solid$_2$-liquid$_2$-liquid$_1$ three phase line; – – : liquid$_2$-liquid$_1$-vapor three phase line; ▲ : upper critical endpoint of the l_2l_1v three phase line; — : critical lines.

From this lower quadruple point, three lines originate: the dashed-dotted blue line of s_2s_1ve, the dashed-dashed blue line of s_2s_1le, and a third line of s_1l_1ve ending in the triple point of O_2. This last three phase line is not represented in Figure 6.28 since the $s_2s_1l_1v$ quadruple point is close to the triple point of N_2.

Eight main isobars are indicated in Figure 6.21: P0 (0.01 MPa), P1 (0.1 MPa), P2 (0.6 MPa), P3 (3 MPa), P4 (3.6 MPa), P5 (6 MPa), P6 (10 MPa), and P7 (20 MPa). The Tx-CSs corresponding to pressures P0, P1, P2, and P3 are portrayed in Figure 6.30 in the range 50 K – 300 K, while the Tx-CSs corresponding to pressures P4, P5, P6, and P7 are portrayed in Figure 6.31 in the same range of temperature. Pressures P0-P4 are also indicated in the calculated PT-EP of Figure 6.29.

The Tx-CSs corresponding to pressures P0-P2 are of the same type of the isobars P0-P2 of the system O_2+C_2H_6.

To sum up, at P0 there are two three phase equilibria: the s_2s_1ve (62.2 K), and the s_2l_2ve (90.4 K). At P1 there are 3 three phase equilibria: the $s_2s_1l_1e$ (63.2 K), the s_2l_1ve (77.5 K), and the s_2l_2ve (89.8 K). At P2, greater than pressure at the $s_2l_2l_1v$ quadruple point (0.028 MPa) the three phase lines involved are: the $s_2s_1l_1$ (63.3 K), the $s_2l_2l_1$ (87.7 K), and the l_2l_1v (96.9 K). Immiscibility in the liquid phase occurs, and the immiscibility gap ends in the vapor-liquid lens yielding the l_2l_1ve.

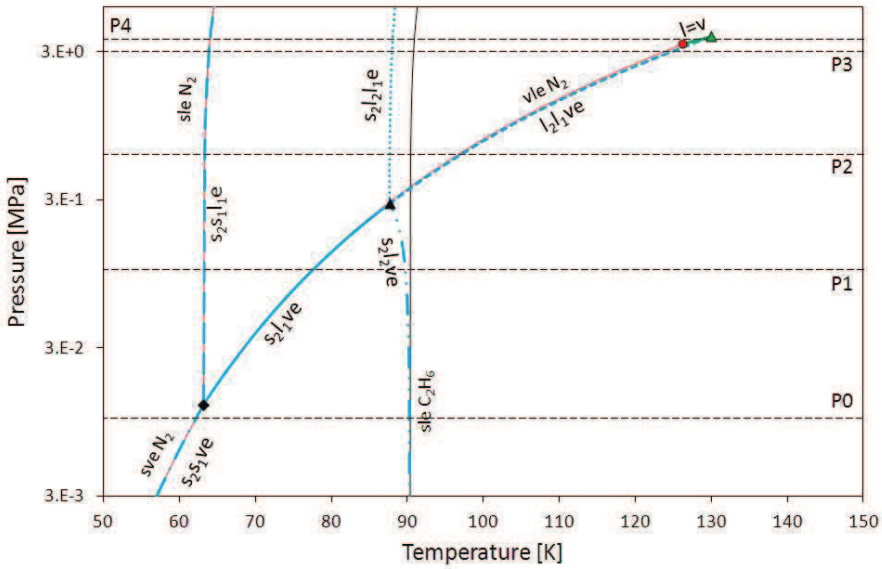

Figure 6.29: Mixture N_2+C_2H_6: calculated pressure-temperature equilibrium projection in the proximity of the triple point of N_2. ♦ : solid$_2$-solid$_1$-liquid$_1$-vapor equilibrium; ▲ : solid$_2$-liquid$_2$-liquid$_1$-vapor equilibrium; — : solid$_2$-liquid$_1$-vapor three phase line; — — : solid$_2$-solid$_1$-liquid$_1$ three phase line; — • — : solid$_2$-solid$_1$-vapor three phase line; — • • — : solid$_2$-liquid$_2$-vapor three phase line; ••• : solid$_2$-liquid$_2$-liquid$_1$ three phase line; – – : liquid$_2$-liquid$_1$-vapor three phase line; ▲ : upper critical endpoint of the l_2l_1v three phase line; — : vapor-liquid critical line.

At P3 (3 MPa) the vl_2e extends itself at higher temperatures, and the $l_{21}ve$ also moves to a temperature higher than the corresponding value in P2. The Tx-CS related to P3 in Figure 6.30 shows again the $s_2s_1l_1e$ (63.9 K) and the $s_2l_2l_1e$ (88.0 K).

The immiscibility in the liquid phase persists with increasing pressures, and at P4 (3.6 MPa) it is located at 128.8 K, beyond the critical temperature of pure N_2. As a consequence, in the Tx-CS related to P4 in Figure 6.31 there is a liquid-vapor critical point at a temperature lower than the l_2l_1ve temperature.

The temperature difference between the l_2l_1ve and the liquid-vapor critical point becomes zero at the l_2l_1ve UCEP, while a l=v point at higher temperatures occurs at P5 (6 MPa), namely when the pressure is greater than the critical pressure of C_2H_6.

The extent of the l_2l_1e reduces with increasing pressures, as it can be observed in the Tx-CSs related to P6 and P7 in Figure 6.31. As a consequence, there is a pressure at which the immiscibility between phases L_1 and L_2 vanishes, and this pressure corresponds to the UCEP of the $s_2l_2l_1e$.

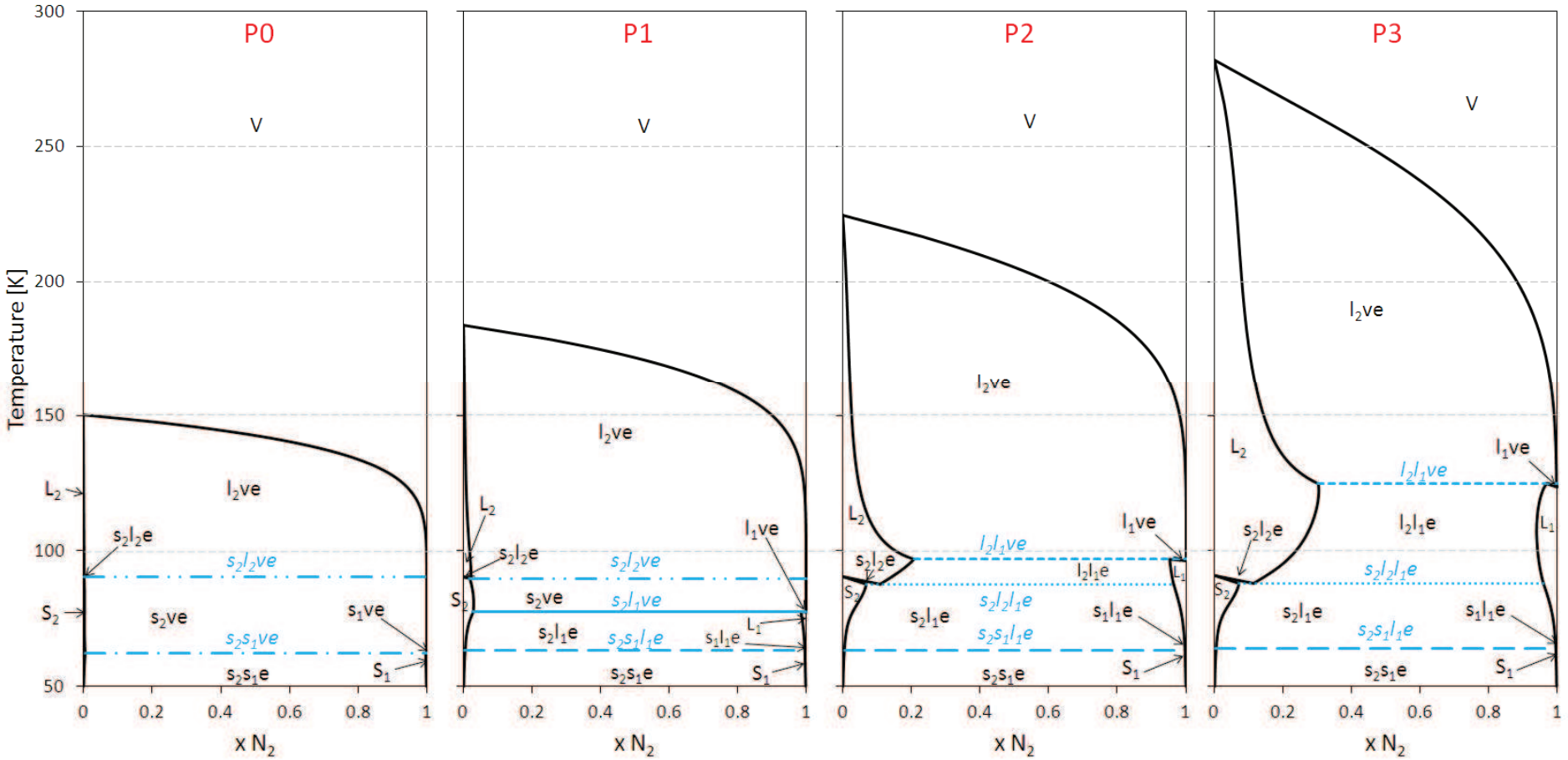

Figure 6.30: Mixture N_2+C_2H_6: evolution of the phase equilibrium behavior with pressure in the range 50 K – 300 K up to 3 MPa.
P0 = 0.01 MPa; P1 = 0.1 MPa; P2 = 0.6 MPa; P3 = 3 MPa. — : solid$_2$-liquid$_1$-vapor equilibrium temperature; — • — : solid$_2$-solid$_1$-vapor equilibrium temperature; — • • — : solid$_2$-liquid$_2$-vapor equilibrium temperature; — — : solid$_2$-solid$_1$-liquid$_1$ equilibrium temperature; – – : liquid$_2$-liquid$_1$-vapor equilibrium temperature; ••• : solid$_2$-liquid$_2$-liquid$_1$ equilibrium temperature; $S_{1,2}$: solid phase; $L_{1,2}$: liquid phases; V : vapor phase; $s_{1,2}$ve : solid-vapor equilibrium; $s_{1,2}l_{1,2}$e : solid-liquid equilibrium; $vl_{1,2}$e : vapor-liquid equilibrium; s_2s_1e : solid$_2$-solid$_1$ equilibrium; l_2l_1e : liquid$_2$-liquid$_1$ equilibrium.

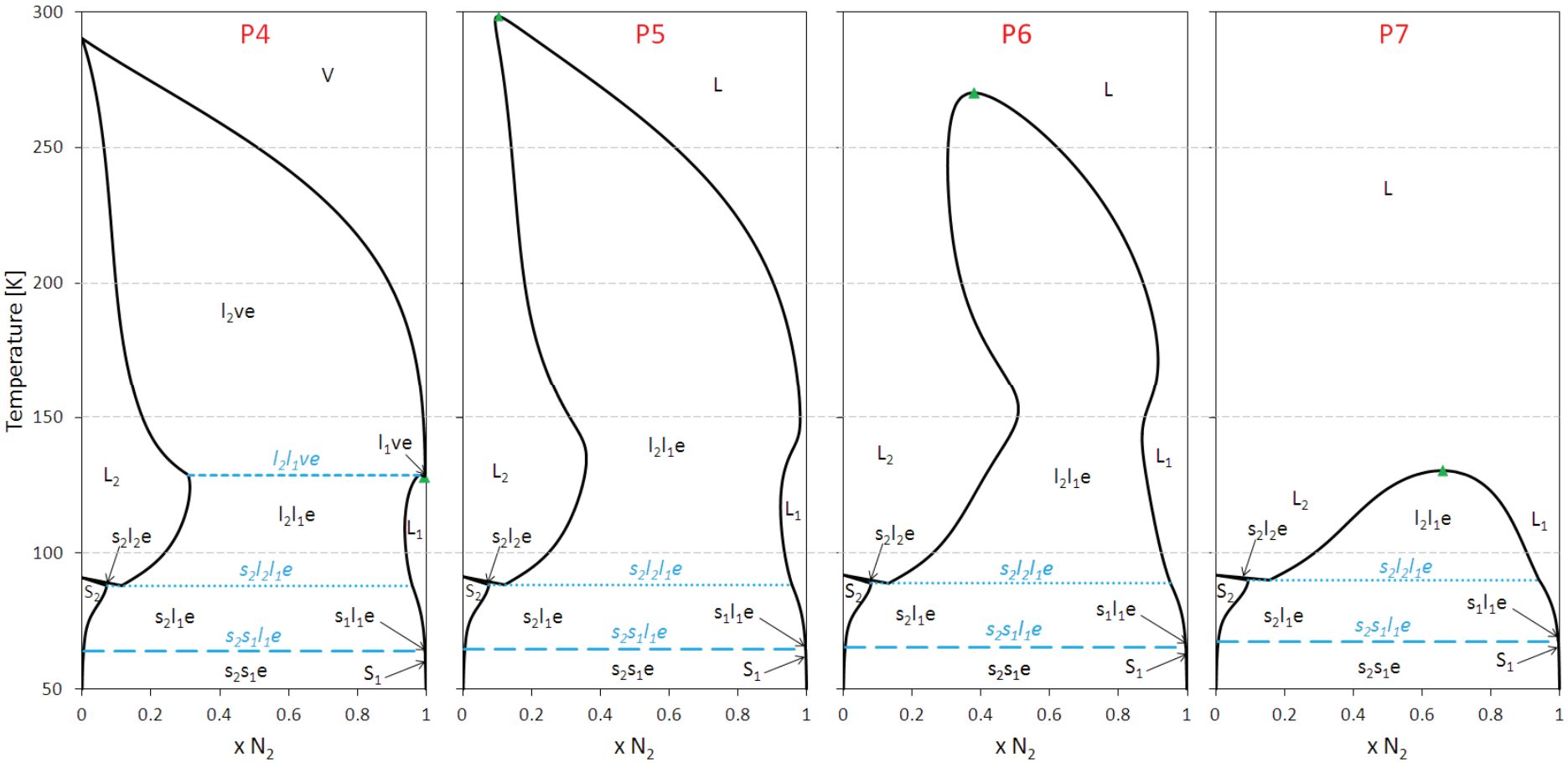

Figure 6.31: Mixture N_2+C_2H_6: evolution of the phase equilibrium behavior with pressure in the range 50 K – 300 K for P > 3 MPa.
P4 = 3.6 MPa; P5 = 6 MPa; P6 = 10 MPa; P7 = 20 MPa. — — : solid$_2$-solid$_1$-liquid$_1$ equilibrium temperature; – – : liquid$_2$-liquid$_1$-vapor equilibrium temperature; ••• : solid$_2$-liquid$_2$-liquid$_1$ equilibrium temperature; $S_{1,2}$: solid phase; $L_{1,2}$: liquid phases; $s_{1,2}l_{1,2}e$: solid-liquid equilibrium; s_2s_1e : solid$_2$-solid$_1$ equilibrium; l_2l_1e : liquid$_2$-liquid$_1$ equilibrium; ▲ : critical points.

6.3.5 Type IIIb+d PT-EP: system Ar+CO_2

Only two values of solubility of solid CO_2 in liquid Ar have been found in the literature, so any Tx-CS concerning the SLE for this mixture has been presented in this section.

The qualitative comparison between experimental and calculated values of the vapor-liquid equilibrium is illustrated in Figure 6.32 for 233 K, 273 K, and 288 K.

The model is in a quite good agreement with data at 233 K, whereas higher deviations occur while approaching the critical temperature of pure CO_2 (304 K).

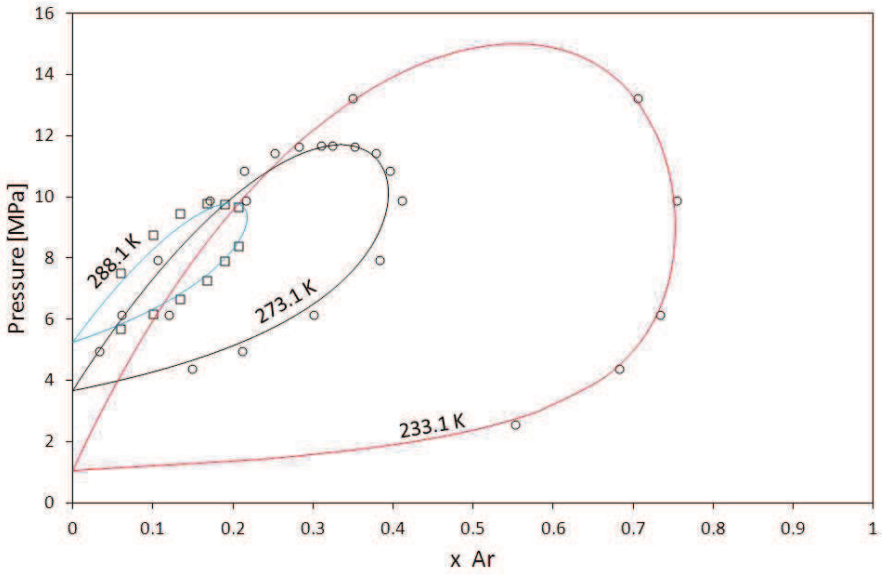

Figure 6.32: Mixture Ar+CO_2: comparison between experimental and calculated values of VLE.
Experimental values: ○ : 172 K, [119]; □ : 220 K, [120]; Δ : 260 K, [121].
Calculated values: 172 K (—), 220 K (—), 260 K (—).

Figure 6.33 resumes the qualitative PT-EP for the mixture Ar+CO_2. Red and black lines are the saturation, sublimation, and melting lines of Ar and CO_2, respectively. Keeping the same distinction in terms of color, triple and critical points of the pure components are indicated by squares and circles, respectively.

The blue lines in Figure 6.33 represent the temperature and pressure conditions at which three phases coexist at equilibrium.

With reference to the classification proposed by van Konynenburg and Scott, the PT-EP of the system Ar+CO_2 is again of type III, even if the behavior differs from the system N_2+C_2H_6.

A liquid-vapor critical line (l=v) joins the critical point of CO_2 and the upper critical endpoint (UCEP) of the solid$_2$-liquid$_2$-vapor three phase line originating at the triple point of CO_2.

A second l=v line joins the critical point of Ar and the UCEP of the solid$_2$-liquid$_1$-vapor three phase line.

The UCEPs of the $s_2l_2$ve and the $l_2l_1$ve are represented in Figure 6.33 by green triangles.

Conversely to the system N_2+C_2H_6, the mixture Ar+CO_2 present only one quadruple point. This point is the black diamond in Figure 6.33, and represents the solid$_2$-solid$_2$-liquid$_1$-vapor equilibrium.

The $s_2s_1$ve joins the $s_2s_1l_1$v quadruple point from the low temperature region. From the quadruple point, the $s_2s_1l_1$e extends in the high pressure region, the $s_1l_1$ve joins the triple point of Ar, and the $s_2l_1$ve reaches its upper critical endpoint. In this UCEP, the composition of liquid$_1$ is equal to the composition in the vapor phase.

Figure 6.34 represents the calculated PT-EP for the system Ar+CO_2.

The notations sve, sle, and vle have been added in Figure 6.34 for indicating the sublimation, melting, and saturation lines of the two pure components

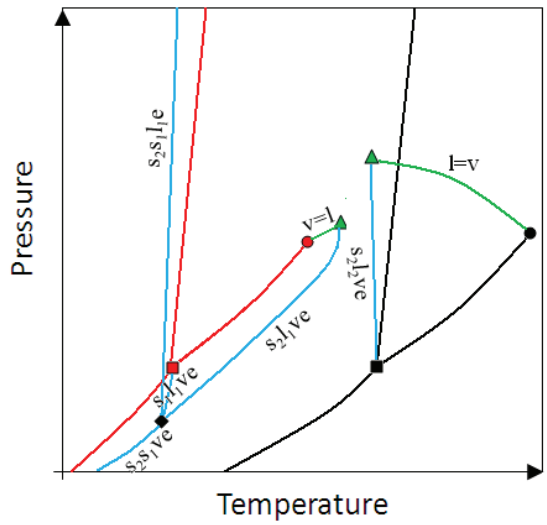

Figure 6.33: Mixture Ar+CO_2: qualitative pressure-temperature equilibrium projection.
Ar: triple point ■; critical point ●; equilibria —.
CO_2: triple point ■; critical point ●; equilibria —.
♦ : $solid_2$-$solid_1$-$liquid_1$-vapor equilibrium; — : three phase lines; ▲ : upper critical endpoints; — : critical lines.

The s_2l_2v three phase line exits the triple point of CO_2 (217 K, 0.52 MPa) and extends itself with negative slope up to a first upper critical endpoint (214 K, 17 MPa).

The s2s111v quadruple point is close to the triple point of Ar (83 K, 0.07 Ma), thus the s_1l_1v three phase line is not portrayed in Figure 6.34. The dashed-dotted blue line represents the s_2s_1ve extending in the low pressure region, the dashed blue line the $s_2s_1l_1e$ extending at high pressures.

The continuous blue line represents temperature and pressure conditions of $solid_2$-$liquid_1$-vapor equilibrium, which leaves the quadruple point ending at the second UCEP of the PT-EP. This UCEP has been calculated at 151 K and 4.9 MPa, thus it is close to the critical point of Ar.

Five main pressures have been chosen for describing the evolution of phase equilibria with pressure: P0 (0.02 MPa), P1 (0.3 MPa), P2 (1.5 MPa), P3 (9 MPa), and P4 (25 MPa). The phase equilibrium behaviors at these five pressures are summarized in Figure 6.35 for temperatures from 50 K up to 300 K.

At 0.02 MPa (P0), a $solid_2$-$solid_1$-vapor equilibrium occurs at 75.5 K. The compositions of the equilibrium phases there are close to 1 for the $solid_1$ and vapor phases, and close to 0 for the phase $solid_2$. According to Figure 6.35, at P0 the system Ar+CO_2 can present a $solid_2$-vapor equilibrium, a $solid_1$-vapor equilibrium, and a $solid_2$-$solid_1$ equilibrium depending on the system temperature.

When the pressure exceeds the triple point pressure of Ar (P1), a liquid phase rich in Ar separates the $solid_1$ and vapor phases, while a s_2ve persists at higher temperatures. As a consequence, the s_2s_1ve ceases to exist, and a s_2l_1e occurs. The s_2s_1ve is replaced by the $s_2s_1l_1e$ (83.9 K), and the presence of the s_2l_1e and s_2ve entails the presence of a s_2l_1ve, whose temperature is 99.1 K. The s2ve ends at higher temperature at the sublimation temperature of pure CO_2 at P1 (~209 K).

A second liquid phase rich in CO_2 appears when pressure bypasses the triple point temperature of pure CO_2. This case is represented by the Tx-CS related to P2 in Figure 6.35. This liquid phase yields the vl_2e and the s_2l_2e at high temperatures, whereas the liquid phase rich in Ar is confined at low temperatures under the $s_2s_1l_1e$ temperature (84.2 K). The other two three phase lines are the s_2l_1ve (123.8 K) and the s_2l_2ve (216.4 K): the former involves the solid phase rich in CO_2 and a liquid and a vapor phase rich in Ar, the latter involves the same solid phase which is at equilibrium with the vapor and the liquid phase rich in CO_2.

The s_2l_1ve disappears when the pressure overcomes the pressure of the UCEP placed to the left of Figure 6.34. The corresponding Tx-CS is similar to the one at P3, the only difference being the

absence of a vapor-liquid critical point when the pressure is lower than the critical point pressure of pure CO_2 (7.4 MPa). This Tx-CS has been omitted for sake of simplicity.

When the pressure becomes supercritical with respect to the critical point pressure of pure CO_2, the vl_2e ends at high temperatures at the vapor-liquid critical point. This case is represented in Figure 6.35 by the Tx-CS at P4 (9 MPa).

At P4, both components are supercritical in the fluid region, and notations v, l_2, and l_1 have been maintained for analogy with the Tx-CSs at lower pressures. As it can be seen in Figure 6.35, at P4 the s_2l_1ve is no longer present, and the remaining three phase lines are the $s_2s_1l_1e$ (86.2 K) and the s_2l_2ve (214.9 K)

The extend of the vl_2e reduces with increasing pressures, and behind the UCEP placed to the right of Figure 6.34 it ceases to exist. This case is portrayed in the Tx-CS related to P4 (25 MPa) in Figure 6.35.

To sum up, when a pressure is fixed between the triple point pressure of pure CO_2 and 17 MPa (the pressure at the s_2l_2ve UCEP), partial immiscibility in the liquid phase occurs from the corresponding temperature on the s_2l_2v three phase line up to a temperature placed on the vapor-liquid critical line (l=v).

In addition to that and contrary to the previous PT-EPs, in the PT-EP of the system Ar+CO_2 any combination of three phase lines allows joining the two triple points of the pure components. Furthermore, according to Figure 6.35, the system presents partial miscibility in either the solid or liquid phases only for temperature greater than the critical point temperature of pure Ar (151 K.)

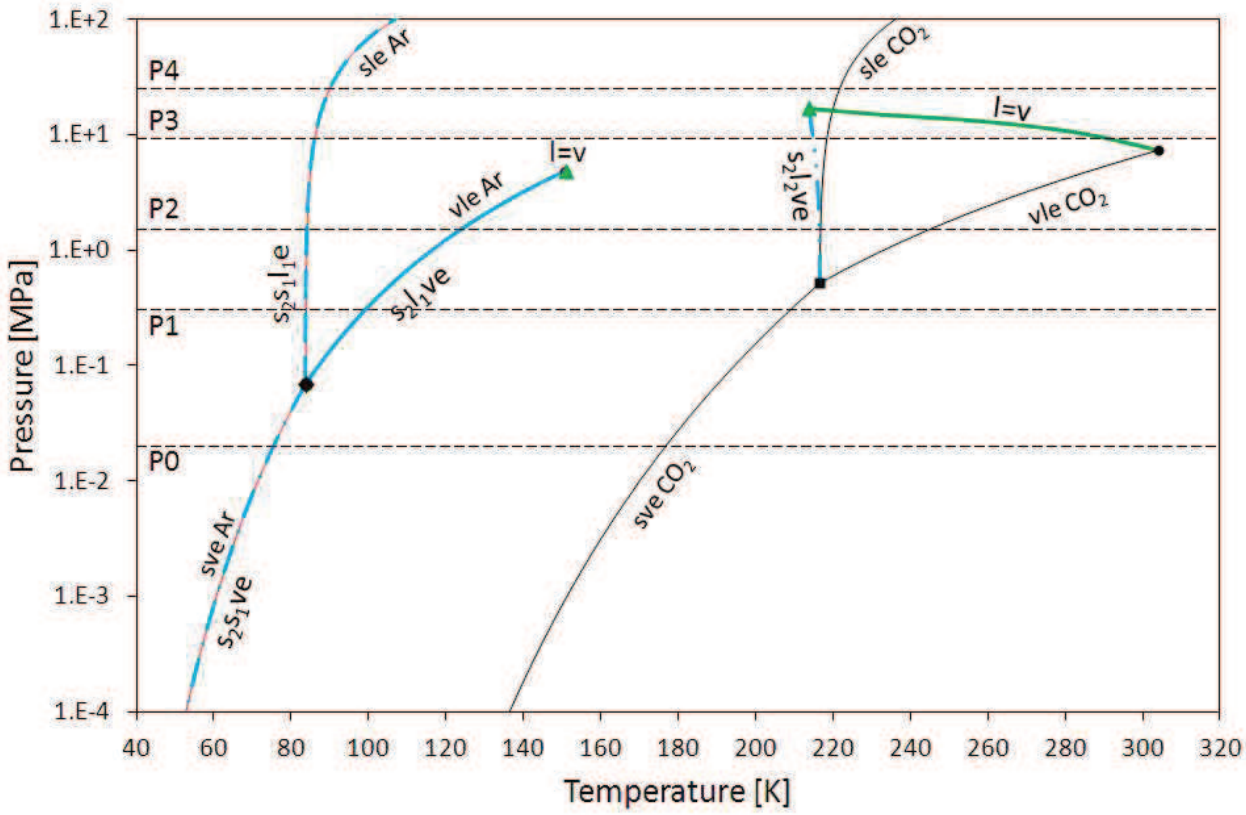

Figure 6.34: Mixture Ar+CO_2: calculated pressure-temperature equilibrium projection.
Ar: triple point ■; critical point ●; solid-liquid, solid-vapor, and vapor-liquid equilibria —.
CO_2: triple point ■; critical point ●; solid-liquid and vapor-liquid equilibria —.
♦ : $solid_2$-$solid_1$-$liquid_1$-vapor equilibrium; — : $solid_2$-$liquid_1$-vapor three phase line; — — : $solid_2$-$solid_1$-$liquid_1$ three phase line; — • — : $solid_2$-$solid_1$-vapor three phase line; — • • — : $solid_2$-$liquid_2$-vapor three phase line; ▲ : upper critical endpoints; — : critical lines.

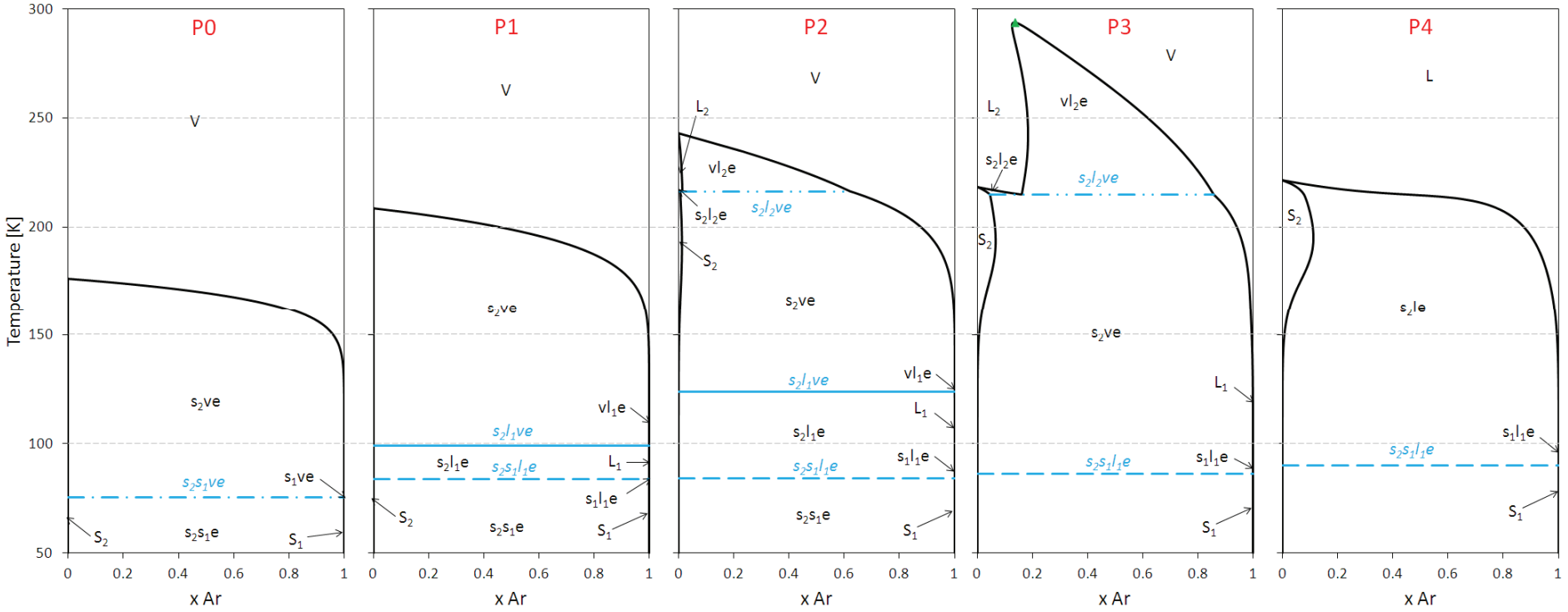

Figure 6.35: Mixture Ar+CO_2: evolution of the phase equilibrium behavior with pressure in the range 50 K – 300 K.
P0 = 0.02 MPa; P1 = 0.3 MPa; P2 = 1.5 MPa; P3 = 9 MPa, P4 = 25 MPa. — : solid$_2$-liquid$_1$-vapor equilibrium temperature; — • — : solid$_2$-solid$_1$-vapor equilibrium temperature; — • • — : solid$_2$-liquid$_2$-vapor equilibrium temperature; — — : solid$_2$-solid$_1$-liquid$_1$ equilibrium temperature; $S_{1,2}$: solid phase; $L_{1,2}$: liquid phases; V : vapor phase; $s_{1,2}ve$: solid-vapor equilibrium; $s_{1,2}l_{1,2}e$: solid-liquid equilibrium; $vl_{1,2}e$: vapor-liquid equilibrium; s_2s_1e : solid$_2$-solid$_1$ equilibrium; ▲ : critical point.

6.4 Considerations about the binary interaction parameters

For almost all the binary mixtures of interest in this work, asymmetric binary interaction parameters were used in the mixing rules for representing the phase equilibrium behavior by means of the SLV EoS in a wide range of temperature and pressure.

Furthermore, the representation of equilibria involving dense phases required considerably modifying the binary interaction parameters (m_{ij}, n_{ij}, and l_{ij}) related to the volumetric parameters within the EoS (solid covolume b, liquid covolume c and parameter d) with respect to null values. As a consequence, temperature dependent functions have been used seeing that:

1. the relation $b(T) < c < d$ must holds in the whole range of temperature;
2. values of binary interaction parameters m_{ij}, n_{ij}, and l_{ij} regressed for representing the solid-fluid equilibria rarely allow the quantitative representation of equilibria occurring in the fluid region, namely the vapor-liquid and liquid-liquid equilibria, and vice versa.

In addition to that, simple polynomials of second or third order leading to continuous functional forms for the temperature-dependent functions have been found to suffer an inconvenient.

For instance, when the solid-liquid equilibrium presents an eutectic behavior with partial immiscibility in the solid phase, like the system Ar+CH_4 presented in section 6.3.2, two sets of parameters are needed for the solid-liquid and the vapor-liquid equilibria. Using polynomials for the temperature dependences of the binary interaction parameters m_{ij}, n_{ij}, and l_{ij} for representing these two sets entails the disappearance of the eutectic behavior with increasing pressures. To make this point clearer, it means that the $solid_2$-$solid_1$-liquid equilibrium in Figure 6.12 ceases to exist at some pressure, and the SLE becomes of the azeotropic form.

In the framework of this thesis it has been considered that pressure variations should modify only the position of the solid-solid and solid-liquid equilibria in the Tx-CS according to the melting temperatures of the pure components, while effects should not involve the variation of the kind of equilibrium in the dense region (solid solution, eutectic, and azeotrope).

The binary interaction parameters and the temperature dependent functions used in this work are protected by confidentiality with the Air Liquide group, but a qualitative understanding of the functional form needed for quantitatively representing the phase equilibrium behavior is illustrated in Figure 6.36. In Figure 6.36 the functional form for a generic binary interaction parameter z_{ij} has been reported: a_0+a_1 and a_0 are the values of z_{ij} at T = 0 and T = ∞, respectively, a_2 is the temperature where $z_{ij} = a_0$+0.5×a_1, and a_3 is related to the slope of the central part of the curve in Figure 6.36 (how rapidly z_{ij} varies in proximity of the temperature a_2).

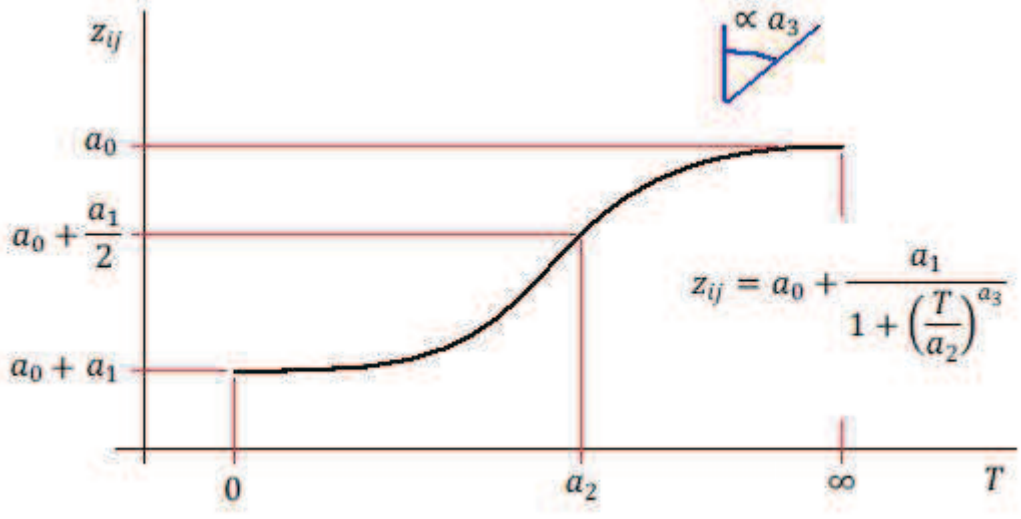

Figure 6.36: Form of a typical temperature dependent function used for the binary interaction parameters.

In Figure 6.36, values of z_{ij} at T = 0 (a_0+a_1) and T = a_2 (a_0+0.5×a_1) are lower than a_0 considering a negative value of a_1. The equation in Figure 6.36 can then be used in both cases of having a higher or a lower value of z_{ij} at T = 0 with respect to the value assumed at T = ∞.

For the author attempts, it has not been possible representing the phase equilibrium behaviors in a wide range of temperature and pressure with constant parameters, and using the temperature dependent function in Figure 6.36 basically results in using two sets of parameters for the dense and the fluid regions. Moreover, tests have not been done concerning derived properties and the representation of equilibrium properties other than equilibrium pressures and temperatures. This point could then be faced as future development.

It is worth mentioning that such a functional form for the temperature dependency of the parameters has been used is some cases also for the parameter k_{ij}. For instance, the calculated PT-EPs of the system N_2+C_2H_6 presented in Figure 6.28 has been obtained with the parameter *a* in the SLV EoS from the function in Figure 6.36. This function is needed for k_{ij} in order to account for the sudden variation of the form of the vapor-liquid equilibrium for increasing temperature while approaching the critical point of C_2H_6. This variation is due to the shape of the l_2=l_1 critical line which becomes a l=v critical line, as it can be observed in Figure 6.27.

6.5 Modeling O_2+impurity binary mixtures at the reboiler-condenser of the ASU

As discussed in Chapter 1, the main critical area within an ASU with reference to the potential accumulation of impurities and safety hazards is the reboiler-condenser. Since it contains liquid oxygen, the part of the reboiler located in the sump of the Low Pressure Column (*LPC*) is mainly concerned, and the presence and the accumulation of hydrocarbons (eventually promoted by solid phase deposition) should be avoided there. Monitoring the composition of the multicomponent mixture at the level of the *LPC* sump is then an important operation.

Table 6.1 displays the composition in ppm of some impurities [CH_4, C_nH_m (mainly C_2H_6, C_3H_8, and C_2H_4), CO_2, and N_2O] in the liquid phase sampled in the air separation unit FlexiNord in Dunkerque (Air Liquide, [122]) at level of the liquid oxygen bath in the *LPC* sump.

Table 6.3: Liquid compositions at level of the *LPC* sump.
C_nH_m groups ethane, ethylene, and propane. Values are related to a period of sampling from 18/11/1999 to 22/02/2006, [122].

Sample	CH_4 / ppm	C_nH_m / ppm	CO_2 / ppm	N_2O / ppm
1	22 ± 1	ND	0.1 ± 0.1	0.2 ± 0.1
2	48 ±3	0.4 ± 0.1	0.1 ± 0.1	0.2 ± 0.1
3	170 ± 10	ND	ND	0.6 ± 0.3
4	160 ± 10	0.4 ± 0.1	ND	0.7 ± 0.1
5	160 ± 10	0.5 ± 0.1	0.2 ± 0.1	0.1 ± 0.1
6	175 ± 5	1.5 ± 0.2	ND	0.3 ± 0.1
7	160 ± 10	0.2 ± 0.1	ND	0.4 ± 0.1
8	160 ± 10	0.4 ± 0.1	ND	0.5 ± 0.1
9	180 ± 10	0.1 ± 0.1	ND	0.1 ± 0.05
10	44 ± 2	0.7 ± 0.1	1.2 ± 0.2	0.8 ± 0.1
11	45 ± 3	0.4 ± 0.2	0.3 ± 0.1	0.4 ± 0.1
12	48 ± 3	0.6 ± 0.1	0.3 ± 0.1	0.6 ± 0.1
13	42 ± 4	0.5 ± 0.1	0.2 ± 0.1	0.7 ± 0.1

For each compound within Table 6.1, each sample composition has been considered as the composition in the liquid phase at equilibrium with a second phase in the correspondent binary mixture with oxygen at the temperature at the *LPC* sump, which can be fixed at 94 K.

The triple point temperatures of C_2H_6, C_2H_4, and C_3H_8 are about 90 K, 104 K, and 85 K, respectively. With the aim of considering the presence of solid phases responsible for hydrocarbons ac-

cumulation, the compositions of C_nH_m have been associated to C_2H_4 seeing that its triple point temperature is greater than 94 K and it can then solidify. According to the pressure-temperature equilibrium behavior of the mixtures O_2+C_2H_6 and O_2+C_3H_8 obtained by the SLV EoS, it is instead possible to state that solid phases do not appear since such systems at 94 K show equilibria involving only fluid phases.

As a result, the model has been applied for representing the binary mixtures O_2+CH_4, O_2+C_2H_4, O_2+N_2O, and O_2+CO_2 at 94 K in order to determine the phases in equilibrium with the liquid phases in Table 6.1.

At 94 K, the mixture O_2+CH_4 shows a vapor-liquid equilibrium extending from the saturation pressure of pure CH_4 (0.0175 MPa) up to the saturation pressure of pure O_2 (0.149 MPa), Figure 6.37. As a consequence, each liquid phase whose CH_4 content is in Table 6.1 is in equilibrium with a vapor phase.

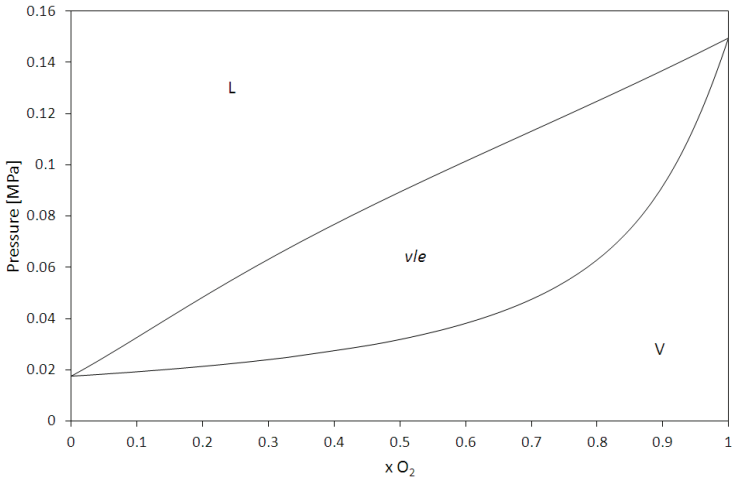

Figure 6.37: Phase equilibrium behavior of the system O_2+CH_4 at 94 K.
— : SLV EoS; L : liquid phase; V : vapor phase; vle : vapor-liquid equilibrium.

The phase equilibrium behavior of the system O_2+C_2H_4 at 94 K is illustrated in Figure 6.38.

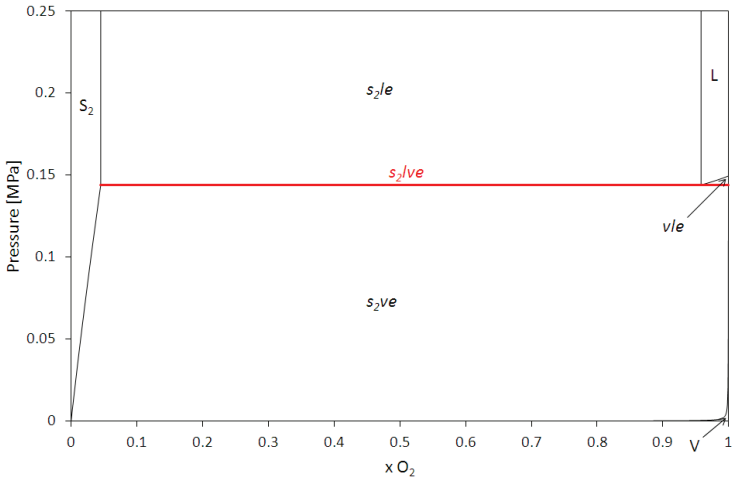

Figure 6.38: Phase equilibrium behavior of the system O_2+C_2H_4 at 94 K.
— and — : SLV EoS; S_2 : solid phase rich in C_2H_4; L : liquid phase; V : vapor phase; vle : vapor-liquid equilibrium; $s_2$le: solid$_2$-liquid equilibrium; $s_2$ve : solid$_2$-vapor equilibrium; $s_2$lve : solid$_2$-liquid-vapor equilibrium.

At 94 K, a three phase equilibrium occurs at about 0.144 MPa in the mixture O_2+C_2H_4. The equilibrium phases are a solid phase rich in ethylene (S_2), a liquid phase (L), and a vapor phase (V). The $s_2$lve pressure is lower than 0.149 MPa, which is the calculated saturation pressure of pure O_2 at 94 K. The calculated equilibrium compositions at $s_2$lve are: xS_2 = 0.045, xL = 0.958; xV = 0.999. In terms of ppm of C_2H_4, the composition in the liquid phase is $xL_{C2H4} = (1- xL)\times10^6 = 42\times10^3$ ppm.

A zoom of the pressure-composition cross section in Figure 6.38 for $xO_2 \geq 0.92$ is shown in Figure 6.39.

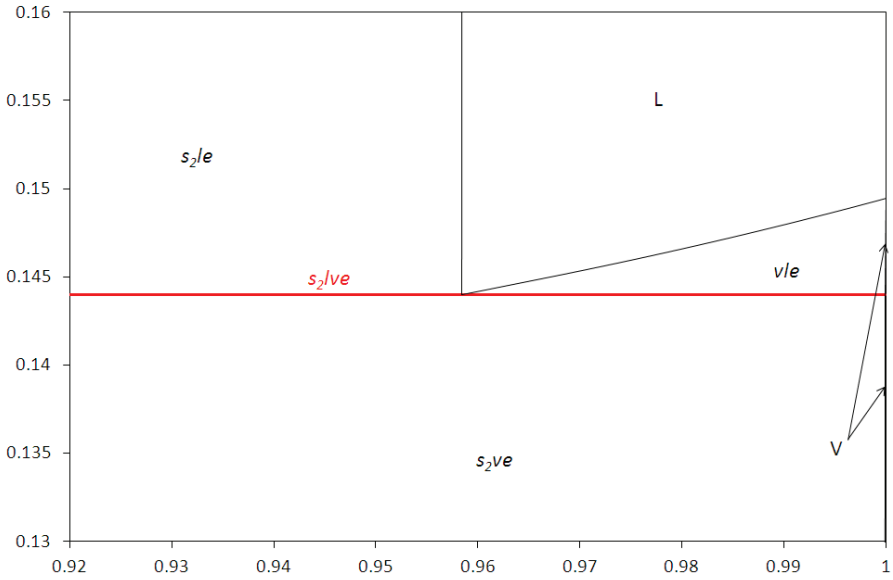

Figure 6.39: Phase equilibrium behavior of the system O_2+C_2H_4 at 94 K for $xO_2 \geq 0.92$.
— and — : SLV EoS; S_2 : solid phase rich in C_2H_4; L : liquid phase; V : vapor phase; vle : vapor-liquid equilibrium; $s_2$le: solid$_2$-liquid equilibrium; $s_2$ve : solid$_2$-vapor equilibrium; $s_2$lve : solid$_2$-liquid-vapor equilibrium.

According to Figure 6.38-Figure 6.39 and the calculated composition of ethylene in the liquid phase (42×10^3 ppm), it is possible to state that a solid-liquid equilibrium (more precisely a $s_2$le) occurs only when the global composition (in terms of O_2 mole fraction) of the binary mixture is lower than the composition of the liquid phase at the $s_2$lve pressure (xL = 0.958).

All the sample compositions (in terms of O_2 mole fraction) in the second column of Table 6.1 are higher than this values.

As a consequence, all the samples in Table 6.1 are related to a liquid phase in equilibrium with a vapor phase. The equilibrium liquid phases (in term of O_2 mole fraction) are located on the liquid branch of the vapor-liquid equilibrium (vle) of Figure 6.39.

At 94 K, same phase equilibrium behavior occurs for the binary mixtures O_2+N_2O and O_2+CO_2. The composition of the liquid phase at the $s_2$lve pressure is xL_{N2O} = 284 ppm for O_2+N_2O, and xL_{CO2} = 8 ppm for O_2+ CO_2.

All the sample compositions in Table 6.1 are lower than these values, then it is possible to state that the phase at equilibrium with each liquid phase in Table 6.1 is a vapor phase, and any solid phase is present according to the model.

Conclusions

The Equation of State proposed by A. Yokozeki in 2003 has been applied for the representation of phase equilibria of binary mixtures of interest in the cryogenic air distillation process. The approach used for solving the equilibrium condition is based on the isofugacity condition and the minimization of the Gibbs free energy of mixing.

The pressure-explicit functional form of the Yokozeki EoS introduces a discontinuity in the solid-liquid transition, and allows evaluating the non ideality in all the phases (solid, liquid, and vapor) in terms of fugacity coefficient. Furthermore, different attractive terms can be considered.

A rigorous procedure for calculating the pure compound parameters has been established; the capability of the Yokozeki EoS with different attractive terms in qualitatively representing equilibrium properties of argon has then been challenged. Limitations have mainly been found with respect to solid-liquid equilibrium densities and latent heats of transition. Based on this comparison, the attractive term of the van der Waals EoS has been considered in the functional form of the Yokozeki EoS as the best compromise for quantitatively representing the phase equilibrium data (pressure and temperature) and qualitatively representing densities and latent heats of transition. As a result, the model used in this work (renamed Solid-Liquid-Vapor EoS) has the same functional form used by A. Yokozeki, but differently from his works the EoS parameters for the pure compounds are regressed considering also solid-liquid, vapor-liquid, and solid-vapor equilibrium values obtained from auxiliary equations.

Nevertheless, limitations remain in the representation of the solid-liquid equilibrium densities, and this suggested investigating other temperature-dependent functions for parameters a and solid covolume b. This study has not been presented in this work seeing that (for the author attempts) the possibility of improving the representation of solid-liquid equilibrium properties entails worsening the representation of the vapor-liquid ones, unless introducing temperature-dependent functions also for the liquid covolume c and the parameter d.

The cited procedure for regressing the parameters has been applied to the SLV EoS, allowing obtaining a good representation of the SLE, SVE, and VLE in a wide range of temperature and pressures up to 100 MPa for the fluids: nitrogen, oxygen, argon, krypton, xenon, neon, helium, carbon dioxide, hydrogen, nitrous oxide, methane, ethane, ethylene, propane and propylene.

As presented in Chapter 4, the AAD averaged with respect to all the compounds obtained calculating equilibrium temperature at fixed pressure is about 0.1% for VLE, SLE, and SVE. The AAD averaged with respect to all the compounds obtained calculating equilibrium pressure at fixed temperature is about 1% for VLE and SVE. Higher deviations are encountered for the SLE, since high relative errors occur between auxiliary equations and calculated pressures for temperatures approaching the triple point temperatures, where in some case the pressure is very low (order of magnitude of $10^{-4} – 10^{-10}$ for light hydrocarbons).

Even if high pressures may not be meaningful from a point of view of the application to real processes like the cryogenic distillation of air, considering the SLE branch up to 100 MPa has been judged as fundamental for showing that the equation is robust when it is included in a process simulator and it has to be mathematically solved also for high variable values.

Now that the robustness of the SLV EoS has been proved, better representations would be achieved for producing sets of EoS parameters regressed in a range of temperature and pressure more specific for the actual conditions of the air separation process. In this way, the performance of the equation – with respect to SLE, VLE and SVE – could be further improved.

Three main drawbacks have been encountered in applying the SLV EoS to binary mixtures.

The first one is the capability of the SLV EoS without Binary Interaction Parameters of qualitatively representing only solid solution, namely SLE where the two pure components are totally miscible in the solid phase and the liquid phase is never stable at temperatures lower than the lowest triple point temperature between the two components (as instead it happens in case of solid-liquid azeotrope). This resulted in the need of regressing the BIPs.

The second problem that has been faced is the lack of SLE and/or VLE data, which sometimes hinders the possibility of regressing the binary interaction parameters. A great amount of data (more than 10 literature works) is available for 10 mixtures out of the 58 of interest in this work: N_2+O_2, N_2+Ar, N_2+He, N_2+CO_2, N_2+H_2, N_2+CH_4, N_2+C_2H_6, N_2+C_3H_8, O_2+Ar, and Ar+CH_4. Among others, for the binary mixtures hydrocarbon+O_2 few VLE data are available, while discrepancies have been found in the SLE data proposed by different authors. Literature data are not available for 5 mixture (Ar/Kr+N_2O, Ar+C_2H_4, and Ar/Kr+C_3H_8), then it would be interesting carrying out experimental measurements for these systems.

In order to overcome these two drawbacks, the SLV EoS has been applied to binary mixtures of Lennard-Jones fluids with the aim of evaluating the binary interaction parameters starting from the LJ parameters σ and ε for the fluids of interest in this work. The BIPs obtained in this way allowed qualitatively representing the SLE of mixtures behaving like LJ fluids (as for instance the mixture N_2-Ar), and provided initial values used in the regression algorithm.

The third inconvenient related to using the SLV EoS is the necessity of respecting the relation between volumetric parameters (*b*, *c*, and *d*) for solving the equation and getting the solid, liquid, and vapor volumes without changing the isothermal pressure-volume behavior of the EoS. This required introducing BIPs in all the parameters within the EoS, which often cannot represent the phase equilibrium behavior just operating on the solid covolume *b*. This sometime caused reducing the quantitative representation of the VLE experimental values.

It is worth saying that the regressed BIPs and the temperature-dependent functions needed for representing SLE and VLE in a wide range of temperature are of course related to the mixing rules used in this work, which correspond to the quadratic rules proposed by A. Yokozeki.

A consequence of this last drawback is the difficulty encountered in representing cases of total immiscibility in the solid phase which, even if not confirmed by experimental values in the solid phase, can be inferred observing the available data of the liquid composition at SLE. It can be stated that the SLV EoS represents the solid phase like a dense liquid phase, and the considered mixing rules with regressed BIPs usually give solid phases more miscible than expected. For this reason, future improvements could be trying different mixing rules.

Despite the cited limitations in applying the SLV EoS to binary mixtures, this model allows evaluating their thermodynamic behavior in a wide range of temperature, and it can be applied also in cases of infinite dilution (as in the systems O_2+CO_2/N_2O). A classification in terms of pressure-temperature equilibrium projections has been proposed for almost all the binary mixtures of interest, thus providing a description of the whole phase diagrams sought at the beginning of this work.

The SLV EoS could then be an important aid for designing and optimizing industrial cryogenic processes, and applied in process simulation when coupled with aspects of kinetics of solidification. Knowing at which conditions in a mixture the solid-fluid equilibria appears and a solid phase deposits represents an opportunity of great interest, because it could be used for improving the cryogenic processes and avoiding some drawbacks as solidification of the impurities.

The phase diagrams, as Px and Tx equilibrium cross sections at cryogenic conditions, can give important information for evaluating new air separation techniques, exploiting the capability of the SLV EoS in representing phase equilibrium values in which also the solid phase is involved.

These information could also be implemented in a thermodynamic package which could be used for evaluating the thermodynamic behavior in a wide range of temperature and pressure.

The thermodynamic model proposed by A. Yokozeki can be seen as a further improvement in the representation of the phase equilibrium behavior of pure components. The proper covolume of the molecules and the attractive forces among them were introduced in the ideal gas equation by van der Waals in 1873 in order to better representing the behavior of real fluid phases.

Now we are moving towards the solid phase just introducing two other volumetric parameters in the functional form of the van der Waals EoS. The pressure-temperature equilibrium behavior presented in Chapter 4 and Annex D are then the results of the need of deeply investigating the real behavior of fluids in a wide range of temperature and pressure.

Author appreciated the possibility of investigating and representing the complex phase equilibrium behavior of binary mixtures in the dense region with the SLV EoS. He challenged himself in understanding/discovering all the possible equilibria occurring at fixed conditions of temperature or pressure, and in evaluating how the phase equilibria evolve with temperature and pressure variations. Furthermore, it is his firm opinion that the main strength of the model is the possibility of (at least qualitatively) representing the real behavior of binary mixture, which increases the comprehension of the whole phase diagram.

This model obviously presents some limitations as the representation of equilibrium densities or compositions at the SLE, but author feels it is the interest of global knowledge to further research along these lines in order to improve the representation of the equilibrium behavior.

Bibliography

[1] P. Arpentinier, F. Cavani and F. Trifirò, The technology of catalytic oxidations, Paris: Editions Technip, 2001, pp. 1-47.

[2] A. Liquide, "Air Distillation - Trainee Book," 2007.

[3] E. Lemmon, M. Huber and M. McLinden, "NIST Standard Reference Database 23: Reference Fluid Thermodynamic and Transport Properties-REFPROP, Version 8.0, National Institute of Standards and Technology, Standard Reference Data Program, Gaithersburg," 2007.

[4] B. F. Dodge, "Isotherms and isobars for air separation studies," *Chemical and Metallurgical Engineering,* vol. 35, no. 10, p. 622, 1928.

[5] I. Burn and F. Din, "Liquid-vapor equilibrium of the system argon+oxygen at pressures up to 10 atmospheres," *Trans. Faraday Soc.,* vol. 58, pp. 1341-1356, 1962.

[6] E. Lemmon, R. Jacobsen, S. Penoncello and D. Friend, "Thermodynamic properties of air and mixtures of nitrogen, argon, and oxygen from 60 to 2000 K at pressures to 2000 MPa," *J. Phys. Chem. Ref. Data,* vol. 29, no. 3, pp. 331-385, 2000.

[7] D. Meneses, J.-Y. Thonnelier, C. Szulman and E. Werlen, "Trace contaminant behavior in air separation units," in *Cryogenics 2000 Conference*, Prague, 2000.

[8] R. M. Hardeveld, M. J. Groeneveld, J.-Y. Lehman and D. C. Bull, "Investigation of an air separation unit explosion," *Journal of Loss Prevention in the Process Industries,* vol. 14, pp. 167-180, 2001.

[9] W. Schmidt, K. Winegardner, M. Dennetry and H. Castle-Smith, "Safe design and operation of a cryogenic air separation unit," *Process Safety Progress,* vol. 20, no. 4, pp. 269-279, 2001.

[10] M. Masson, A. Roger, J. Currie, P.-E. Isaksson, A. Mariotti, H. Puype, F. Ruhland and I. Uriarte, "Safe practices guide for cryogenic air separation plants," European Industrial Gases Association, Brussels, 2008.

[11] S. Pasquetto and L. Patrone, Chimica Fisica: stati di aggregazione-termodinamica chimica-equilibri di fase, VI ed., Italia: Zanichelli, 1997.

[12] G. Tammann, Kristallisieren und Schmelzen, Metzger und Wittig, Leipzig, 1903.

[13] H. D. Leudemann and G. C. Kennedy, "Melting curves of lithium, sodium and potassium, and rubidium to 80 kilobars," *J.Geophys. Res,* vol. 73, pp. 2795-2805., 1968.

[14] N. Dass, "Melting maximum in alkali metals," *Phys. Rev. B,* vol. 52, no. 5, p. 3023–3025, 1995.

[15] K. Kapoor, N. Dass and R. Kumar, "Melting temperature of H2, D2, N2 and CH4 under high pressure," *PRANAMA Journal of Physics,* vol. 62, no. 1, pp. 95-100, 2004.

[16] L. Schames, "Eine neue Hypothese über das Wesen der verschiedenen Aggregatzustände und Modifikationen," *Ann. Physik,* vol. 343, no. 9, pp. 830-848, 1912.

[17] P. W. Bridgman, "The melting parameters of nitrogen and argon under pressure, and the nature of melting," *Phys. Rew.,* vol. 46, pp. 930-933, 1934.

[18] J. E. Lennard-Jones and A. F. Devonshire, "Critical and cooperative phenomena. IV: a theory of disorder in solids and liquids and the process of melting," *Proceedings of the Royal Society of London Series A,* vol. 170, no. 943, pp. 464-484, 1939.

[19] C. Domb, "Some theoretical aspects of melting," *In Nuovo Cimento,* vol. 9, no. 1, pp. 9-26, 1958.

[20] F. Simon and G. Glatzel, "Bemerkungen zur Schmelzdruckkurve," *Zeitschrift für anorganische und allgemeine Chemie,* vol. 178, no. 1, p. 309–316, 1929.

[21] H. Mori, H. Okamoto and S. Isa, "A simplified theory of the liquid-solid transitions. I," *Progress of the Theoretical Phys.,* vol. 47, no. 4, pp. 1087-1109, 1972.

[22] D. Furman, S. Dattagupta and R. B. Griffiths, "Global phase diagram for a three-component model,"

Physical Review B, vol. 15, no. 1, pp. 441-464, 1977.

[23] P. van Konynenburg and R. Scott, "Critical lines and phase equilibria in binary van der Waals mixtures," *Phil. Trans. R. Soc. Lond. A,* vol. 298, p. 495–540, 1980.

[24] J. D. v. d. Waals, Doctoral Dissertation, Leiden, 1873.

[25] R. J. Sadus, High pressure phase behaviour of multicomponent fluid mixtures, Amsterdam: Elsevier, 1992.

[26] A. Bolz, U. K. Deiters, C. J. Peters and T. W. de Loos, "Nomenclature for phase diagrams with particular reference to vapor-liquid and liquid-liquid equilibria," *Pure & Appl. Chem.,* vol. 70, no. 11, pp. 2233-2257, 1998.

[27] M. Matsuoka, "Solid liquid equilibria of binary organic mixtures," *Bunri Gijutsu (Separation Process Engineering),* vol. 7, p. 245–249, 1977.

[28] M. Matsuoka, "Advances in industrial crystallization," London, Butterworth-Heinemann Ltd. Oxford, 1991, pp. 229-224.

[29] A. S. Shirinyan, A. M. Gusak and M. Wautelet, "Phase diagrams versus diagram of solubility: what is the difference for nanosystems?," *Acta Materialia,* vol. 53, pp. 5025-5032, 2005.

[30] D. C. Garcia and K. D. Luks, "Patterns of solid-fluid phase equilibria: new possibilities?," *Fluid Phase Equilibria,* vol. 161, pp. 91-106, 1999.

[31] J. A. Labadie, D. C. Garcia and K. D. Luks, "Patterns of solid-fluid phase equilibria II. Interplay with fluid phase criticality and stability," *Fluid Phase Equilibria,* vol. 171, pp. 11-26, 2000.

[32] J. M. Prausniz, R. N. Lichtenthaler and E. G. de Azevedo, Molecular Thermodynamics of Fluid-Phase Equilibria, Third Edition ed., New Jersey 07458: Prentice Hall PTR, 1999.

[33] H. Renon and J. M. Prausnitz, "Local compositions in thermodynamic excess functions for liquid mixtures," *AIChE Journal,* vol. 14, no. 1, pp. 135-144, 1968.

[34] D. S. Abrams and J. M. Prausnitz, "Statistical thermodynamics of liquid mixtures: a new expression for the excess Gibbs energy of partly or completely miscible systems," *AIChE Journal,* vol. 21, no. 1, pp. 116-128, 1975.

[35] A. Fredenslund, R. L. Jones and J. M. Prausnitz, "Group-contribution estimation of activity coefficients in nonideal liquid mixtures," *AIChE Journal,* vol. 21, no. 6, pp. 1086-1099, 1975.

[36] G. S. Soave, "Equilibrium constants for modified Redlich-Kwong equation of state," *Chem. Eng. Sci.,* vol. 4, pp. 1197-1203, 1972.

[37] D. Peng and D. Robinson, "A new two parameters equation of state," *Industrial and Engineering Chemistry Fundamentals,* vol. 15, pp. 59-64, 1976.

[38] N. C. Patel and A. S. Teja, "A new cubic equation of state for fluids and fluid mixtures," *Chem. Eng. Sci.,* vol. 37, no. 3, pp. 463-473, 1982.

[39] G. W. H. Schmidt, "A modified van der Waals type equation of state," *Chem. Eng. Sci.,* vol. 35, pp. 1503-1512, 1980.

[40] C. H. Twu, W. D. Sim and V. Tassone, "A versatile liquid activity model for SRK, PR and a new cubic equation-of-state TST," *Fluid Phase Equilibria,* Vols. 194-197, pp. 385-399, 2002.

[41] P. Salim and M. Trebble, "Thermodynamic property predictions from the Trebble-Bishnoi-Salim equation of state," *Fluid Phase Equilibria,* vol. 65, pp. 41-57, 1991.

[42] P. M. Mathias and T. W. Copeman, "Extension of the Peng Robinson equation of state to complex misture: evaluation of the various forms of the local composition concept," *Fluid phase equilibrium,* vol. 13, pp. 91-108, 1983.

[43] C. H. Twu, J. E. Coon and J. R. Cunningham, "A new generalized alpha function for a cubic equation of state. Part 1. Peng Robinson Equation," *Fluid Phase Equilib.,* vol. 105, p. 45.59, 1995.

[44] C. H. Twu, J. E. Coon and J. R. Cunningham, "A new generalized alpha function for a cubic equation of state. Part 2. Redlich Kwong equation," *Fluid Phase Equilib.,* vol. 105, pp. 61-69, 1995.

[45] C. Coquelet, A. Chapoy and D. Richon, "Development of a new alpha function for the Peng-Robinson equation of state: comparative study of alpha function models for pure gases (natural gas components) and water-gas systems," *Int. J. Thermophys.,* vol. 25, no. 1, pp. 133-158, 2004.

[46] L. E. Baker, A. C. Pierce and D. L. Kraemer, "Gibbs energy analysis of phase equilibria," *Society of Petroleum Engineers Journal,* pp. 731-742, 1982.

[47] M. L. Michelsen, "The isothermal flash problem. Part I. Stability," *Fluid Phase Equilibr.,* vol. 9, pp. 1-19, 1982.

[48] Division Scientifique, Gas Encyclopedia, Amsterdam: ELSEVIER, 1976.

[49] H. Lee, "The volume expansion factor for solid-liquid transition a the triple point," *Korean J. of Chem. Eng.,* vol. 4, no. 1, pp. 9-14, 1987.

[50] G. S. Soave, "Application of the Redlich-Kwong-Soave equation of state to solid-liquid equilibria calculations," *Chem. Eng. Sci.,* vol. 34, no. 2, pp. 225-229, 1979.

[51] C. H. Twu, V. Tassone and D. W. Sim, "New solid equation of state combining excess energy mixing rule for solid-liquid equilibria," *AIChE J.,* vol. 49, no. 11, pp. 2957-2965, 2003.

[52] S. B. Rodrigues-Reartes, M. Cismondi and M. S. Zabaloy, "Computation of solid-fluid-fluid equilibria for binary asymmetric mixtures in wide ranges of conditions," *J. of Supercritical Fluids,* vol. 57, pp. 9-24, 2011.

[53] J. A. P. Coutinho, "Predictive UNIQUAC: a new model for the description of multiphase solid-liquid equilibria in complex hydrocarbon mixtures," *Ind. Eng. Chem. Res.,* vol. 37, pp. 4870-4875, 1998.

[54] J. A. P. Coutinho and E. H. Stenby, "Predictive local composition models for solid/liquid equilibrium in n-Alkane systems: Wilson equation for multicomponent systems," *Ind. Eng. Chem. Res.,* vol. 35, pp. 918-925, 1996.

[55] P. J. Flory, "Thermodynamics of polymer solutions," *Discuss. Farad. Soc.,* vol. 49, pp. 7-29, 1970.

[56] G. B. Wilson, "Vapor-liquid equilibrium. XI. A new expression for the excess free energy of mixing," *J. Am. Chem. Soc.,* vol. 86, pp. 127-130, 1964.

[57] K. Kan, "An equation of state and the gas-liiquid-solid equilibrium in argon," *Chinese Journal of Physics,* vol. 17, pp. 32-43, 1979.

[58] H. Wenzel and G. Schmidt, "A modified van der Waals equation of state for the representation of phase equilibria between solids, liquids, and gases," *Fluid Phase Equilib.,* vol. 5, pp. 3-17, 1980.

[59] F. d. J. Guevara-Rodriguez and A. Romero-Martinez, "An empirical extension for a generalized cubic equation of state, applied to a pure substance with small molecules," *Fluid Phase Equilibr,* vol. 347, pp. 22-27, 2013.

[60] P. Salim and M. Trebble, "Modeling of solid phases in thermodynamic calculations via translation of a cubic equation of state at the triple point," *Fluid Phase Equilibria,* vol. 93, pp. 75-99, 1994.

[61] R. Heidemann and J. Prausnitz, "A van der Waals-type equation of state for fluids with associating molecules," *Proc. Natl. Acad. Sci.,* vol. 73, pp. 1773-1776, 1976.

[62] E. Lang and H. Wenzel, "Extension of a cubic equation of state to solids," *Fluid Phase Equilib.,* vol. 51, pp. 101-117, 1989.

[63] D. Geaña and H. Wenzel, "Solid–liquid–gas equilibrium by cubic equations of state and association," *J. Supercritical Fluids,* vol. 15, pp. 97-108, 1999.

[64] A. Yokozeki, "Analytical equation of state for solid-liquid-vapor phases," *International Journal of Thermophysics,* vol. 24, no. 3, pp. 589-620, May 2003.

[65] A. Yokozeki, "Phase equilibria of benzene-cyclohexane binary mixtures using a solid-liquid-vapor equation of state," *Applied Energy,* vol. 81, pp. 334-349, 2005.

[66] A. Yokozeki, "Methane gas hydrates viewed through unified solid-liquid-vapor equation of state," *Int J Thermophys.,* vol. 26, pp. 743-765, 2005.

[67] A. Yokozeki, "Solid-liquid-vapor phases of water and water-carbon dioxide mixtures using a simple analytical equation of state," *Fluid Phase Equilibria,* Vols. 55-56, pp. 222-223, 2004.

[68] A. Yokozeki, "Phase behaviors of binary hard-sphere mixtures using simple analytical equation of state," *Int. J. Thermophys.,* vol. 25, no. 3, pp. 643-667, 2004.

[69] A. Yokozeki, "Solid-liquid phase equilibria of binary indole mixtures with some aromatic compounds using a solid-liquid-vapor equation-of-state," *Applied Energy,* vol. 81, pp. 322-333, 2005.

[70] J. H. Lee, M. S. Shin, H. Kim and K.-P. Yoo, "Extended Veytsamn statistics for the solid-fluid

transition in the framework of lattice fluid," *J. Chem. Thermodynamics,* vol. 42, pp. 891-899, 2010.

[71] B. A. Veytsman, "Are lattice models valid for fluids with hydrogen bonds?," *J. Phys. Chem.,* vol. 94, pp. 8449-8500, 1990.

[72] J. H. Lee and K.-P. Yoo, "Comments on "Analytic Equation of State for Solid-Liquid-Vapour Phases"," *Internationa Journal of Thermopysics,* vol. 32, p. 553:558, 2011.

[73] B. Alder, W. G. Hoover and T. Wainwright, "Cooperative motion of hard disk leading to melting," *Phys. Lett. Rev.,* vol. 11, no. 6, pp. 241-243, 1963.

[74] J. H. Lee, M. S. Shin and K.-P. Yoo, "Development of single insertion probability for equation of state applicable to three phases of matter," *Ind. Eng. Chem. Data,* vol. 50, pp. 4166-4176, 2011.

[75] J. E. Lennard-Jones, "On the determination of molecular fields," *Proc. R. SOc. Lond. A,* vol. 106, no. 31, p. 463.477, 1924.

[76] H. Adidharma and M. Radosz, "The LJ-solid equation of state extended to thermal properties, chain molecules, and mixtures," *Ind. Eng. Chem. Res.,* vol. 43, pp. 6890-6897, 2004.

[77] T. W. Cochran and Y. C. Chiew, "Perturbed-chain equation of state for the solid phase," *J. Chem. Phys.,* vol. 126, p. 224901, 2006.

[78] S. P. Tan, H. Adidharma, J. S. Kargel and G. M. Marion, "Equation of state for solid solution-liquid-vapor equilibria at cryogenic conditions," *Fluid Phase Equilibr.,* vol. 360, pp. 320-331, 2013.

[79] T. W. Cochran and Y. C. Chiew, "Application of perturbed chain equation of state to solid-liquid equilibria. I. Pure component," *Fluid Phase Equilibr.,* vol. 262, pp. 37-43, 2007.

[80] T. W. Cochran and Y. C. Chiew, "Application of perturbed chain equation of state to solid-liquid equilibria. II. Binary mixtures," *Fluid Phase Equilibr.,* vol. 262, pp. 44-50, 2007.

[81] U. K. Deiters, "Calculation of densities from cubic equation of state," *AIChE J.,* vol. 48, pp. 882-886, 2002.

[82] O. Redlich and J. Kwong, *Chemical Reviews,* vol. 44, pp. 233-244, 1949.

[83] D. Peng e D. Robinson, *Industrial and Engineering Chemistry Fundamentals,* vol. 15, pp. 59-64, 1976.

[84] P. Stringari, M. Campestrini, C. Coquelet and P. Arpentinier, "An equation of state for solid–liquid–vapor equilibrium applied to gas processing and natural gas liquefaction," *Fluid Phase Equilibr.,* vol. 326, pp. 258-267, 2014.

[85] T. de Loos, J. O'Connell and C. McCabe, "Concerning inconsistent equation of state formulations," *Fluid Phase Equilibr.,* vol. 342, p. iii, 2013.

[86] W. H. Press, S. A. Teukolsky, W. T. Vetterling and B. F. Flannery, Numerical recipes in Fortran90. The art of parallel scientific computing, 2 ed., vol. II, New York: Press Syndicate of University of Cambridge, 1986, p. 572.

[87] J. A. Schouten, A. Deerenberg and N. J. Trappeniers, "Vapor-liquid and gas-gas equilibria in simple systems: IV the system argon + krypton," *Physica A,* vol. 81, no. 151-160, 1975.

[88] R. Heastie, "The solid-liquid equilibrium diagram of argon and krypton," *Nature,* vol. 175, pp. 747-748, 1955.

[89] B. F. Dodge and A. K. Dunbar, "An investigation of the coexisting liquid and vapor phases of solutions of oxygen and nitrogen," *J. Am. Chem. Soc.,* vol. 49, p. 591–610, 1927.

[90] M. Ruhemann, A. Lichter and P. Komarov, "Zustandsdiagramme niedrig schmelzender gemische," *Phys. Z. Sowjetunion,* vol. 8, pp. 326-336, 1935.

[91] N. E. Kosyakov, N. P. Yakimenko and L. L. Chobotko, "Production of medicinal nitrous oxide," *Zh. Prid. Khim.,* vol. 57, p. 2591, 1984.

[92] M. B. Iomtev, N. Yakimenko, G. Glukh and L. Polishchukova, "Solubility of solid nitrous oxide in nitrogen," *Russ. J. Phys. Chem.,* vol. 3, no. 450-451, p. 50, 1976.

[93] P. Stringari and M. Campestrini, "Application of the SLV-EoS for representing phase equilibria of binary Lennard–Jones mixtures including solid phases," *Fluid Phase Equilibr.,* vol. 358, pp. 68-77, 2013.

[94] A. Lotfi, J. Vrabec and J. Fischer, *Mol. Phys.,* vol. 76 , p. 1319–1333, 1992.

[95] M. A. Barroso and A. L. A.L. Ferreira, *J. Chem. Phys. ,* vol. 116 , p. 7145–7150, 2002.

[96] M. H. Lamm and C. K. Hall, *AIChE J.,* vol. 47, p. 1664–1675, 2001.

[97] M. Campestrini, P. Stringari and P. Arpentinier, "Solid–liquid equilibrium prediction for binary mixtures of Ar, O2, N2, Kr, Xe, and CH4 using the LJ-SLV-EoS," *Fluid Phase Equilibr.,* vol. 379, pp. 139-147, 2014.

[98] F. Cuadros, I. Cachadiña and W. Ahumada, *Molecular Engineering,* vol. 6, pp. 319-325, 1996.

[99] F. Cuadros, I. Cachadiña and W. Ahumada, *Int. Rev. Phys. Chem.,* vol. 14 , pp. 205-213, 1995.

[100] M. F. Fedorova, *Zh. Eksp. Teor. Fiz.,* vol. 8, pp. 425-435, 1938.

[101] P. van't Zelfde, M. Omar, H. le Pair-Schroten and Z. Dokoupil, *Physica ,* vol. 38, pp. 241-252, 1968.

[102] H. Veith and E. Schroeder, *Z. Phys. Chem. Abt. A,* vol. 179, pp. 16-22, 1937.

[103] F. Din, K. Goldmann and A. G. Monroe, *Proc. 9 Int. Congr. Refr.,* pp. 1003-1010, 1955.

[104] H. M. Long and F. S. Di Paolo, *Bull. Int. Inst. Refr.,* pp. 253-265, 1958.

[105] R. A. Heidemann and A. M. Khalil, "The Calculation of Critical Points," *AIChE J.,* vol. 5, p. 769, 1980.

[106] M. L. Michelsen, "Calculation of phase envelopes and critical points for multicomponent mixtures," *Fluid Phase Equilibr.,* vol. 4, pp. 1-10, 1980.

[107] H. M. Long and F. S. Di Paolo, "Condensed phase diagram of the system argon-nitrogen," *Chem. Eng. Prog. Symp. Ser.,* vol. 59, no. 44, pp. 30-35, 1963.

[108] F. Din, K. Goldmann and G. A. Monroe, "The solid-liquid equilibria of the systems argon-nitrogen and argon-oxygen," *Proc. 9 Int. Congr. Refr.,* pp. 1003-1010, 1955.

[109] A. Baba-Ahmed, P. Guibot and D. Richon, "New equipment using a static analytic method for the study of vapour-liquid equilibria at temperatures down to 77K," *Fluid Phase Equilibr.,* vol. 166, pp. 225-236, 1999.

[110] D. Gravelle and B. C.-Y. Lu, "Vapor-liquid equilibria in the argon + methane system," *Can. J. Chem. Eng.,* vol. 49, pp. 144-146, 1971.

[111] L. J. Christiansen, A. Fredenslund and J. Mollerup, "Vapour-liquid equilibrium of the CH4–Ar, CH4–CO, and Ar–CO systems at elevated pressures," *Cryogenics,* vol. 13, pp. 405-413, 1973.

[112] D. Houssin-Abbomson, Artist, *Solubilité des hydrocarbures dans l'oxygène liquide.* [Art]. Thesis, MINES ParisTech, 2007.

[113] C. McKinley and E. S. J. Wang, "Hydrocarbon-oxygen systems solubility," *Chem. Eng. Progr.,* vol. 53, p. 112, 1957.

[114] F. Himmelberger, *Chem. Eng. Progr.,* vol. 55, no. 6, pp. 54-64., 1959.

[115] A. L. Cox and T. De Vries, "The solubility of solid ethane, ethylene, and propylene in liquid nitrogen and oxygen," *J. Phys. Colloid. Chem.,* vol. 54, pp. 665-670, 1950,.

[116] E. Karwat and G. Klein, "Hydrocarbon in Air Separating Plants," *Linde Ber. Tech. Wiss.,* vol. 4, pp. 3-10, 1958.

[117] C. McKinley and E. S. J. Wang, *Adv. Cryog. Eng.,* vol. 4, pp. 11-25, 1958.

[118] E. Szczepaniec-Cieciak, V. Kondaurov and S. Melikova, "Study on the solubility light alkanes in liquid nitrogen," *Cryogenics,* vol. 20, no. 1, pp. 48-51, 1980.

[119] R. Stryjek, P. S. Chappelear and R. Kobayashi, "Low-temperature vapor-liquid equilibria of nitrogen–ethane system," *J. Chem. Eng. Data,* vol. 19, pp. 340-343, 1974.

[120] T. S. Brown, E. D. Sloan and A. J. Kidnay, "Vapor-liquid equilibria in the nitrogen + carbon dioxide + ethane system," *Fluid Phase Equilibr.,* vol. 51, pp. 299-313, 1989.

[121] M. K. Gupta, G. C. Gardner, M. J. Hegarty and A. J. Kidnay, "Liquid-vapor equilibriums for the N2 + CH4 + C2H6 system from 260 to 280 K," *J. Chem. Eng. Data,* vol. 25, pp. 313-318, 1980.

[122] "Air separation unit FlexiNord, Dunkerque, Air Liquide Group.," 1999-2006.

Communications

Articles

Stringari, P.; Campestrini, M.
Application of the SLV-EoS for representing phase equilibria of binary Lennard–Jones mixtures including solid phases
Fluid Phase Equilibr., **2013**, *358*, 68–77

Stringari, P.; Campestrini, M.; Coquelet, C.; Arpentinier, P.
An equation of state for solid–liquid–vapor equilibrium applied to gas processing and natural gas liquefaction
Fluid Phase Equilibr., **2014**, *362*, 258-267

Campestrini, M.; Stringari, P.; Arpentinier, P.
Solid–liquid equilibrium prediction for binary mixtures of Ar, O_2, N_2, Kr, Xe, and CH_4 using the LJ-SLV-EoS
Fluid Phase Equilibr., **2014**, *379*, 139-147

Riva, M.; Campestrini, M.; Toubassy, J.; Clodic, D.; Stringari, P.
Solid-liquid-vapor equilibrium models for cryogenic biogas upgrading
Ind. Eng. Chem. Res., **2014**, 53, 17506-16514

Conferences

Stringari, P.; Campestrini, M.; Coquelet, C.; Arpentinier, P.
Development of an equation of state for the representation of solid-liquid, solid-vapor, and liquid-vapor equilibria of substances of interest for the air distillation process
Poster, *12th Cryogenics 2012*, September 11-14, **2012**, Dresden, Germany

Stringari, P.; Campestrini, M.; Coquelet, C.; Arpentinier, P.
An equation of state for solid-liquid-vapor equilibrium applied to gas processing and liquefied natural gas
Poster, *13th PPEPPD 2013*, May 26-30, **2013**, Iguaçu Falls, Argentina-Brazil

Professional presentations

24th November **2011**, Air Liquide. Progress report of the thesis

24th May **2012**, Air Liquide. Mixture O_2+Ar

14th February **2013**, Air Liquide. Mixture O_2+Ar, solid-liquid equilibrium

23rd May **2013**, Air Liquide. Mixture Kr+CH_4

6th February **2014**, Air Liquide. On the representation of the Ar and O_2 phase diagrams by Solid-Liquid-Vapor equations of state having the Yokozeki-functional form

29th April **2014**, Air Liquide. Flash calculation for the mixture N_2 + CH_4 + C_2H_6: check for the presence of a solid phase

Professional reports

Annual report, Air Liquide, December **2011**. Development of an equation of state for the representation of vapor-liquid, solid-liquid, and solid-vapor equilibria of pure compounds of interest in the air distillation process

Bibliographic study, Air Liquide, March **2012**. Study of solid-fluid-fluid equilibria (phase diagrams, models overview and database)

Gas Processor Association, Project No. 112, October **2012**. Modeling existing solid-vapor and solid-liquid data in hydrocarbon-carbon dioxide systems

Report, Air Liquide, November **2012**. Representation of binary mixtures with the SLV PR EoS: Ar+O_2 at 50 bar, CH_4+CO_2 from -160°C up to -120°C, N_2+O_2

Annual report, Air Liquide, December **2012**. Thermodynamic study of solid-liquid-vapor equilibrium: application to cryogenics and air separation unit

Annual report, Air Liquide, December **2013**. Thermodynamic study of solid-liquid-vapor equilibrium: application to cryogenics and air separation unit

Appendix A

DATA COLLECTION

LIST OF TABLES **A2**

NOMENCLATURE **A4**

1 PURE COMPOUNDS A5
1.1 Bibliography *A6*
2 BINARY MIXTURES A9
2.1 Bibliography *A31*

List of tables

Table A.1: References for the phase equilibrium experimental values of the pure compounds. A5
Table A.2: Melting auxiliary equations for neon....A5
Table A.3: Sublimation and melting auxiliary equations for nitrous oxide....A5
Table A.4: Melting auxiliary equations and values of the parameters for the substances of interest....A8
Table A.5: Sublimation auxiliary equations and values of the parameters for the substances of interest....A9
Table A.6: Mixtures of interest and kind of data....A9
Table A.7: Literature data for the system nitrogen-oxygen....A10
Table A.8: Literature data for the system nitrogen-argon. A11
Table A.9: Literature data for the system nitrogen-krypton. A12
Table A.10: Literature data for the system nitrogen-xenon....A12
Table A.11: Literature data for the system neon-nitrogen....A12
Table A.12: Literature data for the system helium-nitrogen. A13
Table A.13: Literature data for the system nitrogen-carbon dioxide....A13
Table A.14: Literature data for the system hydrogen-nitrogen. A14
Table A.15: Literature data for the system nitrogen-nitrous oxide. A15
Table A.16: Literature data for the system nitrogen-methane....A15
Table A.17: Literature data for the system nitrogen-ethane....A17
Table A.18: Literature data for the system nitrogen-ethylene....A18
Table A.19: Literature data for the system nitrogen-propane....A18
Table A.20: Literature data for the system nitrogen-propylene. A19
Table A.21: Literature data for the system argon-oxygen....A19
Table A.22: Literature data for the system oxygen-krypton....A20
Table A.23: Literature data for the system oxygen-xenon. A20
Table A.24: Literature data for the system neon-oxygen. A20
Table A.25: Literature data for the system helium-oxygen....A20
Table A.26: Literature data for the system oxygen-carbon dioxide. A21
Table A.27: Literature data for the system hydrogen-oxygen....A21
Table A.28: Literature data for the system oxygen-nitrous oxide. A21
Table A.29: Literature data for the system oxygen-methane. A21
Table A.30: Literature data for the system oxygen-ethane....A22
Table A.31: Literature data for the system oxygen-ethylene. A22
Table A.32: Literature data for the system oxygen-propane. A22
Table A.33: Literature data for the system oxygen-propylene. A22
Table A.34: Literature data for the system argon-krypton. A23
Table A.35: Literature data for the system argon-xenon....A23
Table A.36: Literature data for the system neon-argon. A23
Table A.37: Literature data for the system helium-argon....A23
Table A.38: Literature data for the system argon-carbon dioxide....A24
Table A.39: Literature data for the system hydrogen-argon....A24
Table A.40: Literature data for the system argon-methane A24
Table A.41: Literature data for the system argon-ethane A25
Table A.42: Literature data for the system argon-propylene....A25
Table A.43: Literature data for the system krypton-xenon....A26
Table A.44: Literature data for the system krypton-carbon dioxide....A26
Table A.45: Literature data for the system methane-krypton....A26
Table A.46: Literature data for the system krypton-ethane....A26
Table A.47: Literature data for the system krypton-ethylene....A27
Table A.48: Literature data for the system krypton-propylene. A27
Table A.49: Literature data for the system xenon-neon. A27
Table A.50: Literature data for the system xenon-carbon dioxide. A27
Table A.51: Literature data for the system xenon-nitrous oxide. A27
Table A.52: Literature data for the system methane-xenon. A28
Table A.53: Literature data for the system xenon-ethane....A28

Table A.54: Literature data for the system ethylene-xenon. A28
Table A.55: Literature data for the system xenon-propane. A28
Table A.56: Literature data for the system xenon-propylene. A28
Table A.57: Literature data for the system helium-neon. A29
Table A.58: Literature data for the system hydrogen-neon. A29
Table A.59: Literature data for the system helium-hydrogen. A29
Table A.60: Literature data for the system nitrogen-argon-oxygen. A30

Nomenclature

Symbol	*Meaning*	*Unit*
T	Temperature	K
P	Pressure	MPa
C_1	Parameter	
C_2	Parameter	
C_3	Parameter	
C_4	Parameter	
g	Parameter	
h	Parameter	
j	Parameter	
Y	Parameter	
e_1	Parameter	
e_2	Parameter	
e_3	Parameter	
e_4	Parameter	
n_1	Parameter	
n_2	Parameter	
n_3	Parameter	
n_4	Parameter	
VLE	Vapor-liquid equilibrium	
SLE	Solid-liquid equilibrium	
SVE	Solid-vapor equilibrium	
CP	Critical curve	
UCEP	Upper critical endpoint	
LLE	Liquid- liquid equilibrium	
VLLE	Vapor-liquid-liquid equilibrium	
SVLE	Solid-liquid-vapor equilibrium	

Superscripts

^{t}	Triple point property
^{c}	Critical point property
^{r}	Reduced property or quantity
^{i}	Index for the i^{th} point
^{m}	Melting property
^{s}	Sublimation property
	Triple point property

1 Pure compounds

Table A.1 shows the references of the equilibrium values collected for the pure substances. These values are common pressure-temperature couples of a pure compound phase equilibrium behavior. The references have been organized on the basis of the kind of equilibrium. P-T values for SLE and SVE have been used in form of equations [1], [2], [3], whereas the VLE values have been generated using equations of the software REFPROP 8.0, [1]. For simplicity, we denoted all these P-T values as "auxiliary values", and as "auxiliary equations" the equations we used to obtain the equilibrium values. As it can be seen in Table A.1, SVE auxiliary equations are not available for the compounds He, C_2H_6, C_2H_4, C_3H_8, C_3H_6.

Table A.1: References for the phase equilibrium experimental values of the pure compounds.

Compound	VLE	SVE	SLE
N_2	[1]	[1]	[1]
O_2	[1]	[1]	[1]
Ar	[1]	[1]	[1]
Kr	[1]	[1]	[1]
Xe	[1]	[1]	[1]
Ne	[1]	[1]	[2]
He	[1]		[1]
CO_2	[1]	[1]	[1]
H_2	[1]	[1]	[1]
N_2O	[1]	[3]	[3]
CH_4	[1]	[1]	[1]
C_2H_6	[1]		[1]
C_2H_4	[1]		[1]
C_3H_8	[1]		[1]
C_3H_6	[1]		[1]

The analytical form of the SLE and SVE auxiliary equations [1], [2], [3] for all the compounds is here reported.

The solid-liquid equilibrium equations used for neon [2] are presented in Table A.2.

Table A.2: Melting auxiliary equations for neon.

Compound	Auxiliary SLE equations	C_1	C_2	C_3	C_4	Range of validity
Ne	$P = C_1[T - C_2]^{C_3} - C_4$	0.0157	11.685	1.41852	0.5877	P<300 MPa
	$P = C_1 T^{C_2} - C_3$	0.012062	1.4587	1.478		P>300 MPa

Table A.3 presents the SLE and SVE equations [3] used for N_2O.

Table A.3: Sublimation and melting auxiliary equations for nitrous oxide.

Compound	Auxiliary Equations	Parameters			
N_2O	SLE	g	h		
	$P_m = P_t + g\left[\frac{T^h}{T_t} - 1\right]$	330.4	3.27		
	SVE	e1	e2	j	υ
	$lnP_s = lnP_t + \frac{e_1\theta + e_2\theta^j}{T/T_c}$	-6.6551	-9.8076	1.0364	$1 - \frac{T}{T_t}$

The analytical form of the SLE and SVE auxiliary equations [1] for all the other compounds is presented in Table A.4 and Table A.5. With reference to the parameters that are used in the SLE and SVE auxiliary equations, P_r and T_r are the reducing triple pressure and the reducing triple temperature. P_r and T_r are used in the auxiliary equations only as parameters and not as real property of each compound. This explains the difference between the values of P_r and T_r. and the triple point coordinates shown in Table 4.5, Chapter 4.

For the fluids not present in Table A.2-Table A.5 auxiliary equations are not available.

1.1 Bibliography

[1] E. Lemmon, M. Huber e M. McLinden, «NIST Standard Reference Database 23: Reference Fluid Thermodynamic and Transport Properties-REFPROP, Version 8.0, National Institute of Standards and Technology, Standard Reference Data Program, Gaithersburg,» 2007.

[2] W. Vos e J. Schouten, «The melting curve of neon at high pressure,» *Journal of Chemical Physics,* vol. 94, n. 5, p. 3835:3838, March 1991.

[3] A. Ferreira e L. Lobo, «Nitrous oxide: Saturation properties and the phase diagram,» *Journal of Chemical Thermodynamics,* vol. 41, p. 1394–1399, 2009.

[4] 2004. [Online]. Available: http://webook.nist.gov.

[5] O. Kunz, R. Klimeck, W. Wagner e M. Jaeschke, «The GERG-2004 wide-range equation of state for natural gases and other mixtures,» *GERG TM15 2007.*

[6] E. Lemmon, R. Jacobsen, S. Penoncello e D. Friend, «Thermodynamic properties of air and mixtures of nitrogen, argon, and oxygen from 60 to 2000 K at pressures to 2000 MPa,» *J. Phys. Chem. Ref. Data,* vol. 29, pp. 331-385, 2000.

[7] A. Kidnay, R. Miller, E. Sloan e M. Hiza, «A review and evaluation of the phase equilibria, liquid-phase heats of mixing and excess volumes, and gas-phase PVT measurements for nitrogen + methane,» *J. Phys. Chem. Ref. Data ,* vol. 14, pp. 681-694, 1985.

[8] J. Estela-Uribe, «An improved Helmholtz energy model for air and related systems,» *Fluid Phase Equilibria ,* vol. 287, pp. 95-105, 2010.

[9] D. Diller e M. J.W., «Thermophysical properties of mixtures of natural gas components: a bibliography of experimental data,» *Physical and Chemical Properties Division, Chemical Science and Technology Laboratory, National Institute of Standards and Technology,* October 2000.

[10] M. Hiza, A. Kidnay e R. Miller, «Equilibrium properties of fluid mixtures-2: a bibliography of data on selected fluids».

[11] M. Hiza, A. A. J. Kidnay e R. Miller, «Equilibrium properties of fluid mixtures: a bibliography of data on fluids of cryogenic interest,» *Plenum Press,* 1975.

[12] E. a. A. Liquide, Encyclopedie des Gaz, 1976.

[13] A. V. e. al., «Thermophysical properties of air and air components, lzdatel'atvo "Nauska" Moscou, 1966,» in *Encyclopedie des Gaz, Elsevier and Air Liquide*, 1976, p. 1019:1023.

[14] R. Jacobsen, «The thermodynamic properties of nitrogen from 65 to 2000 K with pressures to 10000 atmospheres, 1972, Thèse, Washington State University,» in *Encyclopedie des Gaz, Elsevier and Air Liquide*, 1976, p. 1019:1023.

[15] R. Powell, H.C.V. e P. Lilely, «Thermal conductivity of selected materials, National standard reference data series, National Bureau of Standards, 8, 1966,» in *Encyclopedie des Gaz, Elsevier and Air Liquide*, 1976, p. 1019:1023.

[16] V. J. Johnson, «Wadd technical report 60-56, A compendium of the properties of materials at low temperature, Part I, National Bureau of Standards, 1960,» in *Encyclopedie des Gaz, Elsevier and Air Liquide*, 1976, p. 1019:1023.

[17] F. Din, «Thermodynamic functions of gases, Volume 3, Butterworths, London, 1961,» in *Encyclopedie des Gaz, Elsevier and Air Liquide*, 1976, p. 1019:1023.

[18] E. B. e. al., «The vapor pressure of nitrogen at low temperatures, Soviet Physics, 5,506, 1960,» in *Encyclopedie des Gaz, Elsevier and Air Liquide*, 1976, p. 1019:1023.

[19] R. Mills e E. Grilly, «Phys. Rev, 99, 480, 1955,» in *Encyclopedie des Gaz, Elsevier and Air Liquide*, 1976, p. 1079:1083.

[20] J. M. e. al., «Advances in cryogenic engineering, 8, 126, 1968,» in *Encyclopedie des Gaz, Elsevier and Air Liquide*, 1976, p. 1079:1083.

[21] L. Weber, «Thermodynamic and related properties of oxygen from the triple point to 300 K at pressures to 300 atmospheres, NBS report 9710, 1968,» in *Encyclopedie des Gaz, Elsevier and Air Liquide*, 1976, p. 1079:1083.

[22] D. Mc Carty e A. Weber, «Thermophysical properties of oxygen from the freezing liquid line to 600° R for pressures to 500 Psia NBS TN 384, 1971,» in *Encyclopedie des Gaz, Elsevier and Air Liquide*, 1976, p. 1079:1083.

[23] A. S. e B. Armstrong, «International thermodynamic tables of the fluid state, argon, Butterworths, London, 1971,» in *Encyclopedie des Gaz, Elsevier and Air Liquide*, 1976, p. 58:89.

[24] F. Din, «Thermodynamic functions of gases, Volume 2, Butterworths, London, 1962,» in *Encyclopedie des Gaz, Elsevier and Air Liquide*, 1976, p. 85:89.

[25] W. H. e. al, «J. Chem. Phys. 54, 3, 1055, 1971,» in *Encyclopedie des Gaz, Elsevier and Air Liquide*, 1976, p. 85:89.

[26] F. Din, «Thermodynamic functions of gases, Volume 1, Butterworths, London, 1962,» in *Encyclopedie des Gaz, Elsevier and Air Liquide*, 1976, p. 333:337.

[27] E. Bender, «Equations of state exactly representing the phase behavior of pure substances, Proceedings of the fifth symposium on thermophysical properties A.S.M.E., 227, 1970,» in *Encyclopedie des Gaz, Elsevier and Air Liquide*, 1976, p. 333:337.

[28] «AIR LIQUIDE calculation,» in *Encyclopedie des Gaz, Elsevier and Air Liquide*, 1976, p. 333:337.

[29] V. Zagoruchenko e A. Zhuravler, «Thermophysical properties of gaseous and liquid methane, Izdatel'stvo Nauka, Moscou, 1970,» in *Encyclopedie des Gaz, Elsevier and Air Liquide*, 1976, p. 273:277.

[30] R. Goodwin, «The thermophysical properties of methane from 90 to 500 K at pressure 700 bar, NBSIR 73-342, 1973,» in *Encyclopedie des Gaz, Elsevier and Air Liquide*, 1976, p. 273:277.

[31] S. Miller, «Ethylene and its industrial derivates, Ernest Benn Limited, London, 1969,» in *Encyclopedie des Gaz, Elsevier and Air Liquide*, 1976, p. 459:463.

[32] S. A. e. al., «Final Ethylene Tables, IUPAC, Thermodynamic Tables Project Centre, Londres, Juillet 1972,» in *Encyclopedie des Gaz, Elsevier and Air Liquide*, 1976, p. 459:463.

[33] T. Das e P. Eubank, «Thermodynamic properties of propane: vapor liquid coexistence curve, Adv. Cryog. Engng, 18, 208, 1973,» in *Encyclopedie des Gaz, Elsevier and Air Liquide*, 1976, p. 601:603.

[34] L. K. e. al., «Thermodynamic functions of gases, Vol II (F. DIN. Ed.), Butterworths, London, 1962,» in *Encyclopedie des Gaz, Elsevier and Air Liquide*, 1976, p. 601:603.

Table A.4: Melting auxiliary equations and values of the parameters for the substances of interest.

Compound	Auxiliary SLE equation	T_{max} K	P_r / MPa	T_r / K	n_1	e_1	n_2	e_2	n_3	e_3	n_4	e_4
N_2	$\frac{P_m}{P_r} = 1 + \sum_{i=1}^{2} n_i \left[\left(\frac{T}{T_r} \right)^{e_i} - 1 \right]$	2000	1.2523E-2	63.151	12798.61	1.78963	0	0				
O_2	$\frac{P_m}{P_r} = exp\left\{ \sum_{i=1}^{4} n_i \left(\frac{T}{T_r} - 1 \right)^{e_i} \right\}$	300	1.4633E-4	54.361	-32.463	0.0625	142.78	0.125	-147.023	0.187	52.001	0.25
Ar	$\frac{P_m}{P_r} = 1 + \sum_{i=1}^{2} n_i \left[\left(\frac{T}{T_r} \right)^{e_i} - 1 \right]$	700	6.8891E-2	83.8058	-7476.27	1.05	9959.061	1.275				
Kr	$\frac{P_m}{P_r} = \sum_{i=1}^{2} n_i \left(\frac{T}{T_r} \right)^{e_i}$	800	1.01325E-1	115.775	-2345.757	0	1.08	1.617				
Xe	$\frac{P_m}{P_r} = \sum_{i=1}^{2} n_i \left(\frac{T}{T_r} \right)^{e_i}$	1300	1.01325E-1	161.405	-2573.936	0	0.798	1.589				
He	$\frac{P_m}{P_r} = \sum_{i=1}^{2} n_i \left(\frac{T}{T_r} \right)^{e_i}$	1500	1	2.1768	-1.7455837	0	1.6979793	1.555414				
CO_2	$\frac{P_m}{P_r} = 1 + \sum_{i=1}^{2} n_i \left[\left(\frac{T}{T_r} \right)^{e_i} - 1 \right]$	1100	5.1795E-1	216.592	1955.539	1	2055.459	2				
H_2	$\frac{P_m}{P_r} = 1 + \sum_{i=1}^{2} n_i \left[\left(\frac{T}{T_r} \right)^{e_i} - 1 \right]$	400	0.0073578	13.957	5626.3	1	2717.2	1.83				
CH_4	$\frac{P_m}{P_r} = 1 + \sum_{i=1}^{2} n_i \left[\left(\frac{T}{T_r} \right)^{e_i} - 1 \right]$	625	1.1696E-2	90.6941	24756.8	1.85	-7366.02	2.1				
C_2H_6	$\frac{P_m}{P_r} = 1 + \sum_{i=1}^{2} n_i \left[\left(\frac{T}{T_r} \right)^{e_i} - 1 \right]$	2000	1.1421E-6	90.368	223626315	1	105262374	2.55				
C_2H_4	$\frac{P_m}{P_r} = \sum_{i=1}^{3} n_i \left(\frac{T}{T_r} \right)^{e_i}$	450	1	103.986	0.0001225	0	357.924	2.0645	-357.924	0		
C_3H_8	$\frac{P_m}{P_r} = 1 + n_1 \left[\left(\frac{T}{T_r} \right)^{e_1} - 1 \right]$	2000	1.7E-10	85.48	4.23E+12	1.283						
C_3H_6	$\frac{P_m}{P_t} = \sum_{i=1}^{2} n_i \left(\frac{T}{T_r} \right)^{e_i}$	2000	4.85E-08	87.953	-6.59E+09	0	6.59E+09	2.821				

Table A.5: Sublimation auxiliary equations and values of the parameters for the substances of interest.

Compound	Auxiliary SVE Equation	P_r / MPa	T_r / K	n_1	e_1	n_2	e_2	n_3	e_3
N_2	$\frac{P_s}{P_r} = exp\left\{\frac{n_1 T}{T_r}\left[\left(1-\frac{T}{T_r}\right)^{e_1}\right]\right\}$	1.25198E-2	63.151	-13.089	1				
O_2	$\frac{P_s}{P_r} = exp\left\{\frac{n_1 T}{T_r}\left[\left(1-\frac{T}{T_r}\right)^{e_1}\right]\right\}$	1.4628E-4	54.361	-20.714	1.06				
Ar	$\frac{P_s}{P_r} = exp\left\{\frac{n_1 T}{T_r}\left[\left(1-\frac{T}{T_r}\right)^{e_1}\right]\right\}$	6.8891E-2	83.8058	-11.131	1				
Kr	$\frac{P_s}{P_r} = exp\left\{\frac{n_1 T}{T_r}\left[\left(1-\frac{T}{T_r}\right)^{e_1}\right]\right\}$	7.3197E-2	115.775	-11.562	1				
Xe	$\frac{P_s}{P_r} = exp\left\{\sum_{i=1}^{2}\frac{n_i T}{T_r}\left[\left(1-\frac{T}{T_r}\right)^{e_i}\right]\right\}$	8.175E-2	161.405	-13.9	1.06	14	3.1		
Ne	$\frac{P_s}{P_r} = exp\left\{\frac{n_1 T}{T_r}\left[\left(1-\frac{T}{T_r}\right)^{e_1}\right]\right\}$	4.3464E-2	24.556	-10.65	1				
CO_2	$\frac{P_s}{P_r} = exp\left\{\sum_{i=1}^{3}\frac{n_i T}{T_r}\left[\left(1-\frac{T}{T_r}\right)^{e_i}\right]\right\}$	5.1795E-1	216.592	-14.741	1	2.433	1.9	-5.306	2.9
H_2	$\frac{P_s}{P_r} = exp\left\{\frac{n_1 T}{T_r}\left[\left(1-\frac{T}{T_r}\right)^{e_1}\right]\right\}$	0.0077	13.957	-8.065	0.93				
CH4	$\frac{P_s}{P_r} = exp\left\{\frac{n_1 T}{T_r}\left[\left(1-\frac{T}{T_r}\right)^{e_1}\right]\right\}$	1.1696E-2	90.6941	-12.84	1				

2 Binary mixtures

The sources used for the bibliographic research of mixture data referred to the mixture of interest are:

- NIST database TDE (ThermoData Engine) [4];
- DDB (Dortmund Data Bank) database;
- GERG-2004 [5];
- EoS Air 2000 (Lemmon et al.) [6];
- GPA research reports;
- Review N_2+CH_4 (Kidnay et al.) [7];
- EoS Air Estela-Uribe 2010 [8];
- NISTIR 2000 [9];
- NISTIR 1982[10];
- NISTIR 1975 [11];
- other sources: research with science direct and other searching tools in scientific journals and books.

The mixtures of interest and the available references are summarized in Table A.6. The third column of Table A.6 presents the kind of available data.

The following abbreviations have been used: VLE: liquid-vapor equilibrium; SLE, solid-liquid equilibrium; SVE, solid-vapor equilibrium; CP, critical point; UCEP, upper critical endpoint; SVLE, solid-vapor-liquid equilibrium; LLE, liquid-liquid equilibrium; VLLE, vapor-liquid-liquid equilibrium; SFE, solid-fluid equilibrium.

For all the mixtures contained in Table A.6, all the references are indicated from Table A.7 to Table A.60.

Table A.6: Mixtures of interest and kind of data.

Mixture	Number of references	Kind of data
$N_2 – O_2$	20	VLE, CP, SLE, SLE
$N_2 – Ar$	22	VLE, CP, SLE
$N_2 – Kr$	3	VLE, SLE, SVLE
$N_2 – Xe$	1	SVLE
$Ne – N_2$	5	VLE
$He – N_2$	19	CP, VLE, SVE, LLE, SVLE
$N_2 – CO_2$	33	CP, VLE, SVE, SLE
$H_2 – N_2$	17	CP, VLE, SVE, SLE, SVLE
$N_2 – N_2O$	5	VLE, SLE, SVE, CP
$N_2 – CH_4$	37	CP, VLE, SLE, SLE, SVLE
$N_2 – C_2H_6$	25	CP, VLE, SLE, VLLE, UCEP
$N_2 – C_2H_4$	8	VLE, SLE
$N_2 – C_3H_8$	17	CP, VLE, SLE, VLLE, UCEP, LLE
$N_2 – C_3H_6$	6	VLE, SLE
$Ar – O_2$	17	VLE, SLE, CP
$O_2 – Kr$	5	VLE, SLE
$O_2 – Xe$	1	SLE
$Ne – O_2$	3	VLE, CP
$He – O_2$	4	VLE
$O_2 – CO_2$	9	VLE, CP, SLE
$H_2 – O_2$	2	SVE
$O_2 – N_2O$	2	VLE, SLE
$O_2 – CH_4$	6	VLE, CP, SLE

Table A.6 (continued)

Mixture	Number of references	Kind of data
$O_2 – C_2H_6$	6	VLE, SLE
$O_2 – C_2H_4$	5	VLE, SLE
$O_2 – C_3H_8$	3	VLE, SLE
$O_2 – C_3H_6$	5	SLE, LLE
Ar – Kr	9	VLE, SLE
Ar – Xe	1	SLE
Ne – Ar	6	VLE, CP, SLE
He – Ar	8	CP, VLE, LLE, SVE, SVLE
$Ar – CO_2$	4	VLE, SLE
$H_2 – Ar$	5	VLE, CP, SVE, SVLE
$Ar – CH_4$	17	CP, VLE, SLE, SLE, SVLE
$Ar – C_2H_6$	4	VLE
$Ar – C_3H_6$	2	VLE
Kr – Xe	6	VLE, CP, SLE, SVLE
$Kr – CO_2$	1	VLE, CP
$CH_4 – Kr$	6	VLE, SLE, CP
$Kr – C_2H_6$	3	VLE, CP
$Kr – C_2H_4$	1	VLE
$Kr – C_3H_6$	1	VLE
Ne – Xe	4	VLE, LLE, CP, SLE
$Xe – CO_2$	1	CP
$Xe – N_2O$	2	VLE
$CH_4 – Xe$	1	VLE, CP
$Xe – C_2H_6$	2	VLE, CP
$C_2H_4 – Xe$	2	VLE, CP
$Xe – C_3H_8$	1	VLE
$Xe – C_3H_6$	1	VLE
He – Ne	3	VLE, SVE
$H_2 – Ne$	2	VLE, VLLE
$He – H_2$	9	VLE
$N_2 – Ar – O_2$	9	VLE, CP

In all the following tables, the most volatile component is cited as first in the binary mixture; compositions are expressed in term of the most volatile component of each mixture. The critical temperature is considered as the information for stating which component is the more volatile in a mixture.

Table A.7 to Table A.60 present the literature data available for each mixture. For each mixture, all the available references are listed in the relative table. For each reference, the number of data, the kind of data, the temperature, pressure, and composition range of the data are reported. Empty rows mean that the bibliographic research has not yet provided us the correspondent articles. All the references are indicated with the first three letters of the first author followed by the year of publication. When more than one reference was available with the same three letters and year, letters a, b, c (and so on) have been used for distinguishing among them. All the references are listed in alphabetical order in section 2.1.

Table A.7: Literature data for the system nitrogen-oxygen.

Reference	Number of data points total	Kind of data	Temperature T/K	Pressure P/MPa	Composition liquid phase x	Composition vapor phase y
$xN_2 + (1-x)O_2$						
[ARM1955]	71	VLE	64.8 – 77.9	0.003 – 0.1	0.03 – 0.94	0.24 – 0.99
[BAB1999]	45	VLE	100.1 – 122.7	0.3 – 3.0	0.0 – 1.0	0.0 – 1.0
[BAL1900]	28	VLE	77.5 – 91.0	0.1	0.0 – 1.0	0.0 – 1.0

Table A.7 (continued)

Reference	Number of data points total	Kind of data	Temperature T/K	Pressure P/MPa	Composition liquid phase x	Composition vapor phase y
[COC1957]	40	VLE	81.1 – 91.0	0.12 – 0.14	0.065 – 0.81	0.21 – 0.93
[DIN1960]	116	VLE	79.1 – 115.6	0.11 – 1.0	0.1 – 0.89	0.19 – 0.97
[DOD1927a]	50	VLE	76.8 – 125.1	0.06 – 3.0	0.05 – 0.91	0.13 – 0.96
[DOD1927b]	204	VLE	75.0 – 125.0	0.015 – 3.2	0.0 – 1.0	0.0 – 1.0
[DOM1981]	9	VLE	60.2 – 79.8	0.005 – 0.1	0.62 – 0.71	0.9 – 0.94
[DUN1966]	11	VLE	63.1	0.002 – 0.01	0.0 – 1.0	
[HIZ1990]						
[HIZ1999]						
[JON1963]	6	CP	126.2 – 155.0		0.0 – 1.0	
[KRI1936]	42	VLE	100.0 – 125.0	0.25 – 3.2	0.0 – 1.0	0.0 – 1.0
[KUE1922]	28	VLE	132.2 – 147.6	2.8 – 4.6	0.25 – 0.5	
[MEY1936]	6	VLE	77.6 – 86.6	0.11	0.43 – 1.0	0.43 – 1.0
[POO1962]	11	VLE	83.8	0.05 – 0.2	0.0 – 1.0	
[RUH1935]	11 13	SLE SLE	50.1 – 63.1 50.1 – 54.1		0.23 – 1.0 0.0 – 0.23	
[THO1963]	13	VLE	88.2 – 90.3	0.1 – 0.11	0.0 - 0.08	0.0 – 0.27
[WIL1964]	138	VLE	77.8 – 136.2	0.1 – 2.6	0.05 – 0.99	0.11 – 1.0
[YOR1978]	20	VLE	79.9 – 88.3	0.03 – 0.12	0.002 – 0.85	0.01 – 0.93

Table A.8: Literature data for the system nitrogen-argon.

Reference	Number of data points total	Kind of data	Temperature T/K	Pressure P/MPa	Composition liquid phase x	Composition vapor phase y
xN_2 + (1-x)Ar						
[BAB1999]	51	VLE	95.0 – 121.2	0.2 – 2.7	0.0 – 1.0	0.0 – 1.0
[DIN1955]	26	SLE	63.1 – 83.8		0.0 – 1.0	
[DOL1919]	11	VLE	85.1	0.08 – 0.23	0.0 – 1.0	0.0 – 1.0
[ELS1975]	7	VLE	100.0	0.4 – 0.74	0.14 – 0.9	
[FAS1956a]	20	VLE	80.4 – 100.7	0.12 – 0.39	0.1 – 0.78	0.21 – 0.92
[FED1938]	10	SLE	62.9 – 82.8		0.0 – 0.75	
[HAM1915]	24	VLE	71.3 – 90.1	0.04 – 0.16	0.0 – 0.99	0.24 – 0.74
[HIZ1990]						
[HIZ1999]						
[JON1963]	6	CP	126.2 – 150.9		0.0 – 1.0	
[LEW1975]	8	VLE	84.5	0.07 – 0.22	0.0 – 1.0	0.0 – 1.0
[LIU1988]	13	VLE	122.9	1.5 – 2.8	0.05 – 0.97	0.08 – 0.98
[LON1963]	29	SLE	62.5 – 83.8	0.01 – 0.07	0.0 – 1.0	

Table A.8 (continued)

Reference	Number of data points total	Kind of data	Temperature T/K	Pressure P/MPa	Composition liquid phase x	Composition vapor phase y
[MAS1973]	6	VLE	89.9 – 113	0.27 – 1.31	0.503	
[MAS1976]	34	VLE	85.0 – 100.0	0.08 – 0.78	0.0 – 1.0	0.0 – 1.0
[MIL1973]	14	VLE	112.0	0.84 – 1.51	0.11 – 0.85	0.17 – 0.9
[NAR1966]	108	VLE	79.8 – 120.0	0.13 – 2.5	0.0 – 1.0	0.0 – 1.0
[POO1962]	12	VLE	83.8	0.07 – 0.2	0.0 – 1.0	
[SPR1966]	19	VLE	83.8	0.07 – 0.2	0.0 – 1.0	0.0 – 1.0
[THO1968]	69	VLE	80.9 – 115.2	0.13 – 1.1	0.1 – 0.91	0.18 – 0.96
[WIL1964]	179	VLE	72.2 – 133.7	0.1 – 2.63	0.04 – 1.0	0.02 – 1.0
[XIA1990]	18	VLE	100.0	0.35 – 0.74	0.12 – 0.92	0.29 – 0.96

Table A.9: Literature data for the system nitrogen-krypton.

Reference	Number of data points total	Kind of data	Temperature T/K	Pressure P/MPa	Composition liquid phase x	Composition vapor phase y
xN_2 + (1-x)Kr						
[MAS1974]	12	SLE	70.3 – 114.7		0.04 – 0.9	
[MAS1976]	54	VLE	100.0 – 125.0	0.01 – 3.2	0.0 – 1.0	0.0 – 1.0
	12	SVLE	70.3 – 114.7	0.036 – 0.49	0.04 – 0.9	
[TEL1984]	14	SVLE	71.8 – 115.8	0.048 – 0.48	0.0 – 0.89	

Table A.10: Literature data for the system nitrogen-xenon.

Reference	Number of data points total	Kind of data	Temperature T/K	Pressure P/MPa	Composition liquid phase x	Composition vapor phase y
xN_2 + (1-x)Xe						
[TEL1984]	16	SVLE	91.0 – 161.4	0.08 – 4.9	0.014 – 1.0	

Table A.11: Literature data for the system neon-nitrogen.

Reference	Number of data points total	Kind of data	Temperature T/K	Pressure P/MPa	Composition liquid phase x	Composition vapor phase y
xNe + (1-x)N_2						
[BUR1964]	12	VLE	82.7 – 113.0	0.5 – 5.1	0.009 – 0.15	0.08 – 0.93
[SKR1964]	22	VLE	67.4 – 90.3	0.6 – 2.6	0.014 – 0.08	0.7 – 0.98
[SKR1971]	43	VLE	66.0 – 101.3	1.0 – 12.0	0.029 – 0.38	0.61 – 0.97
[STR1965a]	77	VLE	66.1 – 120.6	0.4 – 7.1	0.005 – 0.27	0.1 – 0.98
[STR1968]	33	VLE	66.1 – 114.3	7.4 – 22.0	0.23- 0.6	0.4 – 0.96

Table A.12: Literature data for the system helium-nitrogen.

Reference	Number of data points total	Kind of data	Temperature T/K	Pressure P/MPa	Composition liquid phase x	Composition vapor phase y
xHe + (1-x)N_2						
[BUR1964]	12	VLE	82.7 – 113.1	0.5 – 5.1	0.001 – 0.035	0.08 – 0.95
[BUZ1963]	30	VLE	77.2 – 122.8	1.2 – 6.9	0.002 – 0.08	0.07 – 0.98
[DAV1963]	35	VLE	77.2	0.25 – 6.8	0.003 – 0.015	0.94 – 0.99
[DAV1971]	24	VLE	77.0 – 126.0	2.0 – 10.0		0.11 – 0.98
[DEV1963]	96	VLE	77.0 – 120.0	1.38 – 13.8	0.003 – 0.14	0.17 – 0.99
[FON1989]	55	VLE	64.9 – 125.0	1.4 – 10.0	0.0 – 0.12	0.06 – 1.0
[GON1940a]	29	VLE	78.0 – 109.0	0.11 – 28.9	0.0 – 0.18	0.0 – 0.98
[GON1940b]	5	VLE	90.1	2.9 – 14.7	0.01 – 0.048	
[GON1940c]	29	VLE	78.0 – 109.0	0.11 – 28.9	0.0 – 0.18	0.0 – 0.98
[GON1940d]	5	VLE	90.1	2.9 – 14.7	0.01 – 0.048	5
[KHA1940]	76	VLE	68.0 – 111.5	0.03 – 21.7	0.0 – 0.14	0.0 – 0.99
[ROD1964]	19	VLE	63.3 – 87.1	0.04 – 3.3	0.001-0.005	0.55 – 0.96
	15	SVE	53.9 – 63.8	0.1 – 1.4		0.7 – 0.99
	15	SVLE	63.2 – 65.7	0.01 – 13.9		0.55 – 0.99
[SKR1964]	22	VLE	67.5 – 90.3	0.6 – 2.6	0.001 – 0.009	0.74 – 0.99
[STR1967a]	86	VLE	77.6 – 121.7	6.7 – 82.7	0.012 – 0.56	0.34 – 0.99
	5	LLE	119.9	67.0 – 83.1	0.54 – 0.58	0.63 – 0.73
[STR1970]	101	VLE	77.5 – 119.6	13.1 – 396.5	0.04 – 0.51	0.68 – 0.99
	47	LLE	120.6 – 136.5	97.2 – 413.7	0.33 – 0.64	0.7 – 0.95
	5	SVLE	77.5 – 107.3	93.1 – 405.3	0.07 – 0.21	0.98 – 0.99
[STR1972a]	111	LLE	112.1 – 162.0	110.5 – 1020	0.24 – 0.69	0.82 – 0.98
	6	SVLE	112.1 - 138	492 – 993	0.24 – 0.35	0.96 – 0.98
	5	CP	138.0 – 162.0	416 - 957	0.73 – 0.77	
[TUL1971]	70	VLE	122.0 – 126.0	2.8 – 20.9	0.0 – 0.38	0.0 – 0.49
[VAN1988]	9	CP	155 – 325.6	730 – 8920		
	20	SVLE	153.7 – 303.6	1370 – 9020		
[WIL1992]	33	SLE	175 – 413	1150 – 7440	0.054 – 0.43	
	25	LLE	173.6 – 261.6	1368 – 6020	0.43 – 0.94	
	11	SVLE	154.4 – 375.4	4290 - 16870		

Table A.13: Literature data for the system nitrogen-carbon dioxide.

Reference	Number of data points total	Kind of data	Temperature T/K	Pressure P/MPa	Composition liquid phase x	Composition vapor phase y
xN_2 + (1-x)CO_2						
[ALS1983]	29	VLE	220.0 – 240.0	0.6 – 16.7	0.0 – 0.48	0.0 – 0.83
[ALS1990]	5	VLE	230.0 – 250.0	6.2 – 10.3	0.08 – 0.18	0.61 – 0.77
[ALW1976]	14	VLE	223.2 – 273.2	3.2 – 16.7	0.035 – 0.34	0.24 – 0.82
[ARA1971]	43	VLE	253.0 – 288.0	2.4 – 14.4	0.0 – 0.35	0.0 – 0.57
[BAL1989]	11	VLE	208.5 – 257.8	0.69 – 18.2		0.55

Table A.13 (continued)

Reference	Number of data points total	Kind of data	Temperature T/K	Pressure P/MPa	Composition liquid phase x	Composition vapor phase y
[BIA1992]	23	VLE	293.1 – 299.8	6.2 – 9.2	0.004 – 0.13	0.011 – 0.14
[BIA1993]	12 2	VLE CP	301.3 – 303.3 301.3 – 303.3	6.9 – 8.0 7.8 – 8.0	0.0 – 0.035 0.02 – 0.04	0.0 – 0.039
[BRO1989a]	17	VLE	250.0 – 270.0	1.8 – 14.1	0.0 – 0.3	0.0 – 0.62
[BRO1989b]	69	VLE	220.0 – 270.0	0.5 – 13.0	0.0 – 0.19	0.0 – 0.83
[DUA1995a]	23	VLE	208.9 – 268.0	10.8 – 21.4		0.5 – 0.6
[DUA1995b]	23	VLE	208.9 – 268.0	10.8 – 21.4	0.5 – 0.6	
[ESP1989]	11	VLE	208.5 – 257.8	0.7 – 18.2	0.553	
[FED1940]	5	SLE	67.0 – 98.0		~1	
[FER1980]	5	VLE	273.2	3.5 – 8.4	0.0 – 0.1	
[KAM1966]	17	VLE	233.2 – 298.2	3.7 – 12.7	0.051 – 0.25	0.067 – 0.7
[KRI1962]	27	VLE	288.2 – 303.2	5.6 – 10.3	0.0 – 0.19	0.0 – 0.21
[MUI1965]	4	VLE	273.2	5.5 – 12.0	0.039 – 0.29	0.24 – 0.38
[SHI1984]	14	VLE	288.0 – 288.1	5.6 – 9.9	0.81 – 0.94	0.81 – 0.94
[SOM1978]	39	VLE	270.0	3.2 – 12.3	0.0 – 0.35	0.0 – 0.42
[SON1962]	64	SVE	140 – 190	0.51 – 10.1		0.92 – 1
[SON1963]	72	SVE	140 – 190	5.07 – 20.3		0.95 – 1
[TSI1946]	7	SVE	273.2	392 – 686	0.05 – 0.19	0.15 – 0.57
[WEB1984]	6	VLE	223.0 – 273.0	5.0 – 10.0	0.03 – 0.16	0.21 – 0.8
[WIL1977]	7	VLE	221.2 – 265.3	1.4 – 13.4		0.5
[XU1992a]	20	VLE	288.3 – 293.3	5.1 – 9.7	0.0 – 0.15	0.0 – 0.2
[XU1992b]	12	VLE	298.4	6.5 – 8.4	0.0 – 0.064	0.0 – 0.07
[YAK1975]	29	SLE	78.0 – 115.0	3.6 – 9.12	~1	
[YOR1970]	16	VLE	273.2	3.5 – 11.8	0.0 – 0.3	0.0 – 0.4
[YOR1971a]	5	VLE	273.2	3.5 – 9.4	0.0 – 0.15	0.0 – 0.39
[YOR1985]	34 2	VLE CP	273.2 – 298.2 273.2 – 293.2	4.5 – 12.0 9.8 – 12.0	0.02 – 0.3 0.14 – 0.3	0.06 – 0.4
[YUC1999]	22	VLE	240.0 – 270.0	1.3 – 13.0	0.0 – 0.25	0.0 – 0.7
[ZEC1985]	6	VLE	223.2 – 273.2	5.0 – 10.0	0.03 – 0.16	0.2 – 0.8
[ZEN1963]	31	VLE	218.2 – 273.2	1.3 – 13.9	0.009 – 0.3	0.2 – 0.85

Table A.14: Literature data for the system hydrogen-nitrogen.

Reference	Number of data points total	Kind of data	Temperature T/K	Pressure P/MPa	Composition liquid phase x	Composition vapor phase y
$xH_2 + (1\text{-}x)N_2$						
[AKE1957]	16	VLE	83.2 – 122.0	2.2 – 15.9	0.026 – 0.46	0.08 – 0.9
[AUG1957]	13	VLE	67.0 – 77.7	1.7 – 17.8	0.035 – 0.47	0.84 – 0.97

Table A.14 (continued)

Reference	Number of data points total	Kind of data	Temperature T/K	Pressure P/MPa	Composition liquid phase x	Composition vapor phase y
[DOK1955]	62 7	SVE VLE	25.1 – 62.3 64.9 – 70.4	0.13 – 5.1 2.3 – 5.1		0.94 – 1.0 0.97 – 0.98
[EUB1957]	16	VLE	83.2 – 122.0	2.2 – 15.9	0.026 – 0.46	0.08 – 0.9
[GON1939a]	40	VLE	79.0 – 109.0	0.12 – 17.8	0.0 – 0.46	0.0 – 0.94
[GON1939b]	40	VLE	79.0 – 109.0	0.12 – 17.8	0.0 – 0.46	0.0 – 0.94
[KNA1976]	5	VLE	90.0 – 123.8	3.0		0.0 – 0.78
[KRE1983a]	2	VLE	80.0	5.0 – 10.0	0.11 – 0.23	0.89 – 0.92
[MAI1961]	17	VLE	90.0 – 95.0	0.36 – 4.6	0.0 – 0.11	0.0 – 0.83
[OMA1962a]	30	SLE	26.3 – 32.5	0.61 – 1.7	~1.0	
[STE1939]	23	VLE	90.0 – 113.0	1.6 – 9.6	0.04 – 0.39	0.19 – 0.83
[STR1978]	77 8	VLE CP	63.2 – 110.3 63.2 – 126.2	1.0 – 57.2 3.4 – 58.0	0.018 – 0.54 0.0 – 0.62	0.25 – 0.97
[VER1931]	66 2 12 23	VLE CP SVLE SVE	63.2 – 88.2 78.2 – 88.2 61.2 – 62.1 58.1 – 60.7	0.01 – 22.7 14.0 – 19.4 3.0 – 21.8 1.8 – 21.8	0.0 – 0.55 0.53 – 0.58	0.0 – 0.99 0.93 – 1.0
[XIA1990]	16	VLE	100.0	1.4 – 4.6	0.02 – 0.12	0.37 – 0.69
[YOR1968a]	12	VLE	77.4	0.5 – 15.2	0.02 – 0.36	0.75 – 0.93
[YOR1971a]	17	VLE	77.4 – 88.2	1.7 – 19.0	0.049 – 0.47	0.62 – 0.94
[YOR1971b]	17	VLE	77.4 – 88.2	1.5 – 18.6	0.049 – 0.47	0.62 – 0.94

Table A.15: Literature data for the system nitrogen-nitrous oxide.

Reference	Number of data points total	Kind of data	Temperature T/K	Pressure P/MPa	Composition liquid phase x	Composition vapor phase y
xN_2 + (1-x)N_2O						
[IOM1976]	31	SLE	80.0 – 115.0	4.1 – 12.2	~1	
[KOS1984]	40 5	VLE CP	253.2 – 303.2 253.2 – 303.2	1.8 – 10.7 8.1 – 10.7	0.0 – 0.4 0.05 – 0.4	0.0 – 0.52
[WOJ1975]	5	SLE	63.5 – 77.4		~1	
[YAK1976]	70	SVE	105.0 – 140.0	0.3 – 6.0		~1
[ZEI1972]	38	VLE	213.2 – 253.2	0.4 – 8.2	0.0 – 0.15	0.0 – 0.86

Table A.16: Literature data for the system nitrogen-methane.

Reference	Number of data points total	Kind of data	Temperature T/K	Pressure P/MPa	Composition liquid phase x	Composition vapor phase y
xN_2 + (1-x)CH_4						
[BLO1953]	220 10	VLE CP	91.2 – 188.9 129.6 – 190.5	0.06 – 5.1 3.6 – 5.1	0.03 – 0.95 0.0 – 0.95	0.03 – 0.95

Table A.16 (continued)

Reference	Number of data points total	Kind of data	Temperature T/K	Pressure P/MPa	Composition liquid phase x	Composition vapor phase y
[BLO1955]	32	VLE	113.0 – 173.2	0.69 – 3.4	0.1 – 0.3	0.1 – 0.3
[BRA1958]	9	VLE	137.0 – 174.8	3.4	0.05 – 0.8	0.13 – 0.84
[CHA1966]	10	VLE	171.4	2.8 – 5.1	0.04 – 0.33	0.09 – 0.4
[CHA1967]	28	VLE	122.0 – 171.4	0.35 – 5.0	0.0 – 0.99	0.0 – 0.99
[CHE1964]	20	VLE	91.6 – 124.1	0.02 – 0.56	0.01 – 0.15	0.1 – 0.86
[CIN1953]	28	VLE	122	0.3 – 2.53	0.021 – 0.94	0.25 – 0.98
[COS1959]	9	VLE	137.0 – 174.8	3.45	0.054 – 0.8	0.13 – 0.84
[ELL1959]	196	VLE	78.4 – 186.1	0.1 – 4.8	0.06 – 0.85	0.06 – 0.85
[FAS1941]	5	SLE	70.8 – 79.5		0.31 – 0.55	
[FAS1957a]	37	VLE	81.8 – 149.5	0.15 – 1.6	0.074 – 0.83	0.38 – 1.0
[FED1938]	12	SLE	63.1 – 90.0		0.0 – 1.0	
[FON1989]	176	VLE	112.0 – 183.2	0.2 – 4.9	0.004 – 1.0	0.012 – 1.0
[FUK1967]	20	VLE	84.2 – 90.8	0.09 – 0.24	0.14 – 0.67	
[HAN2012]	83	VLE	100.0 – 123.0	0.04 – 2.9	0.0 – 1.0	0.0 – 1.0
[JAN2000]						
[JAN2007]	27	VLE	130.0 – 180.0	0.58 – 5.1	0.02 – 0.59	0.09 – 0.7
[JIN1993]	10	VLE	122.9	0.4 – 2.6	0.05 – 0.91	0.43 – 0.97
[JON1963]	6	CP	126.2 – 190.3		0.0 – 1.0	
[KID1975a]	91	VLE	112.0 – 180.0	0.1 – 4.9	0.0 – 0.9	0.0 – 0.94
[KRE1982]	34	VLE	140.0 – 160.0	0.64 – 4.9	0.0 – 0.79	0.0 – 0.79
[KRE1983a]	4	VLE	120.0 – 144.3	1.5 – 4.0	0.27 – 0.73	0.66 – 0.9
[LIU1988]	10	VLE	122.9	0.4 – 2.6	0.05 – 0.91	0.43 – 0.97
[MCC1976]	10	VLE	90.7	0.012 – 0.38	0.0 – 1.0	0.0 – 1.0
[MCT1919]	7	VLE	84.5 – 106.5	0.1	0.05 – 0.67	0.13 – 0.85
[MIL1973]	22	VLE	112.0	0.19 – 1.3	0.034 – 0.78	0.45 – 0.96
[OMA1962b]	59 12	SLE SVLE	62.4 – 90.6 60 – 87.5	 0.007 – 0.07	0.0 – 1.0	
[PAR1974a]	60	VLE	95.0 – 120.0	0.02 – 2.5	0.0 – 1.0	0.0 – 1.0
[PAR1974b]	60	VLE	95.0 – 120.0	0.02 – 2.5	0.0 – 1.0	0.0 – 1.0
[ROZ1988]	49	VLE	133.3 – 180.1	0.66 – 4.4		0.068 – 0.4
[SKR1970]	16	VLE	113.2	0.11 – 1.8	0.0 – 1.0	0.0 – 1.0
[SPR1966]	11	VLE	90.7	0.012 – 0.38	0.0 – 1.0	0.0 – 1.0
[STR1972b]	23	VLE	133.7 – 122.0	0.12 – 2.78	0.0 – 1.0	0.0 – 1.0
[STR1974a]	116 8	VLE CP	113.7 – 183.2 126.3 – 183.2	0.12 – 5.0 3.4 – 5.0	0.0 – 1.0 0.23 – 1-0	0.0 – 1.0
[TEL1984]	7	SLE	78.8 – 88.7		0.06 – 0.52	
[TOR1939]	50	VLE	89.8 – 132.9	0.012 – 2.5	0.0 – 1.0	0.0 – 1.0
[WIL1975]	16	VLE	110.9	0.097 – 1.53	0.0 – 1.0	

Table A.17: Literature data for the system nitrogen-ethane.

Reference	Number of data points total	Kind of data	Temperature T/K	Pressure P/MPa	Composition liquid phase x	Composition vapor phase y
$xN_2 + (1\text{-}x)C_2H_6$						
[BRO1989b]	33	VLE	220.0 – 270.0	0.5 – 12.0	0.0 – 0.41	0.0 – 0.83
[CHA1966]	11	VLE	171.4	0.38 – 3.4	0.02 – 0.12	0.57 – 0.94
[CHA1967]	20	VLE	122.0 – 171.4	0.34 – 3.4	0.025 – 0.97	0.57 – 1.0
[CHE1964]	2	VLE	92.8	0.02 – 0.045	0.005 – 0.01	
[COS1959]	3	VLE	144.3 – 199.8	3.4 – 6.9	0.1 – 0.21	0.89 – 0.99
[COX1950]	3	SLE	77.3 – 78.6		0.99 – 1.0	
[EAK1955]	319 6 5	VLE LLE CP	101.8 – 301.8 97.5 – 128.1 131.5 – 301.5	0.53 – 11.98 0.61 – 3.42 4.0 – 9.1	0.05 – 0.98 0.2 – 0.32 0.05 – 0.98	
[ELL1959]	294 9	VLE CP	112.5 – 300.9 131.5 – 284.8	0.69 – 12.8 3.96 – 9.11	0.05 – 0.98 0.05 – 0.98	
[GRA1977a]	35	VLE	200.0 – 290.0	0.2 – 13.2	0.0 – 0.57	0.0 – 0.91
[GUP1980]	67	VLE	260.0 – 280.0	1.7 – 9.9	0.0 – 0.37	0.0 – 0.57
[JAN2000]						
[JAN2007]	24	VLE	150.0 – 270.0	0.56 – 10.1	0.02 – 0.36	0.23 – 0.99
[KOH1984]	15	VLLE	118.0 – 130.8	2.1 – 4.0	0.27 – 0.32 0.93 – 0.96	
	1	UCEP	132.3	4.1	0.32 0.96	
[KRE1982]	21	VLE	120.0 – 133.2	0.64 – 3.6	0.04 – 0.99	1.0
	4	VLLE	120.0 – 133.2	2.3 – 4.1	0.27 – 0.31 0.94 – 0.98	0.99 – 1.0
[KRE1983b]	21	VLE	120.0 – 133.2	0.64 – 3.6	0.04 – 0.99	1.0
	4	VLLE	120.0 – 133.2	2.3 – 4.1	0.27 – 0.31 0.94 – 0.98	0.99 – 1.0
[LLA1985]	15	VLLE	118.0 – 130.8	2.1 – 4.0	0.27 – 0.32 0.93 – 0.96	
	1	UCEP	132.3	4.1	0.32 0.96	
[RAA2001]	24	VLE	150.0 – 270.0	0.56 – 10.1	0.02 – 0.36	0.23 – 0.99
[RAA2004]	31	VLE	119.8 – 138.9	0.6 – 3.3	0.04 – 0.27	
[ROZ1988]	59	VLE	176.8 – 281.3	0.47 – 7.2		
[STR1972b]	52	VLE	138.7 – 194.3	0.0 – 13.5	0.0 – 0.71	0.0 – 0.99
[STR1974b]	49 3	VLE CP	138.7 – 194.3 149.8 – 194.3	0.003 – 13.4 11.9 – 13.5	0.0 – 0.65 0.67 – 0.71	0.0 – 0.99
[SZC1980]	4	SLE	69.5 – 85.5		0.97 – 0.99	
[WIL1975]	15	VLE	110.9	0.2 – 1.5	0.0 – 1.0	
[ZEC1985]	17	VLE	240.0 – 260.0	0.97 – 7.5	0.0 – 0.2	0.0 – 0.72
[ZEC1986a]	17	VLE	240.0 – 260.0	0.97 – 7.5	0.0 – 0.2	0.0 – 0.72

Table A.18: Literature data for the system nitrogen-ethylene.

Reference	Number of data points total	Kind of data	Temperature T/K	Pressure P/MPa	Composition liquid phase x	Composition vapor phase y
xN_2 + (1-x)C_2H_4						
[GAS1981]	68	VL_2E	120.0 – 200.0	0.01 – 9.3	0.0 – 0.8	0.0 – 1.0
	7	VL_1E	125.3 – 140.0	2.9 – 5.4	0.92 – 0.97	0.97 – 1.0
	4	L_1L_2VE	120.0 – 140.0	2.3 – 5.0	0.2 – 0.3	0.96 – 1.0
[GRA1977a]	15	VLE	200.0 – 260.0	0.45 – 11.0	0.0 – 0.47	0.0 – 0.83
[GRA1977b]	15	VLE	200.0 – 260.0	0.45 – 11.0	0.0 – 0.47	0.0 – 0.83
[ROZ1988]	44	VLE	182.6 – 268.0	0.27 – 5.4		0.14 – 0.67
[SZC1979]	3	SLE	68.7 – 80.1		~1	
[TSI1940]	3	SLE	69.0 – 90.1		~1	
[ZEC1985]	17	VLE	240.0 – 260.0	1.8 – 9.1	0.0 – 0.28	0.0 – 0.54
[ZEC1986b]	17	VLE	240.0 – 260.0	1.8 – 9.1	0.0 – 0.28	0.0 – 0.54

Table A.19: Literature data for the system nitrogen-propane.

Reference	Number of data points total	Kind of data	Temperature T/K	Pressure P/MPa	Composition liquid phase x	Composition vapor phase y
xN_2 + (1-x)C_3H_8						
[BOL1954]	8	VLE	298.2	2.5 – 18.1	0.032 – 0.55	0.56 – 0.78
[CHE1964]	6	VLE	91.9 – 128.4	0.12 – 0.58	0.016 – 0.07	
[GRA1977a]	36	VLE	230.0 – 290.0	0.1 – 21.9	0.0 – 0.53	0.0 – 0.96
[HOU2010a]	28	VLE	110.0 – 125.6	0.26 – 3.3	0.011 – 0.12	
[HUD1984]	127	VLE	188.2 – 342.7	0.08 – 5.8		0.26 – 0.91
[KOH1984]	10	VLLE	117.0 – 126.0	2.2 – 3.4	0.13 – 0.14 0.97 – 0.99	
	1	UCEP	126.6	3.45	0.14 0.99	
[KRE1982]	17	VLE	120.0 – 127.0	0.7 – 6.2	0.03 – 0.13	1
	3	VLLE	120.0 – 126.0	2.5 – 3.3	0.11 – 1.0 1	1
[KRE1983b]	17	VLE	120.0 – 127.0	0.7 – 6.2	0.03 – 0.13	1
	3	VLLE	120.0 – 126.0	2.5 – 3.3	0.11 – 1.0 1	1
[LLA1985]	10	VLLE	117.0 – 126.0	2.2 – 3.4	0.13 – 0.14 0.97 – 0.99	
	1	UCEP	126.6	3.45	0.14 0.99	
[LU1969]	9	VLE	113.2 – 125.2	0.15 – 1.78	0.08 – 0.09	1
[POO1974]	32	VLE	114.1 – 122.2	0.15 – 2.8	0.007 – 0.09	1
[ROO1967]	3	CP	311.6 – 365.2	5.2 – 14.8	0.1 – 0.5	
[ROZ1988]	144	VLE	196.1 – 285.3	0.11 – 4.8		0.18 – 0.89
[SCH1966]	70	VLE	103.2 – 353.2	0.01 – 13.8	0.0 – 0.32	0.0 – 1.0
	11	LLE	103.2 – 123.2	1.4 – 13.8	0.08 – 0.14 0.99 – 1.0	

Table A.19 (continued)

Reference	Number of data points total	Kind of data	Temperature T/K	Pressure P/MPa	Composition liquid phase x	Composition vapor phase y
[SZC1980]	5	SLE	64.8 – 101.0		0.995 – 1.0	
[YU1969]	14	VLLE	113.7 – 133.3	1.8 – 4.1	0.25 – 0.33 0.92 – 0.98	0.99 – 1.0
[YUC1999]	41	VLE	240.0 – 330.0	0.15 – 15.1	0.0 – 0.32	0.0 – 0.95

Table A.20: Literature data for the system nitrogen-propylene.

Reference	Number of data points total	Kind of data	Temperature T/K	Pressure P/MPa	Composition liquid phase x	Composition vapor phase y
$xN_2 + (1\text{-}x)C_3H_6$						
[BLA1965]	41	VLE	78.0 – 90.5	0.03 – 0.26	0.004 – 0.34	
[GRA1977a]	22	VLE	260.0 – 290.0	0.38 – 21.4	0.0 – 0.48	0.0 – 0.89
[ROZ1988]	31	VLE	213.2 – 283.2	0.12 – 3.4		0.23 – 0.76
[SZC1979]	3	SLE	71.0 – 90.7		~1.0	
[TSI1940]	3	SLE	67.0 – 83.0		0.93 – 1.0	
[YOR1968b]	20	VLE	194.7 – 295.7	0.53 – 6.3	0.009 – 0.09	0.23 – 0.99

Table A.21: Literature data for the system argon-oxygen.

Reference	Number of data points total	Kind of data	Temperature T/K	Pressure P/MPa	Composition liquid phase x	Composition vapor phase y
$xAr + (1\text{-}x)O_2$						
[BOU1936]	39	VLE	87.0 – 96.3	0.07 – 0.21	0.04 – 0.87	0.06 – 0.88
[BUR1962]	140	VLE	84.8 – 118.3	0.06 – 1.0	0.1 – 0.91	0.12 – 0.92
[CLA1954]	55	VLE	90.0 – 110.0	0.1 – 0.67	0.0 – 1.0	0.0 – 1.0
[DIN1955]	15	SLE	54.3 – 83.8	0 – 0.07	0.0 – 1.0	
[FAS1955]	24	VLE	89.3 – 96.4	0.12 – 0.31	0.21 – 0.83	0.28 – 0.87
[FED1938]	8	SLE	58.8 – 84.1		0.21 – 1.0	
[FED1939]	12	SLE	54.1 – 84.1		0.0 – 1.0	
[HIZ1990]						
[HIZ1999]						
[JON1963]	6	CP	150.9 – 155.0		0.0 – 1.0	
[NAR1957]	63	VLE	90.5 – 120.0	0.1 – 1.21	0.0 – 1.0	0.0 – 1.0
[PAR1997]	24	VLE	92.1 – 115.4	0.12 – 0.94	0.02 – 0.92	0.03 – 0.93
[POO1962]	24	VLE	83.8 – 89.6	0.05 – 0.13	0.0 – 1.0	
[VEI1937]	14	SLE	56.0 – 84.0		0.097 – 1.0	
[WAN1960]	35	VLE	90.4 – 95.9	0.12 – 0.22	0.02 – 1.0	
[WIL1964]	198	VLE	87.4 – 138.7	0.1 – 2.63	0.004 – 0.98	0.01 – 0.98
[YOR1978]	65	VLE	89.4 – 91.5	0.1 – 0.13	0.0 – 0.76	0.0 – 0.79

Table A.22: Literature data for the system oxygen-krypton.

Reference	Number of data points total	Kind of data	Temperature T/K	Pressure P/MPa	Composition liquid phase x	Composition vapor phase y
xO_2 + (1-x)Kr						
[BAR1973]	92	VLE	77.2 – 100.0	0.02 – 0.25	0.5 – 0.98	0.94 – 1.0
[BUR1966]	12	VLE	93.6 – 106.5	0.14 – 0.42	0.9 – 1.0	0.99 – 1.0
[FAS1939]	92	VLE	77.2 – 100.0	0.02 – 0.25	0.5 – 0.98	0.94 – 1.0
[FAS1956b]	20	VLE	95.8 – 137.0	0.14 – 0.69	0.06 – 0.85	0.38 – 0.98
[VON1934]	9	SLE	52.5 – 116.9		0.0 – 0.96	

Table A.23: Literature data for the system oxygen-xenon.

Reference	Number of data points total	Kind of data	Temperature T/K	Pressure P/MPa	Composition liquid phase x	Composition vapor phase y
xO_2+ (1-x)Xe						
[VON1934]	15	SLE	80 – 160.0		0.0 – 0.89	

Table A.24: Literature data for the system neon-oxygen.

Reference	Number of data points total	Kind of data	Temperature T/K	Pressure P/MPa	Composition liquid phase x	Composition vapor phase y
xNe+ (1-x) O_2						
[SKR1964]	25	VLE	67.0 – 90.2	0.6 – 2.6	0.004 – 0.02	0.8 – 1.0
[SKR1971]	90	VLE	64.1 – 118.7	1.96 – 20.6	0.007 – 0.32	0.6 – 1.0
[STR1965b]	113 5	VLE CP	63.4 – 152.3 110.4 – 152.3	0.28 – 35.1 5.9 – 31.0	0.0 – 0.49 0.09 – 0.55	0.0 – 1.0

Table A.25: Literature data for the system helium-oxygen.

Reference	Number of data points total	Kind of data	Temperature T/K	Pressure P/MPa	Composition liquid phase x	Composition vapor phase y
xHe + (1-x)O_2						
[HER1965]	8	VLE	90.0	1.3 – 19.1	0.0 – 0.014	0.92 – 0.99
[SIN1966]	37	VLE	77.4 – 143.2	1.7 – 13.8	0.0 – 0.086	
[SKR1964]	25	VLE	67.5 – 90.3	0.6 – 2.6	0.0 – 0.002	0.78 – 1.0
[SKR1971]	97	VLE	65.1 – 116.2	2.9 – 21.6	0.0 – 0.056	0.57 – 1.0

Table A.26: Literature data for the system oxygen-carbon dioxide.

Reference	Number of data points total	Kind of data	Temperature T/K	Pressure P/MPa	Composition liquid phase x	Composition vapor phase y
xO_2+ (1-x)CO_2						
[BOO1930]	6	CP	154.4 – 304.2	5.0 – 15.0	0.0 – 1.0	
[DES2002]	12	SLE	90.8 – 110.5		~ 1.0	
[FED1940]	5	SLE	67.0 – 98.0		~1.0	
[FRE1970]	72	VLE	223.2 – 283.2	1.0 – 13.2	0.006 – 0.4	0.06 – 0.82
[FRE1972]	11	VLE	223.8	0.93 – 14.2	0.004 – 0.45	0.22 – 0.81
[KAM1966]	22	VLE	233.2 – 298.2	3.7 – 12.7	0.03 – 0.37	0.08 – 0.76
[KEE1903]	36	VLE	283.2 – 296.4	0.01 – 0.14	0.8 – 0.9	0.1 – 0.2
[MUI1965]	4	VLE	273.2	5.5 – 11.7	0.046 – 0.3	0.25 – 0.41
[ZEN1963]	33	VLE	218.2 – 273.2	2.2 – 14.9	0.03 – 0.53	0.25 – 0.85

Table A.27: Literature data for the system hydrogen-oxygen.

Reference	Number of data points total	Kind of data	Temperature T/K	Pressure P/MPa	Composition liquid phase x	Composition vapor phase y
xH_2 + (1-x)O_2						
[MCK1961]	48	SVE	20.9 – 54.5	0.35 – 10.3		~1
[OMA1962c]	24	SVE	40.0 – 54.7	0.51 – 1.52		~1

Table A.28: Literature data for the system oxygen-nitrous oxide.

Reference	Number of data points total	Kind of data	Temperature T/K	Pressure P/MPa	Composition liquid phase x	Composition vapor phase y
xO_2 + (1-x)N_2O						
[DES2002]	14	SLE	90.9 – 112.9		~1	
[ZEI1972]	63	VLE	213.2 – 293.2	0.42 – 9.1	0.0 – 0.68	0.0 – 0.92

Table A.29: Literature data for the system oxygen-methane.

Reference	Number of data points total	Kind of data	Temperature T/K	Pressure P/MPa	Composition liquid phase x	Composition vapor phase y
xO_2 + (1-x)CH_4						
[FAS1941]	5	SLE	69.2 – 74.2		0.33 – 0.47	
[HOD1967]	3	VLE	93.2 – 107.2	0.14 – 0.44	~1	~1
[JON1963]	6	CP	155 – 190.3		0.0 – 1.0	
[MCK1957]	5	SLE	66.5 – 88.7		0.03 – 0.52	
[MCK1958]	6	SLE	67.2 – 90.0		0.0 – 0.46	
[STR2012]	40	VLE	113.0 – 152.6	0.28 – 1.51	0.024 – 0.44	0.09 – 0.81

Table A.30: Literature data for the system oxygen-ethane.

Reference	Number of data points total	Kind of data	Temperature *T/K*	Pressure *P/MPa*	Composition liquid phase *x*	Composition vapor phase *y*
$xO_2 + (1-x)C_2H_6$						
[COX1950]	4	SLE	77.3 – 85.3		0.94 – 0.98	
[HIM1959]	11	SLE	72.0 – 99.8		0.42 – 0.9	
[HOU2007]	31	VLE	112.1 – 139.0	0.26 – 2.64	0.04 – 0.99	
[KAR1958]	1	SLE	90.0		0.872	
[MCK1957]	8	SLE	66.5 – 90.0		0.0 – 0.97	
[MCK1958]	7	SLE	53.3 – 89.1		0.0 – 0.99	

Table A.31: Literature data for the system oxygen-ethylene.

Reference	Number of data points total	Kind of data	Temperature *T/K*	Pressure *P/MPa*	Composition liquid phase *x*	Composition vapor phase *y*
$xO_2 + (1-x)C_2H_4$						
[COX1950]	5	SLE	81.1 – 89.9		0.99 – 1.0	
[HIM1959]	9	SLE	77.6 – 98.8		0.91 – 0.99	
[HOU2007]	5 18	VL1E VL2E	110.1 110.1 – 140.1	0.49 – 0.52 0.013 – 2.82	0.79 – 0.97 0.0 – 0.99	
[KAR1958]	1	SLE	90.0		0.98	
[TSI1940]	5	SLE	69.0 – 101.0		0.83 – 1.0	

Table A.32: Literature data for the system oxygen-propane.

Reference	Number of data points total	Kind of data	Temperature *T/K*	Pressure *P/MPa*	Composition liquid phase *x*	Composition vapor phase *y*
$xO_2 + (1-x)C_3H_8$						
[HIM1959]	4	SLE	73.2 – 83.2		0.93 – 0.94	
[HOU2010b]	24 9	VL1E VL2E	110.2 – 140.0 110.2 – 140.0	0.25 – 2.57 0.54 – 2.61	0.027 – 0.48 0.91 – 0.98	
[KAR1958]	90	SLE	90.0		0.99	

Table A.33: Literature data for the system oxygen-propylene.

Reference	Number of data points total	Kind of data	Temperature *T/K*	Pressure *P/MPa*	Composition liquid phase *x*	Composition vapor phase *y*
$xO_2 + (1-x)C_3H_6$						
[COX1950]	4	SLE	83.0 – 87.4		0.99 – 1.0	
[KAR1958]	1	SLE	90.0		0.996	
[MCK1957]	1	SLLE	78.7		0.18 – 0.82	
[MCK1958]	4	SLE	77.6 – 91.4		0.99 – 1.0	
[TSI1940]	5	SLE	67.0 – 86.5		0.61 – 1.0	

Table A.34: Literature data for the system argon-krypton.

Reference	Number of data points total	Kind of data	Temperature T/K	Pressure P/MPa	Composition liquid phase x	Composition vapor phase y
xAr+ (1-x)Kr						
[CHU1971]	5	VLE	115.8	0.07 – 0.95	0.0 – 1.0	
[DAV1967]	20	VLE	103.9 – 115.8	0.07 – 0.95	0.0 – 1.0	0.0 – 1.0
[HEA1955]	43	SLE	83.7 – 115.7		0.0 – 1.0	
[HOL1992]	22	VLE	125.2 – 151.0	0.19 – 4.0	0.019 – 0.89	0.21 – 0.98
[MAS1974]	7	SLE	84.7 – 110.1		0.15 – 0.78	
[MAS1976]	42 7	VLE SVLE	115.0 – 125.0 84.7 – 110.1	0.07 – 1.58 0.06 – 0.17	0.0 – 1.0 0.16 – 0.78	0.0 – 1.0
[SCH1960]	3	VLE	88.06	0.08 – 0.1	0.65 – 0.89	0.98 – 0.99
[SCH1975]	156	VLE	138.2 – 193.2	0.35 – 6.0	0.0 – 1.0	0.0 – 1.0
[VEI1937]	11	SLE	84.0 – 116.0		0.0 – 1.0	

Table A.35: Literature data for the system argon-xenon

Reference	Number of data points total	Kind of data	Temperature *T/K*	Pressure *P/MPa*	Composition liquid phase *x*	Composition vapor phase *y*
xAr+ (1-x)Xe						
[HEA1960]	10	SLE	82.3 – 83.8		0.7 – 1.0	

Table A.36: Literature data for the system neon-argon.

Reference	Number of data points total	Kind of data	Temperature T/K	Pressure P/MPa	Composition liquid phase x	Composition vapor phase y
xNe+ (1-x)Ar						
[SKR1964]	5	VLE	90.5	0.6 – 2.6	0.004 – 0.02	0.72 – 0.92
[SKR1971]	67	VLE	90.6 – 120.1	2.9 – 19.6	0.03 – 0.31	0.54 – 0.94
[STR1965c]	58	VLE	84.4 – 129.9	0.38 – 7.2	0.002 – 0.09	0.17 – 0.97
[STR1967b]	5 41	CP VLE	95.8 – 129.9 95.8 – 129.9	15.5 – 62.1 7.5 – 62.1	0.39 – 0.59 0.09 – 0.57	 0.46 – 0.92
[STR1971a]	50 6	VLE SLE	87.3 – 93.9 95.8 – 123.8	6.4 – 101.7 120.9 – 393	0.054 – 0.57 0.52 – 0.6	0.65 – 0.96
[TRA1974]	66	VLE	92.8 – 137.8	0.18 – 101.3	0.0 – 1.0	0.0 – 0.94

Table A.37: Literature data for the system helium-argon.

Reference	Number of data points total	Kind of data	Temperature T/K	Pressure P/MPa	Composition liquid phase x	Composition vapor phase y
xHe+ (1-x)Ar						
[KAT1973]	26	VLE	92.0 – 108.2	2.0 – 12.1		0.87 – 0.98
[MUL1965]	21 43 6	SVE VLE SVLE	68.0 – 80.0 86.0 – 108.0 84.4 – 86.3	2.0 – 12.2 2.0 – 12.2 3.0 – 12.2	0.0 – 0.02	0.98 – 1.0 0.85 – 0.99

Table A.37 (continued)

Reference	Number of data points total	Kind of data	Temperature T/K	Pressure P/MPa	Composition liquid phase x	Composition vapor phase y
[SIN1966]	29	VLE	93.2 – 148.2	1.7 – 13.8	0.002 – 0.14	
[SKR1964]	5	VLE	90.5	0.6 – 2.6	0.0 – 0.002	0.74 – 0.94
[SKR1971]	60	VLE	90.7 – 115.1	2.94 – 21.6	0.003 – 0.06	0.47 – 0.98
[STR1969]	4	LLE	147.3	58.4 – 68.9	0.43 – 0.44	0.54 – 0.63
	58	VLE	91.4 – 147.7	1.4 – 68.9	0.001 – 0.41	0.26 – 0.99
	4	CP	147.1 – 150.0	6.9 – 44.2	0.05 – 0.46	
[STR1971b]	196	VLE	98.0 – 159.9	9.6 – 413.7	0.02 – 0.6	0.28 – 0.98
[STR1972a]	66	LLE	150.0 – 199.0	352 – 1040	0.27 – 0.65	0.77 – 0.95
	9	SVLE	150.0 – 199.0	470 – 1050	0.44 – 0.73	0.05 – 0.14
	7	CP	170.0 – 199.0	400 – 980	0.28 – 0.32	

Table A.38: Literature data for the system argon-carbon dioxide

Reference	Number of data points total	Kind of data	Temperature T/K	Pressure P/MPa	Composition liquid phase x	Composition vapor phase y
xAr+ (1-x)CO_2						
[COQ2008]	62	VLE	233.3 – 299.2	1.5 – 14.0	0.006 – 0.41	0.01 – 0.75
[KAM1968]	19	VLE	233.2 – 273.2	2.6 – 13.2	0.03 – 0.35	0.15 – 0.75
[PRE1971]	2	SLE	109 – 115.9		~1	
[SAR1971]	12	VLE	288.2	5.7 – 9.8	0.06 – 0.17	0.06 – 0.21

Table A.39: Literature data for the system hydrogen-argon.

Reference	Number of data points total	Kind of data	Temperature T/K	Pressure P/MPa	Composition liquid phase x	Composition vapor phase y
xH_2+ (1-x)Ar						
[CAL1979]	146	VLE	83.1 – 141.4	0.08 – 51.4	0.0 – 0.62	0.0 – 0.98
	10	CP	84.1 – 141.4	8.2 – 51.8	0.21 – 0.6	
[MUL1965]	18	SVE	68.0 – 79.0	2.03 – 11.2		0.97 – 1.0
	26	VLE	86.9 – 105.0	2.03 – 12.2	0.02 – 0.18	0.71 – 0.95
	6	SVLE	82.6 – 83.4	2.0 – 12.1		
[OST1977]	55	VLE	85.9 – 112.8	0.51 – 4.1	0.0 – 0.07	0.22 – 0.95
[VOL1960]	122	VLE	87.0 – 140.0	1.7 – 10.2	0.019 – 0.13	
[XIA1990]	14	VLE	100.0	0.64 – 4.6	0.004 – 0.06	0.47 – 0.87

Table A.40: Literature data for the system argon-methane

Reference	Number of data points total	Kind of data	Temperature T/K	Pressure P/MPa	Composition liquid phase x	Composition vapor phase y
xAr+ (1-x)CH_4						
[CAL1972]	10	VLE	115.8	0.14 – 0.95	0.0 – 1.0	0.0 – 1.0

Table A.40 (continued)

Reference	Number of data points total	Kind of data	Temperature T/K	Pressure P/MPa	Composition liquid phase x	Composition vapor phase y
[CHE1964]	17	VLE	91.6 – 124.0	0.016 – 0.38	0.01 – 0.38	0.06 – 0.84
[CHR1973]	34	VLE	150.7 – 178.0	1.2 – 5.1	0.02 – 0.94	0.05 – 0.95
[CHR1974]	5	VLE	123.4 – 164.0	1.0 – 3.5	0.038 – 0.69	0.1 – 0.87
[DUN1972]	74	VLE	105.0 – 126.0	0.18 – 1.67	0.15 – 1.0	0.47 – 0.91
[ELS1975]	6	VLE	115.2	0.19 – 0.9	0.05 – 0.96	
[FED1938]	12 12	SLE SLE	71.2 – 90.0 71.2– 84.1		0.0 – 0.6 0.7 – 1.0	0.0 – 0.6 0.7 – 1.0
[GRA1971]	68	VLE	115.2 – 137.1	0.2 – 1.8	0.04 – 0.95	0.17 – 0.99
[JIN1993]	12	VLE	122.9	0.34 – 1.34	0.07 – 0.95	0.33 – 0.98
[JON1963]	6	CP	151.0 – 190.3		0.0 – 1.0	
[KEH1983]	10	VLE	130.6	0.38 – 2.09	0.0 – 1.0	0.0 – 1.0
[KID1975b]	9	VLE	90.7	0.012 – 0.14	0.0 – 1.0	
[LIU1988]	12	VLE	122.9	0.34 – 1.34	0.07 – 0.95	0.33 – 0.98
[SHA1976]	31	VLE	112.6 – 133.0	0.2 – 2.23	0.03 – 0.96	0.14 – 0.99
[SPR1966]	11	VLE	90.7	0.012 – 0.14	0.0 – 1.0	0.0 – 1.0
[VAN1968]	40 40	SLE SVLE	70.1 – 90.6 71.2 – 90.6	 0.01 – 0.07	0.0 – 1.0	
[VEI1937]	22	SLE	68.0 – 90.6		0.0 – 1.0	

Table A.41: Literature data for the system argon-ethane

Reference	Number of data points total	Kind of data	Temperature T/K	Pressure P/MPa	Composition liquid phase x	Composition vapor phase y
xAr+ (1-x)C_2H_6						
[AZE1994]	12	VLE	90.7	0.03 – 0.14	0.062 – 1.0	~ 1.0
[ECK1965]	6	VLE	81.4 – 113.5	0.04 – 0.69	0.31 – 0.66	~ 1.0
[ELS1971]	38	VLE	115.5	0.17 – 0.92	0.07 – 0.98	
[LEW1975]	6	VLE	90.2	0.0 – 0.14	0.0 – 1.0	0.0 – 1.0

Table A.42: Literature data for the system argon-propylene.

Reference	Number of data points total	Kind of data	Temperature T/K	Pressure P/MPa	Composition liquid phase x	Composition vapor phase y
xAr+ (1-x)C_3H_6						
[BLA1963]	76	VLE	74.3 – 91.0	0.003 – 0.13	0.005 – 0.99	
[ORO1968]	65	VLE	100.0 – 150.0	0.14 – 4.7	0.03 – 1.0	

Table A.43: Literature data for the system krypton-xenon.

Reference	Number of data points total	Kind of data	Temperature T/K	Pressure P/MPa	Composition liquid phase x	Composition vapor phase y
xKr+ (1-x)Xe						
[BOR1982]	16	VLE	125.5 – 140.4	0.14 – 0.4	0.88 – 0.99	0.99 – 1.0
[CAL1971a]	13	VLE	161.4	0.08 – 1.1	0.0 – 1.0	0.0 – 1.0
[CAL1983]	139 8	VLE CP	165.6 – 268.7 209.5 – 289.7	0.11 – 6.6 5.5 – 6.7	0.0 – 1.0 0.0 – 1.0	0.0 – 1.0
[CHU1971]	6	VLE	161.4	0.08 – 1.1	0.0 – 1.0	
[MAS1974]	5	SLE	121.9 – 158.4		0.08 – 0.59	
[MAS1976]	32 5	VLE SVLE	150.0 – 170.0 121.9 – 158.4	0.1 – 1.1 0.1 – 0.2	0.04 – 0.67 0.41 – 0.92	0.41 – 0.96

Table A.44: Literature data for the system krypton-carbon dioxide.

Reference	Number of data points total	Kind of data	Temperature T/K	Pressure P/MPa	Composition liquid phase x	Composition vapor phase y
xKr + (1-x)CO_2						
[KUS1991]	94 12	VLE CP	301.1 – 304.1 301.5 – 304.1	7.37 – 7.53 7.40 – 7.53	0.0 – 0.03 0.0 – 0.03	

Table A.45: Literature data for the system methane-krypton.

Reference	Number of data points total	Kind of data	Temperature T/K	Pressure P/MPa	Composition liquid phase x	Composition vapor phase y
xCH_4 + (1-x)Kr						
[CAL1971b]	28	VLE	103.9 – 144.8	0.02 – 0.82	0.0 – 1.0	0.0 – 1.0
[CAL1981]	95 6	VLE CP	160.6 – 204.6 190.6 – 209.5	1.1 – 5.2 4.6 – 5.5	0.0 – 1.0 0.0 – 1.0	0.0 – 1.0
[FUK1967]	32	VLE	110.1 – 118.4	0.07 – 0.12	0.18 – 0.67	
[HOL1992]	36	VLE	125.2 – 188.8	0.17 – 4.1	0.14 – 0.78	0.17 – 0.83
[VEI1937]	11	SLE	90.6 – 116.0		0.0 – 1.0	
[VON1936]	14	SLE	90.5 – 116.0		0.0 – 1.0	

Table A.46: Literature data for the system krypton-ethane.

Reference	Number of data points total	Kind of data	Temperature T/K	Pressure P/MPa	Composition liquid phase x	Composition vapor phase y
xKr + (1-x)C_2H_6						
[CAL1987]	226 8	VLE CP	150.3 – 295.6 209.4 – 305.3	0.01 – 6.61 4.9 – 6.9	0.0 – 1.0 0.0 – 1.0	0.0 – 1.0
[GOM1991]	10	VLE	115.8	0.0 – 0.07	0.0 – 1.0	0.0 – 1.0
[HOL1992]	29	VLE	179.3 – 279.0	0.2 – 4.9	0.046 – 0.92	0.12 – 0.99

Table A.47: Literature data for the system krypton-ethylene.

Reference	Number of data points total	Kind of data	Temperature T/K	Pressure P/MPa	Composition liquid phase x	Composition vapor phase y
xKr + (1-x)C_2H_4						
[CAL1978]	9	VLE	115.8	0.0 – 0.07	0.0 – 1.0	0.0 – 1.0

Table A.48: Literature data for the system krypton-propylene.

Reference	Number of data points total	Kind of data	Temperature T/K	Pressure P/MPa	Composition liquid phase x	Composition vapor phase y
xKr + (1-x)C_3H_6						
[ORO1968]	78	VLE	130.0 – 200.0	0.1 – 2.9	0.06 – 0.96	

Table A.49: Literature data for the system xenon-neon.

Reference	Number of data points total	Kind of data	Temperature T/K	Pressure P/MPa	Composition liquid phase x	Composition vapor phase y
xXe + (1-x)Ne						
[BER1985a]	88 6	LLE CP	246.9 – 411.4 280.3 – 414.7	160 – 1880 300 – 1880	0.14 – 0.53 0.26 – 0.36	
[BER1985b]	7	SLE	380.2 – 450.2	1300 – 2080	0.26 – 0.53	
[DEE1980a]	171 13	VLE CP	162.7 – 279.1 263.8 – 289.7	0.09 - 152 5.84 - 152	0.39 – 1 0.35 – 1	0.015 – 1
[DEE1980b]	87	VLE	262.7 – 283.4	15.2 – 121.6	0.39 – 0.84	0.26 – 0.76

Table A.50: Literature data for the system xenon-carbon dioxide.

Reference	Number of data points total	Kind of data	Temperature T/K	Pressure P/MPa	Composition liquid phase x	Composition vapor phase y
xKr + (1-x)C_3H_6						
[MAR1999]	10	CP	301.7 – 304.1	7.29 – 7.39	0 – 0.042	

Table A.51: Literature data for the system xenon-nitrous oxide.

Reference	Number of data points total	Kind of data	Temperature T/K	Pressure P/MPa	Composition liquid phase x	Composition vapor phase y
xXe + (1-x)N_2O						
[FON1995]	8	VLE	182.3	0.09 – 0.25	0.0 – 1.0	0.0 – 1.0
[MAC1980]	10	VLE	182.3	0.09 – 0.25	0.0 – 1.0	0.0 – 1.0

Table A.52: Literature data for the system methane-xenon.

Reference	Number of data points total	Kind of data	Temperature T/K	Pressure P/MPa	Composition liquid phase x	Composition vapor phase y
xCH_4 + (1-x)Xe						
[DIA2004]	64 6	VLE CP	189.8 – 273.2 208.3 – 273.2	0.35 – 6.5 5.7 – 6.8	0.0 – 1.0 0.21 – 0.85	0.0 – 1.0

Table A.53: Literature data for the system xenon-ethane.

Reference	Number of data points total	Kind of data	Temperature T/K	Pressure P/MPa	Composition liquid phase x	Composition vapor phase y
$xXe + (1-x)C_2H_6$						
[DUA2000]	19	VLE	273.1 – 302.9	2.4 – 5.5	0.0 – 1.0	0.0 – 1.0
[NUN1985]	161 6	VLE CP	210.0 – 304.4 290.3 – 304.4	0.33 – 5.8 5.0 – 5.83	0.0 – 1.0 0.12 – 0.98	0.0 – 1.0

Table A.54: Literature data for the system ethylene-xenon.

Reference	Number of data points total	Kind of data	Temperature T/K	Pressure P/MPa	Composition liquid phase x	Composition vapor phase y
xC_2H_4 + (1-x)Xe						
[CAL1977]	9	VLE	161.4	0.06 – 0.08	0.0 – 1.0	0.0 – 1.0
[NUN1986]	166 11	VLE CP	203.0 – 287.2 282.1 – 289.7	0.5 – 5.7 5.1 – 5.84	0.0 – 1.0 0.04 – 1.0	0.0 – 1.0

Table A.55: Literature data for the system xenon-propane.

Reference	Number of data points total	Kind of data	Temperature T/K	Pressure P/MPa	Composition liquid phase x	Composition vapor phase y
$xXe+ (1-x)C_3H_8$						
[FIL2000]	28	VLE	161.4 – 195.49	0.001 – 0.44	0.0 – 1.0	

Table A.56: Literature data for the system xenon-propylene.

Reference	Number of data points total	Kind of data	Temperature T/K	Pressure P/MPa	Composition liquid phase x	Composition vapor phase y
$xXe+ (1-x)C_3H_6$						
[BLA1967]	51	VLE	156.0 – 185.7	0.006 – 0.12	0.054 – 0.92	

Table A.57: Literature data for the system helium-neon.

Reference	Number of data points total	Kind of data	Temperature T/K	Pressure P/MPa	Composition liquid phase x	Composition vapor phase y
xHe + (1-x)Ne						
[HEC1967]	76	VLE	27.0 – 41.9	0.28 – 20.3	0.009 – 0.36	0.08 – 0.93
[IOM1977]	90	SVE	13.0 – 21.0	0.2 – 12.2		0.96 – 1.0
[KNO1967]	22	VLE	24.7 – 27.0	0.61 – 5.2	0.002 – 0.03	0.97 – 0.998

Table A.58: Literature data for the system hydrogen-neon.

Reference	Number of data points total	Kind of data	Temperature *T/K*	Pressure *P/MPa*	Composition liquid phase *x*	Composition vapor phase *y*
$xH_2 + (1-x)Ne$						
[HEC1966]	90 2	VLE VLLE	26.0 – 42.5 26.0 – 28.0	0.07 – 2.5 0.4 – 0.58	0.0 – 1.0	0.0 – 1.0 0.72 – 0.8
[STR1965d]	113	VLE	24.6 – 33.7	0.04 – 1.4	0.0 – 1.0	0.0 – 1.0

Table A.59: Literature data for the system helium-hydrogen.

Reference	Number of data points total	Kind of data	Temperature T/K	Pressure P/MPa	Composition liquid phase x	Composition vapor phase y
$xHe + (1-x)H_2$						
[HIZ1972]	45	VLE	20.0 – 28.0	0.09 – 2.1	0.0 – 0.057	0.0 – 0.9
[HIZ1981]	45	VLE	20.0 – 28.0	0.09 – 2.1	0.0 – 0.057	0.0 – 0.9
[PAS1981]	137	VLE	14.7 – 30.0	0.01 – 15.4	0.0 – 0.33	0.0 – 0.98
[SMI1952]	106	VLE	17.4 – 21.8	0.19 – 5.9	0.002 – 0.03	0.61 – 0.96
[SNE1968]	76	VLE	15.5 – 29.8	1.97 – 10.3	0.01 – 0.36	0.31 – 0.96
[SON1964]	45	VLE	20.4 – 34.5	0.24 – 3.45	0.002 – 0.18	0.06 – 0.89
[STR1964]	92	VLE	15.5 – 32.5	0.24 – 3.45	0.003 – 0.21	0.03 – 0.97
[STR1973]	104	VLE	26.0 – 100.0	0.59 – 917.0	0.006 – 0.5	0.26 – 0.98
[YAM1992]	13	VLE	17.9 – 19.1	0.07 – 0.16	0.0 – 0.002	0.28 – 0.56

Table A.60: Literature data for the system nitrogen-argon-oxygen.

Reference	Number of data points total	Kind of data	Temperature T/K	Pressure P/MPa	Composition liquid phase		Composition vapor phase	
					x1	x2	y1	y_2
$x_1N_2 + x_2Ar + (1 - x_1 - x_2)O_2$								
[BLA1977]	20	VLE	60.4 – 132.3	0.007 – 3.7	0.78	0.01		
[FAS1957b]	28	VLE	81.2 – 88.3	0.12	0.13 0.68	0.1 0.67	0.32 0.88	0.05 0.54
[FUN1982]	60	VLE	90.0 – 90.2	0.1	0.00 0.01	0.0 0.03	0.0 0.01	0.0 0.04
[JAC1990]	28	VLE	119.5 – 132.6	2.1 – 3.79	0.78	0.01		
	1	CP	132.56	3.79				
[KUE1917]								
[MIC1954]								
[NAR1969]	116	VLE	81.5 – 120.0	0.14 – 2.25	0.04 0.86	0.04 0.78	0.08 0.94	0.02 0.7
[WEI1948]	41	VLE	80.5 – 91.8	0.13	0.01 0.89	0.0 0.93	0.03 0.96	0.0 0.9
[TOR1940]	3	VLE		0.15	0.05 0.08	0.24 0.67	0.09 0.38	0.31 0.45

2.1 Bibliography

[AKE1957] Akers W.W., Eubancks. L. S., *Adv. Cryog. Eng., vol.2, pp.275-293, 1957*.

[ALS1983] Al-Sahhaf, T.A.; Kidnay, A.J.; Sloan, E.D., Liquid + vapor equilibria in the N_2 + CO_2 + CH_4 system. *Ind. Eng. Chem. Fundam., vol.22, pp.372–380, 1983*.

[ALS1990] Al-Sahhaf, T.A., Vapor-liquid equilibria for the ternary system nitrogen + carbon dioxide + methane at 230 and 250 K, *Fluid Phase Equilib., vol.55, pp.159-72, 1990.*

[ALW1976] Al-Wakeel I.M., *Thesis, 1976*.

[ARA1971] Arai Y., Kaminishi G.-I., Saito S., *J. Chem. Eng. Jpn., vol.4(2), p.113, 1971.*

[ARM1955] Armstrong, G.T.; Goldstein, J.M.; Roberts, D.E., Liquid-vapor phase equilibrium in solutions of oxygen and nitrogen at pressures below one atmosphere. *J. Res. Natl. Bur. Stand., vol.55(5), pp.265–277, 1955.*

[AUG1957] Augood D.R., *Trans. Inst. Chem. Engr., vol.35, p.394, 1957.*

[AZE1994] Gomes De Azevedo E.J.S.; Calado J.C.G.; Zollwek J.A., *J. Chem. Thermodyn., vol.26(8), p.847, 1994*.

[BAB1999] Baba-Ahmed, A.; Guibot, P.; Richon, D., New equipment using a static analytic method for the study of vapour-liquid equilibria at temperatures down to 77K, *Fluid Phase Equilibria, vol.166, pp.225-236, 1999.*

[BAR1973] Barsuk S.D., Nenyaminovich O.A., *Gaz. Prom., vol.12, p.38, 1973*.

[BAL1900] Baly E.C.C., *Philos. Mag., vol.49 pp.517-529, 1900.*

[BAL1989] Balley, D.M.; Esper, G.J.; Holste, J.C.; Hall, K.R.; Eubank, P.T.; Marsh, K.M.; Rogers, W.J., Properties of CO_2 mixtures with N_2 and with CH_4, *GPA RR-122, 1989.*

[BER1985a] van den Bergh, L. C.; Schouten, J.A.; Trappeniers, N. J., Phase equilibria in the system Ne-Xe at high pressures: I. Gas-gas equilibrium and the critical line up to 20 kbar, *Physica A*, *132, 537-548, 1985.*

[BER1985b] van den Bergh, L. C.; Schouten, J.A.; Trappeniers, N. J., Phase equilibria in the system Ne-Xe at high pressures: II. Three-phase line, solid-fluid equilibrium and metastable states, *Physica A, 132, 549-556, 1985.*

[BIA1992] Bian B., *Thesis, 1992.*

[BIA1993] Bian, B.; Wang, Y.; Shi, J.; Zhao, E.; Lu, B.C.-Y., Simultaneous determination of vapor-liquid equilibrium and molar volumes for coexisting phases up to the critical temperature with a static method, *Fluid Phase Equilibria, vol.90, pp.177–187, 1993.*

[BLA1963] Blagoi Y.P.; Orobinskii N.P., *Ukr. Fiz. Zh. (Russ. Ed.), vol.8, p.1378, 1963.*

[BLA1965] Blagoi, Y.P.; Orobinskii, N.P., Liquid-vapour phase equilibrium in the propene–nitrogen system, *Zh. Fiz. Khim., vol.39, pp. 2022–2024, (Russ. J. Phys. Chem., Engl. Transl., vol.39, pp.1073–1074), 1965.*

[BLA1967] Blagoi, Y.P.; Orobinskii, N.P., Liquid-vapour phase equilibrium of the propylene - krypton, propylene - xenon systems, *Ukr. Fiz. Zh. Russ. Ed., vol.12, pp. 837–844, 1967.*

[BLA1977] Blanke, W., Proceedings 7th symposium thermophysics properties, *edited by A. Cezairlizau, The American Society of Mechanical Engineers, New York, p. 461, 1977*.

[BLO1953] Bloomer, O.T.; Parent, J.D., Liquid-vapor phase behavior of the methane–nitrogen system. *Chem. Eng. Prog., Symp. Ser., vol.49(6), pp.11–24, 1953.*

[BLO1955] Bloomer, O.T.; Eakin, B.E.; Ellington, R.T.; Gami, D.C., *Inst. Gas Technol. Chicago Res. Bull. 21 , 1955.*

[BOL1954] Bolshakov, P.E.; Linshits, L.R., Phase equilibria in systems liquid - gas at high pressures, *Tr. GIAP, n°3, pp.18-27, 1954.*

[BOO1930] Booth, H.S.; Carter, J.M., The critical constants of carbon dioxide + oxygen mixtures, *J. Phys. Chem., vol.34, p.2801, 1930.*

[BOR1982] Boranbaev N.; Glukhov S.D.; Shevtsvov A.V., *Viniti, CODE 3021-82, 1982.*

[BOU1936] Bourbo, P.; Ischkin, I., Untersuchungen über das Gleichgewicht von Flüssigkeit und Dampf des Systems Argon–Sauerstoff (Research on the equilibrium of liquid and vapor for the system argon–oxygen). *Physica, vol.3, pp.1067–1081, 1936.*

[BRA1958] Brandt, L.W.; Stroud, L., Phase equilibria in natural gas systems. Apparatus with windowed cell for 800 P.S.I.G. and temperatures to -320 °F, *Ind. Eng. Chem., vol. 50, pp.849–85, 1958.*

[BRO1989a] Brown, T.S.; Niesen, V.G.; Sloan, E.D.; Kidnay, A.J., Vapor-liquid equilibria for the binary systems of nitrogen, carbon dioxide, and n-butane at temperatures from 220 to 344 K, *Fluid Phase Equilibria, vol.53, pp.7–14, 1989.*

[BRO1989b] Brown, T.S.; Sloan, E.D.; Kidnay, A.J., Vapor-liquid equilibria in the nitrogen + carbon dioxide + ethane system, *Fluid Phase Equilibria, vol.51, pp.299–313, 1989.*

[BUR1962] Burn, I.; Din, F., Liquid-vapour equilibrium of the system argon + oxygen at pressures up to 10 atmospheres, *Trans. Faraday Soc., vol.58, pp.1341–1356, 1962.*

[BUR1964] Burch, R. J., Low temperature phase equilibria of the gas-liquid system helium + neon + nitrogen, *J. Chem. Eng. Data, vol.9, pp.19-24, 1964.*

[BUR1966] Burch R. J., *Cryogenics, vol.6, pp.77, 1966.*

[BUZ1963] Buzyna, G.; Macriss, R.A.; Ellington, R.T., Vapor-liquid equilibrium in the helium–nitrogen system. *Chem. Eng. Progr. Symp. Ser., vol.59(44), pp.101–111, 1963.*

[CAL1971a] Calado, J.C.G.; Staveley, L.A.K., Thermodynamics of liquid mixtures of krypton and xenon, *Trans. Faraday Soc., vol.67, p.289, 1971.*

[CAL1971b] Calado, J.C.G.; Staveley, L.A.K., *Trans. Faraday Soc., vol.67, p.1261, 1971.*

[CAL1972] Calado, J.C.G.; Staveley, L.A.K., Excess gibbs energy of argon–methane liquid mixtures at 115.77°K, *J. Chem. Phys., vol.56, pp.4718–4719, 1972.*

[CAL1977] Calado, J.C.G.; Soares, V.A.M., Thermodynamics of liquid ethylene + xenon at 161.38 K, *J. Chem. Thermodyn., vol. 9, pp.911-13, 1977*

[CAL1978] Calado, J.C.G.; Nunes da Ponte, M.; Soares, V.A.M.; Staveley, L.A.K., The thermodynamic excess functions of krypton + ethene liquid mixtures, *J. Chem. Thermodyn., vol.10, p.35, 1978.*

[CAL1979] Calado, J.C.G.; Streett, W.B., Liquid-vapor equilibrium in the system H_2 + Ar at temperatures from 83 to 141 k and pressures to 52 MPa, *Fluid Phase Equilib., vol.2, p.275, 1979.*

[CAL1981] Calado, J.C.G.; Streett, W.B.; Dieters U., J., *Chem. Soc., Faraday Trans., vol.77, pp.2503-2513, 1981.*

[CAL1983] Calado, J.C.G.; Chang, E.; Streett, W. B., *Physica A, vol.117, p.127, 1983.*

[CAL1987] Calado, J.C.G.; Chang, E.; Clancy, P.; Streett, W.B., Vapor-liquid equilibrium in the krypton + ethane system, *J. Phys. Chem, vol.91, p.3914., 1987.*

[CHA1966] Chang S.-D., Vapour-liquid equilibria, System nitrogen-methane-ethane. *Master of Science Degree, Department of chemical engineering, University of Ottawa, Canada, May 1966.*

[CHA1967] Chang, S.-D.; Lu, B.C.-Y., Vapor-liquid equilibria in the nitrogen–methane–ethane system. *Chem. Eng. Prog., Symp. Ser. 63, vol.81, pp.18–27, 1967.*

[CHE1964] Cheung, H.; Wang, D.I.-J., Solubility of volatile gases in hydrocarbon soVLEnts at cryogenic temperatures. *Ind. Eng. Chem. Fundam., vol.3, pp.355–361, 1964.*

[CHR1973] Christiansen, L.J.; Fredenslund, A.; Mollerup, J., Vapour-liquid equilibrium of the CH_4–Ar, CH_4–CO, and Ar–CO systems at elevated pressures. *Cryogenics, vol.13, pp.405–413, 1973.*

[CHR1974] Christiansen, L.J.; Fredenslund, A., Cryogenics, *vol.14, p.10, 1974.*

[CHU1971] Chui, C.-H.; Canfield, F.B., Liquid Density and Excess Properties of Argon + Krypton and Krypton + Xenon Binary Liquid Mixtures and Liquid Density of Ethane, *Trans. Faraday Soc., vol.67, p.2933, 1971.*

[CLA1954] Clark, A.M.; Din, F.; Robb, J., The liquid-vapour equilibrium of the binary system argon/oxygen. *Proc. R. Soc. London, Ser. A, vol.221, pp.517–534, 1954.*

[CIN1953] Cines, M.R.; Roach, J.T.; Hogan, R.J.; Roland, C.H., Nitrogen–methane vapor-liquid equilibria. *Chem. Eng. Prog., Symp. Ser., 49, vol.6, p.1–10, 1953.*

[COC1957] Cockett, A.H., The binary system nitrogen–oxygen at 1.3158 atm, *Proc. R. Soc. London, Ser. A, vol.239, pp.76–92, 1957.*

[COQ2008] Coquelet, C.; Valtz, A.; Dieua, F.; Richon, D.; Arpentinier, P.; Lockwood, F., Isothermal P, x, y data for the argon + carbon dioxide system at six temperatures from 233.32 to 299.21K and pressures up to 14MPa, *Fluid Phase Equilibr*., *vol. 273, 38-43, 2008.*

[COS1959] Cosway H.F., Katz D.L., Low temperature vapor-solid equilibria in ternary and quaternary systems containing hydrogen, nitrogen, methane, and ethane, *AIChE J., vol.5, pp.46-50, 1959.*

[COX1950] Cox A.L.; De Vries T., *J. Phys. Colloid. Chem., vol.54, pp.665-670, 1950.*

[DAV1963] Davis, J.A.; Rodewald, N.; Kurata, F., An apparatus for phase studies between 20K. and 300K, *Ind. Eng. Chem., vol.55(11), pp.36–42, 1963.*

[DAV1967] Davies, R.H.; Duncan, A.G.; Saville, G.; Staveley, L.A.K., Thermodynamics of liquid mixtures of argon and krypton, *Trans. Faraday Soc., vol.63, p.855, 1967.*

[DAV1971] Davydov I.A., Budnevich S.S., *Inzh. Fiz. Zh., vol.20, p.1082, 1971.*

[DEE1980a] Deerenberg, A.; Schouten, J. A.; Trappeniers, N.J., Vapour-liquid and gas-gas equilibria in simple systems: V. The system neon-xenon", *Physica A, 101, 459-476, 1980.*

[DEE1980b] Deerenberg, A.; Schouten, J. A.; Trappeniers, N.J., Vapour-liquid and gas-gas equilibria in simple systems: VI. The critical exponents βP and βT of the system neon-xenon, *Physica A, 103, 183-204, 1980.*

[DES2002] De Stefani, V.; Baba-Ahmed, A.; Valtz, A.; Meneses, D.; Richon, D., Solubility measurements for carbon dioxide and nitrous oxide in liquid oxygen at temperatures down to 90K, *Fluid Phase Equilibria, vol.200, pp.19-30, 2002.*

[DEV1963] DeVaney, W.E.; Dalton, B.J.; Meeks, J.C.(Jr.), Vapor-liquid equilibria of the helium– nitrogen system, *J. Chem. Eng. Data, vol.8, pp.473–478, 1963.*

[DIA2004] Dias L.M.B.; Filipe E.J.M.; McCabe, C.; Calado J.C.G.,Thermodynamics of liquid (xenon + methane) mixtures, *J. Phys. Chem., vol.108, pp.7377-7381, 2004.*

[DIN1955] Din F.; Goldmann K.; Monroe A.G., *Proc. 9 Int. Congr. Refr., pp.1003-1010, 1955.*

[DIN1960] Din, F., The liquid-vapour equilibrium of the system nitrogen + oxygen at pressures up to 10 atm. *Trans. Faraday Soc., vol.56, pp.668–681, 1960.*

[DOD1927a] Dodge, B.F.; Dunbar, A.K., An investigation of the coexisting liquid and vapor phases of solutions of oxygen and nitrogen, *J. Am. Chem. Soc., vol.49, pp.591–610, 1927.*

[DOD1927b] Dodge B.F., *Chem. Metall. Eng., vol.10, p.622, 1927.*

[DOK1955] Dokoupil, Z.; van Soest, G.; Swenker, D. P. M., On the equilibrium between the solid phase and the gas phase of the systems H2-N2, H2-CO, and H2-N2-CO, *Appl. Sci. Res*., *5, 182-240,1955.*

[DOL1919] Dolezalek F., *Z. Phys. Chem., vol.93, pp.585–595, 1919.*

[DOM1981] Domashenko A.M., Blinova I.D., *Sb. Teplofiz. Issled. Peregr. Zhidk. (Sverplovsk), 97, 1981.*

[DUA1995a] Duarte-Garza, H.A.; Holste, J.C.; Hall, K.R.; Marsh, K.N.; Gammon, B.E., Isochoric pVT and phase equilibrium measurements for carbon dioxide + nitrogen, *J. Chem. Eng. Data, vol.40, pp.704–711, 1995.*

[DUA1995b] Duarte-Garza, H.; Brugge, H.B.; Hwang, C.-A.; Eubank, P.T.; Holste, J.C.; Hall, K.R., Thermodynamic properties of CO_2+N_2 mixtures, *GPA RR-140, 1995.*

[DUA2000] Duarte, C.M.M.; Guedes, H.J.R.; Nunes Da Ponte, M.,J., *Chem. Thermodyn., vol.32, p.877, 2000.*

[DUN1966] Duncan, A.G.; Staveley, L.A.K., Thermodynamic functions for the liquid systems argon + carbon monoxide, oxygen + nitrogen, and carbon monoxide + nitrogen, *Trans. Faraday Soc., vol.62, pp.548–552, 1966.*

[DUN1972] Duncan, A.G.; Hiza, M.J., Heat of mixing derived from liquid-vapor equilibrium data: a study of the argon–methane, normal hydrogen–neon, and normal deuterium–neon systems, *Ind. Eng. Chem. Fundam., vol.11, pp.38–45, 1972.*

[EAK1955] Eakin, B.E.; Ellington, R.T.; Gami, D.C., Physical-chemical Properties of ethane–nitrogen mixtures, *Institute of Gas Technology, Research Bulletin n°26, pp.1-40, 1955.*

[ECK1965] Eckert, C.A.; Prausnitz, J.M., Phase equilibria for strongly nonideal liquid mixtures at low temperatures, *AIChE J., vol.11, p.886, 1965.*

[ELL1959] Ellington, R.T.; Eakin, B.E.; Parent, J.D.; Gami, D.C.; Bloomer, O.T., Vapor-liquid phase equilibria in the binary systems of methane, ethane and nitrogen, *Thermodynamic and Transport Properties of Gases, Liquids and Solids, McGraw-Hill, New York, pp.180–194, 1959.*

[ELS1971] Elshayal I.M., Lu B.C.-Y., *Cryogenics, vol.11, p.285, 1971.*

[ELS1975] Elshayal, I.M.; Lu, B.C.-Y., Measurement of total pressures for ethylene–propane mixtures, *Can. J. Chem. Eng., vol.53, pp.83–87, 1957.*

[ESP1989] Esper, G.J.; Bailey, D.M.; Holste, J.C.; Hall, K.R., Volumetric behavior of near-equimolar mixtures for carbon dioxide + methane and carbon dioxide + nitrogen, *Fluid Phase Equilib., vol. 49, pp.35-47, 1989.*

[EUB1957] Eubanks L.S., *Thesis, 1957.*

[FAS1939] Fastovsky V.G., Gurvich J.G., *Acta Physicochim. URSS, vol.11, pp.883-898, 1939.*

[FAS1941] Fastovskij, V.G. and Krestinskij, Y.A., *J. Phys. Chem. (Russian), vol.15, pp.525-531, 1941.*

[FAS1955] Fastovskii, V.G.; Petrovskii, Yu.V., Investigation of equilibrium liquid and vapor in systems of argon–oxygen, *Russ. J. Phys. Chem., vol.29, pp.1311–1317, 1955.*

[FAS1956a] Fastovskii, VG.; Petrovskii, Yu.V., Investigation of the equilibrium liquid and vapor in the system argon–nitrogen, *Russ. J. Phys. Chem., vol.30, pp.76–78, 1956.*

[FAS1956b] Fastovskii, V.G.; Petrovskii, Yu.V., Investigation of the liquid-vapor equilibrium in the oxygen - krypton system, *Zh. Fiz. Khim., vol.30, p.589, 1956.*

[FAS1957a] Fastovskii, V.G.; Petrovskii, Yu.V., An investigation of the liquid/vapour equilibrium in the nitrogen–methane system, *Zh. Fiz. Khim., vol. 31, pp.2317–2321, 1957.*

[FAS1957b] Fastovskii, V.G.; Petrovskii, Yu.V., A study of the vapor-liquid equilibrium in the system oxygen–argon–nitrogen (in Russian). Zh. Fiz. Khim., 31 (1957), 836–841.

[FED1938] Fedorova M.F., *Zh. Eksp. Teor. Fiz, vol.8, pp.425-435, 1938.*

[FED1939] Fedorova, M.F., *Acta Physicochimica U.R.S.S. vol.10, p.539, 1939.*

[FED1940] Fedorova, M.F., *Zh. Fiz. Khim, vol.14, pp.422-426, 1940.*

[FER1980] Ferrell, J.K.; Rousseau, R.W.; Matange, J.N., Solubilities of acid gass and nitrogen in methanol, *Interagency Energy/Environment R&D Report, EPA-600/7-80-116, Environmental Protection Agency, May 1980.*

[FIL2000] Filipe, E. J. M.; Gomes de Azevedo, E. J. S.; Martins, L. F. G.; Soares, V. A. M.; Calado, J. C. G.; McCabe, C.; Jackson, G., Thermodynamics of Liquid Mixtures of Xenon with Alkanes: (Xenon + Ethane) and (Xenon + Propane)", *J. Phys. Chem. B., 104, 1315-1321, 2000.*

[FON1989] Fontaine, J.M., Das Phasengleichgewicht Helium–Methan und die Beschreibung mit einer neuen Gemischzustandsgleichung, *Dissertation, Fakultät für Maschinenbau und Elektrotechnik, Technische Universität Carolo-Wilhelmina zu Braunschweig, 1989.*

[FON1995] Fonseca I.M.A.; Lobo L.Q., *Fluid Phase Equilib., vol.113, pp.127-138, 1995.*

[FRE1970] Fredenslund, A.; Sather, G.A., Gas-liquid equilibrium of the oxygen–carbon dioxide system, *J. Chem. Eng. Data, vol.15, pp.17–22, 1970.*

[FRE1972] Fredenslund, A.; Mollerup, J.M.; Persson, O., Gas-liquid equilibrium of oxygen + carbon dioxide system, *J. Chem. Eng. Data, vol.17, p.440, 1972.*

[FUK1967] Fuks, S.; Bellemans, A., Excess free energies and volumes of two simple binary liquid mixtures: methane–krypton and nitrogen–methane, *Bull. Soc. Chim. Belg., vol.76, pp.290–299, 1967.*

[FUN1982] Funada, I.; Yoshimura, S.; Masuoka, H.; Yorizane, M.; Fu, C.-T.; Lu, B.C.-Y., Vapor-liquid equilibrium values for nitrogen–argon–oxygen at high oxygen concentrations, *Adv. Cryog. Eng., vol.27, pp.893–901, 1982.*

[GAS1981] Gasem, K.A.M.; Hiza, M.J.; Kidnay, A.J., Phase behavior in the nitrogen + ethylene system from 120 to 200K, *Fluid Phase Equilib., vol.6, p.181, 1981.*

[GOM1991] Gomes de Azevedo, E.J.S.; Calado, J.C.G., Thermodynamics of liquid mixtures of krypton + ethane, *Fluid Phase Equilib., vol.70, pp.215-25, 1991.*

[GRA1971] Gravelle, D.; Lu, B.C.-Y., Vapor-liquid equilibria in the argon + methane system, *Can. J. Chem. Eng., vol.49, p.144, 1971.*

[GRA1977a] Grauso, L.; Fredenslund, A.; Mollerup, J., Vapor-liquid equilibrium for the systems $C_2H_6 + N_2$, $C_2H_4 + N_2$, $C_3H_8 + N_2$, and $C_3H_6 + N_2$, *Fluid Phase Equilibria, vol.1, p.13–26, 1977.*

[GRA1977b] Grauso, L.; Fredenslund, A., Measurement and correlation of high-pressure vapor-liquid equilibrium data, *Ber. Bunsen-Ges. Phys. Chem., vol.81, p.1088, 1977.*

[GON1939a] Gonikberg, M.G.; Fastovskii, V.G.; Gurvich, I.G., Solubility of gases in liquids at low temperatures and high pressures: I solubility of hydrogen in liquid nitrogen at 79-109 k and at pressures up to 190 atm, *Acta Physicochim. URSS, vol.11, p.865, 1939.*

[GON1939b] Gonikberg G., *Zh. Fiz. Khim., vol.13, pp.1669-1679, 1939.*

[GON1940a] Gonikberg, M.G.; Fastovskii, V.G., Solubility of gases in liquids at low temperatures and high pressures. II. Solubility of helium in liquid nitrogen at temperatures from 78.0 to 109.0K and at pressures up to 295 atmospheres, *Acta Physicochim. URSS, vol.12, pp.67–72, 1940.*

[GON1940b] Gonikberg M.G., Fastovskii V.G., *Zh. Fiz. Khim., vol.14, p.1128, 1940.*

[GON1940c] Gonikberg M.G., Fastovskii V.G., Zh. Fiz. Khim., *vol.14, pp.257–260, 1940.*

[GON1940d] Gonikberg M.G., Fastovskii V.G., *Zh. Fiz. Khim., Acta Physicochim. URSS, vol.13, p.399, 1940.*

[GUP1980] Gupta, M.K.; Gardner, G.C.; Hegarty, M.J.; Kidnay, A.J., Liquid-vapor equilibriums for the $N_2 + CH_4 + C_2H_6$ system from 260 to 280 K, J. *Chem. Eng. Data, vol.25, pp.313-8, 1980.*

[HAM1915] Hamburger, L.; Holst, G., Investigation of the equilibrium liquid-vapour of the system argon-nitrogen, *Koninklijke Nederlandsche Akademie van Wetenschappen Proceedings, vol.18(1), pp.872-894, 1915.*

[HAN2012] Han, X. H; Zhang, Y. J.; Gao, Z. J.; Xu, Y. J.; Wang, Q.; Chen, G. M., Vapor-liquid equilibrium for the mixture nitrogen + methane in the temperature range of 110 to 125K, *J. Chem. Eng. Data*, *57*(*5), 1621-1626, 2012.*

[HEA1955] Heastie, R., *The solid-liquid equilibrium diagram of argon and krypton, Nature, 175(4485), 747-748, 1955.*

[HEA1955] Heastie R., Lefebvre C., Phase equilibria in condensed mixtures of argon and xenon, *Proc. Phys. Soc., 76(2), 180-184, 1960.*

[HEC1966] Heck C.K.; Barrick P.L., *Adv. Cryog. Eng., vol.11, p.714, 1966.*

[HEC1967] Heck C.K.; Barrick P.L., Liquid-vapor equilibria of the neon-helium system, *Adv. Cryog. Eng., vol.12, p.714, 1967.*

[HER1965] Herring R.N., Barrick P.L., *Adv. Cryog. Eng., vol.10, pp.151-159, 1965.*

[HIM1959] Himmelberger, F., *Chem. Eng. Progr., 55 (6), 54-64, 1959.*

[HIZ1972] Hiza M.J., Liquid-vapor equilibrium in the binary systems of He4 and He3 with nD2 and nH2, *Cryogenics Division*, *National Bureau of Standards*, *Boulder, Colorado, 1972*.

[HIZ1981] Hiza M.J., *Fluid Phase Equilib., vol.6, p.203, 1981.*

[HIZ1990] Hiza, M.J.; Kidnay, A.J.; Haynes, W.M., Liquid-vapor equilibria in binary systems containing nitrogen, oxygen, and argon between 63 and 100K, *Preliminary unpublished results, National Institute of Standards and Technology, Boulder, CO, 1990.*

[HIZ1999] Hiza, M.J., Kidnay, A.J.; Haynes, W.M., *Int. J. Thermophys. (unpublished results 1999).*

[HOD1967] Hodges, R.J.; Burch, R.J., The equilibrium distribution of methane between the liquid and vapour phases of oxygen, *Cryogenics, vol.7, pp.112–113, 1967.*

[HOL1992] Holcomb C.D.; Zollweg J.A., *Fluid Phase Equilibria, vol.75, pp.213-224, 1992.*

[HOU2007] Houssin-Agbomson, D., Solubilité des hydrocarbures dans l'oxygène liquide, *MINES ParisTech, Thesis, 2007.*

[HOU2010a] Houssin-Agbomson, D.; Coquelet, C.; Richon., D.; Arpentinier, P., Equipment using a static-analytic method for solubility measurements in potentially hazardous binary mixtures under cryogenic temperatures, *Cryogenics, vol.50, pp.248-256, 2010.*

[HOU2010b] Houssin-Agbomson, D.; Coquelet, C.; Arpentinier, P; Delcorso, F.; Richon, D., Equilibrium data for the oxygen+propane binary system at temperatures of (110.22, 120.13, 130.58, and 139.95) K, *J. Chem. Eng. Data, vol.55, pp. 4412-4415, 2010.*

[HUD1984] Hudziak, J. A.; Kahvand, H.; Yassale, M.; Leipziger, S., Dew point measurements for nitrogen–propane and nitrogen–butane mixtures, *J. Chem. Eng. Data, vol.29, pp.296–301, 1984.*

[IOM1976] Iomtev, M. B.; Yakimenko, N.P.; Glukh, G.M.; Polishchukova, L.I., Solubility of solid nitrous oxide in nitrogen, *Russ. J. Phys. Chem., 50(3), 450-451., 1976.*

[IOM1977] Iomtev, M. B.; Doroshenko, A. I.; Kushner, L. S.; Sarov, K. M.; Kalinichenko, L. T., Solubility of solid neon in gaseous helium, *Zh. Fiz. Khim., 51(6), 1373-1376, 1977.*

[JAC1990] Jacobsen R.T.; Clarke W.P.; Beyerlein S.W.; Rosseau M.F.; van Poolen L.J.; Rainwater J.C., *Int. J. Thermophys., vol.11(1), p.179, 1990.*

[JAN2000] Janisch, J., Vapor-liquid phase equilibria including saturated densities for systems containing nitrogen, methane and ethane from 130 K to 270 K and pressure up to 10 MPa, *Final report to GERG WG 1.34, Institut für Thermodynamik, Technische Universität Braunschweig, 2000.*

[JAN2007] Janish J., Raabe G., Kohler J., Vapor-liquid equilibria and saturated liquid densities in binary mixtures of nitrogen, methane, and ethane and their correlation using the VTPR and PSRK GCEOS, *J. Chem. Eng. Data, vol.52, pp.1897-1903, 2007.*

[JIN1993] Jin, Z.-L.; Liu, K.-Y.; Sheng, W.-W., Vapor-liquid equilibrium in binary and ternary mixtures of nitrogen, argon, and methane, *J. Chem. Eng. Data, vol.38, pp.353–355, 1993.*

[JON1963] Jones, I.W.; Rowlinson, J.S., Gas-liquid critical temperatures of binary mixtures, *Trans. Faraday Soc., vol.59, p.1702, 1963.*

[KAM1966] Kaminishi, G.; Toriumi, T., Vapor-liquid phase equilibrium in the CO_2–H_2, CO_2–N_2 and CO_2–O_2 systems, *Kogyo Kagaku Zasshi, vol.69, pp.175–178, 1966.*

[KAM1968] Kaminishi G.; Arai, Y.; Saito S.; Maeda S., Vapor liquid equilibria for binary and ternary systems containing carbon dioxide, *J. Chem. Eng. Japan, vol.1, pp.109-116, 1968.*

[KAR1958] Karwat, E.; Klein, G., Hydrocarbon in Air Separating Plants, *Linde Ber. Tech. Wiss., 4, 3-10, 1958.*

[KAT1973] Kate Jr., F. H.; Robinson Jr., R.L., Vapor + solid equilibrium for helium + krypton, *J. Chem. Thermodyn., vol.5(2), pp.259-271, 1973.*

[KEE1903] Keesom, W.H., *Commun. Phys. Lab. Univ. Leiden, vol.1, p88, 1903.*

[KEH1983] Kehlen, V.H.; Schneider, F.U.; Haufe, S.; Barnitzke, W., Evaluation of vapor pressure measurements of binary systems in the medium pressure range., *Z. Phys. Chem. (Leipzig), vol.264, pp.801-6, 1983.*

[KHA1940] Kharakhorin F.F., *Zh. Tekh. Fiz., vol.10, p.1533, 1940.*

[KID1975a] Kidnay, A.J.; Miller, R.C.; Parrish, W.R.; Hiza; M.J., Liquid-vapour phase equilibria in the N_2- CH_4 system from 130 to 180K, *Cryogenics, vol.15, p.531, 1975.*

[KID1975b] Kidnay A.J.; Lewis K.L.; Calado J.C.G.; Staveley L.A.K., *J. Chem. Thermodyn., vol.7, pp.847-854, 1975.*

[KNO1967] Knorn M., Vapour-liquid equilibria of the neon-helium system, *Cryogenics, vol.7, p.177, 1967.*

[KOH1984] Kohn, J.P.; LLave, F.M.; Luks, K.D., Liquid-liquid-vapor equilibria in cryogenic LNG mixtures-phase IV nitrogen rich systems, *GPA RR-79, 1984.*

[KOS1984] Kosyakov, N.E.; Yakimenko, N.P.; Chobotko, L.L., *Zh. Prikl. Khim. (Leningrad), vol.57, p.2591, 1984.*

[KNA1976] Knapp H., Schmoelling K., Neumann A., *Cryogenics, vol.16, p.231, 1976.*

[KRE1982] Kremer, H., Experimentelle untersuchung und berechnung von hochdruck-flussigkeits-dampf und flussigkeits-flussigkeits-dampf-gleichgewichten fur tiefsiedende gemische, *Ph.D. Dissertation, University of Berlin, 1982.*

[KRE1983a] Kremer, H.; Knapp, H., Vapor-liquid equilibria in ternary mixtures of H_2, N_2, CO and CH_4., *Fluid Phase Equilib., vol.11, p.289-310, 1983.*

[KRE1983b] Kremer, H.; Knapp, H., *Hydrocarbon Process., vol.62, p.79, 1983.*

[KRI1936] Krichevskii I.R., Toroshechnikov N.S., *Zh. Fiz. Khim., vol.8, p.273, 1936.*

[KRI1962] Krichevskii, I.R.; Khazanova, N.E.; Lesnevskaya, L.S.; Sandalova, L.Yu, Equilibrium of liquid-gas at high pressures in the system nitrogen–carbon dioxide, *Khim. Promst. (Moscow), vol.38(3), pp.169–171, 1962.*

[KUE1917] Kuenen, J.P.; Clark, A.L., *Communs. Phys. Lab. Univ. Leiden, vol.150, p.55, 1917.*

[KUE1922] Kuenen, J.P.; Verschoyle, T.; Van Urk, A.T., Isotherms of diatomic substances and their binary mixtures: II the critical curve of oxygen + nitrogen mixtures, the critical phenomena and some isotherms of two mixtures with 50% and 75% by volume of oxygen…, *Versl. Gewone Vergad. Afd.Natuurk-d., K. Ned. Akad. Wet., vol.31, pp.511-26 (Comm. No. 161, Kamerlingh Onnes Lab.), 1922.*

[KUS1991] Kuskova, N. V.; Kukarin, V. F.; Martynets, V. G.; Matizen, E. V., Study of the phase equilibrium of {(1 − x) CO2 + xKr} for x < 0.032 near the critical point of CO2, J. *Chem. Thermodyn.*, *23, 523-530, 1991.*

[LEW1975] Lewis, K. L.; Staveley, L. A.K, Excess enthalpies of the liquid mixtures nitrogen + oxygen, nitrogen + argon, argon + ethane, and methane + carbon tetrafluoride. J. Chem. Thermodynamics, 7 (1975), 855–864.

[LIU1988] Liu K., Wang W., *J. Chem. Eng. (China), vol.16, pp.58–63, 1988.*

[LLA1985] Llave, F.M.; Luks, K.D.; Kohn, J.P., Three-phase liquid-liquid-vapor equilibria in the binary systems nitrogen + ethane and nitrogen + propane, *J. Chem. Eng. Data, vol.30(4), pp.435-438; 1985.*

[LON1963] Long H.M.; Di Paolo F.S., Condensed phase diagram of the system argon-nitrogen, *Chem. Eng. Prog. Symp. Ser., 59, 30-35, 1963.*

[LU1969] Lu, B.C.; Chang, S.-D.; Elshayal, I.M.; Yu, P.; Gravelle, D.; Poon, D.P.L., *Proceedings of the 1st International Conference on Calorimetry Thermodynamics, Warsaw, 1969.*

[MAC1980] Machado J.R.S., Gubbins K.E., Lobo L.Q.; Staveley L.A.K., *J. Chem. Soc., Faraday Trans., vol.76, pp.2496-2506, 1980.*

[MAI1961] Maimoni, A., Liquid-vapor equilibria in the hydrogen–nitrogen and deuterium–nitrogen systems, *AIChE J., vol.7, pp.371–375, 1961.*

[MAR1999] Martynets, V. G.; Kuskova, N. V.; Matizen, E. V.; Kukarin, V. F., Critical line of xenon + carbon dioxide, *J. Chem. Thermodyn.*, *31, 191-195, 1999.*

[MAS1973] Massengill D.R., Miller R.C., *J. Chem. Thermodyn., vol.5, p.207, 1973.*

[MAS1974] Mastera S.-G.J., *Kfa Kernforschungsanlage Jeulich Gmbh, n°1380, 1974.*

[MAS1976] Mastera S.-G.J., *Thesis, pp.69–85, 1976.*

[MCC1976] McClure, D.W.; Lewis, K.L.; Miller, R.C.; Staveley, L.A.K., Excess enthalpies and Gibbs free energies for nitrogen + methane at temperatures below the critical point of nitrogen, *J. Chem. Thermodynamics, vol.8, pp.785–792, 1976.*

[MCK1957] McKinley C.; Himmelberger F., *Chem. Eng. Progr., vol.53, pp.112-121, 1957.*

[MCK1958] McKinley C.; Wang E.S.J., *Adv. Cryog. Eng., vol.4, pp.11-25, 1958.*

[MCK1961] McKinley C., Brewer J., Wang E.S.J., *Adv. Cryog. Eng., vol.6, p.114, 1961.*

[MCT1919] McTaggart, H.A.; Edwards, E., Composition of the vapour and liquid phases of the system methane–nitrogen, Proc. Trans. Roy. Soc. Can., vol.13, pp.57–65, 1919.

[MEY1936] Meyer L., *Z. Phys. Chem. vol.175, p.275, 1936.*

[MIC1954] Michelis A.; Wassenaar T.; van Seventer W., *Appl. Sci. Res., vol.4, p.52, 1954.*

[MIL1973] Miller, R.C.; Kidnay, A.J.; Hiza, M.J., Liquid-vapor equilibria at 112.00K for systems containing nitrogen, argon, and methane, *AIChE J., vol.19, pp.145–151, 1973.*

[MUI1965] Muirbrook N.K., Prausnitz J.M., *AIChE J., vol.11(6), pp.1092-1102, 1965.*

[MUL1965] Mullins, J.C.; Ziegler, W.T., Phase equilibria in the argon - helium and argon - hydrogen systems from 68 to 108K and pressures to 120 atmospheres, *Adv. Cryog. Eng., vol.10, pp.171-81, 1965.*

[NAR1957] Narinskii, G.B., Investigation of the equilibrium of liquid-vapor in the system oxygen–argon, *Kislorod, vol.10(3), pp.9–16, 1957.*

[NAR1966] Narinskii, G.B., Liquid-vapour equilibrium in the argon–nitrogen system. I. Experimental data and their verification, *(Russ. J. Phys. Chem., Engl. Transl., vol.40, pp.1093–1096, 1966), Zh. Fiz. Khim., vol.40, pp.2022–2029, 1966.*

[NAR1969] Narinskii, G.B., Liquid-vapour equilibrium in the oxygen–argon–nitrogen system. I. Experimental data, *(Russ. J. Phys. Chem., Engl. Transl., vol.43, pp.219–221, 1969), Zh. Fiz. Khim., vol.43, pp.408–412, 1969.*

[NUN1985] Nunes da Ponte, M.; Chokappa, D.; Calado, J.C.G.; Clancy, P.; Streett, W.B., Vapor-liquid equilibrium in the xenon + ethane system, *J. Phys. Chem., vol.89, p.2746, 1985.*

[NUN1986] Nunes da Ponte, M.; Chokappa, D.; Calado, J.C.G.; Zollweg, J.A.; Streett, W. B., Vapor-Liquid Equilibrium in the Xenon + Ethene System, *J. Phys. Chem., vol.90, p.1147, 1986.*

[OMA1962a] Omar, M.H.; Dokoupil, Z., Solubility of nitrogen and oxygen in liquid hydrogen at temperatures between 27 and 33K, *Physica, vol.28(5), pp.461-471. 1962.*

[OMA1962b] Omar, M.H.; Dokoupil, Z.; Schroten, H.G.M., Determination of the solid – liquid equilibrium diagram for the nitrogen – methane system, *Physica, vol.28, pp.309-329, 1962.*

[OMA1962c] Omar, M.H.; Dokoupil, Z., Solid-gas equilibrium of the binary oxygen-hydrogen system, *Physica, vol.28(5), pp.472-478, 1962.*

[ORO1968] Orobinskii, N.A.; Blagoi, Yu.P.; Semyannikova, E.L., Liquid-vapor phase equilibrium of the argon + propylene and krypton + propylene systems at high temperatures, *Ukr. Fiz. Zh., vol.13, pp.373-80, 1968.*

[OST1977] Ostronov, M.G.; Statskaya, L.V.; Finyagina, R.A.; Brodskaya, L.F.; Zhirnova, N.A., *Zh. Fiz. Khim., vol.51, p.2396, 1977.*

[PAR1974a] Parrish, W.R.; Hiza, M.J., Liquid – vapor equilibria in the nitrogen . methane system between 95 and 120K, *Cryogenic Engineering Conference, Atlanta, Georgia, K-9, August 8-10,1973.*

[PAR1974b] Parrish, W.R.; Hiza, M.J., *Adv. Cryog. Eng., vol.19, p.300, 1974.*

[PAR1997] Parikh, N.C.; Zollweg, J.A., *Energy Week Proceedings, Houston, vol.7, p.58, 1997.*

[PAS1981] Pashkov V.V.; Blagoi Y.P.; Lobko M.P., *Currently undefined in source list, 0, 549, 1981.*

[POO1962] Pool, R.A.H.; Saville, G.; Herrington, T.M.; Shields, B.D.C.; Staveley, L.A.K., Some excess thermodynamic functions for the liquid systems argon + oxygen, argon + nitrogen, nitrogen + oxygen, nitrogen + carbon monoxide, and argon + carbon monoxide, Trans. Faraday Soc., vol.58, pp.1692–1704, 1962.

[POO1974] Poon, D.P.L.; Lu, B.C.-Y., Phase equilibria for systems containing nitrogen, methane and propane. *Adv. Cryog. Eng., vol.19, pp.292–299, 1974.*

[PRE1971] Preston, G.T., Funk E.W., Prausnitz J.M., Solubilities of hydrocarbons and carbon dioxide in liquid methane and in liquid argon, *J. Phys. Chem., vol.75(15), pp.2345-2352, 1971.*

[RAA2001] Raabe G., Janisch J., Kohler J., Experimental studies of phase equilibria mixtures relevant for the description of natural gases, *Fluid Phase Equilibria, vol.185, pp.199-208, 2001.*

[RAA2004] Raabe G., Kohler J., Phase equilibria in the system nitrogen-ethane and their prediction using cubic equations of state with different types of mixing rules, *Fluid Phase Equilibria, vol.3(9), pp.222-223, 2004.*

[ROD1964] Rodewald, N.C.; Davis, J.A.; Kurata, F., The heterogeneous phase behavior of the helium–nitrogen system, AIChE J., vol.10, pp.937–943, 1964.

[ROO1967] Roof, J.G.; Baron, J.D., Critical loci of binary mixtures of propane with methane, carbon dioxide, and nitrogen, *J. Chem. Eng. Data, vol.12, pp.292-3, 1967.*

[ROZ1988] Rozhnov, M.S.; Kozya, V.G.; Zhdanov, V.I., *Khim. Prom-st (Moscow), vol.674, 1988.*

[RUH1935] Ruhemann M.; Lichter A.; Komarov P., *Phys. Z. Sowjetunion, vol.8, pp.326-336, 1935.*

[SAR1971] Sarashina E.; Arai Y.; Saito S., The P-V-T-X relation for the carbon dioxide-argon system, *J. Chem. Eng. Japan, vol.4, pp.379-381, 1971.*

[SCH1960] Schmidt, H., Das thermodynamishe Verhalted des flussigen systems Ar-Kr, *Z. Phys. Chem. Neue Fol.*, *24*, *265-274, 1960.*

[SCH1966] Schindler, D.L.; Swift, G.W.; Kurata, F., More low temperature V-L design data, *Hydrocarbon Process. Pet. Refiner 45, vol.11, pp.205–210, 1966.*

[SCH1975] Schouten, J.A.; Deerenberg, A.; Trappeniers, N. J., Vapor-liquid and gas-gas equilibria in simple systems: IV the system argon + krypton, *Physica A, (Amsterdam), vol.81, pp.151-60, 1975.*

[SHA1976] Shatskaya, L.V.; Zhirnova, N.A., Liquid-vapour phase equilibria in binary systems at low temperatures. I. Argon–methane system, *Russ. J. Phys. Chem., vol.50, p.298, 1976. (Translated from Zh. Fiz. Khim., vol.50, p.515, 1976).*

[SHI1984] Shi, M.; Wei, M.; Zhang, J.; Wang, L., Simple and Speedy Measurement of Bubble Point and Dew Point for VLE Binary System Under Pressure, *Chemical Engineering(China), vol.6, pp.51-54, 1984.*

[SIN1966] Sinor, J.E.; Kurata, F., Solubility of helium in liquid argon, oxygen, and carbon monoxide, *J. Chem. Eng. Data, vol.11, pp.537–539, 1966.*

[SKR1964] Skripka V.G., Dykhno N.M., *Tr. Vses. Nauch. – Issled. Inst. Kislorodn. Kriog. Kompres. Mashinostr., vol.8, p.163, 1964.*

[SKR1970] Skripka, V.G.; Nikitina, I.E.; Zhdanovich, L.A.; Sirotin, A.G.; Benyaminovich, O.A., Liquid-vapor phase equilibrium at low temperatures in binary systems. Components produced from natural gas, *Gazov. Promst., vol.15(12), pp.35–36, 1970.*

[SKR1971] Skripka V.G., Lobanova N.N., *Tr. Vses. Nauch. – Issled. Inst. Kislorodn. Kriog. Kompres. Mashinostr., vol.13, p.90, 1971.*

[SMI1952] Smith S.R., *Thesis, 1952.*

[SNE1968] Sneed C.M.; Sonntag R.E.; Van Wylen G.J., *J. Chem. Phys, vol.49, pp.2410-2414, 1968.*

[SOM1978] Somait, F.A.; Kidnay, A.J., Liquid-vapor equilibria at 270.00K for systems containing nitrogen, methane, and carbon dioxide, *J. Chem. Eng. Data, vol.23, pp.301–305, 1978.*

[SON1962] Sonntag, R. E.; Van Wylen, G. J., The solid-vapor equilibrium of carbon dioxide-nitrogen, *Adv. Cryog. Eng., 7, 99-105, 1962.*

[SON1963] Sonntag, R. E.; Van Wylen, G. J., Solid-vapor equilibrium of the carbon dioxide-nitrogen system at pressures to 200 atmospheres, *Adv. Cryog. Eng., 9, 197-206, 1963.*

[SON1964] Sonntag R.E.; Van Wylen G.J.; Crain R.W., *J. Chem. Phys., vol.41, p.2399, 1964.*

[SPR1966] Sprow, F.B.; Prausnitz, J.M., Vapor-liquid equilibria for five cryogenic mixtures, *AIChE J., vol.12, pp.780–784, 1966.*

[STE1939] Steckel, F.A.; Zinn, N.M., Investigation of the liquid-vapor phase behavior of the system methane–nitrogen–hydrogen. *Zurnal Chimiceskoj Promyslennosti, vol.16, pp.24–28, 1939.*

[STR1964] Streett W.B.; Sonntag R.E.; Van Wylen G.J., *J. Chem. Phys, vol.40, p.1390, 1964.*

[STR1965a] Streett, W.B., Liquid-vapour equilibrium in the system neon – nitrogen, *Cryogenics, vol.5, pp.27-33, 1965.*

[STR1965b] Streett, W.B.; Jones, C.H., Liquid-vapor equilibrium in the system neon - oxygen from 63 to 152K and at pressures to 5000 psi, *Adv. Cryog. Eng., vol.11, pp.356-66, 1965.*

[STR1965c] Streett, W.B., Liquid-vapor equilibrium in the system neon-argon, *J. Chem. Phys., vol.42, pp.500-3, 1965.*

[STR1965d] Streett W.B.; Jones C.H., *J. Chem. Phys., vol.42(11), pp.3989-3994, 1965.*

[STR1967a] Streett, W.B., Gas-liquid and fluid-fluid phase separation in the system helium–nitrogen near the critical temperature of nitrogen, *Chem. Eng. Prog., Symp. Ser., vol.63(81), pp.37–42, 1967.*

[STR1967b] Streett, W.B., Liquid-vapor phase behavior and liquid phase density in the system neon - argon at high pressures, *J. Chem. Phys., vol.46, pp.3282-6, 1967.*

[STR1968] Streett, W.B., Density and phase equilibria in the system neon + nitrogen at high pressures, *Cryogenics, vol.8, pp.88-93, 1968.*

[STR1969] Streett, W.B., Gas-liquid and fluid-fluid phase separation in the system helium + argon at high pressures, *Trans. Faraday Soc., vol.65, pp.696–702, 1969.*

[STR1970] Streett, W.B.; Hill, J.L.E., Phase equilibria in fluid mixtures at high pressures: the helium + nitrogen system, *J. Chem. Phys., vol.52, pp.1402-6, 1970.*

[STR1971a] Streett, W.B.; Hill, J.L.E., *J. Chem. Phys., vol.54, p.5088, 1971.*

[STR1971b] Streett, W.B.; Hill, J.L.E., Phase equilibria in fluid mixtures at high pressures: the helium + argon system, *Trans. Faraday Soc., vol.37, pp.622–630, 1971.*

[STR1972a] Streett W.B., Erickson A.L., *Phys. Earth Planet Inter., vol.5, p.357, 1972.*

[STR1972b] Stryjek, R., Chappelear P.S.; Kobayashi R., Low Temperature VLE, *Chemical Engineering Department Monograph, Rice University, Houston, 1972.*

[STR1973] Streett W.B., *Atrophys. J., vol.186, p.1107, 1973.*

[STR1974a] Stryjek, R.; Chappelear, P.S.; Kobayashi, R., Low-temperature vapor-liquid equilibria of nitrogen–methane system, *J. Chem. Eng. Data, vol.19, pp.334–339, 1974.*

[STR1974b] Stryjek, R.; Chappelear, P.S.; Kobayashi, R., Low-temperature vapor-liquid equilibria of nitrogen–ethane system, *J. Chem. Eng. Data, vol.19, pp.340–343,1974.*

[STR1978] Streett, W.B.; Calado, J.C.G., Liquid-vapour equilibrium for hydrogen + nitrogen at temperatures from 63 to 110K and pressures to 57 MPa, *J. Chem. Thermodyn., vol.10, pp.1089-100, 1978.*

[SZC1979] Szczepaniec-Cieciak, Kondaurow V.A.; Melikova S.M., *Cryogenics, vol.2, 1979.*

[SZC1980] Szczepaniec-Cieciak, E., Kondaurov, V.A., Melikova, S.M., Study on the solubility light alkanes in liquid nitrogen, *Cryogenics, vol.20(1), pp.48-51, 1980.*

[TEL1984] Teller, M.; Knapp, H., Measurements of solubilities of solid krypton and xenon in liquid nitrogen, *Cryogenics, vol.24(9), pp.471-476, 1984.*

[THO1963] Thorogood, R.M.; Haselden, G.G., The determination of equilibrium data for the oxygen– nitrogen system at high oxygen concentrations, *Br. Chem. Eng., vol.8, pp.623–625, 1963.*

[THO1968] Thorpe, P.L., Liquid-vapour equilibrium of the system nitrogen + argon at pressures up to 10 atm. *Trans. Faraday Soc., vol.64, pp.2273–2280, 1968.*

[TOR1939] Torocheshnikov, N.S.; Levius, L.A., *Zh. Khim. Prom., vol.16(1), p.19, 1939.*

[TOR1940] Torocheshnikov N.S.; Ershova V.A., *Zh. Khim. Prom., vol.17, pp.30-33, 1940.*

[TRA1974] Trappeniers, N.J.; Schouten, J.A., Vapour-liquid and gas-gas equilibria in simple systems: II the system neon + argon, *Physica (Amsterdam), vol.73, pp.539-45, 1974.*

[TSI1940] Tsin, N.M., Solubility of ethylene and propylene in liquid nitrogen and liquid oxygen, *Zh. Fiz. Khim.*, *14*(*3*), *418-421, 1940.*

[TSI1946] Tsiklis, D.S., Heterogeneous equilibria in binary systems, *Zh. Fiz. Khim., vol.20, pp.181–188, 1964.*

[TUL1971] Tully, P.C.; DeVaney, W.E.; Rhodes, H.L., Phase equilibria of the helium–nitrogen system from 122 to 126K, *Adv. Cryog. Eng., vol.16, pp.88–95, 1971.*

[VAN1968] van't Zelfde, P.; Omar, M.H.; Schroten, H.G.M.; Dokoupil, Z., Solid liquid equilibrium diagram for the argon methane system, *Physica, vol.38, pp.241-252, 1968.*

[VAN1988] van den Bergh, L.C.; Schouten, J.A., The critical line and the three phase line in a molecular helium-nitrogen mixture up to 100 kbar, *Chem. Phys. Lett., vol.145, p.471, 1988.*

[VEI1937] Veith, H.; Schröder, E., *Z. physic. Chem. A, vol.179, pp.16-22, 1973.*

[VER1931] Verschoyle, T. T. H., The ternary system carbon monoxide + nitrogen + hydrogen and the component binary systems between temperatures of -185 and -215°C, and between pressures of 0 and 225 atm, *Philos. Trans. R. Soc. London, A, vol.230, p.189, 1931.*

[VOL1960] Volk, H.; Halsey, G. D.Jr., Solubility of hydrogen and deuterium in liquid argon, J. Chem. Phys., vol.33, p.1132, 1960.

[VON1934] Von Stackelberg M., *Z. Phys. Chem. Leipzig, vol.170A, pp.262-272, 1934.*

[VON1936] Von Stackelberg M.; Quatram F.; Antweiler H.J., *Z. Elektrochem., vol.42, pp.552-557, 1936.*

[WAN1960] Wang, D.I.J., Vapor-liquid equilibrium studies on the system argon–oxygen, *Adv. Cryog. Eng., vol.3, pp.294–304, 1960.*

[WEB1984] Weber, W.; Zeck, S.; Knapp, H., Gas solubilities in liquid soVLEnts at high pressures: apparatus and results for binary and ternary systems of nitrogen, carbon dioxide and methanol, *Fluid Phase Equilib., vol.18, p.253, 1984.*

[WEI1948] Weishaupt, J., Determination of the equilibria of boiling nitrogen–argon–oxygen mixtures at 1000 Torr, *Angewandte Chemie, B, vol.20(12), pp.321–326, 1948.*

[WIL1964] Wilson, G.M.; SiVLErberg, P.M.; Zellner, M.G., Argon–oxygen–nitrogen three-component system experimental vapor-liquid equilibrium data, *Adv. Cryog. Eng., vol.10, pp.192–208, 1965.*

[WIL1975] Wilson, G.M., Vapor-liquid equilibria of nitrogen, methane, ethane and propane binary mixtures at LNG temperatues from total pressure measurements, *Adv. Cryog. Eng., vol.20, pp.164–171, 1975.*

[WIL1977] Wilson G.M., Cunningham J.R., Nielsen P.F., Enthalpy and phase boundary measurements on mixtures of nitrogen with methane, carbon dioxide, and hydrogen sulfide, *GPA RR-24, 1977.*

[WIL1992] Willem L.; Vos, J.; Schouten, A., The phase diagram of the binary mixture nitrogen-helium at high pressure, *Physica A: Statistical Mechanics and its Applications, vol.182(3), pp.365-387, 1992.*

[WOJ1975] Wojtaszek, Z.; Szczepaniec-Cieciak, E.; Morzyniec, A., The solubility of solid nitrous oxide in liquid nitrose in the 77.4 – 63.5 K temperature range, *Cryogenics*, *351-353, 1975.*

[XIA1990] Xiao, J.; Liu, K.; Du, Y.; Jin, Z.; Lu, H., Measurement on and Correlation of VLE of H_2-N_2-Ar System, *Chemical Engineering (China), vol.18(2), pp.8-12, 1990.*

[XU1992a] Xu, N.; Dong, J.; Wang, Y.; Shi, J., High pressure vapor liquid equilibria at 293K for systems containing nitrogen, methane and carbon dioxide, *Fluid Phase Equilibria, vol.81, pp.175–186, 1992.*

[XU1992b] Xu, N., Dong, J., Wang, Y., Shi, J., *J. Chem. Ind. (China), vol.43, p.640, 1992.*

[YAK1975] Yakimenko, N.P.; Glukh, G.M.; Iomotev, M.B.; Abramova, R.I., *Russ. J. Chem., vol.49, pp.116-117, 1975.*

[YAK1976] Yakimenko, N.P.; Glukh, G.M.; Iomtev, M.B.; Polishchukova, L.I.; Dobrovol'skaya, V.E.; Fik,A.S., Solid-gas phase equilibrium in the system nitrogen-nitrous oxide, *Zh. Fiz. Khim*., *50(7), 1909-1910, 1976.*

[YAM1992] Yaminishi, T.; Okuno, K.; Naruse, Y.; Sada, E., *J. Chem. Phys, vol.96, p.2284, 1992.*

[YOR1968a] Yorizane, M.; Yoshimura, S.; Masuoka, H.; Toyama, A., Low temperature vapour-liquid equilibria of hydrogen-containing binaries, *Proc. 1st Int. Cryog. Eng. Conf., pp. 57–62, 1968.*

[YOR1968b] Yorizane, M.; Yoshimura, S.; Sadamoto, S., *Kagaku Kogaku, vol.32, pp.257-264, 1968.*

[YOR1970] Yorizane, M.; Yoshimura, S.; Masuoka, H., Vapor-liquid equilibrium at high pressures (N_2–CO_2, H_2–CO_2), *Kagaku-kogaku, vol.34, pp.953–957, 1970.*

[YOR1971a] Yorizane, M., *Asahi Garasu Kogyo, vol.18, pp.61-76, 1971.*

[YOR1971b] Yorizane, M., Yoshimura, S., Masuoka, H., Naka, T., *Kagaku Kogaku, vol.35, p.691, 1971.*

[YOR1978] Yorizane, M.; Yoshimura, S.; Masuoka, H.; Toyama, A.; Nakako, Y.; Funada, I., Measurement and estimation of low temperature vapor-liquid equilibrium for the system oxygen–argon at high oxygen concentrations, *Chem. Eng. Sci., vol.33, pp.641–649, 1978.*

[YOR1985] Yorizane, M.; Yoshimura, S.; Masuoka, H.; Miyano, Y.; Kakimoto, Y., New procedure for vapor-liquid equilibria. Nitrogen + carbon dioxide, methane + freon22, and methane + freon12, *J. Chem. Eng. Data, vol.30, pp.174–176, 1985.*

[YU1969] Yu, P.; Elshayal, J. M.; Lu, B. C.-Y., Liquid-liquid-vapor equilibria in the nitrogen-methane-ethane system, *Can. J. Chem. Eng*., *47, 495-498, 1969.*

[YUC1999] Yucelen, B.; Kidnay, A.J., Vapor-liquid equilibria in the nitrogen + carbon dioxide + propane system from 240 to 330K at pressures to 15 MPa, *J. Chem. Eng. Data, vol.44, pp.926–931, 1999.*

[ZEC1985] Zeck S., Beitrag zur experimentellen untersuchung und berechnung von gas-flussigkeits-phasengleichgewichten, *Thesis, 1985.*

[ZEC1986a] Zeck, S.; Knapp, H., Vapor-liquid and vapor-liquid-liquid phase equilibria for binary and ternary systems of nitrogen, ethane and methanol: experiment and data reduction, *Fluid Phase Equilib., vol.25, pp.303-322, 1986.*

[ZEC1986b] Zeck, S.; Knapp, H., Vapor-liquid and vapor-liquid-liquid phase equilibria for binary and ternary systems of nitrogen, ethene and methanol: experiment and data evaluation, *Fluid Phase Equilib., vol.26, pp.37-58, 1986.*

[ZEI1972] Zeininger, H., Liquid-vapor equilibriums of the binary systems nitrous oxide - nitrogen, nitrous oxide - oxygen, and nitrous oxide - methane at low temperatures and high pressures, *Chem. Ing. Tech., vol.44, p.607, 1972.*

[ZEN1963] Zenner, G.H.; Dana, L.I., Liquid-vapor equilibrium compositions of carbon dioxide–oxygen–nitrogen mixtures, *Chem. Eng. Prog., Symp. Ser., vol.59(44), pp.36–41, 1963.*

Appendix B

PHASE DIAGRAMS INCLUDING SOLID PHASES

LIST OF TABLES **B2**

LIST OF FIGURES **B2**

NOMENCLATURE **B3**

1 PHASE DIAGRAM INCLUDING SOLID PHASE B4

1.1.1 Type II PT-EP B5

1.1.2 Type III PT-EP B7

1.1.3 Type IV PT-EP B11

1.1.4 Type V PT-EP B14

1.1.5 Type VI PT-EP B16

BIBLIOGRAPHY **B18**

List of tables

Table B.1: Abbreviations used in the diagrams for the different types of phase equilibria. B4
Table B.2: Line styles and symbols used in the PT-EPs. B4

List of figures

Figure B.1: Qualitative PT-EP for type II systems as presented in van Konynenburg and Scott [1]. B5
Figure B.2: Qualitative PT-EP for type II including the solid phase B6
Figure B.3: Qualitative PT-EP for type II including the solid-solid equilibrium. B6
Figure B.4: Qualitative PT-EP for type III systems as presented in van Konynenburg and Scott [1]. B7
Figure B.5: Qualitative PT-EP for type IIIa including the solid phase B8
Figure B.6: Qualitative PT-EP for type IIIb including the solid phase. B8
Figure B.7: Qualitative PT-EP for type IIIc including the solid phase B9
Figure B.8: Qualitative PT-EP for type IIIa including the solid-solid equilibrium. B9
Figure B.9: Qualitative PT-EP for type IIIb including the solid-solid equilibrium. B10
Figure B.10: Qualitative PT-EP for type IIIc including the solid-solid equilibrium. B10
Figure B.11: Qualitative PT-EP for type IV systems as presented in van Konynenburg and Scott [1]. B11
Figure B.12: Qualitative PT-EP for type IV including the solid phase. B12
Figure B.13: Qualitative PT-EP for type IV* systems as presented in van Konynenburg and Scott [1]. B12
Figure B.14: Qualitative PT-EP for type IV* including the solid phase. B13
Figure B.15: Qualitative PT-EP for type IV including the solid-solid equilibrium. B13
Figure B.16: Qualitative PT-EP for type IV* including the solid-solid equilibrium. B14
Figure B.17: Qualitative PT-EP for type V systems as presented in van Konynenburg and Scott [1] B14
Figure B.18: Qualitative PT-EP for type V including the solid phase. B15
Figure B.19: Qualitative PT-EP for type V including the solid-solid equilibrium. B15
Figure B.20: Qualitative PT-EP for type VI systems as presented in van Konynenburg and Scott [1]. B16
Figure B.21: Qualitative PT-EP for type VI including the solid phase. B17
Figure B.22: Qualitative PT-EP for type VI including the solid-solid equilibrium. B17

Nomenclature

Symbol	*Meaning*
PT-EP	Pressure-temperature equilibrium projection
Px-CS	Pressure-composition cross section
Tx-CS	Temperature-composition cross section
UCEP	Upper critical endpoint
LCEP	Lower critical endpoint
F	Degrees of freedom
N	Number of components
π	Number of phases
φ	Number of constraints
l	Liquid phase
v	Vapor phase
s	Solid phase
P	Pressure
T	Temperature
R	Gas constant
v	Volume
a	EoS parameter
b	Liquid covolume
λ	Latent heat

Superscripts

^{1,2}	Phases with the same state of aggregation that coexist at the same P-T

1 Phase diagram including solid phase

This appendix presents the classification from type II to type V projections of the phase diagram as proposed by van Konynenburg and Scott [1]. Type VI PT-EP has been also considered.

In order to maintain the representation as simple as possible, the possible presence of an azeotrope has not been considered. The abbreviations used in the diagrams for indicating the different types of phase equilibria and their meaning are listed in Table B.1.

Table B.1: Abbreviations used in the diagrams for the different types of phase equilibria.

Abbreviation	Meaning
l=v	Liquid – vapor critical curve
l=l	Liquid – liquid critical curve
lv	Liquid – vapor equilibrium curve (pure component)
sl	Solid – liquid equilibrium curve (pure component)
sv	Solid – vapor equilibrium curve (pure component)
llv	Liquid – liquid – vapor equilibrium curve
slv	Solid – liquid – vapor equilibrium curve
sll	Solid – liquid – liquid equilibrium curve
ssv	Solid – solid – vapor equilibrium curve
ssl	Solid – solid – liquid equilibrium curve

Table B.2 explains the meaning of different line styles and symbols used in the diagrams of this section.

Table B.2: Line styles and symbols used in the PT-EPs.

Equilibrium state	Representation
Pure component vapor pressure curve	———
Critical curve	———
Three-phase curve	- · - · -
Pure component critical point	○
Pure component triple point	●
Quadruple point	□
Upper critical endpoint	▲
Lower critical endpoint	▼

In Table B.2, the critical endpoints represent a critical phase coexisting with another non-critical phase. Two relations hold for the two coexisting phases ($\pi = 2$), then the phase rule gives:

$$F = N - \pi + 2 - \varphi = 2 - 2 + 2 - 2 = 0 \qquad (B.1)$$

Critical endpoints (CEP) are the upper and lower limits (upper critical endpoint, UCEP, and lower critical endpoint, LCEP, respectively) of a three phase curve, as a L_1L_2V curve. In a PT-EP or Px-CS, UCEP is the upper pressure limit of a three phase curve and LCEP is the lower pressure limit of a three phase curve. In a Tx-CS, UCEP is the upper temperature limit of a three phase curve and LCEP is the lower temperature limit of a three phase curve.

The PT-EPs are presented from section 1.1.1 to section 1.1.5.

It must be kept in mind that for identifying the components of a binary mixture, the subscript 1 indicates the component with the lowest critical temperature and so the subscript 2 means the component with the highest.

1.1.1 Type II PT-EP

The qualitative pressure-temperature equilibrium projection (PT-EP) for type II systems as presented in van Konynenburg and Scott, [1], is shown in Figure B.1. As reported in [1], this behavior is typical of systems like CO_2 – *n*-octane, CO_2 – *n*-decane, and n-pentane – nitrobenzene

As it is possible to observe in Figure B.1, the usual liquid-vapor critical line links up the critical points of the two substances. Another critical line is present: this $liquid_1$-$liquid_2$ critical line extends from the UCEP of the $liquid_1$-$liquid_2$-vapor line. This three phase line is placed between the vapor pressure curves of the two pure components.

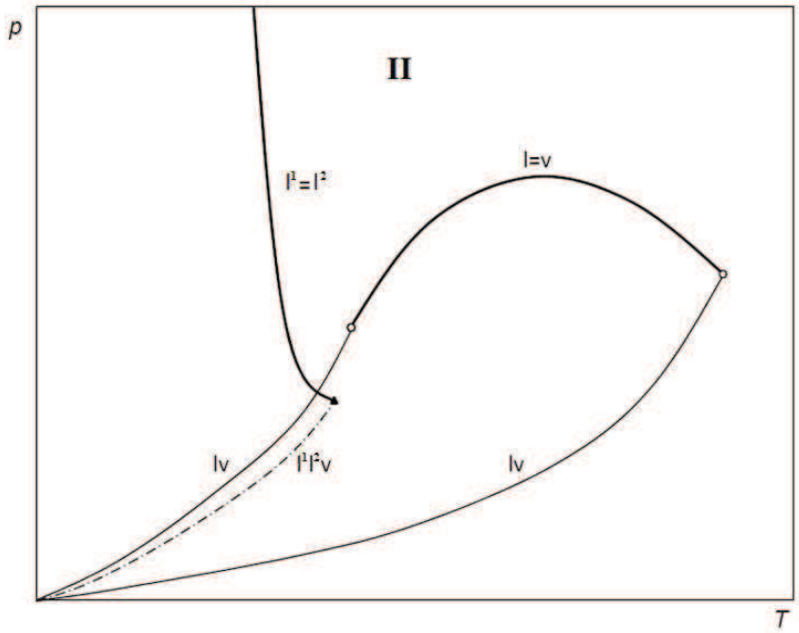

Figure B.1: Qualitative PT-EP for type II systems as presented in van Konynenburg and Scott **[1]**.

The PT-EP of type II including the solid phase, Figure B.2, shows that the $liquid_1$-$liquid_2$ critical curve ends where it joins together a solid-$liquid_1$-$liquid_2$ line. This three phase line extends up to a quadruple point where the solid, $liquid_1$, $liquid_2$, and vapor phases coexist. From this quadruple point other three lines branch off.

One is the $liquid_1$-$liquid_2$-vapor curve that ends in its UCEP, as reported in Figure B.1. The other two lines come from the triple point curve that is split in two: the solid-$liquid_1$-vapor and solid-$liquid_2$-vapor lines, respectively.

The presence of the solid phase in type II diagrams has been studied by Garcia and Lucks [2]. They have associated the $liquid_1$-$liquid_2$-vapor branch to the partial immiscibility between the two components.

Figure B.3 presents the type II PT-EP in presence of immiscibility in the solid phase. In this configuration, a quadruple point occurs where two solid phases and a vapor and a homogeneous liquid phase coexist.

From this point four triple lines originates, a $solid_1$-$solid_2$-vapor line, two solid-liquid-vapor lines, and a $solid_1$-$solid_2$-liquid line. The two solid-liquid-vapor lines involve the two partially or totally immiscible solids.

To sum up, type II PT-EP with immiscibility in the solid phase shows 2 quadruple points and seven triple lines.

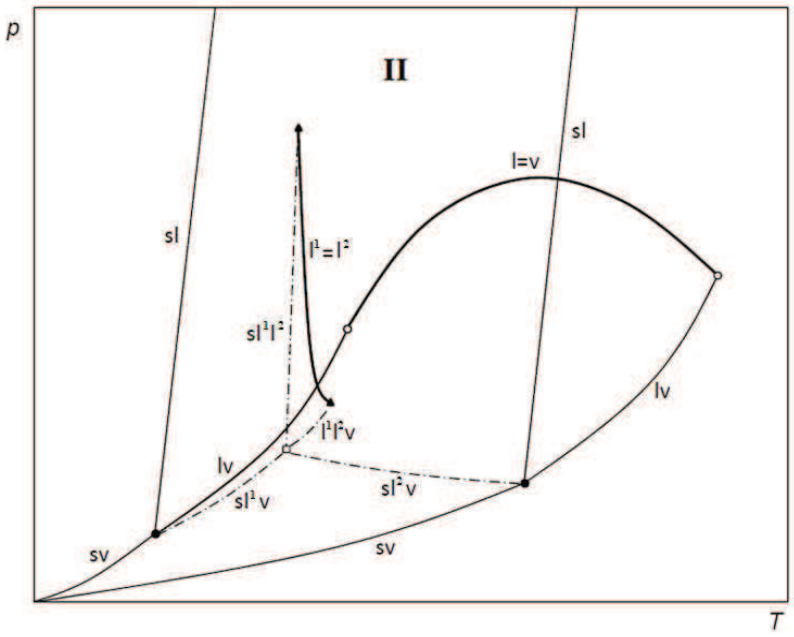

Figure B.2: Qualitative PT-EP for type II including the solid phase.

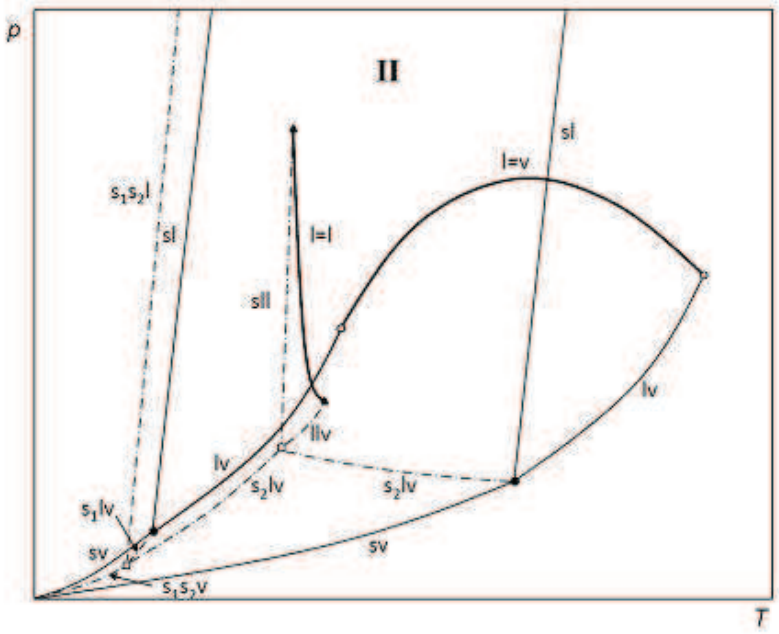

Figure B.3: Qualitative PT-EP for type II including the solid-solid equilibrium.

1.1.2 Type III PT-EP

Type III is the usual behavior for asymmetric binary systems of supercritical gases and non-volatile components, like He – Xe, Ne – Kr, and CH_4 – *n*-heptane.

The qualitative PT-EP for type III systems as presented in van Konynenburg and Scott [1] is shown in Figure B.4, while Figure B.5-Figure B.7 present the effect of the solid.

As shown in Figure B.4, also in this case a $liquid_1$-$liquid_2$-vapor line is present, but differently from type II, see Figure B.1, in this case this three phase line joins together a liquid-vapor critical line. This is one of the two critical line that are present, and it origins in the critical point of the more volatile component. The second critical line extends from the critical point of the other component and it is initially a vapor-liquid critical line changing to a $liquid_1$-$liquid_2$ critical line.

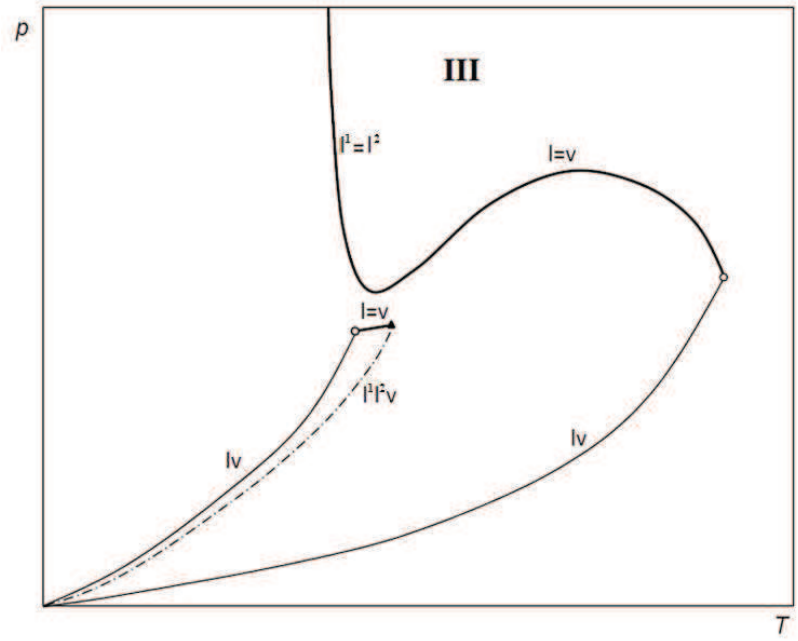

Figure B.4: Qualitative PT-EP for type III systems as presented in van Konynenburg and Scott **[1]**.

As for the type II, the presence of the solid phase in type III, Figure B.5, gives a quadruple point where four phases coexist: solid, $liquid_1$, $liquid_2$, and vapor. This point is the point where four three-phase lines branch off: in terms of pressure, it represents the lower point for the solid-$liquid_1$-$liquid_2$ and $liquid_1$-$liquid_2$-vapor lines, and the higher point for the solid-$liquid_1$-vapor and solid-$liquid_2$-vapor lines.

The solid-$liquid_1$-$liquid_2$ lines joins at it UCEP the $liquid_1$-$liquid_2$ critical line, while the two triple point curves solid-$liquid_1$-vapor and solid-$liquid_2$-vapor join the triple point of the first and second components, respectively.

Figure B.6 and Figure B.7 present the effects due to an increasing shifting of the quadruple point toward higher temperature and pressure.

In the first case, Figure B.6, the solid-$liquid_1$-vapor branch increases progressively till joining the quadruple point with the liquid-vapor critical line that extends from the critical point of the first component. In this case at the quadruple point it is also verified the critical conditions between the liquid2 and the vapor phases.

In the second case, Figure B.7, the solid-liquid-vapor branch starting from the triple point of component 2 joins directly the liquid-vapor critical curve originating from the critical point of component 2. The other solid-liquid-vapor branch joins the liquid-vapor critical curve originating from the critical point of component 1.

The presence of the solid phase in type III diagrams has been studied by Garcia and Lucks [2], Th. W. de Loos [3], , Flöter et al. [4] and Scurto et al. [5], Shaw and Béhar [6], and in Zou and Shaw [7].

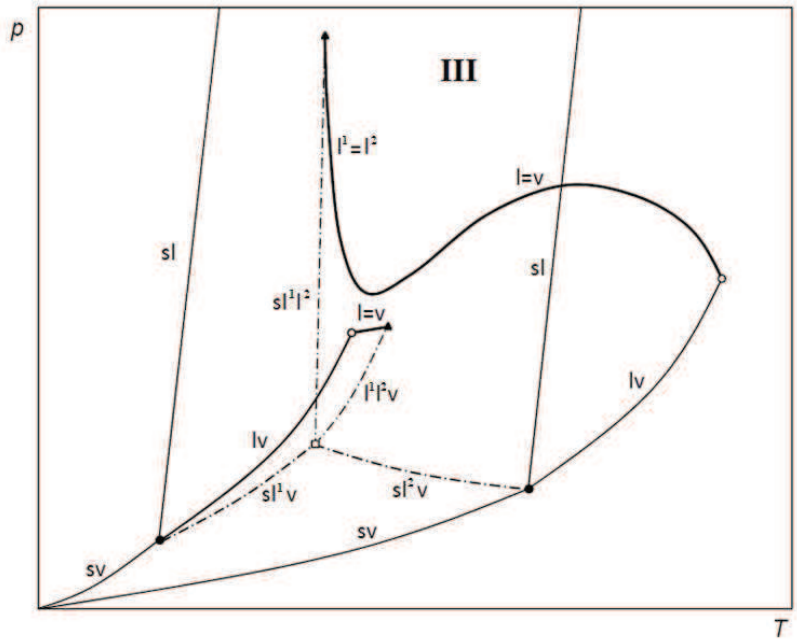

Figure B.5: Qualitative PT-EP for type IIIa including the solid phase.

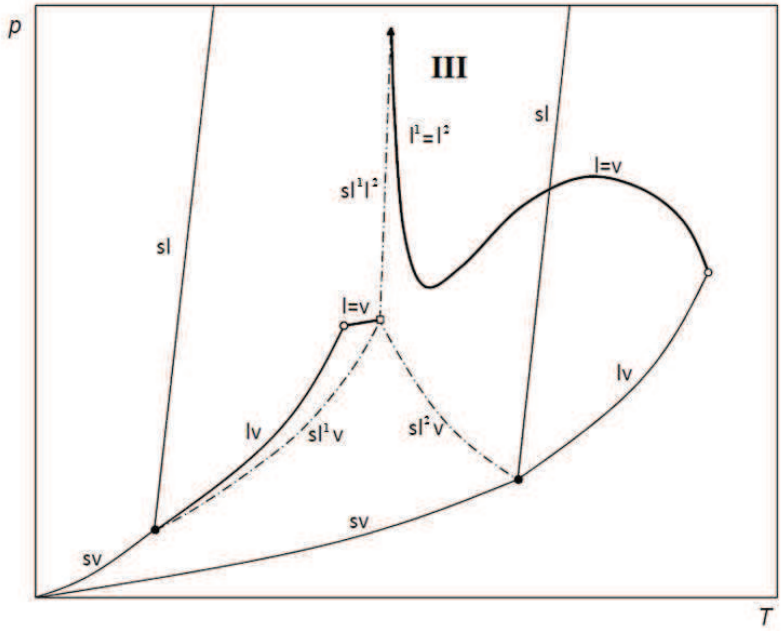

Figure B.6: Qualitative PT-EP for type IIIb including the solid phase.

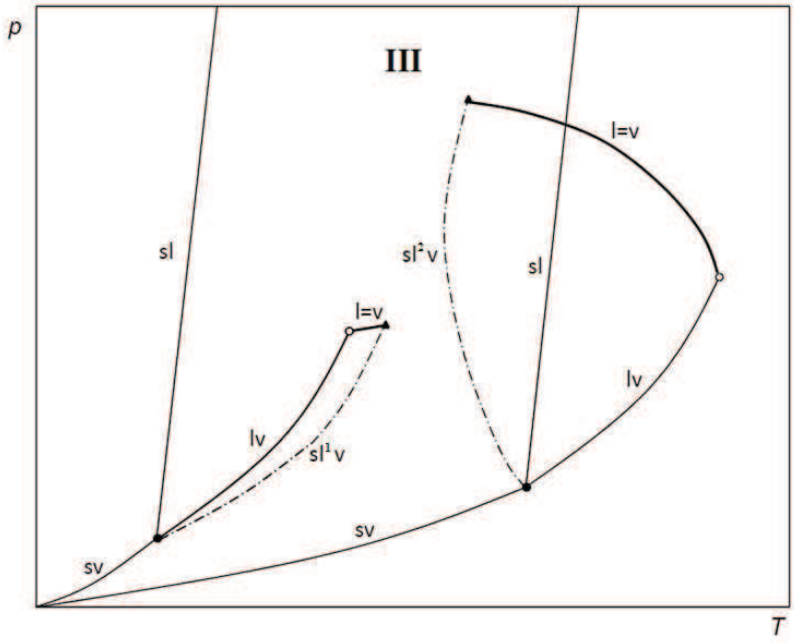

Figure B.7: Qualitative PT-EP for type IIIc including the solid phase.

Figure B.8-Figure B.10 shown the equilibrium projections presented in Figure B.5-Figure B.7 in case of solid-solid equilibrium.

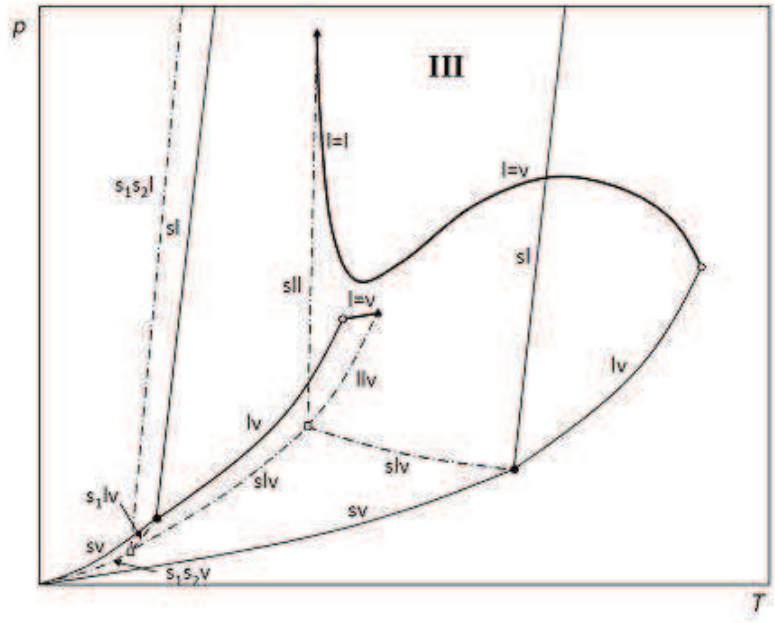

Figure B.8: Qualitative PT-EP for type IIIa including the solid-solid equilibrium.

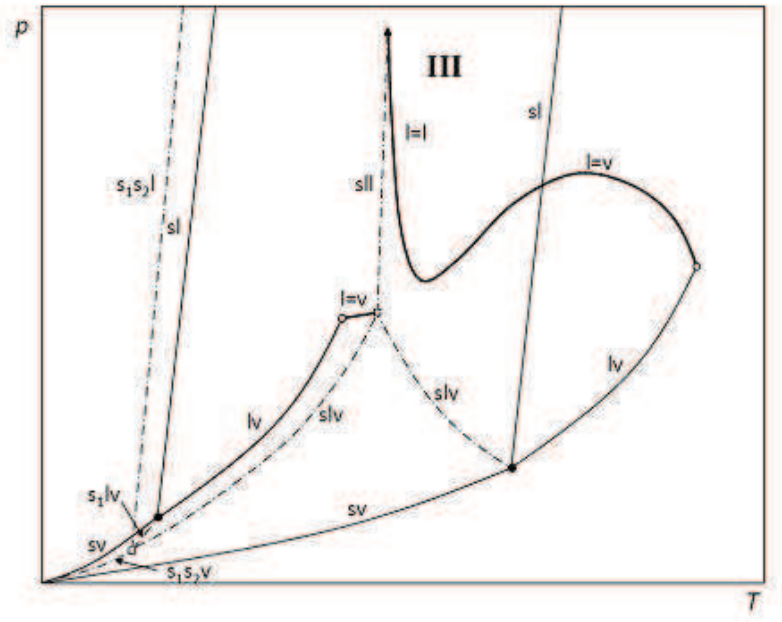

Figure B.9: Qualitative PT-EP for type IIIb including the solid-solid equilibrium.

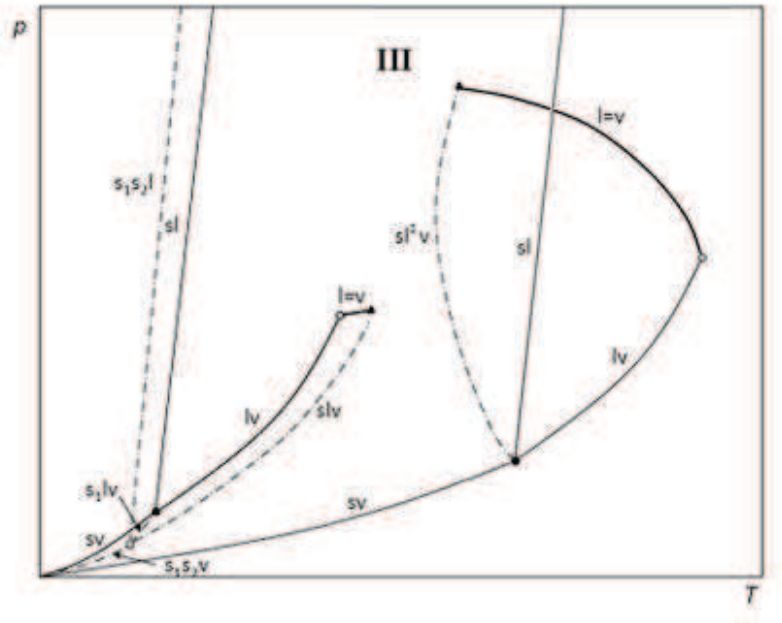

Figure B.10: Qualitative PT-EP for type IIIc including the solid-solid equilibrium.

1.1.3 Type IV PT-EP

The qualitative PT-EP for type IV systems as presented in van Konynenburg and Scott [1] is shown in Figure B.11. This phase behavior is typical of systems as methane – n-hexane, benzene – polyisobutene, and cyclohexane – polystyrene.

As shown in Figure B.11, the PT-EP of type IV for the fluid phases presents three critical line. The first exits the critical point of the less volatile component as liquid-vapor critical line and changes to a liquid$_1$-liquid$_2$ critical line at lower temperatures. The second critical line starts from the critical point of component 1. These two critical lines join at its LCEP and UCEP, respectively, a liquid$_1$-liquid$_2$-vapor line. The third critical line is a liquid$_1$-liquid$_2$ critical line extending from the UCEP of the second liquid$_1$-liquid$_2$-vapor line, placed at lower temperatures and pressures than the other one.

Figure B.12 represents the presence of a solid phase in the type IV PT-EP of Figure B.11. The triple point curve is split in two branches: solid-liquid$_1$-vapor and solid-liquid$_2$-vapor. These two branches join together in a quadruple point, where four phases coexist: solid, liquid$_1$, liquid$_2$, and vapor. A solid-liquid$_1$-liquid$_2$ curve exits the quadruple point and it joins at its UCEP the liquid-liquid critical curve (at high pressures). The "lower" liquid$_1$-liquid$_2$-vapor curve in Figure B.11 joins the quadruple point.

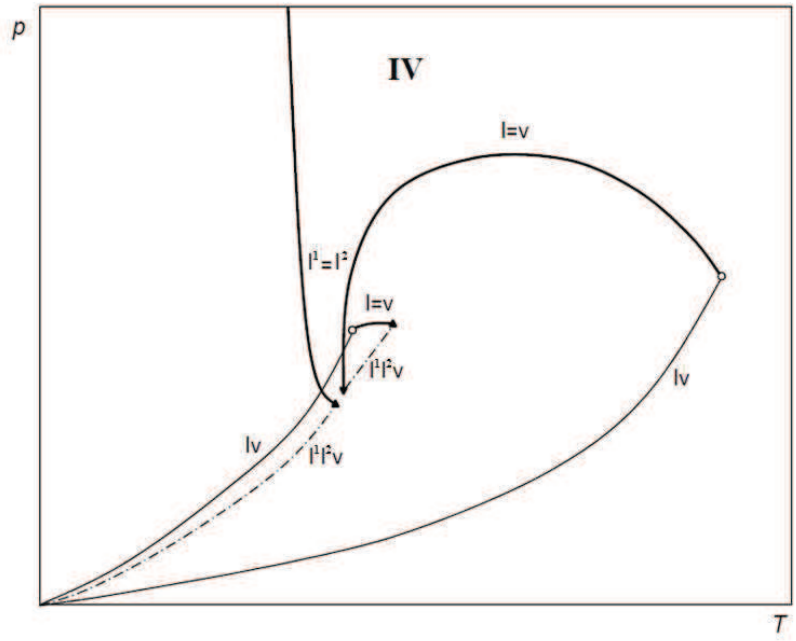

Figure B.11: Qualitative PT-EP for type IV systems as presented in van Konynenburg and Scott **[1]**.

The presence of the solid phase in type IV diagrams has been studied by Garcia and Lucks [2]. They have attributed this behavior to binary systems with both "upper" and "lower" liquid-liquid-vapor branches.

As seen for the type III, the solid-liquid$_1$-liquid$_2$ branch can increase progressively till joining the quadruple point with the liquid-vapor critical line that extends from the critical point of the first component, Figure B.13.

In this case, classified as IV*, at the quadruple point the critical conditions between the liquid2 and the vapor phases holds.

Furthermore, the liquid-liquid part of the first critical line, that exits the critical point of component 2, moves up to higher temperature, and the solid-liquid$_1$-liquid$_2$ curve joins always at its UCEP the liquid-liquid critical line.

The corresponding diagram with the presence of the solid phase is shown in Figure B.14.

Shaw and Béhar [6] studied the solidification of the solute in a Type IV* binary mixture, while Zou and Shaw [7] presented the phase behavior of type IV* systems including solids.

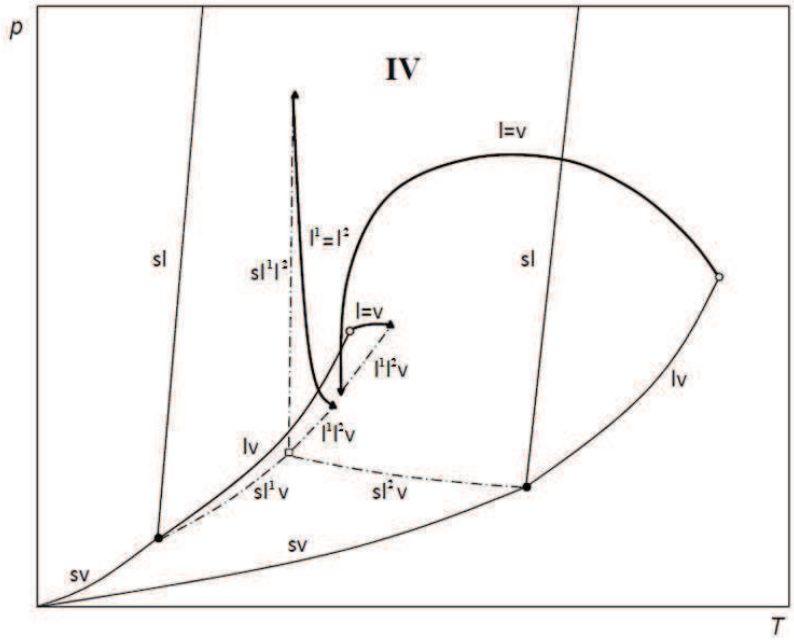

Figure B.12: Qualitative PT-EP for type IV including the solid phase.

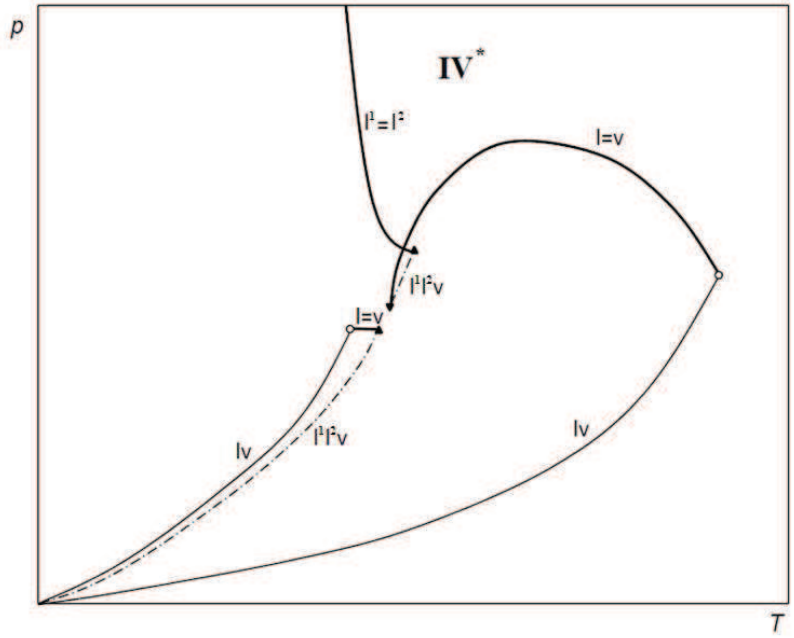

Figure B.13: Qualitative PT-EP for type IV* systems as presented in van Konynenburg and Scott **[1]**.

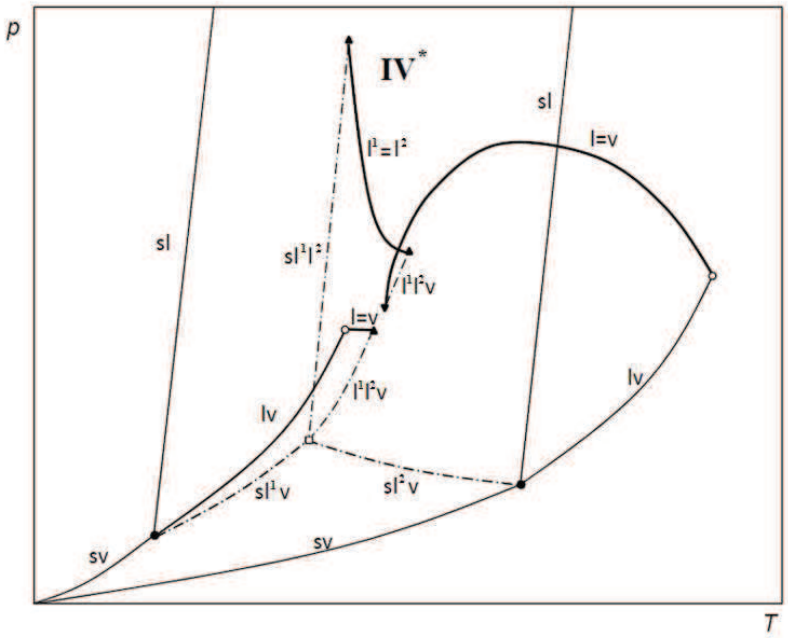

Figure B.14: Qualitative PT-EP for type IV* including the solid phase.

Figure B.15-Figure B.16 shown the equilibrium projections presented in Figure B.12 and Figure B.14 in case of solid-solid equilibrium.

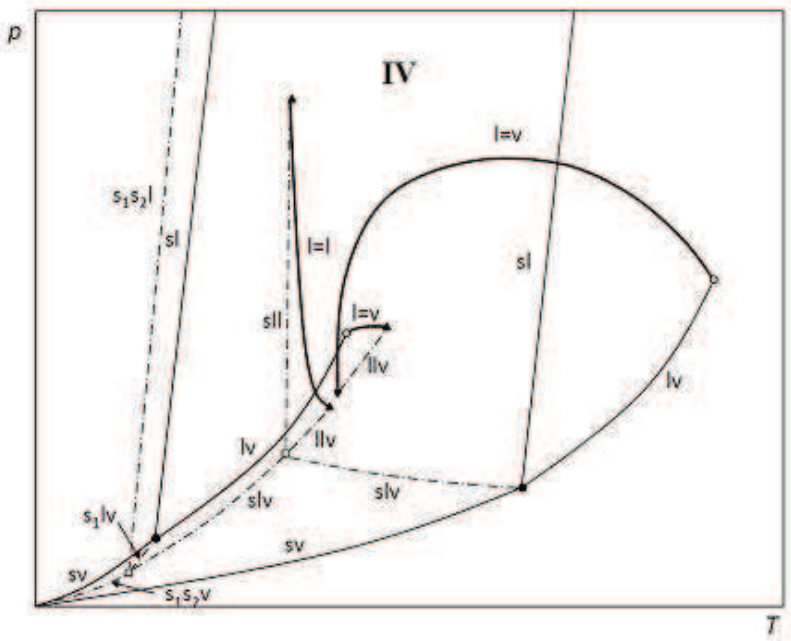

Figure B.15: Qualitative PT-EP for type IV including the solid-solid equilibrium.

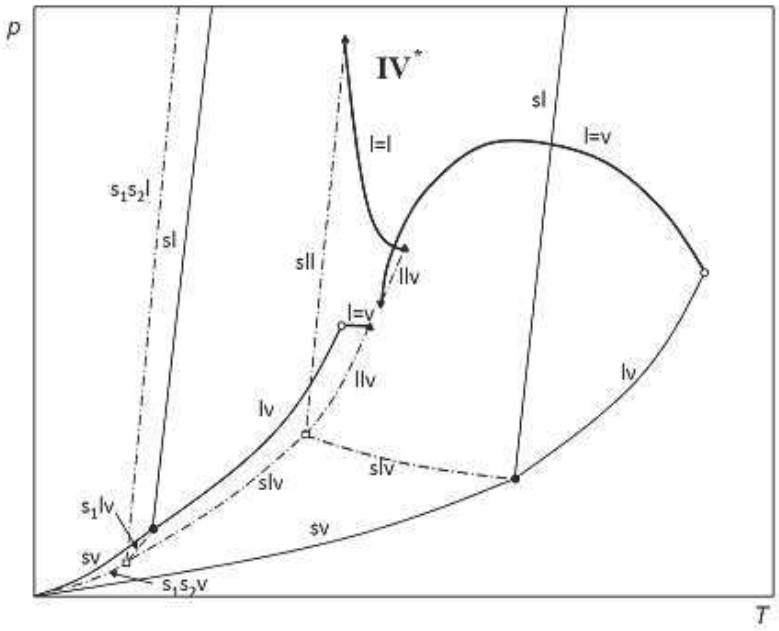

Figure B.16: Qualitative PT-EP for type IV* including the solid-solid equilibrium.

1.1.4 Type V PT-EP

The qualitative PT-EP for type V systems as presented in van Konynenburg and Scott [1] is shown in Figure B.17, while Figure B.18 presents the PT-EP of type V including the solid phase.

Type V PT-EP corresponds to a type IV projection without the upper liquid$_1$-liquid$_2$-vapor branch, see Figure B.11. Therefore the presence of the solid phase gives origin to a continuous solid-liquid-vapor curve extending from the triple point of component 1 to the triple point of component 2. Type V PT-EP including the solid phase has been studied in literature by Shaw and Béhar [6] and by Zou and Shaw [7].

Figure B.19 presents the type I PT-EP in presence of immiscibility in the solid phase.

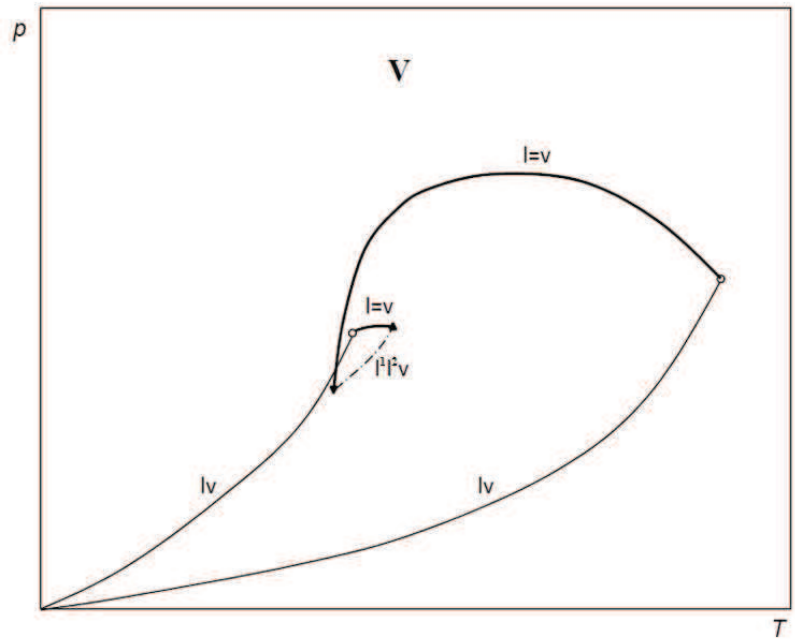

Figure B.17: Qualitative PT-EP for type V systems as presented in van Konynenburg and Scott **[1]**.

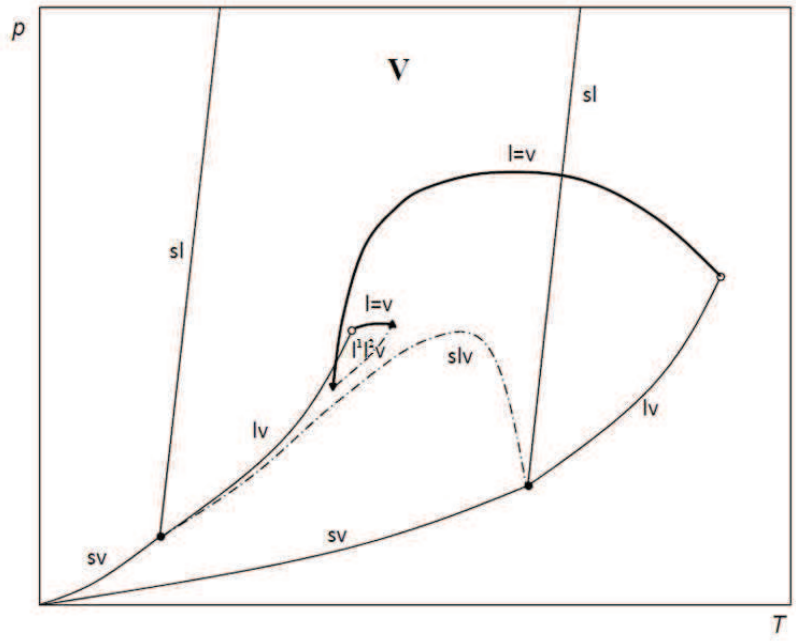

Figure B.18: Qualitative PT-EP for type V including the solid phase.

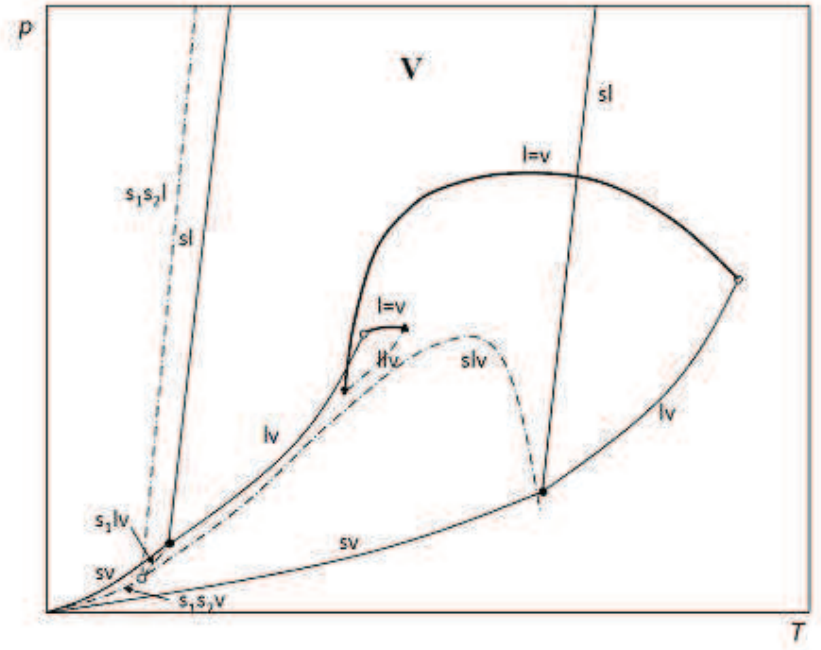

Figure B.19: Qualitative PT-EP for type V including the solid-solid equilibrium.

1.1.5 Type VI PT-EP

The qualitative PT-EP for type VI systems as presented in van Konynenburg and Scott [1] is shown in Figure B.20, while Figure B.21 presents the PT-EP of type V including the solid phase.

In Figure B.20 it can be seen that a type VI corresponds a the type I projection, wherein there are two more lines. A liquid-liquid-vapor curve exists between the vapor pressure curves of the pure components, and, a second critical curve exists; it is a liquid-liquid critical curve joining the LCEP and the UCEP of the liquid-liquid-vapor curve.

No examples of type VI projection including the solid phase have been found in the literature. Nevertheless, the absence of a lower liquid-liquid-vapor equilibrium curve let think to the presence of a continuous solid-liquid-vapor curve joining the triple points of the pure components, as shown in Figure B.21. Figure B.22 presents the type I PT-EP in presence of immiscibility in the solid phase.

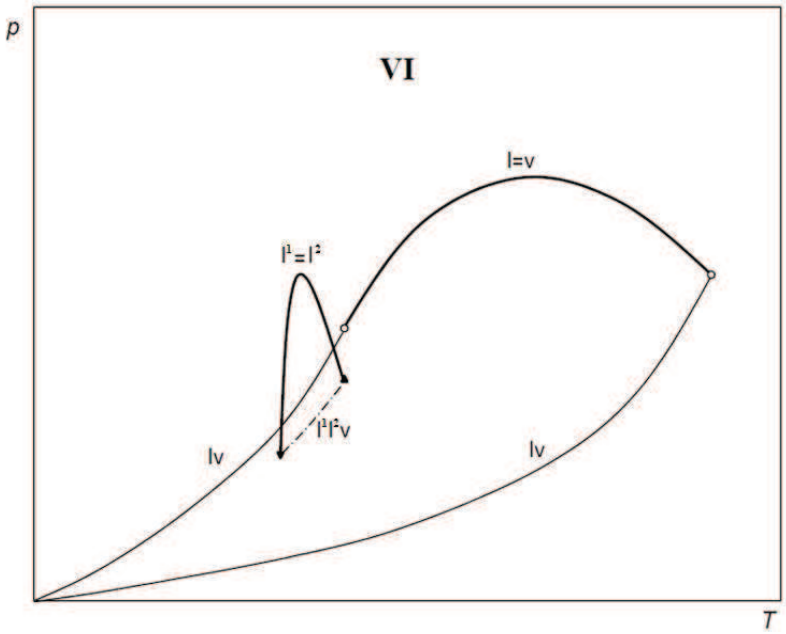

Figure B.20: Qualitative PT-EP for type VI systems as presented in van Konynenburg and Scott **[1]**.

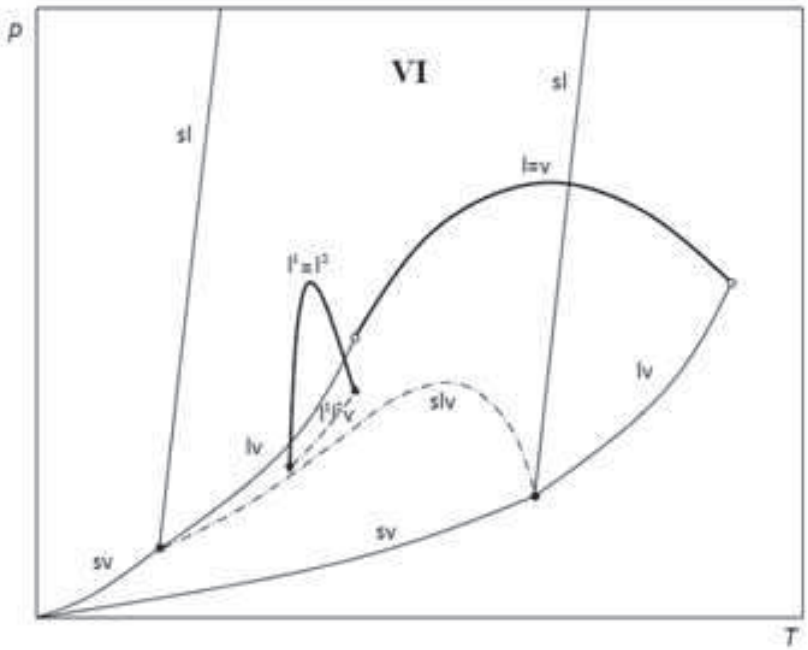

Figure B.21: Qualitative PT-EP for type VI including the solid phase.

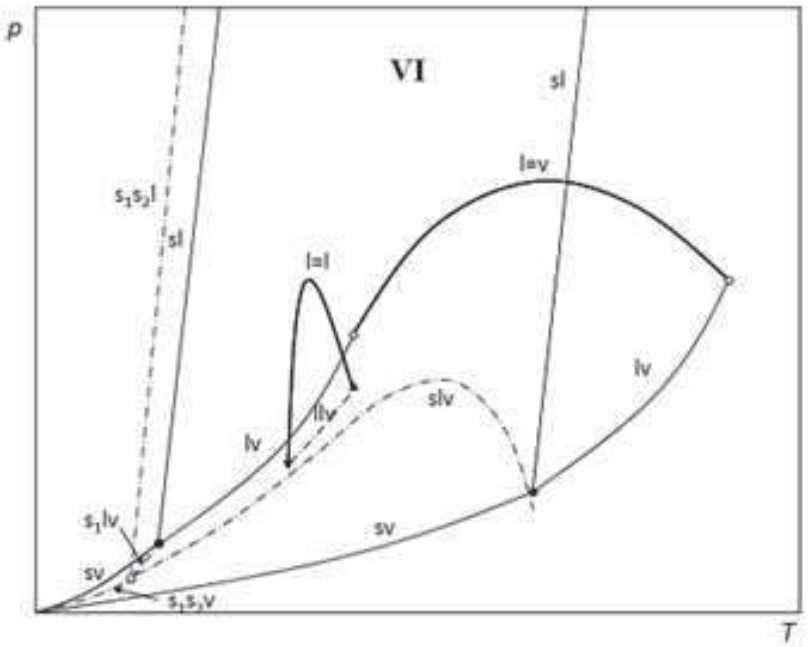

Figure B.22: Qualitative PT-EP for type VI including the solid-solid equilibrium.

Bibliography

[1] P. van Konynenburg e R. Scott, «Critical lines and phase equilibria in binary van der Waals mixtures,» *Phil. Trans. R. Soc. Lond. A,* vol. 298, p. 495–540, 1980.

[2] D. Garcia e K. Lucks, «Patterns of solid – fluid phase equilibria: new possibilities?,» *Fluid Phase Equilibria,* vol. 161, pp. 91-106, 1999.

[3] T. de Loos, «On the phase behaviour of asymmetric systems: the three-phase curve solid–liquid–gas,» *J. of Supercritical Fluids,* vol. 39, p. 154–159, 2006.

[4] E. Flöter, T. de Loos e J. de Swaan Arons, «High pressure solid–fluid and vapour–liquid equilibria in the system (methane+tetracosane),» *Fluid Phase Equilibria,* vol. 127, pp. 129-146, 1997.

[5] A. Scurto, G. Xu, J. Brennecke e M. Stadtherr, «Phase behavior and reliable computation of high pressure solid – fluid equilibrium with cosolvents,» *Ind. Eng. Chem. Res.,* vol. 42, p. 6464–6475, 2003.

[6] J. Shaw e E. Béhar, «SLLV phase behavior and phase diagram transitions in asymmetric hydrocarbon fluids,» *Fluid Phase Equilibria,* vol. 209, p. 185–206, 2003.

[7] X.-Y. Zou e J. Shaw, «Phase behavior of hydrocarbon mixtures,» in *Encyclopedia of Chemical Processing*, Taylor & Francis, 2007.

[8] S. Pasquetto e L. Patrone, Chimica Fisica: stati di aggregazione-termodinamica chimica-equilibri di fase, VI a cura di, Italia: Zanichelli, 1997.

[9] J. D. v. d. Waals, Doctoral Dissertation, Leiden, 1873.

Appendix C

MODELING METHODS FOR SOLID-FLUID EQUIBRIUM

LIST OF FIGURES C2

1 FUNDAMENTAL THERMODYNAMIC RELATIONS C3
2 SOLID-FLUID EQUILIBRIUM MODELS C6
2.1 Classical Approach (CA) C6
2.1.1 CA from the Fundamental Property Relation C7
2.1.2 CA from the Gibbs State Function C8
2.1.3 Soave C11
2.1.4 Twu et al. C12
2.1.5 Rodriguez-Reartes et al. C13
2.1.6 Coutinho et al. C14
2.2 Modified Cubic Equation of State (MCEoS) C16
2.2.1 Kan C16
2.2.2 Wenzel and Schmidt C17
2.2.3 Rodriguez et al. C17
2.3 System of Cubic Equations of State (SCEoSs) C18
2.4 Molecular Association (MA) C18
2.5 Quartic Equation of State (QEoS) C20
2.5.1 Theorical limits of the Yokozeki EoS C22
2.6 Insertion Probability (IP) C25
2.7 Unified Lattice Fluid Equation of State (ULFEoS) C26
2.8 Thermodynamic Perturbation Theory (TPT) C27
2.8.1 Tan et al. C28
2.8.2 Cochran and Chiew C28

BIBLIOGRAPHY C29

List of Figures

Figure C.1: Qualitative Pressure-Temperature Equilibrium Projection of a pure compound. C6
Figure C.2: Path 1: SLE from liquid and solid fugacities..... C6
Figure C.3: Path 2: SLE from entropy and enthalpy variations..... C6
Figure C.4: Qualitative Pressure-Temperature Equilibrium Projection of a long-chain n-alkane with two solid phases. C14
Figure C.5: Schematic isothermal *P*-*v* diagram of the Yokozeki EoS with *k* = odd at the triple point and *v*>*b*. C21
Figure C.6: Schematic isothermal *P*-*v* diagram of the Yokozeki EoS with *k* = even at the triple point and *v*>*b*..... C21
Figure C.7: Function *a*(*T*) for argon, [26]. C21
Figure C.8: Function *b*(*T*) for argon, [26]. C21
Figure C.9: Qualitative behavior of the function 1/(v-c). C23
Figure C.10: Qualitative behavior of the function $1/(v-c)^2$..... C23
Figure C.11: Qualitative insertion probability of the QEoS with *a* = 0 and *k* = 1. ..... C24
Figure C.12: Correlated cell proposed by Alder, [36]. C25
Figure C.13: Qualitative insertion probability by the IP model for SFE. C26
Figure C.14: Qualitative subcritical pressure-density phase diagrams from IP. C26

1 Fundamental thermodynamic relations

This first part of Appendix C concerns the mathematical steps involved in deriving fundamental thermodynamic relations which can be applied to account for phase equilibria.

In a multiphase system of j components, the total Gibbs energy G of a generic α phase can be expressed as follows:

$$G^{\alpha} = n^{\alpha} g^{\alpha} = f\left(P, T, n_1^{\alpha}, n_2^{\alpha}, \ldots, n_j^{\alpha}\right) \qquad (C1)$$

In eq. (C1), g^{α} is the molar Gibbs free energy, and $n_i{}^{\alpha}$ indicates the moles of component i in the phase α. The total differential of G^{α} results in a Fundamental Property Relation (*FPR*), eq. (C2), in which the molar entropy s, the molar volume v, and the chemical potential μ replace the derivatives.

$$dG^{\alpha} = \left(\frac{\partial G^{\alpha}}{\partial T}\right)_{P,n_j} dT + \left(\frac{\partial G^{\alpha}}{\partial P}\right)_{T,n_j} dP + \sum_{i=1}^{j} \left(\frac{\partial G^{\alpha}}{\partial n_i}\right)_{T,P,n_j} dn_i = -n^{\alpha} s^{\alpha} dT + n^{\alpha} v^{\alpha} dP + \sum_{i=1}^{j} \mu_i^{\alpha} dn_i^{\alpha} \qquad (C2)$$

Fundamental Property Relation dG=f(T,P,n)	$dG^{\alpha} = -S^{\alpha} dT + V^{\alpha} dP + \sum_{i=1}^{j} \mu_i^{\alpha} dn_i^{\alpha}$ (C3)

An important consequence of the *FPR* is that μ represents the partial molar Gibbs free energy, eq. (C4), that is the variation of G with changes in the molar composition of i in the phase at constant temperature, pressure, and composition of the other components.

$$\mu_i^{\alpha} = \left(\frac{\partial G^{\alpha}}{\partial n_i}\right)_{T,P,n_j} = \bar{G}_i^{\alpha} \qquad (C4)$$

A different but equivalent expression for the *FPR*, eq. (C9), can be obtained considering the differential of the ratio G/RT, where R is the has constant and T the temperature.

$$d\left(\frac{G^{\alpha}}{RT}\right) = \frac{1}{RT} d(G^{\alpha}) + \frac{G^{\alpha}}{R} d\left(\frac{1}{T}\right) \qquad (C5)$$

By introducing eq. (C2) for dG^{α} and remembering that $G = H - TS$, eq. (C5) becomes:

$$d\left(\frac{G^{\alpha}}{RT}\right) = \frac{1}{RT}\left(-n^{\alpha} s^{\alpha} dT + n^{\alpha} v^{\alpha} dP + \sum_{i=1}^{j} \mu_i^{\alpha} dn_i^{\alpha}\right) + \frac{(H^{\alpha} - TS^{\alpha})}{R}\left(-\frac{1}{T^2}\right) dT \qquad (C6)$$

$$d\left(\frac{G^{\alpha}}{RT}\right) = -\frac{n^{\alpha} s^{\alpha}}{RT} dT + \frac{n^{\alpha} v^{\alpha}}{RT} dP + \frac{1}{RT} \sum_{i=1}^{j} \mu_i^{\alpha} dn_i^{\alpha} - \frac{n^{\alpha} h^{\alpha}}{RT^2} dT + \frac{n^{\alpha} s^{\alpha}}{RT} dT \qquad (C7)$$

$$d\left(\frac{G^{\alpha}}{RT}\right) = \frac{n^{\alpha} v^{\alpha}}{RT} dP - \frac{n^{\alpha} h^{\alpha}}{RT^2} dT + \frac{1}{RT} \sum_{i=1}^{j} \mu_i^{\alpha} dn_i^{\alpha} \qquad (C8)$$

Fundamental Property Relation dG=f(T,P,n)	$d\left(\frac{G^{\alpha}}{RT}\right) = \frac{V^{\alpha}}{RT} dP - \frac{H^{\alpha}}{RT^2} dT + \sum_{i=1}^{j} \frac{\mu_i^{\alpha}}{RT} dn_i^{\alpha}$ (C9)

Removing the Ideal Gas (*ig*) contribution from eq. (C9) leads to the residual form of the *FPR*, eq. (C11)

$$d\left(\frac{G^{\alpha}}{RT}\right)-d\left(\frac{G^{\alpha,id}}{RT}\right)=\frac{V^{\alpha}-V^{\alpha,ig}}{RT}dP-\frac{H^{\alpha}-H^{\alpha,ig}}{RT^{2}}dT+\sum_{i=1}^{j}\frac{\mu_i^{\alpha}-\mu_i^{\alpha.ig}}{RT}dn_i^{\alpha} \qquad (C10)$$

$$d\left(\frac{G^{\alpha,R}}{RT}\right)=-\frac{H^{\alpha,R}}{RT^{2}}dT+\frac{V^{\alpha,R}}{RT}dP+\sum_{i=1}^{j}\frac{\mu_i^{\alpha,R}}{RT}dn_i^{\alpha} \qquad (C11)$$

By comparing eq. (C11) with the second term of eq. (C2) it can be inferred that:

$$-\frac{H^{\alpha,R}}{RT^{2}}=\frac{\partial}{\partial T}\left(\frac{G^{\alpha,R}}{RT}\right)_{P,n_j} \quad , \quad \frac{V^{\alpha,R}}{RT}dP=\frac{\partial}{\partial P}\left(\frac{G^{\alpha,R}}{RT}\right)_{T,n_j} \qquad (C12)$$

The first identity in eq. (12) represents the residual form of the Gibbs-Helmholtz equation. Furthermore, the residual μ can be examined in terms of the partial molar *G*, eq. (C13), and in terms of fugacity *f*, eq. (C14).

$$\frac{\mu_i^{\alpha,R}}{RT}=\frac{\mu_i^{\alpha}-\mu_i^{\alpha.ig}}{RT}=\frac{\bar{G}_i^{\alpha}-\bar{G}_i^{\alpha,ig}}{RT}=\frac{\bar{G}_i^{\alpha,R}}{RT} \qquad (C13)$$

$$\frac{\mu_i^{\alpha,R}}{RT}=\frac{\mu_i^{\alpha}-\mu_i^{\alpha.ig}}{RT}=\frac{RTln\hat{f}_i^{\alpha}-RTln\hat{f}_i^{\alpha,ig}}{RT}=ln\frac{\hat{f}_i^{\alpha}}{y_i^{\alpha}P}=ln\hat{\varphi}_i^{\alpha} \qquad (C14)$$

In eq. (C14), *y* is the composition in the ideal gas, φ is the fugacity coefficient, and *P* the system pressure. Combining eqs. (C13)-(C14) yields the relation between partial molar *G* and fugacity coefficient of component *i* in the multicomponent phase α, eq. (C15), thus the final version of the residual *FPR* is eq. (C16)

Partial molar fugacity coefficient	$\frac{\bar{G}_i^{\alpha,R}}{RT}=\frac{\partial}{\partial n_i}\left(\frac{G^{\alpha,R}}{RT}\right)_{T,P,n_j}=ln\hat{\varphi}_i^{\alpha}$ (C15)

Fundamental Residual-Property Relation $dG^R=f(T,P,n)$	$d\left(\frac{G^{\alpha,R}}{RT}\right)=-\frac{H^{\alpha,R}}{RT^{2}}dT+\frac{V^{\alpha,R}}{RT}dP+\sum_{i=1}^{j}ln\hat{\varphi}_i^{\alpha}dn_i^{\alpha}$ (C16)

Following the procedure of eq. (C10)-(C14), the excess form of the *FPR*, eq. (C18), is obtained by removing the Ideal Mixture (*idmix*) contribution from eq. (C9).

$$d\left(\frac{G^{\alpha}}{RT}\right)-d\left(\frac{G^{\alpha,idmix}}{RT}\right)=\frac{V^{\alpha}-V^{\alpha,idmix}}{RT}dP-\frac{H^{\alpha}-H^{\alpha,idmix}}{RT^{2}}dT+\sum_{i=1}^{j}\frac{\mu_i^{\alpha}-\mu_i^{\alpha.idmix}}{RT}dn_i^{\alpha} \qquad (C17)$$

$$d\left(\frac{G^{\alpha,E}}{RT}\right)=-\frac{H^{\alpha,E}}{RT^{2}}dT+\frac{V^{\alpha,E}}{RT}dP+\sum_{i=1}^{j}\frac{\mu_i^{\alpha,E}}{RT}dn_i^{\alpha} \qquad (C18)$$

The last term of eq. (C18) can be expressed in term of activity coefficient, γ, remembering the definition of excess partial molar *G*, eq. (C19)

$$\bar{G}_i^{\alpha,E}=\bar{G}_i^{\alpha}-\bar{G}_i^{\alpha,idmix}=\mu_i^{\alpha,E}=RTln\hat{f}_i^{\alpha}-RTln\hat{f}_i^{\alpha,idmix}=RTln\frac{\hat{f}_i^{\alpha}}{x_i^{\alpha}f_i^{0}}=RTln\gamma_i^{\alpha} \qquad (C19)$$

In eq. (C19), x is the composition in the ideal multicomponent phase, γ is the activity coefficient, and $f_i^{\,0}$ is the fugacity of the pure component at the system temperature and pressure. eq. (C20), the relation between partial molar excess G_i and activity coefficient of component i in the multicomponent phase α, follows from eq. (C19). The final version of the excess *FPR* is then eq. (C21).

Partial molar activity coefficient	$\frac{\bar{G}_i^{\alpha,E}}{RT} = \frac{\partial}{\partial n_i}\left(\frac{G^{\alpha,E}}{RT}\right)_{T,P,n_j} = ln\gamma_i^{\alpha}$	$(C20)$

Fundamental Excess-Property Relation dG^E=f(T,P,n)	$d\left(\frac{G^{\alpha,E}}{RT}\right) = -\frac{H^{\alpha,E}}{RT^2}dT + \frac{V^{\alpha,E}}{RT}dP + \sum_{i=1}^{j} ln\gamma_i^{\alpha} dn_i^{\alpha}$	$(C21)$

Eqs. (C15) and (C20) assert that $ln\hat{\varphi}_i^{\alpha}$ and $ln\gamma_i^{\alpha}$ are the partial molar properties with respect to $G^{\alpha,R}/RT$ and $G^{\alpha,E}/RT$, respectively. It follows that:

$$\frac{G^{\alpha,R}}{RT} = \sum_{i=1}^{j} n_i \frac{\bar{G}_i^{\alpha,R}}{RT} = \sum_{i=1}^{j} n_i ln\hat{\varphi}_i^{\alpha} \quad , \quad \frac{G^{\alpha,E}}{RT} = \sum_{i=1}^{j} n_i \frac{\bar{G}_i^{\alpha,E}}{RT} = \sum_{i=1}^{j} n_i ln\gamma_i^{\alpha} \qquad (C22)$$

The total differential of the expressions in eq. (C22) are summarized in eq. (C23).

$$d\left(\frac{G^{\alpha,R}}{RT}\right) = \sum_{i=1}^{j} n_i dln\hat{\varphi}_i^{\alpha} + \sum_{i=1}^{j} ln\hat{\varphi}_i^{\alpha} dn_i \quad , \quad d\left(\frac{G^{\alpha,E}}{RT}\right) = \sum_{i=1}^{j} n_i dln\gamma_i^{\alpha} + \sum_{i=1}^{j} ln\gamma_i^{\alpha} dn_i \qquad (C23)$$

Eq. (C24) represents the Gibbs-Duhem Equation in terms of residual properties obtained comparing the first identity of eq. (C23) and the *FPR* in eq. (C16). The Gibbs-Duhem Equation in terms of excess properties, eq. (C25), derives from the comparison between the second identity of eq. (C23) and the *FPR* in eq. (C21).

Residual Gibbs-Duhem Equation	$\sum_{i=1}^{j} n_i dln\hat{\varphi}_i^{\alpha} = \sum_{i=1}^{j} n_i d\left(\frac{\bar{G}_i^{\alpha,R}}{RT}\right) = \frac{V^{\alpha,R}}{RT}dP - \frac{H^{\alpha,R}}{RT^2}dT$	$(C24)$

Excess Gibbs-Duhem Equation	$\sum_{i=1}^{j} n_i dln\gamma_i^{\alpha} = \sum_{i=1}^{j} n_i d\left(\frac{\bar{G}_i^{\alpha,E}}{RT}\right) = \frac{V^{\alpha,E}}{RT}dP - \frac{H^{\alpha,E}}{RT^2}dT$	$(C25)$

Eqs. (C3), (C9), and (C16) give eqs. (C26)-(C28) when dealing with pure compounds.

Fundamental Property Relation dG=f(T,P)	$dG^{\alpha} = -S^{\alpha}dT + V^{\alpha}dP$	$(C26)$

Fundamental Property Relation dG=f(T,P)	$d\left(\frac{G^{\alpha}}{RT}\right) = \frac{V^{\alpha}}{RT}dP - \frac{H^{\alpha}}{RT^2}dT$	$(C27)$

Fundamental Residual-Property Relation dG^R=f(T,P)	$d\left(\frac{G^{\alpha,R}}{RT}\right) = -\frac{H^{\alpha,R}}{RT^2}dT + \frac{V^{\alpha,R}}{RT}dP$	$(C28)$

2 Solid-fluid equilibrium models

The second part of Appendix C provides a detailed description of the Solid-Fluid Equilibrium (SFE) models presented in chapter 3. These SFE models have been classified on the basis of the device used to tackle the problem of representing the solid phase. The resulting categories are Classical Approach (*CA*), Modified Cubic Equation of State (*MCEoS*), System of Cubic Equations of States (*SCEoSs*), Molecular Association (*MA*), Quartic Equation of State (*QEoS*), Insertion Probability (*IP*), Unified Lattice Fluid Equation of State (*ULFEoS*), and Thermodynamic Perturbation Theory (*TPT*).

2.1 Classical Approach (*CA*)

The classical approach used for relating the solid and liquid fugacities in a pure compound system can be obtained from classical thermodynamic relations.

With reference to the qualitative Pressure-Temperature Equilibrium Projection (*PT-EP*) of Figure C.1, the relation between the fugacities of the solid and liquid phases at melting temperature T and pressure P can be derived either from the paths of Figure C.2 Figure C.3. As it has been shown later by mathematical steps, the final relation is the same, independently from the path.

Path 1 in Figure C.2 consists in obtaining the liquid and solid fugacities starting from the triple point conditions, whereas path 2 in Figure C.3 considers all the entropy and enthalpy variations between solid and liquid at melting passing through the triple point phases.

Each vertical line of paths 1 and 2 involves an isothermal step and an isobaric step. In path 1 the pressure and temperature variations are evaluated in terms of fugacity, in path 2 in terms of enthalpy and entropy.

In path 2, the horizontal line represents the solid-liquid transition at the triple point, which occurs at constant temperature and pressure.

In the framework of path 1, the solid and liquid fugacities at melting are evaluated starting from the Fundamental Property Relation (*FPR*) of a pure compound system, eq. (C27).

On the other hand, the differential of the Gibbs State Function (*GSF*) is considered to examine all the steps within path 2.

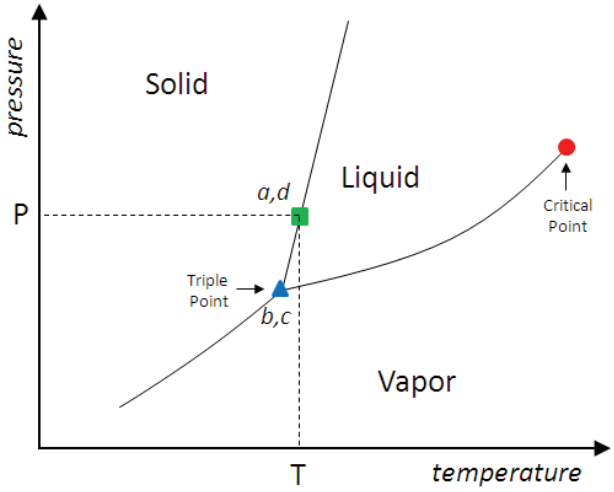

Figure C.1: Qualitative Pressure-Temperature Equilibrium Projection of a pure compound.
— : equilibrium branches; ● : critical point; ▲ : triple point; ■ : solid-liquid equilibrium; P : melting pressure; T : melting temperature; a,d : solid and liquid phases at P, T; b,c : solid and liquid phases the triple point.

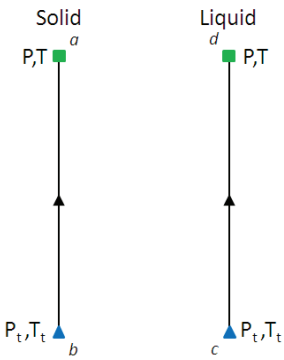

Figure C.2: Path 1: SLE from liquid and solid fugacities.

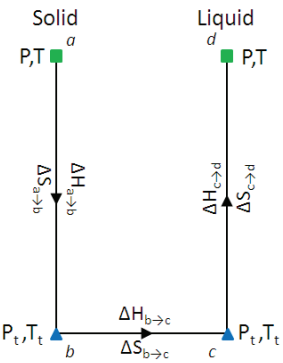

Figure C.3: Path 2: SLE from entropy and enthalpy variations.

Pt : triple point pressure; Tt : triple point temperature.

2.1.1 CA from the Fundamental Property Relation

The *FPR* (in terms of volume *V* and enthalpy *H*) of a pure compound in a generic α phase is reported in eq. (C29) for the reader convenience. In eq. (C29), the last terms have been added considering the relation between Gibbs free energy *G*, chemical potential μ, and fugacity *f*. The superscript *0* stresses the validity of eq. (C29) for a pure compound.

$$d\left(\frac{G^\alpha}{RT}\right) = \frac{V^\alpha}{RT}dP - \frac{H^\alpha}{RT^2}dT = d\left(\frac{\mu^\alpha}{RT}\right) = d\left(\frac{RTlnf^{\alpha,0}}{RT}\right) = d(lnf^{\alpha,0}) \qquad (C29)$$

The variation of the total Gibbs free energy in an isothermal and an isobaric step are represented by the first and the second identity of eq. (C30), respectively.

$$\left(\frac{dlnf^{\alpha,0}}{dP}\right)_T = \frac{V^\alpha}{RT} \quad , \quad \left(\frac{dlnf^{\alpha,0}}{dT}\right)_P = -\frac{H^\alpha}{RT^2} \qquad (C30)$$

From the terms in eq. (C30) it follows that the variation of the fugacity in the phase α from the point (P_1,T_1) to the point (P_2,T_2) is:

$$\iint_{P_1T_1}^{P_2T_2} dlnf^{\alpha,0}\,dTdP = \int_{P_1}^{P_2}\frac{V^\alpha}{RT}dP + \int_{T_1}^{T_2} -\frac{H^\alpha}{RT^2}dT \qquad (C31)$$

With the assumptions within eq. (C32), eq. (C31) becomes eq. (C35) after resolution of the integrals.

$$V^\alpha_{P1,T1} = V^\alpha_{P2,T2} \qquad H^\alpha = H^\alpha_{P1,T1} + Cp^\alpha(T - T_1) \qquad Cp^\alpha_{P1,T1} = Cp^\alpha_{P2,T2} \qquad (C32)$$

$$\boldsymbol{ln\frac{f^{\alpha,0}(P_2,T_2)}{f^{\alpha,0}(P_1,T_1)}} = \frac{V^\alpha_{P1,T1}}{RT}\int_{P_1}^{P_2} dP - \frac{1}{R}\int_{T_1}^{T_2}\frac{H^\alpha_{P1,T1}}{T^2}dT - \frac{1}{R}\int_{T_1}^{T_2}\frac{Cp^\alpha_{P1,T1}(T-T_1)}{T^2}dT = \qquad (C33)$$

$$= \frac{V^\alpha_{P1,T1}(P_2-P_1)}{RT} - \frac{H^\alpha_{P1,T1}}{R}\left(-\frac{1}{T_2}+\frac{1}{T_1}\right) - \frac{Cp^\alpha_{P1,T1}}{R}\left[ln\left(\frac{T_2}{T_1}\right)+\frac{T_1}{T_2}-1\right] = \qquad (C34)$$

$$= \boldsymbol{\frac{V^\alpha_{P1,T1}(P_2-P_1)}{RT} + \frac{H^\alpha_{P1,T1}}{RT_1}\left(\frac{T_1}{T_2}-1\right) - \frac{Cp^\alpha_{P1,T1}}{R}\left[\frac{T_1}{T_2}-1-ln\left(\frac{T_1}{T_2}\right)\right]} \qquad (C35)$$

Eq. (C35) can be applied independently to the solid and liquid fugacities from the triple point temperature and pressure, *Tt* and *Pt*, up to the melting temperature and pressure, *T* and *P*, according to path 1 in Figure C.2. Results are summarized in eq. (C36) for the liquid phase and in eq. (C37) the solid phase.

$$ln\frac{f^{L,0}(P,T)}{f^{L,0}(P_t,T_t)} = \frac{V^L_{Pt,Tt}(P-P_t)}{RT} + \frac{H^L_{Pt,Tt}}{RT_t}\left(\frac{T_t}{T}-1\right) - \frac{Cp^L_{Pt,Tt}}{R}\left[\frac{T_t}{T}-1-ln\left(\frac{T_t}{T}\right)\right] \qquad (C36)$$

$$ln\frac{f^{S,0}(P,T)}{f^{S,0}(P_t,T_t)} = \frac{V^S_{Pt,Tt}(P-P_t)}{RT} + \frac{H^S_{Pt,Tt}}{RT_t}\left(\frac{T_t}{T}-1\right) - \frac{Cp^S_{Pt,Tt}}{R}\left[\frac{T_t}{T}-1-ln\left(\frac{T_t}{T}\right)\right] \qquad (C37)$$

Removing eq. (C37) from eq. (C36), considering the isofugacity condition between the solid and the liquid phases at the triple point, results in the following:

$$ln\frac{f^{L,0}(P,T)}{f^{S,0}(P,T)} = \frac{\left(H^{L}_{Pt,Tt} - H^{S}_{Pt,Tt}\right)}{RT_t}\left(\frac{T_t}{T} - 1\right) - \frac{\left(Cp^{L}_{Pt,Tt} - Cp^{S}_{Pt,Tt}\right)}{R}\left[\frac{T_t}{T} - 1 - ln\left(\frac{T_t}{T}\right)\right] + \frac{\left(V^{L}_{Pt,Tt} - V^{S}_{Pt,Tt}\right)(P - P_t)}{RT} \quad (C38)$$

$$ln\frac{f^{L,0}(P,T)}{f^{S,0}(P,T)} = \frac{\Delta H^{SLE}_{Pt,Tt}}{RT_t}\left(\frac{T_t}{T} - 1\right) - \frac{\Delta Cp^{SLE}_{Pt,Tt}}{R}\left[\frac{T_t}{T} - 1 - ln\left(\frac{T_t}{T}\right)\right] + \frac{\Delta V^{SLE}_{Pt,Tt}(P - P_t)}{RT} \quad (C39)$$

Eq. (C39) is the *CA* equation expressing the relation between solid and liquid fugacity for a pure compound obtained following path 1 in Figure C.2. All the properties involved in this equation are triple point properties, due to the assumptions made in eq. (C32).

2.1.2 CA from the Gibbs State Function

The difference between liquid and solid chemical potentials at melting is related to the total Gibbs energy variation upon fusion, eq. (C40).

$$\mu^{L,0}(T,P) - \mu^{S,0}(T,P) = \Delta G^{SLE}_{P,T} = RTln\frac{f^{L,0}(P,T)}{f^{S,0}(P,T)} \quad (C40)$$

The Gibbs State Function, *GSF*, and the differential of the Gibbs energy in terms of temperature and pressure are expressed in eq. (C41) and eq. (C42), respectively.

$$G(T,P) = H(T,P) - TS(T,P) \quad (C41)$$

$$dG(T,P) = dH(T,P) - TdS(T,P) \quad (C42)$$

The differential of the entropy specified in eq. (C43) has been obtained considering the heat capacity and the Maxwell equation relating the derivative of entropy with respect to the pressure and the derivative of volume with respect to the temperature. The volumetric thermal expansion coefficient β has been introduced in the last term of eq. (C.43). Eq. (C44) follows from eq. (C43).

$$dS(T,P) = \left(\frac{\partial S}{\partial T}\right)_P dT + \left(\frac{\partial S}{\partial P}\right)_T dP = \frac{Cp}{T}dT - \left(\frac{\partial V}{\partial T}\right)_P dP = \frac{Cp}{T}dT - V\beta dP \quad , \quad \beta = \frac{1}{V}\left(\frac{\partial V}{\partial T}\right)_P \quad (C43)$$

$$dH(T,P) = TdS(T,P) + VdP = CpdT + V(1 - T\beta)dP \quad (C44)$$

With reference to Figure C.3, it is possible to write that:

$$\Delta G^{SLE}_{P,T} = \underset{a \to d}{\Delta H} - T\underset{a \to d}{\Delta S} \quad (C45)$$

, thus the enthalpy and entropy variations from the solid phase at melting temperature and pressure towards the liquid phase at same conditions can be evaluated starting from eqs. (C43) and (C44). The enthalpy and entropy variations from point *a* to point *d* are the sum of three contributions:

$$\underset{a \to d}{\Delta H} = \underset{a \to b}{\Delta H} + \underset{b \to c}{\Delta H} + \underset{c \to d}{\Delta H} \quad , \quad \underset{a \to d}{\Delta S} = \underset{a \to b}{\Delta S} + \underset{b \to c}{\Delta S} + \underset{c \to d}{\Delta S} \quad (C46)$$

The details of these contributions are specified in the following equations, where superscript *S* and *L* refer to the solid and the liquid phase, respectively.

It is worth remembering that the global variations along the vertical line referred to the solid phase in Figure C.3 can be evaluated as the sum of an isobaric variation from point (*P*,*T*) to (*P*,*Tt*), and a successive isothermal variation from point (*P*,*Tt*) to point (*Pt*,*Tt*).

A similar approach is adopted for the liquid phase.

$$\begin{cases} \overset{\Delta H}{a \to b} = \int_{T}^{T_t} Cp^S dT + \int_{P}^{P_t} V^S(1 - T\beta^S)dP \\ \overset{\Delta H}{b \to c} = \Delta H_{Pt,Tt}^{SLE} \\ \overset{\Delta H}{c \to d} = \int_{T_t}^{T} Cp^L dT + \int_{P_t}^{P} V^L(1 - T\beta^L)dP \end{cases} \quad (C47)$$

$$\boldsymbol{\overset{\Delta H}{a \to d}} = \int_{T}^{T_t} Cp^S dT + \int_{P}^{P_t} V^S(1 - T\beta^S)dP + \Delta H_{Pt,Tt}^{SLE} + \int_{T_t}^{T} Cp^L dT + \int_{P_t}^{P} V^L(1 - T\beta^L)dP =$$

$$= \int_{T_t}^{T} (Cp^L - Cp^S)dT + \int_{P_t}^{P} (V^L - V^S)dP - \int_{P_t}^{P} T(V^L\beta^L - V^S\beta^S)dP + \Delta H_{Pt,Tt}^{SLE} = \quad (C48)$$

$$= \int_{\boldsymbol{T_t}}^{\boldsymbol{T}} \boldsymbol{\Delta Cp^{SLE} dT} + \int_{\boldsymbol{P_t}}^{\boldsymbol{P}} \boldsymbol{\Delta V^{SLE} dP} - \int_{\boldsymbol{P_t}}^{\boldsymbol{P}} \boldsymbol{T\left(V^L\beta^L - V^S\beta^S\right)dP} + \boldsymbol{\Delta H_{Pt,Tt}^{SLE}}$$

$$\begin{cases} \overset{\Delta S}{a \to b} = \int_{T}^{T_t} \frac{Cp^S}{T} dT - \int_{P}^{P_t} V^S\beta^S dP \\ \overset{\Delta S}{b \to c} = \Delta S_{Pt,Tt}^{SLE} = \frac{\Delta H_{Pt,Tt}^{SLE}}{T_t} \\ \overset{\Delta S}{c \to d} = \int_{T_t}^{T} \frac{Cp^L}{T} dT - \int_{P_t}^{P} V^L\beta^L dP \end{cases} \quad (C49)$$

$$\boldsymbol{\overset{\Delta S}{a \to d}} = \int_{T}^{T_t} \frac{Cp^S}{T} dT - \int_{P}^{P_t} V^S\beta^S dP + \frac{\Delta H_{Pt,Tt}^{SLE}}{T_t} + \int_{T_t}^{T} \frac{Cp^L}{T} dT - \int_{P_t}^{P} V^L\beta^L dP =$$

$$= \int_{T_t}^{T} \frac{(Cp^L - Cp^S)}{T} dT - \int_{P_t}^{P} (V^L\beta^L - V^S\beta^S)dP + \frac{\Delta H_{Pt,Tt}^{SLE}}{T_t} = \quad (C50)$$

$$= \int_{\boldsymbol{T_t}}^{\boldsymbol{T}} \frac{\boldsymbol{\Delta Cp^{SLE}}}{\boldsymbol{T}} \boldsymbol{dT} - \int_{\boldsymbol{P_t}}^{\boldsymbol{P}} \boldsymbol{\left(V^L\beta^L - V^S\beta^S\right)dP} + \frac{\boldsymbol{\Delta H_{Pt,Tt}^{SLE}}}{\boldsymbol{T_t}}$$

The total Gibbs energy variation at melting can then be written introducing eqs. (C48) and (C50) in eq. (C45).

$$\Delta \boldsymbol{G_{P,T}^{SLE}} = \int_{T_t}^{T} \Delta Cp^{SLE} dT + \int_{P_t}^{P} \Delta V^{SLE} dP - \int_{P_t}^{P} T(V^L \beta^L - V^S \beta^S) dP + \Delta H_{Pt,Tt}^{SLE} - T\left[\int_{T_t}^{T} \frac{\Delta Cp^{SLE}}{T} dT - \int_{P_t}^{P} (V^L \beta^L - V^S \beta^S) dP + \frac{\Delta H_{Pt,Tt}^{SLE}}{T_t}\right] = \quad (C51)$$

$$= \int_{\boldsymbol{T_t}}^{\boldsymbol{T}} \boldsymbol{\Delta Cp^{SLE} dT} + \int_{\boldsymbol{P_t}}^{\boldsymbol{P}} \boldsymbol{\Delta V^{SLE} dP} + \Delta \boldsymbol{H_{Pt,Tt}^{SLE}} \left(\mathbf{1} - \frac{\boldsymbol{T}}{\boldsymbol{T_t}}\right) - \boldsymbol{T} \int_{\boldsymbol{T_t}}^{\boldsymbol{T}} \frac{\boldsymbol{\Delta Cp^{SLE}}}{\boldsymbol{T}} \boldsymbol{dT}$$

With the assumptions within eq. (C52), eq. (C51) becomes eq. (C55) after resolution of the integrals.

$$\Delta Cp^{SLE} = \Delta Cp_{Pt,Tt}^{SLE} \qquad \Delta V^{SLE} = \Delta V_{Pt,Tt}^{SLE} \quad (C52)$$

$$\Delta \boldsymbol{G_{P,T}^{SLE}} = \Delta Cp_{Pt,Tt}^{SLE} \int_{T_t}^{T} dT + \Delta V_{Pt,Tt}^{SLE} \int_{P_t}^{P} dP + \Delta H_{Pt,Tt}^{SLE} \left(1 - \frac{T}{T_t}\right) - T\Delta Cp_{Tt}^{SLE} \int_{T_t}^{T} \frac{1}{T} dT = \quad (C53)$$

$$= \Delta Cp_{Pt,Tt}^{SLE} (T - T_t) + \Delta V_{Pt,Tt}^{SLE} (P - P_t) + \Delta H_{Pt,Tt}^{SLE} \left(1 - \frac{T}{T_t}\right) - T\Delta Cp_{Tt}^{SLE} ln\left(\frac{T}{T_t}\right) = \quad (C54)$$

$$= \boldsymbol{\Delta Cp_{Pt,Tt}^{SLE}} \left[\boldsymbol{T - T_t - T ln}\left(\frac{\boldsymbol{T}}{\boldsymbol{T_t}}\right)\right] + \boldsymbol{\Delta V_{Pt,Tt}^{SLE}} (\boldsymbol{P - P_t}) + \Delta \boldsymbol{H_{Pt,Tt}^{SLE}} \left(\mathbf{1} - \frac{\boldsymbol{T}}{\boldsymbol{T_t}}\right) \quad (C55)$$

Combining eqs. (40) and (C55) gives eq. (C56), from which eq. (C57) follows.

$$ln \frac{f^{L,0}(P,T)}{f^{S,0}(P,T)} = \frac{\Delta G_{P,T}^{SLE}}{RT} = \frac{\Delta H_{Pt,Tt}^{SLE}}{RT} \left(1 - \frac{T}{T_t}\right) + \frac{\Delta Cp_{Pt,Tt}^{SLE}}{RT} \left[T - T_t - T ln\left(\frac{T}{T_t}\right)\right] + \frac{\Delta V_{Pt,Tt}^{SLE}}{RT} (P - P_t) \quad (C56)$$

$$ln \frac{f^{L,0}(P,T)}{f^{S,0}(P,T)} = \frac{\Delta H_{Pt,Tt}^{SLE}}{RT_t} \left(\frac{T_t}{T} - 1\right) - \frac{\Delta Cp_{Pt,Tt}^{SLE}}{R} \left[\frac{T_t}{T} - 1 - ln\left(\frac{T_t}{T}\right)\right] + \frac{\Delta V_{Pt,Tt}^{SLE} (P - P_t)}{RT} \quad (C57)$$

It is interesting to notice that eq. (C57) and eq. (C39) are identical.

A simplified version deeply used in dealing with solid-liquid equilibrium is obtained from eq. (C57):

1. neglecting pressure effects, eq. (C58);
2. expanding in series the logarithmic function, eq. (59).

$$\left.\frac{\Delta V_{Pt,Tt}^{SLE} (P - P_t)}{RT}\right|_{P \sim P_t} \approx 0 \quad (C58)$$

$$ln \frac{T_t}{T} = \left(\frac{T_t}{T} - 1\right) - \frac{1}{2}\left(\frac{T_t}{T} - 1\right)^2 + \frac{1}{3}\left(\frac{T_t}{T} - 1\right)^3 + \cdots \overset{T \sim T_t}{\cong} \left(\frac{T_t}{T} - 1\right) \quad (C59)$$

Eq. (C59) implies the second term on the right hand side of eq. (C57) to vanish, then the simplified versions of eq. (C57) is:

$$ln \frac{f^{L,0}(P,T)}{f^{S,0}(P,T)} = \frac{\Delta H_{Pt,Tt}^{SLE}}{RT_t} \left(\frac{T_t}{T} - 1\right) \quad (C60)$$

For a pure substance, the fugacity of the liquid phase, $f^{L,0}$, can be evaluated from a common Cubic EoS (*CEoS*). The fugacity of the solid phase ,$f^{S,0}$, is successively and analytically defined at the same temperature *T* and pressure *P* by using the ratio reported in eq. (C57).

Depending on the values of the enthalpy of fusion (ΔH^{SLE}), the change in heat capacity upon fusion (ΔCp^{SLE}), and the change in volume upon fusion (ΔV^{SLE}), the fugacity of the solid phase is calculated in terms of a liquid-phase reference state. It must be kept in mind that the thermodynamic properties needed in the *CA* (ΔH^{SLE}, ΔCp^{SLE}, and ΔV^{SLE}) are all taken for the pure substance at its triple point.

Eq. (C57) can be applied to mixtures considering the isofugacity condition required for equilibrium in a mixture:

$$z_i\gamma_i^S f_i^{S,0} = x_i\gamma_i^L f_i^{L,0} \qquad (C61)$$

With reference to the simplified version of the *CA*, eq. (C60), eq. (C61) turns in eq. (C62).

$$z_i\gamma_i^S = x_i\gamma_i^L \frac{f_i^{L,0}}{f_i^{S,0}} = x_i\gamma_i^L exp\left[\frac{\Delta H_{Pt,Tt}^{SLE}}{RT_t}\left(\frac{T_t}{T}-1\right)\right] = x_i\gamma_i^L \frac{1}{\psi_i} \qquad (C62)$$

In case of total immiscibility in the solid phase (z_i=1) and of ideal solid phase (γ_i^S=1), the SLE condition of component *i* in a mixture becomes:

$$x_i\gamma_i^L = \psi_i \qquad (C63)$$

One limit of the *CA* is its inability to predict thermodynamic properties of the solid phase, such as density or heat capacity. Furthermore, it requires additional models for evaluating the non ideality in the solid phase and applying eq. (C61) to cases of solid solution, namely when a partial miscibility in the solid phase occurs. The main advantage is to allow the representation of SLE of mixtures in case of total immiscibility in the solid phase knowing only triple point temperature and enthalpy of fusion for each component.

Some applications of the *CA* are presented in the following part of this section.

2.1.3 Soave

In 1978, Soave applied the SRK EoS and the *CA* to SLE calculations in mixtures of carbon dioxide and light hydrocarbons, [1]. In [1], two pure component parameters (the critical pressure and the acentric factor) were adjusted wishing to improve the accuracy of the SRK EoS in representing the Vapor-Liquid Equilibrium, VLE, of the pure compounds involved, namely CO_2, CH_4, C_2H_6, and C_3H_8.

Neglecting the effects of pressure and assuming a constant average value of the difference of liquid and solid heat capacities, Soave applied the *CA* in the form of eq. (C64) for obtaining the solid fugacity from the liquid fugacity, eq. (C65)

$$ln\frac{f^{L,0}(P,T)}{f^{S,0}(P,T)} = \frac{\Delta H_{Pt,Tt}^{SLE}}{RT_t}\left(\frac{T_t}{T}-1\right) - \frac{\Delta Cp_{Pt,Tt}^{SLE}}{R}\left[\frac{T_t}{T}-1-ln\left(\frac{T_t}{T}\right)\right] \qquad (C64)$$

$$f^{S,0}(P,T) = f^{L,0}(P,T)exp\left\{-\frac{\Delta H_{Pt,Tt}^{SLE}}{RT_t}\left(\frac{T_t}{T}-1\right) + \frac{\Delta Cp_{Pt,Tt}^{SLE}}{R}\left[\frac{T_t}{T}-1-ln\left(\frac{T_t}{T}\right)\right]\right\} \qquad (C65)$$

The pure-CO_2 Solid-Vapor Equilibrium (SVE), eq. (C66), were then rewritten by use of eq. (C65) giving eq. (C67).

$$f^{V,0}(P^{SVE},T^{SVE}) = f^{S,0}(P^{SVE},T^{SVE}) = f^{L,0}(P^{SVE},T^{SVE})exp\left\{-\frac{\Delta H^{SLE}_{Pt,Tt}}{RT_t}\left(\frac{T_t}{T}-1\right)+\frac{\Delta Cp^{SLE}_{Pt,Tt}}{R}\left[\frac{T_t}{T}-1-ln\left(\frac{T_t}{T}\right)\right]\right\} \quad (C66)$$

$$ln\frac{f^{V,0}(P^{SVE},T^{SVE})}{f^{L,0}(P^{SVE},T^{SVE})} = -\frac{\Delta H^{SLE}_{Pt,Tt}}{RT_t}\left(\frac{T_t}{T}-1\right)+\frac{\Delta Cp^{SLE}_{Pt,Tt}}{R}\left[\frac{T_t}{T}-1-ln\left(\frac{T_t}{T}\right)\right] \quad (C67)$$

According to eq. (C67), the fugacity of the fluid phases were evaluated solving the SRK EoS at the SVE of pure CO_2, and the triple point properties ΔH and ΔCp were regressed to make the right hand side equal to the left hand side.

Once these values obtained, Soave regressed a binary interaction parameter within the original mixing rule suggested by Redlich and Kwong, [2], for representing experimental values of solubilities of CO_2 in liquid CH_4, C_2H_6, and C_3H_8. In order to do that, author solved the Solid-Liquid-Vapor Equilibrium, SLVE, in eq. (C68) at the experimental temperature, T^{exp}, and liquid composition, x_i^{exp}.

$$f^{S,0}(P,T^{exp}) = x^{exp}_{CO2}\hat{\varphi}^{L}_{CO2}P = y_{CO2}\hat{\varphi}^{V}_{CO2}P \quad (C68)$$

In eq. (C68), y is the composition of CO_2 in the vapor phase, P is the SLVE pressure, and φ is the fugacity coefficient of CO_2 in the fluid phases. Solving eq. (C68) require to evaluate the fugacity coefficients by means of the SRK EoS and successively combining the liquid fugacity and the *CA* of eq. (C64) for evaluating the fugacity of the pure solid CO_2.

The approach proposed by Soave involves the regression of 3 parameters (ΔH, ΔCp, and a binary interaction parameter) on SVE of pure CO_2 and on SLE of binary mixtures.

2.1.4 Twu et al.

Twu et al. [3] represented the SLE and predicted the solid solubility in the liquid phase using the Twu-Sim-Tassone EoS, eq. (C69). The correspondent expressions for the fugacity and reduced volume both at zero pressure limit are eq. (C70) and eq. (C71), respectively.

$$P = \frac{RT}{v-b}-\frac{a}{(v+ub)(v+wb)} \quad (C69)$$

$$\ln\frac{f}{P} = -1-\ln b^* - \ln(v^*-1) - \frac{a^*}{(w-u)b^*}\ln\left(\frac{v^*+w}{v^*+u}\right) \quad (C70)$$

$$v^* = \frac{1}{2}\left[\left(\frac{a^*}{b^*}-u-w\right)\pm\sqrt[2]{\left(u+w-\frac{a^*}{b^*}\right)^2-4\left(uw+\frac{a^*}{b^*}\right)}\right] \quad (C71)$$

The term $v^*=v/b$ in the previous equations is the reduced volume at zero pressure, obtained from eq. (C69) setting $P = 0$.

The parameters a^* and b^* in eqs. (C70)-(C71) are defined as $a^*=Pa/R^2T^2$ and $b^*=Pb/RT$. The parameters a and b take into account respectively the attractive forces among the molecules and the own volume of the molecules. In [3], a is a temperature-dependent value, while b is the same for the liquid and solid phases.

Since correlations are available for the temperature dependence of the term a in the liquid phase, a^L, and not available for the solid phase, a^S, authors proposed to evaluate the temperature dependence of a^S exploiting the *CA* at the zero-pressure limit, eq. (C60).

At a fixed temperature, the smallest value of eq. (71) gives the liquid reduced volume, then the liquid fugacity can be computed from eq. (C70).

The identity of the *CA* in eq. (C72) is then solved introducing eq. (70) for the solid fugacity.

$$\ln\frac{f^{S,0}}{P} = \ln\frac{f^{L,0}}{P} - \frac{\Delta H^{SLE}_{Pt,Tt}}{RT_t}\left(\frac{T_t}{T} - 1\right) \tag{C72}$$

$$-1 - \ln b^* - \ln(v^{*,S} - 1) + \frac{2a^{*,S}}{7b^*}\ln\left(\frac{v^{*,S} + 0.5}{v^{*,S} + 3}\right) = \ln\frac{f^{L,0}}{P} - \frac{\Delta H^{SLE}_{Pt,Tt}}{RT_t}\left(\frac{T_t}{T} - 1\right) \tag{C73}$$

The right hand side of eq. (C73) is known at a fixed temperature. The only unknown in the left hand side of eq. (C73) is instead a^S, seeing that the solid reduced volume, $v^{*,S}$, depends on a^S as indicated in eq. (C71). Solving eq. (C73) for different temperatures provides as many values of a^S which can successively used to find a correlation for the temperature dependence of a^S.

Even thought the methodology developed for the solid a function is at zero pressure, a^S obtained as discussed has been used in the TST EoS to predict the solid fugacity at elevated pressures, because the expression of a for the solid phase is temperature-dependent only, not pressure-dependent.

In [3], authors incorporated G^E mixing rules in the TST EoS to handle SLE in highly non-ideal systems, considering only the case of total immiscibility in the solid phase, eq. (C63). The partial molar fugacity coefficient of component i in both phases is calculated from the TST EoS with G^E mixing rules, using the temperature dependences of a^L and a^S.

In the Twu model, SLE data are needed for regressing the parameters within the G^E mixing rules.

2.1.5 Rodriguez-Reartes et al.

Qualitative Solid-Fluid Equilibrium (SFE) behavior for binary asymmetric mixtures have been presented by Rodriguez-Reartes et al. in [4].

Authors fitted the binary interaction parameters of mixing rules to reproduce experimental binary Fluid-Fluid Equilibrium (FFE) data by means of the PR EoS, [5]. The PR EoS has then be used for evaluating the partial molar fugacities of the fluid phases.

When dealing with SFE, the fluid fugacities have been coupled with the solid fugacity of the pure heavy compound (subscript 2) in the mixture, defined in eq. (C74). For fixed values of temperature and pressure, the PR EoS is used for evaluating the volume (v_0) and the fugacity (f_2^L) of a pure subcooled liquid phase. Then, the pure solid fugacity at same temperature, pressure, and volume, is obtained by the *CA*, resumed in the term *U*. The term *U* has been obtained in [4] assuming a linear temperature dependency of the liquid-solid heat capacity difference, eq. (C75). As a result, a fourth term occurs in developing the *CA* through the paths of Figure C.2 and Figure C.3.

$$f_2^S(P,T,v_0) = f_2^{L,PR}(P,T,v_0^{PR})exp(U) \tag{C74}$$

$$\Delta Cp^{SLE}_{Pt,Tt} = A + BT \tag{C75}$$

$$U = \frac{\Delta H^{SLE}_{Pt,Tt}}{RT_t}\left(1 - \frac{T_t}{T}\right) + \frac{A}{R}\left[\frac{T_t}{T} - 1 + ln\left(\frac{T}{T_t}\right)\right] + \frac{BT_t}{R}\left[\frac{T}{2T_t} + \frac{T_t}{2T} - 1\right] - \frac{\Delta V^{SLE}_{Pt,Tt}(P - P_t)}{RT} \tag{C76}$$

With

$$C_1 = \frac{\Delta H^{SLE}_{Pt,Tt}}{\Delta V^{SLE}_{Pt,Tt}} \quad , \quad C_2 = \frac{AT_t}{\Delta V^{SLE}_{Pt,Tt}} \quad , \quad C_3 = \frac{BT_t^2}{\Delta V^{SLE}_{Pt,Tt}} \tag{C77}$$

eq. (C76) becomes:

$$U = \frac{\Delta V^{SLE}_{Pt,Tt}}{RT_t}\left[C_1\left(1 - \frac{T_t}{T}\right) + C_2\left[\frac{T_t}{T} - 1 + ln\left(\frac{T}{T_t}\right)\right] + C_3\left[\frac{T}{2T_t} + \frac{T_t}{2T} - 1\right] - \frac{T_t(P - P_t)}{T}\right] \tag{C78}$$

The parameters C_1, C_2, and C_3 in eq. (C77) are regressed for reproducing experimental SLE of the pure heavy component, considering that at melting U=0. Binary SFE experimental values are

instead used for fitting the volume change at melting, seeing that this value does not affect the pure heavy component melting curve at set values of C_1, C_2, and C_3.

In the approach proposed in [4], binary FFE data are needed for regressing two binary interaction parameters in the mixing rules for the PR EoS.

2.1.6 Coutinho et al.

The *CA*, namely the relation between activity coefficients of the solid and liquid phases, has been deeply used in several works of Coutinho et al. for representing the appearance of a solid paraffinic phase, known as wax, in a hydrocarbon fluid. Examples are references [6] and [7]. In these works, same authors proposed to use a free-volume model for the non ideality of the liquid phase, [8], and developed a local composition model for the non ideality in the solid phase, [9]. This last model is a predictive version of the local composition model of Wilson, [10].

Long-chain n-alkanes are the main components of waxes, thus a good understanding of the deposition of paraffinic waxes from hydrocarbon fluids require to handle the thermodynamic behavior of Long-Chain N-Alkanes (*LCNA*).

A pure *LCNA* can present a number of crystal lattices ranging from 2 up to 4, thus multicomponent hydrocarbon systems usually involve more than one solid phase in addition to the liquid phase. Nevertheless, in wax formation only the liquid and the low temperature solid phases are considered due to the fact that the temperature of appearance of the solid deposit, called cloud point, usually occurs at a temperature lower than the solid-solid transition temperature of pure *LCNAs*, [7].

The qualitative Pressure-Temperature Equilibrium Projection (*PT-EP*) of a pure *LCNA* can be schematized as in Figure C.4 considering two crystal lattices, thus two solid phases, solid1 and solid2 (*S1* and *S2*). In Figure C.4, a *S1-S2*-vapor triple point (▼) occurs in addition to the *S1*-liquid-vapor triple point (▲). *P* and *T* are *S1-S2* equilibrium temperature and pressure, and the *S1-S2* equilibrium is portrayed by violet square.

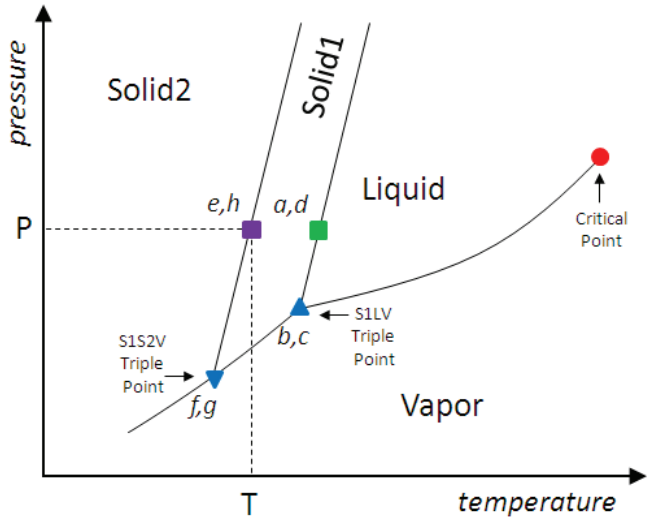

Figure C.4: Qualitative Pressure-Temperature Equilibrium Projection of a long-chain n-alkane with two solid phases.
— : equilibrium branches; ● : critical point; ▲ : solid1-liquid-vapor triple point; ■ : solid1-liquid equilibrium; ▼ : solid1-solid2-vapor triple point; ■ : solid1-solid2 equilibrium; P : solid1-solid2 equilibrium pressure; T : solid1-solid2 equilibrium temperature; a,d : solid1 and liquid phases; b,c : solid1 and liquid phases the s1lv triple point; e,h : solid1 and solid2 phases at T, P; g,f : solid1 and solid2 phases at s1s2v triple point.

With reference to Figure C.4, it is possible to obtain the relation between the fugacities of the two solid phases following the procedure shown in details for the solid-liquid equilibrium. The result is the *CA* applied to the Solid1-Solid2 Equilibrium (S1S2E), eq. (C79):

$$ln\frac{f^{S1,0}(P,T)}{f^{S2,0}(P,T)}=\frac{\Delta H^{S1S2E}_{Pt^*Tt^*}}{RT^*_t}\left(\frac{T^*_t}{T}-1\right)-\frac{\Delta Cp^{S1S2E}_{Pt^*Tt^*}}{R}\left[\frac{T^*_t}{T}-1-ln\left(\frac{T^*_t}{T}\right)\right]+\frac{\Delta V^{S1S2E}_{Pt^*Tt^*}(P-P^*_t)}{RT} \qquad (C79)$$

In eq. (C79), asterisk has been used for remembering that the properties are evaluated at the *S1-S2*-vapor triple point.

Since wax depositions involve principally the liquid and the low temperature solid phase, which is the solid2 phase in the case of Figure C.4, a relation between liquid and solid2 fugacities is required. Eq. (C57) has been here rewritten for the solid1-liquid equilibrium, and then adding eq. (C79) to eq. (C80) provides the expected relation.

$$ln\frac{f^{L,0}(P,T)}{f^{S1,0}(P,T)}=\frac{\Delta H^{S1LE}_{Pt,Tt}}{RT_t}\left(\frac{T_t}{T}-1\right)-\frac{\Delta Cp^{S1LE}_{Pt,Tt}}{R}\left[\frac{T_t}{T}-1-ln\left(\frac{T_t}{T}\right)\right]+\frac{\Delta V^{S1LE}_{Pt,Tt}(P-P_t)}{RT} \qquad (C80)$$

$$ln\frac{f^{L,0}(P,T)}{f^{S1,0}(P,T)}+ln\frac{f^{S1,0}(P,T)}{f^{S2,0}(P,T)}=ln\frac{f^{L,0}(P,T)}{f^{S2,0}(P,T)}=$$

$$\frac{\Delta H^{S1LE}_{Pt,Tt}}{RT_t}\left(\frac{T_t}{T}-1\right)-\frac{\Delta Cp^{S1LE}_{Pt,Tt}}{R}\left[\frac{T_t}{T}-1-ln\left(\frac{T_t}{T}\right)\right]+\frac{\Delta V^{S1LE}_{Pt,Tt}(P-P_t)}{RT}+ \qquad (C81)$$

$$\frac{\Delta H^{S1S2E}_{Pt^*Tt^*}}{RT^*_t}\left(\frac{T^*_t}{T}-1\right)-\frac{\Delta Cp^{S1S2E}_{Pt^*Tt^*}}{R}\left[\frac{T^*_t}{T}-1-ln\left(\frac{T^*_t}{T}\right)\right]+\frac{\Delta V^{S1S2E}_{Pt^*Tt^*}(P-P^*_t)}{RT}$$

It is worth seeing that the liquid and solid1 fugacities in eq. (C80) are evaluated at the same temperature and pressure of the solid1-solid2 equilibrium. The trick is to consider a hypothetical subcooled liquid at *T* and *P*. This is what is commonly done for obtaining the *CA* at zero pressure limit for the solid1-liquid equilibrium by means of a thermodynamic cycle other than those presented in Figure C.2 and Figure C.3, [11].

From eq. (C81) it clearly appears that when *j* triple points are present (then *j* solid phases), the *CA* can be generalized in the form of eq. (C82). Also in this case, the solid fugacity is expressed in terms of a hypothetical subcooled liquid phase. In eq. (C82), $T^*_{t\,(i-1,i)}$ and $P^*_{t\,(i-1,i)}$ are temperature and pressure at the triple point involving the solid(*i-1*) and solid(*i*) phases.

$$ln\frac{f^{L,0}(P,T)}{f^{Sj,0}(P,T)}=ln\frac{f^{L,0}(P,T)}{f^{S1,0}(P,T)}+\sum_{i=2}^{j}\frac{\Delta H^{S_{i-1}S_iE}_{Pt^*Tt^*(i-1,i)}}{RT^*_{t(i-1,i)}}\left(\frac{T^*_{t(i-1,i)}}{T}-1\right)-$$
$$\sum_{i=2}^{j}\frac{\Delta Cp^{S_{i-1}S_iE}_{Pt^*Tt^*(i-1,i)}}{R}\left[\frac{T^*_{t(i-1,i)}}{T}-1-ln\left(\frac{T^*_{t(i-1,i)}}{T}\right)\right]+\sum_{i=2}^{j}\frac{\Delta V^{S_{i-1}S_iE}_{Pt^*Tt^*(i-1,i)}\left(P-P^*_{t(i-1,i)}\right)}{RT} \qquad (C82)$$

At the zero pressure limit and neglecting the difference between the heat capacities of the solid phases ($\Delta Cp^{S1LE}=\Delta Cp^{S1S2E}$), the *CA* in eq. (C81) can be rewritten as in eq. (C83), and in eq. (C84) for representing the solid2-liquid equilibrium in mixtures.

$$ln\frac{f^{L,0}(P,T)}{f^{S2,0}(P,T)}=\frac{\Delta H^{S1LE}_{Pt,Tt}}{RT_t}\left(\frac{T_t}{T}-1\right)+\frac{\Delta H^{S1S2E}_{Pt^*Tt^*}}{RT^*_t}\left(\frac{T^*_t}{T}-1\right)-\frac{\Delta Cp^{S1LE}_{Pt,Tt}}{R}\left[\frac{T_t}{T}-1-ln\left(\frac{T_t}{T}\right)\right] \qquad (C83)$$

$$ln\frac{z_i\gamma^S_i}{x_i\gamma^L_i}=\frac{\Delta H^{S1LE}_{Pt,Tt}}{RT_t}\left(\frac{T_t}{T}-1\right)+\frac{\Delta H^{S1S2E}_{Pt^*Tt^*}}{RT^*_t}\left(\frac{T^*_t}{T}-1\right)-\frac{\Delta Cp^{S1LE}_{Pt,Tt}}{R}\left[\frac{T_t}{T}-1-ln\left(\frac{T_t}{T}\right)\right] \qquad (C84)$$

In eq. (C84), z_i and x_i are compositions of component i in the solid and liquid phases, γ_i^S and γ_i^L the correspondent activity coefficients. Eq. (C84) is formalism of the *CA* adopted by Coutinho et al. in dealing with the thermodynamic behavior of multicomponent hydrocarbon systems.

At the beginning of section 2.1.6, mentions have been reported about the activity models proposed over the years by the authors here involved. A detailed presentation of these models is beyond the scope of this discussion. It is instead interesting to stress the predictive character of the approach proposed Coutinho et al..

In [6] and [7], the non ideality of the liquid phase is obtained coupling the Flory free volume equation, [12] (for representing entropic effects, such as size difference, and free-volume effects), and the UNIFAC model,[13] (for the residual contribution of energetic interactions), without reestimation of the parameters.

In [6] and [7], the non ideality of the solid phase is obtained adopting modified versions of the Wilson model, [10], and the UNIQUAC model, [14], respectively. Briefly, both models contains parameters that have been related to known properties, as the experimental latent heat of sublimation of the *LCNAs*, the number of carbons in the chain, and the length of the crystal cell.

As a consequence, any regression have been done in these works.

One of the main inconvenient of the *CA* in eq. (C84) is that it does not involve the system pressure. Extensions to the wax formation under high pressures has been the object of further and more recent works of Coutinho et al. An example is given in reference [15]. In [15], the *CA* in eq. (C84), without the term involving the heat capacity difference, has been applied for the representation of solid-liquid-vapor equilibria in multicomponent systems. Non idealities in the liquid and solid phases have been calculated as in [6] and [7], while the fugacity of fluid phases under high pressures are obtained coupling the SRK EoS with G^E mixing rules (as done by Twu et al. in 2003), [3].

2.2 Modified Cubic Equation of State (*MCEoS*)

MCEoS models introduce a second S-loop in the *PT-EP* of a pure compound to account for the solid-liquid transition, and represent the SLE via S-loop using the Maxwell's Equal Area Rule (*MEAR*).

The idea of a S-loop comes from what is usually done for obtaining the liquid phase starting from the ideal gas. The *CEoSs* are normally obtained by adding some parameters to the ideal gas EoS.

These parameters are needed for taking into account the characteristic volume of the molecules and the attractive forces among them.

The result is a S-loop connecting the high temperature region of a *PT-EP* with the low temperature and high pressure region.

The S-loop allows obtaining the transition between the vapor and the liquid phases and evaluating the VLE pressure via the *MEAR*, eq. (C85).

For the application of the *MEAR*, the Helmholtz energy must be convergent in the phase transition region. In practice, the integral of the pressure between two general volumes v^α - v^β in eq. (C85) must be convergent.

$$P\left(v^\alpha - v^\beta\right) = \int_{v^\beta}^{v^\alpha} P dv \qquad (C85)$$

Three examples of *MCEoS* have been here presented.

2.2.1 Kan

In [16], Kan added a 9-order term in the repulsive part of the three virial Sengers et al. EoS [17] for improving the prediction of the liquid phase of argon, and obtained the solid phase from the liq-

uid phase via S-loop using a second correction term. The resulting *MCEoS* is presented in eq. (C86).

$$P = \frac{RT}{v}\left(1 + \frac{B(T)}{v} + \frac{C(T)}{v^2}\right) + \frac{I}{v^9} + \frac{\alpha}{(v-\beta)^2 + \gamma^2} \qquad (C86)$$

In eq. (C86), P is pressure, T is absolute temperature, R is the gas constant, v is molar volume, $B(T)$ and $C(T)$ are the second and third virial coefficients, I, α, β, and γ are parameters.

The parameter I has been fitted on experimental PVT curves in the region of small volume and high pressure, while α, β, and γ have been regressed with respect to SLE data.

Owing to the presence of a S-loop for the solid-liquid equilibrium, the behavior of this modified EoS gives at some temperature and pressure conditions a solid-liquid critical point and this fact is not in agreement with the experimental observations.

2.2.2 Wenzel and Schmidt

The *MCEoS* of Wenzel and Schmidt was obtained by adding a term of order 6 in the Redlich-Kwong EoS, eq. (C87), [18].

$$P = \frac{RT}{v-b} - \frac{a}{v(v+b)} - \frac{c}{(v-0.97b)^6} \qquad (C87)$$

In eq. (C87), P is pressure, T is absolute temperature, R is the gas constant, v is molar volume, b is liquid covolume, a and c are temperature dependent parameters. The functional forms of parameters a and c contain 4 parameters, thus giving a total of 5 considering also the liquid covolume.

Eq. (C87) has been applied to pure compounds; the 5 parameters have been regressed on experimental values of saturation pressure, melting pressure, solid density, and heats of melting and vaporization. The application of eq. (C87) requires instead to fix two binary interaction parameters which were obtained from the literature.

Being similar to the Kan approach, also the behavior of this modified EoS gives at some temperature and pressure conditions a solid-liquid critical point and this fact is not in agreement with experimental observations.

2.2.3 Rodriguez et al.

Eq. (C88) shows the pressure explicit form of the *MCEoS* proposed by Rodriguez et al. in [19],

$$P = \frac{RT}{v-b} - \frac{aT(e^{\frac{\varepsilon}{RT}} - 1)}{(v-c)(v-d)} - \frac{fT}{(v-e)^{10}} \qquad (C88)$$

where P is pressure, T is absolute temperature, R is the gas constant, v is molar volume, and a, b, c, d, e, f, ε are parameters.

When $f = 0$, eq. (C88) becomes a *CEoS*. Parameters of the *CEoS* (a, b, c, d, ε) are evaluated imposing the *CEoS* to match the critical point conditions ($P=P_C$, $\angle P/\angle v=0$, $\angle^2 P/\angle v^2=0$), the saturation pressure and the experimental vapor volume at reduced temperature $T/T_C=0.7$. The experimental values for the acentric factor and the compressibility factor are used as inputs.

Starting from these values, an iterative procedure is carried out in order to update the parameters and match the critical point and triple point conditions with eq. (C88). The triple point conditions are solid-liquid and liquid-vapor isofugacities, and triple point temperature and pressure.

Authors guarantee the absence of any solid-liquid critical point, ensuring that an indefinite solid branch never connects its corresponding liquid branch.

In [19], the *MCEoS* in eq. (C88) has been applied for representing *PT-EPs* of pure argon and carbon dioxide, then it remains to verify the possibility of extending this EoS to binary mixtures.

2.3 System of Cubic Equations of State (*SCEoSs*)

Salim and Trebble proposed a System of two Cubic EoSs, eqs. (C89)-(C90), for representing solid, liquid, and vapor phases, [20].

$$\begin{cases} P = \dfrac{RT}{v - b_c} - \dfrac{a_c \alpha(T)}{v^2 + v(b_c + c_c) - (b_c c_c + d_c^2)} & (C89) \\ P = \dfrac{RT}{v - \bar{b}} - \dfrac{\bar{a}\hat{\alpha}(T)}{v^2 + v(\bar{b} + \bar{c}) - (\bar{b}\bar{c} + \bar{d}^2)} & (C90) \end{cases}$$

The first EoS is used for representing the liquid-vapor equilibrium behavior, and it corresponds to the Trebble-Bishnoi-Salim *CEoS*. The second EoS of the system is obtained forcing the first EoS to represent the solid density at the triple point by refitting of the parameters, and used to represent the solid-vapor equilibrium behavior. Eq. (C89) and eq. (90) are called Original EoS (*OEoS*) and Translated EoS (*TEoS*), respectively.

In the system of two *CEoSs*, a_c, b_c, c_c, d_c, and α are parameters of the *OEoS*, while $\bar{a}$, $\bar{b}$, $\bar{c}$, $\bar{d}$, and $\hat{\alpha}$ are the corresponding parameters of the *TEoS*. For the *OEoS*, authors used the pure component parameters presented in a previous work, [21].

In order to avoid discontinuities between the two equations, the *TEoS* parameters were regressed in order to satisfy four constraints at the triple point:

- solid density from the *TEoS* equals to the experimental value;
- pressure from the *TEoS* equals to the correspondent value from the *OEoS*;
- solid phase fugacity from the *TEoS* equals to the vapor phase fugacity from the *TEoS*;
- vapor phase fugacities from the *OEoS* and the *TEoS* must match.

After calculation of the parameters of the *TEoS* at the triple point, the temperature-dependence of $\hat{\alpha}(T)$ were obtained from SVE experimental values: sublimation pressure, solid and vapor densities, solid heat capacity, and heat of sublimation. The total number of parameters that has to be regressed for the *TEoS* is 6.

At this point, the *SCEoSs* is complete. For temperatures higher than the triple point temperature, the *OEoS* is used twice for the liquid and the vapor phases that coexist at the VLE. For SLE, the solid phase is from the *TEoS* and the liquid phase is from the *OEoS*. For representing the SVE at temperatures lower than the triple point temperature, both the solid and vapor phases are from the *TEoS*. At the triple point temperature, the solid phase is from the *TEoS*, the liquid phase from the *OEoS*, the vapor phase can be from both the EoSs because of the fourth constraint.

In [20], the *SCEoSs* has been extended to the representation of binary solid-vapor and solid-liquid equilibria. 4 mixing rules were used for evaluating mixture properties of the *OEoS* and other 4 mixing rules for evaluating those of the *TEoS*. Only 3 among the 8 mixing rules contain a binary interaction parameter, regressed on SVE, VLE, and SLE data.

It is possible with this approach either to assume a pure solid phase or to match solubility data if they are available. However, the Salim and Trebble model does not describe analytically the solid-fluid transition. Furthermore, it used twice a *CEoS*, one for the liquid-vapor equilibrium and the other for the solid-vapor equilibrium, considering the dense branch valid alternatively for the liquid or for the solid phase.

2.4 Molecular Association (*MA*)

Heidemann and Prausnitz proposed a modified van der Waals EoS applicable for to all fluid densities and able to represent the behavior of pure substances containing polar and hydrogen-bonding molecules, [22]. Their theory is based on the fact that all pure substances can be interpreted as mixtures of their own molecules.

Depending on the temperature, the monomer molecules of a pure substance can associate to form dimers, trimers and so on. For this reason they introduced mixing rules for taking into account the different chemical equilibria among monomers, dimers, trimers and *N*-mers, where *N* stands for the aggregated molecule formed by the association of *N* monomers.

Consequently, these authors proposed specific expression for evaluating the correct values of the repulsive and attractive terms presented in the van der Waals EoS. In the Heidemann and Prausnitz EoS, eq. (C91), P_{hs} and P_{att} are the repulsive and attractive terms, respectively.

$$P = P_{hs} + P_{att} = \frac{n_T}{n_0}\frac{RT}{b}\xi z_{hs} - \frac{a}{b^2}\pi_{att} \qquad (C91)$$

The repulsive term of the EoS depends on the temperature *T*, the gas constant *R*, the own volume *b* of the monomer molecules (the molecules are treated as hard spheres, that's explains the subscript *hs*), the reduced density ξ, the compressibility factor z_{hs}, and finally it depends also on n_T and n_0, the total number of moles in presence and in absence of association, respectively. In turn, these two last parameters depend on the equilibrium constants referred to the monomer–*N*-mers chemical equilibria.

For evaluating the attractive term P_{att}, Heidemann and Prausnitz proposed also expressions for the parameters *a* and π_{att}, where *a* depends on the degree of association and π_{att} is a density-dependent parameter.

Applying this EoS to monomers and to *N*-mers (with not so high value for *N*) and using only critical properties (temperature, pressure, and volume), Heidemann and Prausnitz represented the liquid-vapor transition and the critical isotherm of argon. Furthermore, for temperatures below the critical isotherm and above the triple temperature, their EoS shows two maximums in a *P*-*v* diagram depending on the value of *N*. One maximum occurs at moderate densities, and so is a part of the S-loop in the liquid-vapor. The other maximum occurs when the degree of association is high and it is so placed at high densities.

This leaded the authors thinking the possibility of representing the solid phase of a pure substance as a self-associated molecular aggregate (with high value for *N*) and to attribute the maximum at high densities to the solid-liquid transition. Moreover, no critical point was observed for the solid-liquid transition.

Using the Heidemann and Prausnitz approach to the monomers for representing the vapor phase and to *N*-mers with different values of *N*, it is possible to represent alternatively the liquid-vapor and the solid-liquid equilibria. As a consequence, this approach does not represent solid, liquid, and vapor phases with a single equation.

Lang and Wenzel, [23], and Geaña and Wenzel, [24], proposed similar approaches based on the SW EoS, [25], to extend the *MA* approach to the representation of the solid-fluid phase equilibrium behavior of mixtures. The starting points of their models were always the possibility of representing substances as mixtures of their own molecules, and to represent the solid phase as a self associated molecular aggregate. As a result, these models remains do not allow the representation of solid, liquid, and vapor phases with a single equation.

5 pure component parameters within the Lang and Wenzel model were tuned in order to respect triple point properties, as temperature, molar volume change on melting, and heat of melting. Other inputs data are critical temperature and pressure, and the acentric factor. Authors proposed expressions for evaluating equilibrium constants and fugacity coefficients including molecular association in the SW EoS, and regressed two binary interaction parameter on SLE data in dealing with binary mixtures.

Following the approach of Land and Wenzel, Geaña and Wenzel assumed the solid phase to consist of agglomerates of molecules. In [24], authors applied the SW EoS and the PR EoS together with the *MA* approach for representing both pure component phase diagrams and solid solubilities in supercritical gases. For pure components, experimental values of heat of melting, volume change upon melting, critical temperature and pressure, triple point pressure, and acentric factor were used

to regress the 5 parameters of each *CEoS*. With reference to binary mixtures, two binary interaction parameters were regressed on SVE data.

2.5 Quartic Equation of State (*QEoS*)

A. Yokozeki proposed a single equation for representing solid, liquid and vapor phases, [26]. This EoS was developed imposing the respect of some known facts:

- when $v \rightarrow :$, the EoS approach the ideal gas form $Pv=RT$;
- the thermodynamically stable state, including metastable states, must satisfy the mechanical stability condition of $(\partial P/\partial v)_T \leq 0$;
- the existence of the vapor-liquid critical point;
- the existence of the stable solid phase, which has a liquid-like steep slope in $(\partial P/\partial v)_T$, having a region with $P>0$, in addition to the liquid and vapor phases;
- no critical point exists between the solid and fluid phases. Besides the vapor-liquid transition S-loop, it is not possible introducing the solid phase through a continuous transition from the liquid phase, by adding an high order polynomial function in v. Therefore the solid phase branch must be separated from the fluid phase branches and analytically discontinuous at solid-liquid transition.
- the existence of the first order phase transition between liquid and vapor, solid and liquid, and solid and vapor. The so-called van der Waals S-loop exists in the isothermal PV diagram for the VLE, and the Maxwell's equal area rule can be applied over the S-loop;
- the existence of negative pressure regions and the condition of $(\partial P/\partial v)_T>0$ are allowed within the S-loop.

In the cubic EoSs, these conditions are satisfied only with reference to the liquid and vapor phases, because these EoSs do not include the solid phase.

With reference to the above considerations, Yokozeki proposed the eq. (C92) as extension of the van der Waals fluid EoS, [26]. This equation is the first introducing a discontinuity for the solid-fluid transition in the isothermal P-v behavior of a fluid.

The equation is composed of a hard-core repulsive part, P_{HC} and an intermolecular attractive part, P_A, and its pressure explicit form considering a generic attractive part is:

$$P(T,v) = P_{HC} + P_A = \frac{RT}{v-b(T)}\left(\frac{v-d}{v-c}\right)^k - \frac{a(T)}{v^2+qb(T)v+r[b(T)]^2} \qquad (C92)$$

$$a(T) = \frac{R^2T_c^2a_r(T_r)}{P_c} \quad , \quad a_r(T_r) = a_{rc}[a_0 + a_1T_r exp(-a_2T_r^n)] \qquad (C93)$$

$$b(T) = v_c b_r(T_r) \quad , \quad b_r(T_r) = b_{rc}[b_0 + b_1 exp(-b_2T_r^n)] \qquad (C94)$$

Details concerning the EoS parameters are presented in eqs. (C93)-(C94).

Eq. (C92) with $k = 0$ becomes the vdW EoS with $q = r = 0$, the RK EoS with $q = 1$, $r = 0$, and $a = 1/(T^{1/2})$, [2], the PR EoS with $q = 2$, $r = 1$ and a general T-dependence of a, and so on.

Z_c, a_0, a_1, a_2, n, b_0, b_1, b_2, m, c, d and k, q, r are the EoS parameters: b is the covolume of the solid phase, c is the liquid covolume, Z_c is the compressibility factor at the critical point. The subscript r in eqs. (C93)-(C94) refers to reduced values.

The physically valid region is $v>b$; the parameters a, b, c, and d are all positive numbers, with $b<d<c$, and k is integer. Another important relations introduced by Yokozeki for using his EoS is $k \langle 1$ and integer.

The schematic isothermal behaviors behind this equation are illustrated in Figure C.5 and Figure C.6 with reference to the triple point, [26]. In [26], both cases of k odd and even integers possess physically acceptable shapes, although the shape in the solid branch is different.

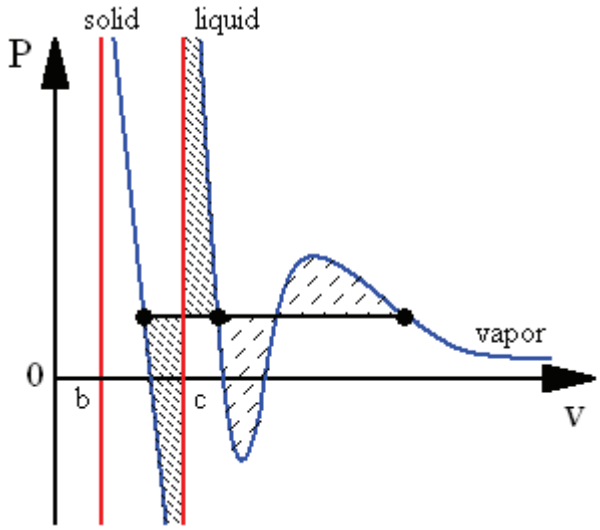

Figure C.5: Schematic isothermal *P*-*v* diagram of the Yokozeki EoS with k = odd at the triple point and $v>b$.

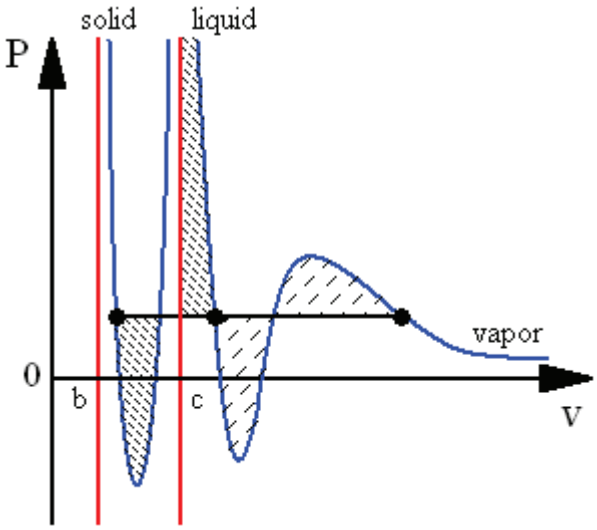

Figure C.6: Schematic isothermal *P*-*v* diagram of the Yokozeki EoS with k = even at the triple point and $v>b$.

— : asymptotes referred to solid and liquid covolumes; — : isothermal *P*-*v* diagram of the Yokozeki EoS; ● : solid, liquid and vapor equilibrium phases; — : triple point pressure; hatched areas are the Maxwell's equal area construction.

The regions with $\partial P/\partial v>0$ are of course thermodynamically unstable, being similar to the case of the vdW EoS within the S- loop. In the Yokozeki EoS, the solid and liquid branches do not possess the ordinary continuous S-loop, but here the S-loop forms an "infinite-size" S loop. This is because $P_{HC}\rightarrow 6$: at $v=c$. The important consequence of this mathematical behavior is that this "infinite-size S" loop does not lead to any solid-liquid critical point, [26].

In [26], Yokozeki used eq. (C92) with k = 1 and the van der Waals attractive term, founding that the proposed EoS respects the three common critical point conditions ($P=P_C$, $\partial P/\partial v=0$, $\partial^2 P/\partial v^2=0$) with the physically correct isotherm of Figure C.5 only for proper values of compressibility factor and solid covolume. Therefore, starting from a total of 5 parameters in eq. (C92) written at the critical point (Z_c, a_c, b_c, d, c), Yokozeki obtained three parameters (a_c, c, and d) solving the system of the three common critical point conditions for fixed proper values for Z_c and b_c.

By keeping Z_c, d, and c constant, new values of a and b at the triple point (a_t, b_t) can be obtained solving the isofugacity conditions by means of the Maxwell's equal area rule for the SLE and the VLE.

Regarding the temperature-dependence of the functions $a(T)$ and $b(T)$, Yokozeki assumed finite values for all the temperatures (including T = 0,∞ K), and a maximum for $a(T)$. The $a(T)$ and $b(T)$ proposed in [26] for argon are presented in Figure C.7 and Figure C.8, respectively.

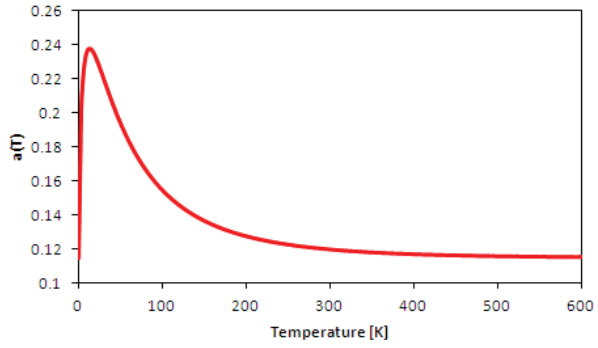

Figure C.7: Function $a(T)$ for argon, **[26]**.

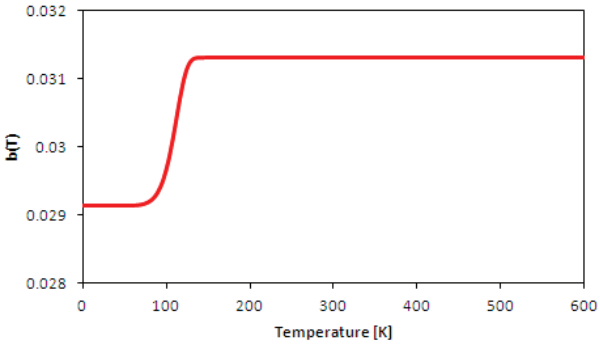

Figure C.8: Function $b(T)$ for argon, **[26]**.

4 of the 8 parameters in the functional form of $a(T)$ and $b(T)$, see eqs. (C93)-(C94), can be calculated because two values of each parameter are known, a_c and a_t for a, and b_c and b_t for b. In [26], other constraints for the evaluation of the other 4 parameters within eqs. (C93)-(C94) are the Boyle's temperature and the maximum inversion temperature of Joule-Thomson's coefficient.

In [26], the *QEoS* has been applied for representing phase equilibrium behavior of pure compounds (argon, methane, and carbon dioxide) and the mixture methane - carbon dioxide by means of four mixing rules. The mixing rule for the parameter a was the sole containing a binary interaction parameters, evaluated by trials and errors for representing SLE and VLE.

Quadratic mixing rules, eqs. (C96)-(C98), were proposed for the EoS parameters b, c, and d, in dealing with phase equilibria in the benzene-cyclohexane binary mixture, [27]. Eq. (C95) is the same used in [26] with $k_{ij} = k_{ji}$. These binary mixtures contain 4 binary interaction parameters, K_{ij}, m_{ij}, n_{ij}, and l_{ij}.

$$a = \sum_{i=1}^{N}\sum_{j=1}^{N}\sqrt{a_i a_j}\left(1 - K_{ij}\right)x_i x_j \quad , \quad K_{ij} = \frac{k_{ij}k_{ji}\left(x_i + x_j\right)}{k_{ij}x_j + k_{ji}x_i} \quad , \quad k_{ii} = 0 \qquad (C95)$$

$$b = \frac{1}{2}\sum_{i=1}^{N}\sum_{j=1}^{N}\left(b_i + b_j\right)\left(1 - m_{ij}\right)x_i x_j \quad , \quad m_{ij} = m_{ji} \quad , \quad m_{ii} = 0 \qquad (C96)$$

$$c = \frac{1}{2}\sum_{i=1}^{N}\sum_{j=1}^{N}\left(c_i + c_j\right)\left(1 - n_{ij}\right)x_i x_j \quad , \quad n_{ij} = n_{ji} \quad , \quad n_{ii} = 0 \qquad (C97)$$

$$d = \frac{1}{2}\sum_{i=1}^{N}\sum_{j=1}^{N}\left(d_i + d_j\right)\left(1 - l_{ij}\right)x_i x_j \quad , \quad l_{ij} = l_{ji} \quad , \quad l_{ii} = 0 \qquad (C98)$$

In addition to these works, the *QEoS* has been applied for representing phase equilibrium behavior of mixtures involving hydrates, [28] and [29], hard sphere, [30], and indoles, [31].

2.5.1 Theorical limits of the Yokozeki EoS

Among the thermodynamic models applicable to solid, liquid, and vapor phases, the *QEoS* is considered as the first repulsion-based analytical EoS in which a discontinuity is introduced in the isotherm. However, concerning the exponent k, other authors found that the model violates some physically important behaviors [32].

The first problem concerns the hard-sphere behavior as described by the Yokozeki EoS. The Yokozeki EoS can be applied for representing the hard-sphere behavior imposing $a=0$ in the attractive term of eq. (C92).

In these cases the EoS with k odd shows a negative pressure in the regions $b<v<c$, as qualitatively shown in Figure C.5 (this figure represents the phase equilibrium behavior as described by the EoS with k odd and a not null attractive part, but the qualitative behavior of the solid phase is the same of the hard-sphere model).

Molecular simulation results [33] confirm that a hard-sphere fluid without attraction has a positive pressure in all density regions, including the solid-fluid transition region. This is in contrast with the Yokozeki model for hard-sphere which presents a negative pressure in the solid phase branch.

The second problem concerns the application of the Maxwell's Equal Area Rule (*MEAR),* eq. (C85), to the solid-liquid phase transition. For the same authors, [32], the case with k even has a mathematical problem: it cannot be applied to the modeling of the solid-liquid phase transition via the *MEAR*. To describe this transition with this rule, the Helmholtz energy should be convergent in the phase transition region and while it is true for the k odd, the same does not happen for k even. Therefore it is not verified the possibility to use even values for k.

This feature can be briefly discussed considering the residual Helmholtz energy, eq. (C99), where the pressure explicit functional form of the QEoS (with $a = 0$) has been introduced.

$$a^R(T,v) = \frac{1}{RT}\int_{\infty}^{v}\left[\frac{RT}{v} - P(T,v)\right]dv = \frac{1}{RT}\int_{\infty}^{v}\left[\frac{RT}{v} - \frac{RT}{v-b(T)}\left(\frac{v-d}{v-c}\right)^k\right]dv \qquad (C99)$$

Considering two volumes so that $b < v_1 < c < v_2$, the differences $a^R(T,v_2)$ - $a^R(T,v_1)$ for $k = 1$ (*QEoS1*) and $k = 2$ (*QEoS2*) are:

$$a^R_{QEoS1}(T,v_2) - a^R_{QEoS1}(T,v_1) = A_1 + A_2\int_{v_1}^{v_2}\frac{1}{v-c}dv \qquad (C99)$$

$$a^R_{QEoS2}(T,v_2) - a^R_{QEoS2}(T,v_1) = B_1 + B_2\int_{v_1}^{v_2}\frac{1}{(v-c)^2}dv \qquad (C100)$$

The form of the quantities A_1, A_2, B_1, and B_2 in eqs. (C99)-(C100) is not of interest in this discussion. The basic difference between eqs. (C99)-(C100) is qualitatively illustrated in Figure C.9 and Figure C.10, having density in the x-axis and $1/(v\text{-}c)$ and $1/(v\text{-}c)^2$ in the y-axis, respectively.

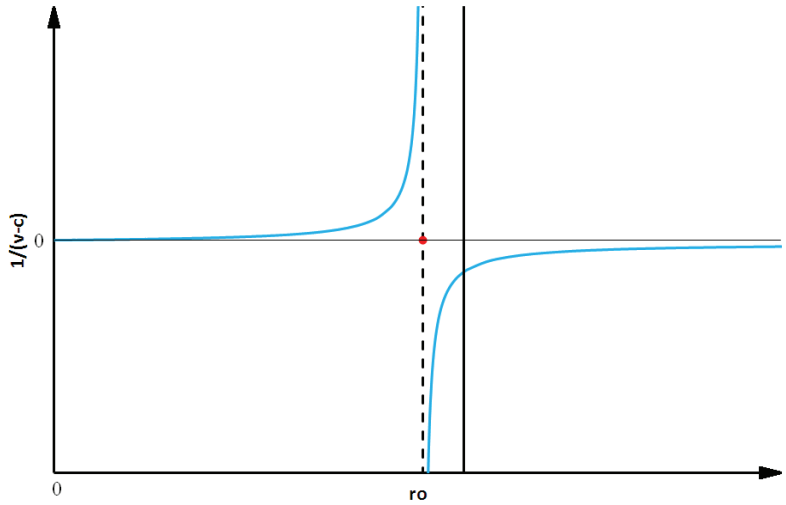

Figure C.9: Qualitative behavior of the function 1/(v-c).
— : 1/b; – – : 1/c; — : 1/(v-c); ● : point of symmetry.

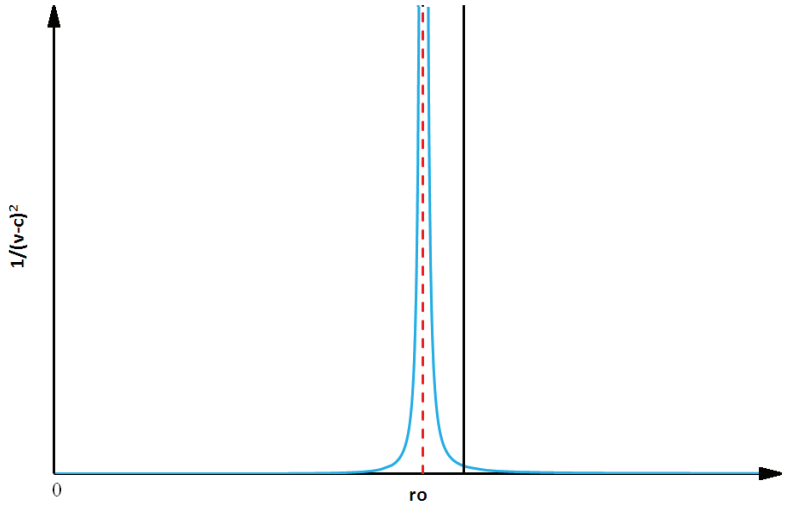

Figure C.10: Qualitative behavior of the function $1/(v\text{-}c)^2$.
— : 1/b; – – : 1/c and line of symmetry; — : $1/(v\text{-}c)^2$.

The definite integral in eq. (C99) is convergent in spite of the singular point $v = c$, because the ratio $1/(v\text{-}c)$ is point symmetrical about this singular point. The red circle ($\rho = 1/c$) in Figure C.9 is the point of symmetry of the function $1/(v\text{-}c)$.

The definite integral in eq. (C100) is instead not convergent in the integration region, because $1/(v\text{-}c)^2$ is line symmetrical, not point symmetrical, thus the *QEoS* with k even cannot be applied for representing the SLE via the *MEAR*. The red dashed line ($\rho = 1/c$) in Figure C.10 is the line of symmetry of the term $1/(v\text{-}c)^2$.

In addition to that, in [32] authors questioned the *QEoS* with $a = 0$ and $k = 1$ (*QEoS1*) in the framework of the Scaled-Particle Theory, (*SPT*). The *SPT* is a strategy applied to the equilibrium behavior of hard sphere systems representing a statistical mechanical device for the description of the hard sphere fluid phase. The SPT was developed by Reiss et al., [34], and its detailed description is beyond the scope of this work. In the framework of the *SPT*, the insertion probability p^* is the probability that the insertion of a molecule in a hard sphere system occurs without overlapping the existing molecules. The insertion probability can be related to the compressibility factor Z by means of eq. (C101), [32]:

$$\ln p^*\left(\theta = \frac{b}{v}, \beta = \frac{1}{k_B T}\right) = 1 - Z(\theta,\beta) - \int_0^{\theta} \frac{Z(\theta,\beta) - 1}{\theta} d\theta \qquad (C101)$$

In eq. (C101), θ is the volume fraction, b the solid covolume, and β contains the Boltzmann constant k_B. According to [32], the insertion probability should satisfy the following boundary conditions: $p^*(\theta{=}0){=}1$, since there are no molecules in the system hindering the insertion, and $p^*(\theta{=}1){=}0$, because the insertion is impossible due to the maximum packing state of the system.

Introducing the expression of compressibility factor derived from *QEoS1* (namely from eq. (C92) with $a = 0$ and $k = 1$), in eq. (C101) gives the following insertion probability:

$$p^*(\theta,\beta) = |1-\theta|^{x_0}|1-c_r\theta|^{x_1} exp\left(-\frac{x_0\theta}{1-\theta}\right) exp\left(-\frac{x_1 c_r \theta}{1-c_r\theta}\right) \qquad (C102)$$

$$x_0 = \frac{d_r - 1}{c_r - 1} \quad , \quad x_1 = \frac{c_r - d_r}{c_r - 1} \quad , \quad c_r = \frac{c}{b}, \quad d_r = \frac{d}{b} \qquad (C103)$$

The quantities in eq. (C102) are detailed in eq. (C103). The presence of a discontinuity in the solid-liquid transition region leads to a discontinuous behavior of the insertion probability.

This can be appreciated in Figure C.11, where p^* is plotted against the volume fraction θ; the discontinuity is here represented by the ratio b/c.

Starting from an empty system ($\theta{=}0$), p^* decreases monotonically as the volume fraction approaches the asymptote b/c, the black dashed line of Figure C.11.

The probability goes to positive infinity at b/c, because of the last exponential term in eq. (C102).

As a consequence, in the *QEoS1* the insertion probability becomes larger than unity approaching the liquid covolume violating a physical constraint.

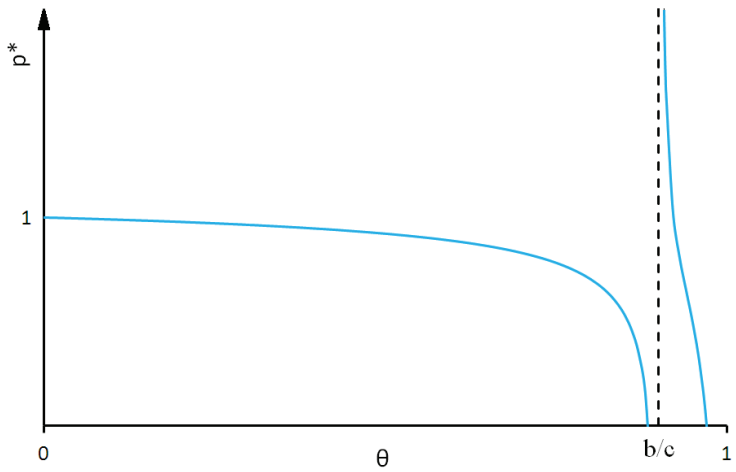

Figure C.11: Qualitative insertion probability of the QEoS with $a = 0$ and $k = 1$.
– – : b/c; — : p*.

2.6 Insertion Probability (*IP*)

Based on the previous comments regarding the *QEoS* of Yokozeki, in 2011 Lee et al. investigated the possibility of obtaining an EoS applicable to the three phases of matter, exploiting the relation between the compressibility factor and the Insertion Probability (*IP*), [35].

As anticipated in section 2.5.1, the *IP* is defined as the probability that a randomly selected molecule can enter into the system without overlapping the existing molecules, thus finding a cavity large enough to accommodate it.

On the basis of this concept, in [35] authors reinterpreted the correlated cell model of Alder et al., [36], in terms of *IP*, proposing an EoS for representing SLE, SVE, and SVE of pure substances ranging from simple gases to organic compounds.

The correlated cell model for the solid phase of Alder et al. is represented in Figure C.12. The solid is thought made of a single unit cell with periodic boundary conditions. The unit crystallographic cell is a hexagonal lattice containing two kinds of particles. Gray filled circles represent particles fixed at lattice positions, while open circles include the central wanderer and some of its neighbors. These latter move in unison with reference to the fixed particles.

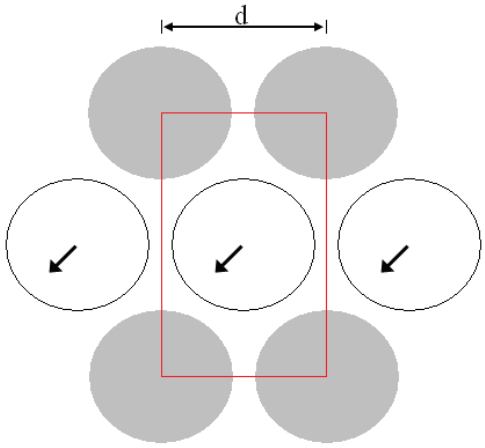

Figure C.12: Correlated cell proposed by Alder, [36].
Gray particles are fixed, empty particles move in unison, d is the characteristic of the cell.

$$Z = \frac{\partial \ln a_f}{\partial \ln d^2} \qquad (C104)$$

In this configuration, the free area a_f available to the central wanderer depends on the cooperative behavior corresponding to the row of atoms sliding relative to the fixed particles.

On the basis of the correlated cell, an expression for a_f has been obtained in [36], and successively converted in an equation of state thanks to the relation between a_f and the compressibility factor, eq. (C104).

In the *IP* approach, Lee et al. considered the free area of a rectangular correlated cell, and obtained an expression for the insertion probability as function of the free area. From this relations, not re-proposed here, these authors obtained the following EoS:

$$\frac{Pb}{k_B T} = \frac{\theta}{r}(1-r) + \frac{\theta^2}{1-\theta} - a \ln\left|1 - \frac{\theta}{a}\right| - \frac{\varepsilon}{k_B T}\theta^2 \qquad (C105)$$

Eq. (C105), contains the volume fraction θ, the Boltzmann constant k_B, the temperature T, the pressure P, and four parameters a, b, r, and ε.

The EoS parameters are determined by minimizing an objective functions involving the average absolute deviation of VLE pressure and liquid density, and solid density.

A qualitative representation of the insertion probability behavior of eq. (C105) is given in Figure C.13. Unlike the unphysical behavior of the Yokozeki *QEoS1* shown in Figure C.11, it is possible to see that in this case p^* is never larger than unity, as required in the *SPT* of hard sphere systems.

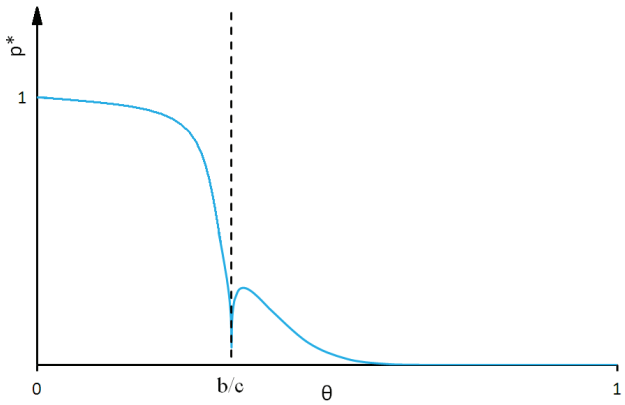

Figure C.13: Qualitative insertion probability by the IP model for SFE.
– – : b/c; — : p*.

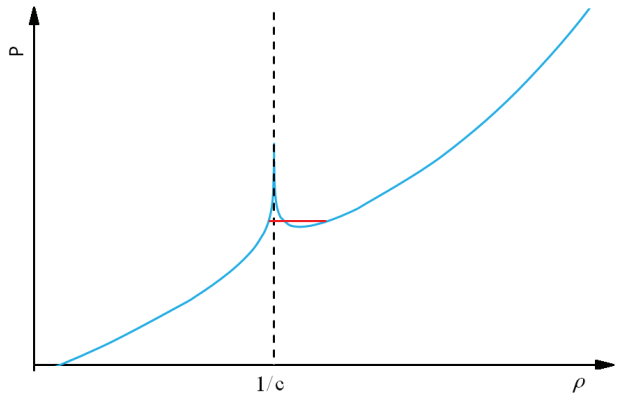

Figure C.14: Qualitative subcritical pressure-density phase diagrams from IP.
– – : 1/c; — : system pressure; — : Maxwell's equal area construction.

The qualitative subcritical pressure-density phase diagram related to eq. (C105) in the solid-liquid transition region is portrayed in Figure C.14. Eq. (C105) implies the classical S-loop for the liquid-vapor transition, while Figure C.14 shows that the solid-liquid one is obtained applying the Maxwell's equal area rule to a cusp which never yields a solid-liquid critical point.

Eq. (C105) have been applied in [35] for representing SLE, VLE, and SVE of pure compounds, while extensions to mixtures are still missing.

2.7 Unified Lattice Fluid Equation of State (*ULFEoS*)

The Unified Lattice Fluid Equation of State (*ULFEoS*) was suggested by Lee et al. in 2010, [37].

The SLE transition was obtained considering the solid phase as a highly associated matter and introducing a probability function concerning the solid bonding network.

Authors devised this approach with reference to the lattice model proposed by Veytsman for fluids with hydrogen bonds, [38], which illustration is beyond the scope of this analysis.

The probability function obtained was used for formulating the canonical partition function for the solid phase, from which authors derived the expression for the pressure and configurational chemical potential due to association in the solid phase. This partition function contains the internal bonding energy and entropy change due to solid formation, U_{SB} and S_{SB}, respectively.

At this point, the obtained SLE contribution was incorporated into a lattice based EoS yielding the vapor-liquid transition to account for the three phase behavior, [37].

Eq. (C106) is the resulting *ULFEoS*: it contains the temperature T, the pressure P, the Boltzmann constant k_B, the density ρ, and a series of parameters related to the lattice based EoS and the molecular association.

$$\frac{Pv_L}{k_BT} = \frac{z}{2} ln\left[1 + \rho\left(\frac{q}{r} - 1\right)\right] - \ln(1-\rho) - \frac{z\beta}{2}\varepsilon\theta_1^2\left[1 - \frac{\beta\varepsilon}{2}\theta_0(2\theta_1 - \theta_0)\right] - m\frac{N_{SB}}{N}\frac{\rho^m}{r} \qquad (C106)$$

The parameters of the lattice based EoS are the lattice cell volume v_L, the coordination number z (set to 10), the surface area parameter q, the molecular pair interaction energy ε, the surface area fraction of hole and molecules θ_0 and θ_1, and the parameter r.

The parameters related to the partition function are number of solid bonding pair N_{SB}, the total number of solid bonding molecules N, and a parameter m needed for shifting the association effect of the Veytsman model to the high density region.

In [37], the *ULFEoS* was tested against equilibrium properties of eight pure compounds, providing a close representation of SLE, VLE, and SVE.

Nevertheless, the application of the *ULFEoS* needs the regression of six parameters.

Three parameters (v_L, r, ε) come from the lattice based part of eq. (C106), namely the first three terms in the right hand side of the equation. Since the solid-liquid contribution is negligible in the vapor-liquid region, v_L, r, and ε have been regressed considering saturated liquid density as well as saturated vapor pressure.

Three parameters (m, U_{SB}, S_{SB}) are contained in the solid-liquid contribution of eq. (C106), namely the last term in the equation. Parameters U_{SB} and S_{SB} are regressed considering experimental sublimation vapor pressure, while m has been imposed.

Authors imposed the value of m because the use of eq. (C106) entails the appearance of a S-loop for describing the solid-liquid transition. The imposed m allows avoiding the solid-liquid critical point while using eq. (C106). In addition to that, limiting value for U_{SB} and S_{SB} are suggested in [37] to make the solid-liquid transition be always first order.

2.8 Thermodynamic Perturbation Theory (*TPT*)

The perturbation theory has been developed for handling the necessity of finding the exact solution of a Complex Problem *CP*. The basic concept of the perturbation theory rests on finding the solution of a initial Solvable Problem, *SP*, and considering further terms to account for the deviation *D* from the *SP* to obtain the solution of the *CP*.

The Thermodynamic Perturbation Theory, *TPT*, represents the application of this concept to the evaluation of the energetic state of a thermodynamic system. In such a case, the Helmholtz free energy (A), the reference value (A^{REF}) and the perturbation term (A^{PERT}) represent the complex problem, the solvable problem and the deviation, respectively.

According to the *TPT*, the Helmholtz free energy of a system can be expressed as in eq. (C107).

$$A = A^{REF} + A^{PERT} \qquad (C107)$$

Since only one term has been added to the *SP* (A^{REF}), eq. (C106) represents a first-order perturbation approximation of A.

The advantage of deriving an expression for the Helmholtz free energy is that the residual Helmholtz can be calculated from an EoS like eq. (C107) and directly used for evaluating the equilibrium condition in pure compounds and mixtures a s well.

The *TPT* has been widely applied in the past to model simple molecules and chains in the fluid state, while extension to the solid phase and to the solid-liquid equilibrium has received significant attention only from the beginning of the new century.

Two examples of the *TPT* applied to solid phase are briefly presented in this section.

Adidharma and Radosz in 2004, [39], extended the Weeks-Chandler-Andersen *TPT* to the solid phase, while Cochran and Chiew in 2006, [40], made use of the Wertheim *TPT*. In both [39] and [40], authors considered the reference system interacting with the Lennard-Jones potential, and a solid phase consisting of orientationally disordered chain connecting different segments of hard spheres.

The resulting LJ-solid EoSs are eq. (C108) and eq. (C109), respectively.

$$\frac{A}{Nk_BT} = \frac{A^{ID}}{Nk_BT} + \frac{A^{SEG}}{Nk_BT} + \frac{A^{CHAIN}}{Nk_BT} \quad , \quad \frac{A^{SEG}}{Nk_BT} = m\left(\frac{\boldsymbol{A^{HS}_{RES}}}{\boldsymbol{N_S k_B T}} + \frac{A^{PERT}}{N_S k_B T}\right) \qquad (C108)$$

$$\frac{A}{Nk_BT} = \frac{\boldsymbol{A^{HSC}_{REF}}}{\boldsymbol{Nk_BT}} + \frac{A^{PERT}}{Nk_BT} \quad , \quad \frac{A^{HSC}}{Nk_BT} = \frac{A^{ID}}{Nk_BT} + \frac{A^{SEG}}{Nk_BT} + \frac{A^{CHAIN}}{Nk_BT} \qquad (C109)$$

In eqs. (C108)-(C109), N is the number of molecular chains, k_B is the Boltzmann constant, T is the temperature, A^{ID} is the Helmholtz energy for the ideal monatomic gas, A^{SEG} is the energy due to the segment-segment interaction, A^{PERT} is the perturbation term, and A^{CHAIN} is the energy due to chain formation.

In eq. (C108), m is the number of segment for chain molecule, N_S is the total number of segments, and $A_{RES}{}^{HS}$ is the reference residual Helmholtz energy. In eq. (C109), A^{HSC} is the reference hard-spheres chain Helmholtz energy.

The main point differentiating these models is the choice of the reference state undergoing perturbation, the bold terms in eqs. (C108)-(C109). In the EoS of Adidharma and Radosz, eq. (C108), perturbation occurs in the segment-segment energy involving the intermolecular interaction as deviation from the hard-sphere reference system ($A_{RES}{}^{HS}$).

Conversely, in eq. (C109) the reference state is the ideal hard-sphere chain ($A_{REF}{}^{HSC}$) and perturbation is added to account for the energetic interaction within the chains.

2.8.1 Tan et al.

Tan et al. coupled the LJ-solid EoS proposed by Adidharma et Radosz with the Perturbed Chain Statistical Associating Fluid Theory (*PC-SAFT*), [41], for representing solid-liquid-vapor equilibria in non-associating and non-polar systems, [42].

The system consists then of two EoSs based on the *TPT*. The physical properties involved in each *TPT* within the system are m, the effective number of spherical segments, σ, the segment size, and ε, the segment interaction energy.

Thus, a total of 6 parameters need to be regressed for applying the system to the representation of solid-liquid-vapor equilibria of pure substances. 3 parameters are in the *PC-SAFT*, fitted to VLE data (vapor pressure and saturated liquid density), and 3 parameters are in the LJ-solid EoS, fitted to SLE and SVE data (melting and sublimation pressure).

For binary mixtures, VLE and SLE data are used for regressing two binary interaction parameters, one for the fluid phase and one for the solid phase, [42].

2.8.2 Cochran and Chiew

In 2007, the perturbed hard chain model proposed by Cochran and Chiew has been coupled with an analogous EoS for the fluid phase. The system of two *EoSs* has been applied to pure compounds and binary mixtures of *n*-alkanes, [43], [44].

Since the fluid-phase hard chain model obtained in [43] is similar to the solid-phase model developed in [40], it follows that parameters m, σ, and ε, are the same for both *EoSs* within the system.

In the framework of the hard chain model, m is the length of the chain, σ is the size of the segment in the chain, and ε is the chain interaction energy.

For the pure n-alkanes presented in [43], the regression of the three parameters has been conducted minimizing an objective function involving experimental SLE data (temperature, solid and liquid densities).

In [44], the perturbed hard chain models have been extended to solid and liquid mixtures, and applied to the representation of Solid-Fluid Equilibrium (*SFE*) data regarding the solubility of waxes in n-alkanes solvents.

In [44], authors adopted the pure n-alkanes parameters obtained in [43], replaced the LJ potential with the Mie model for the intermolecular potential, [11], and compared 5 different mixing rules containing each one binary interaction parameter, regressed on SFE data.

Bibliography

[1] G. S. Soave, "Application of the Redlich-Kwong-Soave equation of state to solid-liquid equilibria calculations," *Chem. Eng. Sci.,* vol. 34, no. 2, pp. 225-229, 1979.

[2] O. Redlich e J. Kwong, *Chemical Reviews,* vol. 44, pp. 233-244, 1949.

[3] C. Twu, V. Tassone e W. Sim, «New solid equation of state combining excess energy mixing rule for solid-liquid equilibria,» *AIChE Journal,* vol. 49, n. 11, pp. 2957-2965, 2003.

[4] S. B. Rodrigues-Reartes, M. Cismondi and M. S. Zabaloy, "Computation of solid-fluid-fluid equilibria for binary asymmetric mixtures in wide ranges of conditions," *J. of Supercritical Fluids,* vol. 57, pp. 9-24, 2011.

[5] D. Peng e D. Robinson, «A new two parameters equation of state,» *Industrial and Engineering Chemistry Fundamentals,* vol. 15, pp. 59-64, 1976.

[6] J. A. P. Coutinho, "Predictive UNIQUAC: a new model for the description of multiphase solid-liquid equilibria in complex hydrocarbon mixtures," *Ind. Eng. Chem. Res.,* vol. 37, pp. 4870-4875, 1998.

[7] J. A. P. Coutinho and E. H. Stenby, "Predictive local composition models for solid/liquid equilibrium in n-Alkane systems: Wilson equation for multicomponent systems," *Ind. Eng. Chem. Res.,* vol. 35, pp. 918-925, 1996.

[8] J. A. P. Coutinho, S. I. Andersen and E. H. Stenby, "Evaluation of activity coefficient models in prediction of alkane solid-liquid equilibria," *Fluid Phase Equilibr,* vol. 103, pp. 23-39, 1995.

[9] J. A. P. Coutinho, K. Knudsen, S. I. Andersen and E. H. Stenby, "A local composition model for paraffinic solid solutions," *Chem. Eng. Sci.,* vol. 51, no. 12, pp. 3273-3282, 1996.

[10] G. B. Wilson, "Vapor-liquid equilibrium. XI. A new expression for the excess free energy of mixing," *J. Am. Chem. Soc.,* vol. 86, pp. 127-130, 1964.

[11] J. Prausnitz, R. Lichtenthaler e E. de Azevedo, Molecular thermodynamics of fluid-phase equilibria, 2nd a cura di, E. Cliffs, A cura di, Prentice-Hall, Chap. 9, NJ, 1985.

[12] P. J. Flory, "Thermodynamics of polymer solutions," *Discuss. Farad. Soc.,* vol. 49, pp. 7-29, 1970.

[13] A. Fredenslund, R. L. Jones e J. M. Prausnitz, «Group-contribution estimation of activity coefficients in nonideal liquid mixtures,» *AIChE Journal,* vol. 21, n. 6, pp. 1086-1099, 1975.

[14] D. S. Abrams and J. M. Prausnitz, "Statistical thermodynamics of liquid mixtures: a new expression for the excess Gibbs energy of partly or completely miscible systems," *AIChE Journal,* vol. 21, no. 1, pp. 116-128, 1975.

[15] J. A. P. Coutinho, F. Mirante and J. Pauly, "A new predictive UNIQUAC for modeling of wax formation in hydrocarbon fluids," *Fluid Phase Equilibr,* vol. 247, pp. 8-17, 2006.

[16] K. Kan, «An equation of state and the gas-liiquid-solid equilibrium in argon,» *Chinese Journal of Physics,* vol. 17, pp. 32-43, 1979.

[17] J. Levelt Sengers, M. Kleim e J. Gallagher, 3rd a cura di, A. I. o. P. Handbook, A cura di, N.Y.: McGraw-Hill Co., 1972, pp. 204-210.

[18] H. Wenzel e G. Schmidt, «A modified van der Waals equation of state for the representation of phase equilibria between solids, liquids, and gases,» *Fluid Phase Equilib.,* vol. 5, pp. 3-17, 1980.

[19] F. d. J. Guevara-Rodriguez and A. Romero-Martinez, "An empirical extension for a generalized cubic equation of state, applied to a pure substance with small molecules," *Fluid Phase Equilibr,* vol. 347, pp. 22-27, 2013.

[20] P. Salim e M. Trebble, «Modeling of solid phases in thermodynamic calculations via translation of a cubic equation of state at the triple point,» *Fluid Phase Equilibria,* vol. 93, pp. 75-99, 1994.

[21] P. H. Salim and M. A. Trebble, "Thermodynamic property predictions from the Trebble-Bishnoi-Salim equation of state," *Fluid Phase Equilibr.,* vol. 65, pp. 41-57, 1991.

[22] R. Heidemann e J. Prausnitz, «A van der Waals-type equation of state for fluids with associating molecules,» *Proc. Natl. Acad. Sci.,* vol. 73, pp. 1773-1776, 1976.

[23] E. Lang e H. Wenzel, «Extension of a cubic equation of state to solids,» *Fluid Phase Equilib.,* vol. 51, pp. 101-117, 1989.

[24] D. Geaña e H. Wenzel, «Solid–liquid–gas equilibrium by cubic equations of state and association,» *J. Supercritical Fluids,* vol. 15, pp. 97-108, 1999.

[25] G. W. H. Schmidt, «A modified van der Waals type equation of state,» *Chem. Eng. Sci.,* vol. 35, pp. 1503-1512, 1980.

[26] A. Yokozeki, «Analytical equation of state for solid-liquid-vapor phases,» *International Journal of Thermophysics,* vol. 24, n. 3, pp. 589-620, May 2003.

[27] A. Yokozeki, «Phase equilibria of benzene-cyclohexane binary mixtures using a solid-liquid-vapor equation of state,» *Applied Energy,* vol. 81, pp. 334-349, 2005.

[28] A. Yokozeki, «Methane gas hydrates viewed through unified solid-liquid-vapor equation of state,» *Int J Thermophys.,* vol. 26, pp. 743-765, 2005.

[29] A. Yokozeki, «Solid-liquid-vapor phases of water and water-carbon dioxide mixtures using a simple analytical equation of state,» *Fluid Phase Equilibria,* Vol. %1 di %255-56, pp. 222-223, 2004.

[30] A. Yokozeki, "Phase behaviors of binary hard-sphere mixtures using simple analytical equation of state," *Int. J. Thermophys.,* vol. 25, no. 3, pp. 643-667, 2004.

[31] A. Yokozeki, «Solid-liquid phase equilibria of binary indole mixtures with some aromatic compounds using a solid-liquid-vapor equation-of-state,» *Applied Energy,* vol. 81, pp. 322-333, 2005.

[32] J. H. Lee e K.-P. Yoo, «Comments on "Analytic Equation of State for Solid-Liquid-Vapour Phases",» *Internationa Journal of Thermopysics,* vol. 32, p. 553:558, 2011.

[33] B. Alder e T. Wainwright, *Journal of Chemical Physics,* vol. 27, pp. 1208-1209, 1957.

[34] H. Reiss, H. L. Frisch and J. L. Lebowitz, *J. Chem. Phys.,* vol. 31, p. 369, 1959.

[35] J. H. Lee, M. S. Shin and K.-P. Yoo, "Development of single insertion probability for equation of state applicable to three phases of matter," *Ind. Eng. Chem. Data,* vol. 50, pp. 4166-4176, 2011.

[36] B. Alder, W. G. Hoover and T. Wainwright, "Cooperative motion of hard disk leading to melting," *Phys. Lett. Rev.,* vol. 11, no. 6, pp. 241-243, 1963.

[37] J. H. Lee, M. S. Shin, H. Kim and K.-P. Yoo, "Extended Veytsamn statistics for the solid-fluid transition in the framework of lattice fluid," *J. Chem. Thermodynamics,* vol. 42, pp. 891-899, 2010.

[38] B. A. Veytsman, "Are lattice models valid for fluids with hydrogen bonds?," *J. Phys. Chem.,* vol. 94, pp. 8449-8500, 1990.

[39] H. Adidharma and M. Radosz, "The LJ-solid equation of state extended to thermal properties, chain molecules, and mixtures," *Ind. Eng. Chem. Res.,* vol. 43, pp. 6890-6897, 2004.

[40] T. W. Cochran e Y. C. Chiew, «Perturbed-chain equation of state for the solid phase,» *J. Chem. Phys.,* vol. 126, p. 224901, 2006.

[41] J. Gross and G. Sadowski, "Perturbed-Chain SAFT: an equation of state based on a perturbation theory for chain molecules," *Ind. Chem. Eng. Res.,* vol. 40, pp. 1244-1260, 2001.

[42] S. P. Tan, H. Adidharma, J. S. Kargel and G. M. Marion, "Equation of state for solid solution-liquid-vapor equilibria at cryogenic conditions," *Fluid Phase Equilibr.,* vol. 360, pp. 320-331, 2013.

[43] T. W. Cochran e T. W. Chiew, «Application of perturbed chain equation of state to solid-liquid equilibria. I. Pure component,» *Fluid Phase Equilibr.,* vol. 262, pp. 37-43, 2007.

[44] T. W. Cochran and Y. C. Chiew, "Application of perturbed chain equation of state to solid-liquid equilibria. II. Binary mixtures," *Fluid Phase Equilibr.,* vol. 262, pp. 44-50, 2007.

Appendix D

REPRESENTATION OF PHASE EQUILIBRIA I. PURE COMPOUNDS

LIST OF FIGURES **D2**

LIST OF TABLES **D3**

1 FUNCTIONAL FORM OF THE SLV EOS D4
1.1 Reduced pressure, first and second derivatives with respect to volume *D5*
1.2 Analytical solution of the critical point conditions *D6*
1.3 Compressibility factor, fugacity coefficient, and residual properties *D10*
1.3.1 First-order partial derivative of a^R with respect to density D13
1.3.2 First-order partial derivative of a^R with respect to temperature D14
2 SOLUTION OF A 4TH ORDER EQUATION D16
3 QUALI/QUANTITATIVE COMPARISONS FOR PURE COMPOUNDS D17
3.1 Nitrogen *D20*
3.2 Oxygen *D21*
3.3 Argon *D22*
3.4 Krypton *D23*
3.5 Xenon *D24*
3.6 Neon *D25*
3.7 Helium *D26*
3.8 Carbon dioxide *D27*
3.9 Hydrogen *D28*
3.10 Nitrous oxide *D29*
3.11 Methane *D30*
3.12 Ethane *D31*
3.13 Ethylene *D32*
3.14 Propane *D33*
3.15 Propylene *D34*

List of Figures

Figure D.1: Pressure-temperature equilibrium projection of helium.....D18
Figure D.2: PT-EP of N_2 obtained with the SLV EoS.....D20
Figure D.3: Percentage errors in terms of pressure for N_2.....D20
Figure D.4: Percentage errors in terms of temperature for N_2.....D20
Figure D.5: PT-EP of O_2 obtained with the SLV EoS.....D21
Figure D.6: Percentage errors in terms of pressure for O_2.....D21
Figure D.7: Percentage errors in terms of temperature for O_2.....D21
Figure D.8: PT-EP of Ar obtained with the SLV EoS.....D22
Figure D.9: Percentage errors in terms of pressure for Ar. D22
Figure D.10: Percentage errors in terms of temperature for Ar.....D22
Figure D.11: PT-EP of Kr obtained with the SLV EoS.....D23
Figure D.12: Percentage errors in terms of pressure for Kr. D23
Figure D.13: Percentage errors in terms of temperature for Kr.....D23
Figure D.14: PT-EP of Xe obtained with the SLV EoS. D24
Figure D.15: Percentage errors in terms of pressure for Xe. D24
Figure D.16: Percentage errors in terms of temperature for Xe. D24
Figure D.17: PT-EP of Ne obtained with the SLV EoS. D25
Figure D.18: Percentage errors in terms of pressure for Ne. D25
Figure D.19: Percentage errors in terms of temperature for Ne. D25
Figure D.20: PT-EP of He obtained with the SLV EoS. D26
Figure D.21: Percentage errors in terms of pressure for He. D26
Figure D.22: Percentage errors in terms of temperature for He. D26
Figure D.23: PT-EP of CO_2 obtained with the SLV EoS. D27
Figure D.24: Percentage errors in terms of pressure for CO_2. .....D27
Figure D.25: Percentage errors in terms of temperature for CO_2. .....D27
Figure D.26: PT-EP of H_2 obtained with the SLV EoS.....D28
Figure D.27: Percentage errors in terms of pressure for H_2.....D28
Figure D.28: Percentage errors in terms of temperature for H_2.....D28
Figure D.29: PT-EP of N_2O obtained with the SLV EoS.....D29
Figure D.30: Percentage errors in terms of pressure for N_2O.....D29
Figure D.31: Percentage errors in terms of temperature for N_2O.....D29
Figure D.32: PT-EP of CH_4 obtained with the SLV EoS. D30
Figure D.33: Percentage errors in terms of pressure for CH_4. .....D30
Figure D.34: Percentage errors in terms of temperature for CH_4. .....D30
Figure D.35: PT-EP of C_2H_6 obtained with the SLV EoS.....D31
Figure D.36: Percentage errors in terms of pressure for C_2H_6.....D31
Figure D.37: Percentage errors in terms of temperature for C_2H_6.....D31
Figure D.38: PT-EP of C_2H_4 obtained with the SLV EoS.....D32
Figure D.39: Percentage errors in terms of pressure for C_2H_4.....D32
Figure D.40: Percentage errors in terms of temperature for C_2H_4.....D32
Figure D.41: PT-EP of C_3H_8 obtained with the SLV EoS.....D33
Figure D.42: Percentage errors in terms of pressure for C_3H_8.....D33
Figure D.43: Percentage errors in terms of temperature for C_3H_8.....D33
Figure D.44: PT-EP of C_3H_6 obtained with the SLV EoS.....D34
Figure D.45: Percentage errors in terms of pressure for C_3H_6.....D34
Figure D.46: Percentage errors in terms of temperature for C_3H_6.....D34

List of Tables

Table D.1: Triple and critical points for the substances of interest, [3]. D17
Table D.2: Minimum SVE and maximum SLE values for the temperature and pressure used for the regression of the SLV EoS parameters. D18
Table D.3: Errors of the SLV EoS with respect to the auxiliary values for nitrogen. D20
Table D.4: Errors of the SLV EoS with respect to the auxiliary values for oxygen. D21
Table D.5: Errors of the SLV EoS with respect to the auxiliary values for argon. D22
Table D.6: Errors of the SLV EoS with respect to the auxiliary values for krypton. D23
Table D.7: Errors of the SLV EoS with respect to the auxiliary values for xenon. D24
Table D.8: Errors of the SLV EoS with respect to the auxiliary values for neon. D25
Table D.9: Errors of the SLV EoS with respect to the auxiliary values for helium. D26
Table D.10: Errors of the SLV EoS with respect to the auxiliary values for carbon dioxide. D27
Table D.11: Errors of the SLV EoS with respect to the auxiliary values for hydrogen. D28
Table D.12: Errors of the SLV EoS with respect to the auxiliary values for nitrous oxide. D29
Table D.13: Errors of the SLV EoS with respect to the auxiliary values for methane. D30
Table D.14: Errors of the SLV EoS with respect to the auxiliary values for ethane. D31
Table D.15: Errors of the SLV EoS with respect to the auxiliary values for ethylene. D32
Table D.16: Errors of the SLV EoS with respect to the auxiliary values for propane. D33
Table D.17: Errors of the SLV EoS with respect to the auxiliary values for propylene. D34

1 Functional form of the SLV EoS

In eq. (D.1), a generic covolume *x* has been considered in the attractive term of the functional form of the Solid-Liquid-Vapor EoS (SLV EoS) proposed by Yokozeki in [1]:

$$P(T,v) = \frac{RT}{v-b}\frac{v-d}{v-c} - \frac{a}{v^2+qxv+rx^2} \qquad (D.1)$$

In eq. (D.1), q and r are parameters, R is the gas constant, T the temperature, P the pressure, d the volume where repulsive term becomes 0, c is the liquid covolume, and v is the volume.

$a(T)$ and $b(T)$ are T-dependent functions and represent the attractive forces among the molecules and the covolume of the solid phase, respectively. x is either the liquid or the solid covolume.

Expressions of $a(T)$ and $b(T)$ are indicated in eqs. (D.2)-(D.3).

$$a(T) = \frac{R^2T_c^2}{P_c}a_r(T_r) = \frac{R^2T_c^2}{P_c}[a_0 + a_1T_r exp(-a_2T_r^n)] \qquad (D.2)$$

$$b(T) = v_c\, b_r(T_r) = v_c[b_0 + b_1 exp(-b_2T_r^n)] \qquad (D.3)$$

In eqs. (D.2)-(D.3), a_r and b_r are reduced parameters. The mathematical steps in eqs. (D.4) and (D.6) yield the first-order derivatives of functions $a(T)$ and $b(T)$, eqs. (D.5) and (D.7), respectively.

$$\begin{aligned}
\frac{\partial a(T)}{\partial T} &= \frac{R^2T_c^2}{P_c}\frac{\partial a_r(T_r)}{\partial T} = \frac{R^2T_c^2}{P_c}\frac{\partial}{\partial T}\left\{a_0 + a_1\frac{T}{T_c}exp\left[-a_2\left(\frac{T}{T_c}\right)^n\right]\right\} = \\
&= \frac{R^2T_c^2}{P_c}\left\{\frac{a_1}{T_c}exp\left[-a_2\left(\frac{T}{T_c}\right)^n\right] + a_1\frac{T}{T_c}exp\left[-a_2\left(\frac{T}{T_c}\right)^n\right]\left[-a_2n\left(\frac{T}{T_c}\right)^{n-1}\frac{1}{T_c}\right]\right\} = \\
&= \frac{R^2T_c^2}{P_c}\left\{\frac{a_1}{T_c}exp[-a_2T_r^n] + a_1T_r\left(-\frac{a_2nT_r^{n-1}}{T_c}\right)exp[-a_2T_r^n]\right\} = \\
&= \frac{R^2T_c^2}{P_c}\left\{\frac{a_1[1-T_ra_2nT_r^{n-1}]}{T_c}exp[-a_2T_r^n]\right\} = \frac{R^2T_c^2}{P_c}\left\{\frac{a_1}{T_c}(1-na_2T_r^n)exp[-a_2T_r^n]\right\} =
\end{aligned} \qquad (D.4)$$

$$\frac{\partial a(T)}{\partial T} = \frac{R^2T_c}{P_c}a_1(1-na_2T_r^n)exp(-a_2T_r^n) \qquad (D.5)$$

$$\begin{aligned}
\frac{\partial b(T)}{\partial T} &= v_c\frac{\partial b_r(T_r)}{\partial T} = v_c\frac{\partial}{\partial T}\left\{b_0 + b_1exp\left[-b_2\left(\frac{T}{T_c}\right)^m\right]\right\} = \\
&= v_c\left\{b_1exp\left[-b_2\left(\frac{T}{T_c}\right)^m\right]\left[-b_2m\left(\frac{T}{T_c}\right)^{m-1}\frac{1}{T_c}\right]\right\} = v_c\left\{b_1exp[-b_2T_r^m]\left(-b_2mT_r^{m-1}\frac{1}{T_c}\right)\right\} =
\end{aligned} \qquad (D.6)$$

$$\frac{\partial b(T)}{\partial T} = -\frac{v_c}{T_c}b_1b_2mT_r^{m-1}exp(-b_2T_r^m) \qquad (D.7)$$

The attractive term in eq. (D.1) can be developed considering the relations $q = \varepsilon_1\varepsilon_2$ and $r = \varepsilon_1+\varepsilon_2$. Since $v=1/\rho$, eq. (D.9) is eq. (D.8) in terms of temperature and density.

$$P(T,v) = \frac{RT}{v-b}\frac{v-d}{v-c} - \frac{a}{(v+\varepsilon_1 x)(v+\varepsilon_2 x)} \qquad (D.8)$$

$$P(T,\rho) = \frac{RT\rho}{1-b\rho}\frac{1-d\rho}{1-c\rho} - \frac{a\rho^2}{(1+\varepsilon_1 x\rho)(1+\varepsilon_2 x\rho)} \qquad (D.9)$$

Eq. (D.1) in terms of dimensionless parameters and expressions for the residual properties can be obtained from eqs. (D.8)-(D.9).

1.1 Reduced pressure, first and second derivatives with respect to volume

Eq. (D.16) is eq. (D.1) obtained considering the identities in eq. (D.10) and following the procedure in eqs. (D.11)-(D.15). In eqs. (D.10)-(D.16), the subscript *r* is for reduced properties of parameters.

$$P_r = \frac{P}{P_c}\ ;\ T_r = \frac{T}{T_c}\ ;\ Z_c = \frac{P_c v_c}{RT_c}\ ;$$
$$v_r = \frac{v}{v_c}\ ;\ b_r = \frac{b}{v_c}\ ;\ c_r = \frac{c}{v_c}\ ;\ d_r = \frac{d}{v_c}\ ;\ a_r = \frac{aP_c}{R^2T_c^2}\ ;\ x_r = \frac{x}{v_c} \qquad (D.10)$$

$$\frac{P}{P_c} = \frac{1}{P_c}\frac{RT}{(v-b)}\frac{v-d}{v-c} - \frac{1}{P_c}\frac{a}{v^2+qxv+rx^2} \qquad (D.11)$$

$$P_r = \frac{v_c}{Z_cRT_c}\frac{RT}{(v-b)}\frac{v/v_c-d/v_c}{v/v_c-c/v_c} - \frac{v_c}{Z_cRT_c}\frac{a}{v_c^2(v^2/v_c^2+qxv/v_c^2+rx^2/v_c^2)} \qquad (D.12)$$

$$P_r = \frac{1}{Z_c}\frac{T}{T_c}\frac{1}{v/v_c-b/v_c}\frac{v_r-d_r}{v_r-c_r} - \frac{1}{Z_cRT_c}\frac{1}{v_c}\frac{a}{(v_r^2+qx_rv_r+rx_r^2)} \qquad (D.13)$$

$$P_r = \frac{T_r}{Z_c(v_r-b_r)}\frac{v_r-d_r}{v_r-c_r} - \frac{1}{Z_cRT_c}\frac{P_c}{Z_cRT_c}\frac{a}{(v_r^2+qx_rv_r+rx_r^2)} \qquad (D.14)$$

$$P_r = \frac{T_r}{Z_c(v_r-b_r)}\frac{v_r-d_r}{v_r-c_r} - \frac{aP_c}{R^2T_c^2}\frac{1}{Z_c^2(v_r^2+qx_rv_r+rx_r^2)} \qquad (D.15)$$

$$P_r(T_r,v_r) = \frac{T_r}{Z_c(v_r-b_r)}\frac{v_r-d_r}{v_r-c_r} - \frac{a_r}{Z_c^2(v_r^2+qx_rv_r+rx_r^2)} \qquad (D.16)$$

First-order derivative of eq. (D.16) with respect to reduced volume v_r has been obtained following the steps resumed in eqs. (D.17)-(D.18).

$$\frac{\partial P_r}{\partial v_r} = \frac{T_r}{Z_c}\frac{v_r-d_r}{v_r-c_r}\frac{\partial}{\partial v_r}\left[\frac{1}{v_r-b_r}\right] + \frac{T_r}{Z_c(v_r-b_r)}\frac{\partial}{\partial v_r}\left[\frac{v_r-d_r}{v_r-c_r}\right] - \frac{a_r}{Z_c^2}\frac{\partial}{\partial v_r}\left[\frac{1}{(v_r^2+qx_rv_r+rx_r^2)}\right] \qquad (D.17)$$

$$\frac{\partial P_r}{\partial v_r} = \frac{T_r}{Z_c}\frac{v_r-d_r}{v_r-c_r}\left[-\frac{1}{(v_r-b_r)^2}\right] + \frac{T_r}{Z_c(v_r-b_r)}\left[\frac{d_r-c_r}{(v_r-c_r)^2}\right] - \frac{a_r}{Z_c^2}\left[-\frac{(2v_r+qx_r)}{(v_r^2+qx_rv_r+rx_r^2)^2}\right] \qquad (D.18)$$

$$\frac{\partial P_r}{\partial v_r} = -\frac{T_r}{Z_c(v_r-b_r)^2}\frac{v_r-d_r}{v_r-c_r} + \frac{T_r}{Z_c(v_r-b_r)}\frac{d_r-c_r}{(v_r-c_r)^2} + \frac{a_r(2v_r+qx_r)}{Z_c^2(v_r^2+qx_rv_r+rx_r^2)^2} \qquad (D.19)$$

First-order derivative of eq. (D.19) with respect to reduced volume v_r has been obtained following the steps resumed in eqs. (D.20)-(D.21).

$$\frac{\partial^2 P_r}{\partial v_r^2} = -\frac{T_r}{Z_c}\frac{v_r - d_r}{v_r - c_r}\frac{\partial}{\partial v_r}\left[\frac{1}{(v_r - b_r)^2}\right] - \frac{T_r}{Z_c(v_r - b_r)^2}\frac{\partial}{\partial v_r}\left[\frac{v_r - d_r}{v_r - c_r}\right] + \frac{T_r}{Z_c}\frac{d_r - c_r}{(v_r - c_r)^2}\frac{\partial}{\partial v_r}\left[\frac{1}{v_r - b_r}\right] + \frac{T_r}{Z_c(v_r - b_r)}\frac{\partial}{\partial v_r}\left[\frac{d_r - c_r}{(v_r - c_r)^2}\right] + \frac{a_r}{Z_c^2}\frac{\partial}{\partial v_r}\left[\frac{(2v_r + qx_r)}{(v_r^2 + qx_r v_r + rx_r^2)^2}\right] \quad (D.20)$$

$$\frac{\partial^2 P_r}{\partial v_r^2} = -\frac{T_r}{Z_c}\frac{v_r - d_r}{v_r - c_r}\left[-\frac{1}{(v_r - b_r)^3}\right] - \frac{T_r}{Z_c(v_r - b_r)^2}\left[\frac{d_r - c_r}{(v_r - c_r)^2}\right] + \frac{T_r}{Z_c}\frac{d_r - c_r}{(v_r - c_r)^2}\left[-\frac{1}{(v_r - b_r)^2}\right] + \frac{T_r}{Z_c(v_r - b_r)}\left[-\frac{2(d_r - c_r)}{(v_r - c_r)^3}\right] + \frac{a_r}{Z_c^2}\left[\frac{2(v_r^2 + qx_r v_r + rx_r^2)^2 - 2(2v_r + qx_r)^2(v_r^2 + qx_r v_r + rx_r^2)}{(v_r^2 + qx_r v_r + rx_r^2)^4}\right] \quad (D.21)$$

$$\frac{\partial^2 P_r}{\partial v_r^2} = \frac{2T_r}{Z_c(v_r - b_r)^3}\frac{v_r - d_r}{v_r - c_r} - \frac{2T_r}{Z_c(v_r - b_r)^2}\frac{d_r - c_r}{(v_r - c_r)^2} - \frac{2T_r}{Z_c(v_r - b_r)}\frac{d_r - c_r}{(v_r - c_r)^3} + \frac{2a_r}{Z_c^2}\frac{(v_r^2 + qx_r v_r + rx_r^2) - (2v_r + qx_r)^2}{(v_r^2 + qx_r v_r + rx_r^2)^3} \quad (D.22)$$

Eqs. (D.19) and (D.22) can be applied to solve the critical point conditions, as detailed in the following section.

1.2 Analytical solution of the critical point conditions

The critical point conditions are resumed in the system of eq. (D.23), where T_{rc} is the critical reduced temperature, v_{rc} is the critical reduced volume, and $T_{rc} = v_{rc} = 1$ holds.

$$\begin{cases} P_r|_{T_{rc},v_{rc}} = 1 \\ \left.\dfrac{\partial P_r}{\partial v_r}\right|_{T_{rc},v_{rc}} = 0 \\ \left.\dfrac{\partial^2 P_r}{\partial v_r^2}\right|_{T_{rc},v_{rc}} = 0 \end{cases} \quad (D.23)$$

The system in eq. (D.23) turns then in the one in eq. (D.24) by means of eqs. (D.16), (D.19), and (D.22). In eq. (D.24), a_{rc} and b_{rc} are reduced values of a and b at the critical temperature.

$$\begin{cases} \dfrac{1}{Z_c(1 - b_{rc})}\dfrac{1 - d_r}{1 - c_r} - \dfrac{a_{rc}}{Z_c^2(1 + qx_r + rx_r^2)} = 1 \\ -\dfrac{1}{Z_c(1 - b_{rc})^2}\dfrac{1 - d_r}{1 - c_r} + \dfrac{1}{Z_c(1 - b_{rc})}\dfrac{d_r - c_r}{(1 - c_r)^2} + \dfrac{a_{rc}}{Z_c^2}\dfrac{(2 + qx_r)}{(1 + qx_r + rx_r^2)^2} = 0 \\ \dfrac{2}{Z_c(1 - b_{rc})^3}\dfrac{1 - d_r}{1 - c_r} - \dfrac{2}{Z_c(1 - b_{rc})^2}\dfrac{d_r - c_r}{(1 - c_r)^2} - \dfrac{1}{Z_c(1 - b_{rc})}\dfrac{2(d_r - c_r)}{(1 - c_r)^3} + \\ + \dfrac{2a_{rc}}{Z_c^2}\dfrac{(1 + qx_r + rx_r^2) - (2 + qx_r)^2}{(1 + qx_r + rx_r^2)^3} = 0 \end{cases} \quad (D.24)$$

The system in eq. (D.24) can be rewritten as follows:

$$\begin{cases} \dfrac{1}{Z_c(1-b_{rc})}\dfrac{1-d_r}{1-c_r} - \dfrac{a_{rc}}{Z_c^2(1+qx_r+rx_r^2)} = 1 \\ \dfrac{1}{Z_c}\left\{-\dfrac{(1-d_r)}{(1-b_{rc})^2(1-c_r)} + \dfrac{(d_r-c_r)}{(1-b_{rc})(1-c_r)^2} + \dfrac{a_{rc}}{Z_c}\dfrac{(2+qx_r)}{(1+qx_r+rx_r^2)^2}\right\} = 0 \\ \dfrac{2}{Z_c}\left\{\dfrac{(1-d_r)}{(1-b_{rc})^3(1-c_r)} - \dfrac{(d_r-c_r)}{(1-b_{rc})^2(1-c_r)^2} - \dfrac{(d_r-c_r)}{(1-b_{rc})(1-c_r)^3} \right. \\ \left. + \dfrac{a_{rc}}{Z_c}\dfrac{(1+qx_r+rx_r^2)-(2+qx_r)^2}{(1+qx_r+rx_r^2)^3}\right\} = 0 \end{cases} \quad (D.25)$$

By removing $1/Z_c$ and $2/Z_c$ in the second and third equation of the system above, respectively, (D.25) becomes:

$$\begin{cases} \dfrac{1}{Z_c(1-b_{rc})}\dfrac{1-d_r}{1-c_r} - \dfrac{a_{rc}}{Z_c^2(1+qx_r+rx_r^2)} = 1 & (D.26a) \\ -\dfrac{(1-d_r)}{(1-b_{rc})^2(1-c_r)} + \dfrac{(d_r-c_r)}{(1-b_{rc})(1-c_r)^2} + \dfrac{a_{rc}}{Z_c}\dfrac{(2+qx_r)}{(1+qx_r+rx_r^2)^2} = 0 & (D.26b) \\ \dfrac{(1-d_r)}{(1-b_{rc})^3(1-c_r)} - \dfrac{(d_r-c_r)}{(1-b_{rc})^2(1-c_r)^2} - \dfrac{(d_r-c_r)}{(1-b_{rc})(1-c_r)^3} \\ + \dfrac{a_{rc}}{Z_c}\dfrac{(1+qx_r+rx_r^2)-(2+qx_r)^2}{(1+qx_r+rx_r^2)^3} = 0 & (D.26c) \end{cases}$$

Eq. (D.26b) can be rearranged adding and removing 1 in the second term:

$$\begin{aligned} &-\frac{(1-d_r)}{(1-b_{rc})^2(1-c_r)} + \frac{(d_r-c_r)+1-1}{(1-b_{rc})(1-c_r)^2} + \frac{a_{rc}}{Z_c}\frac{(2+qx_r)}{(1+qx_r+rx_r^2)^2} = \\ &= -\frac{(1-d_r)}{(1-b_{rc})^2(1-c_r)} + \frac{(1-c_r)}{(1-b_{rc})(1-c_r)^2} - \frac{(1-d_r)}{(1-b_{rc})(1-c_r)^2} + \frac{a_{rc}}{Z_c}\frac{(2+qx_r)}{(1+qx_r+rx_r^2)^2} = \\ &= -\frac{(1-d_r)}{(1-b_{rc})^2(1-c_r)} + \frac{1}{(1-b_{rc})(1-c_r)} - \frac{(1-d_r)}{(1-b_{rc})(1-c_r)^2} + \frac{a_{rc}}{Z_c}\frac{(2+qx_r)}{(1+qx_r+rx_r^2)^2} \end{aligned} \quad (D.27)$$

The same operation concerning the second and third terms in eq. (D.26c) yields:

$$\begin{aligned} &\frac{(1-d_r)}{(1-b_{rc})^3(1-c_r)} - \frac{(d_r-c_r)+1-1}{(1-b_{rc})^2(1-c_r)^2} - \frac{(d_r-c_r)+1-1}{(1-b_{rc})(1-c_r)^3} + \frac{a_{rc}}{Z_c}\frac{(1+qx_r+rx_r^2)-(2+qx_r)^2}{(1+qx_r+rx_r^2)^3} = \\ &= \frac{(1-d_r)}{(1-b_{rc})^3(1-c_r)} - \frac{(1-c_r)}{(1-b_{rc})^2(1-c_r)^2} + \frac{(1-d_r)}{(1-b_{rc})^2(1-c_r)^2} - \frac{(1-c_r)}{(1-b_{rc})(1-c_r)^3} \\ &\quad + \frac{(1-d_r)}{(1-b_{rc})(1-c_r)^3} + \frac{a_{rc}}{Z_c}\frac{(1+qx_r+rx_r^2)-(2+qx_r)^2}{(1+qx_r+rx_r^2)^3} = \\ &= \frac{(1-d_r)}{(1-b_{rc})^3(1-c_r)} - \frac{1}{(1-b_{rc})^2(1-c_r)} + \frac{(1-d_r)}{(1-b_{rc})^2(1-c_r)^2} - \frac{1}{(1-b_{rc})(1-c_r)^2} \\ &\quad + \frac{(1-d_r)}{(1-b_{rc})(1-c_r)^3} + \frac{a_{rc}}{Z_c}\frac{(1+qx_r+rx_r^2)-(2+qx_r)^2}{(1+qx_r+rx_r^2)^3} \end{aligned} \quad (D.28)$$

The identities defined in eq. (D.29) can be introduced in eqs. (D.26a), (D.27) and (D.28).

$$a_{rc} = A \qquad \frac{1}{(1-b_{rc})} = B \qquad \frac{1}{(1-c_r)} = C \qquad (1-d_r) = D \qquad \frac{1}{Z_c} = Z$$
$$\frac{1}{(1+qx_r+rx_r^2)} = E \qquad \frac{(2+qx_r)}{(1+qx_r+rx_r^2)^2} = F \qquad \frac{(1+qx_r+rx_r^2)-(2+qx_r)^2}{(1+qx_r+rx_r^2)^3} = G \tag{D.29}$$

With reference to the identities in eq. (D.29), the systems of eq. (D.26a)-(D.26c) can then be re-written as in eqs. (D.30a)-(D.30c).

$$\begin{cases} BCDZ - AZ^2E = 1 & (D.30a) \\ -B^2CD + BC - BC^2D + AZF = 0 & (D.30b) \\ B^3CD - B^2C + B^2C^2D - BC^2 + BC^3D + AZG = 0 & (D.30c) \end{cases}$$

The system of eqs. (D.30a)-(D.30c) contains five unknowns, Z_c, a_{rc}, b_{rc}, c_r, and d_r, thus an analytical solution can be obtained whenever two of these are fixed as input values.

One input is the critical compressibility factor, Z_c. For the second value of input one it is convenient to use the same covolume involved in the attractive term.

It is advantageous to fix b_{rc} when $x_r = b_{rc}$, while c_r when $x_r = c_r$. In this way, coefficients E, F, and G in eq. (D.29) are determined when x_r is chosen as input value together with Z_c.

In both cases, coefficient A can be obtained directly from eq. (D.30a) as function of the other coefficients. In eq. (D.31) and in the following, X=B+C and Y=BC.

$$BCDZ - AZ^2E = 1 \rightarrow A = \frac{BCDZ - 1}{Z^2E} = \frac{YDZ - 1}{Z^2E} \tag{D.31}$$

Eq. (D.31) can be introduced in eq. (D.30b) giving:

$$-B^2CD + BC - BC^2D + \left(\frac{YDZ-1}{Z^2E}\right)ZF = 0 = \tag{D.33}$$
$$= -BCD(B+C) + BC + \frac{F(YDZ-1)}{ZE} = \tag{D.34}$$
$$= -YXD + Y + \frac{F(YDZ-1)}{ZE} = \tag{D.35}$$
$$= -YXDZE + YZE + YDZF - F = \tag{D.36}$$
$$= D(-XYZE + YZF) - F + YZE = 0 \tag{D.37}$$

$$D = \frac{F - YZE}{YZF - XYZE} \tag{D.38}$$

The expression of coefficient D can be introduced in eq. (D.31) giving a new expression for A:

$$A = \frac{YDZ-1}{Z^2E} = \frac{ZY}{Z^2E}\left(\frac{F-YZE}{YZF-XYZE}\right) - \frac{1}{Z^2E} = \frac{Y}{ZE}\left(\frac{F-YZE}{YZF-XYZE}\right) - \frac{1}{Z^2E} \tag{D.39}$$

Coefficients X and Y are introduced in eq. (D.30c), then coefficients A and D are replaced by the expressions in eqs. (D.38)-(D.39). The mathematical steps in eqs. (D.40)-(D.54) yields a second-order polynomial, eq. (D.55)

$$B^3CD - B^2C + B^2C^2D - BC^2 + BC^3D + AZG = 0 = \quad (D.40)$$

$$= BCD(B^2 + C^2 + BC) - BC(B + C) + AZG = \quad (D.41)$$

$$= YD(B^2 + C^2 + BC + BC - BC) - YX + AZG = \quad (D.42)$$

$$= YD[(B + C)^2 - BC] - YX + AZG = \quad (D.43)$$

$$= YD(X^2 - Y) - YX + AZG = \quad (D.44)$$

$$= D(X^2Y - Y^2) - YX + AZG = \quad (D.45)$$

$$= \left(\frac{F - YZE}{YZF - XYZE}\right)(X^2Y - Y^2) - YX + \left[\frac{Y}{ZE}\left(\frac{F - YZE}{YZF - XYZE}\right) - \frac{1}{Z^2E}\right]ZG = \quad (D.46)$$

$$= \left(\frac{F - YZE}{YZF - XYZE}\right)(X^2Y - Y^2) - YX + \frac{YG}{E}\left(\frac{F - YZE}{YZF - XYZE}\right) - \frac{G}{ZE} = 0 = \quad (D.47)$$

$$= ZE(F - YZE)(X^2Y - Y^2) - ZE(YZF - XYZE)YX + YGZ(F - YZE) - G(YZF - XYZE) = \quad (D.48)$$

$$= E(F - YZE)(X^2Y - Y^2) - E(YZF - XYZE)YX + YG(F - YZE) - G(YF - XYE) = \quad (D.49)$$

$$= X^2YEF - Y^2EF - X^2Y^2ZE^2 + Y^3ZE^2 - XY^2ZEF + X^2Y^2ZE^2 + YGF - Y^2ZEG - YGF + XYGE = \quad (D.50)$$

$$= X^2YEF - Y^2EF + Y^3ZE^2 - XY^2ZEF - Y^2ZEG + XYGE = \quad (D.51)$$

$$= X^2F - YF + Y^2ZE - XYZF - YZG + XG = 0 = \quad (D.52)$$

$$= (B + C)^2F - BCF + B^2C^2ZE - (B + C)BCZF - BCZG + (B + C)G = \quad (D.53)$$

$$= B^2F + C^2F + 2BCF - BCF + B^2C^2ZE - B^2CZF - BC^2ZF - BCZG + BG + CG = \quad (D.54)$$

$$= B^2F + C^2F + BCF + B^2C^2ZE - B^2CZF - BC^2ZF - BCZG + BG + CG = 0 \quad (D.55)$$

Eq. (D.55) contains the coefficients B, C, Z, E, F, and G. According to eq. (D.29), the correspondent reduced parameters are b_{rc}, c_r, Z_c, and x_r. If the values of these parameters are known, a_{rc} and d_r can be calculated using eq. (D.31) and (D.38), respectively.

Eq. (D.55) is solved in terms of B if the attractive term involves the liquid covolume, so that fixing c_r results in knowing coefficients E, F, and G. Z is calculated from the imposed value of Z_c.

In such a case, B (then b_{rc}) is calculated as follows:

$$B^2F + C^2F + BCF + B^2C^2ZE - B^2CZF - BC^2ZF - BCZG + BG + CG = \quad (D.56)$$

$$= B^2(F + C^2ZE - CZF) + B(CF - C^2ZF - CZG + G) + (C^2F + CG) = \quad (D.57)$$

$$= B^2[F(1 - CZ) + C^2ZE] + B[CF + G - CZ(CF + G)] + [C(CF + G)] = \quad (D.58)$$

$$= B^2[F(1 - CZ) + C^2ZE] + B[(CF + G)(1 - CZ)] + [C(CF + G)] = 0 \quad (D.59)$$

$$B^2 + B\frac{[(CF + G)(1 - CZ)]}{[F(1 - CZ) + C^2ZE]} + \frac{[C(CF + G)]}{[F(1 - CZ) + C^2ZE]} = 0 \quad (D.60)$$

$$B^2 + a_1B + a_2 = 0 \rightarrow B = \frac{-a_1 + \sqrt{a_1^2 - 4a_2}}{2} \quad (D.61)$$

Conversely, eq. (D.55) is solved in terms of C if the attractive term involves the solid covolume at the critical temperature, thus fixing b_{rc} results in imposing coefficients E, F, and G. Z is calculated from the imposed value of Z_c.

In such a case, C (then c_r) is the sole unknown of eq. (D.55) and it is calculated as follows:

$$B^2F + C^2F + BCF + B^2C^2ZE - B^2CZF - BC^2ZF - BCZG + BG + CG = \quad (D.62)$$

$$= C^2(F + B^2ZE - BZF) + C(BF - B^2ZF - BZG + G) + (B^2F + BG) = \quad (D.63)$$

$$= C^2[F(1 - BZ) + B^2ZE] + C[BF + G - BZ(BF + G)] + [B(BF + G)] = \quad (D.64)$$

$$= C^2[F(1 - BZ) + B^2ZE] + C[(BF + G)(1 - BZ)] + [B(BF + G)] = 0 \quad (D.65)$$

$$C^2 + C\frac{[(BF + G)(1 - BZ)]}{[F(1 - BZ) + B^2ZE]} + \frac{[B(BF + G)]}{[F(1 - BZ) + B^2ZE]} = 0 \quad (D.66)$$

$$C^2 + a_1C + a_2 = 0 \rightarrow C = \frac{-a_1 + \sqrt{a_1^2 - 4a_2}}{2} \quad (D.67)$$

In eqs. (D.61)-(D.67), only one root of the second-order polynomial is considered because coefficient a_1 is always positive, thus $-a_1$ is always negative. The term a_1^2-$4a_2$ must be positive.

To fix ideas, the system of critical point conditions is solved fixing Z_c and c_r when the attractive term contains the liquid covolume, and the solid covolume is calculated from eq. (D.61).

The system of critical point conditions is solved fixing Z_c and b_{rc} when the attractive term contains the solid covolume, and the liquid covolume is calculated from eq. (D.67).

In both cases, d_r and a_{rc} are calculated from eq. (D.38) and (D.39), respectively.

1.3 Compressibility factor, fugacity coefficient, and residual properties

The values of compressibility factor Z, fugacity coefficient φ, residual Gibbs energy g^R, residual internal energy u^R, residual enthalpy h^R, and residual entropy s^R can be evaluated knowing the residual Helmholtz free energy a^R and its first derivatives with respect to density and temperature, as indicated in eqs. (D.68)-(D.73).

$$Z(T,\rho) = 1 + \rho a_\rho^R(T,\rho) \tag{D.68}$$

$$\ln\varphi\,(T,\rho) = Z(T,\rho) - 1 - \ln Z(T,\rho) + a^R(T,\rho) \tag{D.69}$$

$$\frac{G^R(T,\rho)}{RT} = g^R(T,\rho) = \ln\varphi\,(T,\rho) \tag{D.70}$$

$$\frac{U^R(T,\rho)}{RT} = u^R(T,\rho) = -Ta_T^R(T,\rho) \tag{D.71}$$

$$\frac{H^R(T,\rho)}{RT} = h^R(T,\rho) = Z(T,\rho) - 1 - Ta_T^R(T,\rho) \tag{D.72}$$

$$\frac{S^R(T,\rho)}{RT} = s^R(T,\rho) = -Ta_T^R(T,\rho) - a^R(T,\rho)R^2T^2 \tag{D.73}$$

The residual Helmholtz free energy a^R in terms of variables temperature and volume can be evaluated from:

$$a^R(T,v) = \frac{1}{RT}\int_\infty^v \left[\frac{RT}{v} - P(T,v)\right] dv \tag{D_A.74}$$

The expression of a^R related to the SLV EoS is obtained introducing the functional form of eq. (D.8) in the last term of eq. (D.74). The integral in eq. (D.75) turns in the sum of three integrals, as detailed in eq. (D.76). The three integrals are solved in eqs. (D.76a)-(D.76c).

$$a^R(T,v) = \frac{1}{RT}\int_\infty^v \left[\frac{RT}{v} - \frac{RT}{v-b}\frac{v-d}{v-c} + \frac{a}{(v+\varepsilon_1 x)(v+\varepsilon_2 x)}\right] dv \tag{D.75}$$

$$a^R(T,v) = \int_\infty^v \frac{1}{v}dv - \int_\infty^v \frac{v-d}{(v-b)(v-c)}dv + \frac{a}{RT}\int_\infty^v \frac{1}{(v+\varepsilon_1 x)(v+\varepsilon_2 x)}dv \tag{D.76}$$

$$\int_\infty^v \frac{1}{v}dv = ln|v|_\infty^v \tag{D.76a}$$

$$\int_\infty^v \frac{v-d}{(v-b)(v-c)}dv = \int_\infty^v \left(\frac{A_1}{v-b} + \frac{A_2}{v-c}\right)dv = \int_\infty^v \frac{A_1}{v-b}dv + \int_\infty^v \frac{A_2}{v-c}dv$$
$$= A_1 ln|v-b|_\infty^v + A_2 ln|v-c|_\infty^v = (*)$$

$$\frac{v-d}{(v-b)(v-c)} = \frac{A_1}{v-b} + \frac{A_2}{v-c} = \frac{A_1(v-c) + A_2(v-b)}{(v-b)(v-c)} = \frac{v(A_1+A_2) - (A_1c + A_2b)}{(v-b)(v-c)} \tag{D.76b}$$

$$\begin{cases} v(A_1+A_2) = v \\ d = A_1c + A_2b \end{cases} \Rightarrow \begin{cases} A_1 = 1 - A_2 \\ d = (1-A_2)c + A_2b \end{cases} \Rightarrow \begin{cases} A_1 = (d-b)/(c-b) \\ A_2 = (c-d)/(c-b) \end{cases}$$

$$(*) = \frac{d-b}{c-b} ln|v-b|_\infty^v + \frac{c-d}{c-b} ln|v-c|_\infty^v$$

$$\frac{a}{RT}\int_{\infty}^{v}\frac{1}{(v+\varepsilon_1 x)(v+\varepsilon_2 x)}dv=\frac{a}{RT}\int_{\infty}^{v}\left(\frac{A_3}{v+\varepsilon_1 x}+\frac{A_4}{v+\varepsilon_2 x}\right)dv$$
$$=\frac{a}{RT}\int_{\infty}^{v}\frac{A_3}{v+\varepsilon_1 x}dv+\frac{a}{RT}\int_{\infty}^{v}\frac{A_4}{v+\varepsilon_2 x}dv$$
$$=\frac{aA_3}{RT}ln|v+\varepsilon_1 x|_{\infty}^{v}+\frac{aA_4}{RT}ln|v+\varepsilon_2 x|_{\infty}^{v}=(**)$$
$$\frac{1}{(v+\varepsilon_1 x)(v+\varepsilon_2 x)}=\frac{A_3}{v+\varepsilon_1 x}+\frac{A_4}{v+\varepsilon_2 x}=\frac{A_3(v+\varepsilon_2 x)+A_4(v+\varepsilon_1 x)}{(v+\varepsilon_1 x)(v+\varepsilon_2 x)}$$
$$=\frac{v(A_3+A_4)+(A_3\varepsilon_2 x+A_4\varepsilon_1 x)}{(v+\varepsilon_1 x)(v+\varepsilon_2 x)} \qquad (D.76c)$$
$$\begin{cases} v(A_3+A_4)=0 \\ 1=A_3\varepsilon_2 x+A_4\varepsilon_1 x \end{cases}\Rightarrow\begin{cases} A_3=-A_4 \\ 1=-A_4\varepsilon_2 x+A_4\varepsilon_1 x \end{cases}\Rightarrow\begin{cases} A_3=1/x(\varepsilon_2-\varepsilon_1) \\ A_4=-1/x(\varepsilon_2-\varepsilon_1) \end{cases}$$
$$(**)=\frac{a}{RTx(\varepsilon_2-\varepsilon_1)}ln|v+\varepsilon_1 x|_{\infty}^{v}-\frac{a}{RTx(\varepsilon_2-\varepsilon_1)}ln|v+\varepsilon_2 x|_{\infty}^{v}$$
$$=\frac{a}{RTx(\varepsilon_2-\varepsilon_1)}ln\left|\frac{v+\varepsilon_1 x}{v+\varepsilon_2 x}\right|_{\infty}^{v}$$

Eq. (D.76) results then in eq. (D.77). Eq. (D.77) yields eq. (D.79). The first parenthesis in eq. (D.79) is null because (*d*-*b*)/(*c*-*b*)+(*c*-*d*)/(*c*-*b*)=1. This last relation allows splitting ln(*v*) in eq. (D.80) in two terms, which can be coupled with the third and fourth term, respectively, see eq. (D.81). The final expression of the residual Helmholtz free energy a^R in terms of variables temperature and volume is eq. (D.82). Eq. (D.83) is the residual Helmholtz free energy in terms of temperature and density obtained considering the relation $v=1/\rho$. Eq. (D.83) can be rearranged giving eq. (D.84).

$$a^R(T,v)=ln|v|_{\infty}^{v}-\frac{d-b}{c-b}ln|v-b|_{\infty}^{v}-\frac{c-d}{c-b}ln|v-c|_{\infty}^{v}+\frac{a}{RTx(\varepsilon_2-\varepsilon_1)}ln\left|\frac{v+\varepsilon_1 x}{v+\varepsilon_2 x}\right|_{\infty}^{v}= \qquad (D.77)$$

$$a^R(T,v)=[ln|v|-ln|\infty|]-\left[\frac{d-b}{c-b}ln|v-b|-\frac{d-b}{c-b}ln|\infty|\right]$$
$$-\left[\frac{c-d}{c-b}ln|v-c|-\frac{c-d}{c-b}ln|\infty|\right]+\frac{a}{RTx(\varepsilon_2-\varepsilon_1)}\left[ln\left|\frac{v+\varepsilon_1 x}{v+\varepsilon_2 x}\right|-ln\left|\frac{\infty}{\infty}\right|\right]= \qquad (D.78)$$

$$a^R(T,v)=\left[-ln|\infty|+\frac{d-b}{c-b}ln|\infty|+\frac{c-d}{c-b}ln|\infty|\right]$$
$$+\left[ln|v|-\frac{d-b}{c-b}ln|v-b|-\frac{c-d}{c-b}ln|v-c|+\frac{a}{RTx(\varepsilon_2-\varepsilon_1)}ln\left|\frac{v+\varepsilon_1 x}{v+\varepsilon_2 x}\right|\right]= \qquad (D.79)$$

$$a^R(T,v)=ln|v|-\frac{d-b}{c-b}ln|v-b|-\frac{c-d}{c-b}ln|v-c|+\frac{a}{RTx(\varepsilon_2-\varepsilon_1)}ln\left|\frac{v+\varepsilon_1 x}{v+\varepsilon_2 x}\right|= \qquad (D.80)$$

$$a^R(T,v)=\frac{d-b}{c-b}ln|v|+\frac{c-d}{c-b}ln|v|-\frac{d-b}{c-b}ln|v-b|-\frac{c-d}{c-b}ln|v-c|$$
$$+\frac{a}{RTx(\varepsilon_2-\varepsilon_1)}ln\left|\frac{v+\varepsilon_1 x}{v+\varepsilon_2 x}\right|= \qquad (D.81)$$

$$a^R(T,v)=\frac{d-b}{c-b}ln\left|\frac{v}{v-b}\right|+\frac{c-d}{c-b}ln\left|\frac{v}{v-c}\right|+\frac{a}{RTx(\varepsilon_2-\varepsilon_1)}ln\left|\frac{v+\varepsilon_1 x}{v+\varepsilon_2 x}\right| \qquad (D.82)$$

$$a^R(T,\rho) = \frac{d-b}{c-b} ln\left|\frac{1}{1-b\rho}\right| + \frac{c-d}{c-b} ln\left|\frac{1}{1-c\rho}\right| + \frac{a}{RTx(\varepsilon_2-\varepsilon_1)} ln\left|\frac{1+\varepsilon_1 x\rho}{1+\varepsilon_2 x\rho}\right| \qquad (D.83)$$

$$a^R(T,\rho) = \frac{1}{b-c}\left[dln\left|\frac{1-b\rho}{1-c\rho}\right| + cln|1-c\rho| - bln|1-b\rho|\right] + \frac{a}{RTx(\varepsilon_2-\varepsilon_1)} ln\left|\frac{1+\varepsilon_1 x\rho}{1+\varepsilon_2 x\rho}\right| \qquad (D.84)$$

Eq. (D.76c) does not hold in case of $q = r = 0$ (thus $\varepsilon_1 = \varepsilon_2 = 0$). In such a case, as in the van der Waals EoS, [2], integration of the attractive term gives a different result, and eq. (D.85) replaces eq. (D.76c).

$$\frac{a}{RT}\int_{\infty}^{v}\frac{1}{v^2}dv = \frac{a}{RT}\left|-\frac{1}{v}\right|_{\infty}^{v} = -\frac{a}{RTv} = -\frac{a\rho}{RT} \qquad (D.85)$$

Consequently, the functional form of the residual Helmholtz free energy a^R in terms of variables temperature and density is eq. (D.86). In the parenthesis of eq. (D.86), the second row is valid for $q = r = 0$.

$$a^R(T,\rho) = \underbrace{\frac{1}{b-c}\left[dln\left|\frac{1-b\rho}{1-c\rho}\right|}_{I} + \underbrace{cln|1-c\rho|}_{II} - \underbrace{bln|1-b\rho|}_{III}\right] + \begin{cases} \frac{a}{RTx(\varepsilon_2-\varepsilon_1)} ln\left|\frac{1+\varepsilon_1 x\rho}{1+\varepsilon_2 x\rho}\right| \\ \underbrace{-\frac{a\rho}{RT}}_{IV} \end{cases} \qquad (D.86)$$

Eq. (D.86) allows evaluating the compressibility factor and the fugacity coefficient needed for solving the isofugacity condition in pure compound.

Residual properties require the first-order derivatives of eq. (D.86) with respect to density and temperature.

1.3.1 First-order partial derivative of a^R with respect to density

The first-order derivative of term *I* in eq. (D.86) with respect to density gives:

$$\frac{\partial}{\partial\rho}\left[\frac{1d}{b-c}dln\left|\frac{1-b\rho}{1-c\rho}\right|\right] = \frac{d}{b-c}\frac{1-c\rho}{1-b\rho}\frac{(-b)(1-c\rho)-(1-b\rho)(-c)}{(1-c\rho)^2} = \\ = \frac{d}{b-c}\frac{(-b+bc\rho+c-bc\rho)}{(1-b\rho)(1-c\rho)} = \frac{d(c-b)}{(b-c)(1-b\rho)(1-c\rho)} \qquad (D.87)$$

The first-order derivative of term *II* and *III* in eq. (D.86) with respect to density gives:

$$\frac{\partial}{\partial\rho}\left[\frac{c}{b-c}ln|1-c\rho|\right] = \frac{c}{b-c}\frac{-c}{1-c\rho} = -\frac{c^2}{(b-c)(1-c\rho)} \qquad (D.88)$$

$$\frac{\partial}{\partial\rho}\left[-\frac{b}{b-c}ln|1-cb|\right] = -\frac{b}{b-c}\frac{-b}{1-b\rho} = \frac{b^2}{(b-c)(1-b\rho)} \qquad (D.89)$$

Coupling eqs. (D.87)-(D.89) results in:

$$\frac{1}{b-c}\left[\frac{d(c-b)}{(1-b\rho)(1-c\rho)} - \frac{c^2}{(1-c\rho)} + \frac{b^2}{(1-b\rho)}\right] = \frac{(b+c-d-bc\rho)}{(1-b\rho)(1-c\rho)} \qquad (D.88)$$

The first-order derivative of the first equation of term *IV* in eq. (D.86) with respect to density gives:

$$\frac{\partial}{\partial\rho}\left[\frac{a}{RTx(\varepsilon_2-\varepsilon_1)}ln\left|\frac{1+\varepsilon_1x\rho}{1+\varepsilon_2x\rho}\right|\right]=\frac{a}{RTx(\varepsilon_2-\varepsilon_1)}\frac{1+\varepsilon_2x\rho}{1+\varepsilon_1x\rho}\frac{\varepsilon_1x(1+\varepsilon_2x\rho)-\varepsilon_2x(1+\varepsilon_1x\rho)}{(1+\varepsilon_2x\rho)^2}=$$
$$=\frac{a}{RTx(\varepsilon_2-\varepsilon_1)}\frac{\varepsilon_1x+\varepsilon_1\varepsilon_2x^2\rho-\varepsilon_2x-\varepsilon_1\varepsilon_2x^2\rho}{(1+\varepsilon_1x\rho)(1+\varepsilon_2x\rho)}=-\frac{a}{RT(1+qx\rho+rx^2\rho^2)} \quad (D.89)$$

In case of $q = r = 0$, the derivation involves the second equation of term *IV*, which turns in:

$$\frac{\partial}{\partial\rho}\left[-\frac{a\rho}{RT}\right]=-\frac{a}{RT} \quad (D.90)$$

Finally, the first-order derivative with respect to density is:

$$a_\rho^R(T,\rho)=\frac{\partial a^R(T,\rho)}{\partial\rho}=\frac{(b+c-d-\rho bc)}{(1-\rho b)(1-\rho c)}-\begin{cases}\dfrac{a}{RT(1+qx\rho+rx^2\rho^2)}\\ \dfrac{a}{RT}\end{cases} \quad (D.91)$$

As in eq. (D.86), the second equation in the parenthesis applies when $q = r = 0$.

1.3.2 First-order partial derivative of a^R with respect to temperature

Parameters *a* and *b* are functions of temperature. In this section, *a'* and *b'* are referred to the derivatives of *a* and *b* with respect to temperature, which expressions are in eq.(D.5) and (D.7), respectively.

The first-order derivative of term *I* in eq. (D.86) with respect to temperature gives:

$$\frac{\partial}{\partial T}\left[\frac{1}{b-c}dln\left|\frac{1-b\rho}{1-c\rho}\right|\right]=-\frac{b'd}{(b-c)^2}ln\left|\frac{1-b\rho}{1-c\rho}\right|+\frac{d}{b-c}\frac{1-c\rho}{1-b\rho}\frac{-b'\rho}{1-c\rho}=$$
$$=-\frac{b'd}{(b-c)^2}ln\left|\frac{1-b\rho}{1-c\rho}\right|-\frac{db'\rho}{(b-c)(1-b\rho)} \quad (D.92)$$

The first-order derivative of term *II* and *III* in eq. (D.86) with respect to temperature gives:

$$\frac{\partial}{\partial T}\left[\frac{c}{b-c}ln|1-c\rho|\right]=-\frac{b'c}{(b-c)^2}ln|1-c\rho| \quad (D.93)$$

$$\frac{\partial}{\partial T}\left[-\frac{b}{b-c}ln|1-b\rho|\right]=-\frac{b'(b-c)-bb'}{(b-c)^2}ln|1-b\rho|-\frac{b}{b-c}\frac{-b'\rho}{1-b\rho}=$$
$$\frac{b'c}{(b-c)^2}ln|1-b\rho|+\frac{bb'\rho}{(b-c)(1-b\rho)} \quad (D.94)$$

It is possible to sum the first term in eq. (D.92) with eq. (D.93) and with the first term of eq. (D.94):

$$-\frac{b'd}{(b-c)^2}ln\left|\frac{1-b\rho}{1-c\rho}\right|-\frac{b'c}{(b-c)^2}ln|1-c\rho|+\frac{b'c}{(b-c)^2}ln|1-b\rho|=\frac{b'(c-d)}{(b-c)^2}ln\left|\frac{1-b\rho}{1-c\rho}\right| \quad (D.95)$$

Furthermore, the second terms of eq. (D.92) and (D.94) sum in:

$$-\frac{db'\rho}{(b-c)(1-b\rho)}+\frac{bb'\rho}{(b-c)(1-b\rho)}=\frac{b'\rho(d-b)}{(c-b)(1-b\rho)} \qquad (D.96)$$

In case of not null q and r, the first-order derivative of term *IV* in eq. (D.86) with respect to temperature is:

$$\begin{aligned}
&\frac{\partial}{\partial T}\left[\frac{a}{RTx(\varepsilon_2-\varepsilon_1)}ln\left|\frac{1+\varepsilon_1x\rho}{1+\varepsilon_2x\rho}\right|\right]= \\
&=\frac{1}{R(\varepsilon_2-\varepsilon_1)}\left[\frac{a'Tx-a(x+Tx')}{T^2x^2}\right]ln\left|\frac{1+\varepsilon_1x\rho}{1+\varepsilon_2x\rho}\right| \\
&\quad+\frac{a}{RTx(\varepsilon_2-\varepsilon_1)}\frac{1+\varepsilon_2x\rho}{1+\varepsilon_1x\rho}\frac{\varepsilon_1x'\rho(1+\varepsilon_2x\rho)-\varepsilon_2x'\rho(1+\varepsilon_1x\rho)}{(1+\varepsilon_2x\rho)^2}= \\
&=\frac{a'Tx-ax-aTx'}{RT^2x^2(\varepsilon_2-\varepsilon_1)}ln\left|\frac{1+\varepsilon_1x\rho}{1+\varepsilon_2x\rho}\right|+\frac{a}{RTx(\varepsilon_2-\varepsilon_1)}\frac{\varepsilon_1x'\rho+\varepsilon_1\varepsilon_2xx'\rho^2-\varepsilon_2x'\rho-\varepsilon_2\varepsilon_1xx'\rho^2}{(1+\varepsilon_1x\rho)(1+\varepsilon_1x\rho)}= \\
&=\frac{a'Tx-ax-aTx'}{RT^2x^2(\varepsilon_2-\varepsilon_1)}ln\left|\frac{1+\varepsilon_1x\rho}{1+\varepsilon_2x\rho}\right|-\frac{ax'\rho}{RTx(1+qx\rho+rx^2\rho^2)}
\end{aligned} \qquad (D.96)$$

In eq. (D.96) *x'* is equal to *b'* when the solid covolume is used in the attractive term of the SLV EoS, whereas is null for functional forms using the liquid covolume in the attractive pressure.

In case of $q = r = 0$, the derivation involves the second equation of term *IV*, which turns in:

$$\frac{\partial}{\partial\rho}\left[-\frac{a\rho}{RT}\right]=-\frac{\rho}{R}\left(\frac{a'}{T}-\frac{a}{T^2}\right)=\frac{\rho(a-a'T)}{RT^2} \qquad (D.97)$$

Finally, the first-order derivative with respect to temperature is:

$$\begin{aligned}
a_T^R(T,\rho)&=\frac{\partial a^R(T,\rho)}{\partial T} \\
&=\frac{b'(c-d)}{(b-c)^2}ln\left|\frac{1-b\rho}{1-c\rho}\right|+\frac{b'\rho(d-b)}{(c-b)(1-b\rho)} \\
&\quad+\begin{cases}\dfrac{a'Tx-ax-aTx'}{RT^2x^2(\varepsilon_2-\varepsilon_1)}ln\left(\dfrac{1+\varepsilon_1x\rho}{1+\varepsilon_2x\rho}\right)-\dfrac{ax'\rho}{RTx(1+qx\rho+rx^2\rho^2)} \\ \dfrac{\rho(a-a'T)}{RT^2}\end{cases}
\end{aligned} \qquad (D.98)$$

As in eq. (D.86), the second equation in the parenthesis applies when $q = r = 0$.

2 Solution of a 4th order equation

Eq. (D.99) is a generic 3rd order equation in the variable x with coefficients a, b, and c.

$$x^3 + x^2 a + xb + c = 0 \qquad (D.99)$$

According to the method of Cardano [3], the quadratic term within eq. (D.99) is eliminated substituting $x = y - a/3$ giving:

$$y^3 = cx + d = 0 \qquad (D.100)$$

where,

$$c = b - \frac{a}{3} \quad , \quad d = c - \frac{ab}{3} + \frac{2a^3}{27} \qquad (D.101)$$

The discriminant of eq. (D.101) is:

$$\Delta = \frac{c^3}{27} + \frac{d^2}{4} \qquad (D.102)$$

Three cases are possible:

- $\Delta>0$: only one real root

$$y_1 = \sqrt[3]{-\frac{d}{2} + \sqrt{\Delta}} + \sqrt[3]{-\frac{d}{2} - \sqrt{\Delta}} \quad , \quad y_2 = y_3 = 0 \qquad (D.103)$$

- $\Delta=0$: two real roots

$$y_1 = -2\sqrt[3]{\frac{d}{2}} \quad , \quad y_2 = y_3 = \sqrt[3]{\frac{d}{2}} \qquad (D.104)$$

- $\Delta<0$: three real roots

$$y_k = 2\sqrt{-\frac{c}{3}}\cos\left(\frac{\tau + 2\pi k}{3}\right) \quad , \quad with \quad \tau = \arccos\left(-\frac{d}{2}\sqrt{-\frac{27}{c^3}}\right) \quad , \quad k = 0,1,2 \qquad (D.105)$$

Once the values of y are known, the relation $x = y - a/3$ yields the roots of eq. (D.99).

The generic 4th order equation with coefficients α, β, γ, and δ in eq. (D.106) can be rearranged in a correspondent 3rd order polynomial, eq. (D.99), by means of the identities in eq. (D.107).

$$v^4 + v^3\alpha + v^2\beta + v\gamma + \delta = 0 \qquad (D.106)$$

$$a = -\beta \quad , \quad b = \alpha\gamma - 4\delta \quad , \quad c = \delta(4\beta - \alpha^2) - \gamma^2 \qquad (D.107)$$

The roots of eq. (D.106) are the roots of the two equations:

$$x^2 + c_1 x + d_1 = 0 \qquad (D.108)$$

$$x^2 + c_2 x + d_2 = 0 \qquad (D.109)$$

$$x_{1,2} = 0.5\left(-c_1 \pm \sqrt{c_1^2 - 4d_1}\right) \quad (D.110)$$

$$x_{3,4} = 0.5\left(-c_2 \pm \sqrt{c_2^2 - 4d_2}\right) \quad (D.111)$$

Coefficients c_1, c_2, d_1, and d_2 in eqs. (D.108)-(D.111) depend on the biggest roots of the 3rd order equation (y_{max}) whose parameters are defined as in eq. (D.107).

Considering y_{max} and the coefficients of the 4th order equations (α, β, γ, δ), coefficients c_1, c_2, d_1, and d_2 are evaluated from eqs. ()-().

$$c_1 = \frac{\alpha}{2} + \sqrt{\left(\frac{\alpha}{2}\right)^2 - \beta + y_{max}} \quad (D.112)$$

$$c_2 = \frac{\alpha}{2} - \sqrt{\left(\frac{\alpha}{2}\right)^2 - \beta + y_{max}} \quad (D.113)$$

$$d_1 = \frac{y_{max}}{2} + \varepsilon\sqrt{\left(\frac{y_{max}}{2}\right)^2 - \delta} \quad (D.114)$$

$$d_2 = \frac{y_{max}}{2} - \varepsilon\sqrt{\left(\frac{y_{max}}{2}\right)^2 - \delta} \quad (D.115)$$

In the previous equations, $\varepsilon = 1$ if $\alpha * y_{max} > 2\gamma$, and $\varepsilon = -1$ if $\alpha * y_{max} < 2\gamma$.

3 Quali/quantitative comparisons for pure compounds

Triple and critical point coordinates of the pure compounds of interest have been already presented in Chapter 4.

For the reader convenience, these values have been re-proposed in this section, together with minimum values of sublimation temperature (T_{min}) and pressure (P_{min}) and the maximum values of melting temperature (T_{max}) and pressure (P_{max}) used for the regression of the EoS parameters. For each compound, the entire saturation line has been considered in the regression procedure.

Table D.1 gives temperatures and pressures of triple and critical points for the compounds.

Table D.1: Triple and critical points for the substances of interest, **[4]**.

Fluid	T_t / K	P_t / kPa	T_c / K	P_c / MPa	N VLE
N_2	63.151	12.5198	126.192	3.3958	102
O_2	54.361	0.14628	154.581	5.043	135
Ar	83.8058	68.891	150.687	4.863	107
Kr	115.775	73.5	209.48	5.525	135
Xe	161.405	81.7724	289.733	5.842	167
Ne	24.556	43.368	44.4918	2.6786	135
He	2.1768	5.0428	5.1953	0.22758	173
CO_2	216.592	517.95	304.1282	7.3773	119
H_2	13.957	7.35783	33.145	1.2964	194
N_2O	182.33	87.84	309.52	7.245	96
CH_4	90.6941	11.697	190.56	4.5992	131
C_2H_6	90.368	0.0011421	305.322	4.8722	98
C_2H_4	103.986	0.12196	282.35	5.0418	117
C_3H_8	85.53	1.724×10^{-7}	369.89	4.2512	110
C_3H_6	87.953	7.4717×10^{-7}	364.211	4.555	120

For each pure compound (except helium), Table D.2 presents the couples T_{min}-P_{min} and T_{max}-P_{max} used for the regression of the EoS parameters described in Chapter 4.

Table D.2: Minimum SVE and maximum SLE values for the temperature and pressure used for the regression of the SLV EoS parameters.

Fluid	SVE			SLE		
	T_{min} / K	P_{min} / kPa	N	T_{max} / K	P_{max} / MPa	N
N_2	41	0.0106	24	82	95.5	56
O_2	48	0.0131	8	65	99.6	43
Ar	48	0.0171	36	106	95.6	59
Kr	66	0.0120	28	143	96.9	56
Xe	91	0.0103	72	197	97.4	59
Ne	14	0.0141	26	37	98.4	82
CO_2	125	0.0112	33	236	99.8	31
H_2	8	0.0131	28	33.145	92.7	194
N_2O	120	0.0207	15	197	95.2	38
CH_4	59	0.0118	33	114	99.4	49
C_2H_6				105	97.4	42
C_2H_4				117	98.7	40
C_3H_8				94	93.2	23
C_3H_6				96	99.5	35

In Table D.1 and Table D.2, *N* is the number of auxiliary values used for the regression.

The pressure-temperature equilibrium projection of helium is represented in Figure D.1 in the range 0-10 K. Red lines are values from auxiliary equations, the green one represents qualitatively the liquid$_1$-liquid$_2$ equilibrium.

Upon reaching the point λ_1 on the saturation line, liquid helium changes from form 1 to form 2. As a consequence, no sublimation curve occurs, whereas the solid phase can be obtained only along the melting line which starts at the point λ_2.

Two triple points exist for helium; a liquid$_1$–liquid$_2$-vapor and a solid-liquid$_1$–liquid$_2$ triple point. In this work, only liquid form 1 has been considered, imposing λ_1 to be the solid-liquid-vapor triple point.

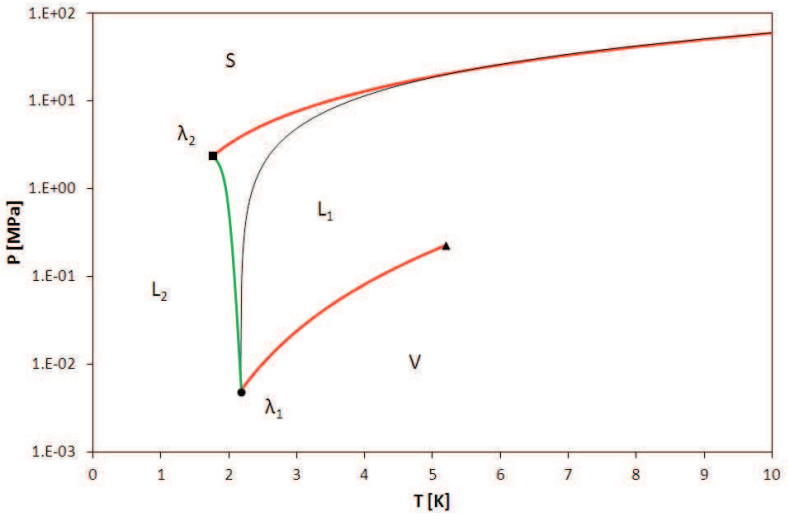

Figure D.1: Pressure-temperature equilibrium projection of helium.
— : saturation and melting equilibria from auxiliary equations; — : qualitative liquid$_1$-liquid$_2$ equilibrium loici; — : SLE from classical approach; ■ : SL_2L_1 triple point; ● : L_2L_1V triple point; ▲ : critical point.

According to Figure D.1, the auxiliary values obtained from the melting equation of helium originate in λ_2. In order to reproduce solid-liquid equilibrium values needed in the regression procedure to set the EoS parameters, the classical approach has been used for the melting line of helium. The experimental values of enthalpy, specific heat and volume changes upon melting have been obtained from [4]. The black line in Figure D.1 represents the melting line from the classical approach.

The results obtained and the capability of the SLV EoS in representing the pressure-temperature equilibrium projection (PT-EP) for the pure compounds of interest are presented in the following sections by means of:

- the qualitative PT-EP obtained with the EoS parameters from T_{min} in Table D.2 up to the critical point temperature. A selected number of auxiliary values have been used to ease the comparison between data and model;
- the details of the percentage errors for SLE, VLE and SVE auxiliary values, with reference to the corresponding ranges shown in Table D.2.
  The quantitative comparison involves equilibrium values (pressure and temperature) calculated from the SLV EoS and values produced with the auxiliary equations. The comparison has been done with reference to the percentage error $err_i\%$ and the percentage deviations: Absolute Average Deviation (AAD), Bias, and Maximum Absolute Deviation (MAD). $err_i\%$, AAD%, Bias%, and MAD% are defined as in eqs. (D.116)-(D.119).

$$err_i\% = 100\left(\frac{M_{calc} - M_{aux}}{M_{aux}}\right)_i \tag{D.116}$$

$$AAD\% = \frac{1}{N}\sum_{i=1}^{N}|err_i\%| \tag{D.117}$$

$$Bias\% = \frac{1}{N}\sum_{i=1}^{N} err_i\% \tag{D.118}$$

$$MAD\% = \underset{i=1,N}{max}\ \{|err_i\%|\} \tag{D.119}$$

- a table that summarizes the deviations in terms of temperatures and pressures with respect to the auxiliary values.

In the framework of the “Contrat Cadre” between Air Liquide and ARMINES the values of the EoS parameters have been considered confidential. Then, the numerical values have not been expressed in Appendix D.

3.1 Nitrogen

Figure D.2 shows the qualitative comparison between calculated and auxiliary values in the PT-EP of nitrogen. The quantitative comparison between calculated and auxiliary values is presented in Table D.3 with reference to deviations in terms of pressure and temperature.

The detail of the percentage errors between the auxiliary and calculated values are presented in Figure D.3 and Figure D.4, respectively.

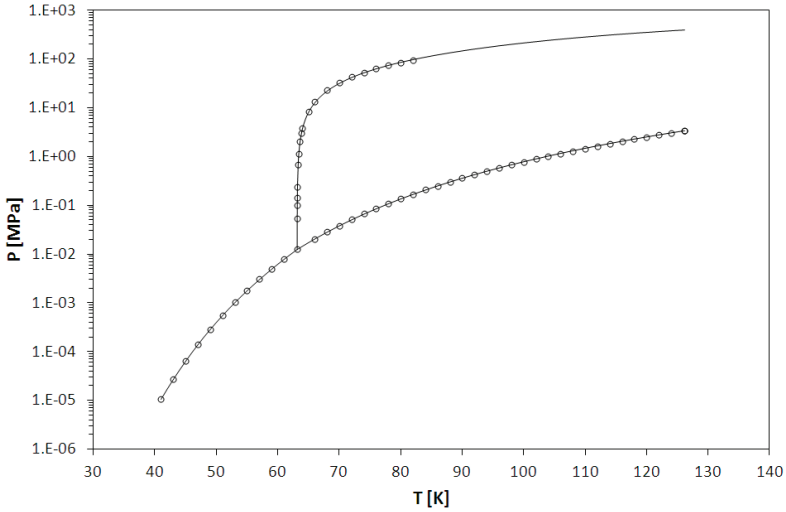

Figure D.2: PT-EP of N_2 obtained with the SLV EoS.
— : SLV EoS; ○ : equilibrium values from auxiliary equations.

Table D.3: Errors of the SLV EoS with respect to the auxiliary values for nitrogen.

For each equilibrium, the first line refers to errors in terms of pressure. The second line refers to errors in terms of temperature.

Fixed value	VLE		
	AAD %	Bias %	MAD %
T	0.68	-0.05	1.26
P	0.08	-0.01	0.20
Fixed value	**SVE**		
	AAD %	Bias %	MAD %
T	0.44	-0.26	0.94
P	0.03	0.02	0.07
Fixed value	**SLE**		
	AAD %	Bias %	MAD %
T	3.60	-3.41	5.70
P	0.15	0.12	0.33

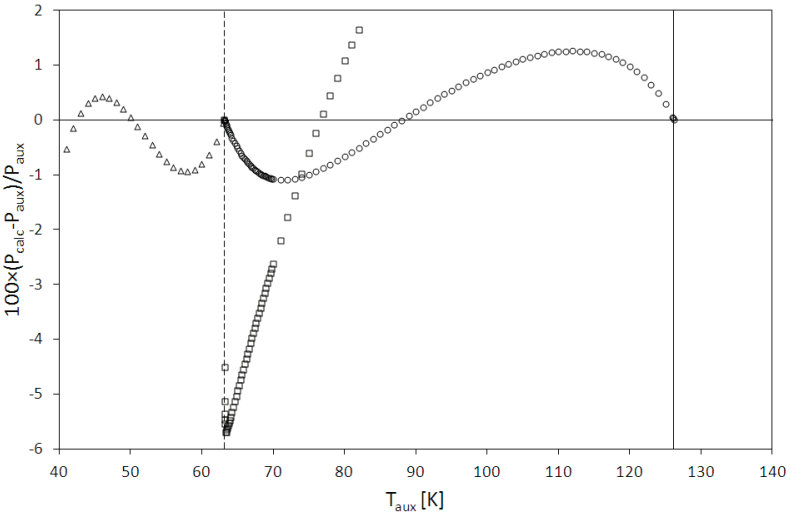

Figure D.3: Percentage errors in terms of pressure for N_2.
○ : VLE; Δ : SVE; □ : SLE.

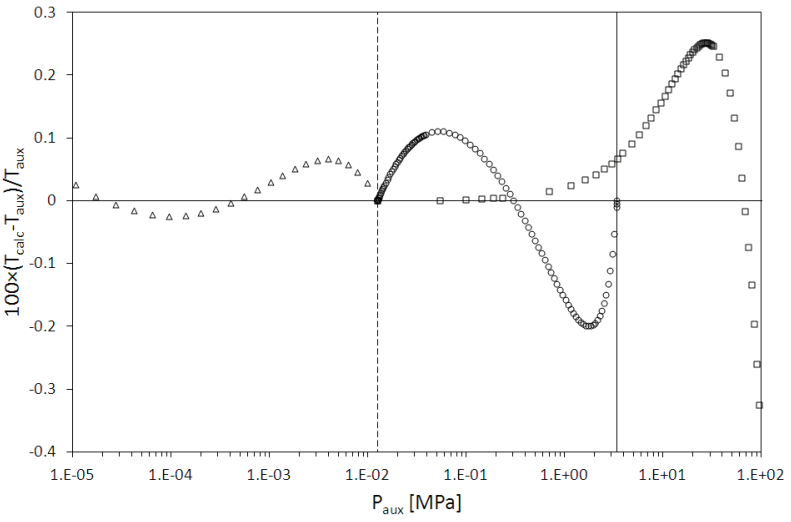

Figure D.4: Percentage errors in terms of temperature for N_2.
○ : VLE; Δ : SVE; □ : SLE.

3.2 Oxygen

Figure D.5 shows the qualitative comparison between calculated and auxiliary values in the PT-EP of oxygen. The quantitative comparison between calculated and auxiliary values is presented in Table D.4 with reference to deviations in terms of pressure and temperature.

The detail of the percentage errors between the auxiliary and calculated values are presented in Figure D.6 and Figure D.7, respectively.

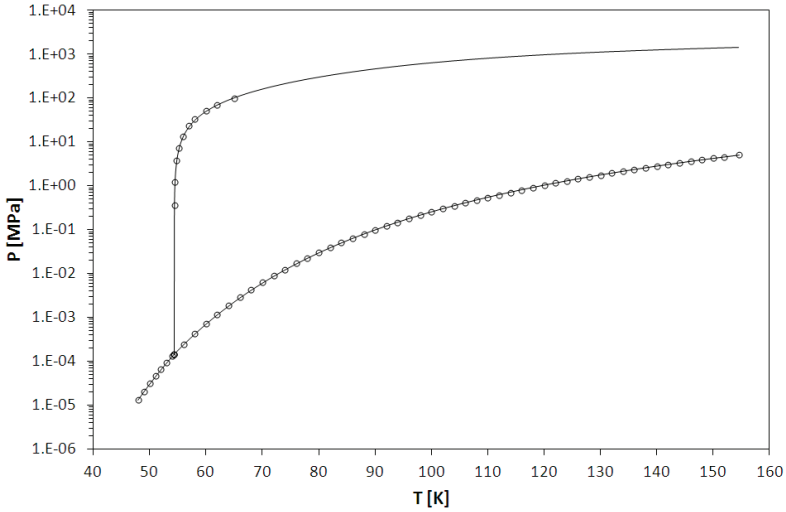

Figure D.5: PT-EP of O_2 obtained with the SLV EoS.
— : SLV EoS; ○ : equilibrium values from auxiliary equations.

Table D.4: Errors of the SLV EoS with respect to the auxiliary values for oxygen.

For each equilibrium, the first line refers to errors in terms of pressure. The second line refers to errors in terms of temperature.

Fixed value	VLE		
	AAD %	Bias %	MAD %
T	1.49	-0.004	3.00
P	0.16	-0.05	0.32
Fixed value	**SVE**		
	AAD %	Bias %	MAD %
T	2.41	-1.52	4.27
P	0.13	0.09	0.23
Fixed value	**SLE**		
	AAD %	Bias %	MAD %
T	4.95	-4.79	11.24
P	0.17	0.15	0.29

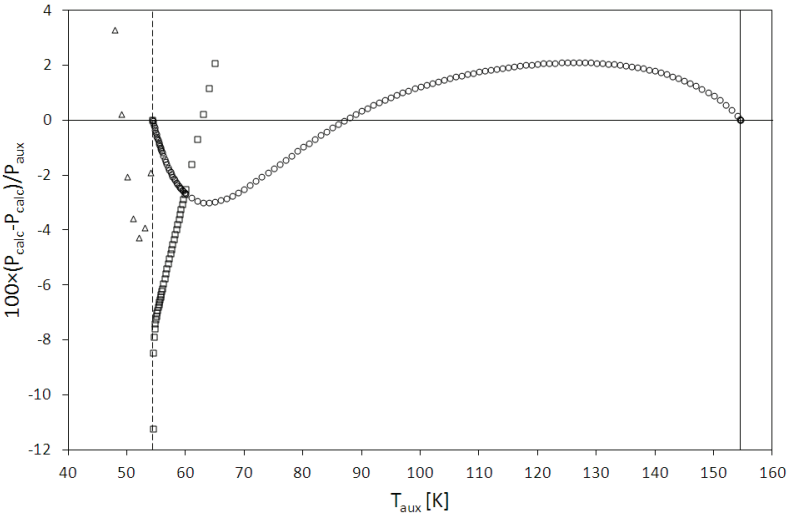

Figure D.6: Percentage errors in terms of pressure for O_2.
○ : VLE; Δ : SVE; □ : SLE.

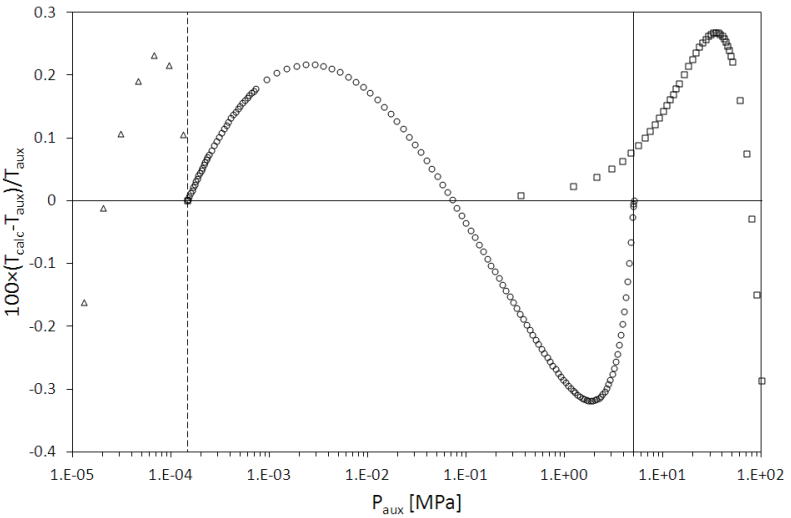

Figure D.7: Percentage errors in terms of temperature for O_2.
○ : VLE; Δ : SVE; □ : SLE.

3.3 Argon

Figure D.8 shows the qualitative comparison between calculated and auxiliary values in the PT-EP of argon. The quantitative comparison between calculated and auxiliary values is presented in Table D.5 with reference to deviations in terms of pressure and temperature.

The detail of the percentage errors between the auxiliary and calculated values are presented in Figure D.9 and Figure D.10, respectively.

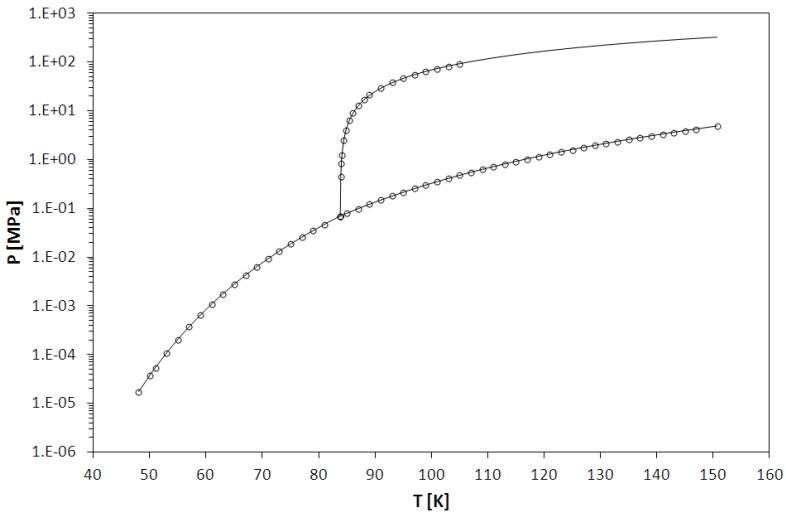

Figure D.8: PT-EP of Ar obtained with the SLV EoS.
— : SLV EoS; ○ : equilibrium values from auxiliary equations.

Table D.5: Errors of the SLV EoS with respect to the auxiliary values for argon.

For each equilibrium, the first line refers to errors in terms of pressure. The second line refers to errors in terms of temperature.

Fixed value	VLE		
	AAD %	Bias %	MAD %
T	0.54	0.32	1.36
P	0.08	-0.06	0.22
Fixed value	**SVE**		
	AAD %	Bias %	MAD %
T	0.61	-0.24	1.15
P	0.04	0.02	0.10
Fixed value	**SLE**		
	AAD %	Bias %	MAD %
T	2.36	-2.02	3.63
P	0.09	0.04	0.34

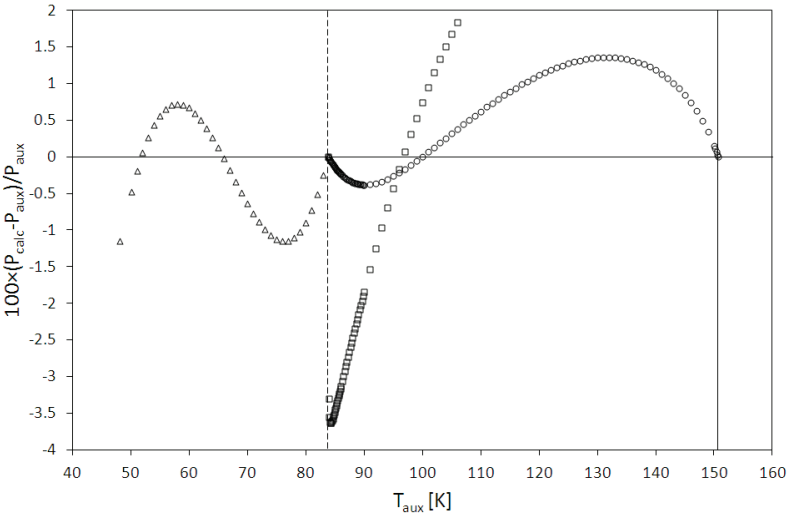

Figure D.9: Percentage errors in terms of pressure for Ar.
○ : VLE; Δ : SVE; □ : SLE.

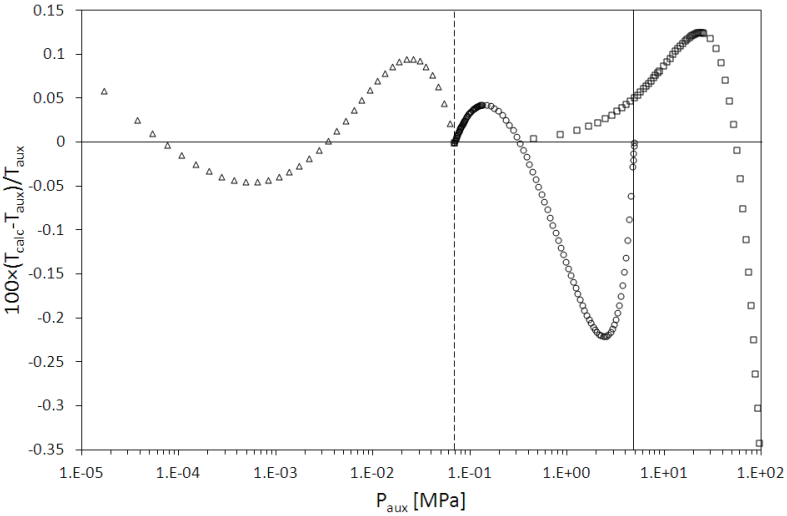

Figure D.10: Percentage errors in terms of temperature for Ar.
○ : VLE; Δ : SVE; □ : SLE.

3.4 Krypton

Figure D.11 shows the qualitative comparison between calculated and auxiliary values in the PT-EP of krypton. The quantitative comparison between calculated and auxiliary values is presented in Table D.6 with reference to deviations in terms of pressure and temperature.

The detail of the percentage errors between the auxiliary and calculated values are presented in Figure D.12 and Figure D.13, respectively.

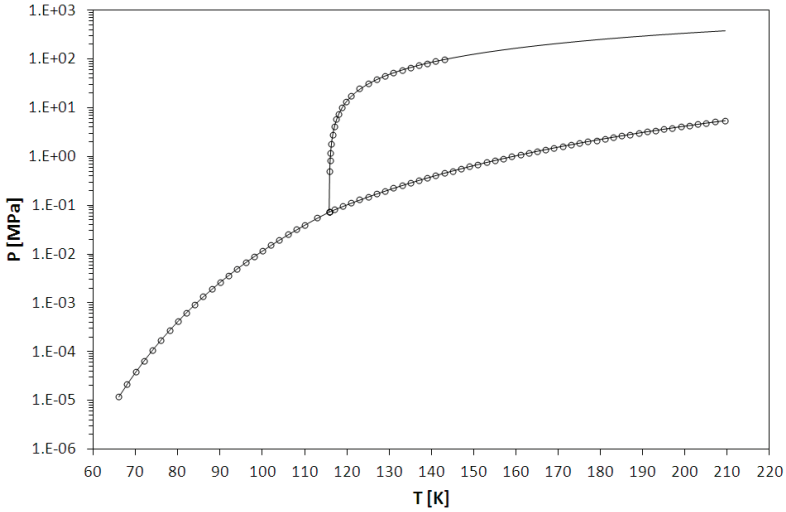

Figure D.11: PT-EP of Kr obtained with the SLV EoS.
— : SLV EoS; ○ : equilibrium values from auxiliary equations.

Table D.6: Errors of the SLV EoS with respect to the auxiliary values for krypton.

For each equilibrium, the first line refers to errors in terms of pressure. The second line refers to errors in terms of temperature.

Fixed value	VLE		
	AAD %	Bias %	MAD %
T	0.72	0.64	1.75
P	0.11	-0.10	0.28
Fixed value	**SVE**		
	AAD %	Bias %	MAD %
T	0.69	-0.21	1.41
P	0.05	0.02	0.10
Fixed value	**SLE**		
	AAD %	Bias %	MAD %
T	2.29	-1.90	5.98
P	0.07	0.01	0.28

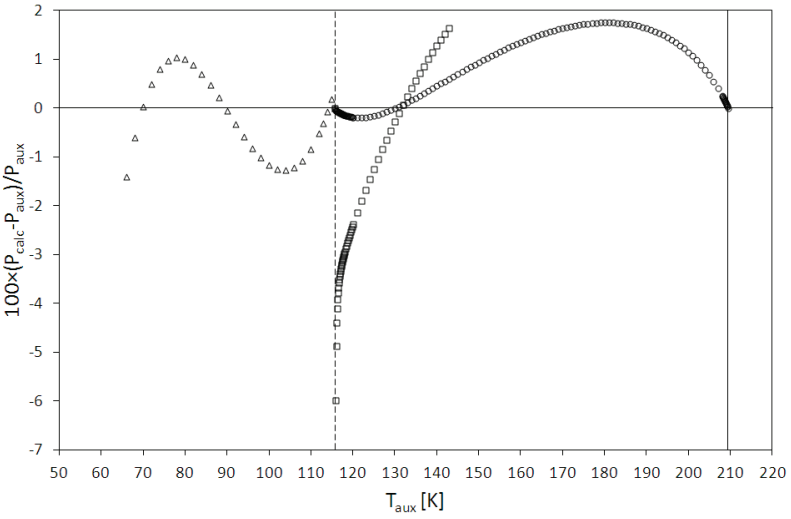

Figure D.12: Percentage errors in terms of pressure for Kr.
○ : VLE; Δ : SVE; □ : SLE.

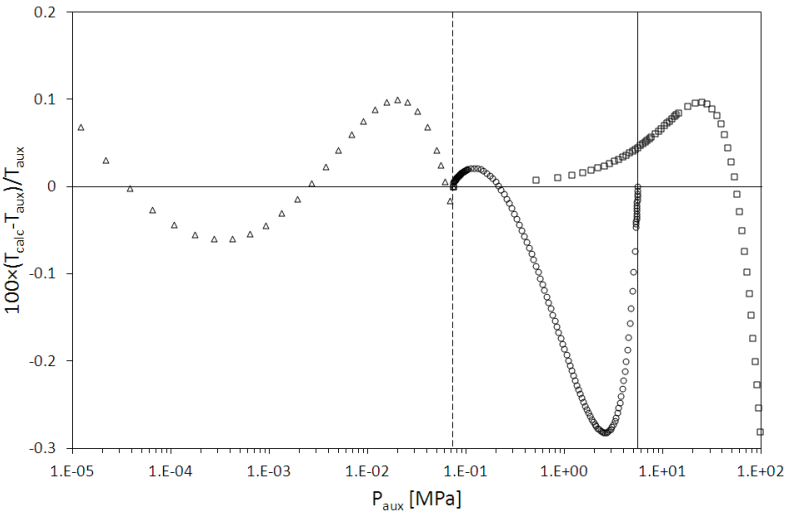

Figure D.13: Percentage errors in terms of temperature for Kr.
○ : VLE; Δ : SVE; □ : SLE.

3.5 Xenon

Figure D.14 shows the qualitative comparison between calculated and auxiliary values in the PT-EP of xenon. The quantitative comparison between calculated and auxiliary values is presented in Table D.7 with reference to deviations in terms of pressure and temperature.

The detail of the percentage errors between the auxiliary and calculated values are presented in Figure D.15 and Figure D.16, respectively.

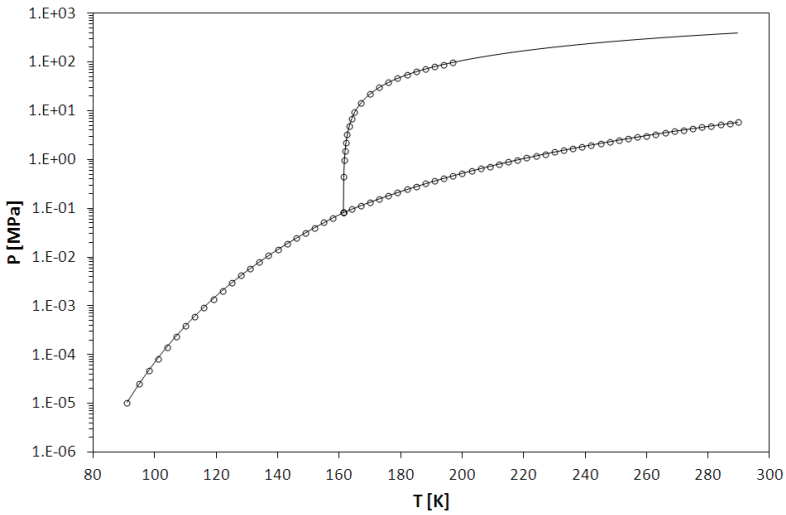

Figure D.14: PT-EP of Xe obtained with the SLV EoS. — : SLV EoS; ○ : equilibrium values from auxiliary equations.

Table D.7: Errors of the SLV EoS with respect to the auxiliary values for xenon.

For each equilibrium, the first line refers to errors in terms of pressure. The second line refers to errors in terms of temperature.

Fixed value	VLE		
	AAD %	Bias %	MAD %
T	0.59	0.50	1.39
P	0.09	-0.08	0.23
Fixed value	**SVE**		
	AAD %	Bias %	MAD %
T	0.42	-0.10	1.29
P	0.03	0.01	0.06
Fixed value	**SLE**		
	AAD %	Bias %	MAD %
T	4.11	-3.48	27.85
P	0.09	-0.002	0.33

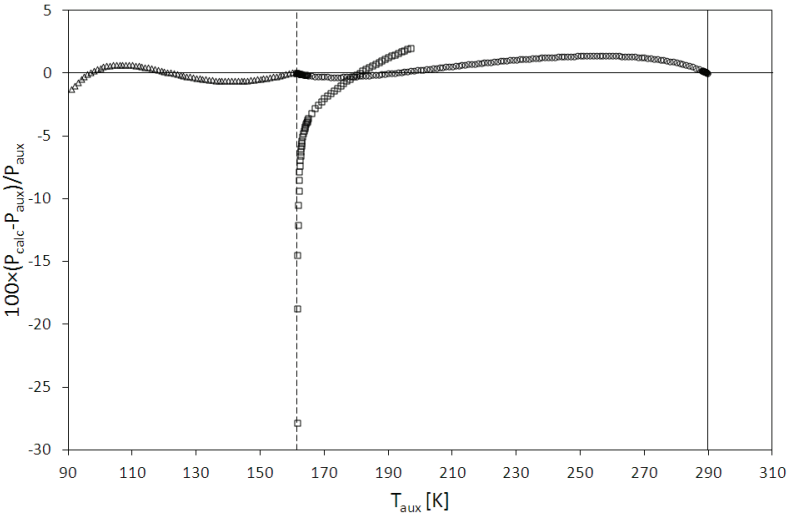

Figure D.15: Percentage errors in terms of pressure for Xe. ○ : VLE; Δ : SVE; □ : SLE.

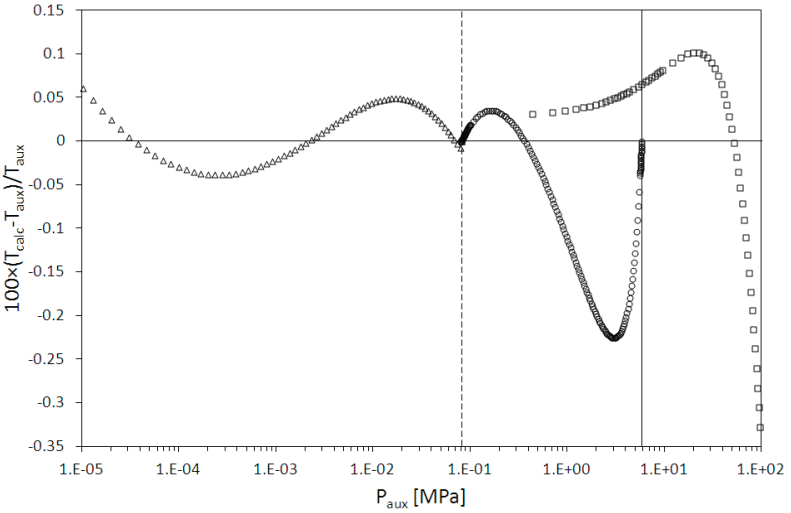

Figure D.16: Percentage errors in terms of temperature for Xe. ○ : VLE; Δ : SVE; □ : SLE.

3.6 Neon

Figure D.17 shows the qualitative comparison between calculated and auxiliary values in the PT-EP of neon. The quantitative comparison between calculated and auxiliary values is presented in Table D.8 with reference to deviations in terms of pressure and temperature.

The detail of the percentage errors between the auxiliary and calculated values are presented in Figure D.18 and Figure D.19, respectively.

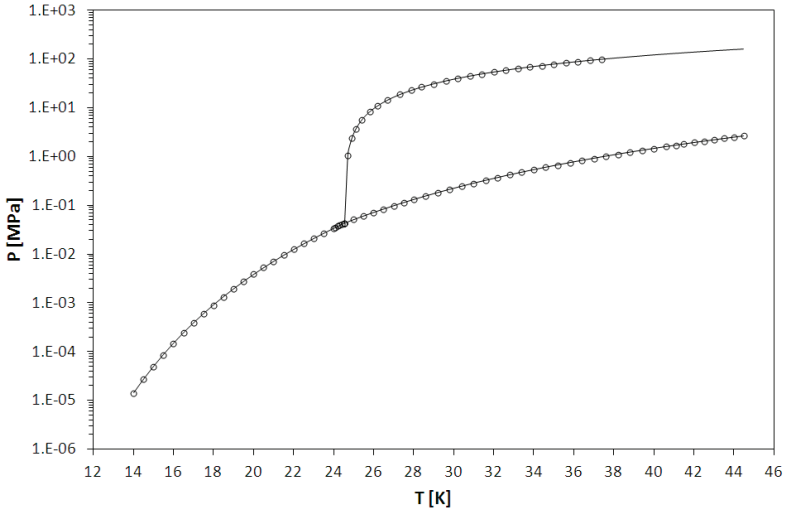

Figure D.17: PT-EP of Ne obtained with the SLV EoS.
— : SLV EoS; ○ : equilibrium values from auxiliary equations.

Table D.8: Errors of the SLV EoS with respect to the auxiliary values for neon.

For each equilibrium, the first line refers to errors in terms of pressure. The second line refers to errors in terms of temperature.

Fixed value	VLE		
	AAD %	Bias %	MAD %
T	0.97	0.97	1.89
P	0.15	-0.15	0.31
Fixed value	**SVE**		
	AAD %	Bias %	MAD %
T	0.90	-0.33	1.75
P	0.07	0.03	0.14
Fixed value	**SLE**		
	AAD %	Bias %	MAD %
T	1.75	1.01	8.18
P	0.30	-0.29	0.68

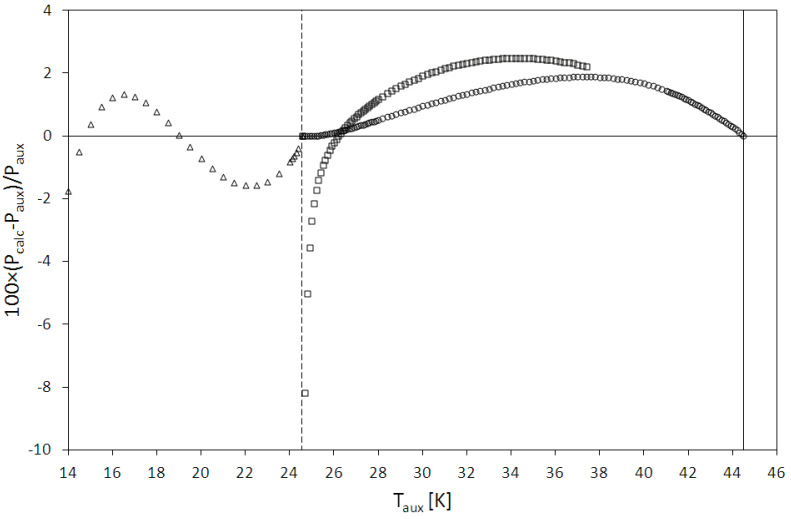

Figure D.18: Percentage errors in terms of pressure for Ne.
○ : VLE; Δ : SVE; □ : SLE.

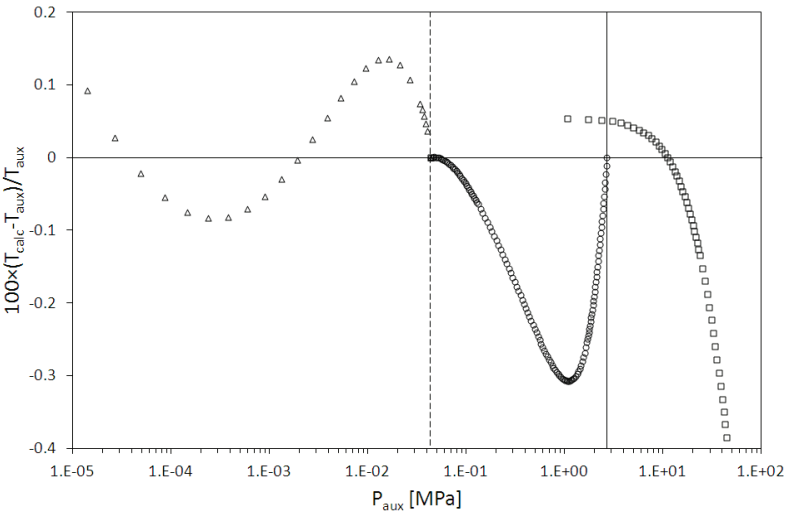

Figure D.19: Percentage errors in terms of temperature for Ne.
○ : VLE; Δ : SVE; □ : SLE.

3.7 Helium

Figure D.20 shows the qualitative comparison between calculated and auxiliary values in the PT-EP of helium. The quantitative comparison between calculated and auxiliary values is presented in Table D.9 with reference to deviations in terms of pressure and temperature.

The detail of the percentage errors between the auxiliary and calculated values are presented in Figure D.21 and Figure D.22, respectively.

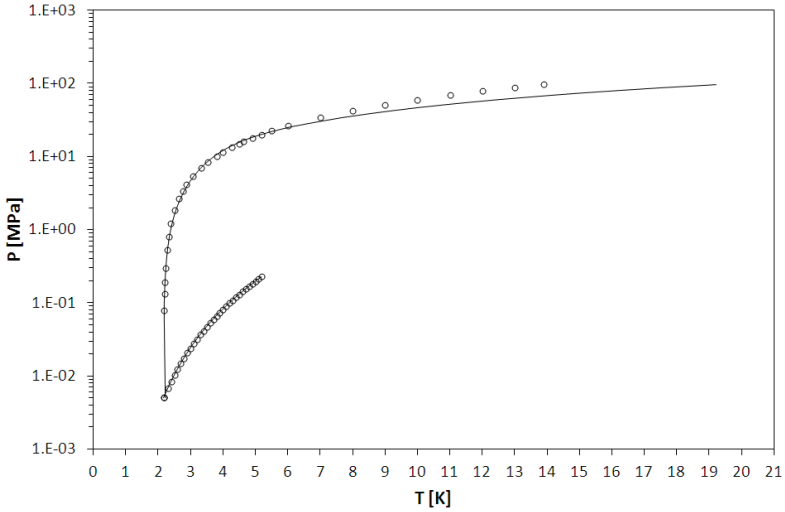

Figure D.20: PT-EP of He obtained with the SLV EoS.
— : SLV EoS; ○ : equilibrium values from auxiliary equations.

Table D.9: Errors of the SLV EoS with respect to the auxiliary values for helium.

For each equilibrium, the first line refers to errors in terms of pressure. The second line refers to errors in terms of temperature.

Fixed value	VLE		
	AAD %	Bias %	MAD %
T	0.29	0.22	0.42
P	0.07	-0.06	0.11

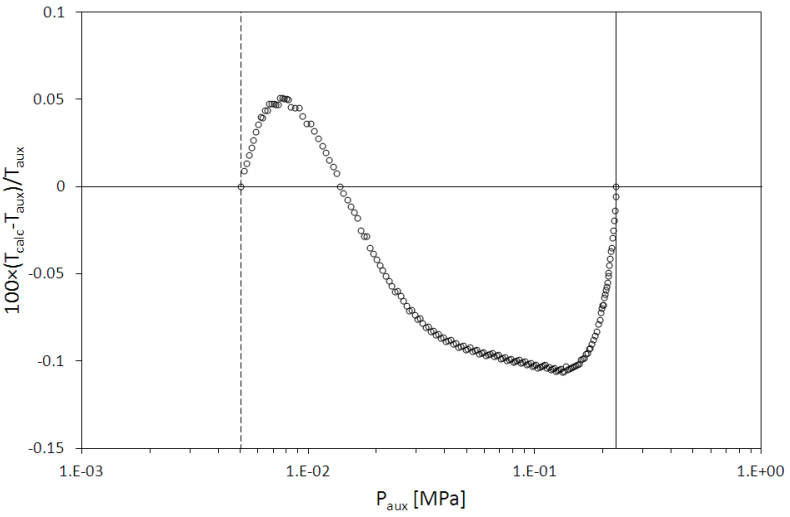

Figure D.21: Percentage errors in terms of pressure for He.
○ : VLE; Δ : SVE; □ : SLE.

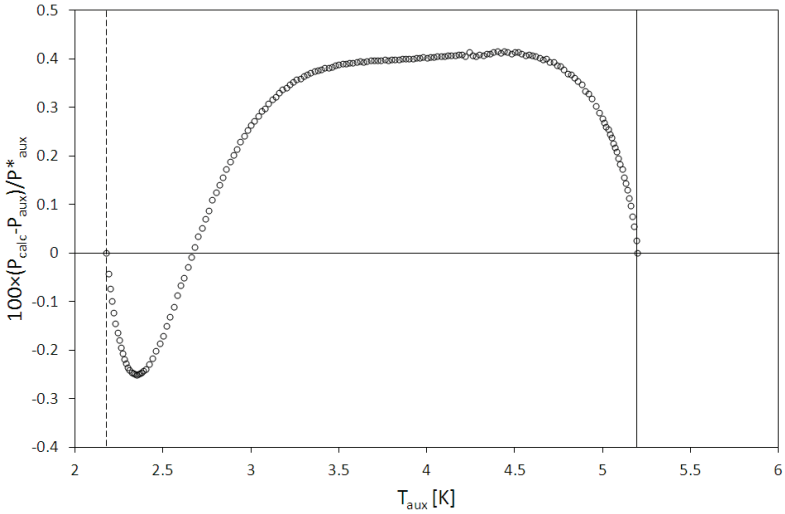

Figure D.22: Percentage errors in terms of temperature for He.
○ : VLE; Δ : SVE; □ : SLE.

3.8 Carbon dioxide

Figure D.23 shows the qualitative comparison between calculated and auxiliary values in the PT-EP of carbon dioxide. The quantitative comparison between calculated and auxiliary values is presented in Table D.4 with reference to deviations in terms of pressure and temperature.

The detail of the percentage errors between the auxiliary and calculated values are presented in Figure D.24 and Figure D.25, respectively.

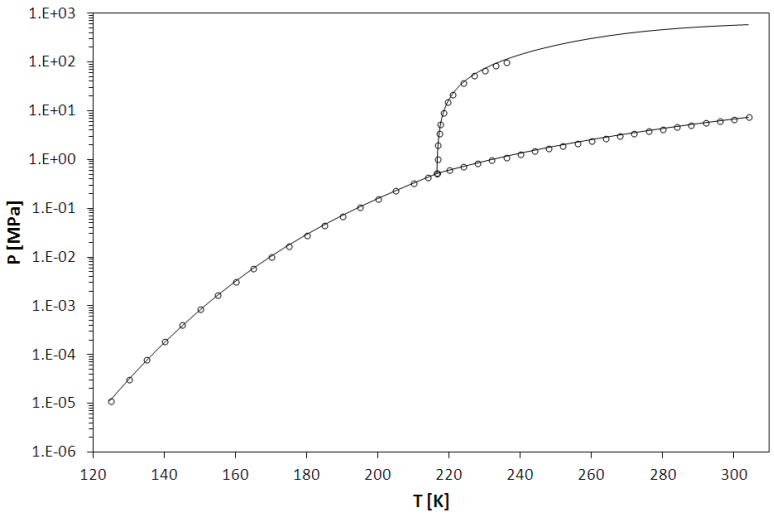

Figure D.23: PT-EP of CO_2 obtained with the SLV EoS. — : SLV EoS; ○ : equilibrium values from auxiliary equations.

Table D.10: Errors of the SLV EoS with respect to the auxiliary values for carbon dioxide.

For each equilibrium, the first line refers to errors in terms of pressure. The second line refers to errors in terms of temperature.

Fixed value	VLE		
	AAD %	Bias %	MAD %
T	3.07	3.07	6.22
P	0.39	-0.39	0.78
Fixed value	**SVE**		
	AAD %	Bias %	MAD %
T	2.08	1.04	6.43
P	0.11	-0.06	0.32
Fixed value	**SLE**		
	AAD %	Bias %	MAD %
T	4.02	4.02	13.57
P	0.16	-0.16	0.84

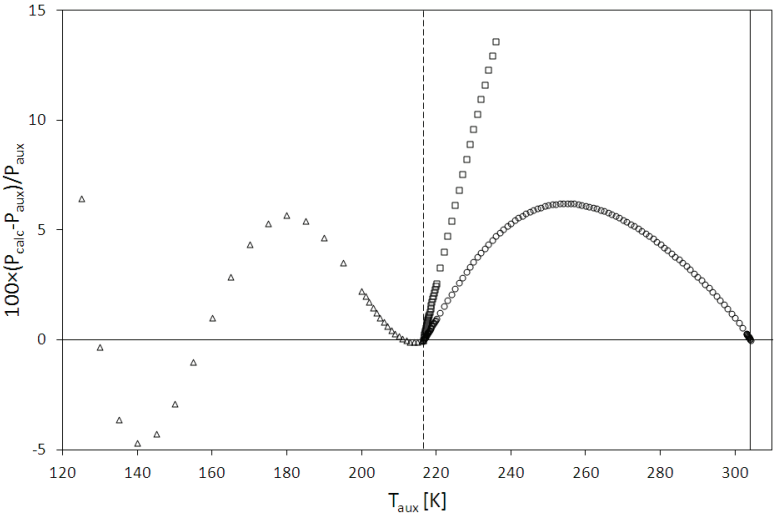

Figure D.24: Percentage errors in terms of pressure for CO_2. ○ : VLE; Δ : SVE; □ : SLE.

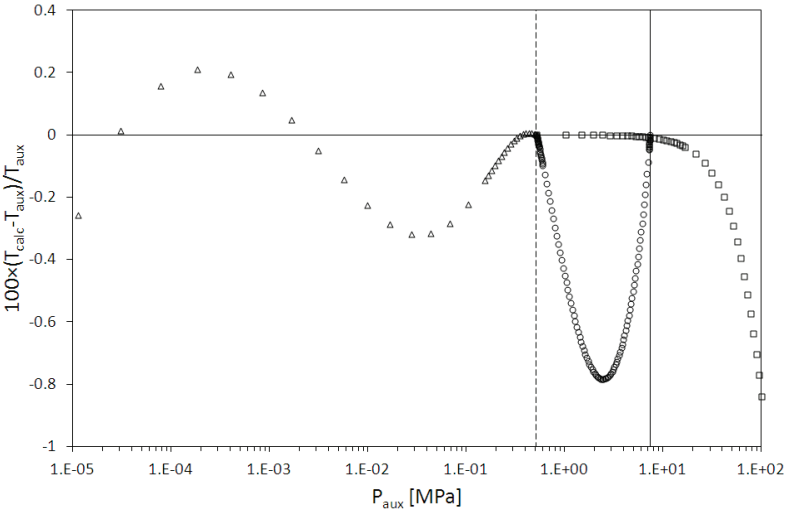

Figure D.25: Percentage errors in terms of temperature for CO_2. ○ : VLE; Δ : SVE; □ : SLE.

3.9 Hydrogen

Figure D.26 shows the qualitative comparison between calculated and auxiliary values in the PT-EP of hydrogen. The quantitative comparison between calculated and auxiliary values is presented in Table D.11 with reference to deviations in terms of pressure and temperature.

The detail of the percentage errors between the auxiliary and calculated values are presented in Figure D.27 and Figure D.28, respectively.

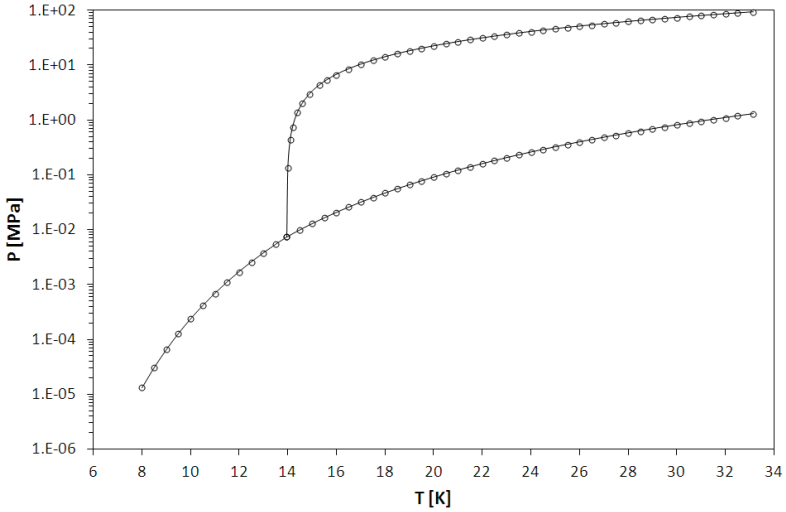

Figure D.26: PT-EP of H_2 obtained with the SLV EoS.
— : SLV EoS; ○ : equilibrium values from auxiliary equations.

Table D.11: Errors of the SLV EoS with respect to the auxiliary values for hydrogen.

For each equilibrium, the first line refers to errors in terms of pressure. The second line refers to errors in terms of temperature.

Fixed value	VLE		
	AAD %	Bias %	MAD %
T	0.54	0.31	1.05
P	0.10	-0.07	0.21
Fixed value	**SVE**		
	AAD %	Bias %	MAD %
T	0.90	0.47	2.31
P	0.09	-0.05	0.26
Fixed value	**SLE**		
	AAD %	Bias %	MAD %
T	0.38	0.33	3.96
P	0.04	-0.03	0.15

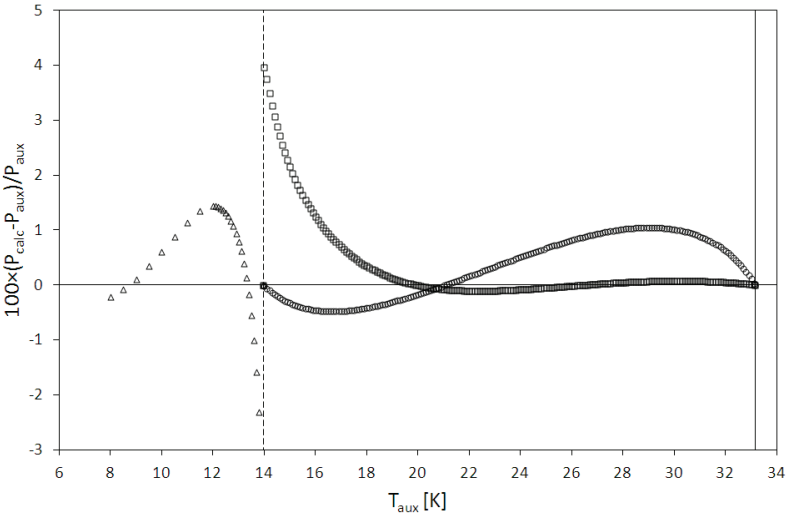

Figure D.27: Percentage errors in terms of pressure for H_2.
○ : VLE; Δ : SVE; □ : SLE.

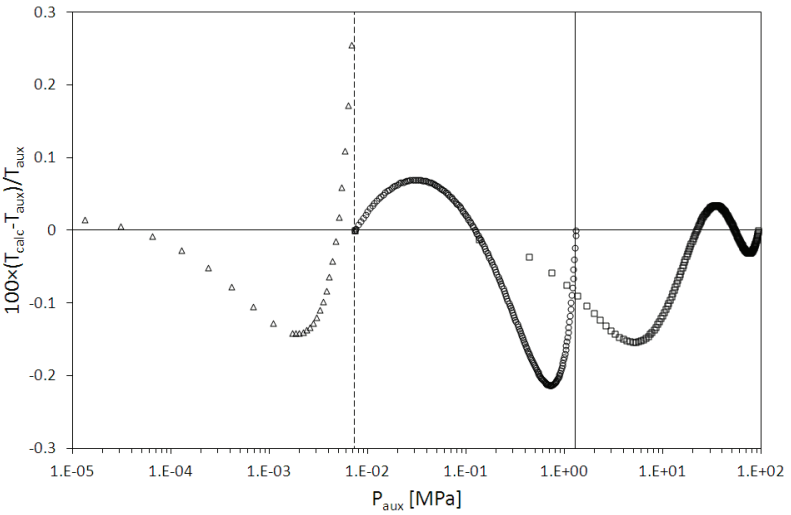

Figure D.28: Percentage errors in terms of temperature for H_2.
○ : VLE; Δ : SVE; □ : SLE.

3.10 Nitrous oxide

Figure D.29 shows the qualitative comparison between calculated and auxiliary values in the PT-EP of nitrous oxide. The quantitative comparison between calculated and auxiliary values is presented in Table D.12 with reference to deviations in terms of pressure and temperature.

The detail of the percentage errors between the auxiliary and calculated values are presented in Figure D.30 and Figure D.31, respectively.

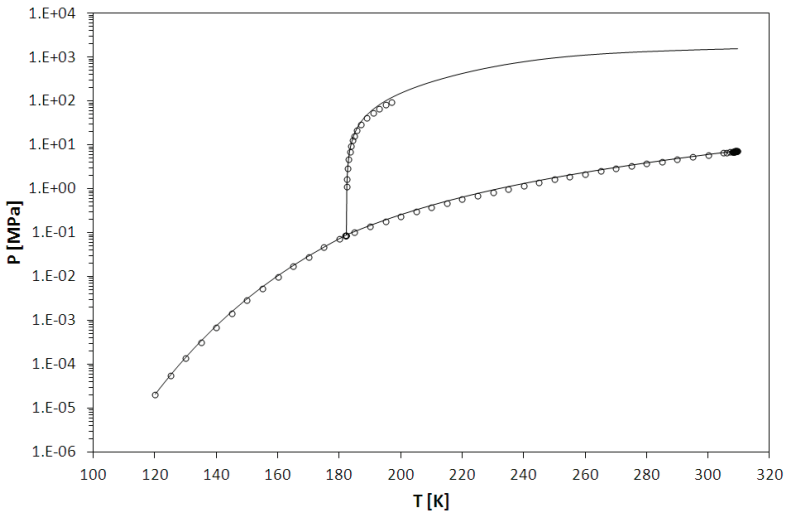

Figure D.29: PT-EP of N_2O obtained with the SLV EoS. — : SLV EoS; ○ : equilibrium values from auxiliary equations.

Table D.12: Errors of the SLV EoS with respect to the auxiliary values for nitrous oxide.

For each equilibrium, the first line refers to errors in terms of pressure. The second line refers to errors in terms of temperature.

Fixed value	VLE		
	AAD %	Bias %	MAD %
T	4.41	4.41	11.41
P	0.46	-0.46	1.25
Fixed value	**SVE**		
	AAD %	Bias %	MAD %
T	2.91	1.78	6.48
P	0.14	-0.09	0.32
Fixed value	**SLE**		
	AAD %	Bias %	MAD %
T	12.14	12.14	23.74
P	0.26	-0.26	1.21

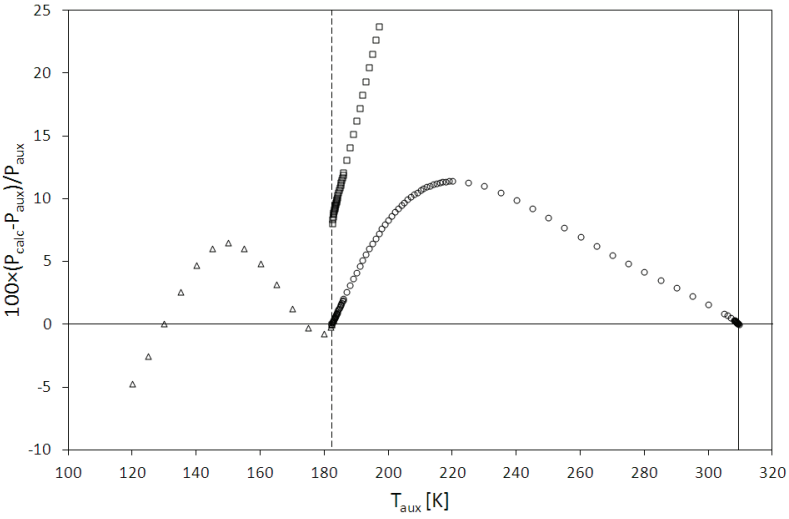

Figure D.30: Percentage errors in terms of pressure for N_2O. ○ : VLE; Δ : SVE; □ : SLE.

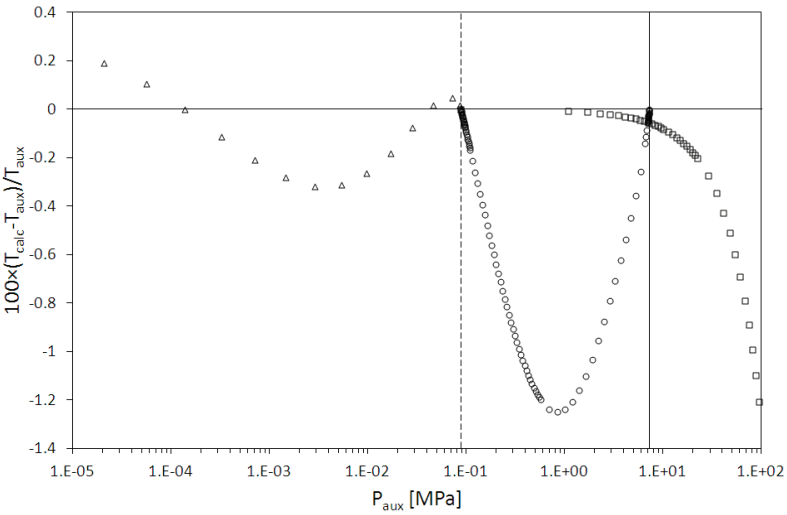

Figure D.31: Percentage errors in terms of temperature for N_2O. ○ : VLE; Δ : SVE; □ : SLE.

3.11 Methane

Figure D.32 shows the qualitative comparison between calculated and auxiliary values in the PT-EP of methane. The quantitative comparison between calculated and auxiliary values is presented in Table D.13 with reference to deviations in terms of pressure and temperature.

The detail of the percentage errors between the auxiliary and calculated values are presented in Figure D.33 and Figure D.34, respectively.

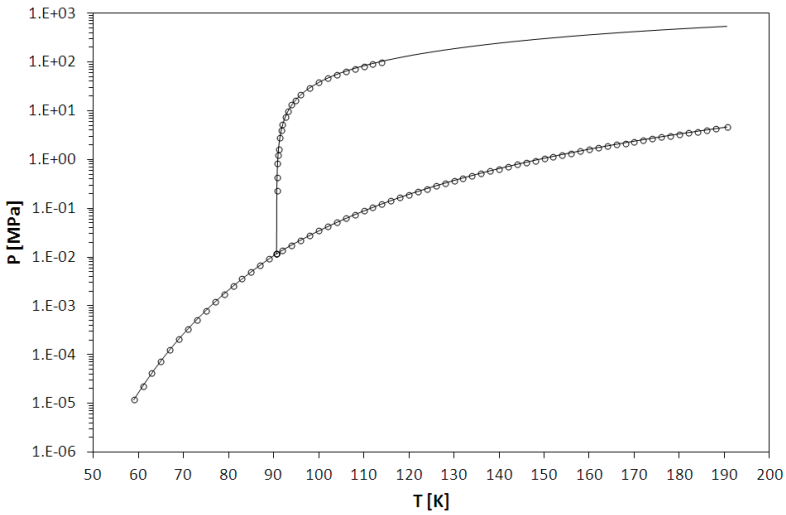

Figure D.32: PT-EP of CH_4 obtained with the SLV EoS. — : SLV EoS; ○ : equilibrium values from auxiliary equations.

Table D.13: Errors of the SLV EoS with respect to the auxiliary values for methane.

For each equilibrium, the first line refers to errors in terms of pressure. The second line refers to errors in terms of temperature.

Fixed value	VLE		
	AAD %	Bias %	MAD %
T	0.71	0.39	1.53
P	0.10	-0.07	0.24
Fixed value	**SVE**		
	AAD %	Bias %	MAD %
T	0.37	-0.05	0.89
P	0.02	0.01	0.05
Fixed value	**SLE**		
	AAD %	Bias %	MAD %
T	2.44	-1.64	3.46
P	0.09	-0.004	0.42

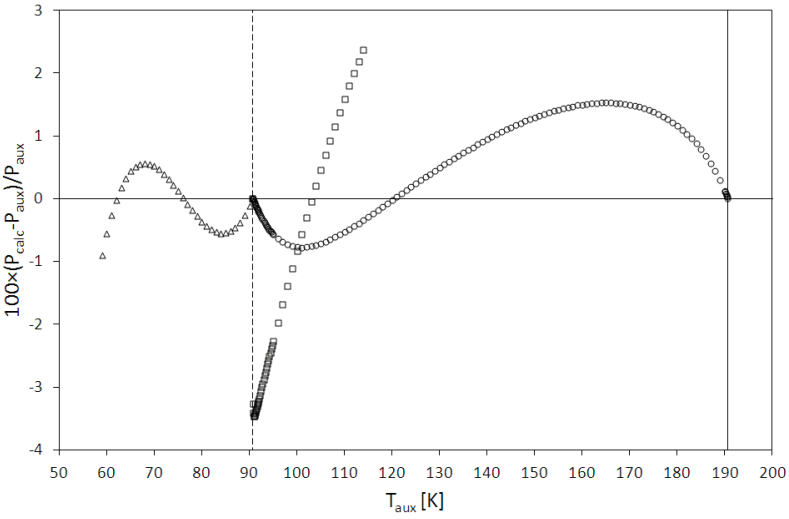

Figure D.33: Percentage errors in terms of pressure for CH_4. ○ : VLE; Δ : SVE; □ : SLE.

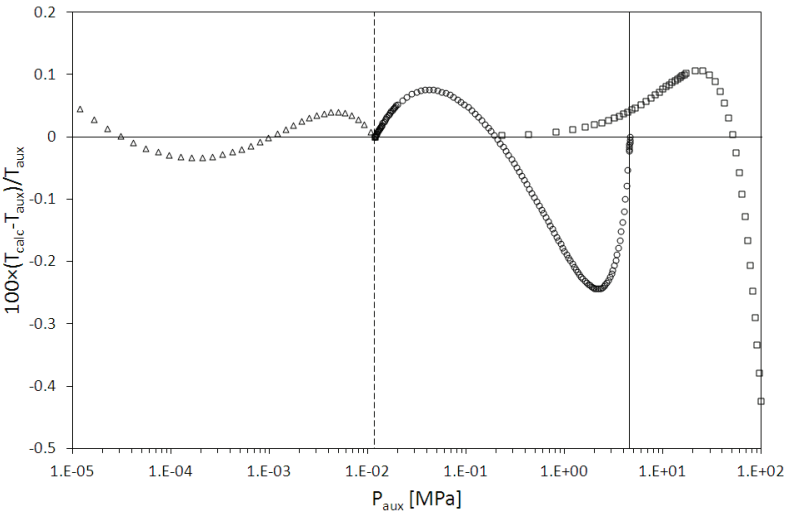

Figure D.34: Percentage errors in terms of temperature for CH_4. ○ : VLE; Δ : SVE; □ : SLE.

3.12 Ethane

Figure D.35 shows the qualitative comparison between calculated and auxiliary values in the PT-EP of ethane.

The quantitative comparison between calculated and auxiliary values is presented in Table D.14 with reference to deviations in terms of pressure and temperature.

The detail of the percentage errors between the auxiliary and calculated values are presented in Figure D.36 and Figure D.37, respectively.

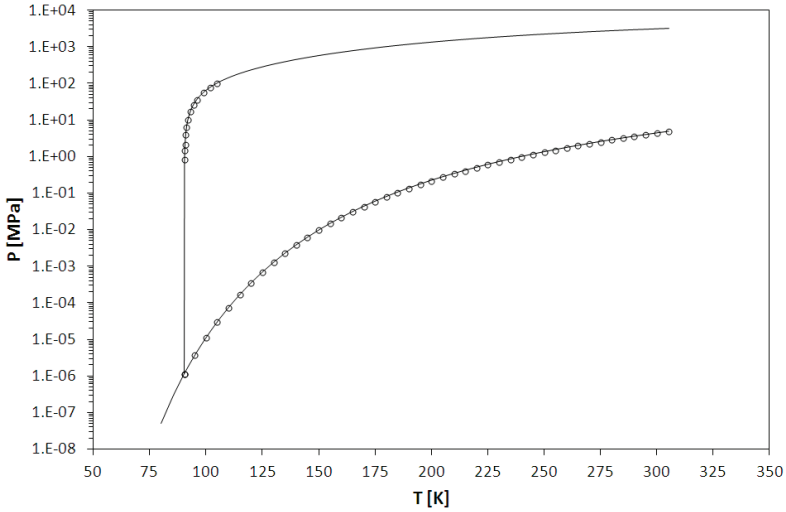

Figure D.35: PT-EP of C_2H_6 obtained with the SLV EoS. — : SLV EoS; ○ : equilibrium values from auxiliary equations.

Table D.14: Errors of the SLV EoS with respect to the auxiliary values for ethane.

For each equilibrium, the first line refers to errors in terms of pressure. The second line refers to errors in terms of temperature.

Fixed value	VLE		
	AAD %	Bias %	MAD %
T	1.22	0.34	3.35
P	0.12	-0.07	0.45
Fixed value	**SLE**		
	AAD %	Bias %	MAD %
T	1.22	-0.07	4.11
P	0.07	-0.05	0.49

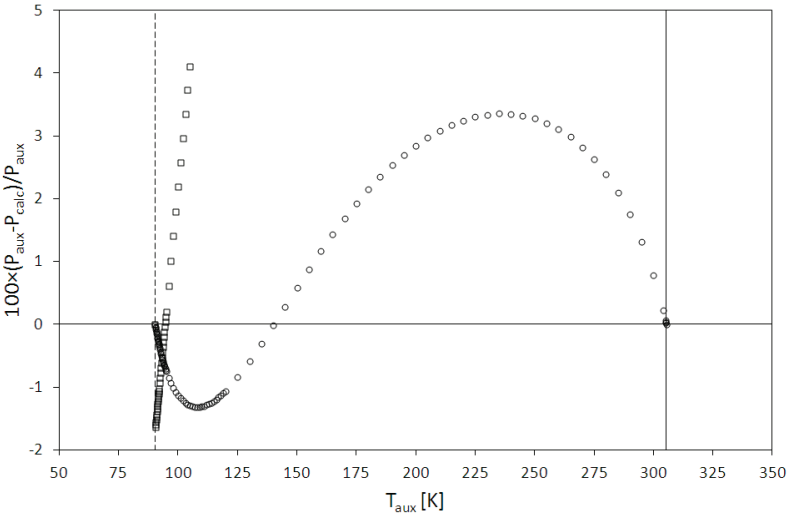

Figure D.36: Percentage errors in terms of pressure for C_2H_6. ○ : VLE; Δ : SVE; □ : SLE.

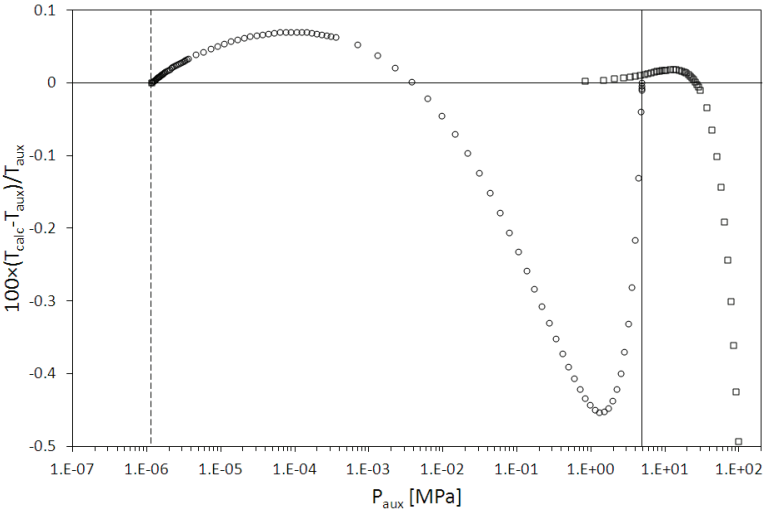

Figure D.37: Percentage errors in terms of temperature for C_2H_6. ○ : VLE; Δ : SVE; □ : SLE.

3.13 Ethylene

Figure D.38 shows the qualitative comparison between calculated and auxiliary values in the PT-EP of ethylene. The quantitative comparison between calculated and auxiliary values is presented in Table D.15 with reference to deviations in terms of pressure and temperature.

The detail of the percentage errors between the auxiliary and calculated values are presented in Figure D.39 and Figure D.40, respectively.

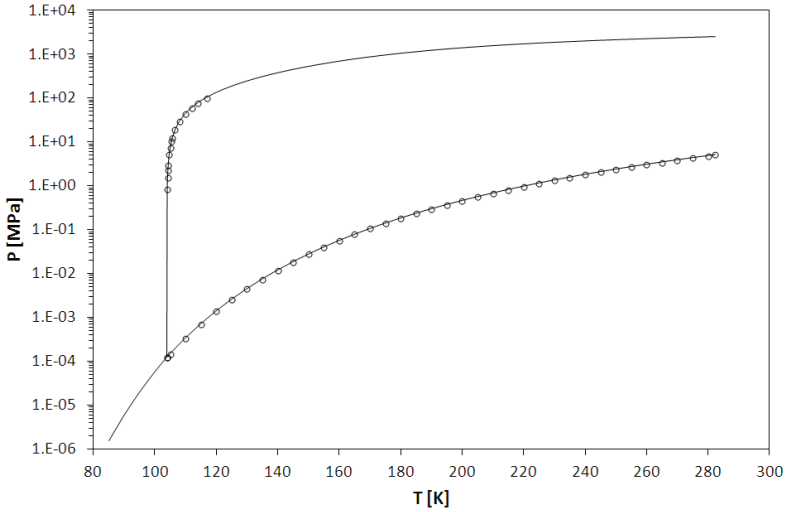

Figure D.38: PT-EP of C_2H_4 obtained with the SLV EoS. — : SLV EoS; ○ : equilibrium values from auxiliary equations.

Table D.15: Errors of the SLV EoS with respect to the auxiliary values for ethylene.

For each equilibrium, the first line refers to errors in terms of pressure. The second line refers to errors in terms of temperature.

Fixed value	VLE		
	AAD %	Bias %	MAD %
T	0.34	0.19	1.47
P	0.04	-0.02	0.22
Fixed value	**SLE**		
	AAD %	Bias %	MAD %
T	3.93	-3.30	5.92
P	0.08	0.03	0.38

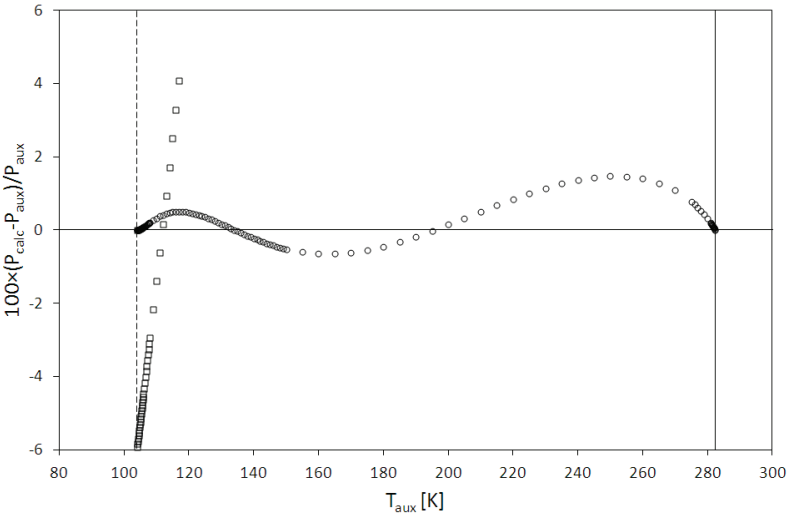

Figure D.39: Percentage errors in terms of pressure for C_2H_4. ○ : VLE; Δ : SVE; □ : SLE.

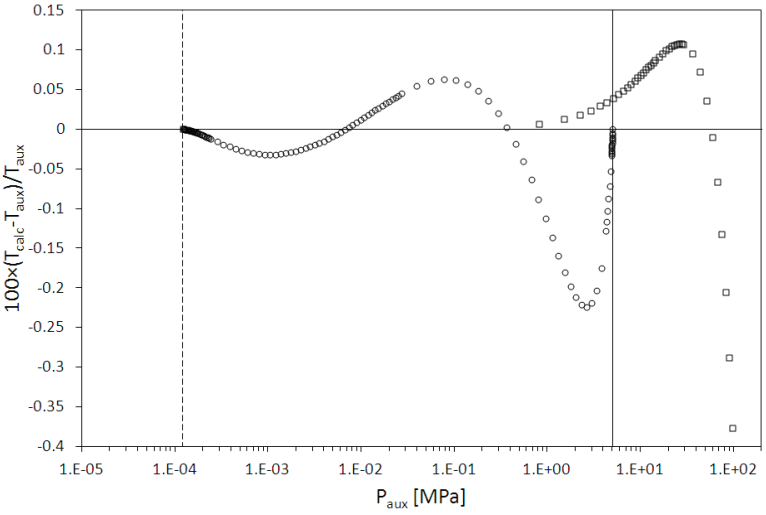

Figure D.40: Percentage errors in terms of temperature for C_2H_4. ○ : VLE; Δ : SVE; □ : SLE.

3.14 Propane

Figure D.41 shows the qualitative comparison between calculated and auxiliary values in the PT-EP of propane. The quantitative comparison between calculated and auxiliary values is presented in Table D.16 with reference to deviations in terms of pressure and temperature.

The detail of the percentage errors between the auxiliary and calculated values are presented in Figure D.42 and Figure D.43, respectively.

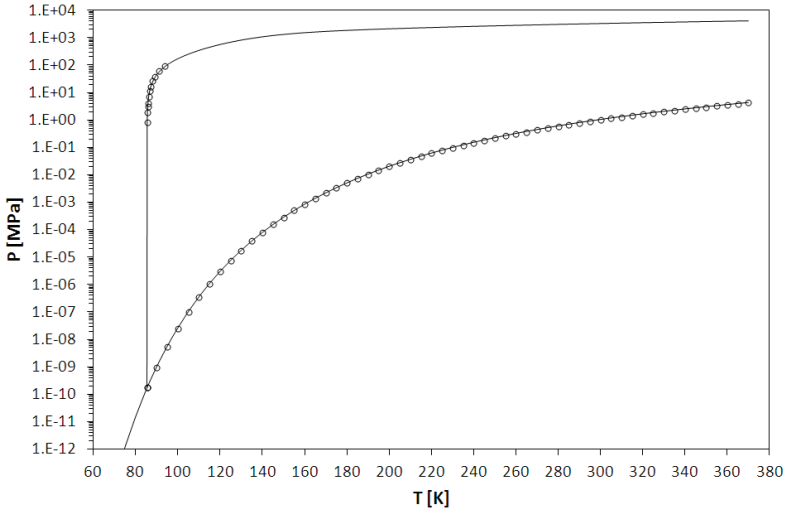

Figure D.41: PT-EP of C_3H_8 obtained with the SLV EoS.
— : SLV EoS; ○ : equilibrium values from auxiliary equations.

Table D.16: Errors of the SLV EoS with respect to the auxiliary values for propane.

For each equilibrium, the first line refers to errors in terms of pressure. The second line refers to errors in terms of temperature.

Fixed value	VLE		
	AAD %	Bias %	MAD %
T	1.01	0.67	3.34
P	0.12	-0.10	0.44
Fixed value	**SLE**		
	AAD %	Bias %	MAD %
T	16.11	-16.11	24.67
P	0.32	0.32	0.70

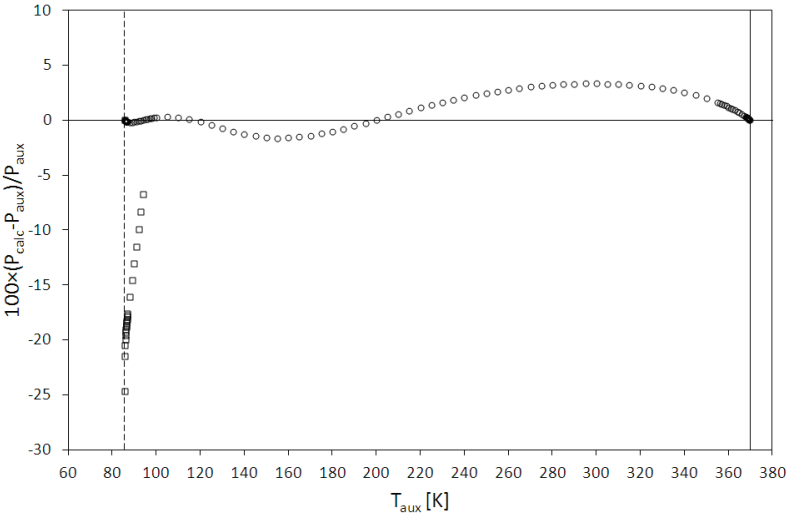

Figure D.42: Percentage errors in terms of pressure for C_3H_8.
○ : VLE; Δ : SVE; □ : SLE.

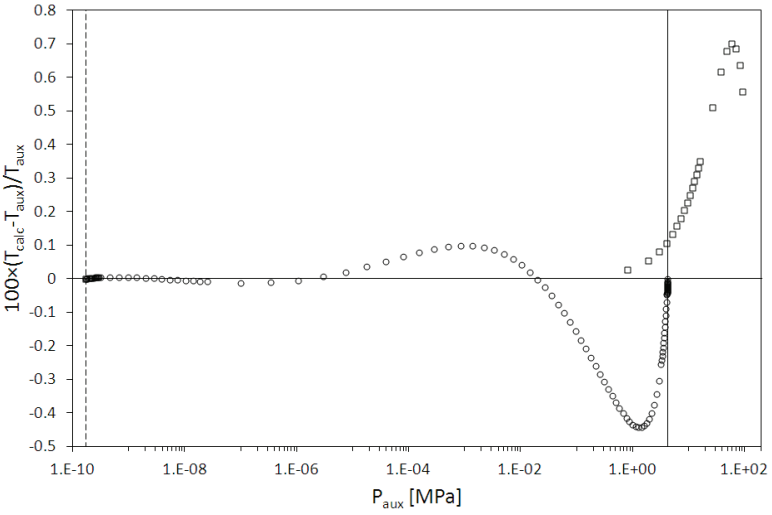

Figure D.43: Percentage errors in terms of temperature for C_3H_8.
○ : VLE; Δ : SVE; □ : SLE.

3.15 Propylene

Figure D.44 shows the qualitative comparison between calculated and auxiliary values in the PT-EP of propylene. The quantitative comparison between calculated and auxiliary values is presented in Table D.17 with reference to deviations in terms of pressure and temperature.

The detail of the percentage errors between the auxiliary and calculated values are presented in Figure D.45 and Figure D.46, respectively.

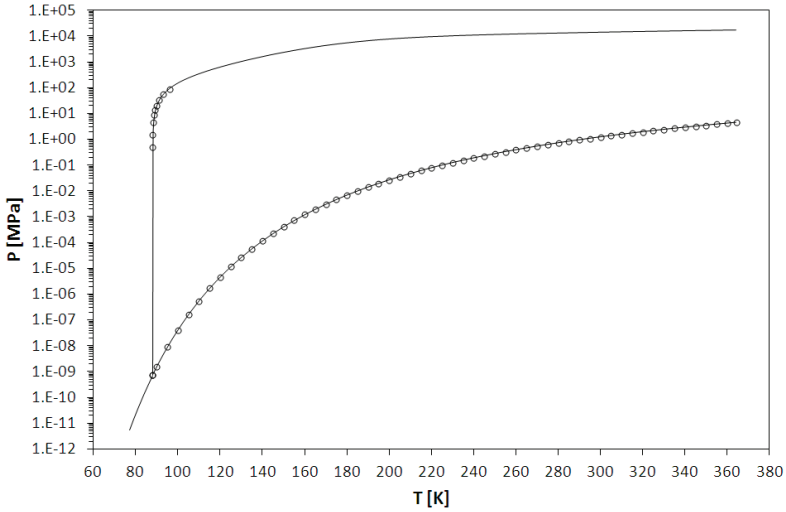

Figure D.44: PT-EP of C_3H_6 obtained with the SLV EoS.
— : SLV EoS; ○ : equilibrium values from auxiliary equations.

Table D.17: Errors of the SLV EoS with respect to the auxiliary values for propylene.

For each equilibrium, the first line refers to errors in terms of pressure. The second line refers to errors in terms of temperature.

Fixed value	VLE		
	AAD %	Bias %	MAD %
T	0.82	0.49	3.07
P	0.09	-0.07	0.42
Fixed value	**SLE**		
	AAD %	Bias %	MAD %
T	1.69	-0.71	5.25
P	0.04	-0.02	0.36

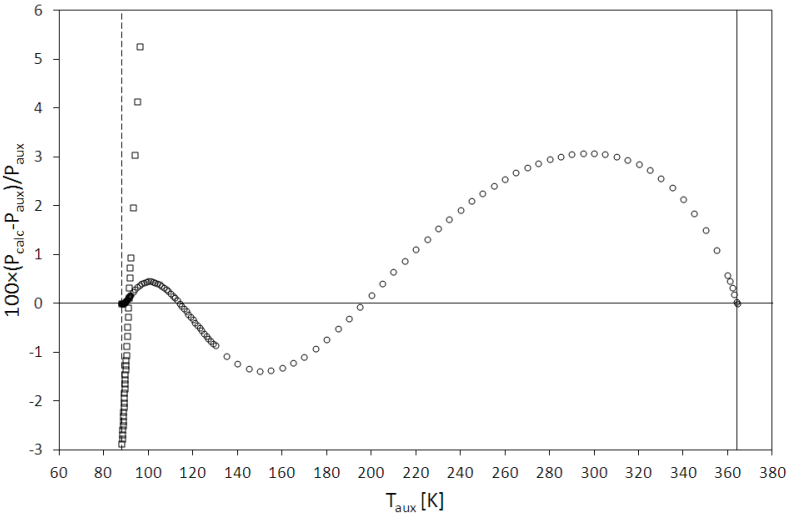

Figure D.45: Percentage errors in terms of pressure for C_3H_6.
○ : VLE; Δ : SVE; □ : SLE.

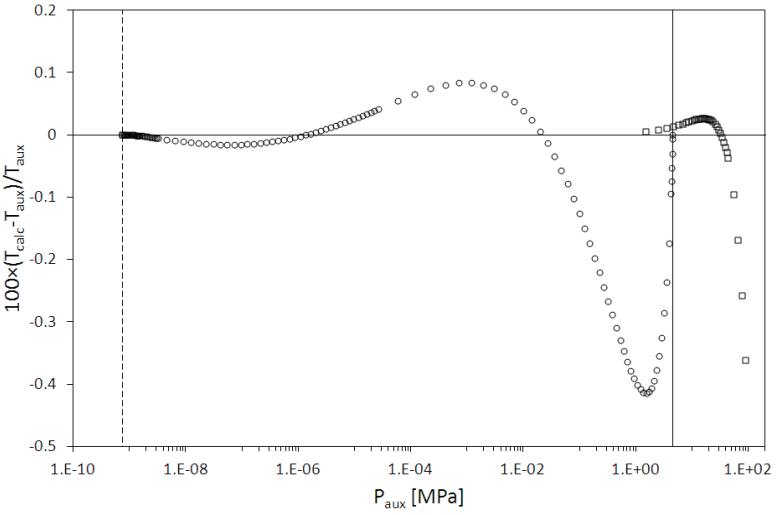

Figure D.46: Percentage errors in terms of temperature for C_3H_6.
○ : VLE; Δ : SVE; □ : SLE.

Appendix E

EXTENSION TO MIXTURES

LIST OF FIGURES **E2**

LIST OF TABLES **E2**

1 SLV EoS APPLIED TO MIXTURES E3

1.1 Derivatives of the mixture parameters *E6*

1.2 Consistency test *E9*

2 MINIMIZATION OF THE GIBBS FREE ENERGY OF MIXING E13

3 THE FUNCTIONAL FORM OF THE LJ-SLV EOS E19

BIBLIOGRAPHY **E20**

List of Figures

Figure E.1: Qualitative pressure-temperature equilibrium behavior of pure component *i*. E13
Figure E.2: Flow diagram of the algorithm for the minimization of the Gibbs free energy of mixing. E14
Figure E.3: Difference between fugacity coefficients of two phases of a pure component as a function of pressure. E15
Figure E.4: Way of cycling the mole fraction of component 1 in the mixture. E17

List of Tables

Table E.1: Temperature and pressure at triple and critical point for carbon dioxide and propane. E10
Table E.2: Parameters of the SLV EoS for carbon dioxide and propane. E10
Table E.3: Evaluation of the partial molar fugacity coefficients for the consistency test. Case A. E10
Table E.4: Evaluation of the numerical derivatives of fugacity coefficients. Case A. E11
Table E.5: Evaluation of the partial molar fugacity coefficients for the consistency test. Case B. E11
Table E.6: Evaluation of the numerical derivatives of fugacity coefficients. Case B. E12
Table E.7: Main thermodynamic properties involved in the algorithm of minimization of the Gibbs free energy of mixing. E13
Table E.8: Criteria for evaluating the stable phase of a pure component at fixed temperature. E16

1 SLV EoS applied to mixtures

Eq. (E.1) is the solid-liquid-vapor equation of state written in terms of mixture parameters a_{mix}, b_{mix}, c_{mix}, and d_{mix}. A generic covolume τ_{mix} ($\tau_{mix} = b_{mix}$ or c_{mix}) has been considered in the attractive term.

$$P(T,v) = \frac{RT}{v - b_{mix}} \frac{v - d_{mix}}{v - c_{mix}} - \frac{a}{v^2 + q\tau_{mix}v + r\tau_{mix}^2} \qquad (E.1)$$

In eq. (E.1), q and r are parameters, R is the gas constant, T the temperature, P the pressure, and v is the volume.

The mixture parameters are expressed in eqs. (E.2)-(E.5)

$$a_{mix} = \sum_{i=1}^{N}\sum_{j=1}^{N} \sqrt{a_i a_j}\left(1 - K_{ij}\right)x_i x_j \quad , \quad K_{ij} = \frac{k_{ij}k_{ji}\left(x_i + x_j\right)}{k_{ij}x_j + k_{ji}x_i} \quad , \quad K_{ii} = 0 \qquad (E.2)$$

$$b_{mix} = \frac{1}{2}\sum_{i=1}^{N}\sum_{j=1}^{N} \left(b_i + b_j\right)\left(1 - M_{ij}\right)x_i x_j \quad , \quad M_{ij} = \frac{m_{ij}m_{ji}\left(x_i + x_j\right)}{m_{ij}x_j + m_{ji}x_i} \quad , \quad M_{ii} = 0 \qquad (E.3)$$

$$c_{mix} = \frac{1}{2}\sum_{i=1}^{N}\sum_{j=1}^{N} \left(c_i + c_j\right)\left(1 - N_{ij}\right)x_i x_j \quad , \quad N_{ij} = \frac{n_{ij}n_{ji}\left(x_i + x_j\right)}{n_{ij}x_j + n_{ji}x_i} \quad , \quad N_{ii} = 0 \qquad (E.4)$$

$$d_{mix} = \frac{1}{2}\sum_{i=1}^{N}\sum_{j=1}^{N} \left(d_i + d_j\right)\left(1 - L_{ij}\right)x_i x_j \quad , \quad L_{ij} = \frac{l_{ij}l_{ji}\left(x_i + x_j\right)}{l_{ij}x_j + l_{ji}x_i} \quad , \quad L_{ii} = 0 \qquad (E.5)$$

These mixing rules contain a maximum of 8 binary interaction parameters (k_{ij}, $k_{ji,}$ m_{ij}, m_{ji}, n_{ij}, n_{ji}, l_{ij}, and l_{ji}). The number of parameters reduces to 4 if symmetric values are fixed for the couples ij and ji. Furthermore, the relation $k_{ii} = m_{ii} = n_{ii} = l_{ii} = 0$ holds.

The application of eq. (E.1) for the representation of the equilibrium in a mixture requires finding the global minimum of the Gibbs free energy of mixing G^M among all the phases. In the φ-φ approach, G^M can be evaluated in a generic phase α from the partial molar fugacity coefficient by:

$$\frac{G^{M\alpha}(T,P,\bar{x})}{nRT} = \sum_{i}^{N} x_i \ln\frac{f_i^{\alpha}(T,P,\bar{x})}{f_i^{0}(T,P)} = \sum_{i}^{N} x_i \ln\frac{x_i\hat{\varphi}_i^{\alpha}(T,P,\bar{x})P}{\varphi_i^{0}(T,P)P} = \sum_{i}^{N} x_i \ln\frac{x_i\hat{\varphi}_i^{\alpha}(T,P,\bar{x})}{\varphi_i^{0}(T,P)} \qquad (E.6)$$

In eq. (E.6), n is the total number of moles, R is the gas constant, P is the pressure, and T is the temperature. x_i, φ_i and f_i are composition, fugacity coefficient and fugacity of component i, respectively. $\bar{x}$ is the composition in the α phase. Finally, ^ is used for the partial molar fugacity coefficient, and superscript 0 refers to properties of the pure component i at the same T and P of the mixture but in its stable phase.

The partial molar fugacity coefficient of the i^{th} component in a phase α is given in eq. (E.7).

$$\ln\hat{\varphi}_i^{\alpha}(T,P,\bar{x}) = \left(\frac{\partial n a^{R,\alpha}}{\partial n_i}\right)_{T,nv,j\neq i} - \ln Z^{\alpha} \qquad (E.7)$$

According to eq. (E.7), $\hat{\varphi}_i^{\alpha}$ is a function of the compressibility factor and the first derivative of the residual free Helmholtz energy with respect to the moles of component i.

The mathematical steps concerning the derivation of the residual Helmholtz free energy are detailed below for the case $q = r = 0$, namely for the case of considering the van der Waals attractive term in eq. (E.1). Similar steps are involved in case of not null values of q and r; these steps have not been reported here in order to avoid a cumbersome discussion, thus for $q, r \neq 0$ only the expression of the partial molar fugacity. Furthermore, no distinction has been made for the kind of phase in the following equations, and subscript *mix* has been neglected to ease the lecture.

The residual Helmholtz free energy in terms of variables temperature and volume has been introduced in Appendix D. That expression times the number of moles n gives:

$$na^R(T,v) = nA_1 \ln\left|\frac{v}{v-b}\right| + nA_2 \ln\left|\frac{v}{v-c}\right| - \frac{na}{RTv} \qquad (E.8)$$

where:

$$A_1 = \frac{d-b}{c-b} \quad , \quad A_2 = \frac{c-d}{c-b} \qquad (E.9)$$

The mixture parameters (here a, b, c, and d) are functions of the composition as introduced in eqs. (E.2)-(E.5). The following identities have been used in eqs. (10)-(18).

$$a_i' = \left(\frac{\partial na}{\partial n_i}\right)_{T,nv,j\neq i} \quad , \quad b_i' = \left(\frac{\partial nb}{\partial n_i}\right)_{T,nv,j\neq i} \quad , \quad c_i' = \left(\frac{\partial nc}{\partial n_i}\right)_{T,nv,j\neq i} \quad , \quad d_i' = \left(\frac{\partial nd}{\partial n_i}\right)_{T,nv,j\neq i} \qquad (E.9)$$

The derivatives of coefficients A_1 and A_2 result in:

$$\left(\frac{\partial A_1}{\partial n_i}\right)_{T,nv,j\neq i} = \frac{\partial}{\partial n_i}\left[\frac{n}{n}\left(\frac{d-b}{c-b}\right)\right] = \frac{(d_i'-b_i')n(c-b) - n(d-b)(c_i'-b_i')}{n^2(c-b)^2} = \frac{c_i'(b-d) + d_i'(c-b) + b_i'(d-c)}{n(c-b)^2} \qquad (E.10)$$

$$\left(\frac{\partial A_2}{\partial n_i}\right)_{T,nv,j\neq i} = \frac{\partial}{\partial n_i}\left[\frac{n}{n}\left(\frac{c-d}{c-b}\right)\right] = \frac{(c_i'-d_i')n(c-b) - n(c-d)(c_i'-b_i')}{n^2(c-b)^2} = \frac{-c_i'(b-d) - d_i'(c-b) - b_i'(d-c)}{n(c-b)^2} \qquad (E.11)$$

Derivation of the logarithms in eq. (E.8) gets:

$$\left[\frac{\partial}{\partial n_i}\left(\ln\left|\frac{v}{v-b}\right|\right)\right]_{T,nv,j\neq i} = \left[\frac{\partial}{\partial n_i}\left(\ln\left|\frac{nv}{nv-nb}\right|\right)\right]_{T,nv,j\neq i} = \frac{b_i'}{n(v-b)} \qquad (E.12)$$

$$\left[\frac{\partial}{\partial n_i}\left(\ln\left|\frac{v}{v-c}\right|\right)\right]_{T,nv,j\neq i} = \left[\frac{\partial}{\partial n_i}\left(\ln\left|\frac{nv}{nv-nc}\right|\right)\right]_{T,nv,j\neq i} = \frac{c_i'}{n(v-c)} \qquad (E.13)$$

Derivation of the first term on the right hand side of eq. (E.8) with respect to n turns in:

$$\left[\frac{\partial n}{\partial n_i}\left(nA_1 \ln\left|\frac{v}{v-b}\right|\right)\right]_{T,nv,j\neq i} = A_1 \ln\left|\frac{v}{v-b}\right| + n\frac{\partial A_1}{\partial n_i}\ln\left|\frac{v}{v-b}\right| + nA_1\frac{\partial}{\partial n_i}\left(\ln\left|\frac{v}{v-b}\right|\right) = \qquad (E.14)$$

$$= A_1 \ln\left|\frac{v}{v-b}\right| + \frac{c_i'(b-d) + d_i'(c-b) + b_i'(d-c)}{(c-b)^2}\ln\left|\frac{v}{v-b}\right| + \frac{A_1 b_i'}{(v-b)} \qquad (E.14)$$

Derivation of the second term on the right hand side of eq. (E.8) with respect to *n* turns in:

$$\left[\frac{\partial n}{\partial n_i}\left(nA_2 \ln\left|\frac{v}{v-c}\right|\right)\right]_{T,nv,j\neq i} = A_2 \ln\left|\frac{v}{v-c}\right| + n\frac{\partial A_2}{\partial n_i}\ln\left|\frac{v}{v-c}\right| + nA_2\frac{\partial}{\partial n_i}\left(\ln\left|\frac{v}{v-c}\right|\right) =$$
$$= A_2 \ln\left|\frac{v}{v-c}\right| - \frac{c_i'(b-d) + d_i'(c-b) + b_i'(d-c)}{(c-b)^2}\ln\left|\frac{v}{v-c}\right| + \frac{A_2 c_i'}{(v-c)} \qquad (E.15)$$

Derivation of the third term on the right hand side of eq. (E.8) with respect to *n* turns in:

$$\left[\frac{\partial}{\partial n_i}\left(-\frac{na}{RTv}\right)\right]_{T,nv,j\neq i} = -\frac{a}{RTv} - \frac{n}{RT}\frac{\partial}{\partial n_i}\left(\frac{a}{v}\right) = -\frac{a}{RTv} - \frac{n}{RT}\frac{\partial}{\partial n_i}\left(\frac{na}{nv}\right) = -\frac{a}{RTv} - \frac{a_i'}{RTv} \qquad (E.16)$$

Some terms of eqs. (E.14)-(E.15) can be coupled:

$$\frac{c_i'(b-d) + d_i'(c-b) + b_i'(d-c)}{(c-b)^2}\ln\left|\frac{v}{v-b}\right| - \frac{c_i'(b-d) + d_i'(c-b) + b_i'(d-c)}{(c-b)^2}\ln\left|\frac{v}{v-c}\right| =$$
$$= \frac{c_i'(d-b) + d_i'(b-c) + b_i'(c-d)}{(c-b)^2}\ln\left|\frac{v-b}{v-c}\right| \qquad (E.17)$$

Then the derivative of na^R becomes:

$$\left(\frac{\partial n a^R}{\partial n_i}\right)_{T,nv,j\neq i} = A_1 \ln\left|\frac{v}{v-b}\right| + A_2 \ln\left|\frac{v}{v-c}\right| + \frac{A_1 b_i'}{(v-b)} + \frac{A_2 c_i'}{(v-c)} - \frac{a}{RTv} - \frac{a_i'}{RTv}$$
$$+ \left[\frac{c_i'(d-b) + d_i'(b-c) + b_i'(c-d)}{(c-b)^2}\right]\ln\left|\frac{v-b}{v-c}\right| \qquad (E.18)$$

The first, second, and the fifth terms on the previous equations give the residual Helmholtz free energy a^R, thus eq. (E.18) becomes:

$$\left(\frac{\partial n a^R}{\partial n_i}\right)_{T,nv,j\neq i} = a^R + \frac{1}{c-b}\left[\frac{b_i'(d-b)}{(v-b)} + \frac{c_i'(c-d)}{(v-c)}\right] - \frac{a_i'}{RTv}$$
$$+ \left[\frac{c_i'(d-b) + d_i'(b-c) + b_i'(c-d)}{(c-b)^2}\right]\ln\left|\frac{v-b}{v-c}\right| \qquad (E.19)$$

The partial molar fugacity coefficient of the i^{th} component is then obtained from eq. (E.19) minus the logarithm of the compressibility factor Z, eq. (E.20).

$$Z = \frac{v}{v-b}\frac{v-d}{v-c} - \frac{a}{RTv} \qquad (E.20)$$

Similar steps are required for obtaining the partial molar fugacity coefficient from eq. (E.1) with not null values for *q* and *r*. The expressions for the correspondent Helmholtz free energy, its first

derivative, and Z are indicated in eqs. (E.21)-(E.23). It is worth remembering that τ equals the solid or the liquid covolume, and that $q = \varepsilon_1+\varepsilon_2$ and $r = \varepsilon_1\times\varepsilon_2$.

$$a^R(T,v) = \frac{d-b}{c-b} ln \left|\frac{v}{v-b}\right| + \frac{c-d}{c-b} ln \left|\frac{v}{v-c}\right| + \frac{a}{RT\tau(\varepsilon_2-\varepsilon_1)} ln \left|\frac{v+\varepsilon_1\tau}{v+\varepsilon_2\tau}\right| \quad (E.21)$$

$$\begin{aligned}\left(\frac{\partial n a^R}{\partial n_i}\right)_{T,nv,j\neq i} &= a^R + \frac{1}{c-b}\left[\frac{b_i'(d-b)}{(v-b)} + \frac{c_i'(c-d)}{(v-c)}\right] \\ &+ \left[\frac{c_i'(d-b) + d_i'(b-c) + b_i'(c-d)}{(c-b)^2}\right] \ln\left|\frac{v-b}{v-c}\right| + \frac{a_i'\tau - a\tau_i'}{RT\tau^2(\varepsilon_2-\varepsilon_1)} \ln\left|\frac{v+\varepsilon_1\tau}{v+\varepsilon_2\tau}\right| \\ &- \frac{av\tau_i'}{RT\tau(v+\varepsilon_1\tau)(v+\varepsilon_2\tau)}\end{aligned} \quad (E.22)$$

$$Z = \frac{v}{v-b}\frac{v-d}{v-c} - \frac{av}{RT(v^2+q\tau v+r\tau^2)} \quad (E.23)$$

Eqs. (E.19)-(E.23) require expressions for the derivatives of the mixture parameters a, b, c, and d. These derivatives are illustrated in the next section for the case of symmetric and asymmetric binary interaction parameters. Since the mixing rules for the volumetric parameters b, c, and d are of the same type, mathematical steps for the solid covolume b has been chosen as example in the following section, but similar derivations have been obtained for c and d.

1.1 Derivatives of the mixture parameters

In case of symmetric binary interaction parameters, eqs. (E.2)-(E.3) are:

$$a = \sum_{i=1}^{N}\sum_{j=1}^{N}\sqrt{a_i a_j}\left(1-k_{ij}\right)x_i x_j \quad , \quad k_{ij} = k_{ji} \quad , \quad k_{ii} = 0 \quad (E.24)$$

$$b = \frac{1}{2}\sum_{i=1}^{N}\sum_{j=1}^{N}\left(b_i+b_j\right)\left(1-m_{ij}\right)x_i x_j \quad , \quad m_{ij} = m_{ji} \quad , \quad m_{ii} = 0 \quad (E.25)$$

Developing eqs. (E.24)-(E.25) for a binary mixture yields to:

$$a = a_i x_i^2 + 2\sqrt{a_i a_j}\left(1-k_{ij}\right) + a_j x_j^2 \quad (E.26)$$

$$b = b_i x_i^2 + \left(b_i+b_j\right)\left(1-m_{ij}\right)x_i x_j + b_j x_j^2 \quad (E.27)$$

The first identity in eq. (E.9) involves the derivative of a:

$$a_i' = \left(\frac{\partial n a}{\partial n_i}\right)_{T,nv,j\neq i} = \frac{\partial}{\partial n_i}\frac{n^2}{n}\left[a_i x_i^2 + 2\sqrt{a_i a_j}\left(1-k_{ij}\right)x_i x_j + a_j x_j^2\right] = \quad (E.28)$$

$$= \frac{\partial}{\partial n_i}\left[\frac{a_i n_i^2 + 2\sqrt{a_i a_j}\left(1-k_{ij}\right)n_i n_j + a_j n_j^2}{n}\right] = \quad (E.29)$$

$$= \frac{2a_i n_i}{n} + \frac{2\sqrt{a_i a_j}\left(1-k_{ij}\right)n_j}{n} - \frac{a_i n_i^2 + 2\sqrt{a_i a_j}\left(1-k_{ij}\right)n_i n_j + a_j n_j^2}{n^2} = \quad (E.30)$$

$$= \frac{2a_i n_i n + 2\sqrt{a_i a_j}\left(1-k_{ij}\right)n_j n - a_i n_i^2 - 2\sqrt{a_i a_j}\left(1-k_{ij}\right)n_i n_j - a_j n_j^2}{n^2} = \quad (E.31)$$

$$= \frac{2a_i x_i n^2 + 2\sqrt{a_i a_j}(1-k_{ij})x_j n^2 - a_i x_i^2 n^2 - 2\sqrt{a_i a_j}(1-k_{ij})x_i x_j n^2 - a_j x_j^2 n^2}{n^2} = \quad (E.32)$$

$$= 2a_i x_i + 2\sqrt{a_i a_j}(1-k_{ij})x_j - a_i x_i^2 - 2\sqrt{a_i a_j}(1-k_{ij})x_i x_j - a_j x_j^2 = \quad (E.33)$$

$$= -a + 2\left[a_i x_i + \sqrt{a_i a_j}(1-k_{ij})x_j\right] \quad (E.34)$$

The partial derivative of the solid covolume is instead:

$$b_i' = \left(\frac{\partial nb}{\partial n_i}\right)_{T,nv,j\neq i} = \frac{\partial}{\partial n_i}\frac{n^2}{n}\left[b_i x_i^2 + (b_i + b_j)(1-m_{ij})x_i x_j + b_j x_j^2\right] = \quad (E.35)$$

$$= \frac{\partial}{\partial n_i}\left[\frac{b_i n_i^2 + (b_i + b_j)(1-m_{ij})n_i n_j + b_j n_j^2}{n}\right] = \quad (E.36)$$

$$= \frac{2b_i n_i}{n} + \frac{(b_i + b_j)(1-m_{ij})n_j}{n} - \frac{b_i n_i^2 + (b_i + b_j)(1-m_{ij})n_i n_j + b_j n_j^2}{n^2} = \quad (E.37)$$

$$= \frac{2b_i n_i n + (b_i + b_j)(1-m_{ij})n_j n - b_i n_i^2 - (b_i + b_j)(1-m_{ij})n_i n_j - b_j n_j^2}{n^2} = \quad (E.38)$$

$$= \frac{2b_i x_i n^2 + (b_i + b_j)(1-m_{ij})x_j n^2 - b_i x_i^2 n^2 - (b_i + b_j)(1-m_{ij})x_i x_j n^2 - b_j x_j^2 n^2}{n^2} = \quad (E.39)$$

$$= 2b_i x_i + (b_i + b_j)(1-m_{ij})x_j - b_i x_i^2 - (b_i + b_j)(1-m_{ij})x_i x_j - b_j x_j^2 = \quad (E.40)$$

$$= -b + 2b_i x_i + (b_i + b_j)(1-m_{ij})x_j \quad (E.41)$$

Similarly, the derivatives of *c* and *d* result in:

$$c_i' = \left(\frac{\partial nc}{\partial n_i}\right)_{T,nv,j\neq i} = -c + 2c_i x_i + (c_i + c_j)(1-n_{ij})x_j \quad (E.42)$$

$$d_i' = \left(\frac{\partial nd}{\partial n_i}\right)_{T,nv,j\neq i} = -d + 2d_i x_i + (d_i + d_j)(1-l_{ij})x_j \quad (E.43)$$

Developing eqs. (E.2)-(E.3) for a binary mixture in case of asymmetric interaction parameters for the couples *ij* and *ji* yields to:

$$a = a_i x_i^2 + 2\sqrt{a_i a_j}x_i x_j\left[1 - \frac{k_{ij}k_{ji}(x_i + x_j)}{k_{ij}x_j + k_{ji}x_i}\right] + a_j x_j^2 \quad (E.44)$$

$$b = b_i x_i^2 + (b_i + b_j)x_i x_j\left[1 - \frac{m_{ij}m_{ji}(x_i + x_j)}{m_{ij}x_j + m_{ji}x_i}\right] + b_j x_j^2 \quad (E.45)$$

The partial derivative of attractive term with respect to the number of moles of component *i* is:

$$a_i' = \left(\frac{\partial na}{\partial n_i}\right)_{T,nv,j\neq i} = \frac{\partial}{\partial n_i}\frac{n^2}{n}\left\{a_i x_i^2 + 2\sqrt{a_i a_j}x_i x_j\left[1 - \frac{k_{ij}k_{ji}(x_i + x_j)}{k_{ij}x_j + k_{ji}x_i}\right] + a_j x_j^2\right\} = \quad (E.46)$$

$$= \frac{\partial}{\partial n_i}\left\{\frac{a_i n_i^2}{n} + \frac{2\sqrt{a_i a_j}n_i n_j}{n}\left[1 - \frac{k_{ij}k_{ji}(n_i + n_j)}{k_{ij}n_j + k_{ji}n_i}\right] + \frac{a_j n_j^2}{n}\right\} = \quad (E.47)$$

$$= \frac{2a_i n_i}{n} + \frac{2\sqrt{a_i a_j} n_j}{n}\left[1 - \frac{k_{ij}k_{ji}(n_i + n_j)}{k_{ij}n_j + k_{ji}n_i}\right] + \frac{2\sqrt{a_i a_j} n_i n_j}{n}\left[-\frac{k_{ij}k_{ji}(k_{ij}n_j + k_{ji}n_i) - k_{ij}k_{ji}^2(n_i + n_j)}{(k_{ij}n_j + k_{ji}n_i)^2}\right] - \frac{a_i n_i^2 + 2\sqrt{a_i a_j} n_i n_j\left[1 - \frac{k_{ij}k_{ji}(n_i + n_j)}{k_{ij}n_j + k_{ji}n_i}\right] + a_j n_j^2}{n^2} = \quad (E.48)$$

$$= 2a_i x_i + 2\sqrt{a_i a_j} x_j\left[1 - \frac{k_{ij}k_{ji}(x_i + x_j)}{k_{ij}x_j + k_{ji}x_i}\right] - 2\sqrt{a_i a_j} x_i x_j\left[\frac{k_{ij}k_{ji}(k_{ij}x_j + k_{ji}x_i) - k_{ij}k_{ji}^2(x_i + x_j)}{(k_{ij}x_j + k_{ji}x_i)^2}\right] - a = \quad (E.49)$$

$$= 2a_i x_i + 2\sqrt{a_i a_j} x_j(1 - K_{ij}) - 2\sqrt{a_i a_j} x_i x_j\left[\frac{k_{ij}^2 k_{ji}x_j + k_{ij}k_{ji}^2 x_i - k_{ij}k_{ji}^2 x_i - k_{ij}k_{ji}^2 x_j}{(k_{ij}x_j + k_{ji}x_i)^2}\right] - a = \quad (E.50)$$

$$= 2a_i x_i + 2\sqrt{a_i a_j} x_j(1 - K_{ij}) - 2\sqrt{a_i a_j} x_i x_j\left[\frac{k_{ij}^2 k_{ji}x_j - k_{ij}k_{ji}^2 x_j}{(k_{ij}x_j + k_{ji}x_i)^2}\right] - a = \quad (E.51)$$

$$= 2a_i x_i + 2\sqrt{a_i a_j} x_j(1 - K_{ij}) - 2\sqrt{a_i a_j} x_i x_j\left[\frac{k_{ij}k_{ji}x_j(k_{ij} - k_{ji})}{(k_{ij}x_j + k_{ji}x_i)^2}\right] - a = \quad (E.52)$$

$$= -a + 2\left\{a_i x_i + \sqrt{a_i a_j} x_j\left[1 - K_{ij} - \frac{k_{ij}k_{ji}x_i x_j(k_{ij} - k_{ji})}{(k_{ij}x_j + k_{ji}x_i)^2}\right]\right\} \quad (E.53)$$

The partial derivative of solid covolume with respect to the number of moles of component *i* is:

$$b_i' = \left(\frac{\partial nb}{\partial n_i}\right)_{T,nv,j\neq i} = \frac{\partial}{\partial n_i}\frac{n^2}{n}\left\{b_i x_i^2 + (b_i + b_j)x_i x_j\left[1 - \frac{m_{ij}m_{ji}(x_i + x_j)}{m_{ij}x_j + m_{ji}x_i}\right] + b_j x_j^2\right\} = \quad (E.54)$$

$$= \frac{\partial}{\partial n_i}\left\{\frac{b_i n_i^2}{n} + \frac{(b_i + b_j)n_i n_j}{n}\left[1 - \frac{m_{ij}m_{ji}(n_i + n_j)}{m_{ij}n_j + m_{ji}n_i}\right] + \frac{b_j n_j^2}{n}\right\} = \quad (E.55)$$

$$= \frac{2b_i n_i}{n} + \frac{(b_i + b_j)n_j}{n}\left[1 - \frac{m_{ij}m_{ji}(n_i + n_j)}{m_{ij}n_j + m_{ji}n_i}\right] + \frac{(b_i + b_j)n_i n_j}{n}\left[-\frac{m_{ij}m_{ji}(m_{ij}n_j + m_{ji}n_i) - m_{ij}m_{ji}^2(n_i + n_j)}{m_{ij}n_j + m_{ji}n_i^2}\right] - \frac{b_i n_i^2 + (b_i + b_j)n_i n_j\left[1 - \frac{m_{ij}m_{ji}(n_i + n_j)}{m_{ij}n_j + m_{ji}n_i}\right] + b_j n_j^2}{n^2} = \quad (E.56)$$

$$= 2b_i x_i + (b_i + b_j)x_j\left[1 - \frac{m_{ij}m_{ji}(x_i + x_j)}{m_{ij}x_j + m_{ji}x_i}\right] - (b_i + b_j)x_i x_j\left[\frac{m_{ij}m_{ji}(m_{ij}x_j + m_{ji}x_i) - m_{ij}m_{ji}^2(x_i + x_j)}{(m_{ij}x_j + m_{ji}x_i)^2}\right] - b = \quad (E.57)$$

$$= 2b_i x_i + (b_i + b_j)x_j(1 - M_{ij}) - (b_i + b_j)x_i x_j\left[\frac{m_{ij}^2 m_{ji}x_j + m_{ij}m_{ji}^2 x_i - m_{ij}m_{ji}^2 x_i - m_{ij}m_{ji}^2 x_j}{(m_{ij}x_j + m_{ji}x_i)^2}\right] - b = \quad (E.58)$$

$$= 2b_i x_i + (b_i + b_j)x_j(1 - M_{ij}) - (b_i + b_j)x_i x_j\left[\frac{m_{ij}^2 m_{ji}x_j - m_{ij}m_{ji}^2 x_j}{(m_{ij}x_j + m_{ji}x_i)^2}\right] - b = \quad (E.59)$$

$$= 2b_i x_i + (b_i + b_j)x_j(1 - M_{ij}) - (b_i + b_j)x_i x_j \left[\frac{m_{ij}m_{ji}x_j(m_{ij} - m_{ji})}{(m_{ij}x_j + m_{ji}x_i)^2}\right] - b = \quad (E.60)$$

$$= -b + 2b_i x_i + (b_i + b_j)x_j \left[1 - M_{ij} - \frac{m_{ij}m_{ji}x_j x_i(m_{ij} - m_{ji})}{(m_{ij}x_j + m_{ji}x_i)^2}\right] \quad (E.61)$$

Similarly, the derivatives of *c* and *d* result in:

$$c_i' = \left(\frac{\partial nc}{\partial n_i}\right)_{T,nv,j\neq i} = -c + 2c_i x_i + (c_i + c_j)x_j \left[1 - N_{ij} - \frac{n_{ij}n_{ji}x_j x_i(n_{ij} - n_{ji})}{(n_{ij}x_j + n_{ji}x_i)^2}\right] \quad (E.62)$$

$$d_i' = \left(\frac{\partial nd}{\partial n_i}\right)_{T,nv,j\neq i} = -d + 2d_i x_i + (d_i + d_j)x_j \left[1 - L_{ij} - \frac{l_{ij}l_{ji}x_j x_i(l_{ij} - l_{ji})}{(l_{ij}x_j + l_{ji}x_i)^2}\right] \quad (E.63)$$

In [1], the EoS in the form of eq. (E.1) has been applied for representing solid-fluid and fluid-fluid equilibria in binary mixtures of carbon dioxide with methane, ethane, and propane. In [1], a qualitative comparison has been made between the cases of null *q* and *r* (as in the van der Waals cubic EoS), and *q* = 2 and *r* = -1 (as in the Peng-Robinson cubic EoS). The liquid covolume *c* has been considered in the latter case.

The EoS has been applied making use of the mixing rules of the kind of eq. (E.25) with symmetric binary interaction parameters for the volumetric parameters *b*, *c*, and *d*, whereas eq. (E.24) and asymmetric values for k_{ij} and k_{ji} have been employed for the attractive parameter *a*.

The thermodynamic consistency test of the solid-liquid-vapor EoS has been proved in the framework of the application of the EoS presented in [1]. Next section give more details about this test.

1.2 Consistency test

The consistency test concerns both pressure and composition-dependent parameters within an EoS, and focuses on the consequences for thermodynamic properties obtained by derivation or integration of the functional forms. The aim of this test is to assure the absence of inconsistency between the Helmholtz energy and the pressure, which gives erroneous fugacity coefficients, partial molar enthalpies and partial molar volumes, [2].

The consistency test, to be proved, requires satisfying the following equality [2]:

$$\ln \hat{\varphi}_i = \left(\frac{\partial \sum_{j=1}^{N} n_j \ln \hat{\varphi}_j}{\partial n_i}\right)_{T,P,n_{j\neq i}} \quad (E.64)$$

Eq. (E.64) is written for a mixture of *N* components, and for a binary mixture it can be written as a system of two equations:

$$\begin{cases} \ln \hat{\varphi}_1 = \left(\dfrac{\partial[n_1 \ln \hat{\varphi}_1 + n_2 \ln \hat{\varphi}_2]}{\partial n_1}\right)_{T,P,n_2} \\ \ln \hat{\varphi}_2 = \left(\dfrac{\partial[n_1 \ln \hat{\varphi}_1 + n_2 \ln \hat{\varphi}_2]}{\partial n_2}\right)_{T,P,n_1} \end{cases} \quad (E.65)$$

The derivatives in the systems avobe can be numerically solved by finite differences, thus:

$$\begin{cases} \ln \hat{\varphi}_1 = \dfrac{(n_1 + \delta)\ln \hat{\varphi}_{1,n_1+\delta} - (n_1 - \delta)\ln \hat{\varphi}_{1,n_1-\delta}}{2\delta} + \dfrac{n_2 \ln \hat{\varphi}_{2,n_1+\delta} - n_2 \ln \hat{\varphi}_{2,n_1-\delta}}{2\delta} \\ \ln \hat{\varphi}_2 = \dfrac{n_1 \ln \hat{\varphi}_{1,n_2+\delta} - n_1 \ln \hat{\varphi}_{1,2-\delta}}{2\delta} + \dfrac{(n_2 + \delta)\ln \hat{\varphi}_{2,n_2+\delta} - (n_2 - \delta)\ln \hat{\varphi}_{2,n_2-\delta}}{2\delta} \end{cases} \quad (E.66)$$

The consistency test is here proposed twice for the mixture carbon dioxide(1)-propane(2); the first test (Case A) is as presented in [1] and involves symmetric binary interaction parameters for *b*, *c*, and *d*, and asymmetric values for k_{ij} and k_{ji}; the second test (case B) involves asymmetric values for the four mixture parameters (randomly taken as the aim of this section is only to prove the consistency of the EoS with the cited mixing rules). The consistency test is here presented only with reference to the case of null values of *q* and *r* in eq. (E.1).

Table E.1 presents temperatures and pressures at the triple and critical points for the two compounds here considered.

Table E.1: Temperature and pressure at triple and critical point for carbon dioxide and propane.

Fluid	P_t / kPa	T_t / K	P_c / MPa	T_c / K
1	517.95	216.592	7.3773	304.1282
2	1.7×10^{-7}	85.53	4.2512	369.89

Pure compounds parameters in Table E.2 are different from those regressed for the Air Liquide Group. Fluid 1 and 2 refer to carbon dioxide and propane, respectively.

Table E.2: Parameters of the SLV EoS for carbon dioxide and propane.

Fluid	Z_c (10^{-1})	b_0 (10^{-1})	b_1 (10^{-1})	b_2	m	d (10^{-2})	c (10^{-2})	a_0 (10^{-2})	a_1	a_2	n
1	3.75038	3.266	-1.897	4.234	3.190	4.228	4.347	33.480	0.498	1.744	2.199
2	3.750008	3.327	-3.326	8.576	0.610	9.065	9.082	2.208	455.26	7.038	0.243

Table E.3 is a summary of the main thermodynamic properties evaluated from the EoS, eq. (E.1). The mixture carbon dioxide-propane has been considered at 100 K and 0.1 MPa, with 0.8 moles of carbon dioxide and 0.2 moles of propane. The total number of moles is then one.

The mole fractions has then been evaluated on these moles, and mixture parameter a_{mix} derives from eq. (E.44) whit k_{ij} and k_{ji} equal to 0.22 and 0.37, respectively. Symmetric values for m_{ij}, n_{ij}, and l_{ij} (0.15, 0.06, and 0.05, respectively) have been used in the mixing rules in the form of eq. (E.27).

The volume has been calculated by solving the 4th order polynomial in terms of volumes, as detailed in Appendix D, thus the residual Helmholtz energy has been computed from eq. (E.8).

Derivatives of the mixture parameters are from eq. (E.53) for a_{mix}, and from eqs. (E.41)-(E.43) for b_{mix}, c_{mix}, and d_{mix}. Finally, eq. (7) is used for the partial molar fugacity of carbon dioxide and propane.

Table E.3: Evaluation of the partial molar fugacity coefficients for the consistency test. Case A.
mij = mji = 0.15; nij = nji = 0.06; lij = lji = 0.05, kij =0.22, kji = 0.37.

Imposed values	T = 100 K, P = 1 MPa, $n_1 = 0.8$; $n_2 = 0.2$; $n_{tot} = 1$.				
Calculated values	Mole fractions		$x_1 = n_1/n_{tot} = 0.8$; $x_2 = n_2/n_{tot} = 0.2$		
	Mixture parameters	a_{mix} eq.(E.44)	b_{mix} eq. (E.27)	c_{mix} eq. (E.27)	d_{mix} eq. (E.27)
		0.533997376	0.03138241	0.051648687	0.050888516
	Volume	7.651663283			
	Compressibility factor eq. (E.20)				0.920282635
	Residual Helmholtz energy eq. (E.8)				-0.079726367
	Derivatives of mixture parameters[1]	$a_1' = 1.131766$	$b_1' = 0.077930$	$c_1' = 0.085665$	$d_1' = 0.086392$
		$a_2' = 0.384555$	$b_2' = 0.019746$	$c_2' = 0.043145$	$d_2' = 0.042013$
	Partial molar fugacity eq. (E.7)	$\ln\varphi_1 = -0.054357683$		$\ln\varphi_2 = -0.164415705$	

[1] – eq. (E.53) for *a*, eqs. (E.41)-(E.43) for *b*, *c*, and *d*.

Table E.4 shows values for almost the same properties within Table E.3 for variations in the number of moles of carbon dioxide and propane. The values of the numerical derivatives from eq. (E.66) are presented at the bottom of Table E.4.

The order of magnitude of the absolute average deviations for the logarithms of the fugacity coefficients from Table E.3 and Table E.4 is about 10^{-6} for both φ_1 and φ_2, thus consistency is verified according to eq. (E.64).

Table E.4: Evaluation of the numerical derivatives of fugacity coefficients. Case A.
mij = mji = 0.15; nij = nji = 0.06; lij = lji = 0.05, kij =0.22, kji = 0.37.

Imposed values		h = 0.000001, T = 100 K, P = 1 MPa			
Calculated values		Numerical derivative $[n_1\times\ln\varphi_1+ n_2\times\ln\varphi_2]/dn_1$		Numerical derivative $[n_1\times\ln\varphi_1+ n_2\times\ln\varphi_2]/dn_2$	
Number of moles		n_1+h; n_2	n_1-h; n_2	n_1; n_2+h	n_1; n_2-h
Mole fractions		$x_1 = (n_1+h)/n_{tot}$ $x_2 = n_2/n_{tot}$	$x_1 = (n_1-h)/n_{tot}$ $x_2 = n_2/n_{tot}$	$x_1 = n_1/n_{tot}$ $x_2 = (n_2+h)/n_{tot}$	$x_1 = n_1/n_{tot}$ $x_2 = (n_2-h)/n_{tot}$
Mixture parameters[1]	a_{mix}	0.533997227	0.533997526	0.533997974	0.533996779
	b_{mix}	0.031382398	0.031382422	0.031382457	0.031382364
	c_{mix}	0.051648679	0.051648696	0.051648721	0.051648653
	d_{mix}	0.050888507	0.050888525	0.050888551	0.05088848
Volume		7.651663484	7.651663083	7.651662482	7.651664085
Compressibility factor eq. (E.20)		0.920282659	0.920282611	0.920282539	0.920282732
Residual Helmholtz energy eq. (E.8)		-0.079726342	-0.079726391	-0.079726463	-0.07972627
Partial molar fugacity eq. (E.7)	$\ln\varphi_1$	-0.164415854	-0.164415556	-0.164415668	-0.164415742
	$\ln\varphi_2$	-0.054357646	-0.054357720	-0.054357692	-0.054357674
Numerical derivatives eq. (E.66)		$\ln\varphi_1$ = -0.054357682			
		$\ln\varphi_2$ = -0.164415700			

[1] – eq. (E.44) for *a*; *b*, *c*, and *d* in the form of eq. (E.25).

Table E.5 show the same values of Table E.3 in case B, namely mixing rules for the four mixture parameters with asymmetric binary interaction parameters. The values chosen are m_{ij} = 0.1 ; m_{ji} = 0.15; n_{ij} = 0.05; n_{ji} = 0.06; l_{ij} = 0.06; l_{ji} = 0.05, while k_{ij} and k_{ji} are as in the previous test.

In this second test, volumetric parameters are evaluated from the mixing rule in eq. (E.45), and the derivatives according to eqs. (E.61)-(E.63).

The partial molar fugacity coefficients are in the last row of Table E.5.

Table E.5: Evaluation of the partial molar fugacity coefficients for the consistency test. Case B.
mij = 0.1 ; mji = 0.15; nij = 0.05; nji = 0.06; lij = 0.06; lji = 0.05, kij =0.22, kji = 0.37.

Imposed values	T = 100 K, P = 1 MPa, n_1 = 0.8; n_2 = 0.2; n_{tot} = 1.				
Calculated values	Mole fractions	$x_1 = n_1/n_{tot}$ = 0.8; $x_2 = n_2/n_{tot}$ = 0.2			
	Mixture parameters	a_{mix} eq.(E.44)	b_{mix} eq. (E.45)	c_{mix} eq. (E.45)	d_{mix} eq. (E.45)
		0.533997376	0.032128262	0.051826504	0.050724917
	Volume	7.652968521			
	Compressibility factor eq. (E.20)				0.920439619
	Residual Helmholtz energy eq. (E.8)				-0.079570041
	Derivatives of mixture parameters[1]	a_1' = 0.384555	b_1'= 0.020065	c_1' = 0.043227	d_1' = 0.041924
		a_2' = 1.131766	b_2'= 0.080381	c_2' = 0.086223	d_2' = 0.085927
	Partial molar fugacity eq. (E.7)	$\ln\varphi_1$ = -0.054297239		$\ln\varphi_2$ = -0.163943773	

[1] – eq. (E.53) for *a*, eqs. (E.61)-(E.63) for *b*, *c*, and *d*.

Being similar to Table E.4, Table E.6 illustrates the values of the thermodynamic properties when the cited asymmetric binary interaction parameters are employed in the mixing rules.

It is possible to appreciate that the logarithms of the fugacity coefficients in Table E.5 and Table E.6 are identical to the 9th digit after decimal point.

Table E.6: Evaluation of the numerical derivatives of fugacity coefficients. Case B.
mij = 0.1 ; mji = 0.15; nij = 0.05; nji = 0.06; lij = 0.06; lji = 0.05, kij =0.22, kji = 0.37.

Imposed values		h = 0.000001, T = 100 K, P = 1 MPa			
Calculated values		Numerical derivative $[n_1\times\ln\varphi_1+ n_2\times\ln\varphi_2]/dn_1$		Numerical derivative $[n_1\times\ln\varphi_1+ n_2\times\ln\varphi_2]/dn_2$	
Number of moles		n_1+h; n_2	n_1-h; n_2	n_1; n_2+h	n_1; n_2-h
Mole fractions		$x_1 = (n_1+h)/n_{tot}$ $x_2 = n_2/n_{tot}$	$x_1 = (n_1-h)/n_{tot}$ $x_2 = n_2/n_{tot}$	$x_1 = n_1/n_{tot}$ $x_2 = (n_2+h)/n_{tot}$	$x_1 = n_1/n_{tot}$ $x_2 = (n_2-h)/n_{tot}$
Mixture parameters[1]	a_{mix}	0.533997227	0.533997526	0.533997974	0.533996779
	b_{mix}	0.03212825	0.032128274	0.03212831	0.032128213
	c_{mix}	0.051826496	0.051826513	0.051826539	0.05182647
	d_{mix}	0.050724908	0.050724925	0.050724952	0.050724881
Volume		7.652968721	7.652968322	7.652967723	7.652969312
Compressibility factor eq. (E.20)		0.920439643	0.920439595	0.920439523	0.920439715
Residual Helmholtz energy eq. (E.8)		-0.079570017	-0.079570065	-0.079570137	-0.079569945
Partial molar fugacity eq. (E.7)	$\ln\varphi_1$	-0.054297248	-0.054297229	-0.054297201	-0.054297277
	$\ln\varphi_2$	-0.163943735	-0.163943810	-0.163943924	-0.163943622
Numerical derivatives eq. (E.66)		$\ln\varphi_1$ = -0.054297239			
		$\ln\varphi_2$ = -0.163943773			

[1] – eq. (E.44) for *a*; *b*, *c*, and *d* in the form of eq. (E.45).

To sum up the information numerically presented in Table E.3-Table E.6, it is possible to state that the EoS in eq. (E.1) with mixing rules in eqs. (E.2)-(E.5) are thermodynamically consistent in both cases of symmetric and asymmetric binary interaction parameters.

2 Minimization of the Gibbs free energy of mixing

This section accounts for the algorithm applied for the minimization of the Gibbs free energy of mixing in a binary mixture. This algorithm has been realized in Fortran90, and makes use of some numerical recipes protected by copyright and published in [3].

The algorithm has been introduced in Chapter 4, while there it has been more deeply discussed from the thermodynamic point of view. The flow diagram in Figure E.2 and the nomenclature in Table E.7 ease the discussion. In Figure E.2, numbers in brackets are the steps number.

Table E.7: Main thermodynamic properties involved in the algorithm of minimization of the Gibbs free energy of mixing.

Symbol	Meaning
T , P	System temperature and pressure
P_{min} , P_{max}	Lower and upper pressure imposed for the flash calculation
ΔP	Pressure increase
i	i^{th} component
T_{ti} , P_{ti}	Pure component triple point temperature and pressure
T_{ci} , P_{ci}	Pure component critical point temperature and pressure
P_i^{SVE} / P_i^{SLE} / P_i^{VLE}	Pure component sublimation/melting/saturation pressures
α , β	Phases
φ	Fugacity coefficient
$\bar{z}$, $\bar{x}$	Vector of mole fractions
G^M	Gibbs free energy of mixing
G_L^M	Local minimum of G^M
G_G^M	Global minimum of G^M

First of all, the algorithm here presented involves solving the equilibrium condition at fixed temperature (T) while pressure is increased from a minimum (P_{min}) up to a maximum (P_{max}).

It is however possible to change the input values so that to perform the flash calculation at fixed pressure and varying the system temperature.

As detailed in Figure E.2, input values are T, P_{min}, P_{max}, the pressure increase ΔP, the number of steps P_{step}, and the vector of mole fractions $\bar{z}$ = {z_1,z_2}. Other values are entered as input values, as discussed later in this section.

The initial value of the system pressure P is set equal to P_{min}. The pressure increase ΔP is equal to $(P_{max}–P_{min})/P_{step}$.

For each pure component in the mixture, the first step in the algorithm entails the evaluation of the possible phases in which each component can be at T.

One among three cases is possible on the basis of the value of T, according to the pressure-temperature equilibrium behavior of each pure component, as shown in Figure E.1.

Without considering the cases of equilibrium, the i^{th} component can be in the solid or in the vapor phase for $T = T_1 < T_{ti}$, whit T_{ti} the pure component triple point temperature.

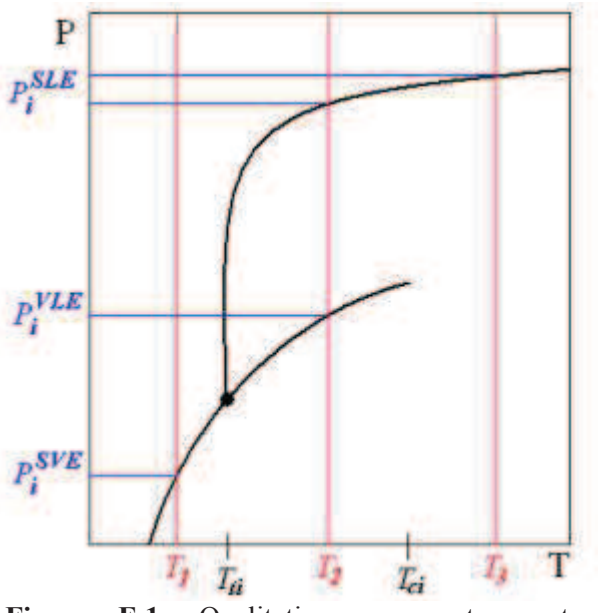

Figure E.1: Qualitative pressure-temperature equilibrium behavior of pure component i.
● : triple point; ■ : critical point; — :equilibrium curves; — : system temperature; equilibrium pressures: saturation (P_i^{VLE}), melting (P_i^{SLE}), sublimation (P_i^{SVE}).

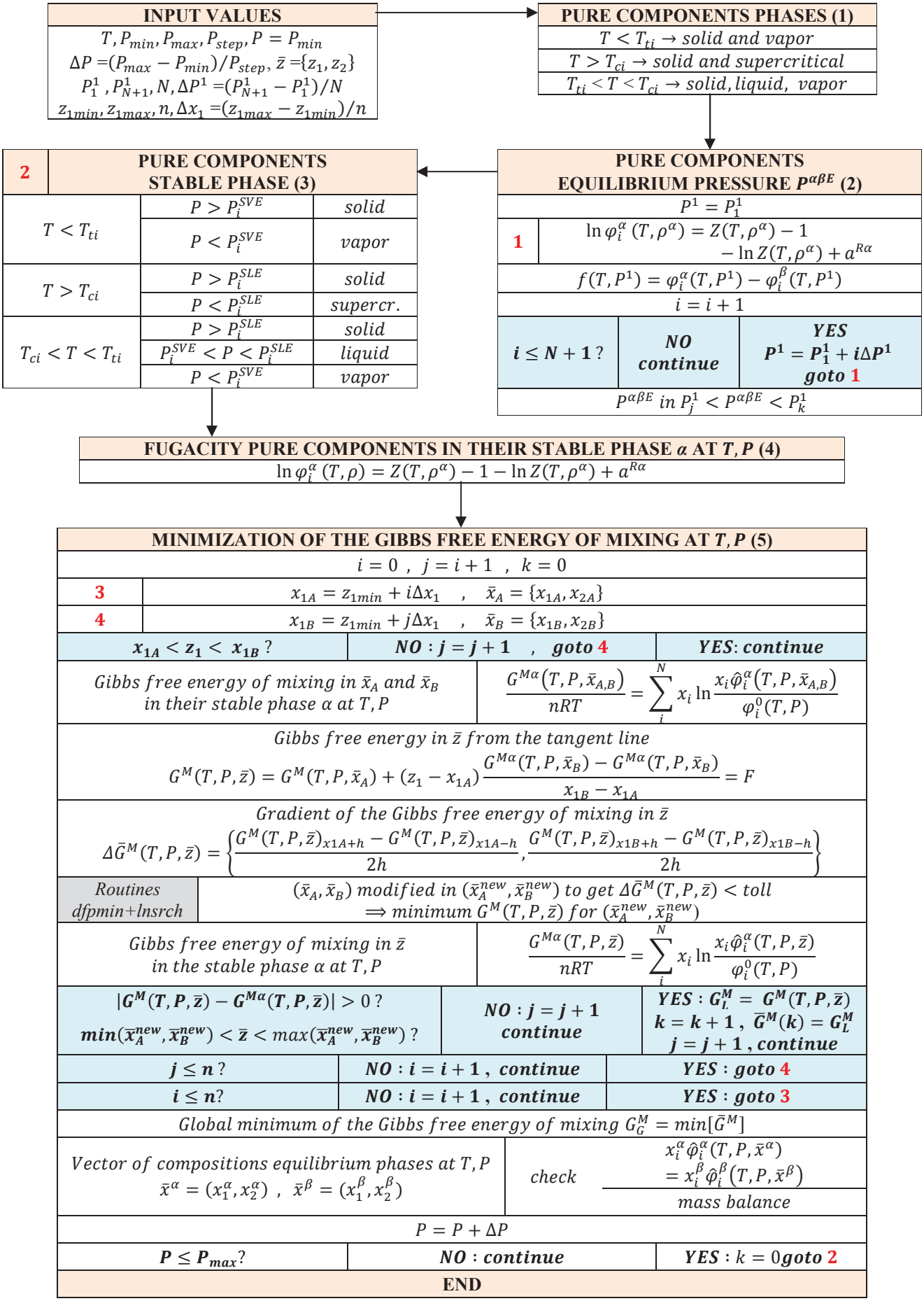

Figure E.2: Flow diagram of the algorithm for the minimization of the Gibbs free energy of mixing.

Again, it can be in the solid or in the supercritical phase for $T = T_3 > T_{ci}$, whit T_{ci} the pure component critical point temperature. Finally, it can be in the solid, liquid, or vapor phase for $T = T_2$, whit $T_{ti} < T_2 < T_{ci}$.

As a consequence, for the i^{th} component only the sublimation pressure (P_i^{SVE}) can be evaluated for $T = T_1 < T_{ti}$, only the melting pressure (P_i^{SLE}) for $T = T_3 > T_{ci}$, while both saturation (P_i^{VLE}) and melting (P_i^{SLE}) pressures are expected for $T = T_2$ and $T_{ti} < T_2 < T_{ci}$.

In any case, finding an equilibrium pressure involves solving the isofugacity condition, which represents the necessary condition for the equilibrium in a pure compound. This point is faced in the second step of the algorithm.

The isofugacity condition is solved between solid and vapor phases for $T = T_1$, solid and supercritical phases for $T = T_3$. Two isofugacity conditions are instead solved when $T = T_2$.

The condition for thermodynamic equilibrium between phases α and β for the component i is solved by imposing the function f in eq. (E.67).

$$f(T, P^1) = \varphi_i^{\alpha}(T, P^1) - \varphi_i^{\beta}(T, P^1) \qquad (E.67)$$

In eq. (E.67), φ_i is the fugacity coefficient of component i, and P^1 is a guess pressure.

The expression for φ_i^{α} in variables temperature and density from the SLV EoS with the van der Waals parameters q and r has been presented in Appendix D, and here re-proposed (analogous expression is valid for φ_i^{β}):

$$\ln \varphi_i^{\alpha}(T, \rho) = Z(T, \rho^{\alpha}) - 1 - \ln Z(T, \rho^{\alpha}) + \frac{1}{b-c}\left[d \ln\left|\frac{1 - b\rho^{\alpha}}{1 - c\rho^{\alpha}}\right| + c \ln|1 - c\rho^{\alpha}| - b \ln|1 - b\rho^{\alpha}|\right] - \frac{a\rho^{\alpha}}{RT} \qquad (E.68)$$

In eq. (E.68), a, b, c, and d are pure component values, while ρ^{α} is the density in the phase α, evaluated solving the SLV EoS at T and P^1.

The difference f between fugacity coefficients defined in eq. (E.67) is a linear function of P^1 and it is zero only if P^1 is the south-after equilibrium pressure between phases α and β at T, $P^{\alpha\beta E}$. The evaluation of the equilibrium pressure at imposed T requires then zeroing f.

f is evaluated for pressures varying between two boundary values. These limits are the pure component triple point pressure (P_{ti}) and critical pressure (P_{ci}) when P^1 is the saturation pressure. P_{ti} represents also the lowest and the highest limit when P^1 is the melting and the sublimation pressure, respectively. The highest pressure for the solid-liquid equilibrium and the lowest for the solid-vapor one have been fixed to 10^5 and 10^{-8} MPa, respectively.

Figure E.3 illustrates the qualitative trend for the function f in eq. (E.67) between a left (P_1^1) and a right (P_{N+1}^1) boundary of pressure. The values of P_1^1, P_{N+1}^1, and N are input values.

The routine *zbrac* from [3] divides the range P_1^1 - P_{N+1}^1 in N intervals, thus f is evaluated for each pressure P_i^1, whit $i = 1, \ldots, N+1$.

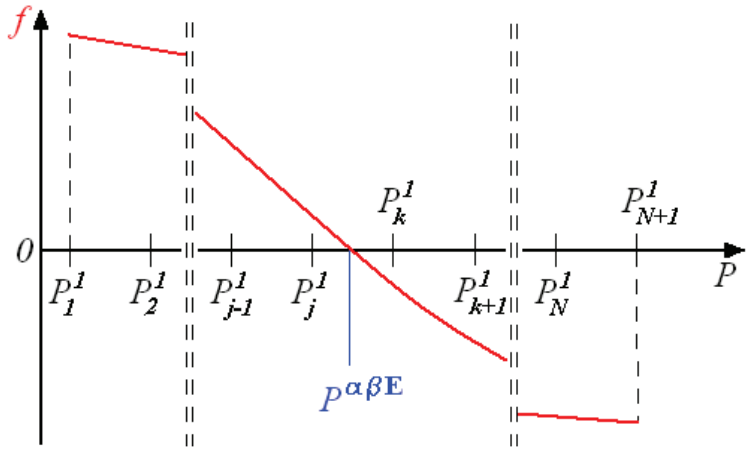

Figure E.3: Difference between fugacity coefficients of two phases of a pure component as a function of pressure.

In such a way, the routine geometrically expands the range P_1^1 - P_{N+1}^1 until the root which zeroes eq. (E.67) is bracketed by the returned values P_j^1 and P_k^1. At this point the equilibrium pressure $P^{\alpha\beta E}$ is known to lie between P_j^1 and P_k^1.

The routine *zbrent* from [3] successively allows evaluating $P^{\alpha\beta E}$, which is refined until a fixed accuracy. This second routine uses the Brent's method for finding the root of a generic function, and the discussion of this method is not treated here.

The second step gives then the equilibrium pressure(s) for both pure components at T. According to what stated above, the calculated pressure is P_i^{SVE} for $T < T_{ti}$, P_i^{SLE} for $T > T_{ci}$, while both P_i^{SLE} and P_i^{VLE} are evaluated for $T_{ti} < T < T_{ci}$.

The system pressure P is now considered in the 3rd and 4th steps for evaluating the stable phases for both components and their fugacity coefficients at T and P, respectively. The stable phases are determined comparing P and the equilibrium pressure(s) of the pure components calculated in the second step.

Table E.8 gives the criteria for determining the stable phase for the generic component i. When $T < T_{ti}$, component i is solid if $P > P_i^{SVE}$, conversely it is vapor. For $T > T_{ci}$, component i is solid if $P > P_i^{SLE}$, conversely it is liquid. If $T_{ti} < T < T_{ci}$, component i is solid if $P > P_i^{SLE}$, vapor if $P < P_i^{VLE}$, liquid if $P_i^{VLE} < P < P_i^{SLE}$.

Table E.8: Criteria for evaluating the stable phase of a pure component at fixed temperature.

System temperature	System pressure	Stable phase
$T < T_{ti}$	$P > P_i^{SVE}$	solid
	$P < P_i^{SVE}$	vapor
$T > T_{ci}$	$P > P_i^{SLE}$	solid
	$P < P_i^{SLE}$	liquid
$T_{ti} < T < T_{ci}$	$P > P_i^{SLE}$	solid
	$P_i^{VLE} < P < P_i^{SLE}$	liquid
	$P < P_i^{VLE}$	vapor

When the stable phase is determined, the 4th polynomial in the variable volume is solved to get the roots, as detailed in Appendix D, and the volume is chosen on the basis of the stable phase.

This volume allows evaluating the fugacity coefficient of component i at T and P in the stable phase from eq. (E.68), and this is the fourth step of the algorithm. This value is successively used for evaluating the Gibbs free energy of mixing, eq. (E.69).

The fugacity coefficients of the pure components are now known, and the last step is faced.

This step represents the core of the algorithm since it provides, if any, the global minimum of the Gibbs free energy of mixing G^M at T, P, and $\bar{x}$. As presented in section 1, G^M in a generic phase α is evaluated as:

$$\frac{G^{M\alpha}(T,P,\bar{x})}{nRT} = \sum_i^N x_i \ln \frac{x_i \hat{\varphi}_i^{\alpha}(T,P,\bar{x})}{\varphi_i^0(T,P)} \qquad (E.69)$$

In eq. (E.69), x_i, $\varphi_i{}^0$, and $\hat{\varphi}_i^{\alpha}$ are mole fraction, pure fugacity coefficient in the stable phase (from the first step), and partial molar fugacity coefficient of the i-th component, respectively. $\hat{\varphi}_i^{\alpha}$ is a function of composition, and its computation requires evaluating parameters a_{mix}, b_{mix}, c_{mix}, and d_{mix} from the mixing rules presented in section 1. $\hat{\varphi}_i^{\alpha}$ is evaluated from eq. (E.7).

Solving the equilibrium conditions in a binary mixture rests on finding the global minimum of G^M, called G_G^M, and a tangent line will join the compositions of the equilibrium phases. This point involves the routines *dfpmin* and *lnsrch* from [3].

G_G^M is sought by dividing the range of composition $z_{1min} < x_1 < z_{2max}$ in n intervals, and considering two vectors of composition.

The first vector is $\bar{x}_A$={x_{1A},x_{2A}}, the second one is $\bar{x}_B$={x_{1B},x_{2B}}. z_{1min}, z_{2max}, (usually set close to 0 and 1, respectively), and n are input values.

The mole fraction increase Δx_1 is equal to $(z_{1max} - z_{1min})/n$.

With reference to the n intervals, molar composition x_{1A} of component 1 in vector $\bar{x}_A$ is $x_{1A} = z_{1min} + i\Delta x_1$ with $i = 0,\ldots,n$. For each value of x_{1A} (then for an imposed $\bar{x}_A$), the molar composition x_{1B} of component 1 in vector $\bar{x}_B$ is $x_{1B} = z_{1min} + j\Delta x_1$ with $j = i+1,\ldots,n$. For component 2, the relations $x_{2A} = 1 - x_{1A}$ in $\bar{x}_A$ and $x_{2B} = 1 - x_{1B}$ in $\bar{x}_B$ hold. When $j = n$ for x_{1B}, then x_{1A} is incremented and x_{1B} cycled again from $j = i+1$.

Figure E.4 gives an idea about how x_{1B} is modified in the range $z_{1min} < x_1 < z_{2max}$ for a fixed x_{1A}. In Figure E.4, the number of intervals n is 8, $i = 2$ for x_{1A}, thus j=3,…,8 for x_{1B}.

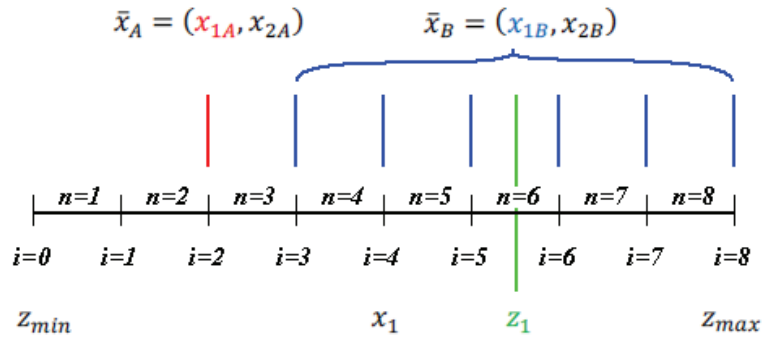

Figure E.4: Way of cycling the mole fraction of component 1 in the mixture.

If the mole fraction of component 1 defined in the input vector $\bar{z}$ satisfies the relation $x_{1A} < z_1 < x_{1B}$, the algorithm computes a local minimum of G^M for the couple ($\bar{x}_A$,$\bar{x}_B$), otherwise j is incremented until this condition is reached. According to Figure E.4, this happens only for the last three values of x_{1B}.

The algorithm makes use of routines *dfpmin* and *lnsrch* to find a local minimum of G^M, called G_L^M. This value is calculated as follows:

1. eq. (E.69) is used for evaluating $G^{M\alpha}(T,P,\bar{x}_A)$ and $G^{M\alpha}(T,P,\bar{x}_B)$, where α stands for the stable phase, not necessary the same for $\bar{x}_A$ and $\bar{x}_B$. For each vector of composition, the stable phase is evaluated comparing the values of eq. (E.69) for the solid, liquid, and vapor phases;
2. eq. (E.70) provides G^M at the input composition $\bar{z}$ placed on the line passing across points [x_{1A},$G^{M\alpha}(T,P,\bar{x}_A)$] and [$x_{1B}$,$G^{M\alpha}(T,P,\bar{x}_B)$]:

$$G^M(T,P,\bar{z}) = G^M(T,P,\bar{x}_A) + (z_1 - x_{1A})\frac{G^{M\alpha}(T,P,\bar{x}_B) - G^{M\alpha}(T,P,\bar{x}_A)}{x_{1B} - x_{1A}} = F \qquad (E.70)$$

3. the gradient of G^M (which is a bi-dimensional vector $\Delta\bar{G}^M$) in $\bar{z}$ is evaluated by means of eqs. (E.69)-(E.70) modifying one at a time the mole fraction x_{1A} and x_{1B} and computing the derivatives by finite differences:

$$\Delta\bar{G}^M(T,P,\bar{z}) = \left\{\frac{G^M(T,P,\bar{z})_{x1A+h} - G^M(T,P,\bar{z})_{x1A-h}}{2h}, \frac{G^M(T,P,\bar{z})_{x1B+h} - G^M(T,P,\bar{z})_{x1B-h}}{2h}\right\} \qquad (E.71)$$

4. the minimization of the function F in eq. (E.70) is performed in the routine *dfpmin*, which uses the Broyden-Fletcher-Goldfarb-Shanno variant of Davidon-Fletcher-Powell minimization, [3].

The function *F* is minimized knowing its value and gradient in a starting point. The starting point is the couple ($\bar{x}_A$,$\bar{x}_B$); its value there is $G^M(T,P,\bar{z})$ from eq. (E.70), and its gradient in same point ($\bar{x}_A$,$\bar{x}_B$) is $\Delta\bar{G}^M(T,P,\bar{z})$ from eq. (E.71).
This routine modifies the global compositions $\bar{x}_A$ and $\bar{x}_B$ till zeroing $\Delta\bar{G}^M(T,P,\bar{z})$ or reducing it under an imposed accuracy. *Dfpmin* makes use of a second routine (*lnsrch*) called to perform the minimization. *Lnsrch* finds new global compositions along the direction $-\Delta\bar{G}^M(T,P,\bar{z})$ from ($\bar{x}_A$,$\bar{x}_B$) where *F* has decreased.
When the gradient $\Delta\bar{G}^M(T,P,\bar{z})$ has been minimized, $G^M(T,P,\bar{z})$ is the lowest value in $\bar{z}$ for the new couple ($\bar{x}_A^{new}$,$\bar{x}_B^{new}$) as calculated from the line in eq. (E.70);

5. eq. (E.69) is used for evaluating $G^{M\alpha}(T,P,\bar{z}\,)$, namely the Gibbs free energy of mixing at *T*, *P*, and $\bar{z}$; α stands again for the stable phase. As for the Gibbs free energy of mixing in $\bar{x}_A$ and $\bar{x}_B$, $G^{M\alpha}(T,P,\bar{z})$ is the lowest among the values for the solid, liquid, and vapor phases;
6. the value $G^M(T,P,\bar{z})$ from point 4 is compared with $G^{M\alpha}(T,P,\bar{z})$ from point 5.
If $G^M(T,P,\bar{z})$>$G^{M\alpha}(T,P,\bar{z})$the system is stable in the phase α, conversely it can split in two equilibrium phases whose compositions are $\bar{x}_1^{new}$ and $\bar{x}_2^{new}$. This test if done computing:

$$\theta = G^M(T,P,\bar{z}) - G^{M\alpha}(T,P,\bar{z}) \qquad (E.72)$$

If $\theta < 0$ then the tangent line does not cross anyone of the G^M of the solid, liquid, and vapor phases. If $\bar{z}$ satisfies the relation min($\bar{x}_A^{new}$,$\bar{x}_B^{new}$) < $\bar{z}$ < max($\bar{x}_A^{new}$,$\bar{x}_B^{new}$), then $G^M(T,P,\bar{z})$ can be considered as a local minimum, G_L^M, and its value is recorded in the vector $\bar{G}^M$;

7. procedure 1-5 is computed for each couple ($\bar{x}_A$,$\bar{x}_B$), cycling x_{1A} and x_{1B} as detailed above. The global minimum G_G^M will correspond to the lowest value of the local minima G_L^M, then it is equal to the lowest value in the vector $\bar{G}^M$.
If no minima are encountered, the system is monophasic at system *T* and *P*. *P* is increased by ΔP to move to a higher pressure. To the contrary, G_G^M lies on a tangent line together with the two equilibrium phases of vectors of compositions $\bar{x}^\alpha = \{x_1^\alpha, x_2^\alpha\}$, $\bar{x}^\beta = \{x_1^\beta, x_2^\beta\}$;
8. if a minima exists, the procedure at *T* and *P* ends verifying the isofugacity conditions for the equilibrium phases α and β:

$$x_1^\alpha \hat{\varphi}_1^\alpha(T,P,\bar{x}^\alpha) = x_1^\beta \hat{\varphi}_1^\beta\left(T,P,\bar{x}^\beta\right) \qquad (E.73)$$
$$x_2^\alpha \hat{\varphi}_2^\alpha(T,P,\bar{x}^\alpha) = x_2^\beta \hat{\varphi}_2^\beta\left(T,P,\bar{x}^\beta\right) \qquad (E.74)$$

and before modifying *P* by ΔP the mass balance is verified to be unitary in order to check the consistency of the calculation:

$$|x_{max}\Phi_{max} + x_{min}(1-\Phi_{max})| + |(1-x_{max})\Phi_{max} + (1-x_{min})(1-\Phi_{max})| \qquad (E.75)$$

where:

$$x_{max} = max\left(x_1^\alpha, x_1^\beta\right) \qquad x_{min} = min\left(x_1^\alpha, x_1^\beta\right) \qquad \Phi_{max} = \frac{z_1 - x_{min}}{x_{max} - x_{min}} \qquad (E.76)$$

After these two controls, P is incremented by ΔP, and the algorithm restarts from the evaluation of the fugacity coefficients of the pure components at T and the new P (third step). If the value P_{max} is achieved, the isothermal calculation ends.

The algorithm here presented performs a flash calculation since it involves solving the equilibrium condition at imposed temperature and pressure. Nevertheless, few modifications are needed for allowing bubble pressure, bubble temperature, dew pressure, and dew temperature calculations, seeing that a cycle can be easily added for modifying the input value of temperature or pressure till matching the wanted composition in a phase.

3 The functional form of the LJ-SLV EoS

The SLV EoS has been applied for the representation of phase equilibria in binary mixtures of Lennard-Jones fluids. The SLV used is in the form:

$$P(T,v) = \frac{RT}{v-\mathrm{b}}\frac{v-\mathrm{d}}{v-\mathrm{c}} - \frac{a}{v^2} \qquad (E.77)$$

In eqs. (E.78)-(E81) the functional form in eq. (E.77) is modified in order to introduce the LJ parameters, namely the collision diameter σ and the well-depth potential ε. For the gas constant R, the relation $R = N_A k_B$ holds. Na and kB are Avogadro number, and the Boltzmann's constant.

$$\frac{\sigma^3 P}{\varepsilon} = \frac{\sigma^3}{\varepsilon}\frac{RT}{v-b}\frac{v-d}{v-c} - \frac{a}{v^2}\frac{\sigma^3}{\varepsilon} \qquad (E.78)$$

$$\frac{\sigma^3 P}{\varepsilon} = \frac{\sigma^3 T}{\varepsilon}\frac{N_A k_B}{v-b}\frac{v-d}{v-c} - \frac{a}{v^2}\frac{\sigma^3}{\varepsilon} \qquad (E.79)$$

$$\frac{\sigma^3 P}{\varepsilon} = \frac{\sigma^3 T}{\varepsilon}\frac{1}{(v/N_A k_B - b/N_A k_B)}\frac{N_A k_B}{N_A k_B}\frac{v-d}{v-c} - \frac{N_A\sigma^3}{N_A\sigma^3}\frac{N_A\sigma^3}{N_A\sigma^3}\frac{a}{v^2}\frac{\sigma^3}{\varepsilon} \qquad (E.80)$$

$$\frac{\sigma^3 P}{\varepsilon} = \frac{\sigma^3 T}{\varepsilon}\frac{1}{(v/N_A k_B - b/N_A k_B)}\frac{(v/N_A k_B - d/N_A k_B)}{(v/N_A k_B - c/N_A k_B)} - \frac{1}{v/N_A\sigma^3}\frac{1}{v/N_A\sigma^3}\frac{a\sigma^3}{N_A^2\sigma^6\varepsilon} \qquad (E.81)$$

$$\frac{N_A\sigma^3 P}{\varepsilon} = \frac{N_A\sigma^3 T}{\varepsilon}\frac{1}{(v/N_A k_B - b/N_A k_B)}\frac{(v/N_A k_B - d/N_A k_B)}{(v/N_A k_B - c/N_A k_B)} - \frac{1}{v/N_A\sigma^3}\frac{1}{v/N_A\sigma^3}\frac{a\sigma^3}{N_A\sigma^6\varepsilon} \qquad (E.82)$$

The following identities can be introduced in eq. (E.82):

$$P^* = \frac{PN_A\sigma^3}{\varepsilon} \qquad T^* = \frac{TN_A k_B}{\varepsilon} \qquad z^* = \frac{z}{N_A\sigma^3},\ z = v,b,c,d \qquad a^* = \frac{a}{N_A\sigma^3\varepsilon} \qquad (E.83)$$

yielding:

$$P^* = \frac{T^*}{v^*-b^*}\frac{v^*-d^*}{v^*-c^*} - \frac{a^*}{v^{*2}} \qquad (E.84)$$

Eq. (E.84) is the Lennard-Jones Solid-Liquid-Vapor Equation of State (LJ-SLV EoS) which can easily be obtained from the SLV EoS, eq. (E.77) substituting the expressions for the reduced variables, eq. (E.83), and considering the gas constant $R = N_A k_B$.

Bibliography

[1] P. Stringari, M. Campestrini, C. Coquelet and P. Arpentinier, "An equation of state for solid–liquid–vapor equilibrium applied to gas processing and natural gas liquefaction," *Fluid Phase Equilibr.,* vol. 326, pp. 258-267, 2014.

[2] T. de Loos, J. O'Connell and C. McCabe, "Concerning inconsistent equation of state formulations," *Fluid Phase Equilibr.,* vol. 342, p. iii, 2013.

[3] W. H. Press, S. A. Teukolsky, W. T. Vetterling and B. F. Flannery, Numerical recipes in Fortran90. The art of parallel scientific computing, 2 ed., vol. II, New York: Press Syndicate of University of Cambridge, 1986, p. 572.

Appendix F

REPRESENTATION OF PHASE EQUILIBRIA II. BINARY MIXTURES

LIST OF FIGURES F3

LIST OF TABLES F6

1.1 N_2+O_2 ..... *F8*
1.2 N_2+Ar *F12*
1.3 N_2+Kr *F16*
1.4 N_2+Xe *F19*
1.5 N_2+Ne *F21*
1.6 N_2+He *F23*
1.7 N_2+CO_2 ..... *F27*
1.8 N_2+H_2 ..... *F31*
1.9 N_2+N_2O *F34*
1.10 N_2+CH_4 ..... *F37*
1.11 $N_2+C_2H_6$ *F42*
1.12 $N_2+C_2H_4$ *F46*
1.13 $N_2+C_3H_8$ *F49*
1.14 $N_2+C_3H_6$ *F53*
1.15 O_2+Ar *F55*
1.16 O_2+Kr *F58*
1.17 O_2+Xe *F60*
1.18 O_2+Ne *F62*
1.19 O_2+He *F64*
1.20 O_2+CO_2 ..... *F66*
1.21 O_2+H_2 ..... *F69*
1.22 O_2+N_2O *F71*
1.23 O_2+CH_4 ..... *F73*
1.24 $O_2+C_2H_6$ *F75*
1.25 $O_2+C_2H_4$ *F78*
1.26 $O_2+C_3H_8$ *F80*
1.27 $O_2+C_3H_6$ *F82*
1.28 $Ar+Kr$ *F84*
1.29 $Ar+Xe$ *F86*
1.30 $Ar+Ne$ *F87*
1.31 $Ar+He$ *F89*
1.32 $Ar+CO_2$ *F91*
1.33 $Ar+H_2$ *F92*
1.34 $Ar+CH_4$ *F94*
1.35 $Ar+C_2H_6$ *F96*
1.36 $Ar+C_3H_6$ *F97*
1.37 $Kr+Xe$ *F98*
1.38 $Kr+CO_2$ *F100*
1.39 $Kr+CH_4$ *F102*
1.40 $Kr+C_2H_6$ *F104*
1.41 $Kr+C_2H_4$ *F105*
1.42 $Kr+C_3H_6$ *F107*
1.43 $Xe+Ne$ *F108*
1.44 $Xe+CO_2$ *F109*
1.45 $Xe+N_2O$ *F111*

1.46 $Xe+CH_4$ F113
1.47 $Xe+C_2H_6$ F114
1.48 $Xe+C_2H_4$ F115
1.49 $Xe+C_3H_8$ F117
1.50 $Xe+C_3H_6$ F118
1.51 Ne+He F119
1.52 $Ne+H_2$ F120
1.53 $He+H_2$ F122

BIBLIOGRAPHY F124

List of Figures

Figure F.1: Available experimental values for the system N_2+O_2. F8
Figure F.2: SLE for the system N_2+O_2. F8
Figure F.3: VLE for the system N_2+O_2 at 0.1 MPa and 0.5 MPa. F9
Figure F.4: VLE for the system N_2+O_2 at 75 K, 85 K, 100 K, and 125 K. F9
Figure F.5: Available experimental values for the system N_2+Ar. F12
Figure F.6: SLE for the system N_2+Ar. F12
Figure F.7: VLE for the system N_2+Ar at 0.2 MPa, 0.4 MPa, and 0.6 MPa. F13
Figure F.8: VLE for the system N_2+Ar at 95 K, 103 K, 115 K, and 121 K. F13
Figure F.9: Available experimental values for the system N_2+Kr. F16
Figure F.10: SLE for the system N_2+Ar. F16
Figure F.11: PT equilibrium projection for the system N_2+Ar in the range 40 K – 120 K. F17
Figure F.12: VLE for the system N_2+Kr at 110 K, 115 K, and 120 K. F17
Figure F.13: Available experimental values for the system N_2+Xe. F19
Figure F.14: SLE for the system N_2+Xe. F19
Figure F.15: PT equilibrium projection for the system N_2+Xe in the range 40 K – 180 K. F20
Figure F.16: Available experimental values for the system N_2+Ne. F21
Figure F.17: VLE for the system N_2+Ne from 66 K up to 114 K. F21
Figure F.18: Available experimental values for the system N_2+He. F23
Figure F.19: SVE for the system N_2+He. F23
Figure F.20: PT equilibrium projection for the system N_2+He in the range 40 K – 120 K. F24
Figure F.21: VLE for the system N_2+He at 77 K, 90 K, and 100 K. F24
Figure F.22: Available experimental values for the system N_2+CO_2. F27
Figure F.23: SVE and SLE for the system N_2+CO_2. F27
Figure F.24: VLE for the system N_2+CO_2 at 220 K, 232 K, and 240 K. F28
Figure F.25: Available experimental values for the system N_2+H_2. F31
Figure F.26: SVE for the system N_2+H_2. F31
Figure F.27: VLE for the system N_2+H_2 at 90 K, 95 K, and 100 K. F32
Figure F.28: Available experimental values for the system N_2+N_2O. F34
Figure F.29: SVE and SLE for the system N_2+N_2O. F34
Figure F.30: VLE for the system N_2+N_2O at 213 K, 233 K, and 253 K. F35
Figure F.31: Available experimental values for the system N_2+CH_4. F37
Figure F.32: SLE for the system N_2+CH_4. F37
Figure F.33: VLE for the system N_2+CH_4 at 91 K, 100 K, and 114 K. F38
Figure F.34: Available experimental values for the system N_2+C_2H_6. F42
Figure F.35: SLE for the system N_2+C_2H_6. F42
Figure F.36: VLE for the system N_2+C_2H_6 at 91 K, 100 K, and 114 K. F43
Figure F.37: Available experimental values for the system N_2+C_2H_4. F46
Figure F.38: SLE for the system N_2+C_2H_4. F46
Figure F.39: VLE for the system N_2+C_2H_6 at 91 K, 100 K, and 114 K. F47
Figure F.40: Available experimental values for the system N_2+C_3H_8. F49
Figure F.41: SLE for the system N_2+C_3H_8. F49
Figure F.42: VLLE for the system N_2+C_3H_8. F50
Figure F.43: Available experimental values for the system N_2+C_3H_6. F53
Figure F.44: SLE for the system N_2+C_3H_6. F53
Figure F.45: VLE for the system N_2+C_3H_6 at 195 K, 218 K, and 290 K F54
Figure F.46: Available experimental values for the system O_2+Ar. F55
Figure F.47: SLE for the system O_2+Ar. F55
Figure F.48: VLE for the system O_2+Ar at 90 K, and 100 K F56
Figure F.49: Available experimental values for the system O_2+Kr. F58
Figure F.50: SLE for the system O_2+Kr. F58
Figure F.51: VLE for the system O_2+Kr at 96 K, 98 K, and 100 K F59
Figure F.52: Available experimental values for the system O_2+Xe. F60
Figure F.53: SLE for the system O_2+Xe. F60

Figure F.54: Available experimental values for the system O_2+Ne. F62
Figure F.55: VLE for the system O_2+Ne from 78 K up to 130 K. F62
Figure F.56: Available experimental values for the system O_2+He. F64
Figure F.57: VLE for the system O_2+He at 91 K, 103 K, and 116 K. F64
Figure F.58: Available experimental values for the system O_2+CO_2. ..... F66
Figure F.59: SLE for the system O_2+CO_2. ..... F66
Figure F.60: VLE for the system O_2+CO_2 at 218 K, 243 K, and 263 K. F67
Figure F.61: Available experimental values for the system O_2+H_2. ..... F69
Figure F.62: SLE for the system O_2+H_2. ..... F69
Figure F.63: Available experimental values for the system O_2+N_2O. F71
Figure F.64: SLE for the system O_2+N_2O. F71
Figure F.65: VLE for the system O_2+N_2O at 213 K, 233 K, and 253 K. F72
Figure F.66: Available experimental values for the system O_2+CH_4. ..... F73
Figure F.67: SLE for the system O_2+CH_4. ..... F73
Figure F.68: Available experimental values for the system O_2+C_2H_6. ..... F75
Figure F.69: SLE for the system O_2+C_2H_6. ..... F75
Figure F.70: VLE for the system O_2+C_3H_6 at 112 K, 120 K, and 129 K F76
Figure F.71: Available experimental values for the system O_2+C_2H_4. ..... F78
Figure F.72: SLE for the system O_2+C_2H_4. ..... F78
Figure F.73: VLE for the system O_2+C_2H_4 at 110 K, and 140 K F79
Figure F.74: Available experimental values for the system O_2+C_3H_8. ..... F80
Figure F.75: SLE for the system O_2+C_3H_8. ..... F80
Figure F.76: VLE for the system N_2+C_3H_6 at 195 K, 218 K, and 290 K F81
Figure F.77: Available experimental values for the system O_2+C_3H_6. ..... F82
Figure F.78: SLE for the system O_2+C_3H_6. ..... F82
Figure F.79: Available experimental values for the system Ar+Kr. F84
Figure F.80: Available experimental values for the system Ar+Xe. F86
Figure F.81: Available experimental values for the system Ar+Ne. F87
Figure F.82: Available experimental values for the system Ar+He. F89
Figure F.83: Available experimental values for the system Ar+CO_2. ..... F91
Figure F.84: Available experimental values for the system Ar+H_2. ..... F92
Figure F.85: Available experimental values for the system Ar+CH_4. ..... F94
Figure F.86: Available experimental values for the system Ar+C_2H_6. ..... F96
Figure F.87: Available experimental values for the system Ar+C_3H_6. ..... F97
Figure F.88: Available experimental values for the system Kr+Xe. F98
Figure F.89: Available experimental values for the system Kr+CO_2. ..... F100
Figure F.90: Experimental critical point and critical line from the SLV EoS for the system Kr+CO_2. ..... F100
Figure F.91: Available experimental values for the system Kr+CH_4. ..... F102
Figure F.92: SLE for the system Kr+CH_4. ..... F102
Figure F.93: Available experimental values for the system Kr+C_2H_6. ..... F104
Figure F.94: Available experimental values for the system Kr+C_2H_4. ..... F105
Figure F.95: VLE for the system Kr+C_2H_4 at 116 K. F105
Figure F.96: Available experimental values for the system Kr+C_3H_6. ..... F107
Figure F.97: Available experimental values for the system Xe+Ne. F108
Figure F.98: Available experimental values for the system Xe+CO_2. ..... F109
Figure F.99: Experimental critical point data and calculated critical line for the system Xe+CO_2. ..... F109
Figure F.100: Available experimental values for the system Xe+N_2O. F111
Figure F.101: VLE for the system Xe+N_2O at 182 K. F111
Figure F.102: Available experimental values for the system Xe+CH_4. ..... F113
Figure F.103: Available experimental values for the system Xe+C_2H_6. ..... F114
Figure F.104: Available experimental values for the system Xe+C_2H_4. ..... F115
Figure F.105: VLE for the system Xe+C_2H_4 at 161 K. F115
Figure F.106: Available experimental values for the system Xe+C_3H_8. ..... F117
Figure F.107: Available experimental values for the system Xe+C_3H_6. ..... F118
Figure F.108: Available experimental values for the system Ne+He. F119
Figure F.109: Available experimental values for the system Ne+H_2. ..... F120

Figure F.110: VLE for the system Ne+H_2 at 26 K. F120
Figure F.111: Available experimental values for the system He+H_2. ..... F122

List of Tables

Table F.1: Quantitative comparison of equilibrium compositions for the system N_2+O_2. ..... F10
Table F.2: Quantitative comparison of equilibrium compositions for the system N_2+Ar. F14
Table F.3: Quantitative comparison of equilibrium compositions for the system N_2+Kr. F18
Table F.4: Quantitative comparison of equilibrium compositions for the system N_2+Xe..... F20
Table F.5: Quantitative comparison of equilibrium compositions for the system N_2+Ne..... F22
Table F.6: Quantitative comparison of equilibrium compositions for the system N_2+He..... F25
Table F.7: Quantitative comparison of equilibrium compositions for the system N_2+CO_2. ..... F28
Table F.8: Quantitative comparison of equilibrium compositions for the system N_2+H_2. ..... F32
Table F.9: Quantitative comparison of equilibrium compositions for the system N_2+N_2O. F35
Table F.10: Quantitative comparison of equilibrium compositions for the system N_2+CH_4. ..... F38
Table F.11: Quantitative comparison of equilibrium compositions for the system N_2+C_2H_6. ..... F43
Table F.12: Quantitative comparison of equilibrium compositions for the system N_2+C_2H_4. ..... F47
Table F.13: Quantitative comparison of equilibrium compositions for the system N_2+C_3H_8. ..... F50
Table F.14: Quantitative comparison of equilibrium compositions for the system N_2+C_3H_6. ..... F54
Table F.15: Quantitative comparison of equilibrium compositions for the system O_2+Ar. F56
Table F.16: Quantitative comparison of equilibrium compositions for the system O_2+Kr. F59
Table F.17: Quantitative comparison of equilibrium compositions for the system O_2+Xe..... F61
Table F.18: Quantitative comparison of equilibrium compositions for the system O_2+Ne..... F63
Table F.19: Quantitative comparison of equilibrium compositions for the system O_2+He..... F65
Table F.20: Quantitative comparison of equilibrium compositions for the system O_2+CO_2. ..... F67
Table F.21: Quantitative comparison of equilibrium compositions for the system O_2+H_2. ..... F70
Table F.22: Quantitative comparison of equilibrium compositions for the system O_2+N_2O. F72
Table F.23: Quantitative comparison of equilibrium compositions for the system O_2+CH_4. ..... F74
Table F.24: Quantitative comparison of equilibrium compositions for the system O_2+C_2H_6. ..... F77
Table F.25: Quantitative comparison of equilibrium compositions for the system O_2+C_2H_4. ..... F79
Table F.26: Quantitative comparison of equilibrium compositions for the system O_2+C_3H_8. ..... F81
Table F.27: Quantitative comparison of equilibrium compositions for the system O_2+C_3H_6. ..... F83
Table F.28: Quantitative comparison of equilibrium compositions for the system Ar+Kr. F84
Table F.29: Quantitative comparison of equilibrium compositions for the system Ar+Xe. F86
Table F.30: Quantitative comparison of equilibrium compositions for the system Ar+Ne. F87
Table F.31: Quantitative comparison of equilibrium compositions for the system Ar+He. F89
Table F.32: Quantitative comparison of equilibrium compositions for the system Ar+CO_2. ..... F91
Table F.33: Quantitative comparison of equilibrium compositions for the system Ar+H_2. ..... F92
Table F.34: Quantitative comparison of equilibrium compositions for the system Ar+CH_4. ..... F94
Table F.35: Quantitative comparison of equilibrium compositions for the system Ar+C_2H_6. ..... F96
Table F.36: Quantitative comparison of equilibrium compositions for the system Ar+C_3H_6. ..... F97
Table F.37: Quantitative comparison of equilibrium compositions for the system Kr+Xe. F98
Table F.38: Quantitative comparison of equilibrium compositions for the system Kr+CO_2. ..... F101
Table F.39: Quantitative comparison of equilibrium compositions for the system Kr+CH_4. ..... F103
Table F.40: Quantitative comparison of equilibrium compositions for the system Kr+C_2H_6. ..... F104
Table F.41: Quantitative comparison of equilibrium compositions for the system Kr+C_2H_4. ..... F106
Table F.42: Quantitative comparison of equilibrium compositions for the system Kr+C_3H_6. ..... F107
Table F.43: Quantitative comparison of equilibrium compositions for the system Xe+Ne. F108
Table F.44: Quantitative comparison of equilibrium compositions for the system Xe+CO_2. ..... F110
Table F.45: Quantitative comparison of equilibrium compositions for the system Xe+N_2O..... F112
Table F.46: Quantitative comparison of equilibrium compositions for the system Xe+CH_4. ..... F113
Table F.47: Quantitative comparison of equilibrium compositions for the system Xe+C_2H_6..... F114
Table F.48: Quantitative comparison of equilibrium compositions for the system Xe+C_2H_4..... F116
Table F.49: Quantitative comparison of equilibrium compositions for the system Xe+C_3H_8..... F117
Table F.50: Quantitative comparison of equilibrium compositions for the system Xe+C_3H_6..... F118
Table F.51: Quantitative comparison of equilibrium compositions for the system Ne+He. F119
Table F.52: Quantitative comparison of equilibrium compositions for the system Ne+H_2..... F121
Table F.53: Quantitative comparison of equilibrium compositions for the system He+H_2..... F122

This Appendix presents the quantitative comparison for all the binary mixtures of interest in this work. Sections 1.1-1.37, 1.43, and 1.51 present the comparison between data and values calculated from the model with regressed Binary Interaction Parameters (BIPs). In the remaining sections null BIPs have been considered in the SLV EoS.

Each section starts with the Pressure-Temperature Equilibrium Projection (PT-EP) for the correspondent mixture. The PT-EP shows (usually up to 100 MPa) the pure components and the available experimental values. Equilibrium values for the pure components are from [1], except He whose melting line is the one calculated from the SLV EoS. If the sublimation line is missing it is because for the component, like hydrocarbons C_nH_m, auxiliary values are not available in [1].

The following symbols have been used in the PT-EPs for representing the different equilibria:

- ● : Fluid-Fluid Equilibrium (FFE);
- × : Solid-Fluid Equilibrium (SFE): Solid-Liquid (SLE) or Solid-Vapor (SVE) Equilibrium;
- ♦ : Critical Point (CP);
- ▲ : Solid-Vapor-Liquid Equilibrium (SLVE) and Vapor-Liquid-Liquid Equilibrium (VLLE);
- ■ : Solid-Solid-Liquid Equilibrium (SSLE).

An arbitrary value of 1 MPa has been chosen for representing the SLE in the PT-EP when experimental pressures are not available. When the literature CP data are expressed only in terms of temperature and mole fraction, the critical pressures have been evaluated as weighted average according to x and the critical pressures of the pure components from [1].

Qualitative comparisons between experimental and calculated values are reported for all the mixtures of N_2 and O_2 by means of some pressure-composition and temperature-composition cross sections. In few cases, the calculated PT-EP has also been presented. Qualitative comparisons have also been reported for a selected number of mixtures where the SLV has been applied with null BIPs.

Each section ends with a table portraying the quantitative comparison between data and model. For each source, the correspondent ranges of temperatures, pressures, and compositions have been introduced in the table. The type of data has been also specified, together with the properties involved: pressure P, temperature T, mole fractions x and y. For instance “VLE PTxy” data is used for VLE data expressed in terms of P, T, and mole fractions in the liquid (x) and vapor (y) phase. For SLE data, x has been considered as the composition in both the liquid and solid phases.

It is worth mentioning that, according to the tables presented in Appendix A, the compositions are referred to the more volatile component. Experimental values of temperature and composition have been rounded: no decimals digit have been considered for temperatures, while 0 and 1 have been used for compositions <0.01 and >0.99, respectively.

The quantitative comparison has been done with reference to AAD%, Bias%, and MAD%, evaluating equilibrium compositions at experimental temperature and pressure. As a consequence, deviations within the tables do not involves experimental values related to pure components (x=0,1). Furthermore, errors have been evaluated in terms of the first component mentioned in the section, which sometimes does not correspond to the more volatile one. For instance, section 1.15 is related to the system O_2+Ar, statistical errors are in terms of O_2 whereas the more volatile component is Ar.

With reference to CP PTx and SLE PTx data, the first and second columns in the section “FLASH” within each table give the comparison in terms of composition between data and values calculated by the SLV EoS at imposed temperature and pressure, respectively. For the SLE PTx data, values from the SLV EoS have been calculated along the triple lines.

For the mixtures N2+H2, O2+H2, and Ne+He, errors related to SVE PTy data at infinite dilution ($y<10^{-3}$) are expressed in terms of AAD, Bias, and MAD instead of AAD%, Bias%, and MAD%.

With reference to SVLE PT data, the first and the second columns in the section “FLASH” within each table give the comparison between data and values calculated by the SLV EoS in terms of temperature and pressure, respectively.

1.1 N_2+O_2

The literature data for the system N_2+O_2 are shown in Figure F.1.

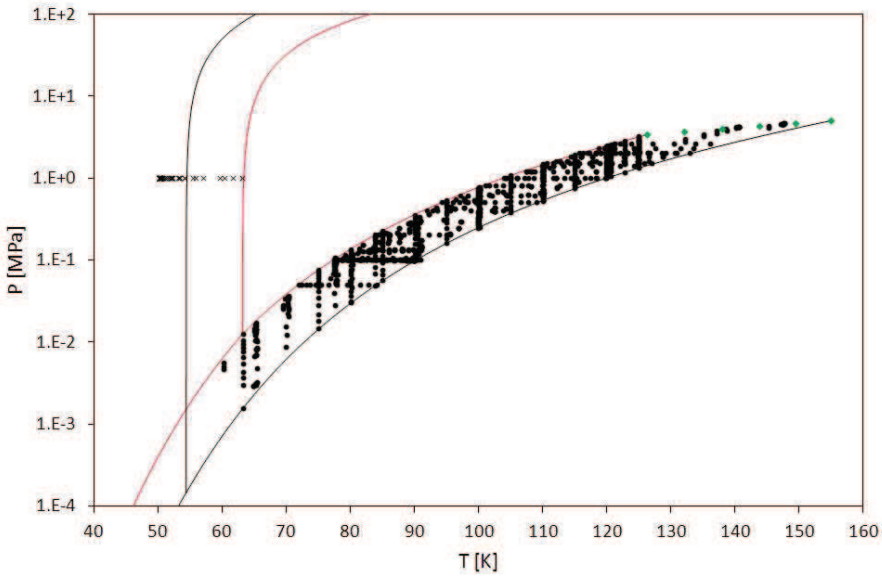

Figure F.1: Available experimental values for the system N_2+O_2.
— : N_2; — : O_2; ● : FFE data; × : SFE data; ♦ : CP data.

The qualitative comparison between model and SLE data is portrayed in Figure F.2. According to [RUH1935], the eutectic temperature is 50.1 K, while compositions of the $solid_2$, liquid, and $solid_1$ phases are 0.16, 0.226, and 0.31 in N_2 mole fraction, respectively. Calculated compositions are 0.156, 0.239, and 0.306. The eutectic temperature from the SLV EoS is 51.05 K.

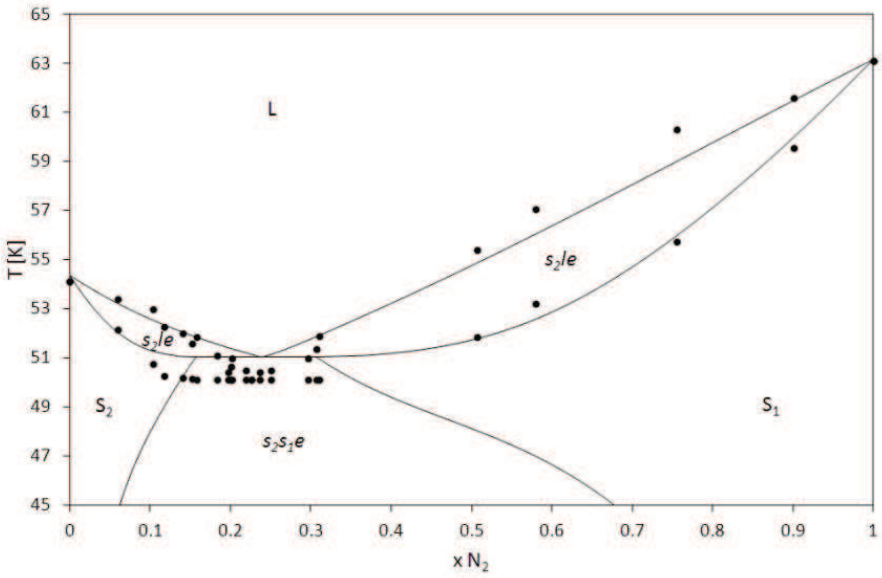

Figure F.2: SLE for the system N_2+O_2.
● : [RUH1935]; — : SLV EoS.

The temperature-composition cross sections at 0.1 MPa and 0.5 MPa are illustrated in Figure F.3, while Figure F.4 represents the qualitative comparison between VLE data and model via the pressure-composition cross sections from 75 K up to 125 K.

Table F.1 gives the quantitative comparison between data and values calculated from the SLV EoS in terms of equilibrium mole fractions of N_2.

The AAD% for both compositions in the liquid (x) and in the vapor (y) phases is lower than 10% for all the references, except for the data presented in [BAL1900], [DUN1966], [KRI1936], [KUE1922], and [THO1963].

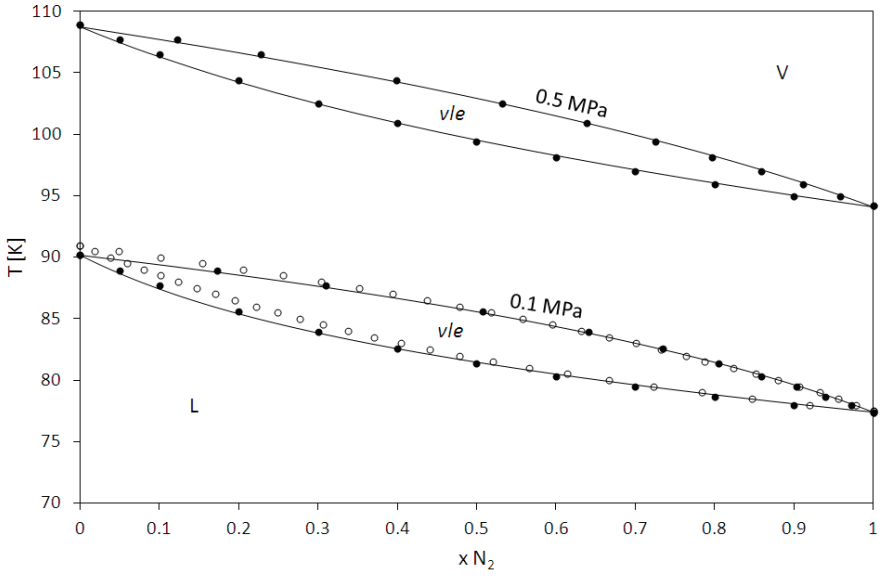

Figure F.3: VLE for the system N_2+O_2 at 0.1 MPa and 0.5 MPa.
● : [DOD1927b]; ○ : [BAL1900]; — : SLV EoS.

The VLE experimental values at 0.1 MPa from [BAL1900] are illustrated in Figure F.3. At this pressure, the model agrees more with the series of data from [DOD1927b] than the values from [BAL1900]. A good agreement between calculated values and data from [DOD1927b] is encountered up to 3.2 MPa, and the case for 0.5 MPa is portrayed in Figure F.3.

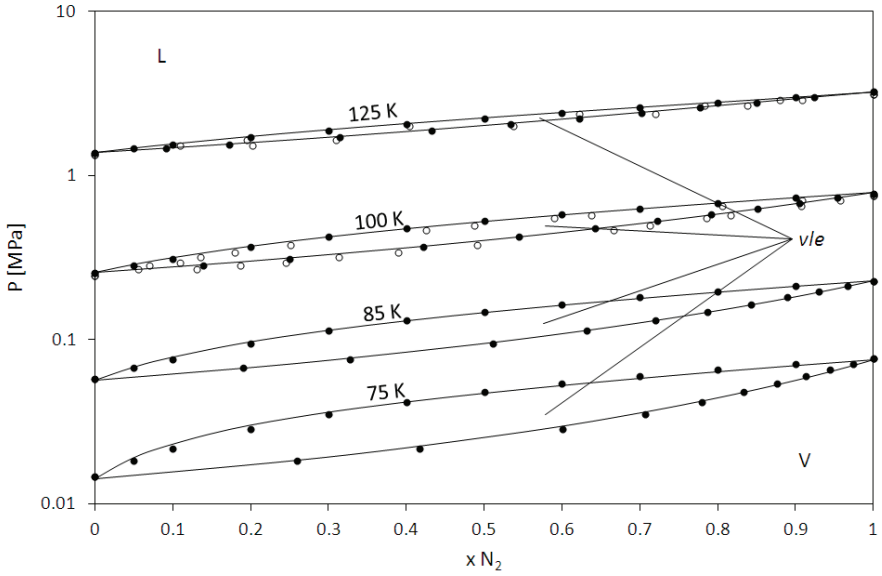

Figure F.4: VLE for the system N_2+O_2 at 75 K, 85 K, 100 K, and 125 K.
● : [DOD1927b]; ○ : [KRI1936]; — : SLV EoS.

The VLE experimental values at 100 K and 125 K from [KRI1936] are illustrated in Figure F.4. Also in this case, model agrees more with the series of data from [DOD1927b].

High deviations with respect to experimental values from [THO1963] occur in the low N_2-composition region. High deviations are encountered also for data from [DIN1960], and are mainly related to the series of 11 experimental values at fixed composition in the liquid phase (xN_2=0.335).

Table F.1: Quantitative comparison of equilibrium compositions for the system N_2+O_2.

xN_2+(1-x)O_2 Ref.	N	Kind of data	T K	P MPa	*x*	*y*		FLASH xN_2	FLASH yN_2
[ARM1955]	71	VLE PTxy	65 – 78	0.003 – 0.1	0.03 – 0.94	0.24 – 0.99	**N calc**	70	71
							AAD%	8.07	1.37
							Bias%	-6.53	-0.37
							MAD%	49.07	13.34
[BAB1999]	45	VLE PTxy	100 – 123	0.3 – 3.0	0 – 1	0 – 1	**N calc**	37	37
							AAD%	3.64	2.99
							Bias%	-2.81	-2.99
							MAD%	16.51	15.61
[BAL1900]	28	VLE PTxy	78 – 91	0.1	0 – 1	0 – 1	**N calc**	24	24
							AAD%	18.32	5.99
							Bias%	-18.3	-5.69
							MAD%	64.57	45.23
[COC1957]	40	VLE PTxy	81 – 91	0.12 – 0.14	0.06 – 0.81	0.21 – 0.93	**N calc**	40	39
							AAD%	4.09	1.43
							Bias%	1.62	0.33
							MAD%	15.38	9.40
[DIN1960]	116	VLE PTxy	79 – 116	0.11 – 1	0.1 – 0.89	0.19 – 0.97	**N calc**	116	116
							AAD%	9.56	6.90
							Bias%	-7.98	-5.15
							MAD%	67.57	54.35
[DOD1927a]	50	VLE PTxy	77 – 125	0.06 – 3.0	0.05 – 0.91	0.13 – 0.96	**N calc**	50	49
							AAD%	4.15	2.67
							Bias%	-3.51	-2.49
							MAD%	31.82	22.55
[DOD1927b]	204	VLE PTxy	75 – 125	0.015 – 3.2	0 – 1	0 – 1	**N calc**	169	168
							AAD%	4.21	2.34
							Bias%	-2.54	-1.71
							MAD%	20.44	16.54
[DOM1981]	9	VLE PTxy	60 – 80	0.005 – 0.1	0.62 – 0.71	0.9 – 0.94	**N calc**	9	9
							AAD%	5.56	1.57
							Bias%	-1.14	-1.07
							MAD%	14.14	3.43
[DUN1966]	11	VLE PTx	63	0.002 – 0.01	0 – 1		**N calc**	9	
							AAD%	16.83	
							Bias%	-16.8	
							MAD%	39.27	
[JON1963]	6	CP Tx	126 – 155		0 – 1		**N calc**	4	
							AAD%	3.16	
							Bias%	-2.98	
							MAD%	7.50	
[KRI1936]	42	VLE PTxy	100 – 125	0.25 – 3.2	0 – 1	0 – 1	**N calc**	34	34
							AAD%	15.75	12.03
							Bias%	-15.7	-12.0
							MAD%	65.62	54.48
[KUE1922]	14	VLE PTx PTy	132 – 148	2.8 – 4.6	0.25 – 0.5	0.25 – 0.5	**N calc**	5	4
							AAD%	19.22	12.73
							Bias%	-19.2	12.73
							MAD%	25.39	13.82
[MEY1936]	6	VLE PTxy	78 – 87	0.1	0.43 – 1	0.43 – 1	**N calc**	6	6
							AAD%	5.48	2.94
							Bias%	5.48	2.94
							MAD%	9.17	3.92
[POO1962]	11	VLE PTx	84	0.05 – 0.2	0 – 1		**N calc**	9	
							AAD%	1.98	
							Bias%	0.17	
							MAD%	5.75	

[RUH1935]	23	SLE Tx	50 – 63		0 – 1		**N calc**	18	
							AAD%	9.00	
							Bias%	1.18	
							MAD%	28.95	
[THO1963]	13	VLE PTxy	88 – 90	0.1 – 0.11	0 – 0.08	0 – 0.27	**N calc**	11	11
							AAD%	32.09	23.19
							Bias%	-32.1	-23.2
							MAD%	57.08	44.85
[WIL1964]	138	VLE PTxy	78 – 136	0.1 – 2.6	0.05 – 0.99	0.11 – 1	**N calc**	138	138
							AAD%	5.12	4.01
							Bias%	-4.19	-3.62
							MAD%	58.15	26.33
[YOR1978]	20	VLE PTxy	80 – 88	0.03 – 0.12	0 – 0.85	0.01 – 0.93	**N calc**	19	19
							AAD%	7.29	2.81
							Bias%	1.63	1.34
							MAD%	17.54	7.75

1.2 N_2+Ar

The literature data for the system N_2+Ar are shown in Figure F.5.

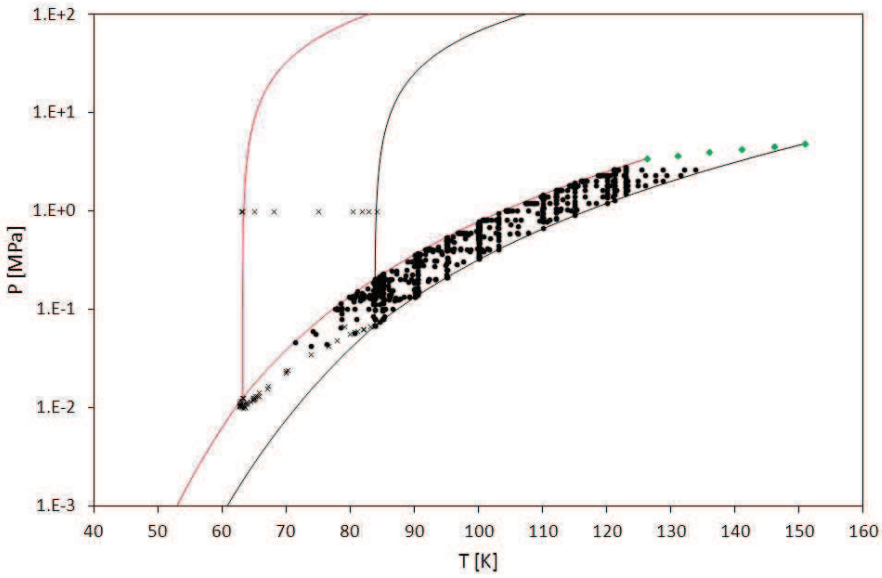

Figure F.5: Available experimental values for the system N_2+Ar.
— : N_2; — : Ar; ● : FFE data; × : SFE data; ♦ : CP data.

The qualitative comparison between model and SLE data is portrayed in Figure F.6. According to [DIN1955], the temperature and composition at the solid-liquid azeotrope are 62.7 K and 0.8 in N_2 mole fraction, respectively. Calculated values are 62.24 K and $xN_2 = 0.807$.

Calculate values are globally in a good agreement with data of [LON1965] and [DIN1955], however deviations increase while approaching the azeotrope. The model is less representative of the data from [FED1938] for compositions close to pure Ar.

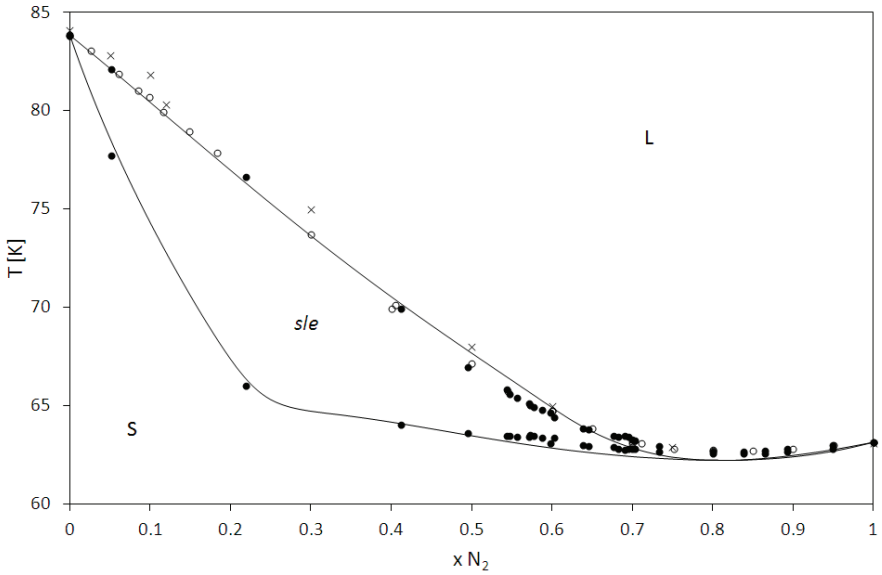

Figure F.6: SLE for the system N_2+Ar.
● : [LON1965]; ○ : [DIN1955]; × : [FED1938]; — : SLV EoS.

The temperature-composition cross sections at 0.2 MPa, 0.4 MPa, and 0.6 MPa are illustrated in Figure F.7; data are from [WIL1964].

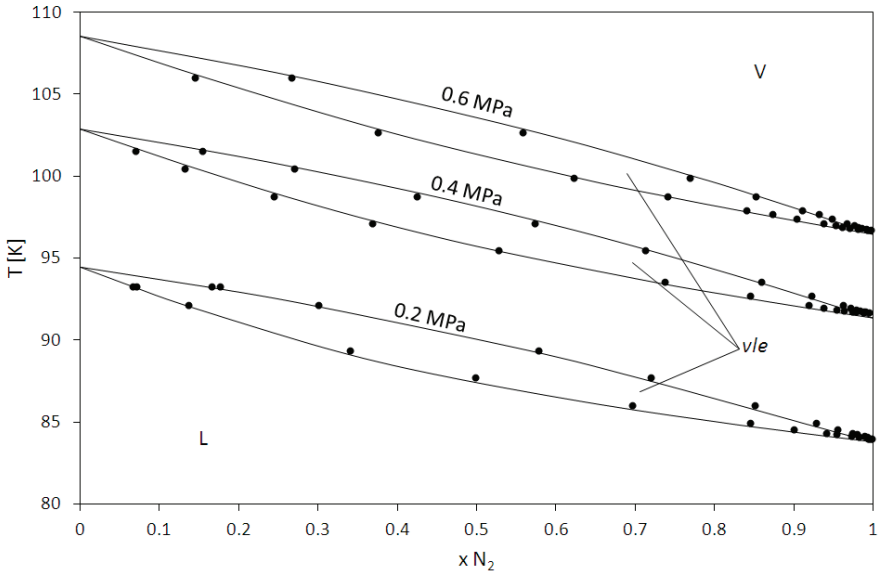

Figure F.7: VLE for the system N_2+Ar at 0.2 MPa, 0.4 MPa, and 0.6 MPa.
● : [WIL1964]; — : SLV EoS.

The pressure-composition cross sections in Figure F.8 show the qualitative comparison between VLE data and model from 95 K up to 121 K; data are from [BAB1999].

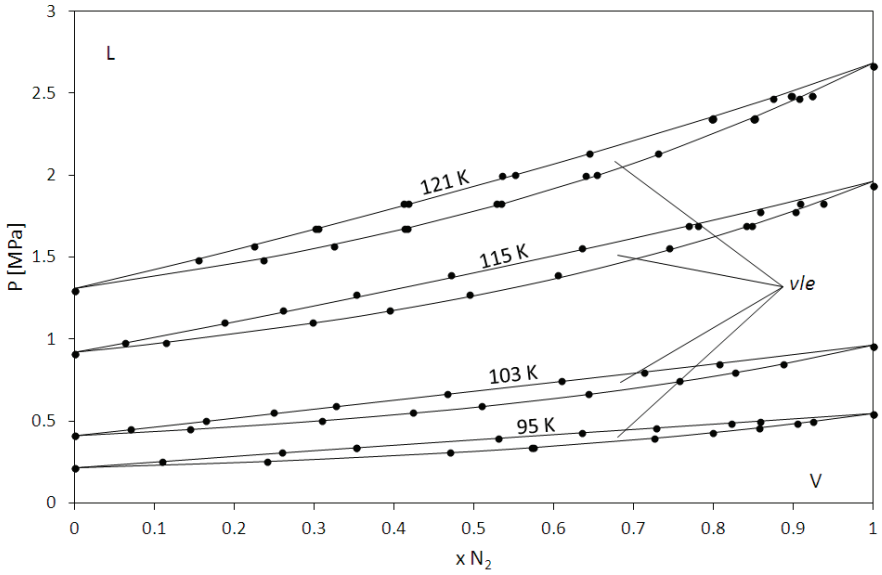

Figure F.8: VLE for the system N_2+Ar at 95 K, 103 K, 115 K, and 121 K.
● : [BAB1999]; — : SLV EoS.

Table F.2 gives the quantitative comparison between data and values calculated from the SLV EoS in terms of equilibrium mole fractions of N_2.

With reference to the VLE, the AAD% for both compositions in the liquid (x) and in the vapor (y) phases is lower than 10% for all the references, except for the data presented in [MAS1973] and [MAS1976]. A maximum value of about 54% for the MAD% has been found with respect to data from [XIA1990].

Table F.2: Quantitative comparison of equilibrium compositions for the system N_2+Ar.

xN_2+(1-x)Ar Ref.	N	Kind of data	T K	P MPa	*x*	*y*		FLASH xN_2	FLASH yN_2
[BAB1999]	51	VLE PTxy	95 – 121	0.2 – 2.7	0 – 1	0 – 1	**N calc**	43	43
							AAD%	2.12	1.32
							Bias%	1.17	0.39
							MAD%	8.74	4.91
[DIN1955]	26	SLE PTx	63 – 84	0.01 – 0.07	0 – 1		**N calc**	24	23
							AAD%	5.40	7.93
							Bias%	-0.77	4.51
							MAD%	17.93	16.00
[DOL1919]	11	VLE PTxy	85	0.08 – 0.23	0 – 1	0 – 1	**N calc**	9	9
							AAD%	6.10	1.17
							Bias%	-5.90	0.22
							MAD%	12.24	2.00
[ELS1975]	7	VLE PTx	100	0.4 – 0.74	0.14 – 0.9		**N calc**	7	
							AAD%	3.28	
							Bias%	3.24	
							MAD%	10.43	
[FAS1956a]	20	VLE PTxy	80 – 101	0.12 – 0.39	0.1 – 0.78	0.21 – 0.92	**N calc**	20	20
							AAD%	8.19	4.72
							Bias%	-0.01	-0.99
							MAD%	32.61	19.68
[FED1938]	10	SLE Tx	63 – 83		0 – 0.75		**N calc**	8	
							AAD%	15.13	
							Bias%	-15.13	
							MAD%	40.62	
[HAM1915]	24	VLE PTx PTy	71 – 90	0.04 – 0.16	0 – 0.99	0.24 – 0.74	**N calc**	12	9
							AAD%	4.98	3.79
							Bias%	-0.97	0.78
							MAD%	13.35	8.98
[JON1963]	6	CP Tx	126 – 151		0 – 1		**N calc**	4	
							AAD%	3.53	
							Bias%	3.53	
							MAD%	4.90	
[LEW1975]	8	VLE PTxy	85	0.07 – 0.22	0 – 1	0 – 1	**N calc**	6	6
							AAD%	2.77	0.85
							Bias%	-2.77	-0.85
							MAD%	4.42	1.18
[LIU1988]	13	VLE PTxy	122.9	1.5 – 2.8	0.05 – 0.97	0.08 – 0.98	**N calc**	12	12
							AAD%	7.00	5.24
							Bias%	3.69	1.08
							MAD%	19.88	24.96
[LON1963]	58	SLE PTx	62 – 84	0.01 – 0.07	0 – 1		**N calc**	54	24
							AAD%	7.24	7.78
							Bias%	-1.59	-7.70
							MAD%	16.95	17.76
[MAS1973]	6	VLE PTx	90 – 113	0.27 – 1.31	0.503		**N calc**	6	
							AAD%	12.82	
							Bias%	12.82	
							MAD%	23.77	
[MAS1976]	34	VLE PTxy	85 – 100	0.08 – 0.78	0 – 1		**N calc**	27	27
							AAD%	14.47	15.55
							Bias%	8.92	10.95
							MAD%	47.73	42.67
[MIL1973]	14	VLE PTx	112	0.84 – 1.51	0.11 – 0.85	0.17 – 0.9	**N calc**	7	7
							AAD%	2.56	2.56
							Bias%	2.42	2.42
							MAD%	6.48	6.48

[NAR1966]	108	VLE PTxy	80 – 120	0.13 – 2.5	0 – 1	0 – 1	**N calc**	98	98
							AAD%	4.00	2.29
							Bias%	0.92	1.14
							MAD%	24.28	13.88
[POO1962]	12	VLE PTx	84	0.07 – 0.2	0 – 1		**N calc**	10	
							AAD%	4.20	
							Bias%	-4.20	
							MAD%	6.92	
[SPR1966]	19	VLE PTxy	84	0.07 – 0.2	0 – 1	0 – 1	**N calc**	17	17
							AAD%	3.35	1.26
							Bias%	-3.35	-1.17
							MAD%	6.68	2.23
[THO1968]	69	VLE PTxy	81 – 115	0.13 – 1.1	0.1 – 0.91	0.18 – 0.96	**N calc**	69	68
							AAD%	4.43	1.99
							Bias%	3.67	1.46
							MAD%	14.86	6.20
[WIL1964]	179	VLE PTxy	72 – 134	0.1 – 2.63	0.04 – 1	0.02 – 1	**N calc**	178	178
							AAD%	3.48	1.99
							Bias%	-1.02	-0.77
							MAD%	22.10	18.78
[XIA1990]	18	VLE PTxy	100	0.35 – 0.74	0.12 – 0.92	0.29 – 0.96	**N calc**	18	18
							AAD%	5.62	4.62
							Bias%	-2.76	-2.39
							MAD%	54.01	53.78

1.3 N_2+Kr

The literature data for the system N_2+Kr are shown in Figure F.9.

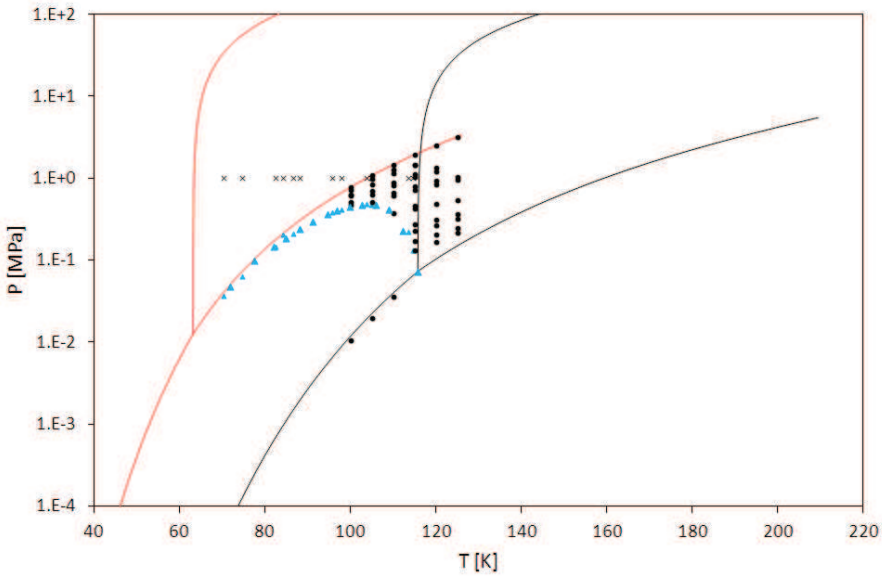

Figure F.9: Available experimental values for the system N_2+Kr.
— : N_2; — : Kr; ● : FFE data; × : SFE data; ▲ : SVLE data.

The qualitative comparison between model and SLE data is portrayed in Figure F.10. Calculated values are in a good agreement with data of [MAS1976] and [TEL1984]. According to the model, the system is of the peritectic type. This entails the presence of a Quadruple Point (QP) of $s_2s_1$lve. The calculated QP temperature is 67.4 K, while compositions in term of N_2 mole fraction of the solid$_2$, solid$_1$, liquid and vapor phases are 0.1, 0.72, and 0.915, and 0.999, respectively.

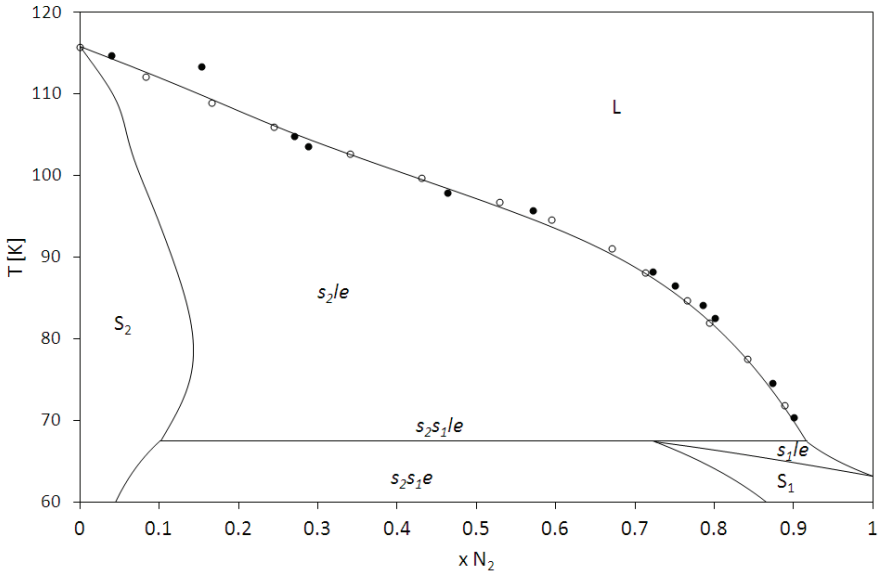

Figure F.10: SLE for the system N_2+Ar.
● : [MAS1976]; ○ : [TEL1984]; — : SLV EoS.

The pressure-temperature equilibrium projection in the range 40 K – 120 K is illustrated in Figure F.11; circles are data from [MAS1976] and [TEL1984]. The red square is the triple point of N_2 (TP N_2), the green one is the Quadruple Point (QP), the black one is the triple point of Kr (TP Kr). Notation used for the three phase lines is the same used in Chapter 6.

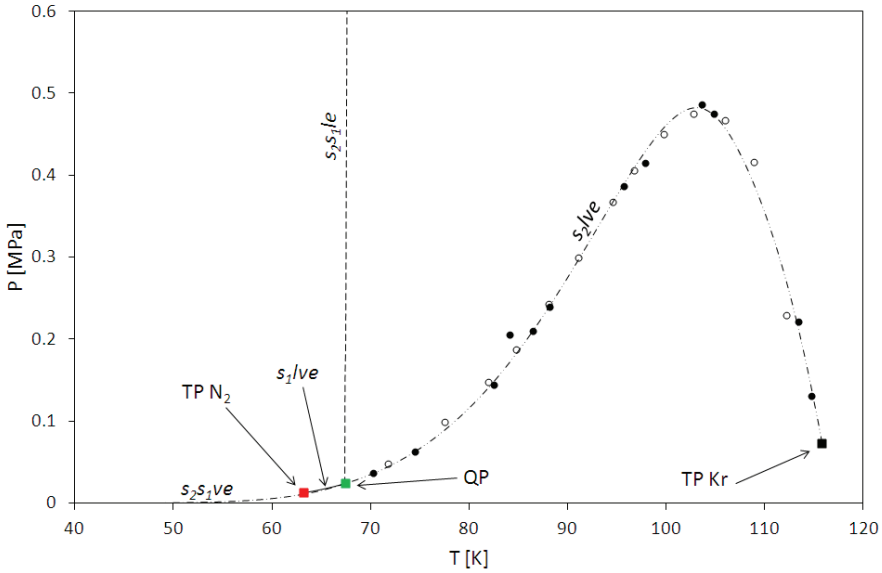

Figure F.11: PT equilibrium projection for the system N_2+Ar in the range 40 K – 120 K.
● : [MAS1976]; ○ : [TEL1984]; — : SLV EoS; ■ : triple point of N_2; ■ : $s_2s_1$lv QP; ■ : triple point of Kr.

The pressure-composition cross sections in Figure F.12 show the qualitative comparison between VLE data and model from 110 K up to 120 K; data are from [MAS1976].

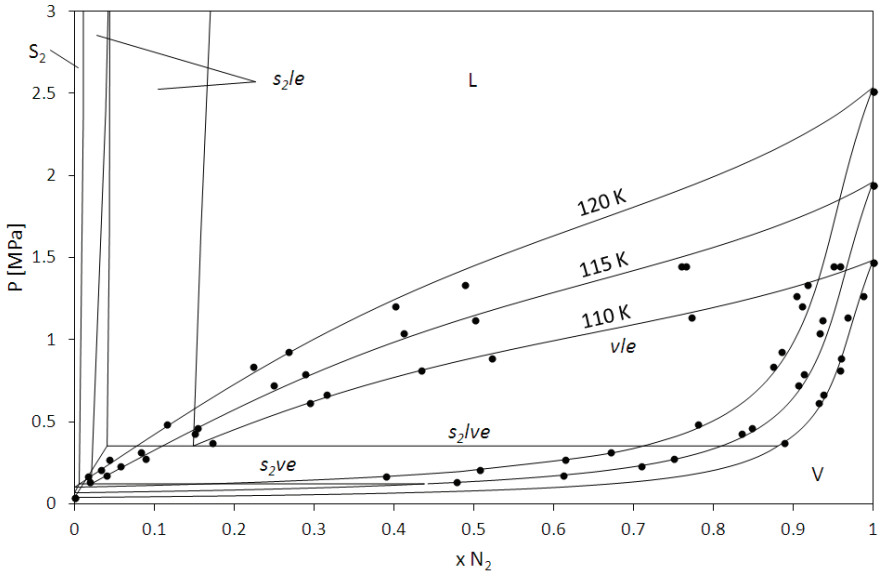

Figure F.12: VLE for the system N_2+Kr at 110 K, 115 K, and 120 K.
● : [MAS1976]; — : SLV EoS.

Table F.3 gives the quantitative comparison between data and values calculated from the SLV EoS in terms of equilibrium mole fractions of N_2.

With reference to the VLE, the AAD% for both compositions in the liquid (x) and in the vapor (y) phases is lower than 10%. A maximum value of about 55% for the MAD% has been found in the low N_2 content region at 125 K.

According to Figure F.12 (and Table F.3), deviations from VLE data in [MAS1976] are mainly encountered along the liquid branch of the VLE for increasing pressures.

Table F.3: Quantitative comparison of equilibrium compositions for the system N_2+Kr.

xN_2+(1-x)Kr Ref.	N	Kind of data	T K	P MPa	*x*	*y*		FLASH xN_2	FLASH yN_2
[MAS1974]	12	SLE Tx	70 – 115		0.04 – 0.9		**N calc**	12	
							AAD%	9.60	
							Bias%	-7.27	
							MAD%	59.09	
[MAS1976]	54	VLE PTxy	100 – 125	0.01 – 3.2	0 – 1	0 – 1	**N calc**	45	45
							AAD%	8.15	0.66
							Bias%	-2.66	0.34
							MAD%	55.12	2.33
	12	SVLE PTx	70 – 115	0.036 – 0.49	0.04 – 0.9		**N calc**	12	11
							AAD%	9.62	11.31
							Bias%	-7.29	-8.91
							MAD%	59.22	55.90
[TEL1984]	14	SVLE PTx	72 – 116	0.048 – 0.48	0 – 0.89		**N calc**	13	13
							AAD%	2.73	5.24
							Bias%	0.63	1.14
							MAD%	14.79	20.82

1.4 N_2+Xe

The literature data for the system N_2+Xe are shown in Figure F.13.

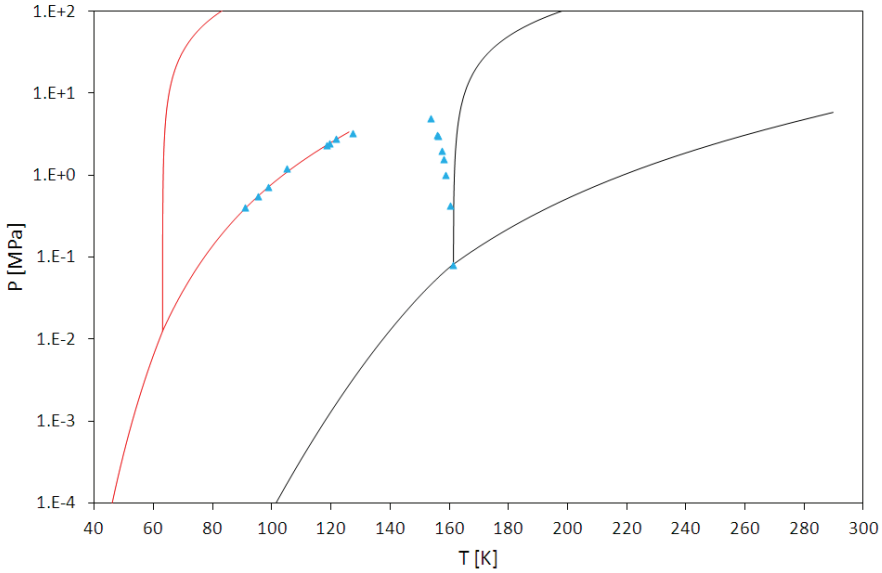

Figure F.13: Available experimental values for the system N_2+Xe.
— : N_2; — : Xe; ▲ : SVLE data.

The qualitative comparison between model and SLE data is portrayed in Figure F.14. Calculated values are in a good agreement with the solubility data along the s_2l_2v three phase line [$xl_2(s_2l_2ve)$]. The model is representative of the solubilities along the s_2l_1v three phase line [$xl_1(s_2l_1ve)$] up to about 105 K, while at higher temperatures calculated values are higher than experimental ones from [TEL1984].

The system presents two Upper Critical Endpoints (UCEP). The first occurring at about 130 K involves a liquid rich in N_2 ($UCEP_1$), the second one occurring at about 150 K involves a liquid richer in Xe ($UCEP_2$).

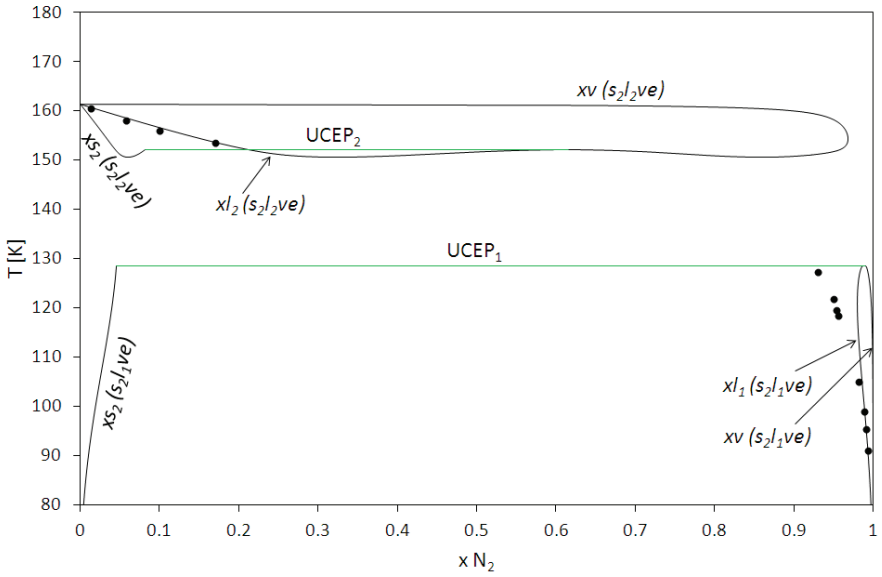

Figure F.14: SLE for the system N_2+Xe.
Experimental values : ●, [TEL1984]. Calculated values : equilibrium compositions (—) and upper critical point temperatures (—).

The pressure-temperature equilibrium projection in the range 40 K – 180 K is illustrated in Figure F.15; circles are data from [TEL1984]. The triple point of N_2 (TP N_2) is covered by the $s_2s_1l_1v$ Quadruple Point (QP), which is indicated by the green square. The black one is the triple point of Xe (TP Xe). Notation used for the three phase lines is the same used in Chapter 6.

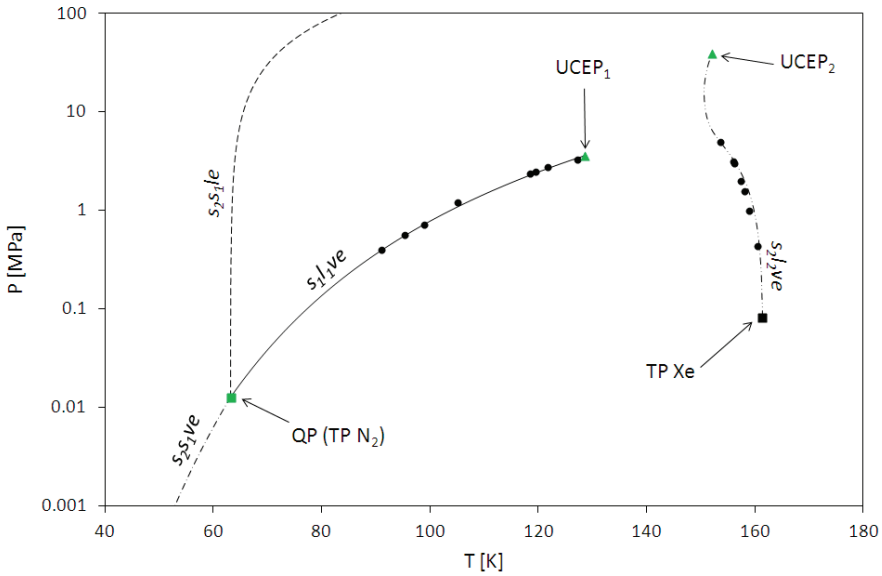

Figure F.15: PT equilibrium projection for the system N_2+Xe in the range 40 K – 180 K.
● : [TEL1984]; — : SLV EoS; ■ : $s_2s_1l_1v$ QP; ■ : triple point of Xe; ▲ : upper critical points.

Table F.4 gives the quantitative comparison between data and values calculated from the SLV EoS in terms of equilibrium mole fractions of N_2.

The AAD% for both compositions in the liquid (x) and in the vapor (y) phases is lower than 10%. The value of 42% for the MAD% (obtained evaluating equilibrium solubilities at imposed temperature) is related to the highest experimental values in terms of temperature, which means the point in Figure F.14 close to pure Xe. The correspondent experimental and calculated values are about 0.013 and 0.02, respectively.

Table F.4: Quantitative comparison of equilibrium compositions for the system N_2+Xe.

xN_2+(1-x)Xe Ref.	N	Kind of data	T K	P MPa	x	y		FLASH xN_2	FLASH yN_2
[TEL1984]	16	SVLE PTx	91 – 161	0.08 – 4.9	0.014 – 1		**N calc**	12	12
							AAD%	7.66	3.43
							Bias%	7.58	0.65
							MAD%	42.21	9.32

1.5 N_2+Ne

The literature data for the system N_2+Ne are shown in Figure F.16.

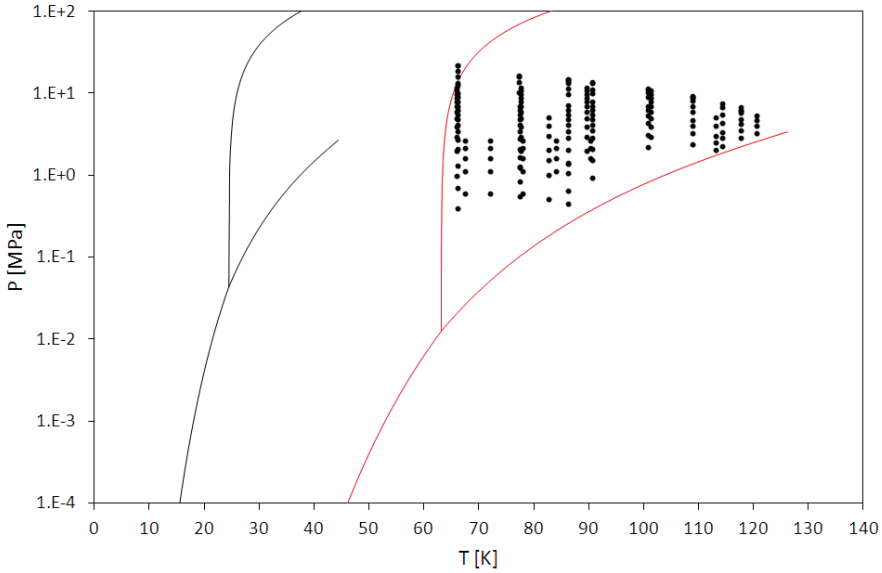

Figure F.16: Available experimental values for the system N_2+Ne.
— : N_2; — : Ne; ● : FFE data.

The pressure-composition cross sections in Figure F.17 show the qualitative comparison between VLE data and model from 66 K up to 114 K; data are from [STR1965a] and [STR1968].

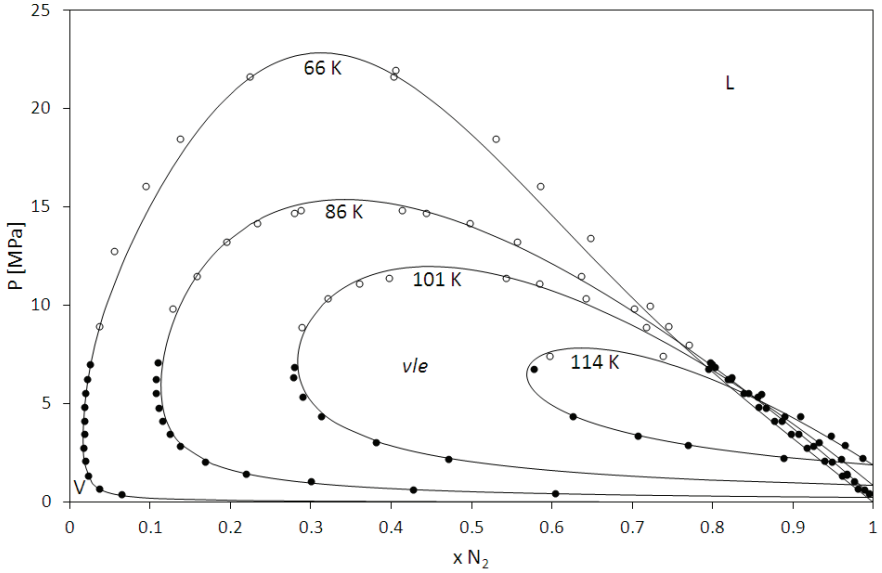

Figure F.17: VLE for the system N_2+Ne from 66 K up to 114 K.
● : [STR1965a]; ○ : [STR1968] ; — : SLV EoS.

Table F.5 gives the quantitative comparison between data and values calculated from the SLV EoS in terms of equilibrium mole fractions of N_2.

With reference to the VLE, the AAD% for both compositions in the liquid (x) and in the vapor (y) phases is lower than 10%. High deviations are related to the vapor phase. A maximum value of about 31% for the MAD% has been found with respect to data from [STR1968] along the vapor branch of the VLE at about 13 MPa (experimental value $yN_2 \approx 0.055$, calculated value $yN_2 \approx 0.073$).

Table F.5: Quantitative comparison of equilibrium compositions for the system N_2+Ne.

xNe+(1-x)N₂ Ref.	N	Kind of data	T K	P MPa	*x*	*y*		FLASH xN_2	FLASH yN_2
[BUR1964]	12	VLE PTxv	83 – 113	0.5 – 5.1	0 – 0.15	0.08 – 0.93	**N calc**	12	12
							AAD%	0.72	7.11
							Bias%	0.12	7.10
							MAD%	2.02	19.93
[SKR1964]	22	VLE PTxy	67 – 90	0.6 – 2.6	0.014 – 0.08	0.7 – 0.98	**N calc**	22	22
							AAD%	0.15	5.46
							Bias%	0.13	4.58
							MAD%	0.48	18.16
[SKR1971]	43	VLE PTxy	66 – 101	1.0 – 12.0	0.029 – 0.38	0.61 – 0.97	**N calc**	43	43
							AAD%	1.39	9.15
							Bias%	-1.38	8.29
							MAD%	5.66	20.92
[STR1965a]	77	VLE PTxy	66 – 121	0.4 – 7.1	0 – 0.27	0.1 – 0.98	**N calc**	72	72
							AAD%	0.64	2.28
							Bias%	-0.56	1.28
							MAD%	3.90	7.32
[STR1968]	33	VLE PTxy	66 – 114	7.4 – 22.0	0.23- 0.6	0.4 – 0.96	**N calc**	30	28
							AAD%	2.06	5.62
							Bias%	-1.26	0.64
							MAD%	4.89	31.04

1.6 N_2+He

The literature data for the system N_2+He are shown in Figure F.18.

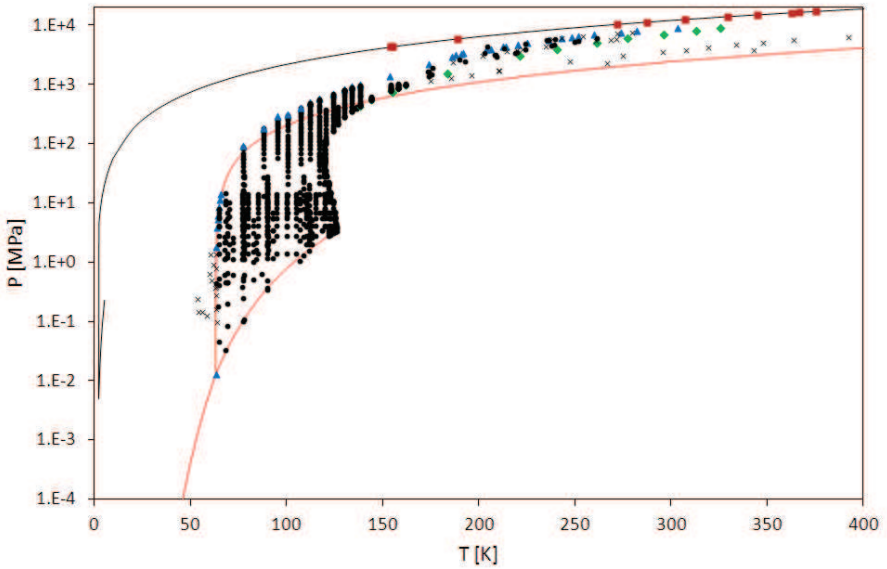

Figure F.18: Available experimental values for the system N_2+He.
— : N_2; — : He; ● : FFE data; × : SFE data; ♦ : CP data; ▲ : SVLE data; ■ : SSLE data.

For the author attempts, it has not been possible representing the phase equilibrium behavior of the system N_2+He for temperature greater than 120 K and pressure greater than 30 MPa. As a consequence, the comparison in this section has been done considering experimental values within these limits.

The qualitative comparison between model and SVE data is portrayed in Figure F.19. In Figure F.19, empty circles are experimental values, while filled ones represent calculated values. Although calculated values are in a good agreement with data, deviations increase while approaching the triple point temperature of N_2 (about 64 K).

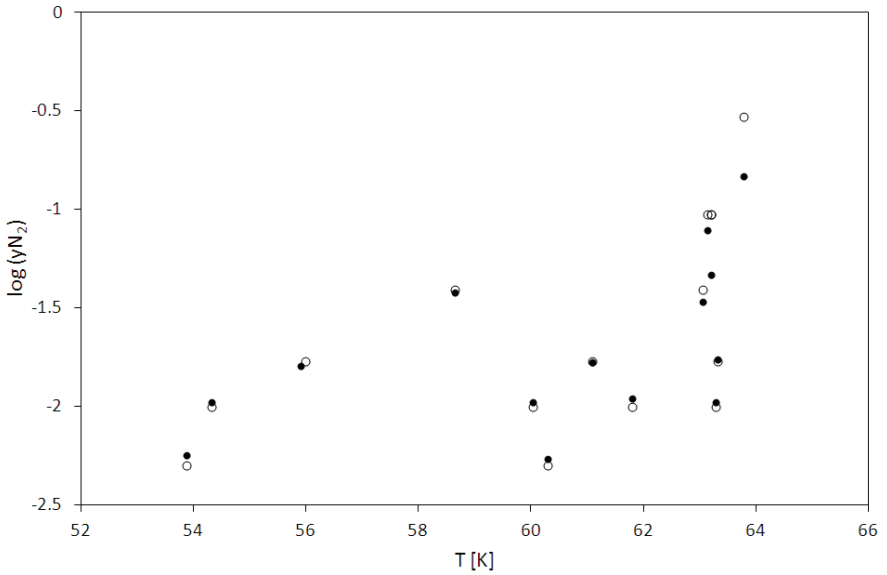

Figure F.19: SVE for the system N_2+He.
○ : [ROD1964]; ● : calculated values.

The qualitative comparison between calculated and experimental values of the vapor compositions along the solid$_1$-liquid$_1$-vapor three phase line is illustrated in Figure F.20. It is worth remembering that 1 is referred to N_2. In Figure F.20, circles are data from [ROD1964].

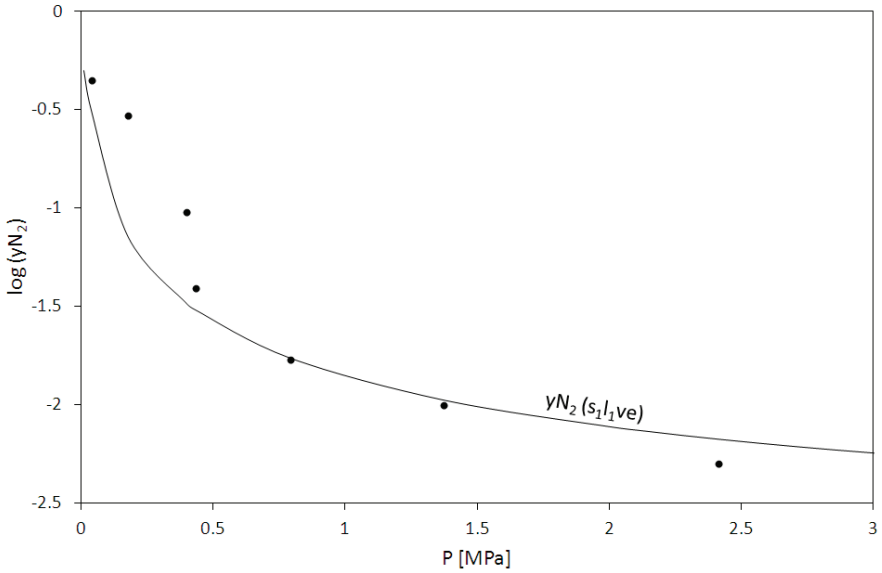

Figure F.20: PT equilibrium projection for the system N_2+He in the range 40 K – 120 K.
● : [ROD1964]; — : SLV EoS.

The pressure-composition cross sections in Figure F.21 show the qualitative comparison between VLE data and model at 77 K, 90 K, and 100 K.

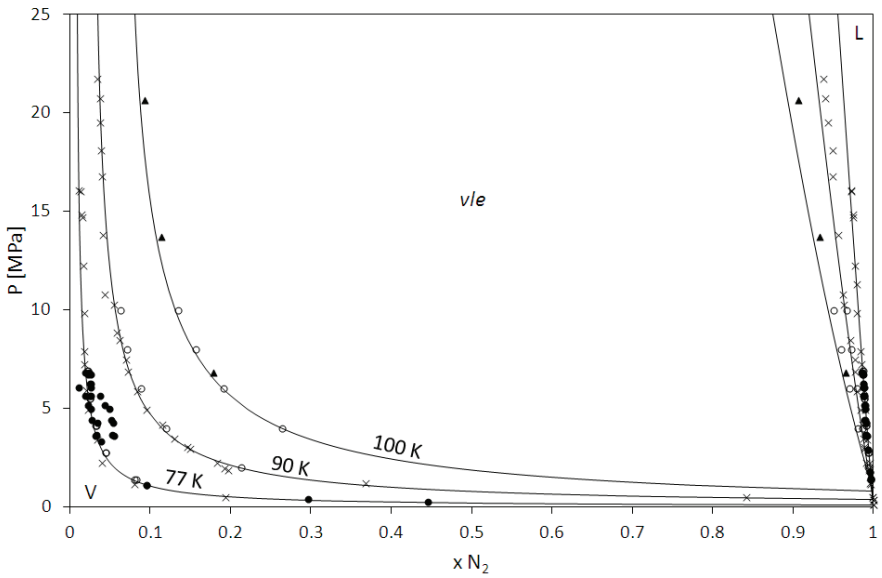

Figure F.21: VLE for the system N_2+He at 77 K, 90 K, and 100 K.
● : [DAV1963]; ○ : [FON1989] ; × : [KHA1940] ; ▲ : [STR1967a] ; — : SLV EoS.

Table F.6 gives the quantitative comparison between data and values calculated from the SLV EoS in terms of equilibrium mole fractions of N_2.

The majority of the literature data are concentrated within the cited limits of temperature and pressure (120 K, 30 MPa), and the EoS is in a good agreement with experimental values concerning the liquid composition of N_2. Higher deviations are encountered for the vapor phase, which is mainly made of He in its supercritical state.

Table F.6: Quantitative comparison of equilibrium compositions for the system N_2+He.

xHe+(1-x)N₂ Ref.	N	Kind of data	T K	P MPa	*x*	*y*		FLASH xN_2	FLASH yN_2
[BUR1964]	12	VLE PTxy	83 – 113	0.5 – 5.1	0 – 0.04	0.08 – 0.95	**N calc**	12	12
							AAD%	0.18	5.29
							Bias%	-0.13	-0.58
							MAD%	0.79	14.38
[BUZ1963]	30	VLE PTxy	77 – 123	1.2 – 6.9	0 – 0.08	0.07 – 0.98	**N calc**	27	27
							AAD%	0.27	7.84
							Bias%	-0.10	-7.28
							MAD%	1.00	24.49
[DAV1963]	35	VLE PTxy	77	0.25 – 6.8	0 – 0.015	0.94 – 0.99	**N calc**	30	29
							AAD%	0.10	20.82
							Bias%	0.10	-11.13
							MAD%	0.32	98.11
[DAV1971]	24	VLE PTy	77 – 126	2.0 – 10.0		0.11 – 0.98	**N calc**		22
							AAD%		5.44
							Bias%		-3.58
							MAD%		15.58
[DEV1963]	96	VLE PTxy	77 – 120	1.38 – 13.8	0 – 0.14	0.17 – 0.99	**N calc**	96	96
							AAD%	0.54	4.33
							Bias%	0.54	-3.55
							MAD%	4.08	18.21
[FON1989]	55	VLE PTxy	65 – 125	1.4 – 10.0	0 – 0.12	0.06 – 1	**N calc**	55	55
							AAD%	0.35	14.87
							Bias%	-0.28	-14.71
							MAD%	5.56	64.54
[GON1940a]	29	VLE PTxy	78 – 109	0.11 – 28.9	0 – 0.18	0 – 0.98	**N calc**	26	25
							AAD%	0.40	29.28
							Bias%	-0.24	-27.96
							MAD%	1.20	46.93
[GON1940b]	5	VLE PTx	90	2.9 – 14.7	0.01 – 0.048		**N calc**	5	
							AAD%	0.11	
							Bias%	-0.09	
							MAD%	0.27	
[KHA1940]	76	VLE PTxy	68 – 112	0.03 – 21.7	0 – 0.14	0 – 0.99	**N calc**	69	69
							AAD%	0.33	13.33
							Bias%	-0.28	-8.29
							MAD%	2.48	65.38
[ROD1964][1]	19	VLE PTxy	63 – 87	0.04 – 3.3	<0.01	0.55 – 0.96	**N calc**	5	14
							AAD%	0.05	22.43
							Bias%	0.04	-22.43
							MAD%	0.12	71.52
	15	SVE PTy	54 – 64	0.1 – 1.4		0.7 – 0.99	**N calc**		15
							AAD%		16.66
							Bias%		-10.29
							MAD%		63.24
	7	SVLE Py		0.04 – 2.4		0 – 0.45	**N calc**		7
							AAD%		33.46
							Bias%		-21.52
							MAD%		75.80
	8	SVLE PT	63 – 66	0.01 – 13.9			**N calc**	7	7
							AAD%	0.22	11.21
							Bias%	0.22	-6.39
							MAD%	0.44	16.87

[SKR1964]	22	VLE PTxy	67 – 90	0.6 – 2.6	0 – 0.01	0.74 – 0.99	**N calc**	22	22
							AAD%	0.02	6.73
							Bias%	-0.01	6.72
							MAD%	0.07	19.85
[STR1967a]	86	VLE PTxy	78 – 122	6.7 – 82.7	0.012 – 0.56	0.34 – 0.99	**N calc**	18	17
							AAD%	1.25	10.94
							Bias%	-0.48	-3.97
							MAD%	3.16	43.84
	5	LLE	129	67.0 – 83.1	0.54 – 0.58	0.63 – 0.73			
[STR1970]	101	VLE PTxy	78 – 120	13.1 – 396.5	0.04 – 0.51	0.68 – 0.99	**N calc**	2	2
							AAD%	1.06	14.61
							Bias%	-1.06	-14.61
							MAD%	1.68	14.99
	47	LLE	121 – 137	97.2 – 413.7	0.33 – 0.64	0.7 – 0.95			
	5	SVLE	78 – 107	93.1 – 405.3	0.07 – 0.21	0.98 – 0.99			
[STR1972a]	111	LLE	112 – 162	111 – 1020	0.24 – 0.69	0.82 – 0.98			
	6	SVLE	112 – 138	492 – 993	0.24 – 0.35	0.96 – 0.98			
	5	CP	138 – 162	416 - 957	0.73 – 0.77				
[TUL1971]	70	VLE	122 – 126	2.8 – 20.9	0 – 0.38	0 – 0.49			
[VAN1988]	9	CP	155 – 326	730 – 8920					
	20	SVLE	154 – 304	1370 – 9020					
[WIL1992]	33	SLE	175 – 413	1150 – 7440	0.054 – 0.43				
	25	LLE	174 – 262	1368 – 6020	0.43 – 0.94				
	11	SLVE	154 – 375	4290 - 16870					

[1] – for SVLE PT data, column xN_2 (yN_2) contains the deviations between calculated and experimental temperatures (pressures) at fixed pressures (temperatures).

1.7 N_2+CO_2

The literature data for the system N_2+CO_2 are shown in Figure F.22.

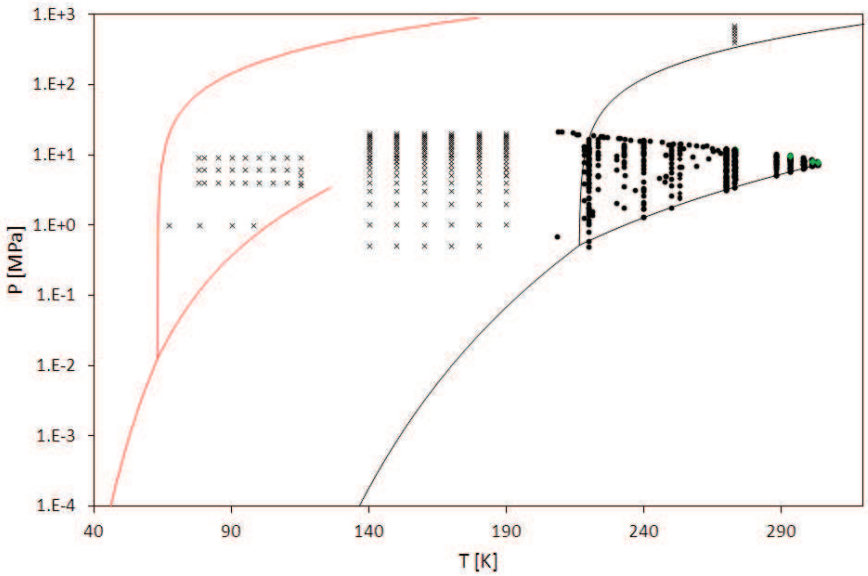

Figure F.22: Available experimental values for the system N_2+CO_2.
— : N_2; — : CO_2; ● : FFE data; × : SFE data; ♦ : CP data.

The qualitative comparison between model and SVE/SLE data is portrayed in Figure F.23. In Figure F.23, the y-axis is the logarithm of the CO_2 mole fraction in either the vapor or the liquid phase. Filled circles are SVE experimental values from [SON1962] and [SON1963], while empty ones represent SLE experimental values from [YAK1975].

The vertical lines in Figure F.23 are placed at the s_2l_1ve pressure, where 1 and 2 are N_2 and CO_2, respectively. The s_2l_1ve ends in an upper critical endpoint close to the critical point of pure N_2, so that for higher temperatures (140 K ≤ T ≤ 190 K) the s_2l_1e disappears and only the s_2ve occurs.

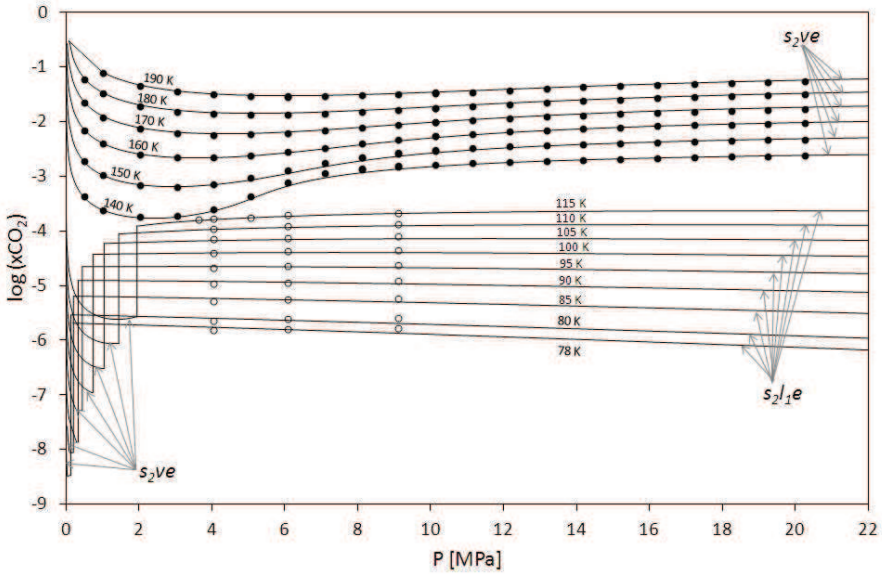

Figure F.23: SVE and SLE for the system N_2+CO_2.
● : [SON1962]+[SON1963]; ○ : [YAK1975]; — : SLV EoS.

The pressure-composition cross sections in Figure F.24 show the qualitative comparison between VLE data and model at 220 K, 232 K, and 240 K.

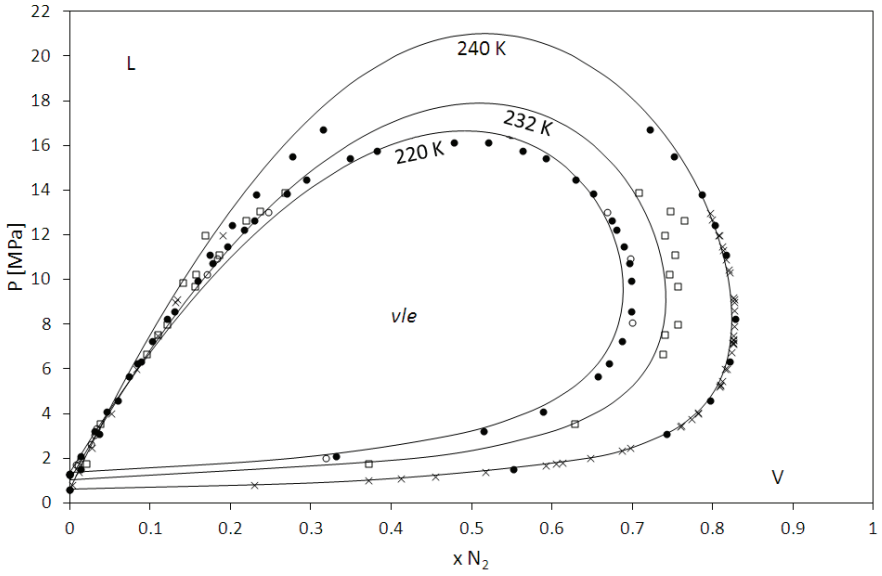

Figure F.24: VLE for the system N_2+CO_2 at 220 K, 232 K, and 240 K. ● : [ALS1983]; ○ : [YUC1999]; □ : [ZEN1963]; × : [BRO1989b]; — : SLV EoS.

According to Figure F.24, calculated values are qualitatively representative of the experimental values, and deviations mainly occur in the liquid phase at 240 K.

Table F.7 gives the quantitative comparison between data and values calculated from the SLV EoS in terms of equilibrium mole fractions of N_2.

With reference to the VLE, the AAD% for both compositions in the liquid (x) and in the vapor (y) phases is globally lower than 15%. Higher deviations are usually related to the liquid phase. The deviation between calculated and experimental values increases for temperatures approaching the critical temperature of pure CO_2, as for the case of [BIA1993].

With reference to Figure F.23 and the deviations related to SVE and SLE data in Table F.7, it is possible to state that model is in a good agreement with experimental values. It is worth remembering that SVE and SLE are the main equilibria involved in an air distillation unit considering the system N_2+CO_2. The model is not able to represent the SVE at 273 K proposed in [TSI1946].

Table F.7: Quantitative comparison of equilibrium compositions for the system N_2+CO_2.

xN_2+(1-x)CO_2 Ref.	N	Kind of data	T K	P MPa	*x*	*y*		FLASH xN_2	FLASH yN_2
[ALS1983]	29	VLE PTxy	220 – 240	0.6 – 16.7	0 – 0.48	0 – 0.83	**N calc**	27	27
							AAD%	7.49	1.86
							Bias%	0.30	-0.43
							MAD%	14.41	8.83
[ALS1990]	5	VLE PTxy	230 – 250	6.2 – 10.3	0.08 – 0.18	0.61 – 0.77	**N calc**	5	5
							AAD%	6.58	1.01
							Bias%	5.42	-0.97
							MAD%	9.77	2.03
[ALW1976]	14	VLE PTxy	223– 273	3.2 – 16.7	0.035 – 0.34	0.24 – 0.82	**N calc**	14	14
							AAD%	8.43	3.54
							Bias%	1.96	-3.50
							MAD%	16.39	10.27
[ARA1971]	43	VLE PTxy	253 – 288	2.4 – 14.4	0 – 0.35	0 – 0.57	**N calc**	9	28
							AAD%	18.16	7.17
							Bias%	18.16	-4.56
							MAD%	23.87	38.76

[BAL1989]	11	VLE PTy	209 – 258	0.69 – 18.2		0.55	**N calc**		11
							AAD%		5.00
							Bias%		1.70
							MAD%		17.54
[BIA1993]	12	VLE PTxy	301 – 303	6.9 – 8.0	0 – 0.035	0 – 0.039	**N calc**	4	4
							AAD%	31.40	2.90
							Bias%	31.40	-2.46
							MAD%	36.35	6.92
	2	CP PTx	301 – 303	7.8 – 8.0	0.02 – 0.04		**N calc**	2	2
							AAD%	19.92	70.68
							Bias%	-19.92	70.68
							MAD%	39.06	91.35
[BRO1989a]	17	VLE PTxy	250 – 270	1.8 – 14.1	0 – 0.3	0 – 0.62	**N calc**	15	15
							AAD%	9.84	4.73
							Bias%	9.38	-4.62
							MAD%	15.90	13.43
[BRO1989b]	69	VLE PTxy	220 – 270	0.5 – 13.0	0 – 0.19	0 – 0.83	**N calc**	22	66
							AAD%	12.86	1.80
							Bias%	6.96	-1.73
							MAD%	19.92	14.67
[DUA1995a]	23	VLE PTy	209 – 268	10.8 – 21.4		0.5 – 0.6	**N calc**		23
							AAD%		15.99
							Bias%		10.38
							MAD%		64.38
[FED1940]	5	SLE Tx	67 – 98		~1		**N calc**	5	
							AAD%	0.001	
							Bias%	-0.001	
							MAD%	0.002	
[FER1980]	5	VLE PTx	273	3.5 – 8.4	0 – 0.1		**N calc**	4	
							AAD%	13.55	
							Bias%	13.55	
							MAD%	20.71	
[KAM1966]	17	VLE PTxy	233 – 298	3.7 – 12.7	0.051 – 0.25	0.067 – 0.7	**N calc**	13	16
							AAD%	15.73	4.50
							Bias%	15.73	-4.50
							MAD%	23.17	8.94
[KRI1962]	27	VLE PTxy	288 – 303	5.6 – 10.3	0 – 0.19	0 – 0.21	**N calc**	7	7
							AAD%	13.82	13.38
							Bias%	1.38	-13.38
							MAD%	32.09	40.78
[MUI1965]	4	VLE PTxy	273	5.5 – 12.0	0.039 – 0.29	0.24 – 0.38	**N calc**	3	3
							AAD%	15.01	2.69
							Bias%	15.01	-2.69
							MAD%	19.66	3.23
[SOM1978]	39	VLE PTxy	270	3.2 – 12.3	0 – 0.35	0 – 0.42	**N calc**	33	33
							AAD%	12.77	8.48
							Bias%	9.37	-7.79
							MAD%	30.80	42.70
[SON1962]	64	SVE PTy	140 – 190	0.51 – 10.1		0.92 – 1	**N calc**		64
							AAD%		0.05
							Bias%		-0.04
							MAD%		0.29
[SON1963]	72	SVE PTy	140 – 190	5.07 – 20.3		0.95 – 1	**N calc**		72
							AAD%		0.08
							Bias%		-0.07
							MAD%		0.31
[TSI1946]	7	SVE PTy	273	392 – 686	0.05 – 0.19	0.15 – 0.57			

[WEB1984]	6	VLE PTxy	223 – 273	5.0 – 10.0	0.03 – 0.16	0.21 – 0.8	**N calc**	6	6
							AAD%	8.50	3.27
							Bias%	4.65	-3.21
							MAD%	14.71	12.10
[WIL1977]	7	VLE PTy	221 – 265	1.4 – 13.4		0.5	**N calc**		6
							AAD%		4.95
							Bias%		-4.95
							MAD%		9.45
[XU1992a]	20	VLE PTxy	288 – 293	5.1 – 9.7	0 – 0.15	0 – 0.2	**N calc**	14	14
							AAD%	11.74	6.74
							Bias%	11.71	-5.44
							MAD%	32.66	17.04
[XU1992b]	12	VLE PTxy	298	6.5 – 8.4	0 – 0.064	0 – 0.07	**N calc**	6	6
							AAD%	22.04	8.06
							Bias%	22.04	-4.89
							MAD%	32.94	16.61
[YAK1975]	29	SLE PTx	78 – 115	3.6 – 9.12	~1		**N calc**	29	
							AAD%	<0.001	
							Bias%	<0.001	
							MAD%	<0.001	
[YOR1970]	16	VLE PTxy	273	3.5 – 11.8	0 – 0.3	0 – 0.4	**N calc**	14	14
							AAD%	14.06	9.33
							Bias%	5.00	-0.94
							MAD%	42.20	31.43
[YOR1985]	36	VLE PTxy	273 – 298	4.5 – 12.0	0.02 – 0.3	0.06 – 0.4	**N calc**	26	26
							AAD%	13.05	5.61
							Bias%	10.76	-5.56
							MAD%	27.22	18.86
	2	CP PTx	273 – 293	9.8 – 12.0	0.14 – 0.3		**N calc**	2	2
							AAD%	6.88	27.06
							Bias%	3.58	27.06
							MAD%	10.46	37.35
[YUC1999]	22	VLE PTxy	240 – 270	1.3 – 13.0	0 – 0.25	0 – 0.7	**N calc**	18	10
							AAD%	15.31	12.82
							Bias%	-6.74	-12.79
							MAD%	38.07	50.52
[ZEC1985]	6	VLE PTxy	223 – 273	5.0 – 10.0	0.03 – 0.16	0.2 – 0.8	**N calc**	6	6
							AAD%	8.50	3.27
							Bias%	4.65	-3.21
							MAD%	14.71	12.10
[ZEN1963]	31	VLE PTxy	218 – 273	1.3 – 13.9	0.009 – 0.3	0.2 – 0.85	**N calc**	31	30
							AAD%	9.53	3.46
							Bias%	2.09	-2.77
							MAD%	45.12	16.21

1.8 N_2+H_2

The literature data for the system N_2+H_2 are shown in Figure F.25.

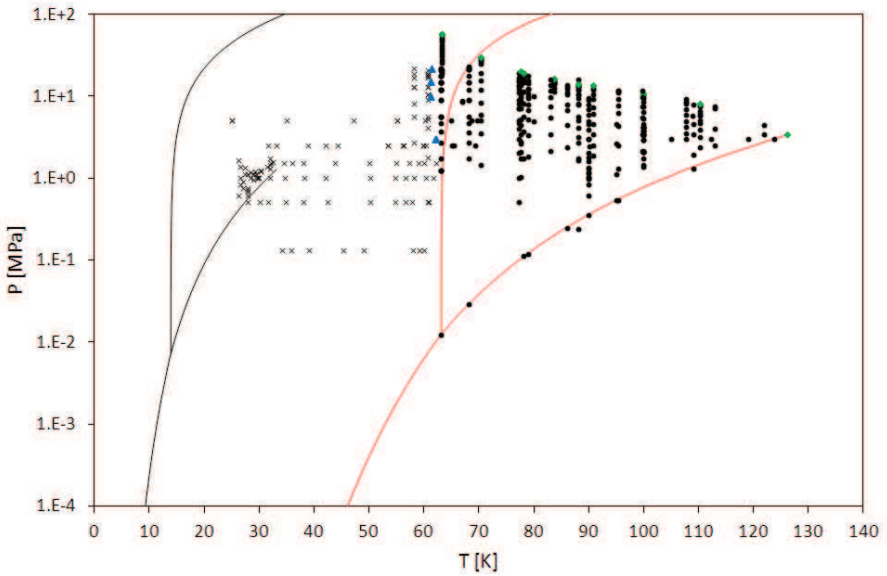

Figure F.25: Available experimental values for the system N_2+H_2. — : N_2; — : H_2; ● : FFE data; × : SFE data; ♦ : CP data; ▲ : SVLE data.

The qualitative comparison between model and SVE data is portrayed in Figure F.26. In Figure F.26, the *y*-axis is the pressure while the *x*-axis is the logarithm of the H_2 mole fraction in the vapor phase. Filled points (squares and circles) are experimental values from [DOK1955], empty ones represent experimental values from [VER1931]. The model is only qualitatively representative of data, and deviations mainly increase in the high pressure region.

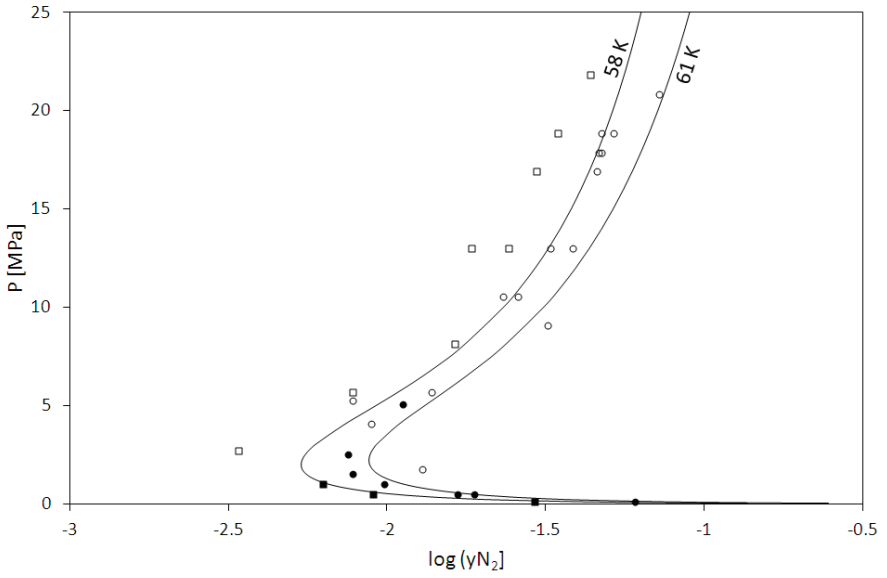

Figure F.26: SVE for the system N_2+H_2.
Experimental values: 58 K : ■ [DOK1955], □ [VER1931]; 61 K : ● [DOK1955], ○ [VER1931]; — : SLV EoS.

Figure F.27 show the qualitative comparison between VLE data and model at 90 K, 95 K, and 100 K.

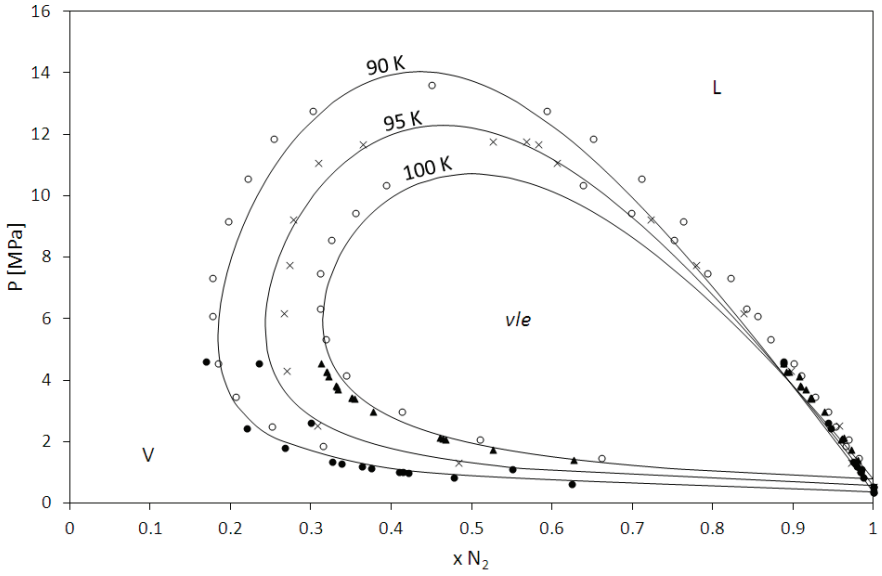

Figure F.27: VLE for the system N_2+H_2 at 90 K, 95 K, and 100 K. ● : [MAI1961]; ○ : [STR1978]; × : [GON1939a]; ▲ : [XIA1990]; — : SLV EoS.

According to Figure F.27, calculated values are qualitatively representative of the experimental values, and the deviations occur in both the liquid vapor branches.

Table F.8 gives the quantitative comparison between data and values calculated from the SLV EoS in terms of equilibrium mole fractions of N_2.

With reference to the VLE, the AAD% for the compositions in the liquid (x) and in the vapor (y) phases is generally lower than 10%. Higher deviations are usually related to the vapor phase. The highest deviations have been found with respect to the experimental values from [AUG1957].

The model is not in a quantitative agreement with SVE and SLE experimental values.

Table F.8: Quantitative comparison of equilibrium compositions for the system N_2+H_2.

xH_2+(1-x)N_2 Ref.	N	Kind of data	T K	P MPa	*x*	*y*		FLASH xN_2	FLASH yN_2
[AUG1957]	13	VLE PTxy	67 – 78	1.7 – 17.8	0.035 – 0.47	0.84 – 0.97	**N calc**	7	10
							AAD%	6.32	39.50
							Bias%	-0.35	38.24
							MAD%	17.92	85.22
[DOK1955][1]	62	SVE PTy	25 – 62	0.13 – 5.1		0.94 – 1	**N calc**		62
							AAD		0.70
							Bias		0.70
							MAD		23.17
	7	VLE PTy	65 – 70	2.3 – 5.1		0.97 – 0.98	**N calc**		7
							AAD%		10.55
							Bias%		8.30
							MAD%		17.5
[EUB1957]	16	VLE PTxy	83 – 122	2.2 – 15.9	0.026 – 0.46	0.08 – 0.9	**N calc**	15	15
							AAD%	2.79	5.83
							Bias%	-2.79	4.62
							MAD%	5.52	11.19
[GON1939a]	40	VLE PTxy	79 – 109	0.12 – 17.8	0 – 0.46	0 – 0.94	**N calc**	34	31
							AAD%	3.15	9.80
							Bias%	-2.95	2.28
							MAD%	9.50	40.11
[KNA1976]	5	VLE PTx	90 – 124	3		0 – 0.78	**N calc**	4	
							AAD%	2.89	
							Bias%	-2.89	
							MAD%	7.832	

[KRE1983a]	2	VLE PTxy	80	5 – 10	0.11 – 0.23	0.89 – 0.92	**N calc**	2	2
							AAD%	2.97	7.39
							Bias%	-2.97	7.39
							MAD%	3.61	8.21
[MAI1961]	17	VLE PTxy	90 – 95	0.36 – 4.6	0 – 0.11	0 – 0.83	**N calc**	11	15
							AAD%	0.54	1.05
							Bias%	-0.54	1.00
							MAD%	1.37	4.56
[OMA1962a][1]	30	SLE PTx	26 – 33	0.61 – 1.7	~1.0		**N calc**	29	
							AAD	9.72	
							Bias	9.72	
							MAD	40.49	
[STE1939]	23	VLE PTxy	90 – 113	1.6 – 9.6	0.04 – 0.39	0.19 – 0.83	**N calc**	19	19
							AAD%	1.69	3.61
							Bias%	-1.44	-1.71
							MAD%	8.54	9.77
[STR1978]	77	VLE PTxy	63 – 110	1.0 – 57.2	0.018 – 0.54	0.25 – 0.97	**N calc**	61	60
							AAD%	4.96	7.25
							Bias%	-4.92	3.86
							MAD%	18.12	33.89
	8	CP PTx	63 – 126	3.4 – 58.0	0 – 0.62		**N calc**	6	6
							AAD%	12.76	14.23
							Bias%	-12.76	-14.23
							MAD%	16.28	15.62
[VER1931][2]	66	VLE	63 – 88	0.01 – 22.7	0 – 0.55	0 – 0.99	**N calc**	45	42
							AAD%	4.97	14.42
							Bias%	-4.28	4.94
							MAD%	13.56	37.80
	2	CP PTx	78 – 88	14.0 – 19.4	0.53 – 0.58		**N calc**	2	2
							AAD%	20.10	19.06
							Bias%	-20.10	-19.06
							MAD%	21.30	19.97
	12	SVLE PT	61 – 62	3.0 – 21.8			**N calc**	12	3
							AAD%	0.36	15.21
							Bias%	0.36	15.21
							MAD%	0.52	27.28
	23	SVE PTy	58 – 61	1.8 – 21.8		0.93 – 1	**N calc**		23
							AAD%		30.02
							Bias%		30.02
							MAD%		77.39
[XIA1990]	16	VLE	100	1.4 – 4.6	0.02 – 0.12	0.37 – 0.69	**N calc**	16	16
							AAD%	0.86	3.35
							Bias%	-0.86	3.35
							MAD%	2.09	4.64
[YOR1968a]	12	VLE	77	0.5 – 15.2	0.02 – 0.36	0.75 – 0.93	**N calc**	11	12
							AAD%	2.54	6.92
							Bias%	-1.38	-3.09
							MAD%	6.84	12.82
[YOR1971a]	17	VLE	77 – 88	1.7 – 19.0	0.049 – 0.47	0.62 – 0.94	**N calc**	16	16
							AAD%	2.47	12.59
							Bias%	-2.12	11.97
							MAD%	5.59	21.08

[1] – for SVE PTy or SLE PTx data deviations are in terms of AAD, Bias, and MAD.

[2] - – for SVLE PT data, column xN_2 (yN_2) contains the deviations between calculated and experimental temperatures (pressures) at fixed pressures (temperatures).

1.9 N_2+N_2O

The literature data for the system N_2+N_2O are shown in Figure F.28.

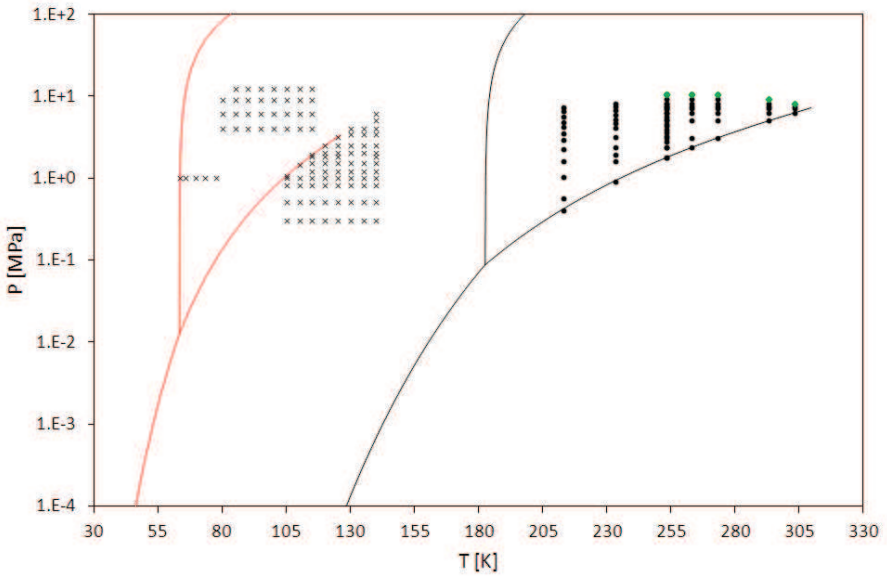

Figure F.28: Available experimental values for the system N_2+N_2O.
— : N_2; — : N_2O; ● : FFE data; × : SFE data; ♦ : CP data.

The qualitative comparison between model and SVE/SLE data is portrayed in Figure F.29. In Figure F.29, the *y*-axis is the logarithm of the N_2O mole fraction in either the vapor or the liquid phase. Filled circles are SVE experimental values from [YAK1976], while empty ones represent SLE experimental values from [IOM1976].

The vertical lines in Figure F.29 are placed at the s_2l_1ve pressure, where 1 and 2 are N_2 and N_2O, respectively. The s_2l_1ve ends in an upper critical endpoint close to the critical point of pure N_2, so that for higher temperatures (T > 130 K) the s_2l_1e disappears and only the s_2ve occurs.

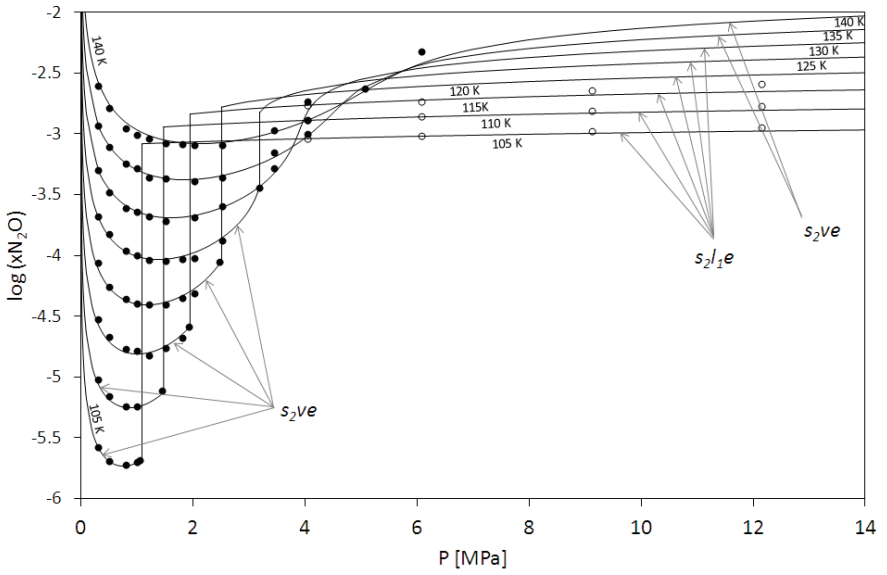

Figure F.29: SVE and SLE for the system N_2+N_2O.
● : [YAK1976]; ○ : [IOM1976]; — : SLV EoS.

The pressure-composition cross sections in Figure F.30 show the qualitative comparison between VLE data and model at 213 K, 233 K, and 253 K.

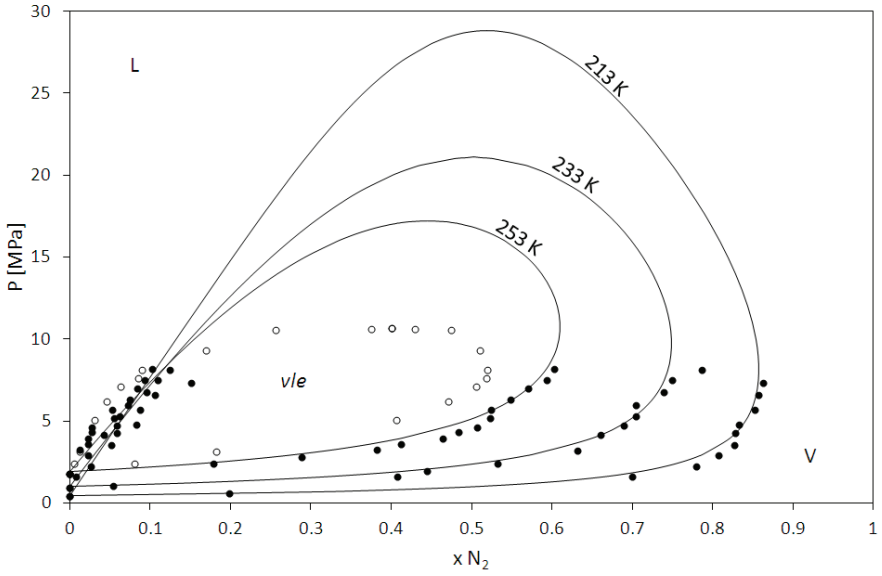

Figure F.30: VLE for the system N_2+N_2O at 213 K, 233 K, and 253 K. ● : [ZEI1972]; ○ : [KOS1984]; — : SLV EoS. Data from [KOS1984] are at 253 K.

According to Figure F.30, calculated values are qualitatively representative of the experimental values. Data from [ZEI1972] and [KOS1984] do not agree at 253 K, and since the model agrees better with respect to data from [ZEI1972], higher deviations are encountered with respect to the experimental values from [KOS1984], as shown in Table F.9.

Table F.9 gives the quantitative comparison between data and values calculated from the SLV EoS in terms of equilibrium mole fractions of N_2. With reference to the VLE, higher deviations are usually related to the liquid phase.

With reference to Figure F.29 and the deviations related to SVE and SLE data in Table F.9, it is possible to state that model is in a good agreement with experimental values. It is worth remembering that SVE and SLE are the main equilibria involved in an air distillation unit considering the system N_2+CO_2.

Table F.9: Quantitative comparison of equilibrium compositions for the system N_2+N_2O.

xN_2+(1-x)N_2O Ref.	N	Kind of data	T K	P MPa	*x*	*y*		FLASH xN_2	FLASH yN_2
[IOM1976]	31	SLE PTx	80 – 115	4.1 – 12.2	~1		**N calc**	31	
							AAD%	0.98	
							Bias%	-0.98	
							MAD%	1.00	
[KOS1984]	40	VLE PTxy	253 – 303	1.8 – 10.7	0 – 0.4	0 – 0.52	**N calc**	34	34
							AAD%	57.36	29.90
							Bias%	39.26	27.58
							MAD%	127.1	91.67
	5	CP PTx	253 – 303	8.1 – 10.7	0.05 – 0.4		**N calc**	5	5
							AAD%	40.63	31.18
							Bias%	40.63	-16.17
							MAD%	89.93	46.26
[WOJ1975]	5	SLE Tx	64 – 77		~1		**N calc**	5	
							AAD%	0.002	
							Bias%	-0.002	
							MAD%	0.005	
[YAK1976]	70	SVE PTy	105 – 140	0.3 – 6.0		~1	**N calc**		70
							AAD%		1.86
							Bias%		1.67
							MAD%		7.55

[ZEI1972]	38	VLE PTxy	213 – 253	0.4 – 8.2	0 – 0.15	0 – 0.86	**N calc**	38	38
							AAD%	25.67	5.53
							Bias%	14.21	14.21
							MAD%	97.00	25.21

1.10 N_2+CH_4

The literature data for the system N_2+CH_4 are shown in Figure F.31.

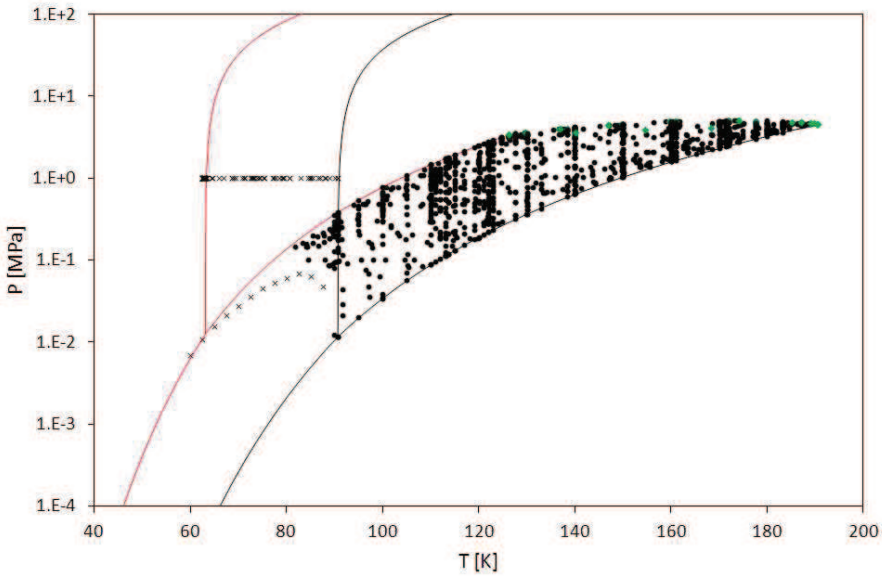

Figure F.31: Available experimental values for the system N_2+CH_4.
— : N_2; — : CH_4; ● : FFE data; × : SFE data; ♦ : CP data.

The qualitative comparison between model and SLE data is portrayed in Figure F.32. According to [OMA1962b], the eutectic temperature is about 62.5 K, while compositions of the $solid_2$ and liquid phases are 0.46, 0.8, and 0.31 in N_2 mole fraction, respectively, whereas the value associated to the $solid_1$ has not been specified by the author.

Calculated compositions are 0.43, 0.83, and 0.87. The eutectic temperature from the SLV EoS is 61.24 K, thus the eutectic temperature is 1 K lower than the experimental value. The calculated liquidus line in equilibrium with solid phase s_2 is in a good agreement with the experimental values, however the $s_1$le is calculated at lower temperature than the experimental value from [OMA1962a]. The model is not representative of the experimental data from [FED1938].

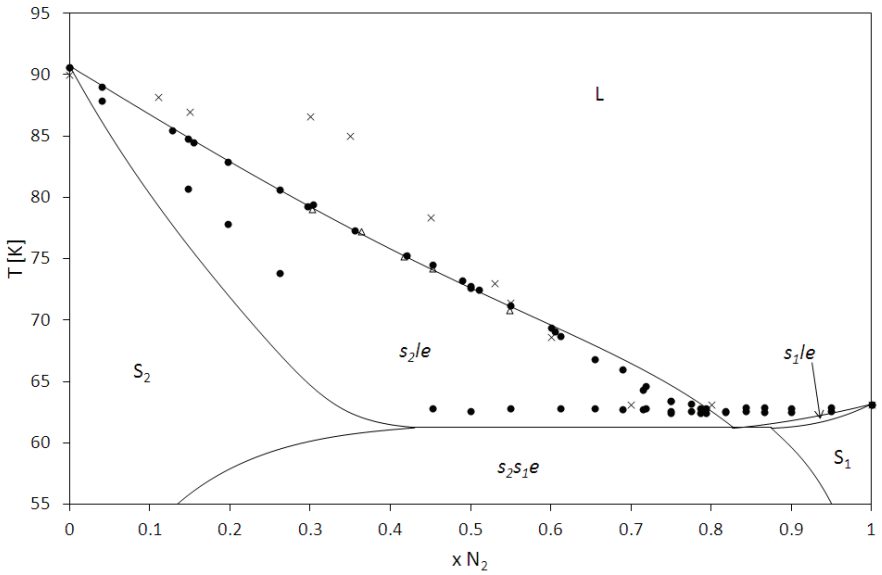

Figure F.32: SLE for the system N_2+CH_4.
● : [OMA1962b]; Δ : [FAS1941] ; × : [FED1938] ; — : SLV EoS.

The pressure-composition cross sections in Figure F.33 show the qualitative comparison between VLE data and model from 91 K up to 114 K.

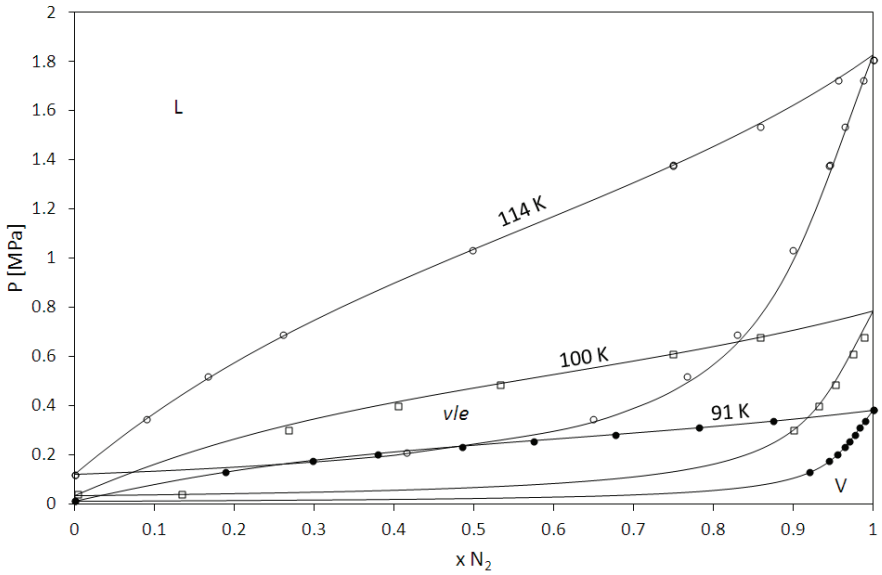

Figure F.33: VLE for the system N_2+CH_4 at 91 K, 100 K, and 114 K.
● : [MCCT1976]; □ : [HAN2012]; ○ : [STR1974a]; — : SLV EoS.

Table F.10 gives the quantitative comparison between data and values calculated from the SLV EoS in terms of equilibrium mole fractions of N_2. With reference to the VLE, the AAD% for both compositions in the liquid (x) and in the vapor (y) phases is lower than 10% for all the references, except for the data presented in [MCT1919] and [TOR1939].

Table F.10: Quantitative comparison of equilibrium compositions for the system N_2+CH_4.

xN_2+(1-x)CH_4 Ref.	N	Kind of data	T K	P MPa	*x*	*y*		FLASH xN_2	FLASH yN_2
[BLO1953]	220	VLE PTx PTy	91 – 189	0.06 – 5.1	0.03 – 0.95	0.03 – 0.95	**N calc**	90	115
							AAD%	3.40	5.56
							Bias%	1.13	0.55
							MAD%	16.17	54.39
	10	CP PTx	130 – 191	3.6 – 5.1	0 – 0.95		**N calc**	9	9
							AAD%	10.06	27.78
							Bias%	10.06	24.45
							MAD%	19.06	79.53
[BLO1955]	32	VLE PTx PTy	113 – 173	0.69 – 3.4	0.1 – 0.3	0.1 – 0.3	**N calc**	16	15
							AAD%	2.32	3.85
							Bias%	-0.62	-2.75
							MAD%	8.72	12.09
[BRA1958]	9	VLE PTxy	137 – 175	3.4	0.05 – 0.8	0.13 – 0.84	**N calc**	9	9
							AAD%	8.23	3.32
							Bias%	5.23	2.41
							MAD%	19.53	11.41
[CHA1966]	10	VLE PTxy	171	2.8 – 5.1	0.04 – 0.33	0.09 – 0.4	**N calc**	9	9
							AAD%	7.61	5.58
							Bias%	-0.13	-3.23
							MAD%	19.76	9.15
[CHA1967]	28	VLE PTxy	122 – 171	0.35 – 5.0	0 – 0.99	0 – 0.99	**N calc**	25	26
							AAD%	11.56	10.17
							Bias%	10.22	8.46
							MAD%	32.78	37.35

[CHE1964]	20	VLE PTxy	92 – 124	0.02 – 0.56	0.01 – 0.15	0.1 – 0.86	**N calc**	20	20
							AAD%	9.39	12.21
							Bias%	-4.08	8.80
							MAD%	54.70	34.15
[CIN1953]	28	VLE PTxy	122	0.3 – 2.53	0.021 – 0.94	0.25 – 0.98	**N calc**	28	28
							AAD%	3.44	2.40
							Bias%	-2.43	1.99
							MAD%	14.43	11.61
[COS1959]	9	VLE PTxy	137 – 175	3.45	0.054 – 0.8	0.13 – 0.84	**N calc**	9	9
							AAD%	8.23	3.32
							Bias%	5.23	2.41
							MAD%	19.53	11.41
[FAS1941]	5	SLE Tx	71 – 80		0.31 – 0.55		**N calc**	5	
							AAD%	1.08	
							Bias%	0.15	
							MAD%	2.01	
[FAS1957a]	37	VLE PTxy	82 – 150	0.15 – 1.6	0.074 – 0.83	0.38 – 1	**N calc**	37	37
							AAD%	5.43	3.59
							Bias%	-0.36	-3.55
							MAD%	54.81	15.31
[FED1938]	12	SLE Tx	63 – 90		0 – 1		**N calc**	10	
							AAD%	26.30	
							Bias%	-22.69	
							MAD%	65.57	
[FON1989]	176	VLE PTxy	112 – 183	0.2 – 4.9	0 – 1	0.012 – 1	**N calc**	163	163
							AAD%	4.13	3.15
							Bias%	-0.42	-1.43
							MAD%	71.41	56.71
[FUK1967]	20	VLE PTx	84 – 91	0.09 – 0.24	0.14 – 0.67		**N calc**	20	
							AAD%	2.42	
							Bias%	-1.89	
							MAD%	4.78	
[HAN2012]	83	VLE PTxy	100 – 123	0.04 – 2.9	0 – 1	0 – 1	**N calc**	69	69
							AAD%	7.79	1.52
							Bias%	-7.58	-1.14
							MAD%	16.09	7.05
[JAN2007]	27	VLE PTxy	130 – 180	0.58 – 5.1	0.02 – 0.59	0.09 – 0.7	**N calc**	25	15
							AAD%	4.69	2.43
							Bias%	3.77	1.44
							MAD%	15.21	12.78
[JON1963]	6	CP Tx	126 – 190		0 – 1		**N calc**	4	
							AAD%	3.81	
							Bias%	3.81	
							MAD%	4.49	
[KID1975a]	91	VLE PTxy	112 – 180	0.1 – 4.9	0 – 0.9	0 – 0.94	**N calc**	81	81
							AAD%	4.17	3.02
							Bias%	0.56	-1.62
							MAD%	22.62	25.66
[KRE1982]	34	VLE PTxy	140 – 160	0.64 – 4.9	0 – 0.79	0 – 0.79	**N calc**	29	29
							AAD%	1.69	1.21
							Bias%	0.16	-0.11
							MAD%	9.41	9.20
[KRE1983a]	4	VLE PTxy	120 – 144	1.5 – 4	0.27 – 0.73	0.66 – 0.9	**N calc**	4	4
							AAD%	2.51	0.56
							Bias%	-1.44	0.21
							MAD%	5.02	1.24

[LIU1988]	10	VLE PTxy	123	0.4 – 2.6	0.05 – 0.91	0.43 – 0.97	**N calc**	10	10
							AAD%	1.32	0.53
							Bias%	0.75	0.36
							MAD%	3.10	2.60
[MCC1976]	10	VLE PTxy	91	0.012 – 0.38	0 – 1	0 – 1	**N calc**	8	8
							AAD%	1.78	0.08
							Bias%	-1.61	0.07
							MAD%	2.86	0.23
[MCT1919]	7	VLE PTxy	85 – 107	0.1	0.05 – 0.67	0.13 – 0.85	**N calc**	7	7
							AAD%	65.41	59.40
							Bias%	-65.41	59.40
							MAD%	75.29	185.68
[MIL1973]	22	VLE PTx PTy	112	0.19 – 1.3	0.034 – 0.78	0.45 – 0.96	**N calc**	11	11
							AAD%	2.68	0.38
							Bias%	-2.62	0.34
							MAD%	14.12	0.75
[OMA1962b][1]	59	SLE Tx	62 – 91		0 – 1		**N calc**	33	
							AAD%	7.02	
							Bias%	-3.92	
							MAD%	39.72	
	12	SVLE PT	60 – 88	0 – 0.07			**N calc**	10	12
							AAD%	0.84	5.61
							Bias%	-0.34	2.70
							MAD%	2.18	10.72
[PAR1974a]	60	VLE PTxy	95 – 120	0.02 – 2.5	0 – 1	0 – 1	**N calc**	48	48
							AAD%	0.98	0.46
							Bias%	-0.66	0.46
							MAD%	3.05	1.12
[ROZ1988]	49	VLE PTy	133 – 180	0.66 – 4.4		0.068 – 0.4	**N calc**		46
							AAD%		11.65
							Bias%		-8.43
							MAD%		34.04
[SKR1970]	16	VLE PTx PTy	113	0.11 – 1.8	0 – 1	0 – 1	**N calc**	6	6
							AAD%	4.71	20.78
							Bias%	-0.50	20.78
							MAD%	12.63	86.90
[SPR1966]	11	VLE PTxy	91	0.012 – 0.38	0 – 1	0 – 1	**N calc**	9	9
							AAD%	7.35	0.13
							Bias%	-7.32	-0.09
							MAD%	12.75	0.27
[STR1972b]	23	VLE PTxy	134 – 122	0.12 – 2.78	0 – 1	0 – 1	**N calc**	19	19
							AAD%	0.78	1.42
							Bias%	-0.21	1.41
							MAD%	3.66	6.38
[STR1974a]	116	VLE PTxy	114 – 182	0.12 – 5	0 – 1	0 – 1	**N calc**	94	95
							AAD%	3.82	2.62
							Bias%	-0.07	-0.79
							MAD%	47.15	46.82
	8	CP PTx	126 – 183	3.4 – 5	0.23 – 1		**N calc**	6	6
							AAD%	7.49	14.64
							Bias%	7.49	-2.54
							MAD%	13.06	31.05
[TOR1939]	50	VLE PTxy	90 – 133	0.012 – 2.5	0 – 1	0 – 1	**N calc**	32	27
							AAD%	84.95	18.14
							Bias%	84.95	17.67
							MAD%	263.07	56.01

[WIL1975]	16	VLE PTx	111	0.097 – 1.53	0 – 1	0 – 1	**N calc**	14
							AAD%	4.50
							Bias%	-4.50
							MAD%	11.42

[1] – for SVLE PT data, column xN_2 (yN_2) contains the deviations between calculated and experimental temperatures (pressures) at fixed pressures (temperatures).

1.11 N_2+C_2H_6

The literature data for the system N_2+C_2H_6 are shown in Figure F.34.

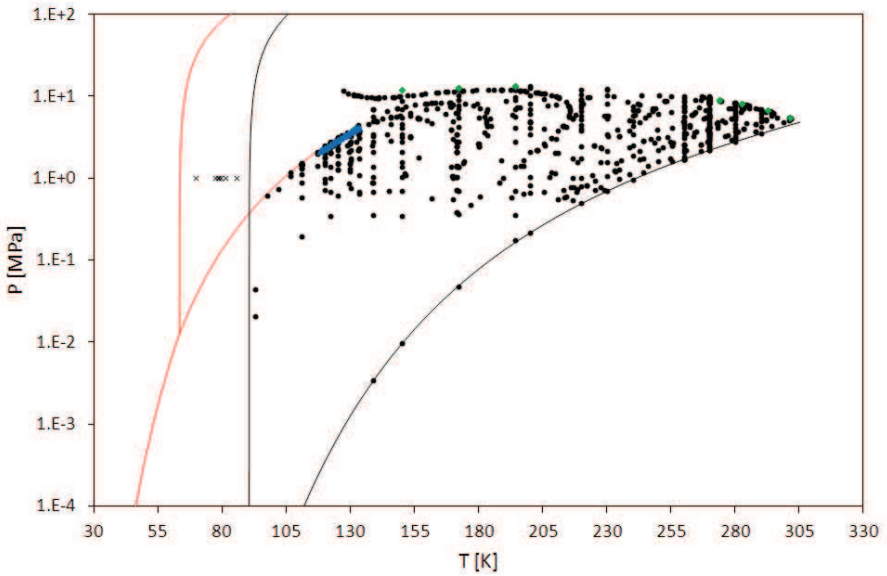

Figure F.34: Available experimental values for the system N_2+C_2H_6.
— : N_2; — : C_2H_6; ● : FFE data; × : SFE data; ♦ : CP data; ▲ : VLLE data.

The qualitative comparison between model and SLE data is portrayed in Figure F.35. Experimental values are from [SZC1980] (filled circles) and [COX1950] (open circles). In Figure F.35, the solid line is the mole fraction of N_2 in the phase liquid$_1$ along the solid$_2$-liquid$_1$-vapor three phase line, where 1 and 2 are related to N_2 and C_2H_6, respectively. This line extends between two Quadruple Points (QP): QP_1 is the solid$_2$-solid$_1$-liquid$_1$-vapor equilibrium calculated at about 63 K; QP_2 is the solid$_2$-liquid$_2$-liquid$_1$-vapor equilibrium calculated at about 87 K. Green points in Figure F.35 represent the composition of the phase liquid$_1$ at the QP_1 and the QP_2. With reference to Figure F.35, model agrees more with data from [SZC1980].

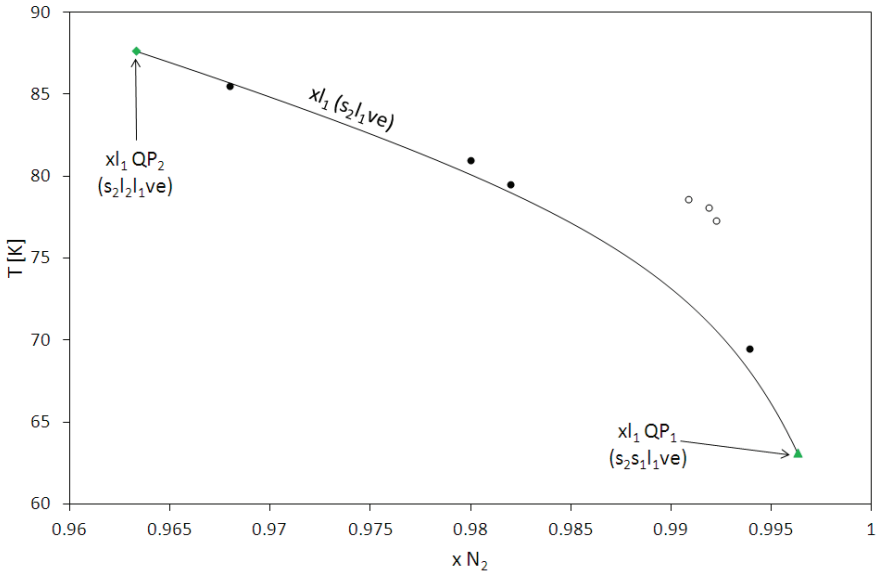

Figure F.35: SLE for the system N_2+C_2H_6.
● : [SZC1980]; ○ : [COX1950] — : SLV EoS; ♦ : xl_1 at $s_2l_2l_1ve$; ▲ : xl_1 at $s_2s_1l_1ve$.

The pressure-composition cross sections in Figure F.36 show the qualitative comparison between VLE data and model at 111 K, 120 K, and 130 K. Immiscibility in the liquid phase occurs at these temperatures, and in Figure F.36 the immiscibility gap is indicated by the red dashed lines. N_2 becomes supercritical at 130 K, and a l_1=v critical point occurs at a pressure slightly greater than the pressure of liquid$_2$-liquid$_1$-vapor equilibrium. In Figure F.36 , the l_1=v critical point is the green triangle.

Calculated values are in agreement with experimental values, however deviations are mainly concentrated in the liquid$_2$ phase at 111 K. Furthermore, the calculated pressure of $l_2l_1$ve is usually higher than the experimental value at 111 K and 120 K.

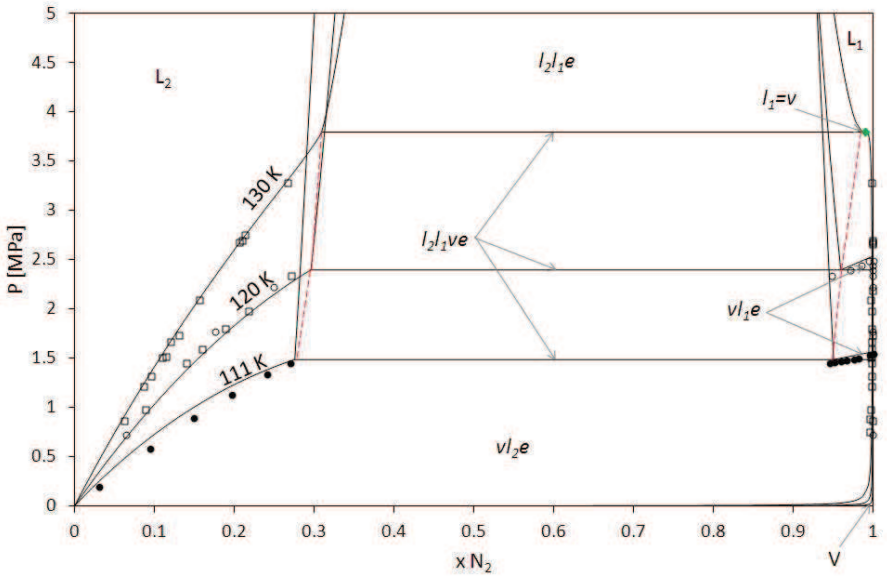

Figure F.36: VLE for the system N_2+C_2H_6 at 91 K, 100 K, and 114 K. ● : [WIL1975]; ○ : [KRE1982]; □ : [RAA2004]; ♦ : critical point (l_1=v); — : SLV EoS; – – : l_2l_1 immiscibility gap.

Table F.11 gives the quantitative comparison between data and values calculated from the SLV EoS in terms of equilibrium mole fractions of N_2. With reference to the VLE, the AAD% for both compositions in the liquid (x) and in the vapor (y) phases is lower than 10% for all the references, except for the data presented in [CHA1966], [CHA1966], and [CHE1964]. A value of about 20% for the AAD% is obtained by evaluating the critical composition at the experimental critical temperatures from [EAK1955].

The errors between model and VLLE data from [KRE1982] have been calculated in the following manner: in the column xN_2 errors are deviations in terms of mole fractions in all the three phases (xl_1,xl_2, xv) at fixed temperature; conversely, in the column yN_2 errors are deviations in terms of mole fractions in same phases (xl_1,xl_2, xv) at fixed pressure.

Table F.11: Quantitative comparison of equilibrium compositions for the system N_2+C_2H_6.

$xN_2+(1-x)C_2H_6$ Ref.	N	Kind of data	T K	P MPa	x	y		FLASH xN_2	FLASH yN_2
[BRO1989b]	33	VLE PTxy	220 – 270	0.5 – 12	0 – 0.41	0 – 0.83	**N calc**	30	31
							AAD%	4.33	2.92
							Bias%	-0.30	0.42
							MAD%	18.22	12.80
[CHA1966]	11	VLE PTxy	171	0.38 – 3.4	0.02 – 0.12	0.57 – 0.94	**N calc**	11	10
							AAD%	26.50	10.77
							Bias%	-8.31	10.77
							MAD%	54.97	55.77

[CHA1967]	20	VLE PTxy	122 – 171	0.34 – 3.4	0.025 – 0.97	0.57 – 1	**N calc**	17	16
							AAD%	21.70	6.31
							Bias%	-3.89	6.31
							MAD%	54.97	55.77
[CHE1964]	2	VLE PTx	93	0.02 – 0.045	0 – 0.01		**N calc**	2	2
							AAD%	13.50	
							Bias%	-13.50	
							MAD%	14.72	
[COS1959]	3	VLE PTxy	144 – 200	3.4 – 6.9	0.1 – 0.21	0.89 – 0.99	**N calc**	3	3
							AAD%	1.32	0.27
							Bias%	0.18	-0.18
							MAD%	2.24	0.55
[COX1950]	3	SLE Tx	77.3 – 78.6		0.99 – 1		**N calc**	3	
							AAD%	0.81	
							Bias%	-0.81	
							MAD%	0.84	
[EAK1955]	319	VLE PTx PTy	102 – 302	0.53 – 11.98	0.05 – 0.98		**N calc**	93	298
							AAD%	5.19	3.44
							Bias%	-1.04	-0.18
							MAD%	33.36	45.39
	6	LLE PTx	98 – 128	0.61 – 3.42	0.2 – 0.32		**N calc**	6	
							AAD%	7.70	
							Bias%	-1.35	
							MAD%	13.84	
	5	CP PTx	132 – 302	4.0 – 9.1	0.05 – 0.98		**N calc**	4	4
							AAD%	18.38	7.97
							Bias%	18.38	7.97
							MAD%	21.72	8.95
[GRA1977a]	35	VLE PTxy	200 – 290	0.2 – 13.2	0 – 0.57	0 – 0.91	**N calc**	31	31
							AAD%	6.51	2.45
							Bias%	-1.28	-1.03
							MAD%	17.40	8.53
[GUP1980]	67	VLE PTxy	260 – 280	1.7 – 9.9	0 – 0.37	0 – 0.57	**N calc**	57	52
							AAD%	7.66	6.32
							Bias%	2.11	-5.29
							MAD%	36.61	39.49
[JAN2007]	24	VLE PTxy	150 – 270	0.56 – 10.1	0.02 – 0.36	0.23 – 0.99	**N calc**	24	22
							AAD%	4.44	1.54
							Bias%	-2.74	-1.40
							MAD%	10.24	6.78
[KOH1984]	15	VLLE PTx	118 – 131	2.1 – 4.0	0.27 – 0.96		**N calc**	13	13
							AAD%	3.64	3.45
							Bias%	3.34	3.11
							MAD%	10.21	9.94
[KRE1982]	21	VLE PTxy	120 – 133	0.64 – 3.6	0.04 – 0.99	1	**N calc**	17	17
							AAD%	2.73	0.04
							Bias%	1.32	0.04
							MAD%	8.37	0.11
	4	VLLE PTxy	120 – 133	2.3 – 4.1	0.27 – 0.98	0.99 – 1	**N calc**	3	3
							AAD%	3.02	2.84
							Bias%	3.02	2.84
							MAD%	9.54	9.14
[RAA2004]	31	VLE PTxy	120 – 139	0.6 – 3.3	0.04 – 0.27	~1	**N calc**	25	27
							AAD%	3.25	0.12
							Bias%	1.43	0.08
							MAD%	8.01	0.35

[ROZ1988]	59	VLE PTy	177 – 281	0.47 – 7.2		0.14 – 0.82	**N calc**		59
							AAD%		4.99
							Bias%		-4.34
							MAD%		25.38
[STR1974b]	49	VLE PTxy	139 – 194	0.003 – 13.4	0 – 0.65	0 – 0.99	**N calc**	45	45
							AAD%	3.91	0.88
							Bias%	-1.75	0.69
							MAD%	16.54	6.92
	3	CP PTx	150 – 194	11.9 – 13.5	0.67 – 0.71		**N calc**	3	3
							AAD%	2.19	2.13
							Bias%	0.46	0.41
							MAD%	2.58	3.65
[SZC1980]	4	SLE Tx	70 – 86		0.97 – 0.99		**N calc**	4	
							AAD%	0.10	
							Bias%	-0.08	
							MAD%	0.18	
[WIL1975]	15	VLE PTx	111	0.2 – 1.5	0 – 1		**N calc**	8	
							AAD%	7.29	
							Bias%	-7.29	
							MAD%	19.33	
[ZEC1985]	17	VLE PTxy	240 – 260	0.97 – 7.5	0 – 0.2	0 – 0.72	**N calc**	15	15
							AAD%	2.89	2.34
							Bias%	-1.56	-2.34
							MAD%	7.54	7.15

1.12 N_2+C_2H_4

The literature data for the system N_2+C_2H_4 are shown in Figure F.37.

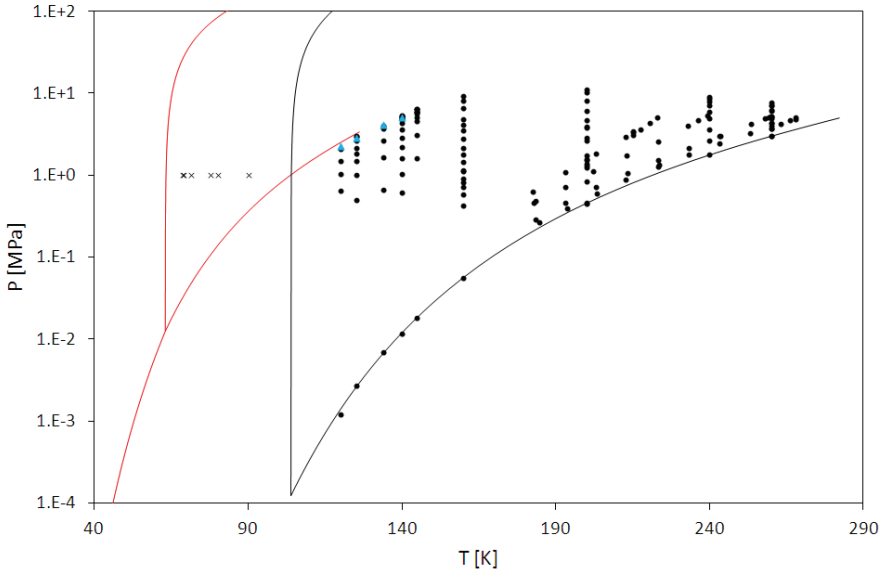

Figure F.37: Available experimental values for the system N_2+C_2H_4.
— : N_2; — : C_2H_4; ● : FFE data; × : SFE data; ▲ : VLLE data.

The qualitative comparison between model and SLE data is portrayed in Figure F.38. Experimental values are from [SZC1979] (filled circles) and [TSI1940] (open circles). In Figure F.38, the solid line is the mole fraction of N_2 in the phase liquid$_1$ along the solid$_2$-liquid$_1$-vapor three phase line, where 1 and 2 are related to N_2 and C_2H_4, respectively.

This line extends between two Quadruple Points (QP): QP_1 is the solid$_2$-solid$_1$-liquid$_1$-vapor equilibrium calculated at about 63 K; QP_2 is the solid$_2$-liquid$_2$-liquid$_1$-vapor equilibrium calculated at about 103 K. The green triangle in Figure F.38 represents the composition of the phase liquid$_1$ at the QP_1.

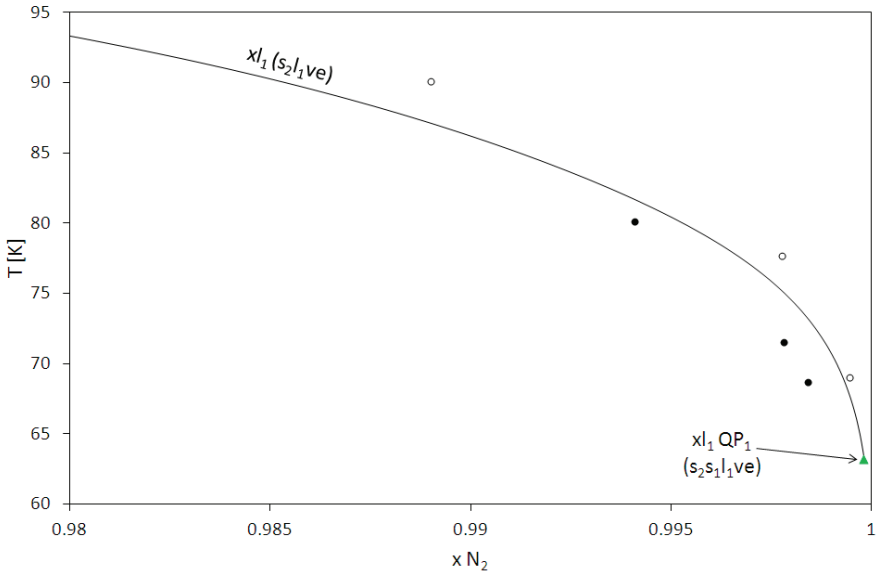

Figure F.38: SLE for the system N_2+C_2H_4.
● : [SZC1979]; ○ : [TSI1940] — : SLV EoS; ▲ : xl_1 at $s_2s_1l_1ve$.

The pressure-composition cross sections in Figure F.39 show the qualitative comparison between VLE data and model at 120 K, 125 K, and 134 K. Immiscibility in the liquid phase occurs at 120 K and 125 K, and in Figure F.39 the immiscibility gap is indicated by the red dashed lines. According to [GAS1981], a liquid$_2$-liquid$_1$-vapor equilibrium ($l_2l_1$ve) exists up to 140 K, where a critical point l_1=v occurs. N_2 becomes supercritical at 130 K, and the calculated upper critical endpoint is at 132 K, thus 8 K lower than the experimental value (140 K). As a consequence, at 134 K the model does not give a $l_2l_1$ve, as it can be observed in Figure F.39.

The calculated values of vapor-liquid$_2$ equilibrium (vl_2e) and of pressures of $l_2l_1$ve are in agreement with the experimental values at 120 K and 125 K.

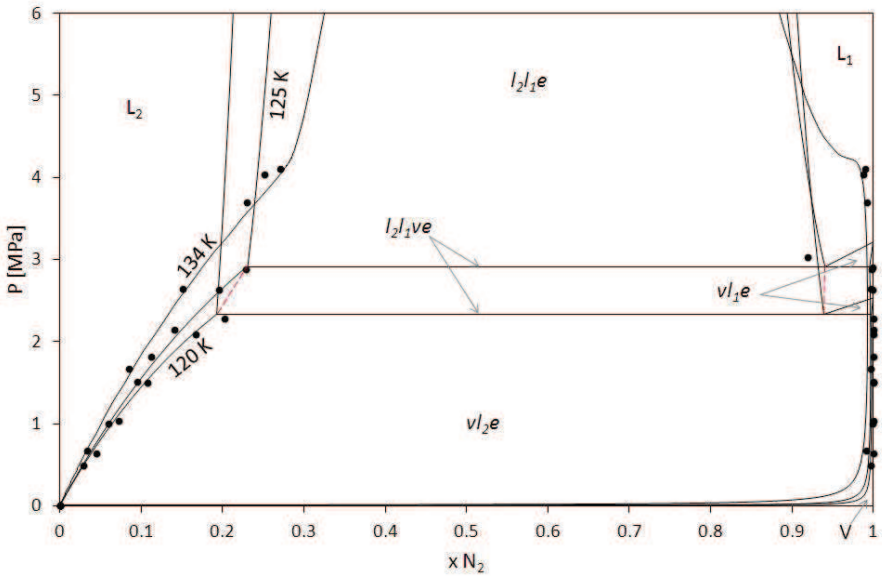

Figure F.39: VLE for the system N_2+C_2H_6 at 91 K, 100 K, and 114 K.
● : [GAS1981]; — : SLV EoS; – – : l_2l_1 immiscibility gap.

Table F.12 gives the quantitative comparison between data and values calculated from the SLV EoS in terms of equilibrium mole fractions of N_2. With reference to the VLE, the AAD% for both compositions in the liquid (x) and in the vapor (y) phases is lower than 13% for all the references.

The maximum MAD% in the vapor phase (27%) has been found at about 194 K and 0.4 MPa with respect to reference [ROZ1988]: the correspondent experimental and calculated values are yN_2 = 0.144 and yN_2 = 0.105, respectively.

The maximum MAD% in the liquid phase (56%) has been found at about 145 K and 6.4 MPa) with respect to reference [GAS1981]: the correspondent experimental and calculated values are xN_2 = 0.8 and xN_2 = 0.35, respectively.

Similarly to the case of data from [KRE1982] for the mixture N_2+C_2H_6, the errors between model and VLLE data from [GAS1981] have been calculated as follows: in the column xN_2 errors are deviations in terms of mole fractions in all the three phases (xl_1,xl_2, xv) at fixed temperature; conversely, in the column yN_2 errors are deviations in terms of mole fractions in same phases (xl_1,xl_2, xv) at fixed pressure.

Table F.12: Quantitative comparison of equilibrium compositions for the system N_2+C_2H_4.

xN_2+(1-x)C_2H_4 Ref.	N	Kind of data	T K	P MPa	*x*	*y*		FLASH xN_2	FLASH yN_2
[GAS1981]	75	VLE PTxy	120 – 200	0.01 – 9.3	0 – 0.8	0 – 1	**N calc**	50	51
							AAD%	7.77	0.73
							Bias%	-4.58	-0.66
							MAD%	56.02	10.40

[GAS1981]	4	VLLE PTxy	120 – 140	2.3 – 5	0.2 – 0.3	0.96 – 1	**N calc**	2	2
							AAD%	2.38	2.24
							Bias%	-0.90	-2.21
							MAD%	4.66	6.46
[GRA1977a]	15	VLE Ptxy	200 – 260	0.45 – 11	0 – 0.47	0 – 0.83	**N calc**	13	13
							AAD%	12.09	1.75
							Bias%	12.09	0.46
							MAD%	18.78	8.09
[ROZ1988]	44	VLE PTy	183 – 268	0.27 – 5.4		0.14 – 0.67	**N calc**		44
							AAD%		3.66
							Bias%		-2.67
							MAD%		27.22
[SZC1979]	3	SLE Tx	69 – 80		~1		**N calc**	3	
							AAD%	0.10	
							Bias%	0.10	
							MAD%	0.12	
[TSI1940]	3	SLE Tx	69 – 90		~1		**N calc**	3	
							AAD%	0.17	
							Bias%	-0.17	
							MAD%	0.38	
[ZEC1985]	17	VLE PTxy	240 – 260	1.8 – 9.1	0 – 0.28	0 – 0.54	**N calc**	15	15
							AAD%	11.37	1.39
							Bias%	11.37	-0.46
							MAD%	14.94	4.77

1.13 N_2+C_3H_8

The literature data for the system N_2+C_3H_8 are shown in Figure F.40.

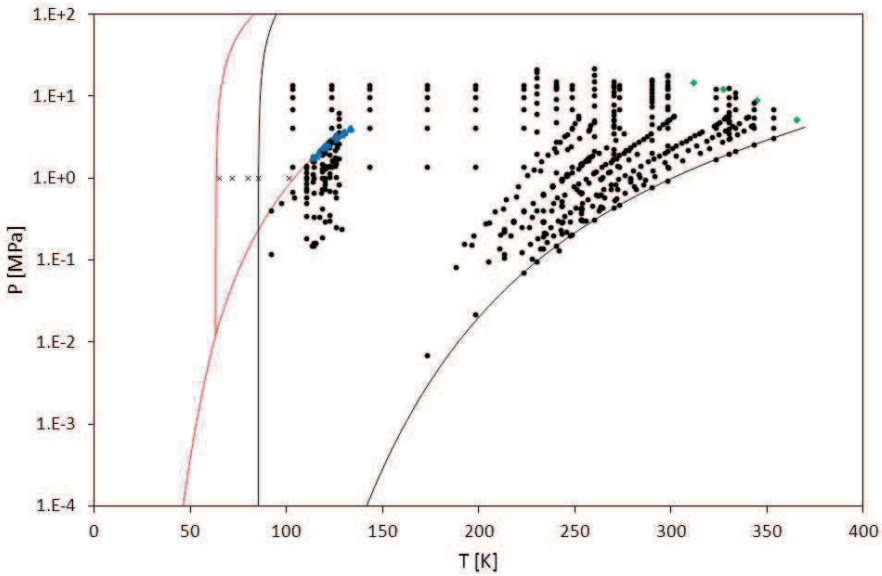

Figure F.40: Available experimental values for the system N_2+C_3H_8. — : N_2; — : C_3H_8; ● : FFE data; × : SFE data; ♦ : CP data; ▲ : VLLE data.

The qualitative comparison between model and SLE data is portrayed in Figure F.41. Experimental values are from [SZC1980]. In Figure F.41, the solid line is the mole fraction of N_2 in the phase liquid$_1$ along the solid$_2$-liquid$_1$-vapor three phase line, where 1 and 2 are related to N_2 and C_3H_8, respectively. This line extends between two Quadruple Points (QP): QP_1 is the solid$_2$-solid$_1$-liquid$_1$-vapor equilibrium calculated at about 63 K; QP_2 is the solid$_2$-liquid$_2$-liquid$_1$-vapor equilibrium calculated at about 85 K. Green points in Figure F.41 represent the composition of the phase liquid$_1$ at the QP_1 and the QP_2. The dashed line in Figure F.41 represents the mole fraction of N_2 in the phase liquid$_1$ along the liquid$_2$-liquid$_1$-vapor three phase line.

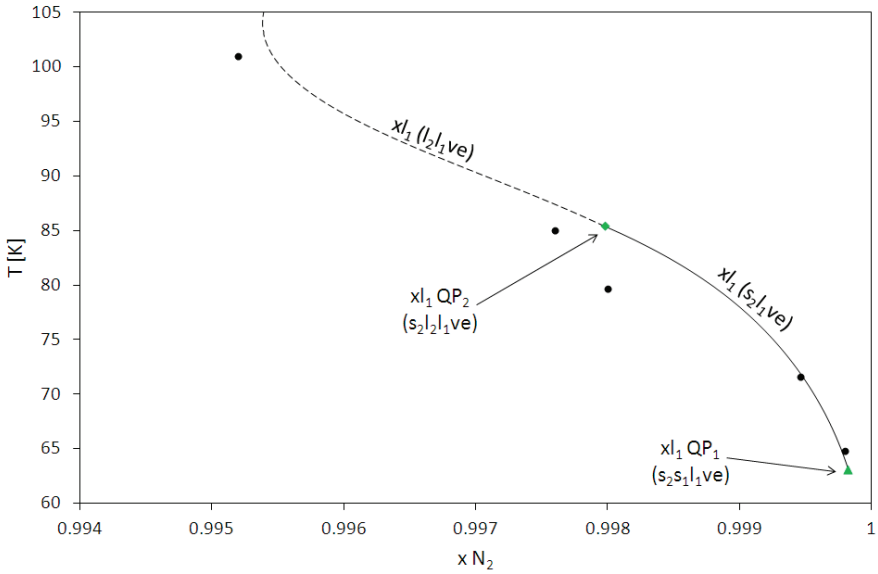

Figure F.41: SLE for the system N_2+C_3H_8. ● : [SZC1980]; — : SLV EoS; ♦ : xl_1 at $s_2l_2l_1ve$; ▲ : xl_1 at $s_2s_1l_1ve$.

The SLV EoS does not represent the experimental value placed at about 100 K as the solubility of solid C_3H_8 in the liquid phase; depending on the value of pressure, at this temperature the model gives a fluid-fluid equilibrium, where fluid means the liquid$_1$, the liquid$_2$, or the vapor phases.

Figure F.42 represents the qualitative comparison between VLLE data and model in the pressure-temperature equilibrium projection in the range 80 K ≤ T ≤ 140 K. The green points are calculated values: the quadruple point (QP_2) is the green diamond, the Upper Critical EndPoint (UCEP) is the green square.

Immiscibility ceases for temperature greater than the temperature at the UCEP. Calculated temperature are 85.4 K for the QP_2, and 126 K for the UCEP.

Red diamond and square are experimental values for the QP_2 (84.8 K) and the UCEP (126.7 K) from [SCH1966]. The blue square is the experimental value for the UCEP (126.6 K) from [KOH1984]. The VLLE data from [YU1969] extend to higher temperatures.

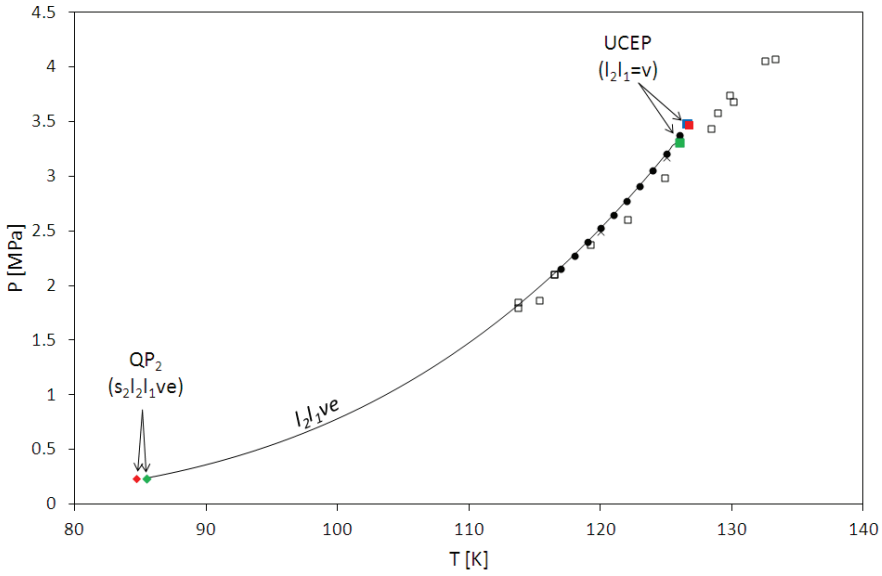

Figure F.42: VLLE for the system N_2+C_3H_8.
● : [KOH1984]; × : [KRE1982]; □ : [YU1969]; — : SLV EoS.
$s_2l_2l_1e$ (QP_2): ♦ [SCH1966]; ♦ : SLV EoS.
l_2l_1=v (UCEP): ■ [SCH1966]; ■ [KOH1984]; ■ : SLV EoS.

Table F.13 gives the quantitative comparison between data and values calculated from the SLV EoS in terms of equilibrium mole fractions of N_2. With reference to the VLE, the AAD% for both compositions in the liquid (x) and in the vapor (y) phases is lower than 13% for all the references, except for the data presented in [CHE1964], and [LU1969].

With reference to the VLLE, deviations occur with respect to the references [SCH1966] and [YU1969]. It is worth mentioning that compositions from [YU1969] differ from those in [KRE1982] and [KOH1984], and same situation is portrayed in Figure F.42 for the VLLE pressure and temperature.

The MAD% between the model and experimental mole fractions along the vapor-liquid critical line from [ROO1967] are about 41% and 21% when evaluating xN_2 at fixed T and P, respectively.

Table F.13: Quantitative comparison of equilibrium compositions for the system N_2+C_3H_8.

xN_2+(1-x)C_3H_8 Ref.	N	Kind of data	T K	P MPa	*x*	*y*		FLASH xN_2	FLASH yN_2
[BOL1954]	8	VLE PTxy	298.2	2.5 – 18.1	0.032 – 0.55	0.56 – 0.78	**N calc**	7	7
							AAD%	8.04	3.38
							Bias%	8.04	-1.69
							MAD%	9.79	5.98

[CHE1964]	6	VLE PTx	92 – 128	0.12 – 0.58	0.016 – 0.07		**N calc**	6	6
							AAD%	46.98	
							Bias%	-46.98	
							MAD%	77.85	
[GRA1977a]	36	VLE PTxy	230 – 290	0.1 – 22	0 – 0.53	0 – 0.96	**N calc**	32	33
							AAD%	5.19	0.92
							Bias%	2.30	-0.42
							MAD%	11.22	4.50
[HOU2010a]	28	VLE PTx	110 – 125	0.26 – 3.3	0.011 – 0.12		**N calc**	28	
							AAD%	6.09	
							Bias%	-6.09	
							MAD%	13.21	
[HUD1984]	127	VLE PTy	188 – 343	0.08 – 5.8		0.26 – 0.91	**N calc**		125
							AAD%		6.53
							Bias%		-5.59
							MAD%		66.66
[KOH1984]	10	VLLE PTx	117 – 126	2.2 – 3.4	0.13 – 0.99		**N calc**	9	9
							AAD%	10.50	10.33
							Bias%	-8.77	-8.60
							MAD%	21.15	21.26
[KRE1982]	17	VLE PTxy	120 – 127	0.7 – 6.2	0.03 – 0.13	1	**N calc**	17	17
							AAD%	5.11	0.03
							Bias%	-5.11	0.03
							MAD%	8.38	0.18
	3	VLLE PTxy	120 – 126	2.5 – 3.3	0.11 – 1	1	**N calc**	2	2
							AAD%	1.45	1.55
							Bias%	-1.33	-1.43
							MAD%	4.19	4.59
[LU1969]	9	VLE PTxy	113 – 125	0.15 – 1.78	0.08 – 0.09	1	**N calc**	9	9
							AAD%	53.8	0.20
							Bias%	-53.8	0.20
							MAD%	91.07	0.23
[POO1974]	32	VLE PTxy	114 – 122	0.15 – 2.8	0 – 0.09	1	**N calc**	21	21
							AAD%	12.82	0.03
							Bias%	12.58	0.03
							MAD%	21.69	0.11
[ROO1967]	4	CP PTx	311 – 365	5.2 – 14.8	0.1 – 0.5		**N calc**	3	3
							AAD%	22.80	12.19
							Bias%	22.80	12.19
							MAD%	40.88	22.76
[ROZ1988]	144	VLE PTy	196 – 285	0.11 – 4.8		0.18 – 0.89	**N calc**		144
							AAD%		2.83
							Bias%		-2.02
							MAD%		29.16
[SCH1966]	70	VLE PTxy	103 – 353	0.01 – 13.8	0 – 0.32	0 – 1	**N calc**	60	59
							AAD%	7.15	1.64
							Bias%	1.62	0.69
							MAD%	66.36	17.63
	11	LLE PTx	103.2 – 123.2	1.4 – 13.8	0.08 – 0.14 0.99 – 1		**N calc**	11	11
							AAD%	16.72	0.05
							Bias%	-16.72	-0.02
							MAD%	30.48	0.14
[SZC1980]	5	SLE Tx	65 – 101		0.995 – 1		**N calc**	4	
							AAD%	0.03	
							Bias%	0.03	
							MAD%	0.08	

[YU1969]	14	VLLE PTxy	114 – 133	1.8 – 4.1	0.25 – 0.98	0.99 – 1	**N calc**	8	8
							AAD%	22.74	22.85
							Bias%	-18.39	-18.51
							MAD%	63.00	63.19
[YUC1999]	41	VLE PTxy	240 – 330	0.15 – 15.1	0 – 0.32	0 – 0.95	**N calc**	36	36
							AAD%	4.39	2.25
							Bias%	0.30	-2.25
							MAD%	22.46	12.34

1.14 N_2+C_3H_6

The literature data for the system N_2+C_3H_6 are shown in Figure F.43.

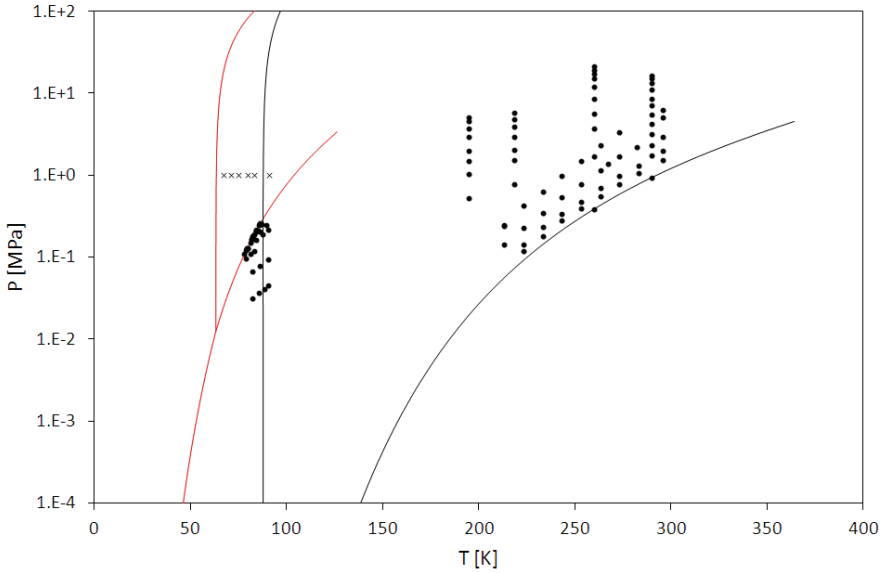

Figure F.43: Available experimental values for the system N_2+C_3H_6.
— : N_2; — : C_3H_6; ● : FFE data; × : SFE data.

The qualitative comparison between model and SLE data is portrayed in Figure F.44. Experimental values are from [SZC1979] (filled circles) and [TSI1940] (open circles). In Figure F.44, the solid line is the mole fraction of N_2 in the phase liquid$_1$ along the solid$_2$-liquid$_1$-vapor three phase line, where 1 and 2 refer to N_2 and C_3H_6, respectively.

This line originates in a quadruple point QP_1, where the solid$_2$-solid$_1$-liquid$_1$-vapor phases are at equilibrium. The calculated temperature at the QP_1 is about 64 K. The green triangle in Figure F.44 represents the composition of the phase liquid$_1$ at the QP_1. Calculated values are qualitatively representative of data, except for the experimental value at $xN_2 = 0.928$.

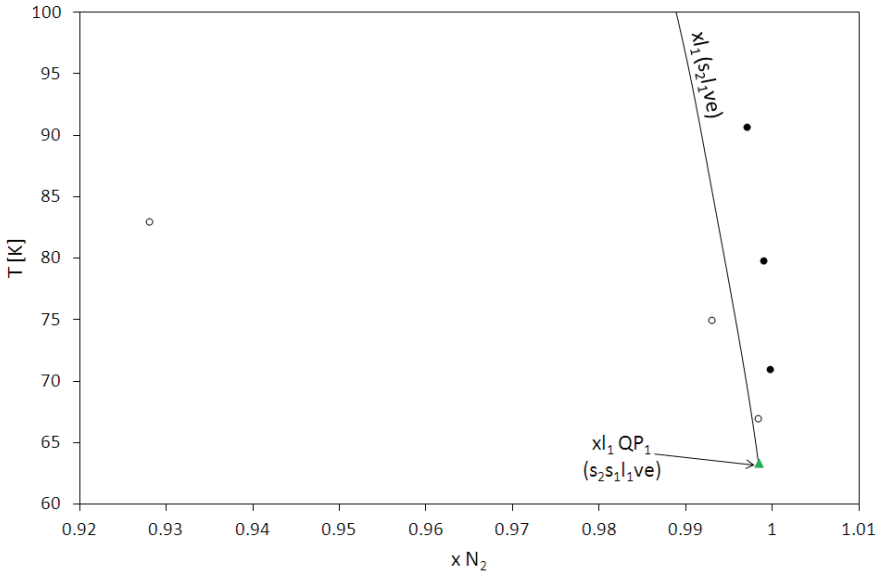

Figure F.44: SLE for the system N_2+C_3H_6.
● : [SZC1980]; ○ :[TSI1940]; — : SLV EoS; ▲ : xl_1 at $s_2s_1l_1ve$.

The pressure-composition cross sections in Figure F.45 show the qualitative comparison between VLE data and model from 195 K up to 218 K; data are from [YOR1968b] and [GRA1977a].

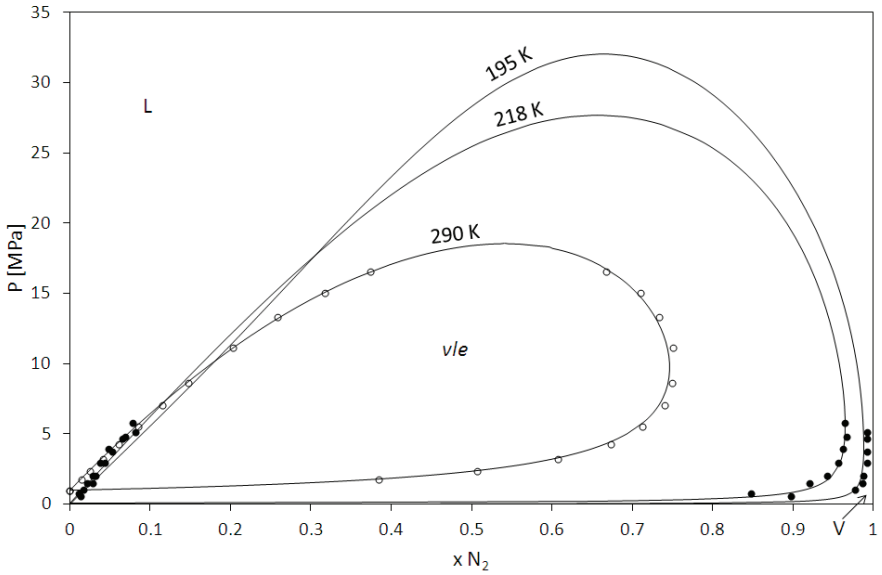

Figure F.45: VLE for the system N_2+C_3H_6 at 195 K, 218 K, and 290 K
● : [YOR1968b]; ○ : [GRA1977a]; — : SLV EoS.

Table F.14 gives the quantitative comparison between data and values calculated from the SLV EoS in terms of equilibrium mole fractions of N_2. With reference to the VLE, the AAD% for both compositions in the liquid (x) and in the vapor (y) phases is lower than 10% for all the references, except for the data presented in [BLA1965] and the liquid phase from [YOR1968b].

Table F.14: Quantitative comparison of equilibrium compositions for the system N_2+C_3H_6.

xN_2+(1-x)C_3H_6 Ref.	N	Kind of data	T K	P MPa	x	y		FLASH xN_2	FLASH yN_2
[BLA1965]	41	VLE PTx	78 – 91	0.03 – 0.26	0 – 0.34		**N calc**	5	
							AAD%	27.89	
							Bias%	-27.89	
							MAD%	44.44	
[GRA1977a]	22	VLE PTxy	260 – 290	0.38 – 21.4	0 – 0.48	0 – 0.89	**N calc**	20	20
							AAD%	5.37	1.82
							Bias%	-5.16	-1.73
							MAD%	13.32	7.97
[ROZ1988]	31	VLE PTxy	213 – 283	0.12 – 3.4		0.23 – 0.76	**N calc**	31	
							AAD%	5.45	
							Bias%	-5.24	
							MAD%	19.95	
[SZC1979]	3	SLE Tx	71 – 91		~1.0		**N calc**	3	
							AAD%	0.42	
							Bias%	-0.42	
							MAD%	0.54	
[TSI1940]	3	SLE Tx	67 – 83		0.93 – 1		**N calc**	3	
							AAD%	2.47	
							Bias%	2.43	
							MAD%	7.08	
[YOR1968b]	20	VLE PTxy	195 – 296	0.53 – 6.3	0 – 0.09	0.23 – 0.99	**N calc**	19	20
							AAD%	15.55	4.23
							Bias%	8.94	-2.77
							MAD%	34.67	33.55

1.15 O_2+Ar

The literature data for the system O_2+Ar are shown in Figure F.46.

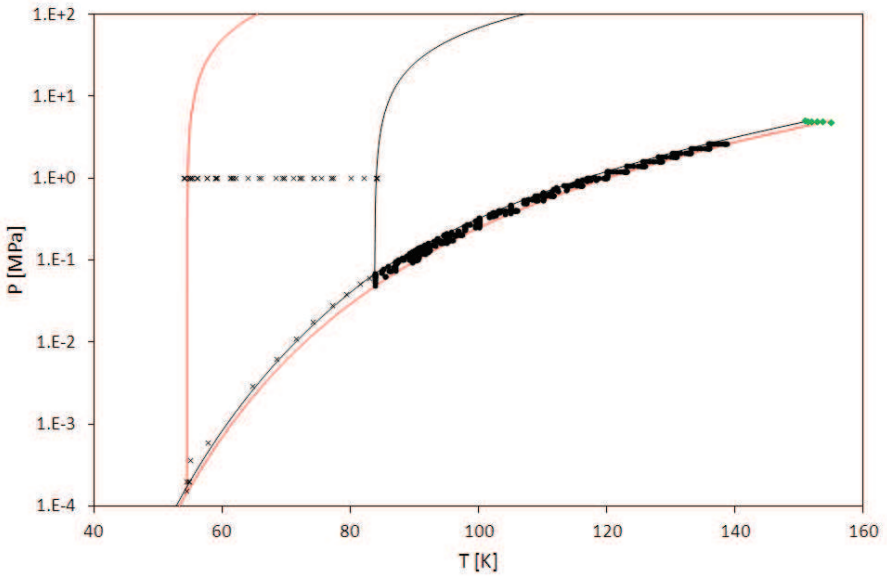

Figure F.46: Available experimental values for the system O_2+Ar.
— : O_2; — : Ar; ● : FFE data; × : SFE data; ♦ : CP data.

The qualitative comparison between model and SLE data is portrayed in Figure F.47. According to [FED1939], the peritectic temperature is 55 K, while compositions of the solid$_2$, solid$_1$, and liquid phases are 0.79, 0.9, and 0.96 in O_2 mole fraction, respectively. Calculated compositions are 0.801, 0.903, and 0.968. The peritectic temperature from the SLV EoS is 54.8 K.

For the author attempts, it has not been possible matching *i*. experimental values of solid and liquid compositions and *ii*. the compositions at the peritectic temperature. This entails the calculated solid$_2$-liquid equilibrium being not in agreement with experimental values for compositions in the range $0.4 \leq x\ O_2 \leq 0.85$, especially for the solid branch.

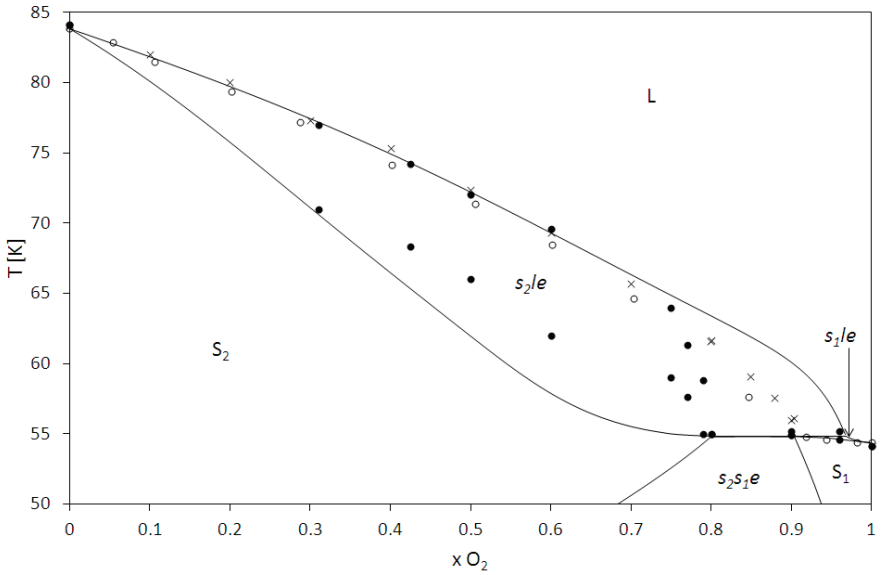

Figure F.47: SLE for the system O_2+Ar.
● : [FED1939]; ○ : [DIN1955]; × : [VEI1937]; — : SLV EoS.

The pressure-composition cross sections in Figure F.48 show the qualitative comparison between VLE data and model at 90 K and 100 K; data are from [CLA1954].

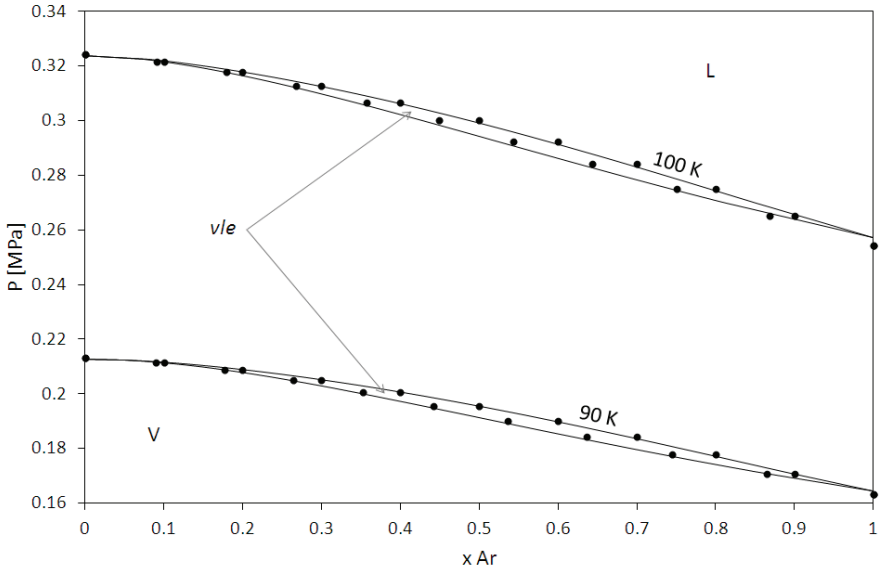

Figure F.48: VLE for the system O_2+Ar at 90 K, and 100 K
● : [CLA1954]; — : SLV EoS.

Table F.15 gives the quantitative comparison between data and values calculated from the SLV EoS in terms of equilibrium mole fractions of O_2.

With reference to the VLE, the AAD% for both compositions in the liquid (x) and in the vapor (y) phases is lower than 14% for all the references, except for the data presented in [NAR1957].

For the critical point data of [JON1963], the AAD% is 24%, with a MAD% of 54%.

Table F.15: Quantitative comparison of equilibrium compositions for the system O_2+Ar.

xAr+(1-x)O₂ Ref.	N	Kind of data	T K	P MPa	*x*	*y*		FLASH xO_2	FLASH yO_2
[BOU1936]	39	VLE PTxy	87 – 96	0.07 – 0.21	0.04 – 0.87	0.06 – 0.88	**N calc**	27	38
							AAD%	8.74	9.98
							Bias%	-8.53	-9.92
							MAD%	26.39	34.22
[BUR1962]	140	VLE PTxy	86 – 118	0.06 – 1	0.1 – 0.91	0.12 – 0.92	**N calc**	138	138
							AAD%	7.89	7.78
							Bias%	3.10	4.46
							MAD%	81.05	86.71
[CLA1954]	55	VLE PTxy	90 – 110	0.1 – 0.67	0 – 1	0 – 1	**N calc**	45	45
							AAD%	4.67	4.54
							Bias%	2.45	3.67
							MAD%	43.78	45.82
[DIN1955]	15	SLE PTx	54 – 84	0 – 0.07	0 – 1		**N calc**	9	9
							AAD%	7.74	9.13
							Bias%	5.52	9.05
							MAD%	11.26	16.24
[FAS1955]	24	VLE PTxy	89 – 96	0.12 – 0.31	0.21 – 0.83	0.28 – 0.87	**N calc**	24	24
							AAD%	9.29	8.21
							Bias%	2.37	1.81
							MAD%	45.19	44.95
[FED1938]	8	SLE Tx	59 – 84		0.21 – 1		**N calc**	7	
							AAD%	5.69	
							Bias%	5.19	
							MAD%	17.17	

[FED1939]	24	SLE Tx	54 – 84		0 – 1		**N calc**	20	
							AAD%	10.51	
							Bias%	-3.86	
							MAD%	24.21	
[JON1963]	6	CP Tx	151 – 155		0 – 1		**N calc**	4	4
							AAD%	23.92	
							Bias%	23.92	
							MAD%	54.44	
[NAR1957]	63	VLE PTxy	90 – 120	0.1 – 1.21	0 – 1	0 – 1	**N calc**	50	50
							AAD%	25.19	26.27
							Bias%	23.78	25.15
							MAD%	141.68	139.54
[PAR1997]	24	VLE PTxy	92 – 115	0.12 – 0.94	0.02 – 0.92	0.03 – 0.93	**N calc**	21	21
							AAD%	13.27	11.96
							Bias%	-12.87	-11.41
							MAD%	35.61	32.21
[POO1962]	24	VLE PTx	84 – 90	0.05 – 0.13	0 – 1		**N calc**	19	
							AAD%	9.83	
							Bias%	8.67	
							MAD%	41.82	
[VEI1937]	14	SLE Tx	56 – 84		0.097 – 1		**N calc**	13	
							AAD%	5.28	
							Bias%	1.99	
							MAD%	9.17	
[WAN1960]	35	VLE PTx	90 – 96	0.12 – 0.22	0.02 – 1		**N calc**	24	
							AAD%	9.23	
							Bias%	-4.87	
							MAD%	52.68	
[WIL1964]	198	VLE TPxy	87 – 139	0.1 – 2.63	0 – 0.98	0.01 – 0.98	**N calc**	63	63
							AAD%	12.10	11.80
							Bias%	11.60	11.17
							MAD%	104.79	94.99
[YOR1978]	65	VLE PTxy	89 – 92	0.1 – 0.13	0 – 0.76	0 – 0.79	**N calc**	25	25
							AAD%	2.84	3.39
							Bias%	0.44	0.21
							MAD%	26.07	21.33

1.16 O_2+Kr

The literature data for the system N_2+Kr are shown in Figure F.49.

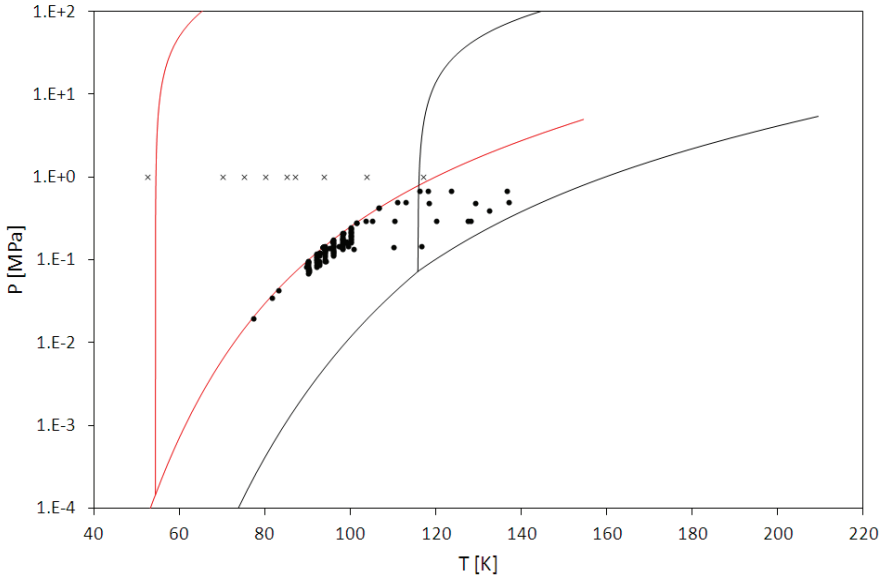

Figure F.49: Available experimental values for the system O_2+Kr.
— : O_2; — : Kr; ● : FFE data; × : SFE data.

The qualitative comparison between model and SLE data is portrayed in Figure F.50. The model is in agreement with the experimental values, and the calculated phase diagram is of the eutectic type. The calculated temperature at the eutectic point is 52.7 K, while calculated compositions of the solid$_2$, liquid, and solid$_1$ phases are 0.005, 0.95, and 0.99 in O_2 mole fraction, respectively.

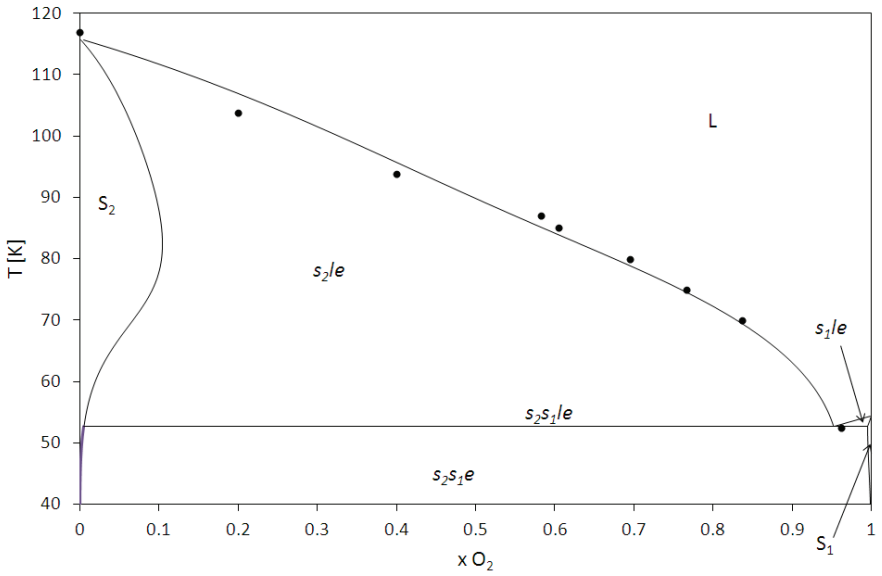

Figure F.50: SLE for the system O_2+Kr.
● : [VON1934]; — : SLV EoS.

The pressure-composition cross sections in Figure F.51 show the qualitative comparison between VLE data and model from 96 K up to 100 K; data are from [FAS1939]. Calculated values are in agreement with experimental values. The VLE in Figure F.51 are at temperatures lower than the triple point temperature of pure Kr (115.7 K), therefore also solid$_2$-liquid ($s_2$le) and solid$_2$-vapor ($s_2$ve) equilibria occur in the phase equilibrium behavior. For each temperature, the $s_2$le, $s_2$ve, and vle meet at the correspondent solid$_2$-liquid-vapor three phase line.

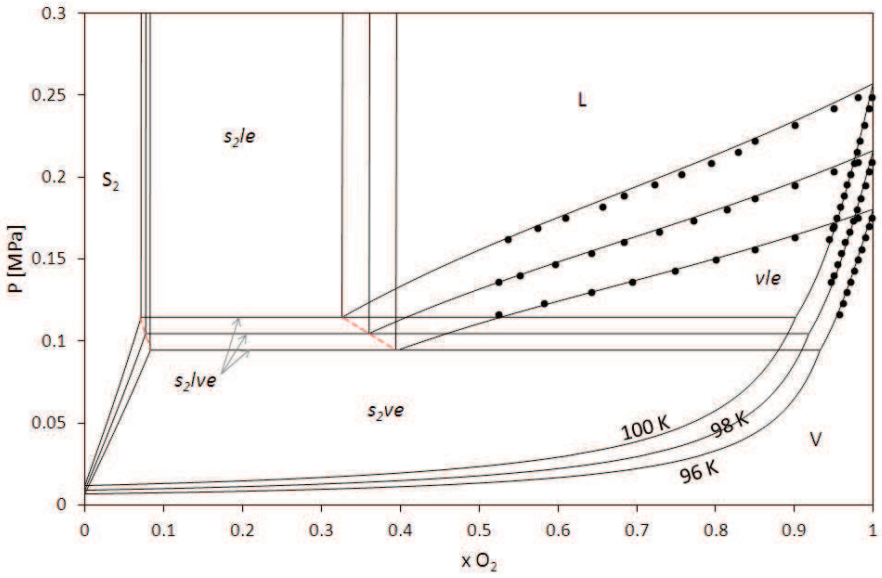

Figure F.51: VLE for the system O_2+Kr at 96 K, 98 K, and 100 K
● : [FAS139]; — : SLV EoS; – – : extent of the $s_2$le.

Table F.16 gives the quantitative comparison between data and values calculated from the SLV EoS in terms of equilibrium mole fractions of O_2.

With reference to the VLE, the AAD% for both compositions in the liquid (x) and in the vapor (y) phases is lower than 7% for all the references. A maximum value of about 25% for the MAD% has been found with respect to data from [FAS1956b].

Table F.16: Quantitative comparison of equilibrium compositions for the system O_2+Kr.

xO_2+(1-x)Kr Ref.	N	Kind of data	T K	P MPa	*x*	*y*		FLASH xO_2	FLASH yO_2
[BUR1966]	12	VLE PTxy	94 – 107	0.14 – 0.42	0.9 – 1	0.99 – 1	**N calc**	12	12
							AAD%	2.35	0.24
							Bias%	0.78	0.06
							MAD%	9.64	0.92
[FAS1939]	92	VLE PTxy	77 – 100	0.02 – 0.25	0.5 – 0.98	0.94 – 1	**N calc**	91	62
							AAD%	2.23	0.15
							Bias%	0.33	-0.04
							MAD%	17.30	0.35
[FAS1956b]	20	VLE PTxy	96 – 137	0.14 – 0.69	0.06 – 0.85	0.38 – 0.98	**N calc**	20	20
							AAD%	6.88	2.48
							Bias%	0.76	-0.60
							MAD%	24.58	14.19
[VON1934]	9	SLE Tx	53 – 117		0 – 0.96		**N calc**	7	
							AAD%	7.20	
							Bias%	3.41	
							MAD%	29.15	

1.17 O_2+Xe

The literature data for the system O_2+Xe are shown in Figure F.52.

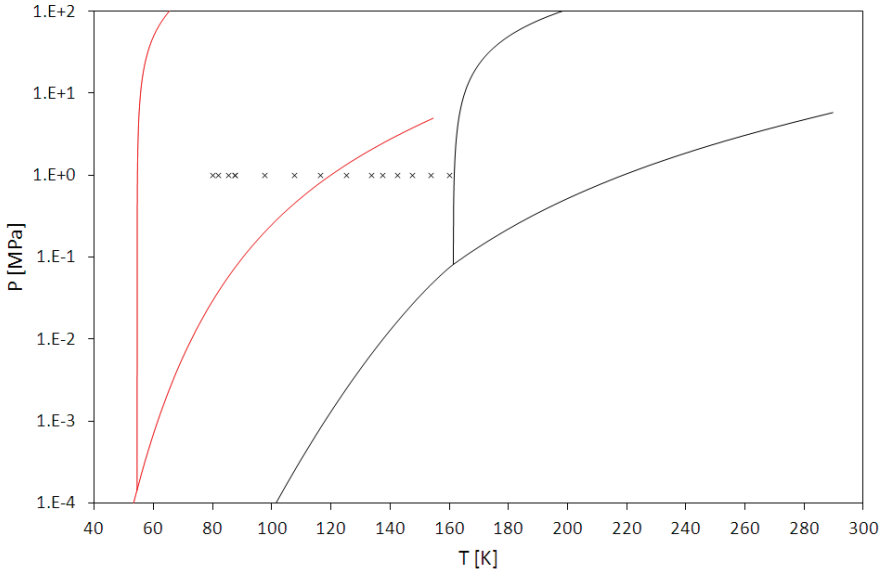

Figure F.52: Available experimental values for the system O_2+Xe.
— : O_2; — : Xe; × : SFE data.

The qualitative comparison between model and SLE data is portrayed in Figure F.53. The model is in agreement with the experimental values, and the calculated phase diagram is of the peritectic type. The calculated temperature at the peritectic point is 57.4 K, while calculated compositions of the solid$_2$, solid$_1$, and liquid phases are 0.013, 0.924, and 0.983 in O_2 mole fraction, respectively.

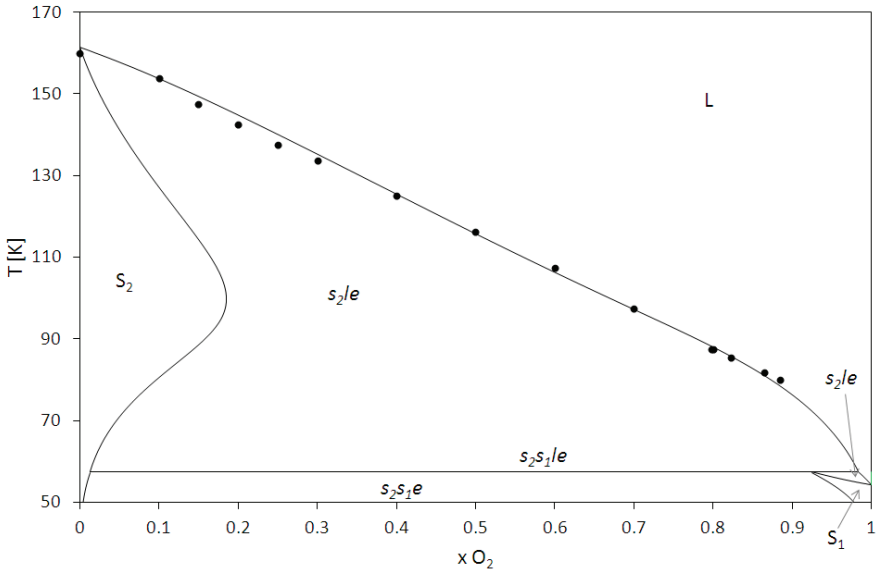

Figure F.53: SLE for the system O_2+Xe.
● : [VON1934]; — : SLV EoS.

Table F.17 gives the quantitative comparison between data and values calculated from the SLV EoS in terms of equilibrium mole fractions of O_2.

Table F.17: Quantitative comparison of equilibrium compositions for the system O_2+Xe.

xO_2+(1-x)Xe Ref.	N	Kind of data	T K	P MPa	*x*	*y*	FLASH	
								yO_2
[VON1934]	15	SLE Tx	80 – 160		0 – 0.89		**N calc**	14
							AAD%	3.83
							Bias%	2.87
							MAD%	13.57

1.18 O_2+Ne

The literature data for the system O_2+Ne are shown in Figure F.54.

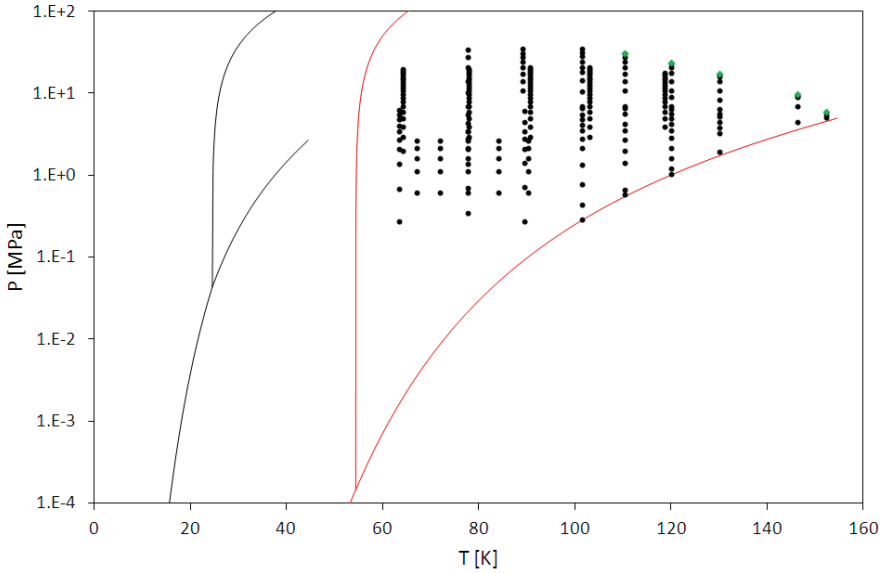

Figure F.54: Available experimental values for the system O_2+Ne.
— : O_2; — : Ne; ● : FFE data; ♦ : CP data.

The pressure-composition cross sections in Figure F.55 show the qualitative comparison between VLE data and model from 78 K up to 130 K; data are from [STR1965b].

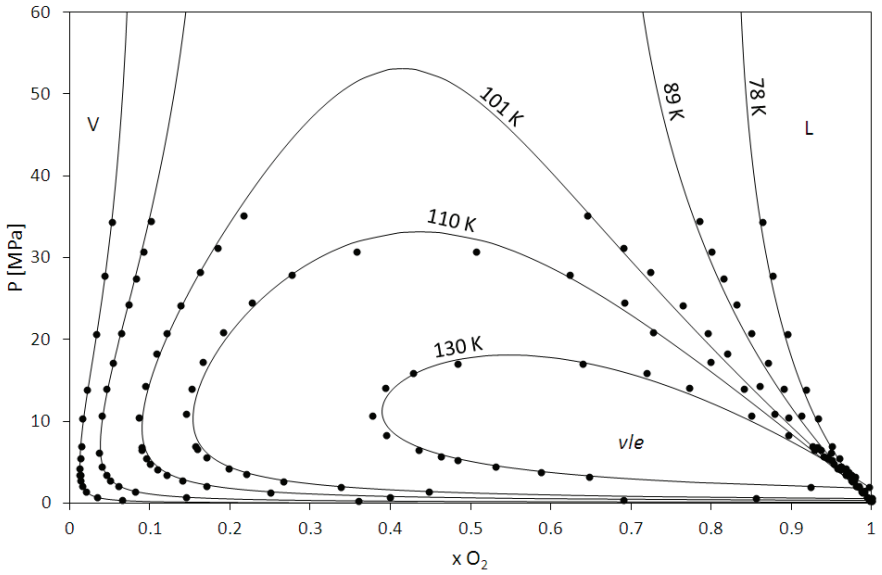

Figure F.55: VLE for the system O_2+Ne from 78 K up to 130 K.
● : [STR1965b]; — : SLV EoS.

Table F.18 gives the quantitative comparison between data and values calculated from the SLV EoS in terms of equilibrium mole fractions of O_2.

The AAD% for both compositions in the liquid (x) and in the vapor (y) phases is lower than 6% for all the references, except for the vapor phase presented in [SKR1971].

Table F.18: Quantitative comparison of equilibrium compositions for the system O_2+Ne.

xNe+(1-x)O₂ Ref.	N	Kind of data	T K	P MPa	*x*	*y*		FLASH xO_2	FLASH yO_2
[SKR1964]	25	VLE PTxy	67 – 90	0.6 – 2.6	0 – 0.02	0.8 – 1	**N calc**	25	25
							AAD%	0.11	4.93
							Bias%	-0.11	1.90
							MAD%	0.22	13.04
[SKR1971]	90	VLE PTxy	64 – 119	1.96 – 20.6	0 – 0.32	0.6 – 1	**N calc**	88	88
							AAD%	1.46	31.44
							Bias%	1.30	-31.44
							MAD%	8.29	62.70
[STR1965b]	113	VLE PTxy	63 – 152	0.28 – 35.1	0 – 0.49	0 – 1	**N calc**	106	106
							AAD%	0.79	5.84
							Bias%	-0.57	4.62
							MAD%	9.48	58.87
	5	CP PTx	110 – 152	5.9 – 31.0	0.09 – 0.55		**N calc**	5	5
							AAD%	5.72	6.35
							Bias%	-5.22	-4.77
							MAD%	10.70	10.68

1.19 O_2+He

The literature data for the system O_2+He are shown in Figure F.56.

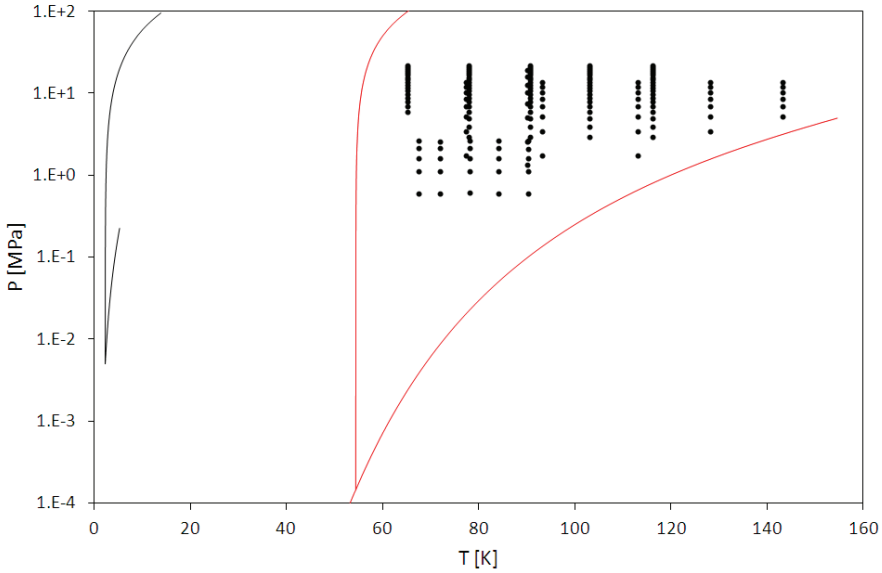

Figure F.56: Available experimental values for the system O_2+He.
— : O_2; — : He; ● : FFE data.

The pressure-composition cross sections in Figure F.57 show the qualitative comparison between VLE data and model from 91 K up to 116 K; data are from [SKR1971].

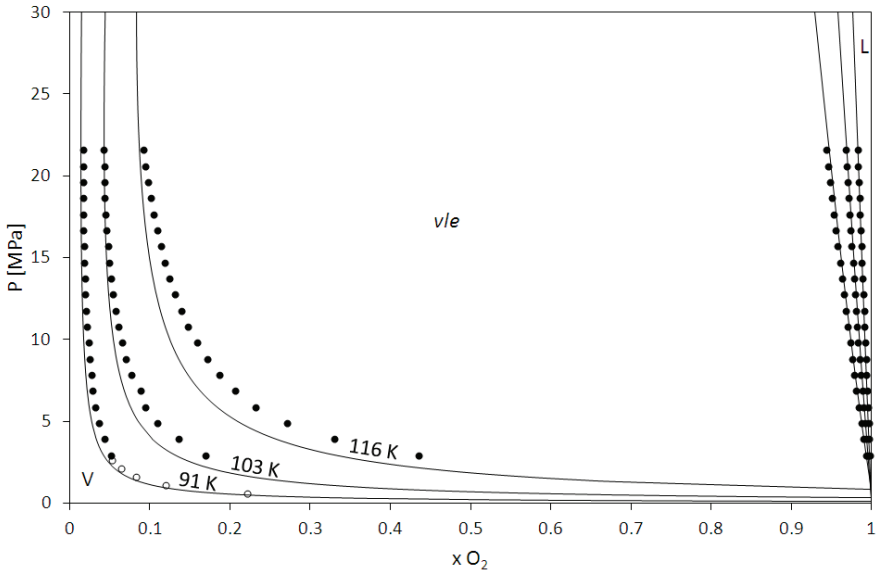

Figure F.57: VLE for the system O_2+He at 91 K, 103 K, and 116 K.
● : [SKR1971]; — : SLV EoS.

According to Figure F.57, calculated values are qualitatively representative of the experimental values, and deviations occur mainly in the vapor phase.

Table F.19 gives the quantitative comparison between data and values calculated from the SLV EoS in terms of equilibrium mole fractions of O_2.

The AAD% for the compositions in the liquid phase is lower than 1% for all the references. For the vapor phase, the maximum MAD% (87%) is related to the isotherm 116 K from [SKR1971] (see Figure F.57).

Table F.19: Quantitative comparison of equilibrium compositions for the system O_2+He.

xHe+(1-x)O₂ Ref.	N	Kind of data	T K	P MPa	*x*	*y*		FLASH xO_2	FLASH yO_2
[HER1965]	8	VLE PTxy	90.0	1.3 – 19.1	0 – 0.014	0.92 – 0.99	**N calc**	6	8
							AAD%	0.03	8.07
							Bias%	0.03	-0.39
							MAD%	0.04	26.37
[SIN1966]	37	VLE PTx	77 – 143	1.7 – 13.8	0 – 0.086		**N calc**	37	
							AAD%	0.18	
							Bias%	-0.16	
							MAD%	0.87	
[SKR1964]	25	VLE PTx	68 – 90	0.6 – 2.6	<0.01	0.78 – 1	**N calc**	25	25
							AAD%	0.01	15.95
							Bias%	0.01	-7.71
							MAD%	0.02	51.19
[SKR1971]	97	VLE PTxy	65 – 116	2.9 – 21.6	0 – 0.056	0.57 – 1	**N calc**	97	97
							AAD%	0.11	26.67
							Bias%	0.10	-26.33
							MAD%	0.32	87.46

1.20 O_2+CO_2

The literature data for the system O_2+CO_2 are shown in Figure F.58. A series of VLE data, [KEE1903], is located under the saturation line of CO_2 at about 0.01 MPa and temperatures from 280 K up to 300 K. Model is not representative of this series of data.

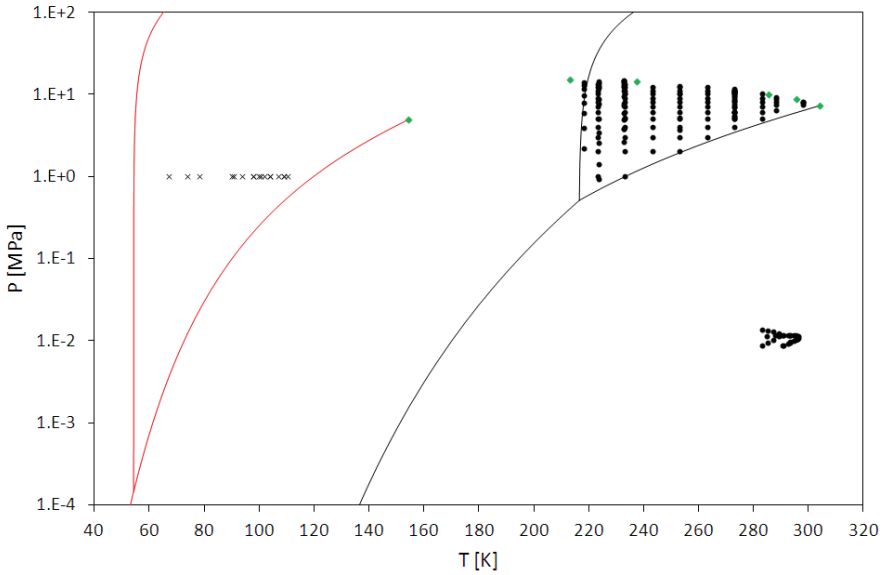

Figure F.58: Available experimental values for the system O_2+CO_2.
— : O_2; — : CO_2; ● : FFE data; × : SFE data; ♦ : CP data.

The qualitative comparison between model and SLE data is portrayed in Figure F.59. Experimental values are from [DES2002] (filled circles) and [FED1940] (open circles). In Figure F.59, the solid line is the mole fraction of O_2 in the phase liquid$_1$ along the solid$_2$-liquid$_1$-vapor three phase line, where 1 and 2 are related to O_2 and CO_2, respectively. The two series of data present two different "slopes", and BIPs have been regressed with reference to the more recent data, namely [DES2002].

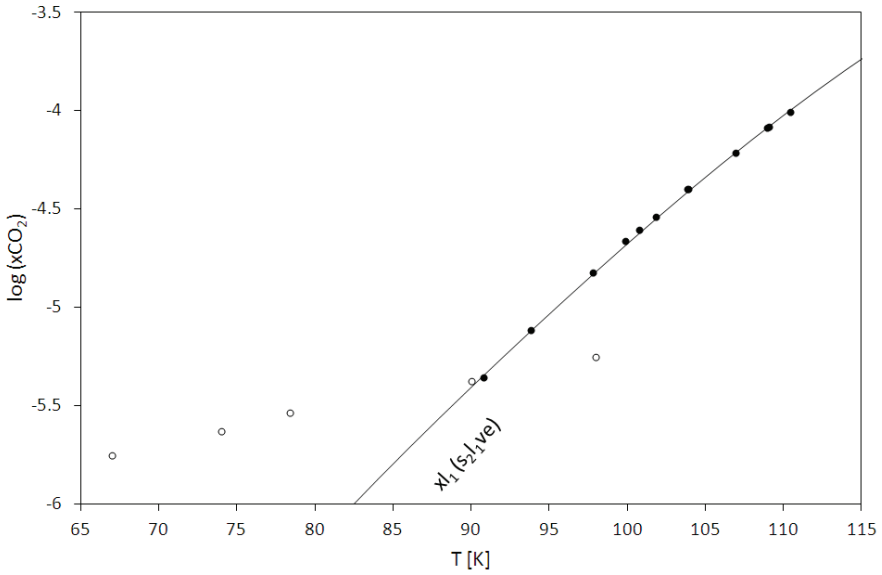

Figure F.59: SLE for the system O_2+CO_2.
● : [DES2002]; ○ : [FED1940]; — : SLV EoS.

The pressure-composition cross sections in Figure F.60 show the qualitative comparison between VLE data and model from 218 K up to 263 K; data are from [ZEN1963] and [FRE1970].

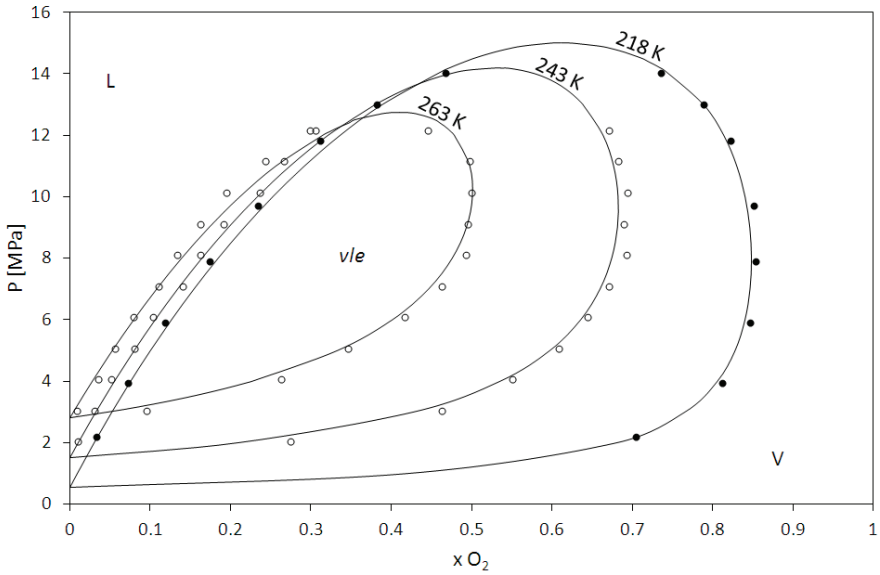

Figure F.60: VLE for the system O_2+CO_2 at 218 K, 243 K, and 263 K.
● : [ZEN1963]; ○ : [FRE1970]; — : SLV EoS.

Table F.20 gives the quantitative comparison between data and values calculated from the SLV EoS in terms of equilibrium mole fractions of O_2.

With reference to the VLE and CP data, the AAD% for both compositions in the liquid (x) and in the vapor (y) phases is lower than 12% for all the references, except for the liquid compositions presented in [KAM1966]. A maximum value of about 40% for the MAD% has been found for both the fluid phases with respect to data from [FRE1970]. These deviations occur at 263 K for experimental compositions lower than $xO_2 = 0.1$.

Table F.20: Quantitative comparison of equilibrium compositions for the system O_2+CO_2.

xO_2+(1-x)CO_2 Ref.	N	Kind of data	T K	P MPa	x	y		FLASH xO_2	FLASH yO_2
[BOO1930]	6	CP PTx	154 – 304	5.0 – 15.0	0 – 1		**N calc**	4	4
							AAD%	10.53	10.44
							Bias%	10.33	10.44
							MAD%	15.21	15.66
[DES2002]	12	SLE Tx	91 – 111		~ 1.0		**N calc**	12	
							AAD%	<0.001	
							Bias%	<0.001	
							MAD%	<0.001	
[FED1940]	5	SLE Tx	67 – 98		~1.0		**N calc**	5	
							AAD%	<0.001	
							Bias%	<0.001	
							MAD%	<0.001	
[FRE1970]	72	VLE PTxy	223 – 283	1.0 – 13.2	0 – 0.4	0.06 – 0.82	**N calc**	69	69
							AAD%	7.26	3.73
							Bias%	3.22	-2.74
							MAD%	40.91	39.46
[FRE1972]	11	VLE PTxy	224	0.93 – 14.2	0 – 0.45	0.22 – 0.81	**N calc**	11	10
							AAD%	19.39	3.38
							Bias%	19.39	2.38
							MAD%	38.91	13.05

[KAM1966]	22	VLE PTxy	233 – 298	3.7 – 12.7	0.03 – 0.37	0.08 – 0.76	**N calc**	17	20
							AAD%	11.16	7.70
							Bias%	8.49	-7.70
							MAD%	23.48	30.73
[KEE1903]	36	VLE PTxy	283 – 296	0.01 – 0.14	0.8 – 0.9	0.1 – 0.2			
[MUI1965]	4	VLE PTxy	273	5.5 – 11.7	0.046 – 0.3	0.25 – 0.41	**N calc**	3	3
							AAD%	8.31	4.24
							Bias%	8.31	-4.24
							MAD%	10.04	6.92
[ZEN1963]	33	VLE PTxy	218 – 273	2.2 – 14.9	0.03 – 0.53	0.25 – 0.85	**N calc**	26	30
							AAD%	5.91	4.11
							Bias%	3.77	-3.98
							MAD%	22.55	14.28

1.21 O_2+H_2

The literature data for the system O_2+H_2 are shown in Figure F.61.

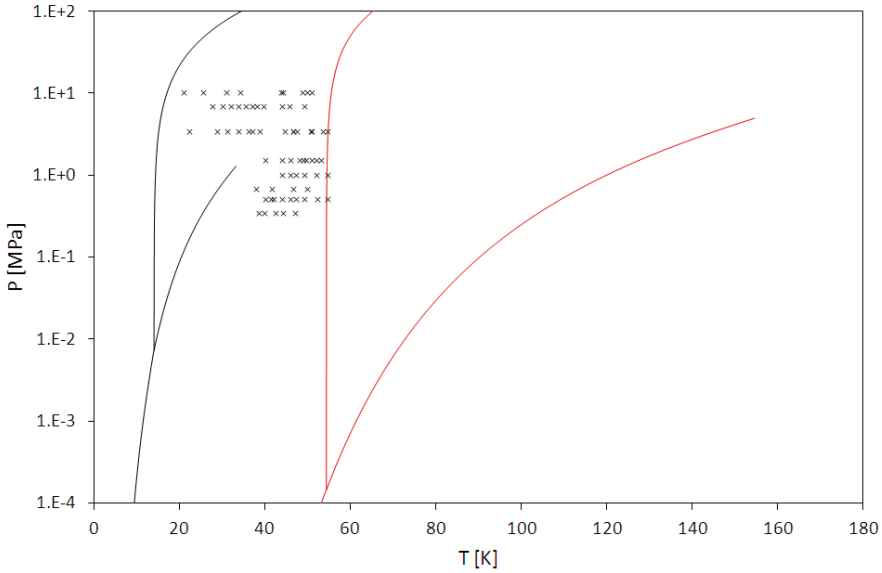

Figure F.61: Available experimental values for the system O_2+H_2.
— : O_2; — : H_2; × : SFE data.

The qualitative comparison between model and SVE data is portrayed in Figure F.62. Experimental values are from [MCK1971] (filled circles) and [OMA1962c] (open circles). The solid lines in Figure F.62 are the mole fraction of O_2 in the vapor phase at 0.35 MPa and 0.51 MPa.

Each line extends up to a solid$_1$-liquid$_1$-vapor equilibrium ($s_1l_1$ve) temperature, where 1 is related to O_2: the green triangles in Figure F.62 represent then the mole fraction of O_2 in the vapor phase at two different $s_1l_1$ve temperatures.

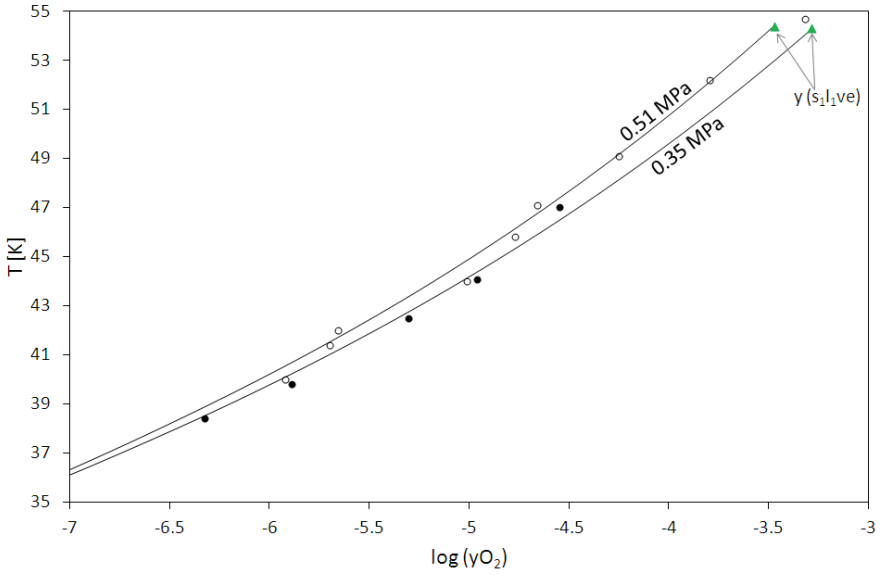

Figure F.62: SLE for the system O_2+H_2.
● : [MCK1971]; ○ : [OMA1962c]; — : SLV EoS; ▲ : yO_2 at $s_2s_1l_1$ve.

Table F.21 gives the quantitative comparison between data and values calculated from the SLV EoS in terms of equilibrium mole fractions of O_2.

The AAD for both the vapor composition is lower than 0.5 for all the references. A maximum value of about 0.8 for the MAD has been found with respect to data from [MCK1975].

Table F.21: Quantitative comparison of equilibrium compositions for the system O_2+H_2.

xH_2+(1-*x*)O_2 Ref.	N	Kind of data	T K	P MPa	*x*	*y*		FLASH
								xO_2 yO_2
[MCK1961][1]	48	SVE PTy	21 – 55	0.35 – 10.3		~1	**N calc**	44
							AAD	0.28
							Bias	-0.60
							MAD	0.75
[OMA1962c][1]	24	SVE PTy	40 – 55	0.51 – 1.52		~1	**N calc**	24
							AAD	0.23
							Bias	0.16
							MAD	0.69

[1] – for SVE PTy data deviations are in terms of AAD, Bias, and MAD.

1.22 O_2+N_2O

The literature data for the system O_2+N_2O are shown in Figure F.63.

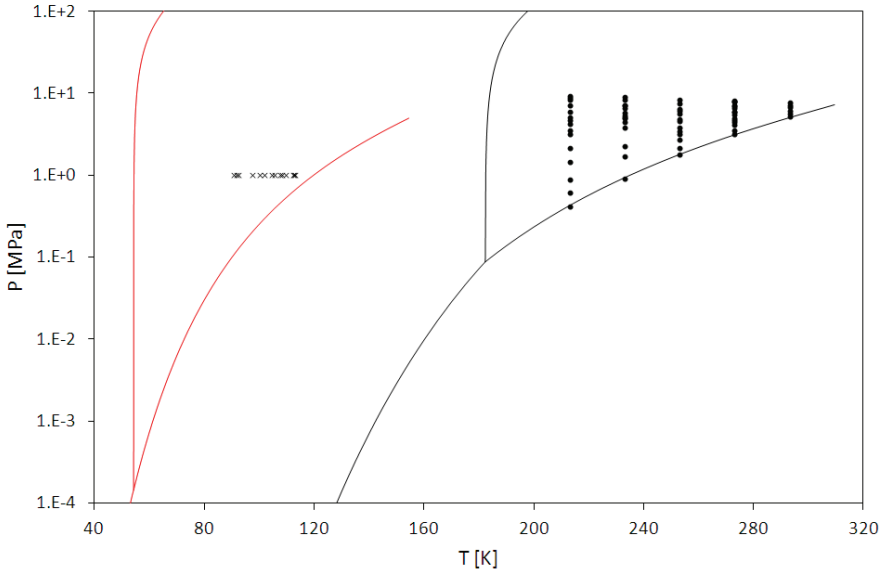

Figure F.63: Available experimental values for the system O_2+N_2O.
— : O_2; — : N_2O; ● : FFE data; × : SFE data.

The qualitative comparison between model and SLE data is portrayed in Figure F.64. Experimental values are from [DES2002]. In Figure F.64, the solid line is the mole fraction of O_2 in the phase liquid$_1$ along the solid$_2$-liquid$_1$-vapor three phase line, where 1 and 2 are related to O_2 and N_2O, respectively.

This line extends between a solid$_2$-solid$_1$-liquid$_1$-vapor equilibrium up to an upper critical endpoint. The calculated quadruple point temperature is 54.7 K, the calculated value for the UCEP temperature is about 160 K.

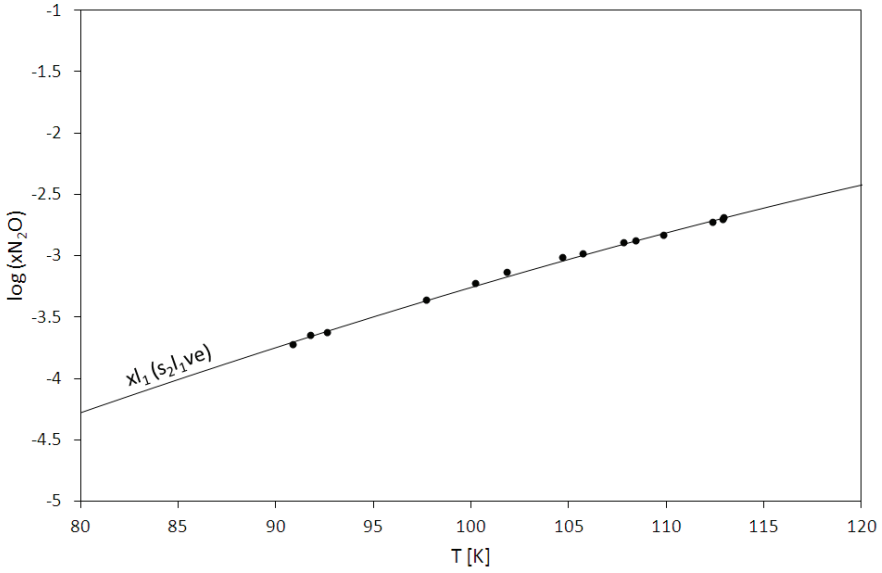

Figure F.64: SLE for the system O_2+N_2O.
● : [DES2002]; — : SLV EoS.

The pressure-composition cross sections in Figure F.65 show the qualitative comparison between VLE data and model from 213 K up to 253 K; data are from [ZEI1972].

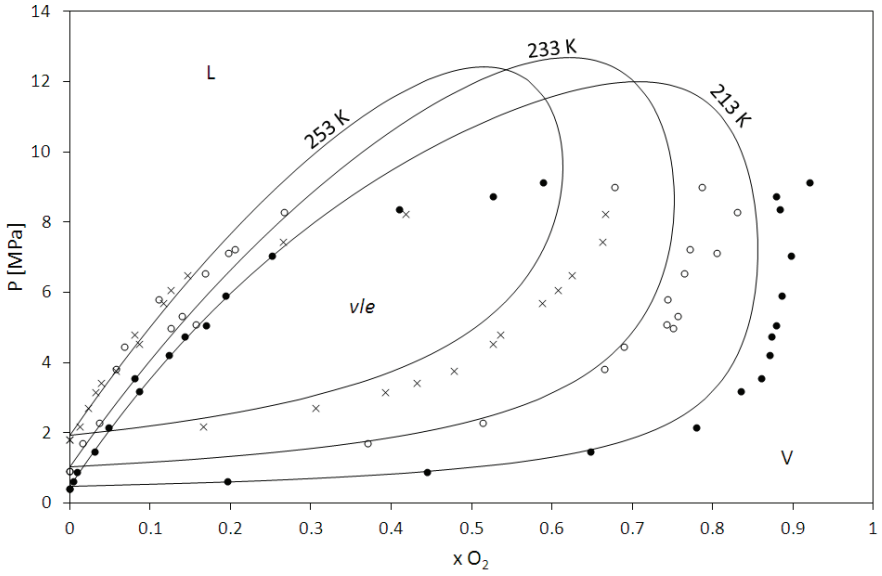

Figure F.65: VLE for the system O_2+N_2O at 213 K, 233 K, and 253 K.
Experimental values [ZEI1972]: ● (213K), ○ (233K), × (253K). — : SLV EoS.

According to Figure F.65, the regressed BIPs do not make the SLV EoS in agreement with data.

Table F.22 gives the quantitative comparison between data and values calculated from the SLV EoS in terms of equilibrium mole fractions of O_2.

As it has previously been pointed out, the model is not representative of the VLE proposed in [ZEI1972], thus important deviations are encountered between calculated and experimental compositions.

Table F.22: Quantitative comparison of equilibrium compositions for the system O_2+N_2O.

O_2+(1-x)N_2O Ref.	N	Kind of data	T K	P MPa	*x*	*y*		FLASH xO_2	FLASH yO_2
[DES2002]	14	SLE Tx	91 – 113		~1		**N calc**	14	
							AAD%	0.003	
							Bias%	0.001	
							MAD%	0.008	
[ZEI1972]	63	VLE PTxy	213 – 293	0.42 – 9.1	0 – 0.68	0 – 0.92	**N calc**	51	51
							AAD%	20.40	8.84
							Bias%	7.15	-8.28
							MAD%	97.18	43.21

1.23 O_2+CH_4

The literature data for the system O_2+CH_4 are shown in Figure F.66.

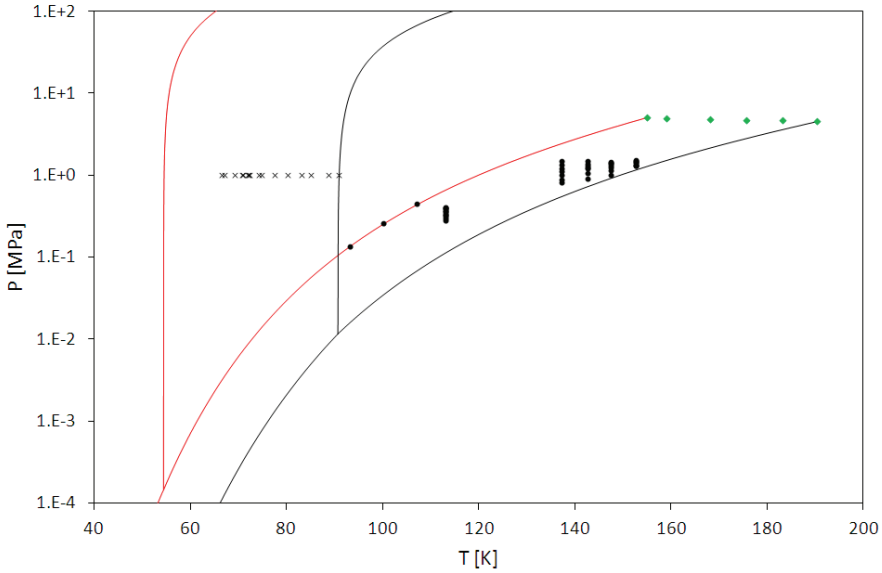

Figure F.66: Available experimental values for the system O_2+CH_4.
— : O_2; — : CH_4; ● : FFE data; × : SFE data; ♦ : CP data.

The qualitative comparison between model and SLE data is portrayed in Figure F.67. The model is in agreement with the experimental values, and the calculated phase diagram is of the eutectic type. The calculated temperature at the eutectic point is 50.6 K, while calculated compositions of the solid$_2$, liquid, and solid$_1$ phases are 0.106, 0.84, and 0.99 in O_2 mole fraction, respectively.

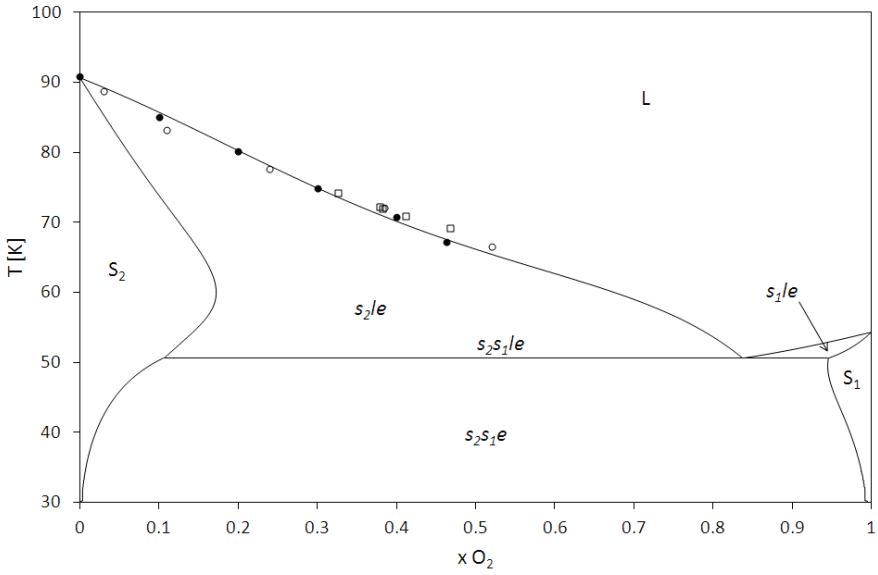

Figure F.67: SLE for the system O_2+CH_4.
● : [MCK1958]; ○ : [MCK1957]; □ : [FAS1941]; — : SLV EoS.

Table F.23 gives the quantitative comparison between data and values calculated from the SLV EoS in terms of equilibrium mole fractions of O_2.

The AAD% is lower than 10% for all the references, except for the SLE data presented in [MCK1957] and the CP data from [JON1963]. The maximum MAD% is related to the SLE data from [MCK1957] and occurs at 88.7 K: the experimental and calculated mole fractions in the liquid phase are $xO_2 = 0.03$ and $xO_2 = 0.042$, respectively.

Table F.23: Quantitative comparison of equilibrium compositions for the system O_2+CH_4.

xO_2+(1-x)CH_4 Ref.	N	Kind of data	T K	P MPa	*x*	*y*		FLASH xO_2	FLASH yO_2
[FAS1941]	5	SLE Tx	69 – 74		0.33 – 0.47		**N calc**	5	
							AAD%	6.37	
							Bias%	-6.37	
							MAD%	9.30	
[HOD1967]	3	VLE PTxy	93 – 107	0.14 – 0.44	~1	~1	**N calc**	3	3
							AAD%	1.31	0.27
							Bias%	-1.31	-0.27
							MAD%	1.90	0.48
[JON1963]	6	CP Tx	155 – 190		0 – 1		**N calc**	4	
							AAD%	10.47	
							Bias%	10.47	
							MAD%	16.38	
[MCK1957]	5	SLE Tx	67 – 89		0.03 – 0.52		**N calc**	5	
							AAD%	18.26	
							Bias%	13.45	
							MAD%	40.49	
[MCK1958]	6	SLE Tx	67 – 90		0 – 0.46		**N calc**	6	
							AAD%	4.55	
							Bias%	3.14	
							MAD%	14.61	
[STR2012]	40	VLE	113 – 153	0.28 – 1.51	0.024 – 0.44	0.09 – 0.81	**N calc**	40	40
							AAD%	2.80	2.01
							Bias%	2.05	-0.65
							MAD%	8.70	9.89

1.24 O_2+C_2H_6

The literature data for the system O_2+C_2H_6 are shown in Figure F.68.

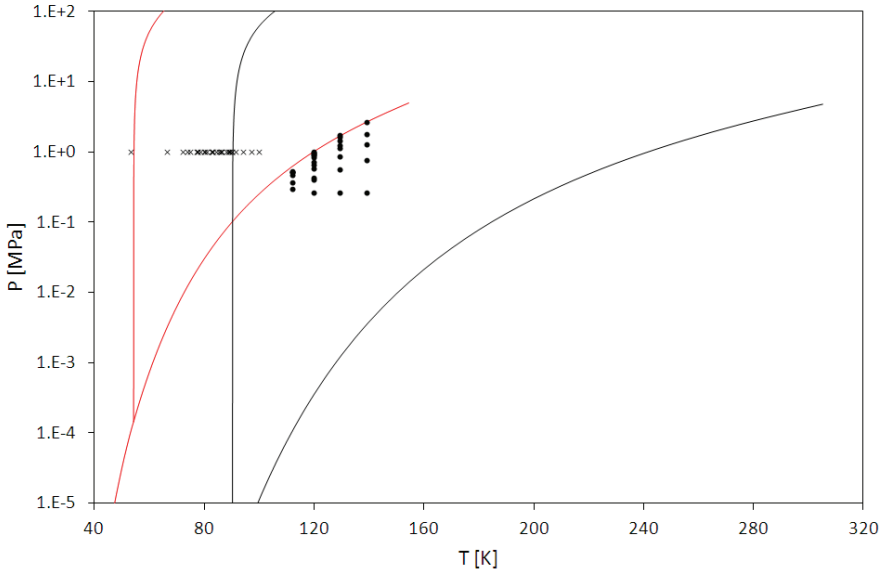

Figure F.68: Available experimental values for the system O_2+C_2H_6.
— : O_2; — : C_2H_6; ● : FFE data; × : SFE data.

The qualitative comparison between model and SLE data is portrayed in Figure F.69. Experimental values are from [COX1950] (circles), [HIM1959] (triangles), [KAR1958] (cross), [MCK1957] (filled squares), and [MCK1958] (open squares).

The calculated phase equilibrium behavior of the system O_2+C_2H_6 presents two Quadruple Point (QP_1 and QP_2) and an Upper Critical EndPoint (UCEP). These points are indicated in Figure F.69 in terms of temperature and O_2 mole fraction.

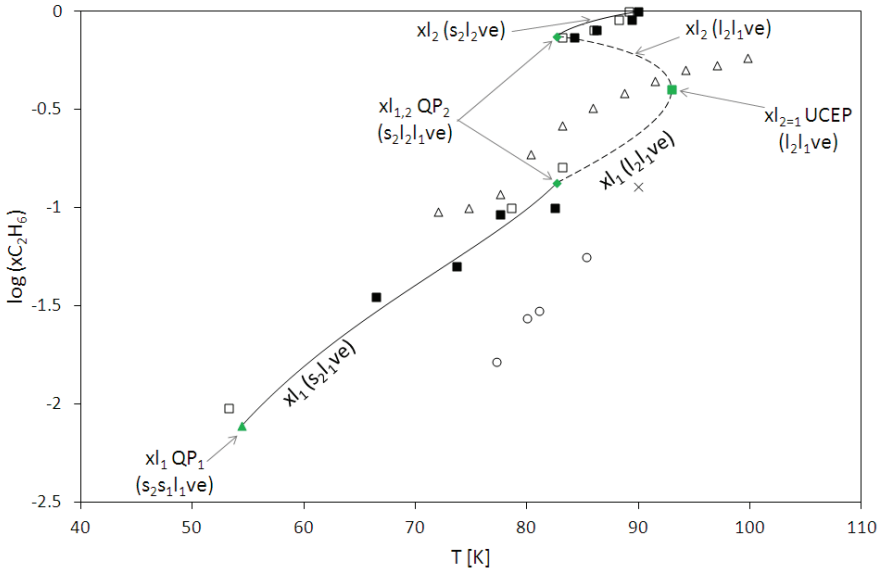

Figure F.69: SLE for the system O_2+C_2H_6.
■ : [MCK1957]; □ : [MCK1958]; ○ : [COX1950]; Δ : [HIM1959]; × : [KAR1958]; — : SLV EoS; ▲ : xl_1 at $s_2s_1l_1ve$; ♦ : xl_1 and xl_2 at $s_2l_2l_1ve$; xl at l_2=l_1ve

The QP_1 is calculated at 54.4 K and it is related to the $solid_2$-$solid_1$-$liquid_1$-vapor equilibrium ($s_2s_1l_1ve$). The QP_1 is represented in Figure F.69 by the green triangle in terms of temperature and the O_2 mole fraction in the phase $liquid_1$.

The QP_2 is calculated at 82.7 K and it is related to the $solid_2$-$liquid_2$-$liquid_1$-vapor equilibrium ($s_2l_2l_1ve$). The QP_2 is represented in Figure F.69 by the green diamonds in terms of temperature and the O_2 mole fraction in the $liquid_1$ and $liquid_2$ phases.

The UCEP is calculated at 93 K and it is associated to the $liquid_2$-$liquid_1$-vapor equilibrium (l_2l_1ve). The UCEP is represented in Figure F.69 by the green square in terms of temperature and the O_2 mole fraction in the critical liquid phase ($l_2=l_1$).

In Figure F.69, the solid lines are the mole fraction of O_2 in the phase $liquid_1$ and $liquid_2$ along the $s_2s_1l_1v$ and the $s_2l_2l_1v$ three phase lines, respectively. Dashed lines are the mole fraction of O_2 in the phase $liquid_1$ and $liquid_2$ along the l_2l_1v three phase line.

The O_2 content in the phase $liquid_1$ at the QP_1 decreases for increasing temperatures till reaching the composition xl_1 at the QP_2 temperature (82.7 K). The O_2 content in the phase $liquid_1$ further decreases up to the UCEP, where the $liquid_1$ and $liquid_2$ phases join together. For temperatures higher than 93 K (UCEP) the two liquid phases becomes totally miscible.

With reference to the phase $liquid_2$, the O_2 content from the UCEP decreases with decreasing temperatures down to the composition xl_2 at the QP_2 temperature (82.7 K), then the O_2 content decreases with increasing temperatures up to the triple point temperature of pure C_2H_6, (placed at y=0 on the *y*-axis).

The SLE experimental values present different equilibrium behaviors, and BIPs have been regressed for matching the presence of immiscibility in the liquid phase proposed in [MCK1957].

The pressure-composition cross sections in Figure F.70 show the qualitative comparison between VLE data and model from 112 K up to 129 K; data are from [HOU2007].

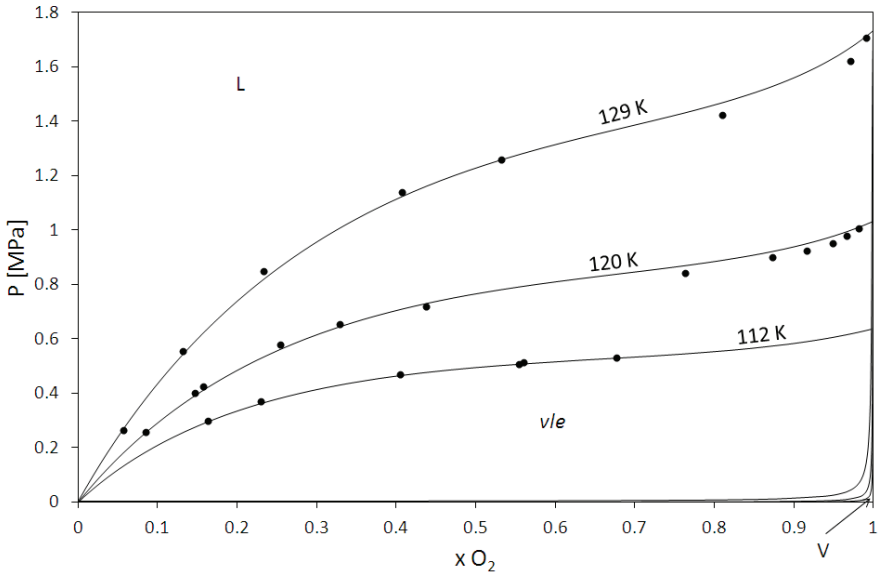

Figure F.70: VLE for the system O_2+C_3H_6 at 112 K, 120 K, and 129 K
● : [HOU2007]; — : SLV EoS.

Table F.24 gives the quantitative comparison between data and values calculated from the SLV EoS in terms of equilibrium mole fractions of O_2.

With reference to the VLE, the AAD% for the composition in the liquid phase is lower than 4%.

With reference to the SLE, only data up to the QP_2 temperature have been considered. The maximum deviations are related to data from [MCK1957] and [MCK1958], and are related to the composition in the phase $liquid_2$.

Table F.24: Quantitative comparison of equilibrium compositions for the system O_2+C_2H_6.

$xO_2+(1-x)C_2H_6$ Ref.	N	Kind of data	T K	P MPa	*x*	*y*	FLASH	
								xO_2 yO_2
[COX1950]	4	SLE Tx	77 – 85		0.94 – 0.98		**N calc**	3
							AAD%	6.09
							Bias%	-6.09
							MAD%	8.37
[HIM1959]	11	SLE Tx	72 – 100		0.42 – 0.9		**N calc**	4
							AAD%	6.18
							Bias%	6.18
							MAD%	10.43
[HOU2007]	31	VLE PTx	112 – 139	0.26 – 2.64	0.04 – 0.99		**N calc**	31
							AAD%	3.15
							Bias%	0.36
							MAD%	9.85
[KAR1958]	1	SLE Tx	90		0.872			
[MCK1957]	8	SLE Tx	67 – 90		0 – 0.97		**N calc**	7
							AAD%	24.83
							Bias%	-23.98
							MAD%	80.78
[MCK1958]	7	SLE Tx	53 – 89		0 – 0.99		**N calc**	4
							AAD%	29.84
							Bias%	-29.06
							MAD%	54.56

1.25 O_2+C_2H_4

The literature data for the system O_2+C_2H_4 are shown in Figure F.71.

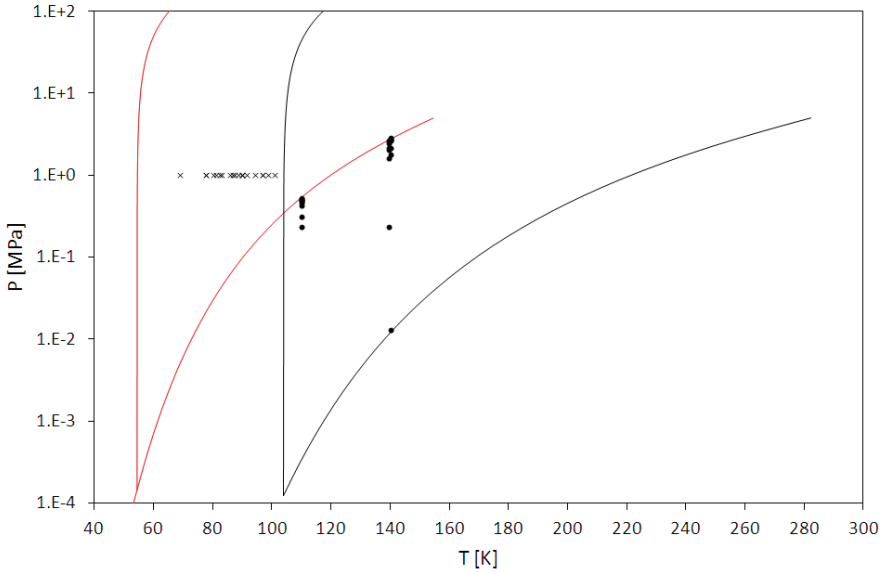

Figure F.71: Available experimental values for the system O_2+C_2H_4.
— : O_2; — : C_2H_4; ● : FFE data; × : SFE data.

The qualitative comparison between model and SLE data is portrayed in Figure F.72. Experimental values are from [COX1950] (filled circles), [HIM1959] (triangles), [KAR1958] (cross), and [TSI1940] (squares). In Figure F.72, the solid line is the mole fraction of O_2 in the phase liquid$_1$ along the solid$_2$-liquid$_1$-vapor three phase line, where 1 and 2 are related to O_2 and C_2H_4, respectively. This line extends up to a QP_2 representing the solid$_2$-liquid$_2$-liquid$_1$-vapor equilibrium, which calculated temperature is about 100 K. The green diamond in Figure F.72 represents the composition of the phase liquid$_1$ at the QP_2.

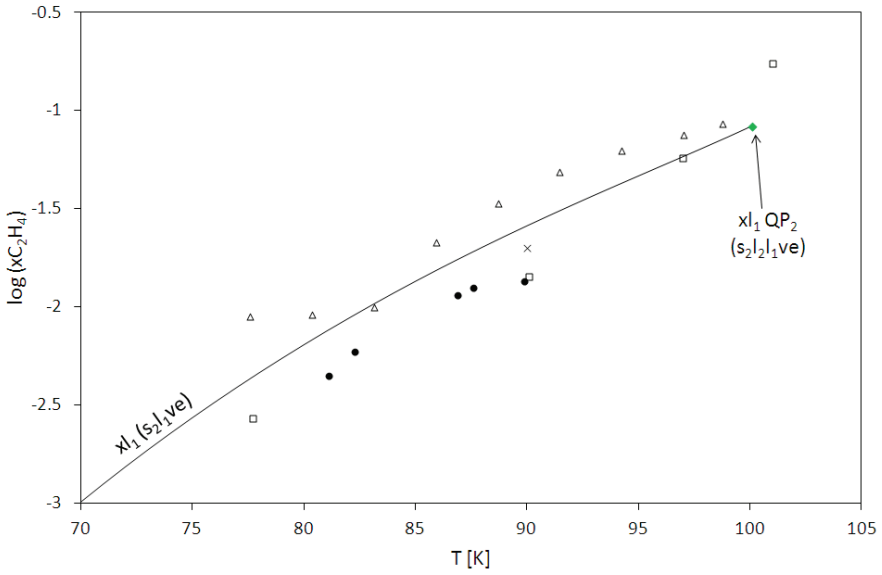

Figure F.72: SLE for the system O_2+C_2H_4.
● : [COX1950]; Δ : [HIM1959]; × : [KAR1958]; □ : [TSI1940]; — : SLV EoS; ♦ : xl_1 at $s_2l_2l_1ve$.

The pressure-composition cross sections in Figure F.73 show the qualitative comparison between VLE data and model at 110 K and 140 K; data are from [HOU2007].

Immiscibility in the liquid phase occurs at 110 K, and at 140 K the two phases are totally miscible. Brackets have been used in Figure F.73 for equilibrium phases and equilibria occurring at 110 K in order to ease the comprehension of the two different phase equilibrium behaviors occurring at 110 K and 140 K. Calculated values are in agreement with experimental values.

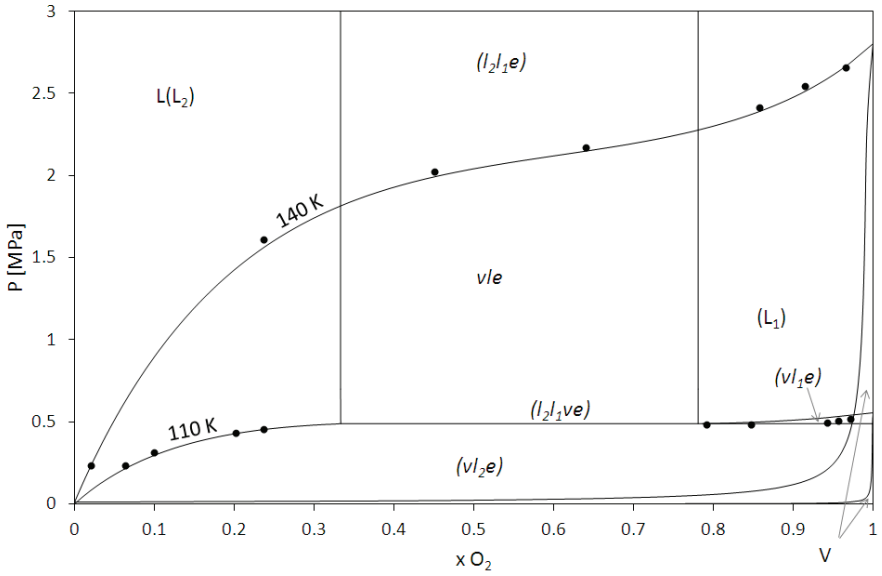

Figure F.73: VLE for the system O_2+C_2H_4 at 110 K, and 140 K
● : [HOU2007]; — : SLV EoS.

Table F.25 gives the quantitative comparison between data and values calculated from the SLV EoS in terms of equilibrium mole fractions of O_2. With reference to the VLE, the AAD% for the composition in the liquid phase is about 5%. With reference to the SLE, only data up to the QP_2 temperature have been considered, and the maximum MAD% is lower than 3%.

Table F.25: Quantitative comparison of equilibrium compositions for the system O_2+C_2H_4.

xO_2+(1-x)C_2H_4 Ref.	N	Kind of data	T K	P MPa	*x*	*y*	FLASH		
								xO_2	yO_2
[COX1950]	5	SLE Tx	81.1 – 89.9		0.99 – 1		**N calc**	5	
							AAD%	0.62	
							Bias%	-0.62	
							MAD%	1.21	
[HIM1959]	9	SLE Tx	77.6 – 98.8		0.91 – 0.99		**N calc**	9	
							AAD%	1.11	
							Bias%	1.10	
							MAD%	2.14	
[HOU2007]	23	VLE PTx	110 – 140	0.013 – 2.82	0 – 0.99		**N calc**	22	
							AAD%	5.14	
							Bias%	1.27	
							MAD%	14.30	
[KAR1958]	1	SLE Tx	90		0.98		**N calc**	1	
							AAD%	0.58	
							Bias%	-0.58	
							MAD%	0.58	
[TSI1940]	5	SLE Tx	69 – 101		0.83 – 1		**N calc**	4	
							AAD%	0.36	
							Bias%	-0.36	
							MAD%	1.20	

1.26 O_2+C_3H_8

The literature data for the system O_2+C_3H_8 are shown in Figure F.74.

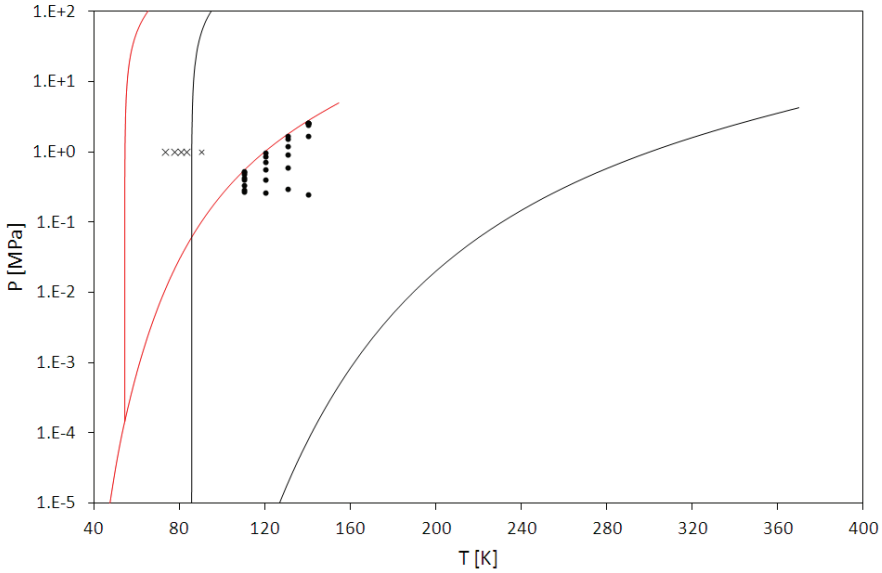

Figure F.74: Available experimental values for the system O_2+C_3H_8.
— : O_2; — : C_3H_8; ● : FFE data; × : SFE data.

The qualitative comparison between model and SLE data is portrayed in Figure F.75. Experimental values are from [KAR1958] (filled circle), [HIM1959] (empty circles).

In Figure F.75, the solid line is the mole fraction of O_2 in the phase liquid$_1$ along the solid$_2$-liquid$_1$-vapor three phase line, where 1 and 2 are related to O_2 and C_3H_8, respectively. This line extends up to a QP_2 representing the solid$_2$-liquid$_2$-liquid$_1$-vapor equilibrium, which calculated temperature is about 83 K. The green diamond in Figure F.75 represents the composition of the phase liquid$_1$ at the QP_2.

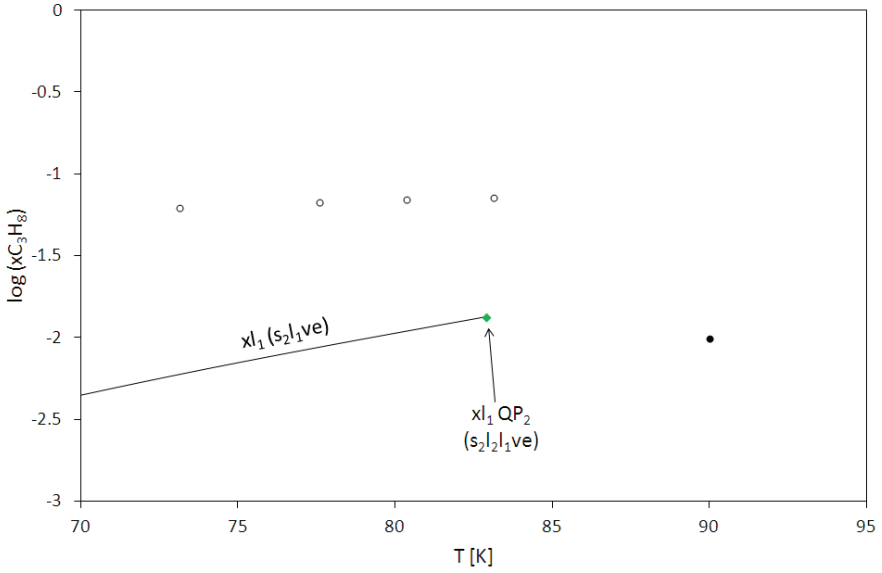

Figure F.75: SLE for the system O_2+C_3H_8.
● : [KAR1958]; ○ : [HM1959]; — : SLV EoS; ♦ : xl_1 at $s_2l_2l_1ve$.

The pressure-composition cross sections in Figure F.76 show the qualitative comparison between VLE data and model from 110 K up to 131 K; data are from [HOU2010b].

Figure F.36 show the qualitative comparison between VLE data and model at 111 K, 120 K, and 130 K. Immiscibility in the liquid phase occurs at these temperatures, and in Figure F.36 the immiscibility gap is indicated by the red dashed lines.

Calculated values are in agreement with experimental values, however the calculated pressure of l_2l_1ve is usually higher than the experimental values of vl_1e.

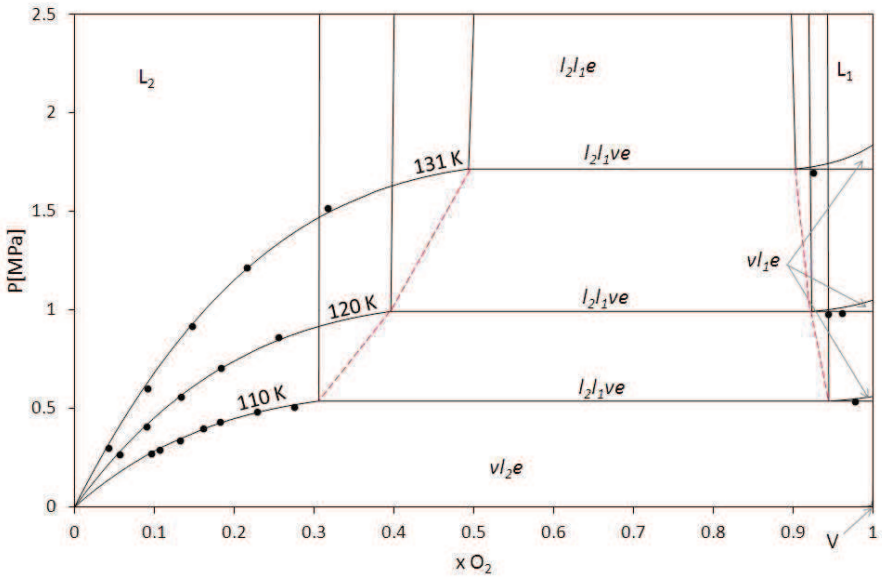

Figure F.76: VLE for the system N_2+C_3H_6 at 195 K, 218 K, and 290 K

● : [HOU2010b]; — : SLV EoS; – – : l_2l_1 immiscibility gap.

Table F.26 gives the quantitative comparison between data and values calculated from the SLV EoS in terms of equilibrium mole fractions of O_2.

With reference to the VLE, the MAD% for the composition in the liquid phase is lower than 10%. With reference to the SLE, only data up to the QP_2 temperature have been considered.

Table F.26: Quantitative comparison of equilibrium compositions for the system O_2+C_3H_8.

$xO_2+(1-x)C_3H_8$ Ref.	N	Kind of data	T K	P MPa	x	y	FLASH		
								xO_2	yO_2
[HIM1959]	4	SLE Tx	73.2 – 83.2		0.93 – 0.94		**N calc**	3	
							AAD%	6.19	
							Bias%	6.19	
							MAD%	6.35	
[HOU2010b]	36	VLE PTx	110 – 140	0.25 – 2.61	0.027 – 0.98		**N calc**	24	
							AAD%	3.57	
							Bias%	-1.59	
							MAD%	9.27	
[KAR1958]	1	SLE Tx	90		0.99				

1.27 O_2+C_3H_6

The literature data for the system O_2+C_3H_6 are shown in Figure F.77

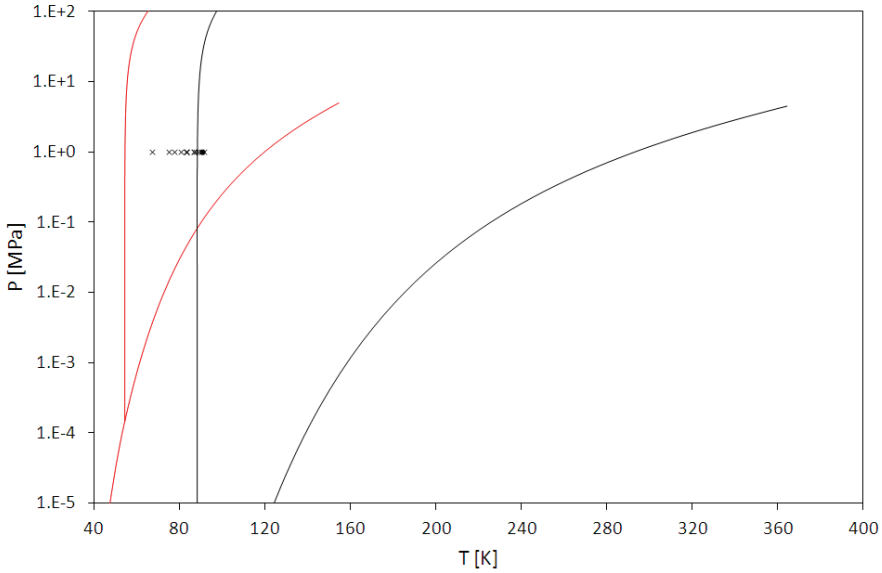

Figure F.77: Available experimental values for the system O_2+C_3H_6.
— : O_2; — : C_3H_6; ● : FFE data; × : SFE data.

The qualitative comparison between model and SLE data is portrayed in Figure F.78. Experimental values are from [MCK1958] (filled circles), [MCK1957] (triangle), [TSI1940] (empty circles), [KAR1958] (cross), and [COX1950] (squares).

In Figure F.78, the solid line is the mole fraction of O_2 in the phase liquid$_1$ along the solid$_2$-liquid$_1$-vapor three phase line, where 1 and 2 are related to O_2 and C_3H_6, respectively. The dashed line is the mole fraction of O_2 in the phase liquid$_2$ along the liquid$_2$-liquid$_1$-vapor three phase line.

These lines meet at the QP_2, namely the solid$_2$-liquid$_2$-liquid$_1$-vapor equilibrium, calculated at 81 K. The green diamond in Figure F.78 represents the composition of the phase liquid$_1$ at the QP_2.

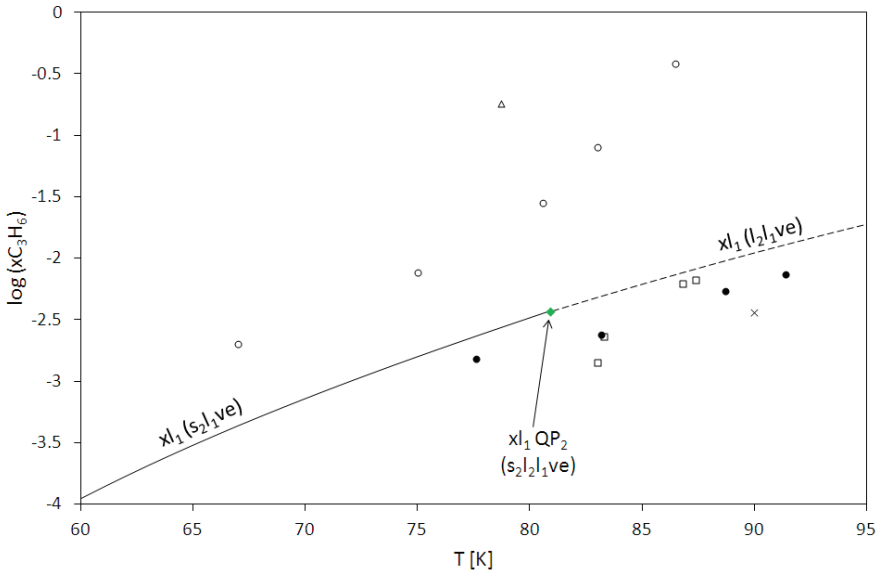

Figure F.78: SLE for the system O_2+C_3H_6.
● : [MCK1958]; Δ : [MCK1957]; ○ : [TSI1940]; × : [KAR1958]; □ : [COX1950]; — : SLV EoS; ♦ : xl$_1$ at $s_2l_2l_1$ve.

Table F.27 gives the quantitative comparison between data and values calculated from the SLV EoS in terms of equilibrium mole fractions of O_2. Only data up to the QP_2 temperature have been considered.

Table F.27: Quantitative comparison of equilibrium compositions for the system O_2+C_3H_6.

$xO_2+(1-x)C_3H_6$ Ref.	N	Kind of data	T K	P MPa	x	y	FLASH	
							xO_2	yO_2
[COX1950]	4	SLE Tx	83 – 87		0.99 – 1			
[KAR1958]	1	SLE Tx	90		~1			
[MCK1957]	1	SLLE Tx	79		0.18 – 0.82		**N calc**	1
							AAD%	0.40
							Bias%	0.40
							MAD%	0.40
[MCK1958]	4	SLE Tx	78 – 91		0.99 – 1		**N calc**	1
							AAD%	0.08
							Bias%	-0.08
							MAD%	0.08
[TSI1940]	5	SLE Tx	67 – 87		0.61 – 1		**N calc**	3
							AAD%	1.11
							Bias%	1.11
							MAD%	2.54

1.28 Ar+Kr

The literature data for the system Ar+Kr are shown in Figure F.79.

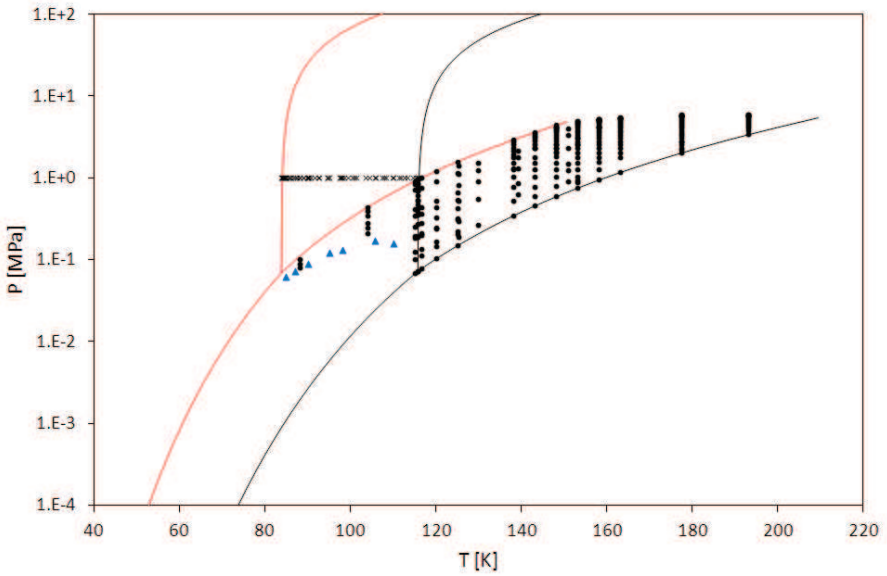

Figure F.79: Available experimental values for the system Ar+Kr.
— : Ar; — : Kr; ● : FFE data; × : SFE data; ▲ : SLVE data.

Table F.28 gives the quantitative comparison between data and values calculated from the SLV EoS in terms of equilibrium mole fractions of Ar. With reference to the VLE, the AAD% for both compositions in the liquid (x) and in the vapor (y) phases is lower than 8% for all the references, except for the data presented in [MAS1976]. For the liquid phase, the maximum value of about 42% for the MAD% has been found with respect to data from [HOL1992]. For the vapor phase, the maximum value of about 30% for the MAD% has been found with respect to data from [SCH1975].

Among the sources of SLE data, the highest deviations occur with respect to [VEI1937].

Table F.28: Quantitative comparison of equilibrium compositions for the system Ar+Kr.

xAr+(1-x)Kr Ref.	N	Kind of data	T K	P MPa	x	y		FLASH xAr	FLASH yAr
[CHU1971]	5	VLE PTx	116	0.07 – 0.95	0 – 1		**N calc**	3	3
							AAD%	1.55	
							Bias%	0.38	
							MAD%	2.69	
[DAV1967]	20	VLE PTxy	104 – 116	0.07 – 0.95	0 – 1	0 – 1	**N calc**	17	17
							AAD%	5.28	1.20
							Bias%	5.14	1.20
							MAD%	14.16	2.25
[HEA1955]	43	SLE Tx	84 – 116		0 – 1		**N calc**	41	
							AAD%	4.83	
							Bias%	-3.49	
							MAD%	38.51	
[HOL1992]	22	VLE PTxy	125 – 151	0.19 – 4.0	0.019 – 0.89	0.21 – 0.98	**N calc**	22	22
							AAD%	6.66	1.56
							Bias%	6.37	-0.44
							MAD%	42.09	7.49
[MAS1974]	7	SLE Tx	85 – 110		0.15 – 0.78		**N calc**	7	
							AAD%	7.82	
							Bias%	6.01	
							MAD%	21.75	

[MAS1976]	42	VLE PTxy	115 – 125	0.07 – 1.58	0 – 1	0 – 1	**N calc**	33	33
							AAD%	17.56	2.34
							Bias%	17.56	1.84
							MAD%	35.93	8.95
	7	SVLE PTx	85 – 110	0.06 – 0.17	0.16 – 0.78		**N calc**	7	5
							AAD%	7.79	7.01
							Bias%	5.98	5.42
							MAD%	21.75	16.94
[SCH1960]	3	VLE PTxy	88	0.08 – 0.1	0.65 – 0.89	0.98 – 0.99	**N calc**	3	3
							AAD%	7.54	0.68
							Bias%	-2.07	0.68
							MAD%	14.41	0.88
[SCH1975]	156	VLE PTxy	138 – 193	0.35 – 6.0	0 – 1	0 – 1	**N calc**	133	135
							AAD%	2.31	1.52
							Bias%	1.48	0.31
							MAD%	34.86	29.90
[VEI1937]	11	SLE Tx	84 – 116		0 – 1		**N calc**	9	
							AAD%	12.52	
							Bias%	-3.88	
							MAD%	44.86	

1.29 Ar+Xe

The literature data for the system Ar+Xe are shown in Figure F.80.

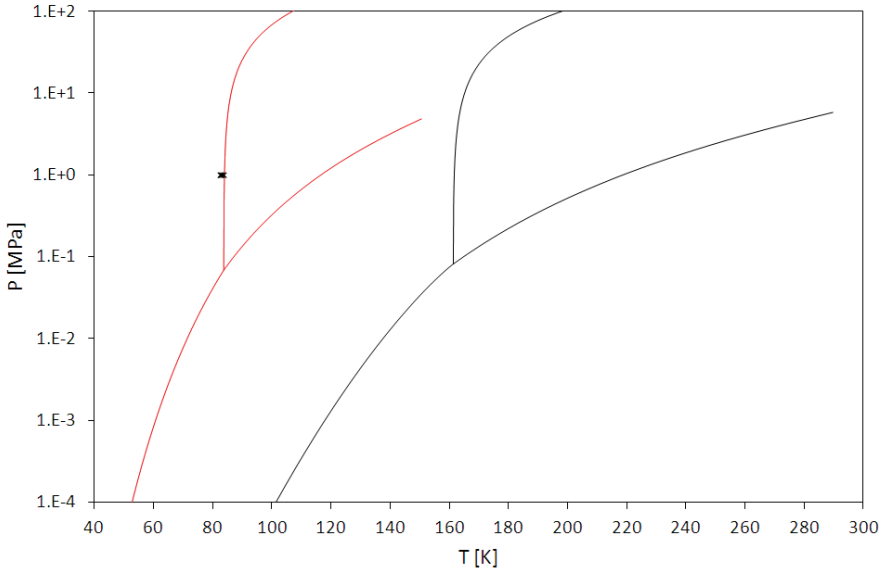

Figure F.80: Available experimental values for the system Ar+Xe.
— : Ar; — : Xe; × : SFE data.

Table F.29 gives the quantitative comparison between data and values calculated from the SLV EoS in terms of equilibrium mole fractions of Ar. AAD% and Bias% are within 10% of error.

Table F.29: Quantitative comparison of equilibrium compositions for the system Ar+Xe.

xAr+(1-x)Xe Ref.	N	Kind of data	T K	P MPa	*x*	*y*	FLASH	
								xAr yAr
[HEA1960]	10	SLE Tx	82 – 84		0.7 – 1		**N calc**	9
							AAD%	9.81
							Bias%	9.81
							MAD%	15.82

1.30 Ar+Ne

The literature data for the system Ar+Ne are shown in Figure F.81.

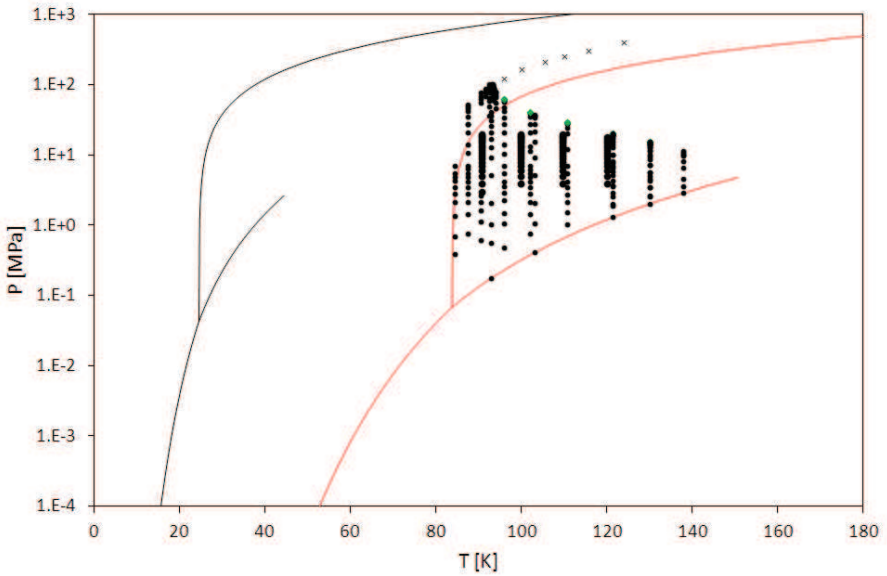

Figure F.81: Available experimental values for the system Ar+Ne.
— : Ar; — : Ne; ● : FFE data; × : SFE data; ♦ : CP data.

Table F.30 gives the quantitative comparison between data and values calculated from the SLV EoS in terms of equilibrium mole fractions of Ar.

With reference to the VLE, the AAD% for both compositions in the liquid (x) and in the vapor (y) phases is lower than 10% for all the references. The maximum values for the MAD% for the liquid (38%) and the vapor (16%) have both been found with respect to data from [STR1967b].

The model is not in agreement with the SLE data at high pressures from [STR1971a].

Table F.30: Quantitative comparison of equilibrium compositions for the system Ar+Ne.

xNe+(1-x)Ar Ref.	N	Kind of data	T K	P MPa	x	y		FLASH xAr	FLASH yAr
[SKR1964]	5	VLE PTxy	90	0.6 – 2.6	0 – 0.02	0.72 – 0.92	**N calc**	5	5
							AAD%	4.26	0.56
							Bias%	-2.93	-0.56
							MAD%	9.67	0.85
[SKR1971]	67	VLE PTxy	91 – 120	2.9 – 19.6	0.03 – 0.31	0.54 – 0.94	**N calc**	67	67
							AAD%	9.18	0.90
							Bias%	-9.18	-0.15
							MAD%	16.65	2.84
[STR1965c]	58	VLE PTxy	84 – 130	0.38 – 7.2	0 – 0.09	0.17 – 0.97	**N calc**	58	58
							AAD%	1.79	0.67
							Bias%	0.57	-0.66
							MAD%	14.69	1.61
[STR1967b]	5	CP PTx	96 – 130	15.5 – 62.1	0.39 – 0.59		**N calc**	5	5
							AAD%	7.14	6.15
							Bias%	-7.14	-6.15
							MAD%	11.89	9.69
	41	VLE PTxy	96 – 130	7.5 – 62.1	0.09 – 0.57	0.46 – 0.92	**N calc**	36	37
							AAD%	4.38	4.34
							Bias%	-0.36	-2.72
							MAD%	37.61	16.19

[STR1971a]	50	VLE PTxy	87 – 94	6.4 – 102	0.054 – 0.57	0.65 – 0.96	**N calc**	46	41
							AAD%	2.72	6.22
							Bias%	1.99	-6.14
							MAD%	22.62	14.16
	6	SLE PTx	96 – 124	120.9 – 393	0.52 – 0.6		**N calc**	6	
							AAD%	49.58	
							Bias%	-49.58	
							MAD%	87.72	
[TRA1974a]	66	VLE PTxy	93 – 138	0.18 – 101.3	0 – 1	0 – 0.94	**N calc**	59	59
							AAD%	1.78	2.58
							Bias%	-1.35	-0.93
							MAD%	7.26	14.01

1.31 Ar+He

The literature data for the system Ar+He are shown in Figure F.82.

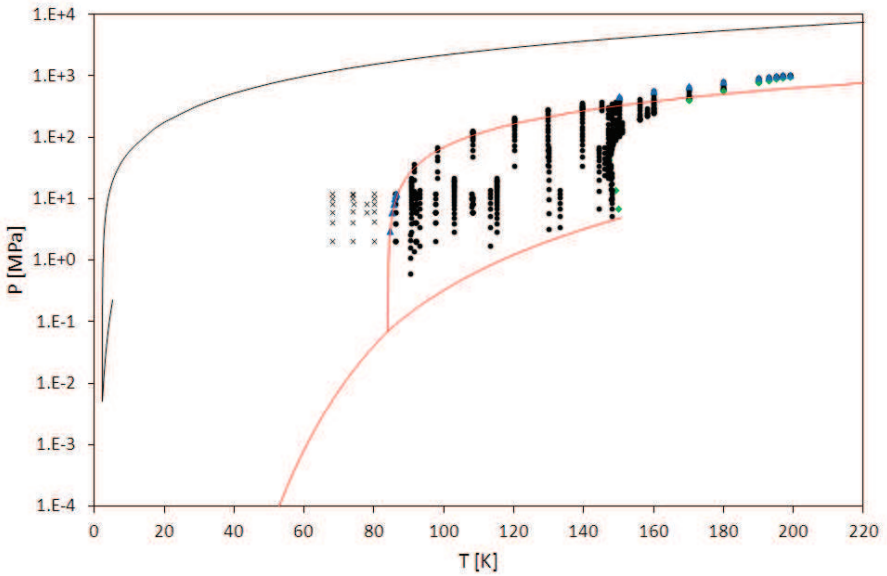

Figure F.82: Available experimental values for the system Ar+He. — : Ar; — : He; ● : FFE data; × : SFE data; ♦ : CP data; ▲ : SVLE and SSLE data.

For the author attempts, it has not been possible representing the phase equilibrium behavior of the system Ar+He for temperature greater than 146 K and pressure greater than 30 MPa. As a consequence, the comparison in this section has been done considering experimental values within these limits.

Table F.31 gives the quantitative comparison between data and values calculated from the SLV EoS in terms of equilibrium mole fractions of Ar. With reference to the VLE, the AAD% for the compositions in the liquid phase is lower than 5% for all the references. For the compositions in the vapor phase, the AAD% is greater than 10% with respect to data proposed in [SKR1971], [STR1969], and [STR1971b].

The maximum values for the MAD% for the liquid (17%) and the vapor (31%) are related to [STR1969] and [STR1971b], respectively.

The model is in agreement with the SVE data from [MUL1965].

Table F.31: Quantitative comparison of equilibrium compositions for the system Ar+He.

xHe+(1-x)Ar Ref.	N	Kind of data	T K	P MPa	*x*	*y*	FLASH	xAr	yAr
[KAT1973]	26	VLE PTy	92 – 108	2.0 – 12.1		0.87 – 0.98	**N calc**		14
							AAD%		2.07
							Bias%		-1.87
							MAD%		4.10
[MUL1965]	21	SVE PTy	68 – 80	2.0 – 12.2		0.98 – 1	**N calc**		21
							AAD%		2.14
							Bias%		-1.79
							MAD%		6.32
	43	VLE PTxy	86 – 108	2 – 12.2	0 – 0.02	0.85 – 0.99	**N calc**	23	26
							AAD%	0.07	2.18
							Bias%	0.06	-2.16
							MAD%	0.52	6.68

[SIN1966]	29	VLE PTx	93 – 148	1.7 – 13.8	0 – 0.14		**N calc**	29	
							AAD%	0.34	
							Bias%	-0.30	
							MAD%	1.28	
[SKR1964]	5	VLE PTxy	90.5	0.6 – 2.6	<0.01	0.74 – 0.94	**N calc**	5	5
							AAD%	0.02	2.60
							Bias%	0.02	-2.60
							MAD%	0.03	7.14
[SKR1971]	60	VLE PTxy	91 – 115	2.94 – 21.6	0 – 0.06	0.47 – 0.98	**N calc**	60	60
							AAD%	0.50	20.59
							Bias%	0.50	-20.19
							MAD%	1.07	31.45
[STR1969]	4	LLE	147	58.4 – 68.9	0.43 – 0.44	0.54 – 0.63			
	58	VLE PTxy	91 – 148	1.4 – 68.9	0. – 0.41	0.26 – 0.99	**N calc**	24	23
							AAD%	2.55	11.02
							Bias%	1.07	-6.57
							MAD%	17.39	27.37
	4	CP	147 – 150	6.9 – 44.2	0.05 – 0.46				
[STR1971b]	196	VLE PTxy	98 – 160	9.6 – 413.7	0.02 – 0.6	0.28 – 0.98	**N calc**	11	11
							AAD%	2.57	15.61
							Bias%	2.35	-10.63
							MAD%	10.04	28.74
[STR1972a]	66	LLE	150 – 199	352 – 1040	0.27 – 0.65	0.77 – 0.95			
	9	SLVE	150 – 199	470 – 1050	0.44 – 0.73				
	7	CP	170 – 199	400 – 980	0.28 – 0.32	0.05 – 0.14			

1.32 Ar+CO_2

The literature data for the system Ar+CO_2 are shown in Figure F.83.

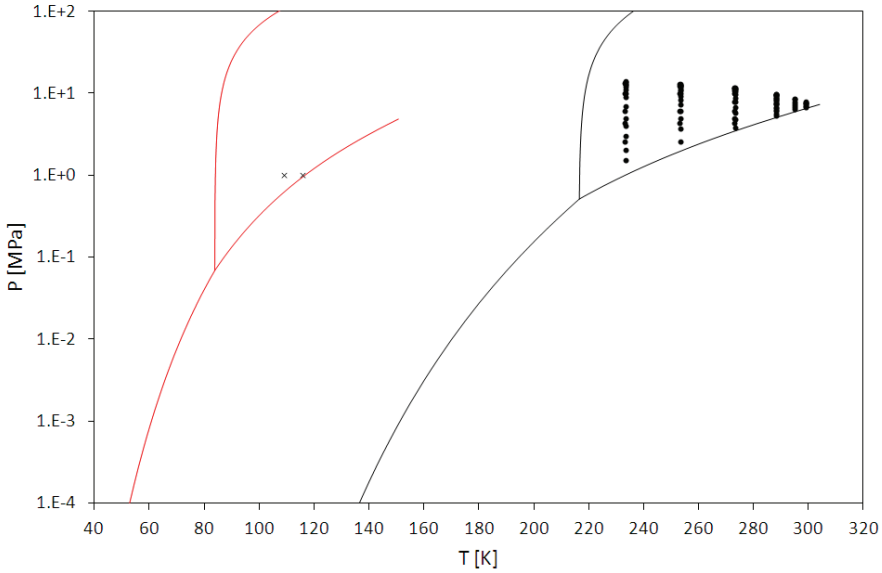

Figure F.83: Available experimental values for the system Ar+CO_2.
— : Ar; — : CO_2; ● : FFE data; × : SFE data.

Table F.32 gives the quantitative comparison between data and values calculated from the SLV EoS in terms of equilibrium mole fractions of Ar.

With reference to the VLE, the AAD% for the compositions in the liquid phase is lower than 11% except for [SAR1971]. For the compositions in the vapor phase, the AAD% is lower than 10% for both references. The maximum values for the MAD% for the liquid and vapor phases are 48% and 53%, respectively. These deviations are encountered for data from [COQ2008], and occur at 273 K and 3.8 MPa: experimental and calculated values for the mole fraction of Ar in the liquid phase are xAr = 0.0069 and xAr = 0.0036, respectively; experimental and calculated values for the mole fraction of Ar in the vapor phase are yAr = 0.058 and yAr = 0.027, respectively.

The model is in agreement with the SLE experimental values from [PRE1971].

Table F.32: Quantitative comparison of equilibrium compositions for the system Ar+CO_2.

xAr+(1-x)CO₂ Ref.	N	Kind of data	T K	P MPa	*x*	*y*		FLASH xAr	FLASH yAr
[COQ2008]	62	VLE PTxy	233 – 299	1.5 – 14.0	0 – 0.41	0.01 – 0.75	**N calc**	58	58
							AAD%	10.76	4.09
							Bias%	6.39	-2.71
							MAD%	47.92	53.44
[KAM1968]	19	VLE PTxy	233.2 – 273.2	2.6 – 13.2	0.03 – 0.35	0.15 – 0.75	**N calc**	14	18
							AAD%	7.70	4.46
							Bias%	4.84	-4.35
							MAD%	14.73	23.39
[PRE1971]	2	SLE Tx	109 – 116		~1		**N calc**	2	
							AAD%	<0.001	
							Bias%	<0.001	
							MAD%	<0.001	
[SAR1971]	12	VLE PTx PTy	288.2	5.7 – 9.8	0.06 – 0.17	0.06 – 0.21	**N calc**	4	6
							AAD%	16.50	8.87
							Bias%	16.50	-8.87
							MAD%	19.79	23.02

1.33 Ar+H_2

The literature data for the system Ar+H_2 are shown in Figure F.84.

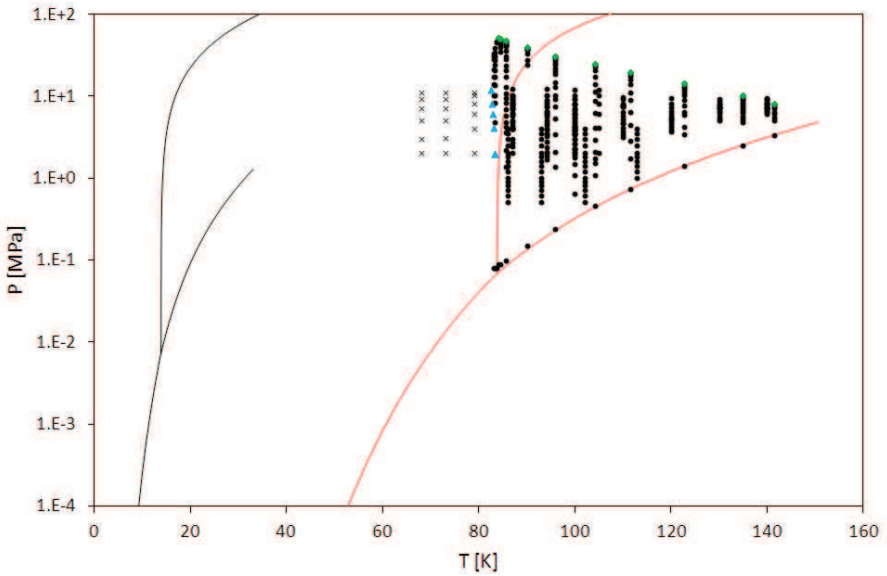

Figure F.84: Available experimental values for the system Ar+H_2. — : Ar; — : H_2; ● : FFE data; × : SFE data; ♦ : CP data; ▲ : SVLE data.

Table F.33 gives the quantitative comparison between data and values calculated from the SLV EoS in terms of equilibrium mole fractions of Ar. With reference to the VLE, the AAD% for both compositions in the liquid (x) and in the vapor (y) phases is lower than 10% for all the references, except for the vapor compositions presented in [CAL1979]. The maximum value for the MAD% for the liquid phases (33%) is related to data from [CAL1979].

The model is in agreement with the SVE experimental values from [MUL1965].

Table F.33: Quantitative comparison of equilibrium compositions for the system Ar+H_2.

xH_2+(1-x)Ar Ref.	N	Kind of data	T K	P MPa	x	y		FLASH xAr	FLASH yAr
[CAL1979]	146	VLE PTxy	83 – 141	0.08 – 51.4	0 – 0.62	0 – 0.98	**N calc**	98	99
							AAD%	4.26	58.00
							Bias%	2.59	57.75
							MAD%	33.76	194.50
	10	CP PTx	84 – 141	8.2 – 51.8	0.21 – 0.6		**N calc**	8	8
							AAD%	3.10	3.24
							Bias%	2.81	3.15
							MAD%	5.78	6.37
[MUL1965][1]	18	SVE PTy	68 – 79	2.03 – 11.2		0.97 – 1	**N calc**		18
							AAD%		2.50
							Bias%		2.50
							MAD%		5.38
	26	VLE PTxy	87 – 105	2.03 – 12.2	0.02 – 0.18	0.71 – 0.95	**N calc**	23	25
							AAD%	0.26	5.54
							Bias%	0.08	5.54
							MAD%	1.06	10.03
	6	SVLE PT	82 – 83	2.0 – 12.1			**N calc**	6	
							AAD%	0.96	
							Bias%	0.96	
							MAD%	1.66	

[OST1977]	55	VLE PTxy	86 – 113	0.51 – 4.1	0 – 0.07	0.22 – 0.95	**N calc**	53	53
							AAD%	0.31	7.43
							Bias%	0.31	2.07
							MAD%	1.74	21.05
[VOL1960]	122	VLE PTx	87 – 140	1.7 – 10.2	0.019 – 0.13		**N calc**	117	
							AAD%	1.56	
							Bias%	-1.52	
							MAD%	10.91	
[XIA1990]	14	VLE PTxy	100	0.64 – 4.6	0 – 0.06	0.47 – 0.87	**N calc**	14	14
							AAD%	0.19	4.95
							Bias%	0.17	4.95
							MAD%	0.49	7.07

[1] – for SVLE PT data, column xAr contains the deviations between calculated and experimental temperatures at fixed pressures. All the experimental temperatures are lower than the minimum temperature along the calculated SVLE (maximum difference about 1.2 K), hindering the possibility of evaluating errors between calculated and experimental pressures. For this reason the column yAr is empty.

1.34 Ar+CH_4

The literature data for the system Ar+CH_4 are shown in Figure F.85.

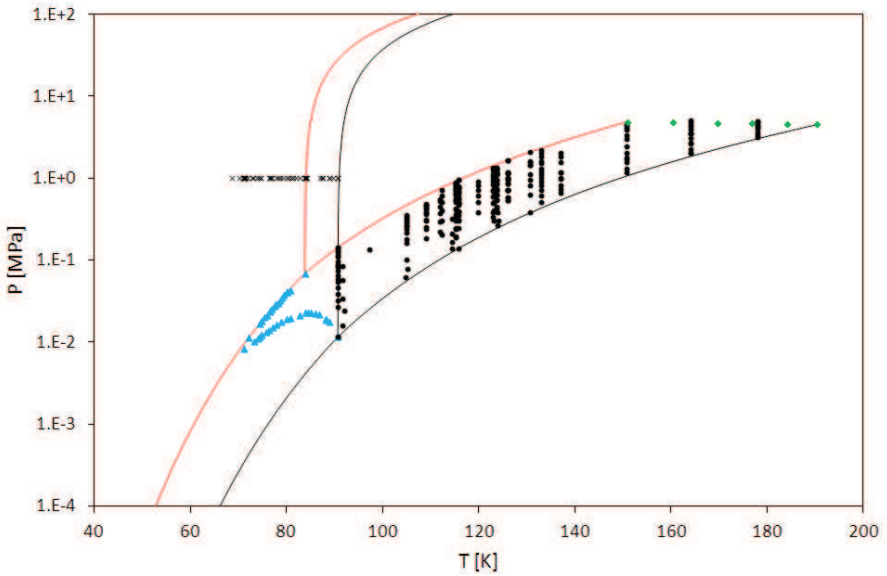

Figure F.85: Available experimental values for the system Ar+CH_4. — : Ar; — : CH_4; ● : FFE data; × : SFE data; ♦ : CP data; ▲ : SVLE data.

Table F.34 gives the quantitative comparison between data and values calculated from the SLV EoS in terms of equilibrium mole fractions of Ar.

With reference to the all the data, the AAD% for both compositions in the liquid (x) and in the vapor (y) phases is lower than 11% for all the references. The maximum values for the MAD% for the liquid (17%) and the vapor (31%) are related to [STR1969] and [STR1971b], respectively.

Considering the VLE, the maximum values for the MAD% for the liquid (57%) and the vapor (34%) have both been found with respect to data from [GRA1971].

The maximum MAD% (81%) among the sources of SLE experimental values is related to data from [VAN1968].The correspondent experimental and calculated values for the solubility of Ar in the liquid phase are xAr = 0.015 and xAr = 0.027, respectively.

Table F.34: Quantitative comparison of equilibrium compositions for the system Ar+CH_4.

xAr+(1-x)CH₄ Ref.	N	Kind of data	T K	P MPa	*x*	*y*		FLASH xAr	FLASH yAr
[CAL1972]	10	VLE PTxy	116	0.14 – 0.95	0 – 1	0 – 1	**N calc**	8	8
							AAD%	4.22	1.04
							Bias%	3.70	1.02
							MAD%	8.09	1.50
[CHE1964]	17	VLE PTxy	92 – 124	0.016 – 0.38	0.01 – 0.38	0.06 – 0.84	**N calc**	17	17
							AAD%	7.39	8.87
							Bias%	-1.09	8.72
							MAD%	18.64	49.49
[CHR1973]	34	VLE PTxy	151 – 178	1.2 – 5.1	0.02 – 0.94	0.05 – 0.95	**N calc**	30	30
							AAD%	4.94	5.27
							Bias%	2.46	-3.56
							MAD%	21.81	38.85
[CHR1974]	5	VLE PTxy	123 – 164	1.0 – 3.5	0.038 – 0.69	0.1 – 0.87	**N calc**	5	5
							AAD%	6.22	6.23
							Bias%	1.55	-3.43
							MAD%	11.68	24.15

[DUN1972]	74	VLE PTx PTy	105 – 126	0.18 – 1.67	0.15 – 1	0.47 – 0.91	**N calc**	63	9
							AAD%	2.97	1.05
							Bias%	2.77	1.05
							MAD%	8.68	1.73
[ELS1975]	6	VLE PTx	115	0.19 – 0.9	0.05 – 0.96		**N calc**	6	6
							AAD%	5.89	
							Bias%	5.77	
							MAD%	10.21	
[FED1938]	24	SLE Tx	71 – 90.0		0 – 1	0 – 1	**N calc**	15	
							AAD%	6.31	
							Bias%	-4.44	
							MAD%	23.25	
[GRA1971]	68	VLE PTxy	115 – 137	0.2 – 1.8	0.04 – 0.95	0.17 – 0.99	**N calc**	67	48
							AAD%	6.98	3.07
							Bias%	6.97	3.07
							MAD%	57.43	34.03
[JON1963]	6	CP Tx	151 – 190		0 – 1		**N calc**	4	
							AAD%	4.97	
							Bias%	4.97	
							MAD%	6.85	
[KEH1983]	10	VLE PTxy	131	0.38 – 2.09	0 – 1	0 – 1	**N calc**	5	8
							AAD%	4.06	3.69
							Bias%	4.06	3.60
							MAD%	9.01	18.20
[KID1975b]	9	VLE PTx	91	0.012 – 0.14	0 – 1		**N calc**	7	
							AAD%	8.85	
							Bias%	-8.85	
							MAD%	18.69	
[LIU1988]	12	VLE PTxy	123	0.34 – 1.34	0.07 – 0.95	0.33 – 0.98	**N calc**	12	12
							AAD%	5.89	1.78
							Bias%	5.51	1.74
							MAD%	12.51	4.57
[SHA1976]	31	VLE PTxy	113 – 133	0.2 – 2.23	0.03 – 0.96	0.14 – 0.99	**N calc**	31	31
							AAD%	10.89	3.70
							Bias%	9.21	2.43
							MAD%	39.43	12.00
[SPR1966]	11	VLE PTxy	91	0.012 – 0.14	0 – 1	0 – 1	**N calc**	11	11
							AAD%	9.46	0.76
							Bias%	-8.79	-0.75
							MAD%	20.12	1.20
[VAN1968]	40	SLE Tx	70 – 91		0 – 1		**N calc**	26	
							AAD%	9.36	
							Bias%	4.25	
							MAD%	81.39	
	40	SVLE PT	71 – 91	0.01 – 0.07			**N calc**	39	39
							AAD%	1.11	7.87
							Bias%	-0.48	5.32
							MAD%	4.18	15.93
[VEI1937]	22	SLE Tx	68 – 91		0 – 1		**N calc**	14	
							AAD%	14.97	
							Bias%	1.25	
							MAD%	31.40	

[1] – for SVLE PT data, column xN_2 (yN_2) contains the deviations between calculated and experimental temperatures (pressures) at fixed pressures (temperatures).

1.35 Ar+C_2H_6

The literature data for the system Ar+C_2H_6 are shown in Figure F.86.

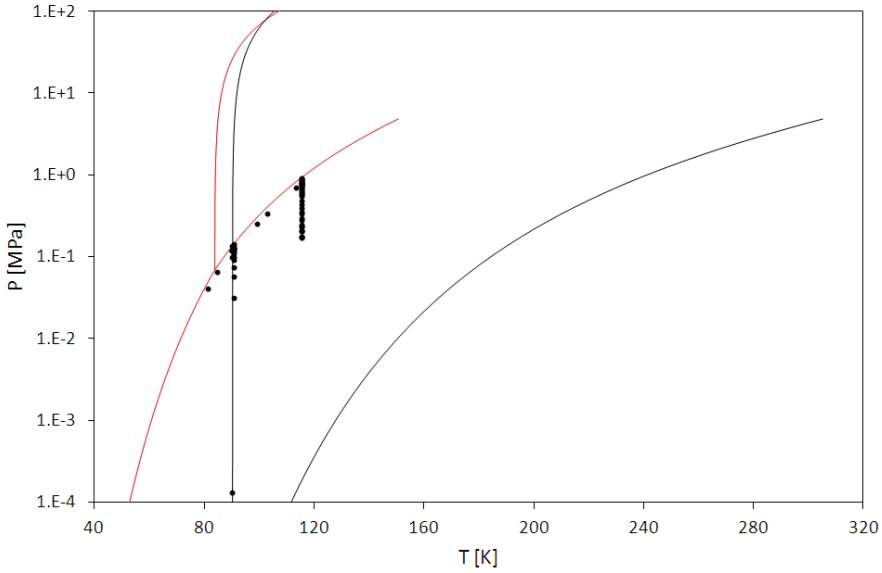

Figure F.86: Available experimental values for the system Ar+C_2H_6.
— : Ar; — : C_2H_6; ● : FFE data.

Table F.35 gives the quantitative comparison between data and values calculated from the SLV EoS in terms of equilibrium mole fractions of Ar.

According to Table F.35, the values calculated from the SLV EoS are quantitatively representative of the experimental values from [AZE1994] and [ELS1971]. Higher deviations in the liquid phase occur for data from [ECK1965] and [LEW1975], whereas the vapor phase remains well represented also in this case.

Table F.35: Quantitative comparison of equilibrium compositions for the system Ar+C_2H_6.

xAr+(1-x)C_2H_6 Ref.	N	Kind of data	T K	P MPa	*x*	*y*		FLASH xAr	FLASH yAr
[AZE1994]	12	VLE PTxy	91	0.03 – 0.14	0.062 – 1	>0.99	**N calc**	11	11
							AAD%	2.91	<0.01
							Bias%	1.18	<0.01
							MAD%	7.34	<0.01
[ECK1965]	6	VLE PTxy	81 – 113	0.04 – 0.69	0.31 – 0.66	>0.99	**N calc**	6	6
							AAD%	31.63	0.13
							Bias%	31.63	0.13
							MAD%	66.60	0.20
[ELS1971]	38	VLE PTx	116	0.17 – 0.92	0.07 – 0.98		**N calc**	38	
							AAD%	3.72	
							Bias%	1.61	
							MAD%	16.42	
[LEW1975]	6	VLE PTxy	90	0 – 0.14	0 – 1	0 – 1	**N calc**	4	4
							AAD%	65.05	0.22
							Bias%	65.05	0.22
							MAD%	182.21	0.57

1.36 Ar+C_3H_6

The literature data for the system Ar+C_3H_6 are shown in Figure F.87.

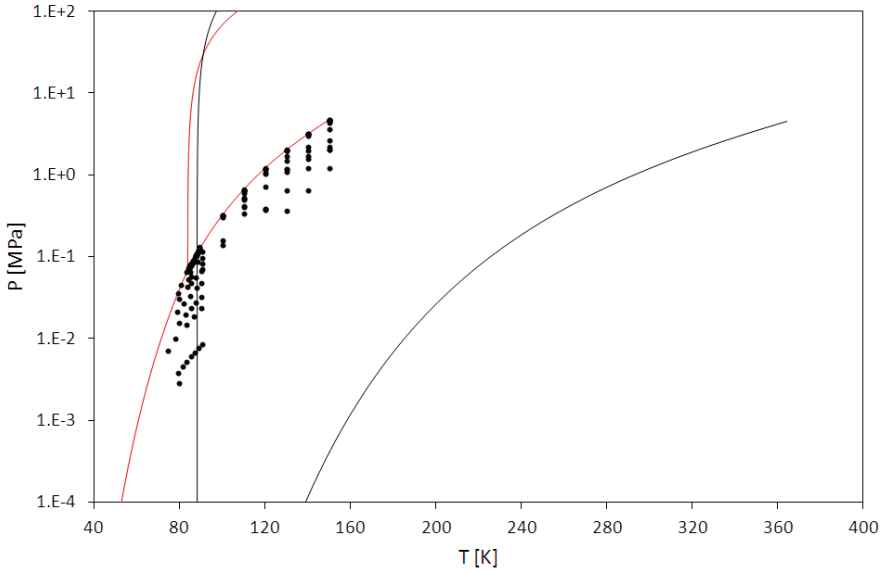

Figure F.87: Available experimental values for the system Ar+C_3H_6.
— : Ar; — : C_3H_6; ● : FFE data.

Table F.36 gives the quantitative comparison between data and values calculated from the SLV EoS in terms of equilibrium mole fractions of Ar.

According to Table F.35, the SLV EoS is in a good agreement with data from [ORO1968]. Nevertheless, calculated values are not representative of the VLE data proposed in [BLA1963], which extend down to temperatures lower than the triple point temperature of pure Ar.

Table F.36: Quantitative comparison of equilibrium compositions for the system Ar+C_3H_6.

xAr+(1-x)C_3H_6 Ref.	N	Kind of data	T K	P MPa	*x*	*y*		FLASH xAr	FLASH yAr
[BLA1963]	76	VLE PTx	74 – 91	<0.01 – 0.13	<0.01 – 0.99		**N calc**	10	
							AAD%	60.00	
							Bias%	-60.00	
							MAD%	76.58	
[ORO1968]	65	VLE PTx	100 – 150	0.14 – 4.7	0.03 – 1		**N calc**	59	
							AAD%	7.52	
							Bias%	1.20	
							MAD%	38.04	

1.37 Kr+Xe

The literature data for the system Kr+Xe are shown in Figure F.88.

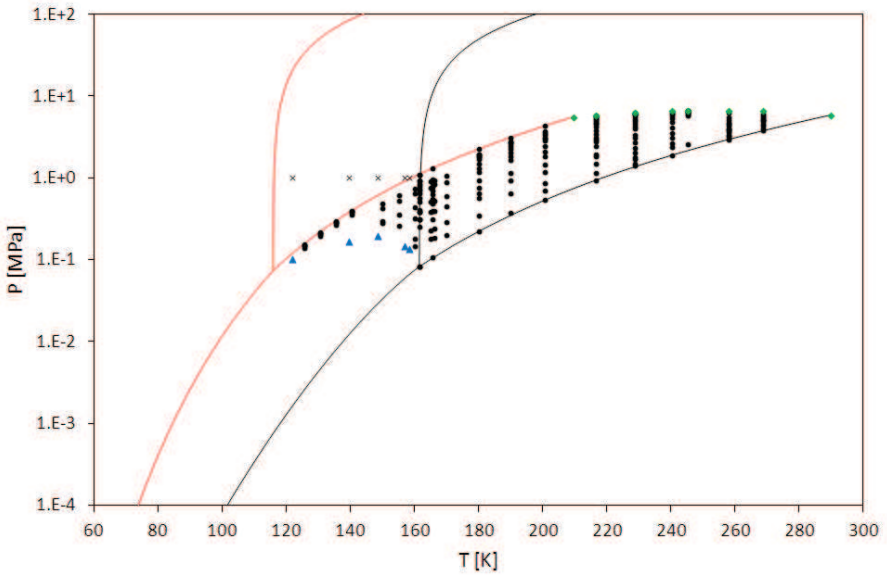

Figure F.88: Available experimental values for the system Kr+Xe. — : Kr; — : Xe; ● : FFE data; × : SFE data; ♦ : CP data; ▲ : VLLE data.

Table F.37 gives the quantitative comparison between data and values calculated from the SLV EoS in terms of equilibrium mole fractions of Kr.

With reference to the VLE, the AAD% for both compositions in the liquid (x) and in the vapor (y) phases is lower than 8% for all the references. A maximum value of about 44% for the MAD% has been found in the liquid phase with respect to data from [MAS1976].

Almost the same experimental values concerning the solubility of solid Xe in liquid Kr are proposed in [MAS1974] and [MAS1976]. The MAD% (42%) related to S(V)LE data in [MAS1974] and [MAS1976] is located at 158 K close to pure Xe. The experimental and calculated values there are xKr = 0.083, and xKr = 0.048, respectively.

Table F.37: Quantitative comparison of equilibrium compositions for the system Kr+Xe.

xKr+(1-x)Xe Ref.	N	Kind of data	T K	P MPa	x	y		FLASH xKr	FLASH yKr
[BOR1982]	16	VLE PTxy	126 – 140	0.14 – 0.4	0.88 – 0.99	0.99 – 1	**N calc**	16	16
							AAD%	0.12	0.03
							Bias%	-0.12	-0.03
							MAD%	0.48	0.13
[CAL1971a]	13	VLE PTxy	161	0.08 – 1.1	0 – 1	0 – 1	**N calc**	11	11
							AAD%	1.57	0.47
							Bias%	0.43	0.46
							MAD%	5.40	1.00
[CAL1983]	139	VLE PTxy	166 – 269	0.11 – 6.6	0 – 1	0 – 1	**N calc**	119	118
							AAD%	4.37	2.59
							Bias%	-3.33	1.27
							MAD%	28.62	23.95
	8	CP PTx	210 – 290	5.5 – 6.7	0 – 1		**N calc**	6	6
							AAD%	2.42	5.02
							Bias%	2.40	-2.06
							MAD%	5.71	12.41

[CHU1971]	6	VLE PTx	161	0.08 – 1.1	0 – 1		**N calc**	4
							AAD%	1.01
							Bias%	-0.11
							MAD%	1.81
[MAS1974]	5	SLE Tx	122 – 158		0.08 – 0.59		**N calc**	5
							AAD%	19.32
							Bias%	-18.42
							MAD%	41.58
[MAS1976]	32	VLE PTxy	150 – 170	0.1 – 1.1	0.04 – 0.67	0.41 – 0.96	**N calc**	32
							AAD%	7.18
							Bias%	4.08
							MAD%	43.92
	5	SVLE PTx	122 – 158	0.1 – 0.2	0.41 – 0.92		**N calc**	5
							AAD%	19.30
							Bias%	-18.40
							MAD%	41.44

N calc	32	4
AAD%	1.62	13.91
Bias%	0.61	-13.91
MAD%	14.59	22.30

1.38 Kr+CO_2

The literature data for the system Kr+CO_2 are shown in Figure F.89.

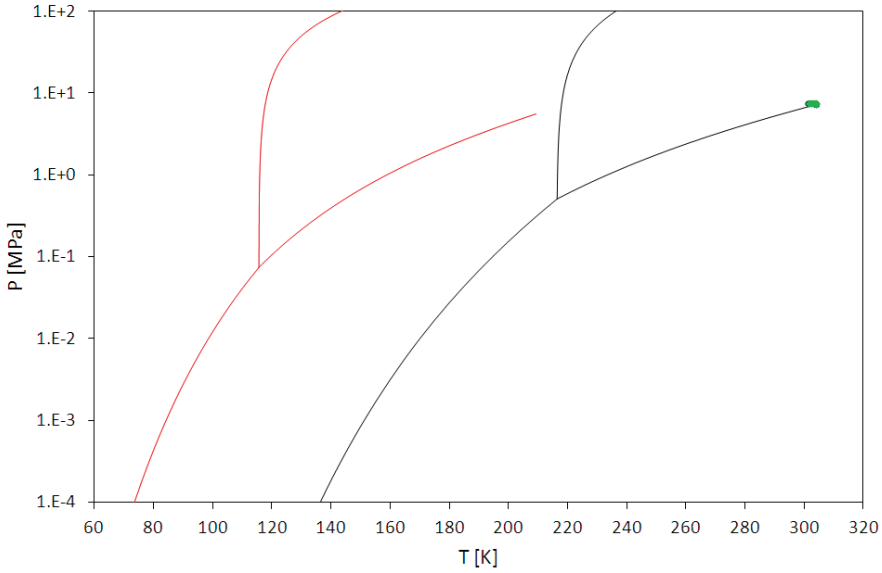

Figure F.89: Available experimental values for the system Kr+CO_2.
— : Kr; — : CO_2; ● : FFE data; ♦ : CP data.

The pressure-temperature equilibrium projection in Figure F.90 shows the comparison between VLE data from [KUS1991] and the critical line from the SLV EoS with null BIPs. The SLV EoS gives a critical locus at temperatures lower than the experimental VLE temperature. As a consequence, deviations cannot be evaluated for the VLE data.

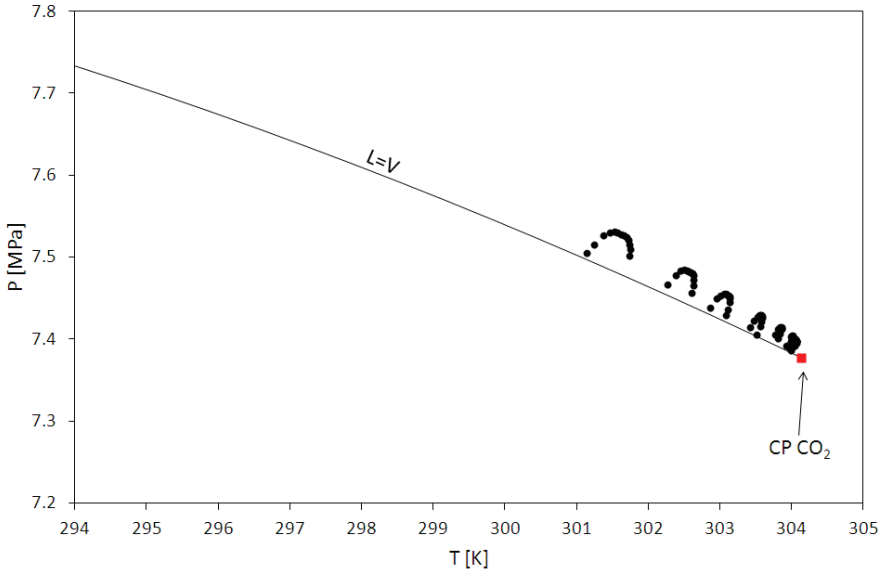

Figure F.90: Experimental critical point and critical line from the SLV EoS for the system Kr+CO_2.
● : [KUS1991]; ■ : critical point of CO_2, [1]; — : SLV EoS (null BIPs).

Table F.38 gives the quantitative comparison between data and values calculated from the SLV EoS with null BIPs in terms of equilibrium mole fractions of Kr. With reference to CP data, the AAD% is lower 20% when critical compositions are evaluated at imposed temperature (column xKr), while a value higher than 100% is encountered when calculation is made at imposed pressure (column yKr).

Table F.38: Quantitative comparison of equilibrium compositions for the system $Kr+CO_2$.

xKr+(1-x)CO₂ Ref.	N	Kind of data	T K	P MPa	*x*	*y*		FLASH xKr	FLASH yKr
[KUS1991]	94	VLE PTx PTy	301 – 304	7.37 – 7.53	0 – 0.03	0 – 0.03	**N calc**		
							AAD%		
							Bias%		
							MAD%		
	12	CP PTx	301 – 304	7.40 – 7.53	0 – 0.03		**N calc**	10	10
							AAD%	16.61	>100
							Bias%	10.70	>100
							MAD%	28.19	>100

1.39 Kr+CH_4

The literature data for the system Kr+CH_4 are shown in Figure F.91.

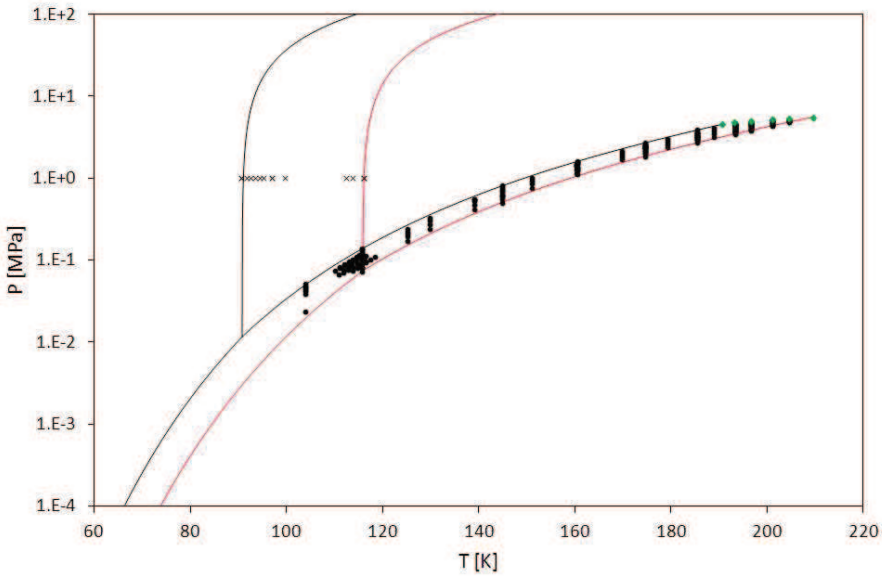

Figure F.91: Available experimental values for the system Kr+CH_4.
— : Kr; — : CH_4; ● : FFE data; × : SFE data; ♦ : CP data.

The temperature-composition cross section in Figure F.92 shows the comparison between SLE data and values calculated from the SLV EoS with null BIPs. The SLV EoS gives a solid solution in agreement with data, and deviations occur mostly with respect to the composition in the solid phase.

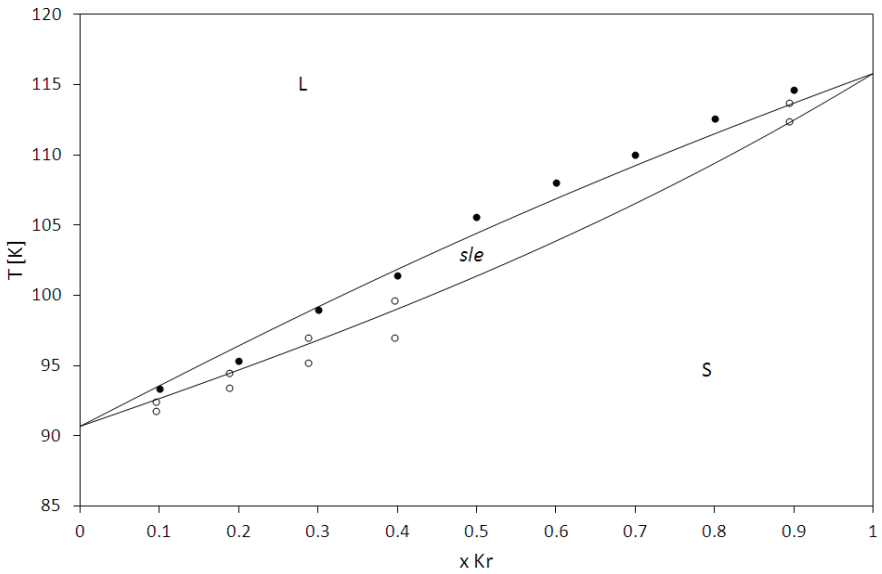

Figure F.92: SLE for the system Kr+CH_4.
● : [VEI1937]; ○ : [VON1936]; — : SLV EoS (null BIPs).

Table F.39 gives the quantitative comparison between data and values calculated from the SLV EoS with null BIPS in terms of equilibrium mole fractions of Kr. With reference to VLE data, the AAD% for both compositions in the liquid (x) and in the vapor (y) phases is lower than 6% for all the references. The calculated critical line agrees well with experimental values from [CAL1981].

Table F.39: Quantitative comparison of equilibrium compositions for the system $Kr+CH_4$.

xKr+(1-x)CH4 Ref.	N	Kind of data	T K	P MPa	*x*	*y*		FLASH xKr	FLASH yKr
[CAL1971b]	28	VLE PTxy	104 – 145	0.02 – 0.82	0 – 1	0 – 1	**N calc**	22	22
							AAD%	5.77	5.37
							Bias%	-2.46	-3.96
							MAD%	20.27	20.80
[CAL1981]	95	VLE PTxy	161 – 205	1.1 – 5.2	0 – 1	0 – 1	**N calc**	87	85
							AAD%	3.73	4.21
							Bias%	3.03	3.67
							MAD%	44.82	50.75
	6	CP PTx	191 – 210	4.6 – 5.5	0 – 1		**N calc**	4	4
							AAD%	2.02	9.86
							Bias%	-1.47	9.86
							MAD%	4.62	17.69
[FUK1967]	32	VLE PTx	110 – 118	0.07 – 0.12	0.18 – 0.67		**N calc**	32	
							AAD%	5.18	
							Bias%	-5.18	
							MAD%	13.24	
[HOL1992]	36	VLE PTxy	125 – 189	0.17 – 4.1	0.14 – 0.78	0.17 – 0.83	**N calc**	36	36
							AAD%	4.08	4.54
							Bias%	0.54	0.80
							MAD%	14.86	16.77
[VEI1937]	11	SLE PTx	91 – 116		0 – 1		**N calc**	9	
							AAD%	7.55	
							Bias%	-0.09	
							MAD%	19.28	
[VON1936]	14	SLE PTx	91 – 116		0 – 1		**N calc**	10	
							AAD%	22.62	
							Bias%	-22.36	
							MAD%	41.37	

1.40 $Kr+C_2H_6$

The literature data for the system $Kr+C_2H_6$ are shown in Figure F.93.

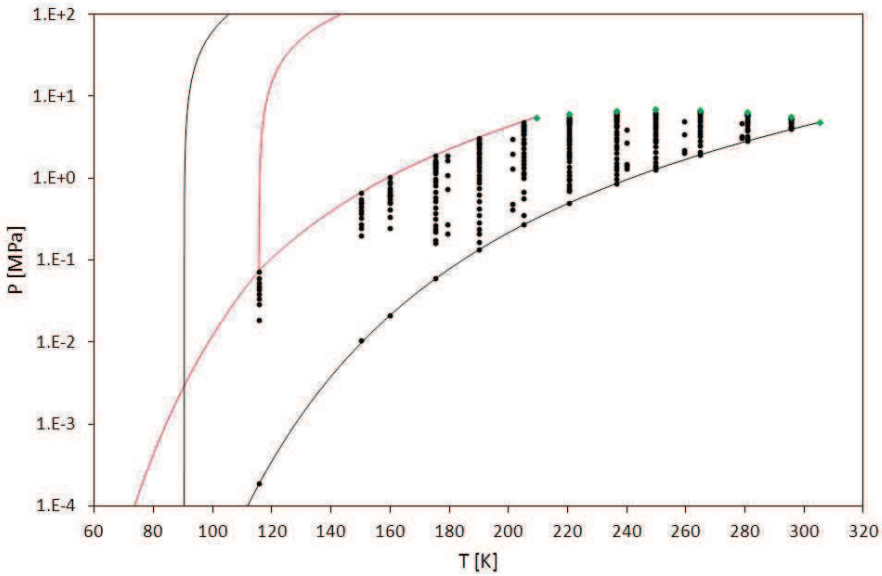

Figure F.93: Available experimental values for the system $Kr+C_2H_6$.
— : Kr; — : C_2H_6; ● : FFE data; ♦ : CP data.

Table F.40 gives the quantitative comparison between data and values calculated from the SLV EoS with null BIPs in terms of equilibrium mole fractions of Kr.

With reference to VLE data, the AAD% for both compositions in the liquid (x) and in the vapor (y) phases is lower than 8% for all the references, except [HOL1992]. The calculated critical line agrees well with experimental values from [CAL1987].

Table F.40: Quantitative comparison of equilibrium compositions for the system $Kr+C_2H_6$.

xKr+(1-x)C₂H₆ Ref.	N	Kind of data	T K	P MPa	*x*	*y*		FLASH xKr	FLASH yKr
[CAL1987]	226	VLE PTxy	150 – 296	0.01 – 6.61	0 – 1	0 – 1	**N calc**	192	168
							AAD%	6.33	2.91
							Bias%	1.08	-0.71
							MAD%	46.71	42.53
	8	CP PTx	209 – 305	4.9 – 6.9	0 – 1		**N calc**	6	6
							AAD%	3.75	7.55
							Bias%	3.75	2.54
							MAD%	6.84	17.46
[GOM1991]	10	VLE PTxy	116	0 – 0.07	0 – 1	0 – 1	**N calc**	8	8
							AAD%	7.01	0.05
							Bias%	7.01	0.05
							MAD%	19.25	0.10
[HOL1992]	29	VLE PTxy	179 – 279	0.2 – 4.9	0.046 – 0.92	0.12 – 0.99	**N calc**	29	29
							AAD%	22.97	14.80
							Bias%	-22.97	-14.80
							MAD%	41.15	38.51

1.41 Kr+C_2H_4

The literature data for the system Kr+C_2H_4 are shown in Figure F.94.

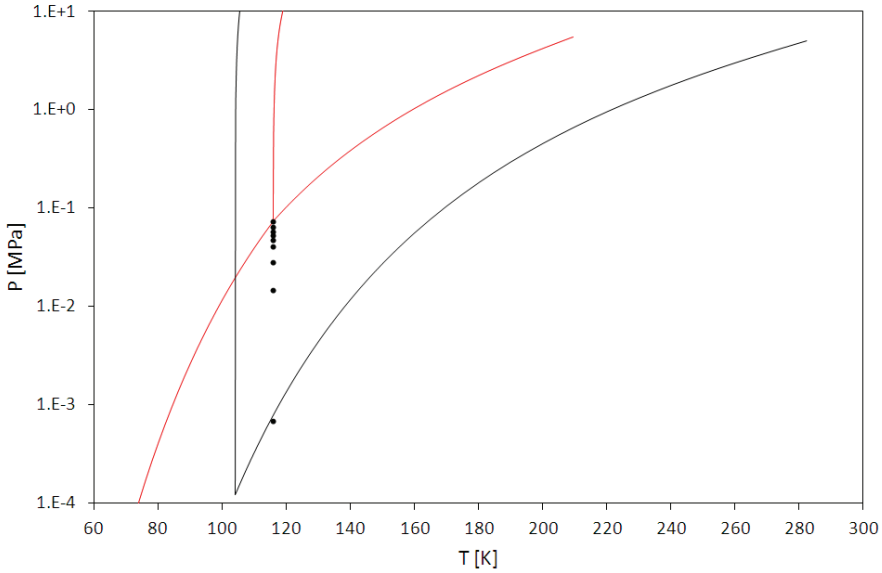

Figure F.94: Available experimental values for the system Kr+C_2H_4.
— : Kr; — : C_2H_4; ● : FFE data.

The pressure-composition cross section in Figure F.95 shows the comparison between experimental values and model with null BIPs at 116 K. The SLV EoS does not represent quantitatively the liquid compositions at VLE from [CAL1978].

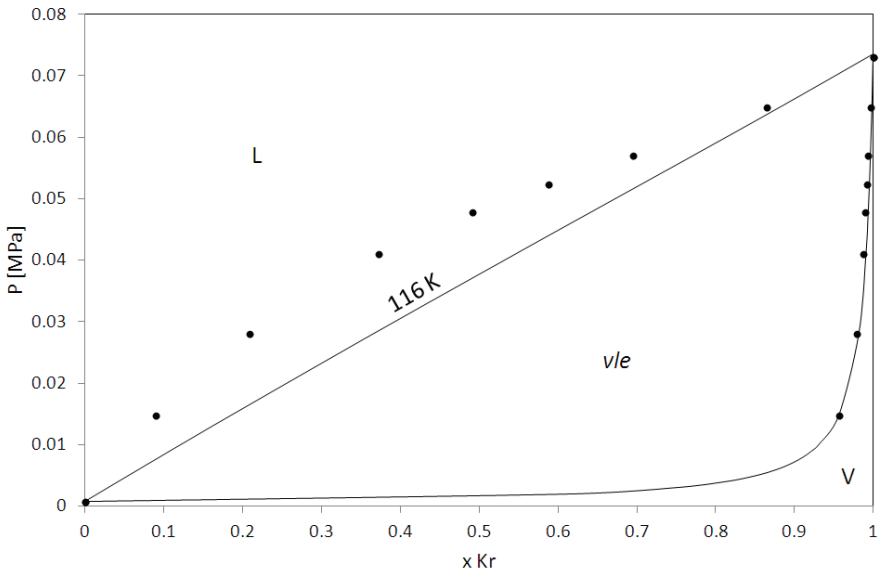

Figure F.95: VLE for the system Kr+C_2H_4 at 116 K.
● : [CAL1978]; — : SLV EoS (null BIPs).

Table F.41 gives the quantitative comparison between data and values calculated from the SLV EoS with null BIPs in terms of equilibrium mole fractions of Kr.

Important deviations are encountered when evaluating compositions in the liquid phase, whereas statistical indexes are less than 0.5% with respect to the mole fraction in the vapor phase.

Table F.41: Quantitative comparison of equilibrium compositions for the system $Kr+C_2H_4$.

xKr+(1-x)C₂H₄ Ref.	N	Kind of data	T K	P MPa	*x*	*y*		FLASH xKr	FLASH yKr
[CAL1978]	9	VLE PTxy	116	<0.001 – 0.07	0 – 1	0 – 1	**N calc**	7	7
							AAD%	41.69	0.26
							Bias%	41.69	0.25
							MAD%	106.07	0.26

1.42 $Kr+C_3H_6$

The literature data for the system $Kr+C_3H_6$ are shown in Figure F.96.

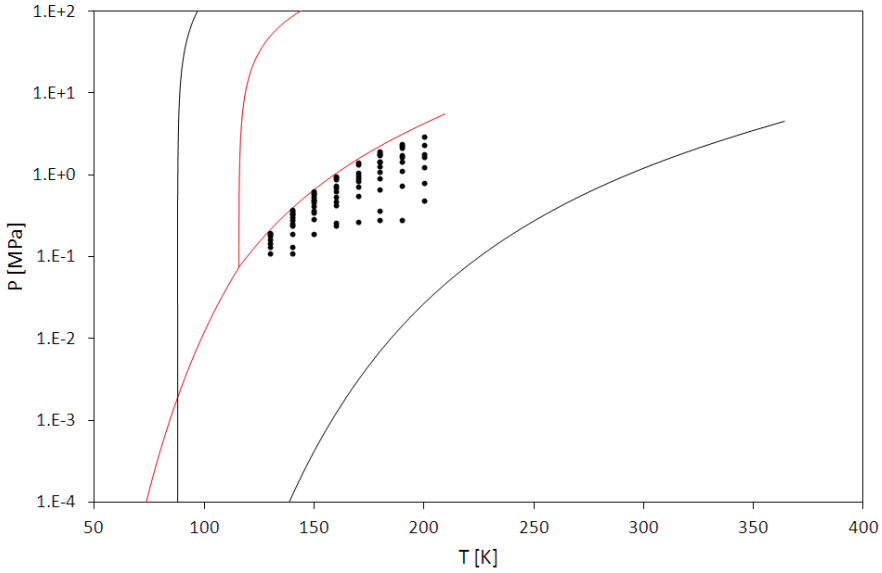

Figure F.96: Available experimental values for the system $Kr+C_3H_6$.
— : Kr; — : C_3H_6; ● : FFE data.

Table F.42 gives the quantitative comparison between data and values calculated from the SLV EoS with null BIPs in terms of equilibrium mole fractions of Kr. Model is not in agreement with the experimental values proposed in [ORO1968].

Table F.42: Quantitative comparison of equilibrium compositions for the system $Kr+C_3H_6$.

xKr+(1-x)C₃H₆ Ref.	N	Kind of data	T K	P MPa	*x*	*y*	FLASH	
								xKr yKr
[ORO1968]	78	VLE PTx	130 – 200	0.1 – 2.9	0.06 – 0.96		**N calc**	72
							AAD%	24.93
							Bias%	24.91
							MAD%	125.25

1.43 Xe+Ne

The literature data for the system Xe+Ne are shown in Figure F.97.

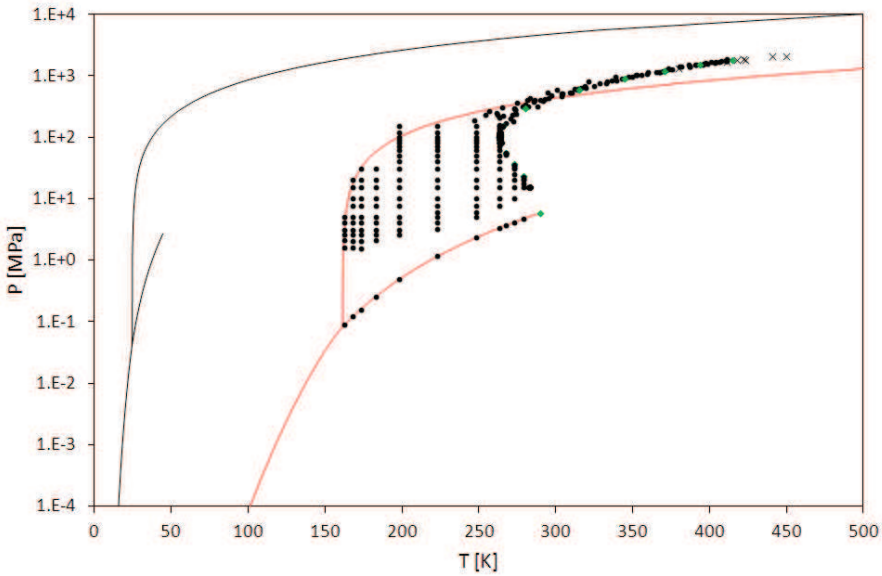

Figure F.97: Available experimental values for the system Xe+Ne.
— : Xe; — : Ne; ● : FFE data; × : SFE data; ♦ : CP data.

For the author attempts, it has not been possible representing the phase equilibrium behavior of the system Xe+Ne for temperature greater than 250 K and pressure greater than 100 MPa. As a consequence, the comparison in this section has been done considering experimental values within these limits.

Table F.43 gives the quantitative comparison between data and values calculated from the SLV EoS in terms of equilibrium mole fractions of Xe.

Only one available reference presents data within the cited limits of temperature and pressure (250 K, 100 MPa), and the EoS is in a good agreement with experimental values concerning both the liquid and the vapor phases.

Table F.43: Quantitative comparison of equilibrium compositions for the system Xe+Ne.

xXe+(1-x)Ne Ref.	N	Kind of data	T K	P MPa	*x*	*y*	FLASH		
								xXe	yXe
[BER1985a]	88	LLE PTx	247 – 411	160 – 1880	0.14 – 0.53				
	6	CP PTx	280 – 415	300 – 1880	0.26 – 0.36				
[BER1985b]	7	SLE PTx	380 – 450	1300 – 2080	0.26 – 0.53				
[DEE1980a]	171	VLE PTxy	163 – 279	0.09 - 152	0.39 – 1	0.015 – 1	**N calc**	61	80
							AAD%	0.60	1.82
							Bias%	-0.56	-0.96
							MAD%	2.57	10.93
	13	CP PTx	264 – 290	5.84 - 152	0.35 – 1				
[DEE1980b]	87	VLE PTxy	263 – 283	15.2 – 121.6	0.26 – 0.76	0.39 – 0.84			

1.44 $Xe+CO_2$

The literature data for the system N_2+O_2 are shown in Figure F.98.

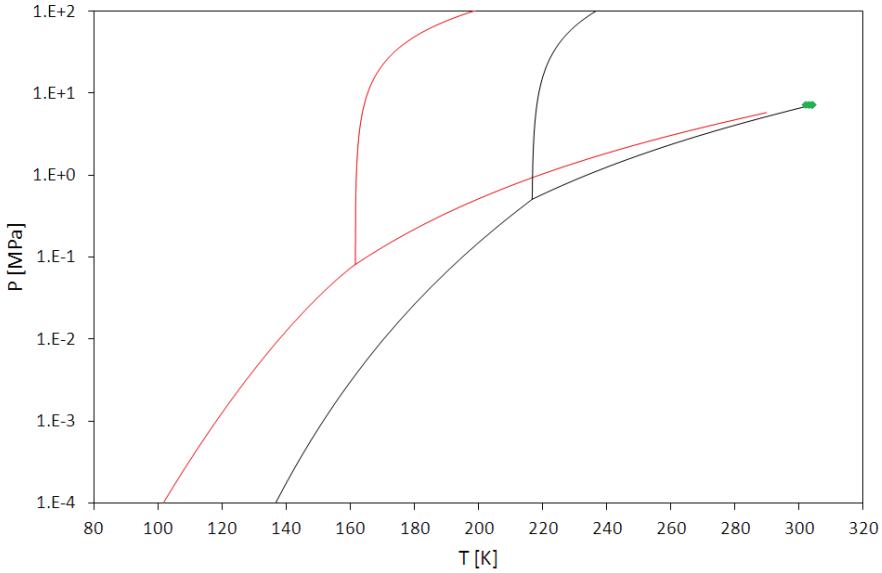

Figure F.98: Available experimental values for the system $Xe+CO_2$.
— : Xe; — : CO_2; ♦ : CP data.

The temperature-composition cross section Figure F.99 shows the comparison between critical point data and the critical line from the model with null BIPs. The SLV EoS is not in agreement with the experimental values from [MAR1999].

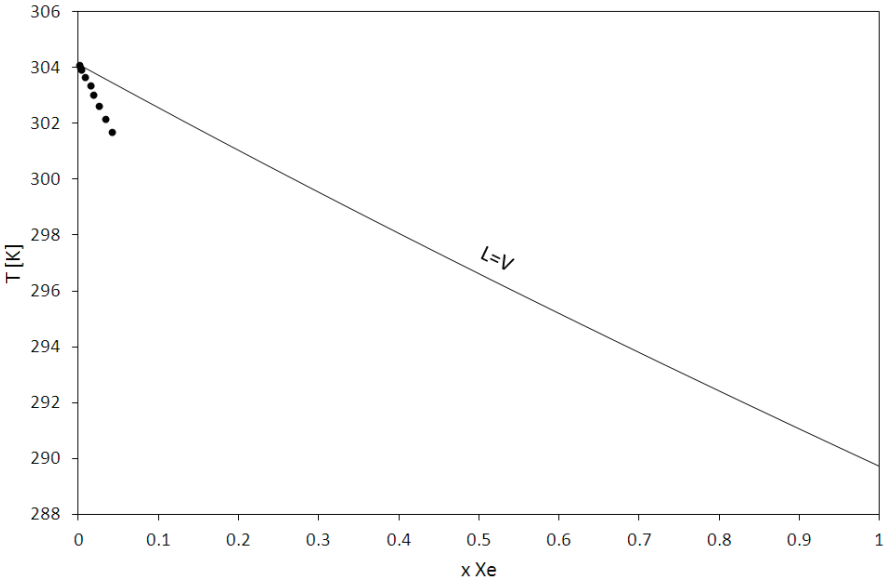

Figure F.99: Experimental critical point data and calculated critical line for the system $Xe+CO_2$.
● : [MAR1999]; — : SLV EoS (null BIPs).

Table F.44 gives the quantitative comparison between data and values calculated from the SLV EoS with null BIPs in terms of equilibrium mole fractions of Xe. Important deviations are encountered when evaluating compositions at fixed temperature, whereas the AAD% is less than 20% when calculation is made at fixed pressure.

Table F.44: Quantitative comparison of equilibrium compositions for the system $Xe+CO_2$.

xXe+(1-x)CO₂ Ref.	N	Kind of data	T K	P MPa	*x*	*y*		FLASH xXe	FLASH yXe
[MAR1999]	10	CP PTx	302 – 304	7.29 – 7.39	0 – 0.042		**N calc**	9	6
							AAD%	>100	18.78
							Bias%	>100	-13.61
							MAD%	>100	50.51

1.45 Xe+N_2O

The literature data for the system N_2+N_2O are shown in Figure F.100.

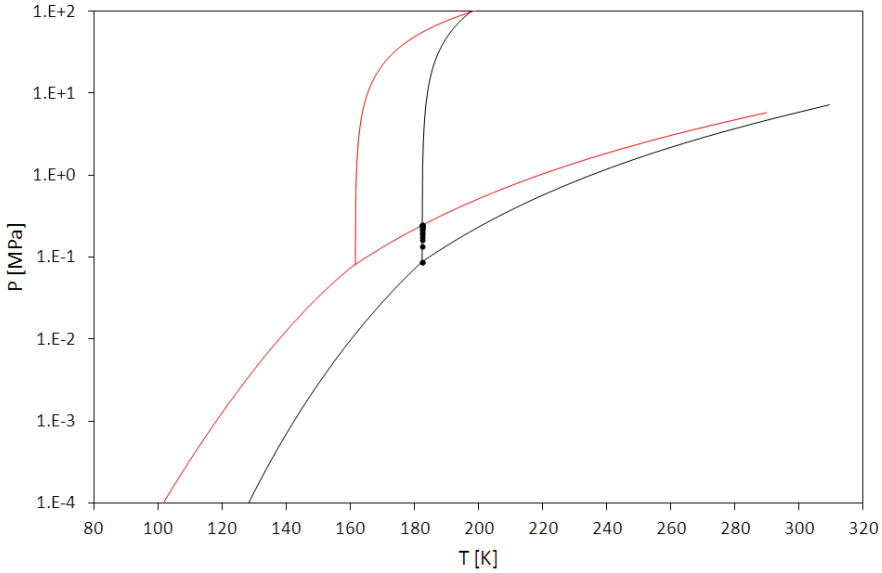

Figure F.100: Available experimental values for the system Xe+N_2O.
— : Xe; — : N_2O; ● : FFE data.

The pressure-composition cross section in Figure F.101 shows the qualitative comparison between VLE data and model with null BIPs at 182 K. The SLV EoS does not represent the azeotropic behavior of the system Xe+N_2O.

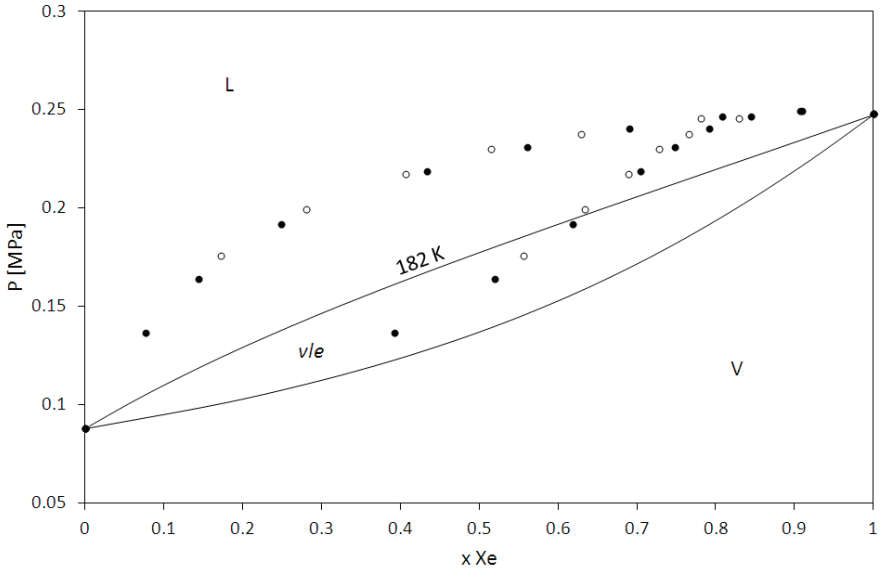

Figure F.101: VLE for the system Xe+N_2O at 182 K.
● : [MAC1980]; ○ [FON1995]; — : SLV EoS (null BIPs).

Table F.45 gives the quantitative comparison between data and values calculated from the SLV EoS with null BIPs in terms of equilibrium mole fractions of Xe. Important deviations are encountered for both the liquid and the vapor phases.

Table F.45: Quantitative comparison of equilibrium compositions for the system $Xe+N_2O$.

xXe+(1-x)N₂O Ref.	N	Kind of data	T K	P MPa	*x*	*y*		FLASH xXe	FLASH yXe
[FON1995]	8	VLE PTxy	182	0.09 – 0.25	0 – 1	0 – 1	**N calc**	5	5
							AAD%	105.65	28.99
							Bias%	105.65	28.99
							MAD%	183.35	30.25
[MAC1980]	10	VLE PTxy	182	0.09 – 0.25	0 – 1	0 – 1	**N calc**	6	6
							AAD%	119.71	26.60
							Bias%	119.71	26.60
							MAD%	212.02	28.33

1.46 Xe+CH_4

The literature data for the system Xe+CH_4 are shown in Figure F.102.

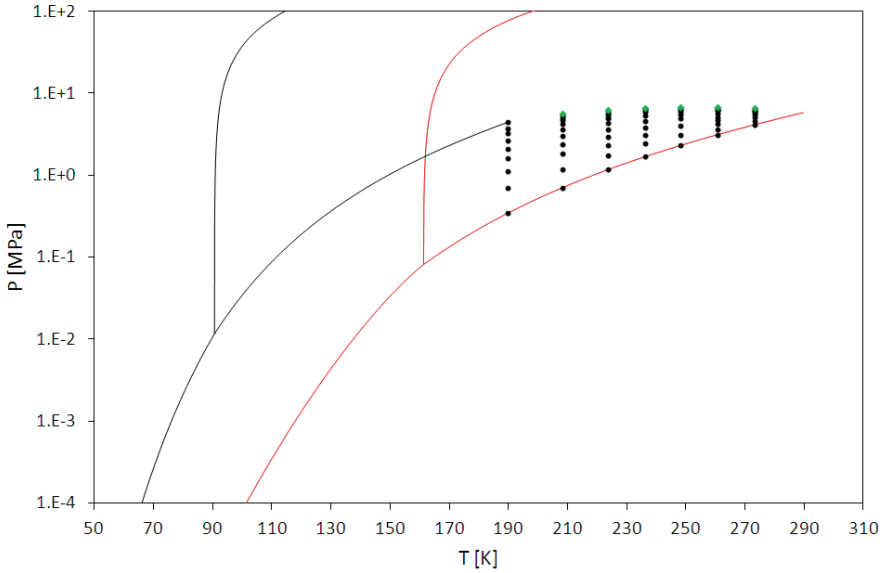

Figure F.102: Available experimental values for the system Xe+CH_4.
— : Xe; — : CH_4; ● : FFE data; ♦ : CP data.

Table F.46 gives the quantitative comparison between data and values calculated from the SLV EoS with null BIPs in terms of equilibrium mole fractions of Xe. With reference to the data, the AAD% for both compositions in the liquid (x) and in the vapor (y) phases is lower than 6%.

Table F.46: Quantitative comparison of equilibrium compositions for the system Xe+CH_4.

xXe+(1-x)CH4 Ref.	N	Kind of data	T K	P MPa	*x*	*y*		FLASH xXe	FLASH yXe
[DIA2004]	64	VLE PTxy	190 – 273	0.35 – 6.5	0 – 1	0 – 1	**N calc**	56	56
							AAD%	1.96	3.90
							Bias%	-0.37	-3.63
							MAD%	12.47	16.09
	6	CP PTx	208 – 273	5.7 – 6.8	0.21 – 0.85		**N calc**	6	4
							AAD%	5.25	3.74
							Bias%	-5.25	-1.07
							MAD%	11.53	7.73

1.47 $Xe+C_2H_6$

The literature data for the system $Xe+C_2H_6$ are shown in Figure F.103.

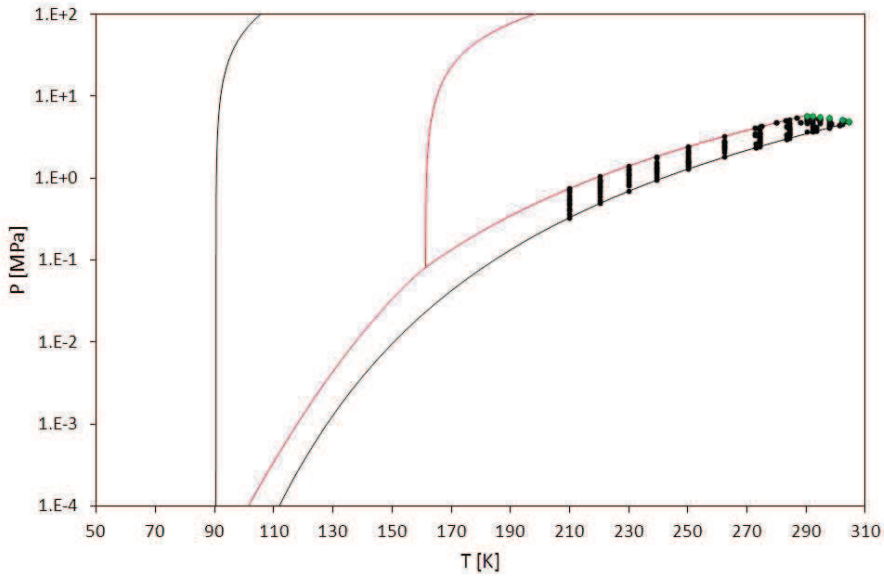

Figure F.103: Available experimental values for the system $Xe+C_2H_6$.
— : Xe; — : C_2H_6; ● : FFE data; ♦ : CP data.

Table F.47 gives the quantitative comparison between data and values calculated from the SLV EoS with null BIPs in terms of equilibrium mole fractions of Xe.

With reference to the VLE, the AAD% for both compositions in the liquid (x) and in the vapor (y) phases is lower than 16% for all the references. Although high values for the MAD% are encountered (at low contents of Xe), the model with null BIPs is in a good agreement with data considering the narrow vapor-liquid equilibrium that the system $Xe+C_2H_6$ presents in the range 210 K ≤ T ≤ 304 K.

Table F.47: Quantitative comparison of equilibrium compositions for the system $Xe+C_2H_6$.

xXe+(1-x)C₂H₆ Ref.	N	Kind of data	T K	P MPa	*x*	*y*		FLASH xXe	FLASH yXe
[DUA2000]	19	VLE PTx PTy	273 – 303	2.4 – 5.5	0 – 1	0 – 1	**N calc**	8	9
							AAD%	14.28	15.10
							Bias%	-14.28	-15.10
							MAD%	35.53	35.44
[NUN1985]	161	VLE PTxy	210 – 304	0.33 – 5.8	0 – 1	0 – 1	**N calc**	109	109
							AAD%	15.70	14.17
							Bias%	-15.70	-14.17
							MAD%	56.18	55.94
	6	CP PTx	290 – 304	5.0 – 5.83	0.12 – 0.98		**N calc**	6	6
							AAD%	15.07	4.52
							Bias%	-15.07	4.48
							MAD%	41.61	7.50

1.48 Xe+C_2H_4

The literature data for the system Xe+C_2H_4 are shown in Figure F.104.

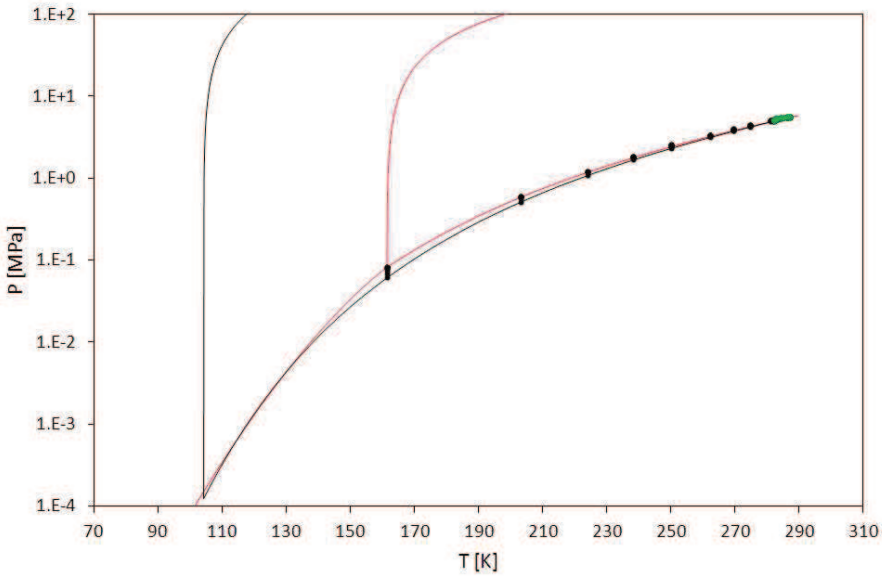

Figure F.104: Available experimental values for the system Xe+C_2H_4.
— : Xe; — : C_2H_4; ● : FFE data; ♦ : CP data.

The pressure-composition cross sections in Figure F.105 show the qualitative comparison between VLE data and model with null BIPs at 161 K. The SLV EoS does not represent the azeotropic behavior of the system Xe+C_2H_4. According to data, this vapor-liquid azeotrope extends up to the critical line.

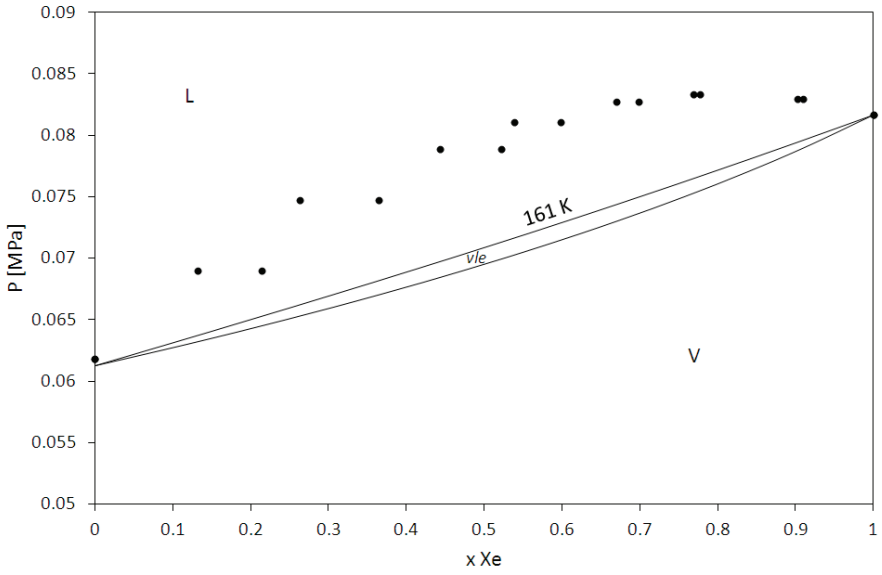

Figure F.105: VLE for the system Xe+C_2H_4 at 161 K.
● : [CAL1977]; — : SLV EoS (null BIPs).

Table F.48 gives the quantitative comparison between data and values calculated from the SLV EoS with null BIPs in terms of equilibrium mole fractions of Xe. Important deviations are encountered for both the liquid and the vapor phases.

Table F.48: Quantitative comparison of equilibrium compositions for the system $Xe+C_2H_4$.

xXe+(1-x)C₂H₄ Ref.	N	Kind of data	T K	P MPa	*x*	*y*		FLASH xXe	FLASH yXe
[CAL1977]	9	VLE PTxy	161	0.06 – 0.08	0 – 1	0 – 1	**N calc**	3	3
							AAD%	155.84	99.73
							Bias%	155.84	99.73
							MAD%	207.87	120.62
[NUN1986]	156	VLE PTxy	203 – 287	0.5 – 5.7	0 – 1	0 – 1	**N calc**	3	3
							AAD%	136.75	124.40
							Bias%	136.75	124.40
							MAD%	199.79	168.18
	10	CP PTx	282 – 290	5.1 – 5.84	0.16 – 0.9		**N calc**	6	10
							AAD%	49.57	13.96
							Bias%	-49.57	-13.96
							MAD%	89.59	23.35

1.49 Xe+C_3H_8

The literature data for the system Xe+C_3H_8 are shown in Figure F.106.

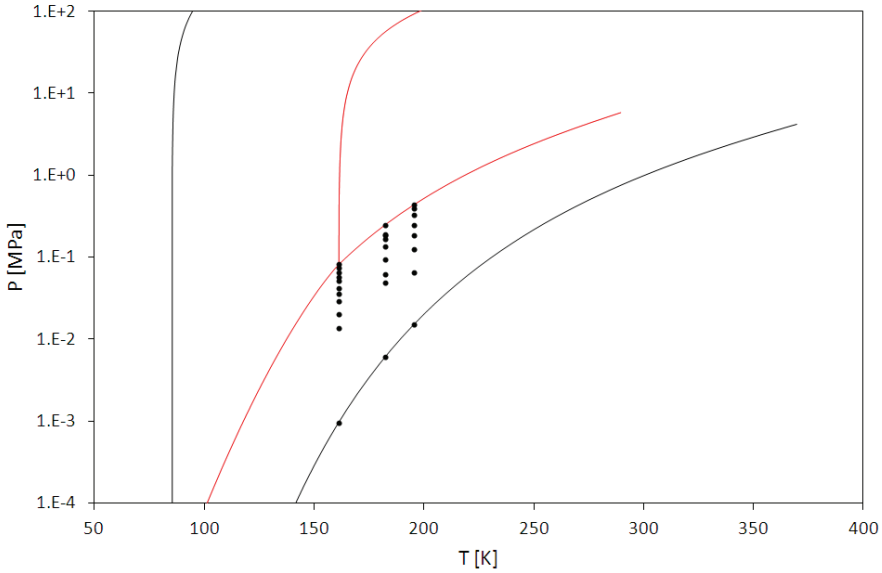

Figure F.106: Available experimental values for the system Xe+C_3H_8.
— : Xe; — : C_3H_8; ● : FFE data.

Table F.49 gives the quantitative comparison between data and values calculated from the SLV EoS with null BIPs in terms of equilibrium mole fractions of Xe. Model is in agreement with the experimental values proposed in [FIL2000].

Table F.49: Quantitative comparison of equilibrium compositions for the system Xe+C_3H_8.

xXe+(1-x)C_3H_8 Ref.	N	Kind of data	T K	P MPa	*x*	*y*	FLASH	
								xXe yXe
[FIL2000]	28	VLE PTx	161 – 195	0.001 – 0.44	0 – 1		**N calc**	22
							AAD%	1.82
							Bias%	-1.70
							MAD%	7.74

1.50 Xe+C_3H_6

The literature data for the system Xe+C_3H_6 are shown in Figure F.107.

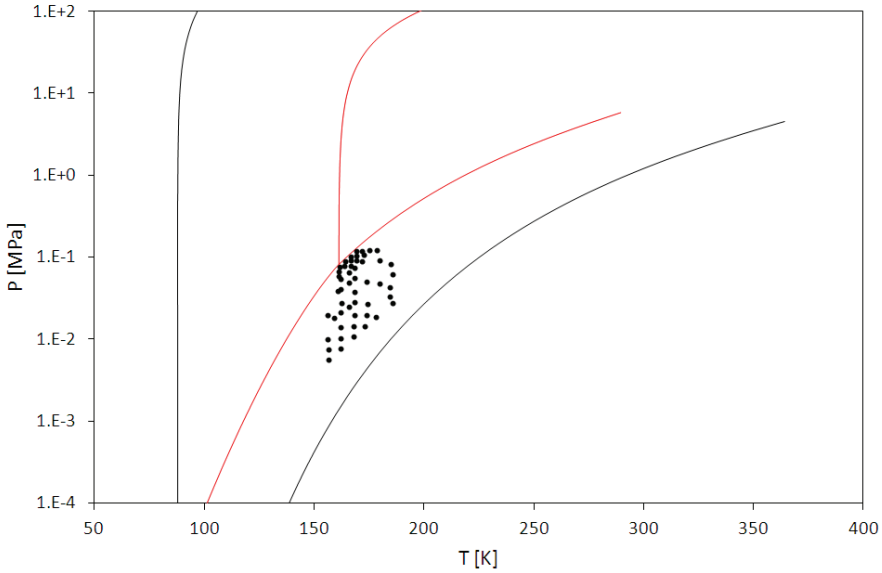

Figure F.107: Available experimental values for the system Xe+C_3H_6.
— : Xe; — : C_3H_6; ● : FFE data.

Table F.50 gives the quantitative comparison between data and values calculated from the SLV EoS with null BIPs in terms of equilibrium mole fractions of Xe. Model is not in agreement with the experimental values proposed in [BLA1967].

Table F.50: Quantitative comparison of equilibrium compositions for the system Xe+C_3H_6.

xXe+(1-x)C_3H_6 Ref.	N	Kind of data	T K	P MPa	*x*	*y*	FLASH	
								xXe yXe
[BLA1967]	51	VLE PTx	156 – 186	0.006 – 0.12	0.05 – 0.92		**N calc**	51
							AAD%	27.29
							Bias%	27.29
							MAD%	64.84

1.51 Ne+He

The literature data for the system Ne+He are shown in Figure F.108.

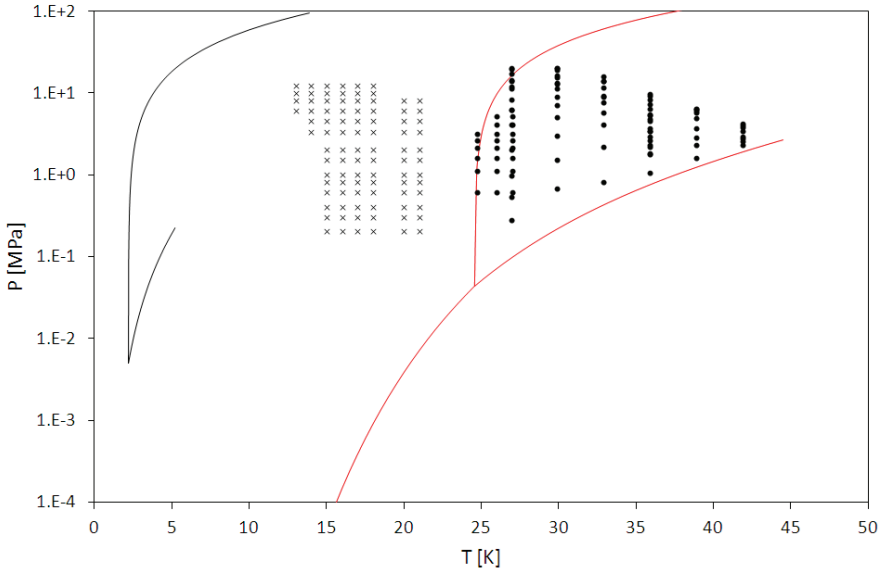

Figure F.108: Available experimental values for the system Ne+He.
— : Ne; — : He; ● : FFE data; × : SFE data.

Table F.51 gives the quantitative comparison between data and values calculated from the SLV EoS in terms of equilibrium mole fractions of Ne. Model agrees well with all the experimental values.

Table F.51: Quantitative comparison of equilibrium compositions for the system Ne+He.

xNe+(1-x)He Ref.	N	Kind of data	T K	P MPa	*x*	*y*		FLASH xNe	FLASH yNe
[HEC1967]	76	VLE PTxy	27 – 42	0.28 – 20.3	<0.01 – 0.36	0.08 – 0.93	**N calc**	52	52
							AAD%	1.46	4.24
							Bias%	-0.81	1.88
							MAD%	4.59	12.71
[IOM1977][1]	90	SVE PTy	13 – 21	0.2 – 12.2		0.96 – 1	**N calc**		90
							AAD		0.05
							Bias		0.01
							MAD		0.97
[KNO1967]	22	VLE PTxy	25 – 27	0.61 – 5.2	<0.01 – 0.03	0.97 – 0.998	**N calc**	22	22
							AAD%	0.19	5.02
							Bias%	0.19	-4.48
							MAD%	0.91	13.13

[1] – for SVE PTy data deviations are in terms of AAD, Bias, and MAD.

1.52 Ne+H_2

The literature data for the system Ne+H_2 are shown in Figure F.109.

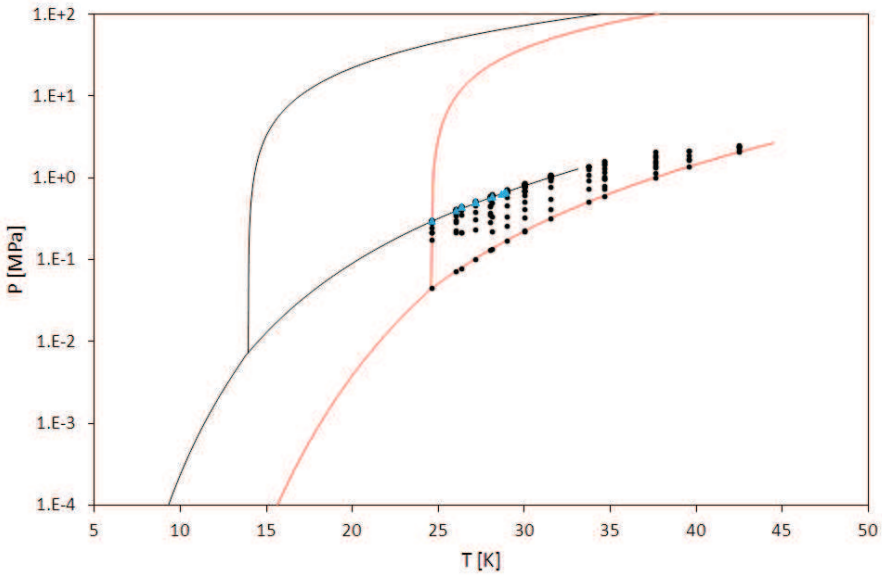

Figure F.109: Available experimental values for the system Ne+H_2.
— : Ne; — : H_2; ● : FFE data; ▲ : VLLE data.

The pressure-composition cross section in Figure F.110 shows the qualitative comparison between VLE data and model with null BIPs at 26 K. The SLV EoS does not represent the azeotropic behavior which is coupled with partial immiscibility in the liquid phase. According to data, this immiscibility occurs in the range 26 K ≤ T ≤ 29 K.

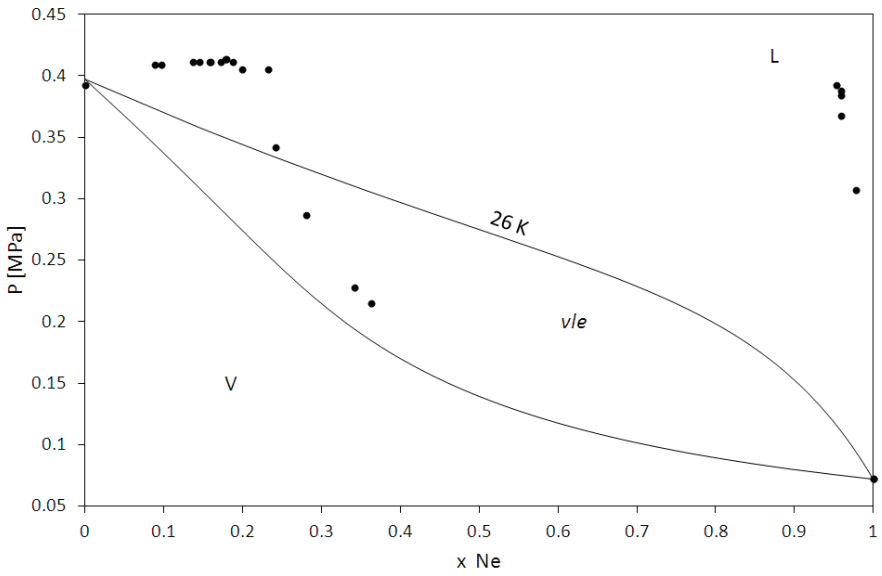

Figure F.110: VLE for the system Ne+H_2 at 26 K.
● : [HEC1966]; — : SLV EoS (null BIPs).

Table F.52 gives the quantitative comparison between data and values calculated from the SLV EoS with null BIPs in terms of equilibrium mole fractions of Ne. Important deviations are encountered for both the liquid and the vapor phases.

Table F.52: Quantitative comparison of equilibrium compositions for the system Ne+H_2.

xNe+(1-x)H_2 Ref.	N	Kind of data	T K	P MPa	*x*	*y*		FLASH xNe	FLASH yNe
[HEC1966]	90	VLE PTxy	26 – 43	0.07 – 2.5	0 – 1	0 – 1	**N calc**	24	31
							AAD%	45.84	26.32
							Bias%	-45.84	-26.32
							MAD%	96.60	88.49
	2	VLLE	26 – 28	0.4 – 0.58		0.72 – 0.8	**N calc**	0	0
							AAD%		
							Bias%		
							MAD%		
[STR1965d]	113	VLE PTxy	25 – 34	0.04 – 1.4	0 – 1	0 – 1	**N calc**	29	29
							AAD%	48.44	38.49
							Bias%	-48.44	-38.49
							MAD%	92.67	86.72
	21	VLLE	25 – 29	0.31 – 0.68	0.03 – 0.83	0.72 – 0.84	**N calc**	0	0
							AAD%		
							Bias%		
							MAD%		

1.53 He+H_2

The literature data for the system He+H_2 are shown in Figure F.111.

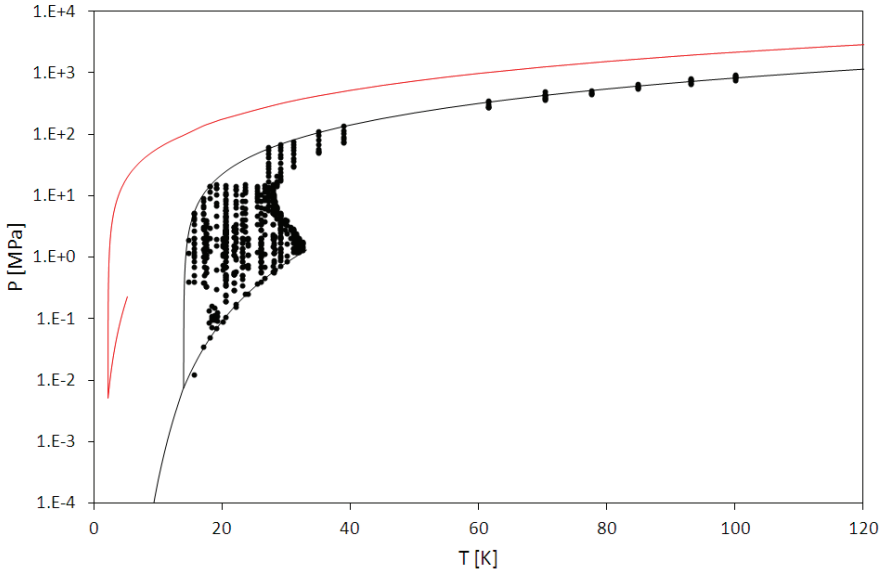

Figure F.111: Available experimental values for the system He+H_2.
— : He; — : H_2; ● : FFE data.

Table F.53 gives the quantitative comparison between data and values calculated from the SLV EoS with null BIPs in terms of equilibrium mole fractions of He.

Important deviations are encountered for both the liquid and the vapor phases. Errors usually increase while approaching the critical temperature of pure H_2 (33 K) and proceeding beyond this value, as in the case of data from [STR1973].

Table F.53: Quantitative comparison of equilibrium compositions for the system He+H_2.

xHe+(1-x)H₂ Ref.	N	Kind of data	T K	P MPa	*x*	*y*		FLASH xHe	FLASH yHe
[HIZ1972]	45	VLE PTxy	20.– 28	0.09 – 2.1	0 – 0.057	0 – 0.9	**N calc**	24	16
							AAD%	7.80	1.43
							Bias%	-1.28	0.79
							MAD%	25.45	4.33
[HIZ1981]	45	VLE PTxy	20 – 28	0.09 – 2.1	0 – 0.057	0 – 0.9	**N calc**	24	16
							AAD%	23.62	1.41
							Bias%	23.62	-1.41
							MAD%	78.16	5.24
[PAS1981]	137	VLE PTxy	15 – 30	0.01 – 15.4	0 – 0.33	0 – 0.98	**N calc**	124	124
							AAD%	83.85	6.14
							Bias%	80.26	<0.01
							MAD%	302.00	36.03
[SON1964]	45	VLE PTxy	20 – 35	0.24 – 3.45	0.002 – 0.18	0.06 – 0.89	**N calc**	45	45
							AAD%	19.51	9.62
							Bias%	14.84	8.85
							MAD%	100.39	77.35
[SMI1952]	106	VLE PTxy	17 – 22	0.19 – 5.9	<0.01 – 0.03	0.61 – 0.96	**N calc**	58	73
							AAD%	77.45	3.38
							Bias%	77.45	-3.15
							MAD%	317.62	28.64

[SNE1968]	76	VLE PTxy	16 – 30	1.97 – 10.3	0.01 – 0.36	0.31 – 0.96	**N calc**	76	76
							AAD%	48.37	15.24
							Bias%	31.89	13.51
							MAD%	236.96	77.26
[STR1964]	92	VLE PTxy	16 – 33	0.24 – 3.45	<0.01 – 0.21	0.03 – 0.97	**N calc**	91	88
							AAD%	31.09	5.37
							Bias%	26.40	2.70
							MAD%	144.20	52.80
[STR1973]	104	VLE PTxy	26 – 100	0.59 – 917	<0.01 – 0.45	0.26 – 0.97	**N calc**	33	33
							AAD%	95.39	11.83
							Bias%	77.88	-9.27
							MAD%	564.02	28.98
[YAM1992]	13	VLE PTxy	18 – 19	0.07 – 0.16	<0.01	0.28 – 0.56	**N calc**	13	5
							AAD%	12.78	12.80
							Bias%	2.49	-12.80
							MAD%	32.55	23.61

Bibliography

[1] E. Lemmon, M. Huber and M. McLinden, "NIST Standard Reference Database 23: Reference Fluid Thermodynamic and Transport Properties-REFPROP, Version 8.0, National Institute of Standards and Technology, Standard Reference Data Program, Gaithersburg," 2007.

Etude thermodynamique des équilibres solide-liquide-vapeur: application à la cryogénie et aux unités de séparation de l'air

RESUME: Dans le cadre du procédé de séparation cryogénique des gaz de l'air (T< 100 K), impuretés telles que le CO_2 et le N_2O peuvent se solidifier au niveau de l'échangeur de chaleur placé entre les deux colonnes de distillation cryogénique.
La formation du solide doit être évitée pour deux principales raisons:

- au niveau opérationnel, le solide constitue une résistance supplémentaire aux transferts de chaleur et de matière, et augmente les chutes de pression dans les colonnes de distillation;
- au niveau sécurité, la présence d'une phase solide peut également favoriser l'accumulation d'hydrocarbures légers qui forment avec l'oxygène liquide des mélanges potentiellement inflammables.

Les conditions de formation thermodynamique de la phase solide doivent être parfaitement maitrisées dans le cadre de la distillation cryogénique. C'est pourquoi, il est indispensable de disposer d'une équation d'état adaptée qui permette de représenter les diagrammes de phases impliquant une phase solide dans les conditions opératoire du procédé.
L'objectif principal de la thèse est de développer un modèle thermodynamique pour représenter les équilibres de phases solide – fluides. Ce travail nécessite de mettre au point des algorithmes de résolution des équilibres bi et triphasiques et de déterminer le meilleur jeu de paramètres du modèle en s'appuyant sur la disponibilité des données expérimentales dans les conditions cryogéniques.
Le modèle permet d'améliorer la connaissance des équilibres et constitue un outil indispensable pour maîtriser les risques associés à la présence de phases solides pour le procédé de distillation cryogénique.

Mots clés: Diagramme de phases, Enthalpie libre de Gibbs, Equation d'état, Modélisation, Equilibre solide-fluide

Thermodynamic study of solid-liquid-vapor equilibrium: application to cryogenics and air separation unit

ABSTRACT: In the framework of the cryogenic air separation, impurities such as CO_2 and N_2O may solidify at the reboiler-condenser placed between the two distillation columns.
The formed solid could provide an additional strength to the heat and material transfers, and increase the pressure drops in the distillation columns.
Furthermore, the presence of a solid phase can promote the accumulation of light hydrocarbons which may form flammable mixtures with liquid oxygen.
Therefore, the presence of solid phases must be controlled see avoided within the cryogenic air distillation process.
The main issue of this thesis is to develop a suitable model for representing solid phases and their equilibrium with the liquid and vapor phases at the operating conditions of the process, and to obtain full phase diagrams which would improve the knowledge of phase equilibria and the control of the risks associated to the presence of solid phases.

Keywords: Phase diagram, Gibbs free energy, Equation of state, Modelling, Solid-fluid equilibrium

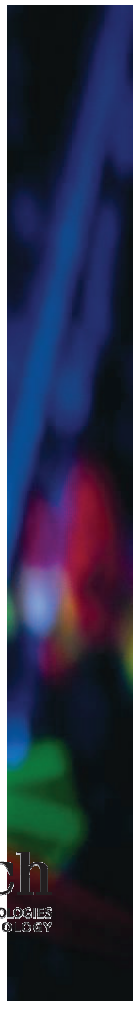

MINES ParisTech

ParisTech
INSTITUT DES SCIENCES ET TECHNOLOGIES
PARIS INSTITUTE OF TECHNOLOGY